THEORETICA CHIMICA ACTA

edenda curat

Hermann Hartmann

adiuvantibus

C. J. Ballhausen, København
R. D. Brown, Clayton
E. Heilbronner, Basel
J. Jortner, Tel-Aviv
M. Kotani, Tokyo
J. Koutecký, Praha
J. W. Linnett, Cambridge
E. E. Nikitin, Moskwa
R. G. Pearson, Evanston
B. Pullman, Paris
K. Ruedenberg, Ames
C. Sandorfy, Montreal
M. Simonetta, Milano
O. Sinanoğlu, New Haven

Vol. 28, 1972/73

Springer-Verlag · Berlin · Heidelberg · New York

The exclusive copyright for all languages and countries, including the right for photomechanical and any other reproductions, also in microform, is transferred to the publisher.

The use of registered names, trademarks, etc. in this publication does not imply, even in the absence of a specific statement, that such names are exempt from the relevant protective laws and regulations and therefore free for general use.

Alle Rechte, einschließlich das der Übersetzung in fremde Sprachen und das der fotomechanischen Wiedergabe oder einer sonstigen Vervielfältigung, auch in Mikroform, vorbehalten. Jedoch wird gewerblichen Unternehmen für den innerbetrieblichen Gebrauch nach Maßgabe des zwischen dem Börsenverein des Deutschen Buchhandels e. V. und dem Bundesverband der Deutschen Industrie abgeschlossenen Rahmenabkommens die Anfertigung einer fotomechanischen Vervielfältigung gestattet. Wenn für diese Zeitschrift kein Pauschalabkommen mit dem Verlag vereinbart worden ist, ist eine Wertmarke im Betrage von DM 0,40 pro Seite zu verwenden. *Der Verlag läßt diese Beträge den Autorenverbänden zufließen.*

Die Wiedergabe von Gebrauchsnamen, Handelsnamen, Warenbezeichnungen usw. in dieser Zeitschrift berechtigt auch ohne besondere Kennzeichnung nicht zu der Annahme, daß solche Namen im Sinne der Warenzeichen- und Markenschutz-Gesetzgebung als frei betrachtet wären und daher von jedermann benutzt werden dürften.

Springer-Verlag Berlin Heidelberg New York
Printed in Germany by Brühlsche Universitätsdruckerei, Gießen
© by Springer-Verlag Berlin Heidelberg 1973

S/02
38966
Date 24.4.76

Index

Commentationes et Relationes

Achatz, M., s. Hensen, K., *et al.* 297

Almlöf, J., Wahlgren, U.: Hydrogen Bond Studies. 66. *Ab initio* Studies of the Conformation of the Oxonium Ion in Solids 161

Andreev, E. A.: On Asymptotic Calculation of the Exchange Interaction 235

Basch, H.: Photodecomposition of Ketene to Form Methylene 151

Becker, R. S., s. Germer, H. A., Jr. 1

Bingel, W. A., Klahn, B.: Der Elektronendichtequotient zweiatomiger Moleküle. I. Allgemeine Theorie und deren Anwendung auf das δ-Modell 37

Bingel, W. A., s. Klahn, B. 53

Blomquist, J., Nordén, B., Sundbom, M.: A Semiempirical MO Study of the Electronic Structure and Excited States of the *Tris*(2,2′-Bipyridyl) Iron(II) and *Tris*(Glyoxal-*Bis*-N-Methylimine)Iron(II) Ions 313

Brown, R. D., Burden, F. R., Hart, B. T., Williams, G. R.: The Electronic Structure of the NF_2 Radical 339

Burden, F. R., s. Brown, R. D., *et al.* 339

Burrows, B. L.: Unrestricted Hartree Fock Perturbation Theory 179

Castro, E. A., Sorarrain, O. M.: Electronic Structure of BF_3-Benzaldehyde 209

Chenot, J. L.: Optimized Extended Hückel Theory for Calculating the Ionization Potentials and Dissociation Energies of Hydrocarbons 201

Clark, P. A.: Electronic Structures of Some Olefins and Their Radical Cations 75

Demuynck, J., Veillard, A.: Electronic Structure of the Nickel Tetracyanonickelate $Ni(CN)_4^{2-}$ and Nickel Carbonyl $Ni(CO)_4$. An *ab initio* LCAO-MO-SCF Calculation. . . . 241

Diercksen, G. H. F., Kraemer, W. P., Niessen, W. von: SCF MO LCGO Studies on Hydrogen Bonding: The System $NH_3 \cdot H_2O$ 67

Dyczmons, V.: No N^4-Dependence in the Calculation of Molecules 307

Ehrenson, S., Wong, M.: On Radial Weighting Effects in Gaussian Expansions of Self-Consistent Field Atomic Orbitals 283

Fraser, S. J., Linnett, J. W.: The Use of Correlated Gaussian Wavefunctions for the Calculation of Chemical Energies for Small Systems 13

Gelus, M., Kutzelnigg, W.: *Ab initio* Calculations of Small Hydrides Iucluding Electron Correlation. VIII. Equilibrium Geometry and Harmonic Force Constants of BH_3 . . . 103

Germer, H. A., Jr., Becker, R. S.: Interpretation of Pentacyclic Aromatic Hydrocarbon Transitions in Terms of Composite System Approximations 1

Gołębiewski, A., Mrozek, J. Nalewajski, R.: A Comparative Study of Approximate SCF MO Treatments of Hydrides 169

Habitz, P., Schwarz, W. H. E.: Vibronic and Spin-Orbit Splitting in Spectra of Systems Exhibiting Jahn-Teller-Effect 267

Hariharan, P. C., Pople, J. A.: The Influence of Polarization Functions on Molecular Orbital Hydrogenation Energies 213

Hart, B. T., s. Brown, R. D., *et al.* 339

Hase, H. L., Meyer, H., Schweig, A.: A Note on the Importance of Including Monoatomic Overlap Densities in the Calculation of CNDO/2 Charge Distributions 99

Hensen, K., Achatz, M., Müller, R.: Statistische Modellrechnungen an den Molekülen CH_4, SiH_4, GeH_4 SnH_4 und PbH_4 nach der Einzentrenmethode 297

Hussonnois, M., s. Malý, J. 363

Jeżowska-Trzebiatowska, B., s. Natkaniec, L., *et al.* 193

Klahn, B., Bingel, W. A.: Der Elektronendichtequotient zweiatomiger Moleküle. II. Anwendung der Theorie auf Moleküle und Entwicklung des Elektronendichtequotienten nach dem Kernabstand 53

Klahn, B., s. Bingel, W. A. 37

Kitaura, K., Nishimoto, K.: An Application of RPA Theory to Conjugated Systems in the Excited States 111

Kraemer, W. P., s. Diercksen, G. H. F., *et al.* 67

Kutzelnigg, W., s. Gelus, M. 103

Ladik, J., s. Suhai, S. 27

Laurenzi, B. J.: Isoelectronic Molecules.
First- and Second-Order Properties and the Continuous Group *L* (*l*) 81

Lehn, J. M., Wipff, G.: The Electronic Structure of Bicyclo [2.1.1] hexane 223

Linnett, J. W., s. Fraser, S. J. 13

Malý, J., Hussonnois, M.: SCF Dirac-Hartree-Fock Calculations in the Periodic System.
I. Calculated Ground States of All Elements from $Z = 1$ to $Z = 120$ 363

Meyer, H., s. Hase, H. L., *et al.* 99

Mrozek, J., s. Gołębiewski, A., *et al.* 169

Müller, R., s. Hensen K., *et al.* 297

Nalewajski, R., s. Gołębiewski, A., *et al.* 169

Natkaniec, L., Rudolf, M. F., Jeżowska-Trzebiatowska, B.: The Electronic Structure of the Oxygen Double-Bridged $\mu\mu'$-Dioxo-bis (Oxodichloroaquo) Dimolybdate (V)-Ion by SCCC MO Method 193

Niessen, W. von, s. Diercksen, G. H. F., *et al.* 67

Nikitin, E. E., Umanskij, S. J.: Wellenfunktionen und Terme des Systems Atom/zweiatomiges Molekül bei großen intermolekularen Abständen 121

Nishimoto, K., s. Kitaura, K. 111

Nordén, B., s. Blomquist, J., *et al.* 313

Pamuk, H. Ö.: Semi-Empirical Effective Pair Correlation Parameters and Correlation Energies of BH, CH, NH, OH, HF, N_2, and CH_4 85

Pople, J. A., s. Hariharan, P. C. 213

Repmann, H.: Die Elektronenstruktur von Steroidhormonen.
2. Die Nebennierenrindenhormone 141

Rudolf, M. F., s. Natkaniec, L., *et al.* 193

Schwarz, W. H. E., s. Habitz, P. 267

Schweig, A., s. Hase, H. L., *et al.* 99

Sieiro, C., s. Smeyers, Y. G. 355

Smeyers, Y. G., Sieiro, C.: Spectres et étude conformationelle des dérivés méthyles de l'acide benzoïque 355

Sorarrain, O. M., s. Castro, E. A. 209

Suhai, S., Ladik, J.: The Electronic Structure of Periodic Protein Models.
I. CNDO/2 and MINDO/2 Energy Band Structures of a Two-Dimensional Formamide Network 27

Sundbom, M., s. Blomquist, J., *et al.* 313

Umanskij, S. J., s. Nikitin, E. E. 121

Veillard, A., s. Demuynck, J. 241

Wahlgren, U., s. Almlöf, J. 161

Williams, G. R., s. Brown, R. D., *et al.* 339

Wipff, G., s. Lehn, J. M. 223

Wong, M., s. Ehrenson, S. 283

Erratum

Kahn, O., Kettle, S. F. A.: Influence du couplage vibronique sur le paramagnétisme d'un complexe cubique dans l'état électronique $^2T_2$. [Theoret. chim. Acta (Berl.) 27, 187 (1972)] 312

Indexed in Current Contents

Theoret. chim. Acta (Berl.) 28, 1—11 (1972)
© by Springer-Verlag 1972

Commentationes

Interpretation of Pentacyclic Aromatic Hydrocarbon Transitions in Terms of Composite System Approximations

Henry A. Germer, Jr. [1]
Department of Biophysical Sciences

Ralph S. Becker
Department of Chemistry
University of Houston, Houston, Texas 77004

Received July 27, 1971/May 29, 1972

The observed electronic transitions and transition assignments of three pentacyclic aromatic hydrocarbons, benz(a)naphthacene, dibenz(a, c) anthracene, and 3,4-benzopyrene, are presented. The transitions of the pentacyclic aromatics are correlated with the transitions of tetracyclic aromatic hydrocarbons contained within the structure of the pentacyclic. The results of the experimental correlation are then compared with the results of a theoretical "molecules in molecule" interpretation of the pentacyclic transitions. The results of this comparison indicate that applying a theoretical composite system concept to the interpretation of pentacyclic spectra is justified for the lower energy transitions.

Es wird über die bei den drei pentacyclischen aromatischen Kohlenwasserstoffen: Benz(a)-naphthacen, Dibenz(a, c) anthracen und 3,4-Benzopyren beobachteten Elektronenübergänge und ihre Zuordnung berichtet. Die Übergänge der pentacyclischen aromatischen Kohlenwasserstoffe werden mit Übergängen bei den tetracyclischen aromatischen Kohlenwasserstoffen verglichen, die als Strukturelemente der pentacyclischen auftreten. Danach werden die Ergebnisse der experimentellen Korrelation mit Resultaten der theoretischen „Molekül im Molekül" Interpretation der pentacyclischen Übergänge verglichen.

Dieser Vergleich zeigt, daß bei den Übergängen niedriger Energie die Verwendung des theoretischen Konzepts zusammengesetzter Systeme gerechtfertigt ist.

Introduction

The similarities noted in the ultraviolet and visible absorption spectra of many polycyclic aromatic hydrocarbons have led to a number of studies which have attempted to interpret the electronic transitions of particular molecules in terms of various parts of the molecules. These studies are best exemplified by the "independent systems" or "molecules in molecule" approaches of Simpson [2] and Longuet-Higgins and Murrell [3]. In the "molecules in molecule" (MIM) method, it is assumed that the molecule is a composite system, R-S, and that electronic transitions may be described in terms of local excitations in the two parts, R and S, and electron-transfer transitions arising from excitation of an electron from a molecular orbital in one part to a molecular orbital in another part. Longuet-Higgins and Murrell [3] applied this method to analysis of the spectra of diphenyl, butadiene, and styrene.

Longuet-Higgins and Murrell's [3] theoretical development has served as the basis of a number of later studies. Heilbronner *et al.* [4] applied this composite system approach to acenaphthylene and fluoranthene. These two molecules are characterized as "weakly" non-alternant, which means that they consist of alternant subunits linked by non-essential double bonds in such a way that the subunits retain much of their individuality. A composite systems approach was used by Mori [5] to calculate the electronic transitions of benzyl radical. Experimental work by Johnson and Albrecht [6] indicates that the composite systems approach of Mori [4] predicts the transitions of benzyl radical much better than the conventional molecular orbital treatment. Favini *et al.* [7] have applied the composite systems or MIM theory to the interpretation of the electronic spectra of a large number of aromatic hydrocarbons. This study was unique in that many of the molecules studied normally have significant conjugation between the parts of the composite system model.

The above studies have all been within the framework of the P-P-P semi-empirical theory. Von Niessen [8] has recently proposed a theory of molecules for use in *ab initio* studies within the Hartree-Fock formalism.

The present investigation was prompted by the observation that many electronic transitions of the pentacyclic aromatic hydrocarbons appear, on the basis of extinction coefficient, vibrational structure, and general appearance, to be quite similar to the electronic transitions observed in the tetracyclic aromatic hydrocarbons. In order to try to understand a phenomenon such as this, the obvious approach is by means of the MIM concept in which these molecules are treated as a composite two-part system. Consequently, a composite systems study has been performed on a representative group of three pentacyclic aromatic hydrocarbons: benz(a)naphthacene (BN), dibenz(a,c)-anthracene (DBA), and 3,4-benzopyrene (BP) (see Fig. 1 for structures). Initially, the observed spectra

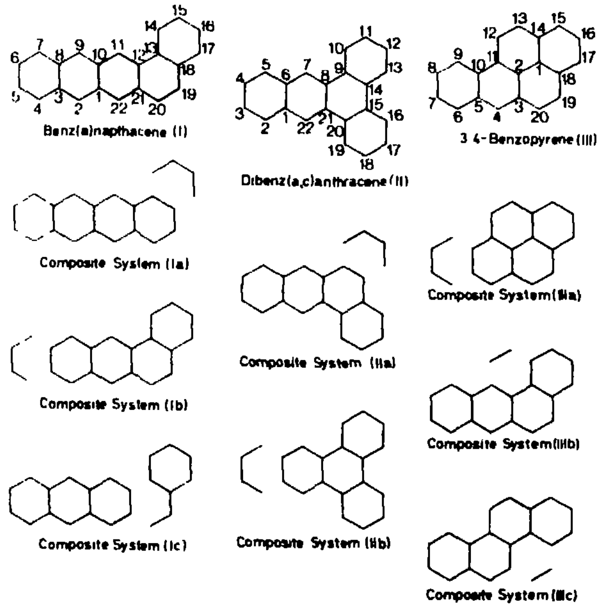

Fig. 1. Structures of compounds and composite system models

of these molecules were systematically examined and, where possible, the transitions correlated to particular tetracyclic aromatic transitions. Following this, the electronic transitions of the pentacyclics were calculated, together with the spectra of various composite system models of each molecule, in order to infer a theoretical composite system basis for the pentacyclic transitions. Finally, the results of the experimental and theoretical MIM interpretations were compared.

Experimental

The experimentally observed transitions of benz(a)naphthacene, dibenz(a,c)anthracene, and 3,4-benzopyrene are given in Tables 1, 2 and 3, respectively. The corresponding calculated transitions are also given in these tables.

The observed transitions and extinction coefficients of the pentacyclics were obtained from the room temperature absorption spectra of the hydrocarbons dissolved in *p*-dioxane. Low temperature absorption spectra (77° K) were used as an aid in making transition assignments. The analysis of the experimental tetracyclic aromatic spectra required for the MIM interpretation was done by Becker *et al.* [9].

Table 1. Experimentally observed maximum of transitions of benz(a)naphthacene and corresponding calculated transitions[a]

Transition number	Observed transition energy (eV)	Extinction coefficient of observed transition (1/mole · cm)	Calculated transition energy (eV)	Calculated oscillator strength
I	2.75	36095	2.98	0.371
II	3.92	61657	3.84	0.892
III	4.09	117057	4.21	1.815
IV	4.81	61657	4.98	0.634
V	5.55	36095	5.25	0.327

[a] Considering molecule as single quantum mechanical system.

Table 2. Experimentally observed maximum of transitions of dibenz(a,c)anthracene and corresponding calculated transitions[a]

Transition number	Observed transition energy (eV)	Extinction coefficient of observed transition (1/mole · sec)	Calculated transition energy (eV)	Calculated oscillator strength
I	3.29	697	3.53	0.000
II	3.52	3465	3.74	0.168
III	4.31	146315	4.37	2.285
IV	4.98	52255	4.84	1.263
V	5.68	40264	5.35	0.364
VI	6.00	–	5.92	0.268

[a] See Table 1.

Table 3. Experimentally observed maximum transitions of 3,4-benzopyrene and corresponding calculated transitions[a]

Transition number	Observed transition energy (eV)	Extinction coefficient of observed transition (l/mole · sec)	Calculated transition energy (eV)	Calculated oscillator strength
I	3.07	4029	3.31	0.000
II	3.22	27637	3.12	0.997
III	4.18	57871	4.42	0.871
IV	4.67	43889	4.72	0.662
V	5.47	24352	5.14	1.055
VI	5.93	–	5.78	0.334

[a] See Table 1

The experimental MIM interpretation of the observed transitions of the pentacyclic aromatic hydrocarbons in terms of observed tetracyclic transitions was based on the correlation of a number of factors. Of primary importance were the relative energies and intensities of the transitions. Other important considerations were the vibrational sequences and general shape of the transitions. Finally the overall aspects of the entire UV spectra of the molecules were considered. The results of this MIM interpretation are summarized in the correlations between columns 4 and 5 of the three correlation diagrams, Figs. 2, 3 and 4.

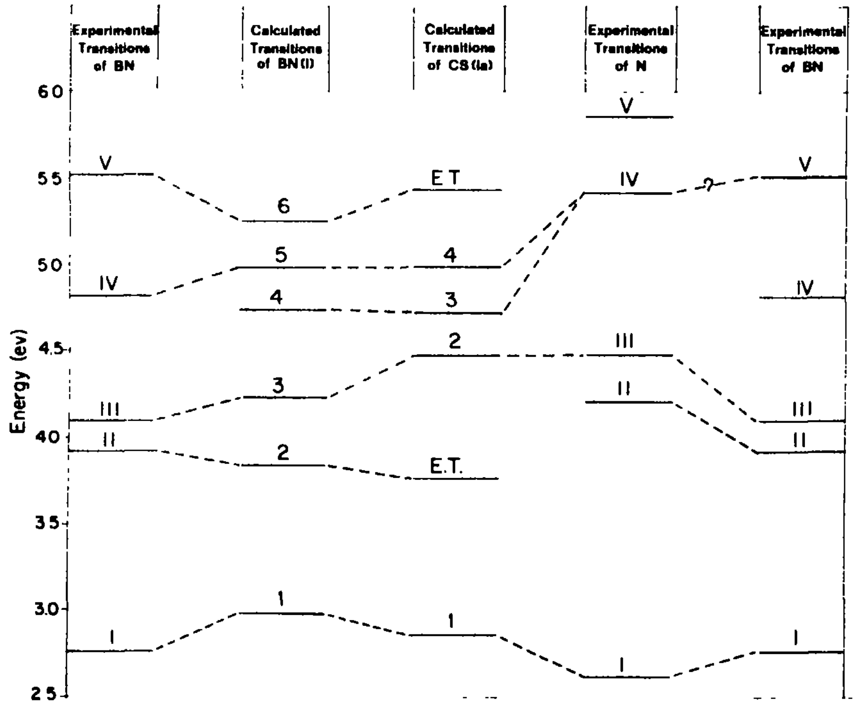
Experimental Transitions of BN
Calculated Transitions of BN (I)
Calculated Transitions of CS (Ia)
Experimental Transitions of N
Experimental Transitions of BN
Energy (ev)
6.0
5.5
5.0
4.5
4.0
3.5
3.0
2.5
V
IV
III
II
I
6
5
4
3
2
1
ET
4
3
2
E.T.
1
V
IV
III
II
I
?
V
IV
III
II
I

Fig. 2. Summary of theoretical and experimental transitions of Benz(a)naphthacene (BN) and its appropriate composite system (CS) model, together with correlations resulting from "molecules in molecule" interpretations. Experimental transitions of Naphthacene (N) from Ref. [9]. E.T. denotes degenerate pair of formally forbidden electron-transfer transitions

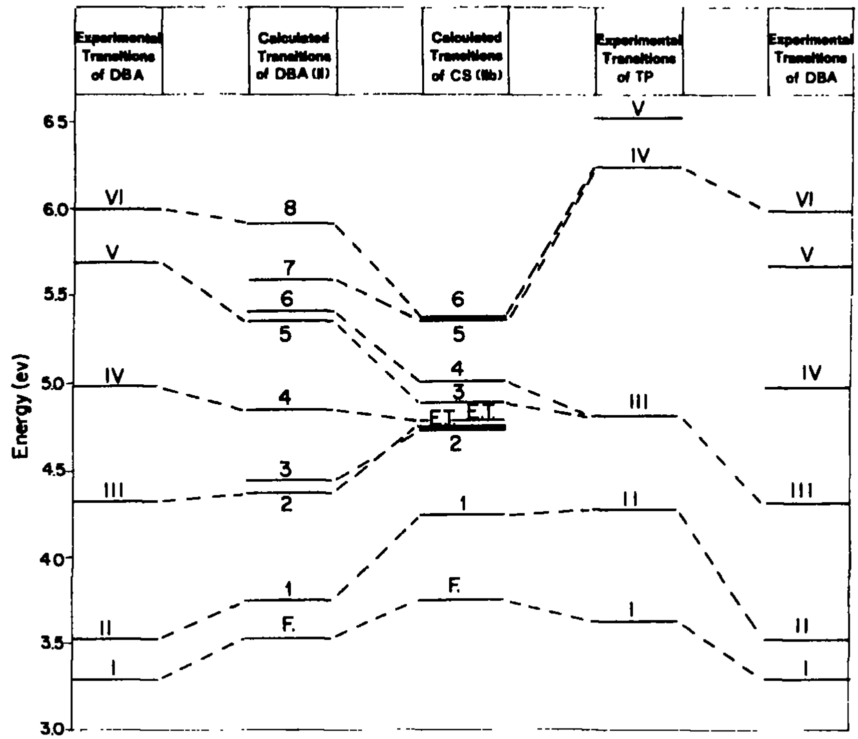

Fig. 3. Summary of theoretical and experimental transitions of Dibenz(a,c)anthracene (DBA) and its appropriate composite system (CS) model, together with correlations resulting from "molecules in molecule" interpretations. Experimental transitions of Triphenylene (TP) from Ref. [9]. E.T. denotes degenerate pair of electron-transfer transitions and F. denotes a formally forbidden transition

In the case of BN, transitions I, II, and III are clearly naphthacene-like, implying a composite system model containing naphthacene and cis-butadiene. Transition IV does not resemble any naphthacene transition; however, transition V may slightly resemble the fourth transition of naphthacene.

On the whole, the transitions of DBA most clearly approximate the observed spectra of triphenylene, implying a composite system model composed of triphenylene and cis-butadiene. Transitions IV and V of DBA cannot be related to any observed triphenylene transitions. In the absorption spectra of triphenylene (see Ref. [9]), a large energy gap exists between the third and fourth observed transitions. It is in this region that transition IV and V of DBA appear. A possible explanation of this phenomenon is that the triphenylene transitions in this region are forbidden due to the high symmetry of triphenylene, but become allowed in the less symmetrical DBA molecule. Transition VI is correlated to the fourth triphenylene transition.

The observed transitions of BP can be clearly correlated with the observed transitions of pyrene. This, of course, implies a composite system model consisting of pyrene and cis-butadiene.

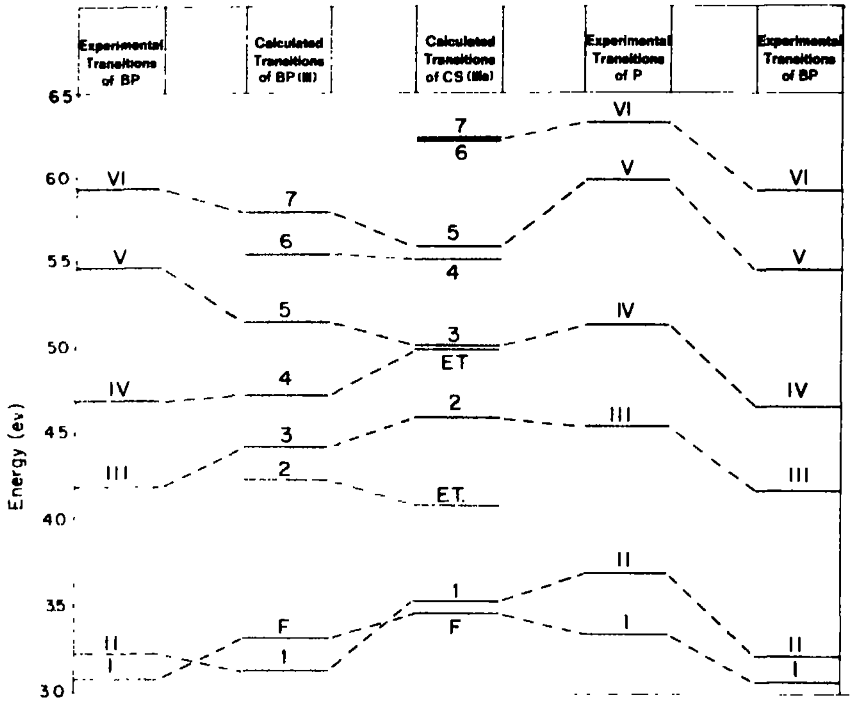
Experimental Transitions of BP
Calculated Transitions of BP (III)
Calculated Transitions of CS (IIIa)
Experimental Transitions of P
Experimental Transitions of BP
Energy (ev)
65
60
55
50
45
40
35
30
VI
V
IV
III
II
I
7
6
5
4
3
2
1
F
ET
E.T.

Fig. 4 Summary of theoretical and experimental transitions of 3,4-Benzopyrene (BP) and its appropriate composite system (CS) model, together with correlations resulting from "molecules in molecule" interpretations. Experimental transitions of Pyrene (P) from Ref. [9]. E.T. denotes degenerate pair of formally forbidden electron-transfer transitions and F. denotes a formally forbidden transition

Theoretical

The theoretical spectra were determined by standard Pariser-Pople-Parr (P-P-P) semi-empirical SCF-MO calculations with configuration interaction. Only π electrons were considered. The Pariser [10] approximation was used for the one-center repulsion integrals, γ_{ii}, while the Mataga [11] approximation was used for two-center repulsion integrals, γ_{ij}. The valence state ionization potential and electron affinity of a $2p\pi$ carbon atom were taken as 11.42 eV and 0.58 eV, respectively. Standard aromatic type geometry was assumed for all calculations with bond lengths equal to 1.40 Å. In the CI calculations, a maximum of 50 of the lowest energy singly excited configurations having an energy within 8.0 eV of the ground state were used to determine the excited state wave functions.

Calculations were performed on all composite system models shown in Fig. 1. Essentially three calculations were made for each composite system model. The spectra were first calculated with the resonance integrals, β_{ij}, between all bonded centers set to -2.318 eV with the exception of the bonds connecting the component parts of the composite system for which β_{ij} was set to 0.0 eV. In the second calculation, the β_{ij} for the bonds connecting the two moieties of the composite system were changed to -1.00 eV. And third, the spectra were calculated with β_{ij} equal to -2.318 eV for all bonded centers including the bonds between the composite system parts.

The theoretical development presented by Longuet-Higgins and Murrell [3] is applicable to the present calculations with the zero resonance integrals between the two parts of the composite system. However, the manner in which the effects of finite resonance integrals between the parts is treated is somewhat different in this present study. In the presence of finite resonance integrals between the component parts, the self-consistent MO's will no longer simply be the orbitals of the two subsystems R and S which would be found if both were treated as separate quantum mechanical systems; instead, they are a set of MO's spanning the entire composite system. Longuet-Higgins and Murrell assumed in their treatment of a molecule as a component system that the MO's of the composite system did not change upon introducing finite resonance integrals between the subsystems. In their concept of a composite system, the increased interaction of the component parts results only in changed configuration interaction and not in alteration of the MO's. In other words, the limit of a strongly interacting composite system is not the subject molecule treated conventionally as a single quantum mechanical system. In the present study, the passing from a weakly interacting composite system to a completely interacting system is accomplished by allowing the resonance integrals to increase in magnitude, starting at zero,

Table 4. Comparison of excitation energies of 3,4-benzopyrene (III) and composite system models (IIIa), (IIIb) and (IIIc) with $\beta_{RS} = -1.0$ eV

3,4-Benzopyrene (III)		Composite system (IIIa)		Composite system (IIIb)		Composite system (IIIc)	
Excitation energy (eV)	f	Excitation energy (eV)	f	Excitation energy (eV)	f	Excitation energy (eV)	f
3.120	0.997	3.357	0.966	3.421	0.000	3.536	0.000
3.312	0.000	3.419	0.000	3.449	0.543	3.615	0.690
4.199	0.000	4.125	0.000	4.276	1.072	4.438	0.000
4.225	0.048	4.237	0.057	4.366	0.000	4.689	0.000
4.419	0.871	4.376	0.003	4.651	0.000	4.712	0.104
4.424	0.000	4.387	0.000	4.759	0.972	4.727	1.583
4.671	0.000	4.678	0.595	4.783	0.000	4.899	0.330
4.719	0.662	4.809	0.710	4.842	0.098	4.955	0.000
5.141	1.055	4.835	0.000	4.934	0.302	5.115	0.828
5.263	0.000	5.081	0.000	5.276	0.000	5.447	0.000
5.432	0.000	5.260	0.000	5.347	0.000	5.576	0.000
5.542	0.046	5.442	0.000	5.457	0.038	5.563	0.000
5.638	0.000	5.447	0.704	5.616	0.000	5.696	0.121
5.782	0.334	5.542	0.236	5.688	0.504	5.793	0.000
5.973	0.000	5.760	0.571	5.817	0.000	5.818	0.148
6.031	0.044	6.059	0.000	5.827	0.633	5.878	0.121
6.146	0.000	6.061	0.004	6.081	0.000	5.967	0.014
6.244	0.324	6.133	0.122	6.123	0.339	6.141	0.000
6.401	0.450	6.234	0.000	6.239	0.365	6.342	0.245
6.448	0.000	6.417	0.173	6.272	0.000	6.360	0.000
		6.445	0.000	6.488	0.000	6.402	0.277
		6.478	0.998			6.483	0.040

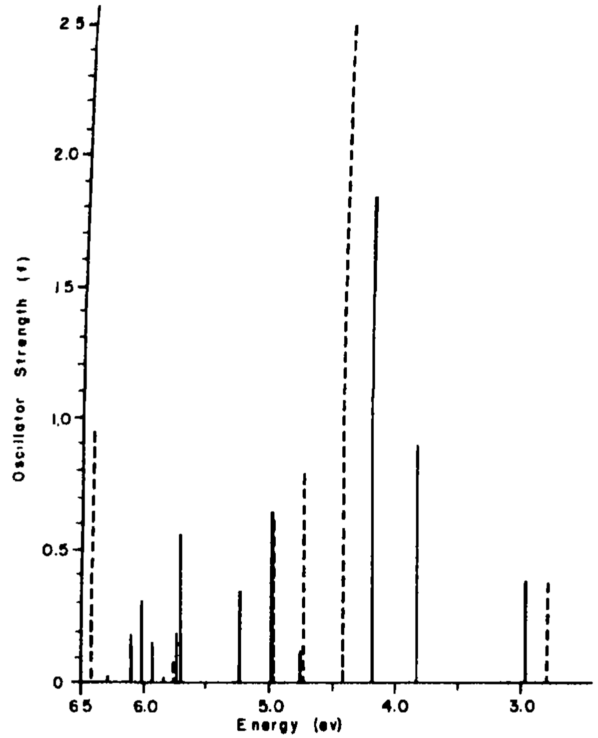

Fig. 5. Calculated absorption spectra of benz(a)naphthacene (I), shown as solid lines, and composite system (Ia), shown as dashed lines

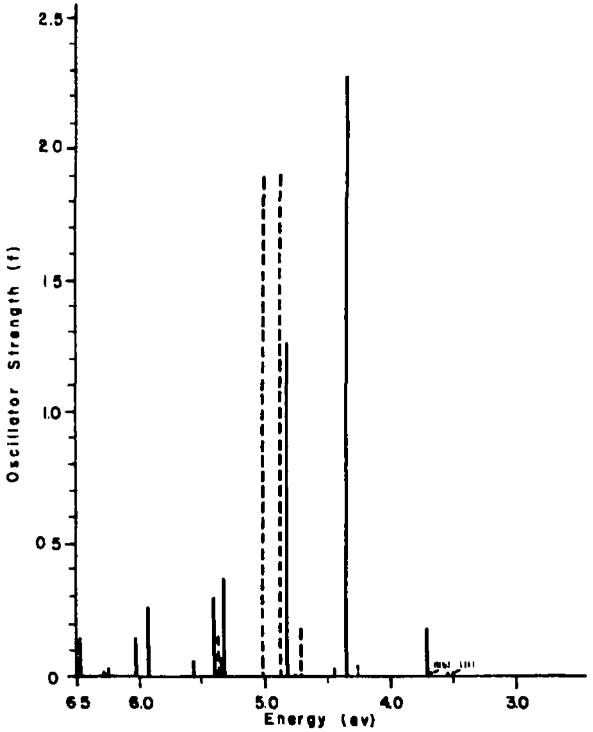

Fig. 6. Calculated absorption spectra of dibenz(a,c)anthracene (II), shown as solid lines, and composite system (IIb), shown as dashed lines

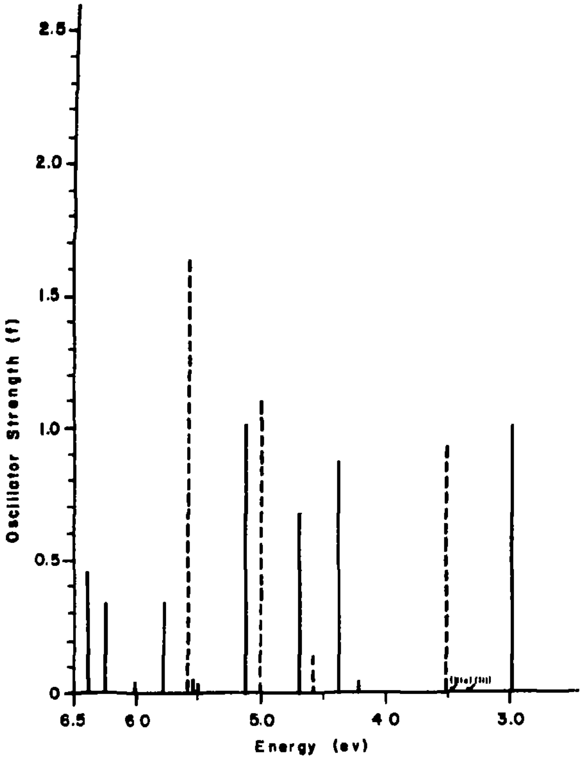

Fig. 7. Calculated absorption spectra of 3,4-benzopyrene (III), shown as solid lines, and composite system (IIIa), shown as dashed lines

in both the solution for the self-consistent MO's and in the determination of the excited state wave functions by configuration interaction. This implies that the molecule treated as a single system gives the best results but that there exists a composite system which is a close approximation to the subject molecule. This is apparently the same viewpoint as that taken by Heilbronner *et al.* [4] in their work.

The purpose of the calculations for the "weakly" interacting composite system, that is, β_{ij} equal to -1.00 eV between the component parts, was two-fold. First, the most appropriate composite system model for a given molecule was chosen primarily on the basis of how closely the spectra of the composite system with intermediate interaction approximated the spectra of the molecule treated as a single system. For an example, Table 4 compares the transitions of the three composite system models of BP, β_{ij} equal to -1.00 eV between the two parts, with the transitions of BP calculated with β_{ij} equal to -2.318 eV between all bonded centers. Second, these intermediate interaction calculations aided in the correlation of composite system transitions with those of the subject molecule.

The calculated spectra of BN, DBA, and BP, together with the superimposed spectra of the most appropriate composite system model ($\beta_{ij} = 0.0$ eV), are given in Figs. 5, 6, and 7. The results of the correlation of the calculated transitions of a composite system model with the calculated transitions of the modeled pentacyclic aromatic are summarized in the correlations between columns 2 and 3 of Figs. 2, 3 and 4.

Discussion

The correlation diagrams shown in Figs. 2, 3 and 4, summarize the results of the study. The diagrams give both the experimental and theoretical MIM correlations discussed above. The correlations of the calculated and observed pentacyclic transitions given in Tables 1, 2 and 3, and the correlations of the calculated and observed tetracyclic transitions, taken from Becker *et al.* [9], complete the diagrams. The agreement between experimental and theoretical spectra was good, considering that no particular effort was made to achieve a precise fit in this study.

Since the correlations presented begin and end with the observed pentacyclic transitions, columns 1 and 5, one may follow the correlation lines from an observed transition in column 1 to the same transition in column 5 if the experimental and theoretical MIM interpretations lead to the same conclusion regarding the transition "origin". This is not possible when the experimental and theoretical MIM interpretations are not in agreement.

No attempt was made to correlate a pentacyclic transition with one of a smaller molecule when it appeared that the pentacyclic transition originated from one of a degenerate pair of forbidden electron-transfer transitions in the non-bonded composite system model. Consequently, no correlation lines appear in these cases.

Conclusion

The comparison of the theoretical and experimental composite system interpretations of the electronic transitions of BN, DBA, and BP reveals generally good agreement. In all cases, there was agreement between the theoretical and experimental results regarding which particular composite system models were the best approximations to the subject molecules. This agreement indicates that the application of the MIM concept in interpreting at least the first three transitions of these pentacyclics seems justified. However, interpretations of the individual transitions disagreed in some instances, particularly in the case of higher energy transitions. Furthermore, the experimental and to some extent the theoretical composite system interpretation of the higher transitions were much less clear. Although the treatment of molecules by means of the MIM method would benefit greatly by a more rigorous theoretical justification, the results of the investigation indicate the soundness of the basic concept.

It must be noted that there possibly are other schemes by which the theoretical interpretation of the transitions could be made to agree more closely with the experimental interpretation for some individual transitions. However, the objective of this work was to verify if the MIM concept was a valid approach for analyzing the complete spectra of the pentacyclic aromatic hydrocarbons. Consequently, all the theoretical interpretations were based on the foregoing premise and agreement or disagreement between the theoretical and experimental interpretations was taken as evidence for or against this objective.

Acknowledgement. Henry A. Germer, Jr. wishes to acknowledge the support of a Public Health Service Postdoctoral Fellowship while he was engaged in this research.

References

1. Taken from a dissertation submitted in partial fulfillment of the requirements for the Ph. D. degree.
2. Simpson, W. I: Theories of electrons in molecules. New York: Prentice-Hall 1962.
3. Longuet-Higgins, H. C., Murrell, J. W.: Proc. physic. Soc. **68** A, 601 (1955).
4. Heilbronner, E., Weber, J., Michl, J., Zahradnik, R.: Theoret. chim. Acta (Berl.) **6**, 141 (1966).
5. Mori, Y.: Bull. chem. Soc. Japan **34**, 1031 (1961); **34**, 1036 (1961).
6. Johnson, P. M., Albracht, A. C.: J. chem. Phys **48**, 851 (1968).
7. Favini, G., Gamba, A., Simonetta, M.: Theoret. chim. Acta (Berl.) **13**, 175 (1969).
8. von Niessen, W.: J. chem. Physics **55**, 1948 (1971).
9. Becker, R. S., Singh, I. S., Jackson, E. A.: J. chem. Physics **38**, 2144 (1968).
10. Pariser, R.: J. chem. Physics **21**, 568 (1953).
11. Mataga, N., Nishimoto, K.: Z. physik. Chem. **13**, 140 (1957).

Dr. Henry A. Germer, Jr.
Department of Physiology
University of Texas Medical Branch
Galveston, Texas 77550
USA

Requests for reprints to:
Dr. R. S. Becker
Department of Chemistry
University of Houston
Houston, Texas 77004
USA

Theoret. chim. Acta (Berl.) 28, 13–26 (1972)
© by Springer-Verlag 1972

The Use of Correlated Gaussian Wavefunctions for the Calculation of Chemical Energies for Small Systems

S. J. Fraser and J. W. Linnett

Department of Physical Chemistry, University of Cambridge

Received December 22, 1971/July 28, 1972

The purpose of this paper was to investigate the use of limited sets of Gaussian functions as bases to calculate dissociation and activation energies. Gaussian functions have the principal advantage that they lead to integrals that can be performed analytically, even when explicit correlation terms are introduced.

Calculations were performed on H_2 and linear H_3 using a restricted 1s-type Gaussian basis, and direct correlation factors were introduced into the wave function in both cases. The best result for the dissociation energy of H_2 was 105.1 kcal/mole. However, the activation energy of the hydrogen atom–hydrogen molecule exchange reaction was calculated to be 15.8 kcal/mole.

Die Anwendungsmöglichkeit von Basissätzen einer beschränkten Zahl von Gaußfunktionen zur Berechnung von Dissoziations- und Aktivierungsenergien wird untersucht. Der Hauptvorteil bei der Verwendung von Gaußfunktionen besteht darin, daß sie auf Integrale führen, die analytisch ausgewertet werden können, sogar im Falle, daß explizite Korrelationsanteile in den Funktionen enthalten sind.

Für H_2 und lineares H_3 wurde eine eingeschränkte Gaußfunktionenbasis vom 1s-Typ unter Einschluß expliziter Korrelationsanteile verwendet. Das beste Ergebnis für die Dissoziationsenergie des H_2 beträgt 105,1 kcal/mol. Dagegen ergibt sich für die Aktivierungsenergie der Austauschreaktion Wasserstoffatom Wasserstoffmolekül ein Wert von 15,8 kcal/mol.

1. Introduction and General Account of Calculations

The calculations in this paper were instigated by the investigation of Reeves [1], who suggested that it was not necessary to achieve high absolute accuracy in calculations in order to estimate energy differences successfully. Reeves' results were extended in this research by using more elaborate wave functions for H_2 and carrying out corresponding calculations for H_3. In this way the validity of this suggestion could be assessed for the calculation of both dissociation energies and activation energies at least for small chemical systems. A set of 1s-like atomic functions was used as a basis in all calculations.

The wave functions for the H_2 or H_3 system were constructed using the following alternatives:

1. The Form of Basis
a) One or two 1s-type Gaussians per atomic 1s-orbital.
b) Spherical or elliptical space functions.
2. The Form of the Complete Wavefunction.
a) Molecular orbital or configuration interaction treatment.
b) Inclusion of explicit correlation terms or uncorrelated function.

Additional constraints appear in the calculations but these are unimportant relative to the above classification. The first calculations employed a basis of single 1*s*-type spherical Gaussians on each nuclear centre. Both molecular orbital and limited configuration interaction wave functions were tested and for each type of function explicit correlation was included in further calculations.

An additional set of calculations using spherical Gaussians was carried out, the atomic 1*s* orbitals being approximated by a double rather than a single Gaussian basis. Only configuration interaction wave functions were investigated in this and subsequent calculations. Calculations on H_3 were continued using elliptical Gaussian functions.

At each stage in the calculation sequence, increased accuracy was achieved. The dissociation energy of H_2 was approximated closely. However, the method of using a limited set of Gaussians was not successful for H_3; at least not in terms of the computational effort required. The reasons for this failure are probably complicated and their discussion is deferred until Section 5.

2. The Hamiltonian and Approximations

All calculations were carried out using the Schrödinger spin-free Hamiltonian:

$$H = H_e + V_{ee} + V_{nn}$$

where H_e, V_{ee}, and V_{nn} are respectively the one-electron, two-electron and nuclear repulsion terms. The operators are given in atomic units.

The one-electron Hamiltonian H_e is given by:

$$H_e = -\tfrac{1}{2}\sum_i \nabla_i^2 - \sum_{ij} \frac{Z_j}{|r_i - A'_j|}\,.$$

The electron coordinates are $\{r_i\}$ and the stationary nuclear coordinates are $\{A'_j\}$ with corresponding charge Z_j. $Z_j = 1$ for all systems considered here.

The two-electron Hamiltonian V_{ee} is given by:

$$V_{ee} = \sum_{i>j} |r_i - r_j|^{-1}\,.$$

The equation was solved in the Born-Oppenheimer approximation in which the electronic and nuclear wavefunctions are regarded as independent; then the separable internuclear potential terms is:

$$V_{nn} = \sum_{i>j} |A'_i - A'_j|^{-1}\, Z_i Z_j\,.$$

Although the equations were solved in the Born-Oppenheimer approximation, no investigation of the validity of this approximation was carried out for the dynamic system H_3.

The trial wavefunctions obeyed neither the nuclear cusp condition nor the interelectron cusp condition. Basically the main object of the work was to examine the extent to which the use of very limited sets of Gaussian functions, which give a poor representation of the behaviour of the wave function near the nuclei and produce poor absolute energies, may be satisfactory for obtaining energy differences.

For all the calculations performed here the energy changes were deduced for changes which did not alter the number of electrons or the number of nuclei. Cancelling of errors is therefore possible. The absence of the inter-electronic cusp condition is of smaller importance.

Although it would have been very interesting to include both nuclear and electronic cusp conditions the improved wavefunctions would have required much longer computations.

3. Types of Wavefunction Used

As indicated in the introduction the types of wavefunction investigated in this paper can be classified firstly according to basis and secondly according to the type of the total space wavefunction. The algebraic form of the correlation function is discussed in the section on bases since the space and correlation functions have similar structure. The way in which the correlation terms are included in the overall wavefunction is discussed in the second section on the form of the total wavefunction.

3.1. Types of Atomic and Gaussian Basis and the Form of the Correlation Functions

3.1.1. Space Basis Functions

The spherical Gaussian functions can be written:

$$G_s(a\underset{\sim}{A}) = \exp(-a(r-\underset{\sim}{A})^2)$$

where a is the exponent and $\underset{\sim}{A}$ the coordinates of the function-centre. The *tilde* indicates a vector. The evaluation of the integrals arising from a basis such as this were first discussed by Boys [2], and summarised, together with an account of the evaluation of the numerical term, by Shavitt [3].

The integrals for correlated terms of the spherical functions were discussed by Boys [4]. Additional techniques for the evaluation of these integrals are given in a paper to be published later.

The space part of the elliptical Gaussians can be written:

$$G_e(\underset{\sim}{a}\underset{\sim}{A}) = \exp(-\sum_{xyz} a_x(x-A_x)^2)$$

where $\{a\}$ are the exponents and $\{A\}$ the function centres.

The matrix formulation of the elliptical integrals was first given by Singer [5]. However, the forms used here are slightly modified to give an overall wavefunction comparable with that obtained using Boys' integrals. The differences required in the integral formulae are indicated in a paper to be published later, together with a method for the factored matrix forms of the integrals for linear systems.

Atomic 1s-type functions $\{\chi\}$ were formed from the Gaussian functions by linear combinations:

$$\chi_i = \sum_j b_{(ij)} G_{(ij)}$$

where the indices are function labels. (ij) is a contracted double index. The relation between atomic and Gaussian sets can be written in matrix notation but many of the matrix elements are zero so this is inconvenient.

Use of molecular orbital wave functions required the transformation of the atomic basis $\{\chi\}$ to a molecular basis $\{\varphi\}$. This transformation can be written:

$$\varphi = C\chi .$$

For H_2, C is the unnormalised orthogonal matrix

$$\begin{bmatrix} 1 & 1 \\ 1 & -1 \end{bmatrix} .$$

For H_3, C is the unnormalised orthogonal matrix

$$\begin{bmatrix} 1 & \lambda & 1 \\ -1 & 0 & 1 \\ 0 & 0 & 0 \end{bmatrix} .$$

λ is an adjustable parameter. The antibonding orbital does not occur in the ground state and for this reason its coefficient vector is set to zero.

All correlated integrals have the same dimension as the coupled electron function-space and require a double index per electron. Thus the two-electron integrals required a four-dimensional supermatrix transformation and the three-electron integrals required a six-dimensional supermatrix transformation. All matrices were held and transformed in a coded vector. Considerable effort was expended on the problem of labelling the unique Gaussian integrals in vectors in order that they could be recovered, summed and transformed if necessary.

3.1.2. Correlation Functions

The general form of the two-electron correlation function used with both elliptical and spherical space functions is given by:

$$G(r_{ij}) = \exp(-d(r_{ij})^2)$$

where the indices refer to electron labels.

Thus the symmetry of the correlation function is hyperspherical. This particular form of two-electron function weights the least probable configurations and therefore the contribution due to these configurations must be *subtracted* from the uncorrelated structure.

The three-electron correlation functions can be built from component two-electron functions in two distinct ways: either a symmetrical sum or product of the two-electron functions can be formed.

For the sum function:

$$G^{s}_{ijk} = \sum_{\alpha} G_{\alpha}$$

where $\alpha (= ij$ etc.) is the index for all distinct unordered pairs of the indices i, j and k.

For the product function:

$$G^p_{ijk} = \prod_{\alpha} G_\alpha .$$

After a preliminary investigation for H_3, G^s_{ijk} was chosen as the more effective correlation function. There are good reasons for thinking that a simple restricted correlation function should have this form. The sum and product functions distinguish different structures, the sum function correlating all electron pairs more effectively.

3.2. Structure of the Total Wavefunction

The overall structure of the H_2 and H_3 wave functions was very simple; conventional uncorrelated molecular orbital or configuration interaction wavefunctions were used and combined with correlation terms to produce correlated functions. The configuration interaction functions incorporated all possible linearly independent Slater determinants that could be formed from the atomic (not Gaussian) basis $\{\chi\}$. Since the correlation functions are always symmetric and the space wavefunction are determinants, the overall wavefunction is antisymmetric.

Correlation destroys the orthogonality properties of the overlap matrix. Thus it is necessary to solve an additional set of secular equations to diagonalise the overlap matrix, in order that both the overlap and Hamiltonian matrices should be simultaneously diagonal.

3.2.1. Space Part of the Wavefunctions

3.2.1.1. Molecular Orbital Wavefunctions

For H_2 the wavefunction is written:

$$\Psi_{\text{mo}}(H_2) = \|\varphi_1(1)\,\alpha(1)\,\varphi_1(2)\,\beta(2)\|$$

where φ_1 is the lowest lying (symmetrical) molecular orbital, corresponding to row 1 of the matrix C, of Section 3.1.1.

For H_3 the wavefunction is written:

$$\Psi_{\text{mo}}(H_3) = \|\varphi_1(1)\,\alpha(1)\,\varphi_2(2)\,\alpha(2)\,\varphi_1(3)\,\beta(3)\|$$

where $\{\varphi\}$ is the molecular basis, corresponding to rows 1 and 2 of C, the molecular coefficient matrix.

The Slater determinants are written conventionally as the sequence of diagonal elements between double bars.

3.2.1.2. Configuration Interaction Wavefunctions

The H_2 configuration interaction wavefunction is written as:

$$\Psi_{\text{ci}}(H_2) = \sum_{\alpha} C_\alpha \|\chi_i(1)\,\alpha(1)\,\chi_j(2)\,\beta(2)\|$$

where the sum is over the contracted double index α corresponding to all i, j pairs that generate distinct Slater determinants. For H_2 there are four such linearly independent determinants. The basis $\{\varphi\}$ may, of course, be used instead of the basis $\{\chi\}$ in the configuration interaction function.

The H_3 configuration interaction wavefunction can be written:

$$\Psi_{ci}(H_3) = \sum_{\alpha} C_\alpha \, \|\chi_i(1)\,\alpha(1)\,\chi_j(2)\,\beta(2)\,\chi_k(3)\,\alpha(3)\|$$

where $k \neq i$ for $\{\chi_i : i = 1, 2, 3\}$. A given sequence of indices i, j, k codes a unique α. There are then nine linearly independent Slater determinants.

For both species the configuration interaction functions may be more briefly written as:

$$\Psi_{ci} = \sum_{\alpha}^{N} C_\alpha \Delta_\alpha$$

where $N = 4$ for H_2 and $N = 9$ for H_3.

3.2.2. Introduction of the Correlation Terms and Correlated Wavefunctions

As mentioned in Section 3.1.2, the correlation factor weights improbable structures preferentially. Thus the structures must be subtracted from the uncorrelated determinant (mo) or determinants (ci).

The correlated molecular orbital wavefunction may be written for both H_2 and H_3 as:

$$\Psi_{mo} = \sum_{i=1}^{2} C_i \Delta_i$$

where

$$\Delta_1 = \Psi_{mo} \quad \text{(for the appropriate species)}$$

$$\Delta_2 = G\,\Psi_{mo} .$$

G is the correlation function, for H_2 or H_3. If C_1 is positive then C_2 is negative because $G(r_{ij})$ is larger the smaller is r_{ij}.

The form of correlated configuration interaction wavefunction closely resembles that of the correlated molecular orbital functions:

$$\Psi_{ci} = \sum_{i=1}^{N} (C_i \Delta_i + C_{i+N} G \Delta_i) .$$

Again $\{C_{i+N}\}$ are negative as they are the coefficients of correlated determinants. Contracting the notation:

$$\Psi_{ci} = \sum_{i=1}^{2N} C_i \Delta_i ,$$

$$\Delta_{i+N} = G \Delta_i \quad \text{for } i = 1(1)\,N .$$

$N = 4$ for H_2 and $N = 9$ for H_3, giving respectively 8 and 18 determinants for the complete configuration interaction correlated wavefunction for H_2 and H_3.

The precise types of calculation carried out are indicated in the next section where the particular constraints on the individual calculations are also listed.

4. Results for Calculations for H_2 and Linear H_3

4.1. *Reeves' Results for the Hydrogen Atom* (Table 1)

Reeves' results [1] for the hydrogen atom are given in Table 1 in order to indicate the scale of absolute accuracy of the calculations reported in this paper. Only when three or more Gaussians are used does the hydrogen atom energy error (1.88 kcal/mole) become comparable with the exchange reaction activation energy (approximately 10 kcal/mole).

In the notation of Section 3.1.1 the hydrogen atom wave function can be written:

$$\Psi_{1s}(\mathrm{H}) = \sum_i b_i G(a_i, 0).$$

Table 1. Summary of Reeves' results for hydrogen atom

Size of Gaussian basis	Exponents a	Linear multipliers b	Energy a.u.	Energy error	
				a.u.	kcal/mole
1	0.2829	0.6515	−0.4244	0.0756	47.5
2	0.2015 1.3320	0.1760 0.2425	−0.4858	0.014	8.91
3	0.1433 0.6577 4.2392	0.1034 0.2164 0.1575	−0.4970	0.003	1.88
Exact	—	—	−0.5000		—

4.2. *Results and Discussion of Present Calculations on* H_2 *and Linear* H_3

4.2.1. Tables of Results

This section refers to three tables of results: Table 2.1 which lists the data for all calculations performed on H_2 and H_3; Table 2.2 which gives the dissociation energies calculated from the H_2 results of Table 2.1; and Table 2.3 which gives the activation energies calculated from the H_2 and H_3 results of Table 2.1, and the H results in Table 1.

The calculations in Table 2.1 are ordered, where possible, in pairs of corresponding H_2 and H_3 calculations. Calculations 1–7 were made with a basis of "single-Gaussian" 1*s* atomic orbitals. Calculations 8–11 use "double-Gaussian" 1*s* atomic orbitals. In calculations 12 and 13 an elliptical double Gaussian basis was used, there being no corresponding calculations for H_2.

4.2.1.1. Notation for All Tables

The first column of all three tables numbers the calculations and to permit easy cross-reference these numbers correspond in all tables. The second column of Tables 2.2 and 2.3 and the third column of Table 2.1 code the type of

Table 2.1. All calculated results for H_2 and H_3

Calc. No.	System	Type code of calc.	Energy a.u.	Nuclear centres A'	Orbital exponents a	Orbital centres A	Linear multipliers b	Correlation exponent d
1	H_2	MSU 1	−0.9808	0	3.70(−1)[a]	0		
				1.56	3.70(−1)	1.56	—	
2	H_3	MSU 1	1.3844	−1.89	3.37(−1)	−1.89	—	—
				0	3.37(−1)	0	—	
				1.89	3.37(−1)	1.89	—	
3	H_2	MSR 1	0.9986	0	4.10(−1)	0		1.03(−1)
				1.57	4.10(−1)	1.57		
4	H_3	MSR 1	1.4156	1.84	3.12(−1)	−1.84		3.80(−1)
				0	5.26(−1)	0		
				1.84	3.12(−1)	1.84		
5	H_2	CSU 1	0.9975	0	3.72(−1)	1.98(−2)		
				1.59	3.72(−1)	1.57		
6	H_2	CSR 1	1.0081	0	4.10(−1)	0		1.03(−1)
				1.59	4.10(−1)	1.59		
7	H_3	CSR 1	−1.4285	−1.83	3.12(−1)	−1.83		3.97(−1)
				0	5.28(−1)	0		
				1.83	3.12(−1)	1.83	—	
8	H_2	CSU 2	−1.1221	0	2.58(−1)	4.83(−2)	2.04(−1)	
					1.71	5.92(−1)	3.38(−1)	
				1.45	2.58(−1)	1.41	2.04(−1)	
					1.71	1.40	3.38(−1)	
9	H_3	CSU 2	1.5767	1.88	2.21(−1)	−1.85	1	
					1.44	−1.83	1.32	
				0	3.09(−1)	0	1	
					1.74	0	1.47	
				1.88	2.21(−1)	1.85	1	
					1.44	1.83	1.32	
10	H_2	CSR 2	−1.1390	0	2.68(−1)	9.37(−2)	1.76(−1)	3.68(−1)
					1.65	9.39(−2)	3.38(−1)	
				1.44	2.68(−1)	1.34	1.76(−1)	
					1.65	1.34	3.38(−1)	
11	H_3	CSR 2	−1.5997	−1.81	2.36(−1)	−1.72	1	[a,b]
					1.53	−1.71	1.32	
				0	3.80(−1)	0	1	
					2.13	0	1.47	
				1.81	2.36(−1)	1.72	1	
					1.53	1.71	1.32	
12	H_3	CEU 2	−1.5779	−1.85	2.19(−1)	0	1	—
					2.33(−1)	−1.83		
					1.47	0	1.32	
					1.30	−1.83		
				0	3.08(−1)	0	1	
					3.40(−1)	0		
					1.74	0	1.47	
					1.75	0		

Table 2.1 (continued)

Calc. No.	System	Type code of calc.	Energy a.u.	Nuclear centres A'	Orbital exponents a	Orbital centres A	Linear multipliers b	Correlation exponent d
12	H_3	CEU2	1.5779	1.85	2.19(−1)	0	1	
					2.33(−1)	1.83		
					1.47	0	1.32	
					1.30	1.83		
13	H_3	CER2	−1.6021	−1.79	2.36(−1)	0	*	*
					2.36(−1)	−1.70		
					1.58	0	*	
					1.27	−1.67		
				0	4.10(−1)	0	*	
					3.80(−1)	0		
					2.30	0	*	
					2.13	0		
				1.79	2.36(−1)	0	*	
					2.36(−1)	1.70		
					1.58	0	*	
					1.27	1.67		

[a] The bracketed numbers are powers of 10.

[b] The asterisk indicates that the data are unavailable, although in all cases the values are not critical.

calculation carried out according to the following scheme:

first letter	M	molecular orbital wavefunction
	C	configuration interaction wavefunction,
second letter	S	spherical Gaussian basis
	E	elliptical Gaussian basis,
third letter	R	explicit correlation terms included
	U	no explicit correlation terms included,
digit	1	one 1*s* Gaussian per atomic 1*s* orbital
	2	two 1*s* Gaussians per atomic 1*s* orbital.

4.2.1.2. Details and Notes for Table 2.1

Column 5 contains the nuclear centre coordinates. As each nuclear centre is associated with one 1*s* atomic function for single 1*s* Gaussians there is one data set corresponding to each nuclear centre. For double-Gaussian atomic orbitals there are two data sets for each nuclear centre. For elliptical Gaussians each Gaussian function is specified by independent axial (z) and radial (x or y) exponents, and each pair is associated with the corresponding Gaussian orbital centre. The exponents are written in the column order $\begin{pmatrix}x\\z\end{pmatrix}$. An asterisk in the table indicates that the data are not available. However, in all cases this is not critical.

The details of the different calculations, as identified by the numbers in the first column of Table 2.1, are the following:

1. Nuclear and corresponding orbital centre are equal.
2. Nuclear and corresponding orbital centres are equal; all Gaussian exponents are the same. $\lambda = 1.489$ (see Section 3.1.1) λ is the only adjustable molecular orbital coefficient matrix element in the symmetric linear configuration for H_3.
3. Nuclear and corresponding orbital centres are the same.
4. Nuclear and corresponding orbital centres are the same. $\lambda = 1.721$.
5. No corresponding calculation performed for H_3. Polarised (floated) orbital centres were used.
6. All data are identical with data for calculation 3. Correlation coefficient d optimised.
7. Single unoptimised calculation with data from calculation 4.
8. Fully minimised wavefunction.
9. Fully minimised wavefunction.
10. Fully minimised wavefunction.
11. Apart from d all parameters were optimised.
12. Orbital exponents, centres and nuclear centres optimised.
13. Orbital exponents, centres and nuclear centres optimised.

The calculations 10–13 all illustrated the great computational difficulty of finding a minimum in a non-linear parameter space. All other minimisations were carried out by Ransil's method [6].

4.2.2. Discussion of Results for All Tables 2

The purpose of the initial calculations 1–8 was to investigate the accuracy of energy differences calculated using the minimum possible 1*s*-type basis.

For the hydrogen molecule it appears that the calculated dissociation energy is not subject to large errors resulting from the absence of cusps in the wavefunctions. (Energy differences in Table 2.2 are, of course, always calculated using the corresponding basis for the hydrogen atom.) The dissociation energy calculated with type 1 function (one Gaussian function per atom) is 83.2, while that using a single Slater orbital per atom is 80.0 kcal/mole. J. P. Chesick *et al.* [7] using two Gaussian functions per centre obtained 83.4. Also in the series using configuration interaction calculation 5 and 8 gave 93.3 and 94.5 kcal/mole, while that using single Slater functions gave 92.2 kcal/mole. In both sets the variation is small despite the fact that the Slater functions have a cusp whereas the Gaussian functions do not. The addition of the correlation term improves the calculated dissociation energy by 10.6 kcal/mole for the calculations using a molecular orbital treatment with a single Gaussian function per atom (calc. 3), but when two Gaussians per atom are used the improvement is only 6.6 kcal/mole (calc. 6). When a correlation term is added to the configuration interaction treatment with two Gaussians per centre, the improvement is 11.0 kcal/mole (calc. 10). It is possible that the last calculation allows particularly effectively for electron correlation because it is included both through configuration interaction and in the correlation term as well. This would provide additional flexibility.

Table 2.2. *Complete energy results for H_2, including dissociation energy*

Calc. No.	Type code of calc.	Absolute energy a.u.	Error in absolute energy	Dissociation energy	Error in dissociation energy
1	MSU 1	−0.9808	0.1938 A	0.1328 A	0.0418 A
			121.6 K	83.4 K	26.1 K
3	MSR 1	−0.9986	0.1860 A	0.1498 A	0.0246 A
			116.8 K	94.0 K	15.5 K
5	CSU 1	−0.9975	0.1771 A	0.1487 A	0.0259 A
			111.2 K	93.3 K	16.1 K
6	CSR 1	−1.0081	0.1665 A	0.1593 A	0.0153 A
			104.5 K	100.0 K	9.5 K
8	CSU 2	−1.1221	0.0525 A	0.1605 A	0.0141 A
			32.5 K	94.5 K	15.4 K
10	CSR 2	−1.1390	0.0356 A	0.1674 A	0.0072 A
			22.9 K	105.1 K	4.4 K
Slater	mo			80.0 K	29.5 K
Slater	ci			92.2 K	17.3 K
Exact	—	−1.1746	—	0.1746 A	--
				109.5 K	

A = atomic units. -- K = kcal/mole.

Table 2.3. Complete energy results for H_3, including activation energy

Calc. No.	Type code of calc.	Energy a.u.	Energy of comparable $H_2 + H$	Activation energy a.u.	Activation energy kcal/mole
2(1)[a]	MSU 1	−1.3844	−1.4052	0.0208	13.1
4(3)	MSR 1	−1.4156	−1.4230	0.0074	4.6
7(6)	CSR 1	−1.4285	−1.4325	0.0040	2.5
9(8)	CSU 2	−1.5767	−1.6079	0.0312	19.6
11(10)	CSR 2	−1.5997	−1.6248	0.0251	15.8
12	CEU 2	−1.5779	--		—
13	CER 2	−1.6021	—	-	--

[a] The numbers in brackets refer to the corresponding calculations for H_2.

The calculations of the activation energy for the reaction of hydrogen atoms with hydrogen molecules are listed in Table 2.3. Activation energies were obtained using the corresponding H, H_2, and H_3 calculations. The absolute accuracy for H_3 increases in the series 2, 4, 7, 9, and 11, as would be expected. However, the calculated activation energy fluctuates in the same series showing that the cancellation of core errors arising from the absence of cusps at the nuclei is not adequate relative to the small activation energy that is being derived. It is possible that this results from the rather special situation of the central proton in H_3.

The first calculations indicate that, for these, the absolute error is so large in comparison with the quantity being calculated that the space wavefunction is *inadequate to allow an accurate predication of the relatively small chemical energy. A further difference between the results for H_2 and H_3 is demonstrated by the fact that on going from calculation 2 to 4, the introduction of a correlation term actually results in a poorer value for the activation energy.* The erratic behaviour of the results for calculations 7, 9, and 11 also demonstrates that the total errors are too large with these functions when interest lies in the calculation of such a small energy.

The use of double Gaussian 1*s* atomic orbitals greatly reduced the effect of the poor space part of the wavefunction near the nuclei. Thus the result of calculation 9 (19 kcal/mole) corresponds well with the result of Bowen and Linnett [8] (22.8 kcal/mole) where comparable exponent variation of a 1*s*-type basis was allowed. The last activation energy calculated from 11 (15.8 kcal/mole) is reasonably satisfactory, though disappointing in terms of the computational effort required.

The purpose of the elliptical Gaussian calculations 12 and 13 was to include polarisation effects more successfully than by merely "floating" spherical Gaussians from their associated nuclear centres. However, the results indicate that the incorporation of elliptical symmetry effects a negligible improvement in the H_3 energy, at least with the limited basis used. For this reason no corresponding calculations with H_2 were attempted.

5. The Computations and Computational Times

The number of Gaussian integrals to be evaluated for a correlated function is of the order of $(N)^{2n}$, where N is the size of the basis set and n is the number of electrons. As a result an energy computation for H_3 is about two hundred times more time-consuming than for H_2 (for the double-Gaussian basis). By far the greatest portion of time was used in integral evaluation. For the H_3 calculation using spherical Gaussian functions roughly 52500 integrals had to be evaluated. For H_2 there were only 990 for the corresponding calculation.

All calculations were performed using the Titan Computer in Cambridge (add-time about 5 micro-seconds). A spherical double Gaussian calculation with correlation required about 8 minutes for H_3, and the corresponding elliptical one about 20. The similar H_2 calculations using spherical Gaussian functions took less than 1 minute.

6. General Discussion

There are two kinds of problem involved in the quantum mechanical computation of activation energies. The first is the difficulty of choosing an adequate wavefunction and of deriving the potential energy surface and barrier height from it. However, in addition, there are the theoretical difficulties such as the assumption of the Born-Oppenheimer approximation, the supposition that the process is adiabatic and also uncertainty regarding tunnelling through the barrier. The last might be particularly important in the present case because protons only are involved. It is not, however, the purpose of this paper to discuss problems of this second kind because they are common to all computations for this system. Moreover, it does seem probable that a good estimate of the activation energy is about 9 kcal/mole.

The idea behind the present calculations was to examine whether the introduction of specific allowance for electron correlation could make it possible to calculate energy changes with reasonable accuracy, even when the basis function was so simple that the absolute value for the energy was bound to be very inaccurate. There was some hope that this might be successful because the dissociation energy of the hydrogen molecule is, as has been pointed out earlier, calculated to be between 80 and 83.5 kcal/mole when a simple molecular orbital treatment is used, whether the basis consists of a single Gaussian, double Gaussian or single Slater orbital on each atom. The error in the absolute energy changes considerably from one of these calculations to another but the calculated energy change does not. The same is true for the configuration interaction calculations.

The absolute energy errors discussed below are shown in Tab. 2.2. For the dissociation energy of hydrogen, calculation 3 (MSR 1) showed that, although the total error was 117, the error in the energy change (dissociation energy) was only 15.5 kcal/mole. For calculation 6 (CSR 1), the corresponding figures were 104 and 9.5; and for calculation 10 (CSR 2) 22.9 and 4.4 kcal/mole. So, for this quantity, the error in the energy change is very much less than the absolute error, though for calculation 10 the ratio of the two errors (4.4/22.9) is rather greater than the ratio of the dissociation energy to the total energy (110/740). Nevertheless, the results do give some satisfaction because electron correlation is involved in the molecule but not in the separated atoms.

The results for the activation energy are not so satisfactory. Calculation 4 (MSR 1) gives 4.6 kcal/mole, calculation 7 (CSR 1) 2.5 and calculation 11 (CSR 2) 15.8. Comparison of calculations 2 and 4, and of 9 and 11, shows that, in both cases, the calculated activation energy is lowered on introducing a correlation term, as would be expected. The actual errors in the energy of activation are no bigger than those for the dissociation energy of H_2, but they are comparable to the energy being calculated.

Therefore, the conclusion of the present work is that this procedure may be useful for the calculation of large energy changes but cannot be expected to be particularly useful for small energy changes. In such cases the absolute accuracy needs to be greater.

S.J.F. wishes to express his gratitude to Pembroke College, Cambridge, for the financial assistance they gave him.

References

1. Reeves, C. M.: J. chem. Physics **39**, 1 (1963).
2. Boys, S. F.: Proc. Roy. Soc. A **200**, 542 (1950).
3. Shavitt, I.: Methods in computational physics, Vol. 2, p. 1. New York: Academic Press 1963.
4. Boys, S. F.: Proc. Roy. Soc. A **258**, 402 (1960).
5. Singer, K.: Proc. Roy. Soc. A **258**, 412 (1960).

6. Ransil, B. J.: Rev. mod. Physics **32**, 239 (1960).
7. Chesick, J P., Fraser, S. J., Linnett, J. W.: Trans. Faraday Soc. **64**, 257 (1968).
8. Bowen, H. C., Linnett, J. W.: Trans. Faraday Soc. **62**, 2953 (1966).

Prof. Dr. J. W. Linnett
Department of Physical Chemistry
University of Cambridge
Lensfield Road
Cambridge CB2 1 EP
England

Theoret. chim. Acta (Berl.) 28, 27—35 (1972)
© by Springer-Verlag 1972

The Electronic Structure of Periodic Protein Models
I. CNDO/2 and MINDO/2 Energy Band Structures of a Two-Dimensional Formamide Network

S. Suhai and J. Ladik

Central Research Institute for Chemistry of the Hungarian Academy of Sciences, Budapest

Received May 29, 1972

The energy band structures of a two-dimensional polyformamide network have been calculated with the aid of the CNDO/2 and MINDO/2 crystal orbital method in the first neighbour's interactions approximation. For comparison also one-dimensional polyformamide chains have been computed with the same methods. The features of the obtained band structures are discussed.

Es wurden die Energiebandenstrukturen eines zweidimensionalen Polyformamid-Netzwerkes in einer Näherung, die die Wechselwirkung der ersten Nachbarn berücksichtigt, mit Hilfe der CNDO/2 und MINDO/2 Kristallorbital-Methoden berechnet. Zum Vergleich wurden auch eindimensionale Polyformamid-Ketten unter Verwendung derselben Methoden berechnet. Die Eigenschaften der erhaltenen Bandenstrukturen werden diskutiert.

Calcul de la structure des bandes d'énergie d'un réseau bidimensionnel de polyformamide à l'aide des méthodes d'orbitales cristallines CNDO/2 et MINDO/2 dans l'approximation d'interaction des premiers voisins. A titre de comparaison les chaînes unidimensionnelles de polyformamide ont été calculées avec les mêmes méthodes. Discussion des caractéristiques des structures de bande obtenues.

Introduction

The electronic structure of proteins is of great importance from obvious reasons. The first approximate Hückel calculation of the π electronic band structure of a $\mathrm{H{-}N{-}C{=}O\cdots H{-}N{-}C{=}O\cdots}$ infinite chain is due to Evans and Gergely [1] back in 1949, who have applied this model to describe the π electrons in proteins following the suggestions of Szent-Györgyi [2], Coulson [3] and Laki [4]. By extrapolating from the semiempirical SCF LCAO MO (PPP) energy levels of a monopeptide, dipeptide and tripeptide, respectively, Suard, Berthier, and Pullman [5] have obtained an approximate band structure of the infinite chain. A similar calculation has been performed by Yomosa [6]. The first proper treatment of the infinite π electron crystal orbitals in the tight binding approximation is due to one of the authors [7], followed by a similar treatment of Suard-Sender [8]. In this paper there is also a calculation of the π electronic structure of an infinite $\mathrm{{-}NCO{-}NCO{-}}$ chain.

On the other hand Brillouin [9] has proposed such a periodic model for proteins in which the $\mathrm{NH{-}CO{-}CH_2}$ group of a protein forms the elementary cell. Introducing further side chain groups we obtain the

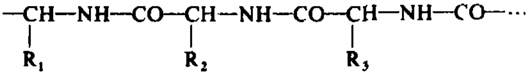

$$-\underset{\underset{R_1}{|}}{\mathrm{CH}}-\mathrm{NH}-\mathrm{CO}-\underset{\underset{R_2}{|}}{\mathrm{CH}}-\mathrm{NH}-\mathrm{CO}-\underset{\underset{R_3}{|}}{\mathrm{CH}}-\mathrm{NH}-\mathrm{CO}-\cdots$$

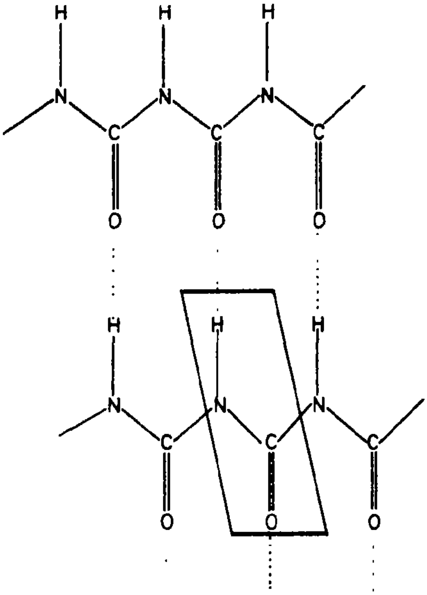

Fig. 1. The two-dimensional polyformamide network. The unit cell is indicated by a quadrangle

chain of the proteins, where the R_1, R_2 and R_3 etc. amino acid residues may play the role of impurities [9]. Following these ideas Fujita and Imamura [10] have performed an CNDO/2 crystal orbital (CO) calculation for the main chain of polyglycine. Most recently a similar calculation has been performed by Beveridge *et al.* for polyglycine in the INDO and MINDO/2 CO approximations [11].

It seems obvious to try to take into account simultaneously the interactions through the hydrogen bonds and along the main chain of polypeptides. Such a calculation requires the treatment of a polypeptide as a two-dimensional system. If we want to treat polyglycine as a two-dimensional periodic system from simple geometrical considerations it is clear that four glycine molecules form the elementary cell. The same difficulty arises in the case of other homopolypeptides. Therefore as a first step of this series of investigations on periodic protein models we have investigated as a very simple model system a two-dimensional formamide network in the CNDO/2 and MINDO/2 approximation. In this case as we can see from Fig. 1 a single formamide molecule forms the unit cell.

Method

It was shown [12] that in the case of a two-dimensional periodic system to obtain the band structure we have to solve the matrix eigenvalue equation

$$F(k_1, k_2)\, c_i(k_1, k_2) = \varepsilon_i(k_1, k_2)\, c_i(k_1, k_2) \qquad (1)$$

for different components k_1 and k_2 of the crystal momentum $\vec{k}$. Here if we introduce first neighbour's interactions only[1],

$$\begin{aligned}F(k_1, k_2) &= F(0,0) + F(+1,0)e^{ik_1a_1} + F(-1,0)e^{-k_1a_1}\\ &\quad + F(0,+1)e^{ik_2a_2} + F(0,-1)e^{-ik_2a_2},\\ F(-1,0) &= F(+1,0)^{\mathrm{tr}}, \quad F(0,-1) = F(0,+1)^{\mathrm{tr}}\end{aligned} \tag{2}$$

where a_1, a_2 are elementary translations along the main chain and the hydrogen bonds, respectively. The matrix $F(0,0)$ belongs to the reference cell and the matrices $F(+1,0)$, $F(-1,0)$, $F(0,+1)$ and $F(0,-1)$ contain the interactions between the reference cell and its four different first neighbours.

The CNDO/2 form of the method has been described elsewhere [13]. In the MINDO/2 version of the method

$$\begin{aligned}F_{\mu,\mu}(0,0) &= U_{\mu,\mu} + \tfrac{1}{2}p_{\mu,\mu}(0,0)\langle\mu\mu|\mu\mu\rangle\\ &\quad + \sum_{\substack{\nu\neq\mu\\(\nu\in \mathrm{A})}} p_{\nu,\nu}(0,0)\left[\langle\mu\mu|\nu\nu\rangle - \tfrac{1}{2}\langle\mu\nu|\mu\nu\rangle\right]\\ &\quad + \sum_{\mathrm{B}\neq\mathrm{A}}\left[p_{\mathrm{B,B}}(0,0) - z_{\mathrm{B}}\right]\gamma_{\mathrm{A,B}}(0,0) + \sum_{\mathrm{B}}\left[p_{\mathrm{B,B}}(0,0) - z_{\mathrm{B}}\right]\left[\gamma_{\mathrm{A,B}}(+1,0)\right.\\ &\quad \left. + \gamma_{\mathrm{A,B}}(-1,0) + \gamma_{\mathrm{A,B}}(0,+1) + \gamma_{\mathrm{A,B}}(0,-1)\right], \quad (\mu\in\mathrm{A})\end{aligned} \tag{3}$$

$$F_{\mu,\nu}(0,0) = p_{\mu,\nu}(0,0)\left[\tfrac{3}{2}\langle\mu\nu|\mu\nu\rangle - \tfrac{1}{2}\langle\mu\mu|\nu\nu\rangle\right] \quad (\mu\neq\nu,\ \mu,\nu\in\mathrm{A}), \tag{4}$$

$$\begin{gathered}F_{\mu,\nu}(0,0) = \Omega_{\mathrm{A,B}}(I_\mu + I_\nu)\,S_{\mu,\nu}(0,0) - \tfrac{1}{2}p_{\mu,\nu}(0,0)\,\gamma_{\mathrm{A,B}}(0,0)\\ (\mu\neq\nu,\ \mu\in\mathrm{A},\ \nu\in\mathrm{B},\ \mathrm{B}\neq\mathrm{A})\end{gathered} \tag{5}$$

and finally

$$\begin{gathered}F_{\mu,\nu}(q_1,q_2) = \Omega_{\mathrm{A,B}}(I_\mu + I_\nu)\,S_{\mu,\nu}(q_1,q_2) - \tfrac{1}{2}p_{\mu,\nu}(q_1,q_2)\,\gamma_{\mathrm{A,B}}(q_1,q_2),\\ (\mu\in\mathrm{A},\ \nu\in\mathrm{B},\ q_1=\pm1 \text{ and } q_2=0, \text{ or } q_1=0 \text{ and } q_2=\pm1).\end{gathered} \tag{6}$$

For the one-center core integrals $U_{\mu,\mu}$ and the valence state ionization potentials appropriate values are given by Dewar *et al.* [15]. For all the one-center two electron integrals occurring in (3) and (4) the usual Slater-Condon parameters have been used [16]. The Coulomb integrals $\gamma_{\mathrm{A,B}}(q_1, q_2)$ were computed with the aid of the Ohno-Klopman expression [17]. Finally

$$p_{\mathrm{A,A}}(0,0) = \sum_{\mu\in\mathrm{A}} p_{\mu,\mu}(0,0), \tag{7}$$

$$\begin{aligned}p_{\mu,\nu}(q_1,q_2) &= \frac{a_1a_2}{(2\pi)^2}\int_{-\pi/a_1}^{+\pi/a_1}\int_{-\pi/a_2}^{+\pi/a_2}\sum_{i=1}^{n^*} e^{i(k_1q_1a_1 + k_2q_2a_2)}\\ &\quad \cdot c^*_{i,\mu}(k_1,k_2)\,c_{i,\nu}(k_1,k_2)\,dk_1\,dk_2, \quad (q_1=0,\pm1,\ q_2=0,\pm1).\end{aligned} \tag{8}$$

The expressions used for the one-dimensional polyformamide systems, can be derived in a trivial way from the formalisms shown here.

---

[1] It seems probable that in more accurate calculations at least second neighbour's interactions should be taken into account. Such investigations are in progress.

Table 1. The CNDO/2 and MINDO/2 band structures of an one-dimensional

CNDO/2				
No. of band	E_{MO} and type of level	$E_{min}(k_2a_2)$	$E_{max}(k_2a_2)$	δE
		$R_{O\cdots H-N} = 2.66$ Å		
1	13.310 (σ)	13.599 (0)	13.654 (π)	0.055
2	11.890 (σ)	11.782 (π)	12.425 (0)	0.643
3	8.555 (σ)	8.274 (0)	9.414 (π)	1.140
4	4.274 (π)	4.486 (0)	4.529 (π)	0.043
5	1.224 (σ)	1.260 (π)	1.591 (0)	0.331
6	−14.023 (π)	−13.933 (π)	−13.743 (0)	0.190
7	−14.819 (σ)	−14.714 (π)	−14.104 (0)	0.610
8	19.149 (σ)	−19.657 (π)	−17.863 (0)	1.794
9	−21.590 (σ)	−21.890 (π)	−21.184 $(\pi/2)$	0.706
10	23.045 (π)	−22.109 (0)	−21.947 (π)	0.162
11	24.611 (σ)	−27.005 (0)	−22.492 (π)	4.513
12	−37.922 (σ)	−39.292 (π)	−36.681 (0)	2.611
13	−44.420 (σ)	−45.173 (0)	−44.230 (π)	0.943
		$R_{O\cdots H-N} = 2.75$ Å		
1	13.310 (σ)	13.558 (0)	13.611 (π)	0.053
2	11.890 (σ)	11.799 (π)	12.375 (0)	0.576
3	8.555 (σ)	8.309 (0)	9.308 (π)	0.999
4	4.274 (π)	4.473 (0)	4.505 (π)	0.032
5	1.224 (σ)	1.271 (π)	1.552 (0)	0.281
6	−14.023 (π)	−13.933 (π)	−13.788 (0)	0.144
7	−14.819 (σ)	−14.742 (π)	−14.237 (0)	0.505
8	−19.149 (σ)	−19.626 (π)	−18.064 (0)	1.562
9	−21.590 (σ)	−22.088 (π)	−21.234 $(\pi/4)$	0.854
10	−23.045 (π)	−22.107 (0)	−21.983 $(\pi/4)$	0.124
11	−24.611 (σ)	−26.622 (0)	−22.526 (π)	4.096
12	37.922 (σ)	−39.070 (π)	−36.877 (0)	2.193
13	−44.420 (σ)	−45.051 (0)	−44.255 (π)	0.796

The criterium of self consistency used in the calculations was

$$|P^{(l+1)}_{\mu,\nu}(q_1,q_2) - P^{(l)}_{\mu,\nu}(q_1,q_2)| \leqq 10^{-3}, \qquad (9)$$

where the upper index l stands for the l-th iteration step. To fulfil this we needed usually 18–20 iterations in the CNDO and 12–14 ones in the MINDO case.

To diagonalize the Hermitian complex matrix (2) of order 13 (the number of valence orbitals in formamide) we have rewritten its eigenvalue equation (1) in the usual way [18] into a real form. The eigenvalue problems have been solved with the aid of a fast modified Givens program written by Neszmélyi [19].

Results

In Table 1 we present the CNDO/2 and MINDO/2 band structures of an one-dimensional polyformamide chain in which we have taken into account interactions only through the hydrogen bonds (see Fig. 1). In the Table the first column polyformamide chain (interactions through hydrogen bonds, all energy values in eV)

MINDO/2				
No. of band	E_{MO} and type of level	$E_{min}(k_2a_2)$	$E_{max}(k_2a_2)$	δE
		$R_{O\cdots H-N} = 2.66$ Å		
1	4.569 (σ)	5.079 (π)	5.115 (0)	0.036
2	3.877 (σ)	4.649 (0)	4.681 (π)	0.032
3	2.506 (σ)	2.785 (0)	2.906 (π)	0.121
4	0.389 (π)	0.509 (0)	0.526 (π)	0.017
5	-1.312 (σ)	-1.186 (π)	-1.134 (0)	0.054
6	-11.102 (π)	-10.962 (π)	-10.879 (0)	0.083
7	-11.496 (σ)	-11.065 (π)	-10.919 (0)	0.144
8	-12.783 (σ)	-13.457 (π)	-12.191 (0)	1.266
9	-14.525 (π)	-14.535 (0)	-14.464 (π)	0.069
10	-15.126 (σ)	-15.417 (π)	-14.827 (0)	0.590
11	-17.632 (σ)	-19.535 (0)	-16.191 (π)	3.344
12	-31.779 (σ)	-33.285 (π)	-29.861 (0)	3.424
13	-38.725 (σ)	-43.356 (0)	-38.122 (π)	2.234
		$R_{O\cdots H-N} = 2.75$ Å		
1	4.569 (σ)	4.884 (π)	4.933 (0)	0.048
2	3.877 (σ)	4.614 (0)	4.652 (π)	0.038
3	2.506 (σ)	2.753 (0)	2.876 (π)	0.122
4	0.389 (π)	0.500 (0)	0.514 (π)	0.012
5	-1.312 (σ)	-1.194 (π)	-1.150 (0)	0.043
6	-11.102 (π)	-10.965 (π)	-10.903 (0)	0.062
7	-11.496 (σ)	-11.131 (π)	-11.036 (0)	0.095
8	-12.783 (σ)	-13.392 (π)	-12.211 (0)	1.183
9	-14.525 (π)	-14.519 (0)	-14.464 (π)	0.054
10	-15.126 (σ)	-15.449 (π)	-14.834 (0)	0.612
11	-17.632 (σ)	-19.256 (0)	-16.217 (π)	3.039
12	-31.779 (σ)	-33.087 (π)	-30.094 (0)	2.993
13	-38.725 (σ)	-40.072 (0)	-38.102 (π)	1.970

contains the corresponding molecular levels, the second and third one, respectively, the lower and upper limits of the bands (their values k_2a_2 are in parenthesis) and finally the last column shows the widths of the bands. The left half of the Table contains the CNDO, the right one the MINDO results. Further the data given in the upper half of the Table refer to O···H—N hydrogen bond distance of 2.66 Å, while the lower one to 2.75 Å.

In Table 2 we give the results obtained again for an one-dimensional polyformamide chain taking into account only interactions along the main chain now. The quantities shown in Table 2 are the same as those in Table 1.

In Table 3 we show our CNDO/2 and MINDO/2 results obtained for the two-dimensional polyformamide model system (see Fig. 1). Here ε_{min} and ε_{max}, respectively, stand for the absolute lower edge and upper edge of the bands (the values k_1a_1 and k_2a_2 belonging to them are again in parenthesis). The results are given here only for the hydrogen bond distances of 2.66 Å.

Table 4 summarizes the forbidden band widths between the valence and conduction bands for all the calculated model systems in both approximations.

Table 2. The CNDO/2 and MINDO/2 band structures of a one-dimensional

No of band	CNDO/2				
	E_{MO} (type)	$E_{min}(k_1 a_1)$	$E_{max}(k_1 a_1)$	δE	
1	13.310 (σ)	13.630 (0)	15.170 (π)	1.540	
2	11.890 (σ)	11.924 ($\pi/4$)	12.686 (π)	0.762	
3	8.555 (σ)	7.412 (0)	9.934 (π)	2.522	
4	4.274 (π)	3.694 (π)	6.953 (0)	3.259	3.259
5	1 224 (σ)	5.572 (0)	6.177 ($\pi/2$)	0.605	
6	14.023 (π)	− 15.516 (π)	− 12.922 ($\pi/4$)	2.594	4.211
7	− 14.819 (σ)	15.868 (π)	− 11.657 (0)	4.211	
8	19.149 (σ)	− 18.520 (0)	− 16.205 (π)	2.315	17.476
9	− 21.590 (σ)	− 25.241 (0)	− 18.796 (π)	7.045	
10	23 045 (π)	− 28.479 (π)	− 16.417 (0)	12.062	
11	− 24.611 (σ)	− 33.681 ($\pi/4$)	− 25.350 (π)	8.331	
12	− 37.922 (σ)	− 43.307 (0)	− 37.135 ($3\pi/4$)	6.172	
13	− 44 420 (σ)	− 53.619 (0)	− 43.890 (π)	9.729	

Table 3. The CNDO/2 and MINDO/2 band structures of the two-dimensional

No. of band	CNDO/2				
	E_{MO} (type)	$E_{min}(k_1 a_1, k_2 a_2)$	$E_{max}(k_1 a_1, \bar{k}_2 a_2)$	δE	
1	13.310 (σ)	13.790 (0, − π)	15 473 (π, 0)	1.683	
2	11.890 (σ)	11.903 (0, − π)	12.774 (π, 0)	0.871	
3	8 555 (σ)	7.429 (0, 0)	10.126 (π, − π)	2.697	
4	4.274 (π)	3.441 (π, − π)	5.997 ($\pi/2$, $\pi/2$)	2.556	
5	1 224 (σ)	6.357 (π, − $\pi/2$)	7.143 (0, − π)	0.785	
6	14 023 (π)	− 15.308 (π, − π)	− 12.703 (0, 0)	2.605	22.433
7	14.819 (σ)	− 14.753 (π, π)	− 11 107 (0, − π)	3.646	
8	− 19.149 (σ)	− 17 705 ($\pi/2$, $\pi/2$)	− 13.841 (0, 0)	3.864	
9	− 21 590 (σ)	− 23.857 ($\pi/2$, 0)	− 17.581 (0, 0)	6.276	
10	− 23.045 (π)	− 27.608 (0, 0)	− 22.465 (0, − π)	5.143	
11	24.611 (σ)	− 33.540 (π, π)	− 26.190 ($\pi/2$, π)	7.350	
12	37.922 (σ)	44.960 (0, − π)	− 38.339 (π, 0)	6.621	15.534
13	− 44.420 (σ)	− 53.873 (0, 0)	− 43.490 (π, π)	10.383	

Table 4 The forbidden band widths between the valence and conduction bands of the different polyformamide systems (R stands for the O···H—N distance, energies are in eV)

		CNDO/2	MINDO/2
H-bonded one-dimensional chain	$R = 2.66$ Å	15.00	9.69
	$R = 2.75$ Å	15.06	9.75
One-dimensional main chain		16.62	9.20
Two-dimensional network	$R = 2.66$ Å	14.52	8.83

Discussion

As we can see from Tables 1–3 we have always three π bands corresponding to the three π molecular levels and ten σ ones. The bands lie in all cases symmetrical with respect to the molecular levels with the exception of the conduction polyformamide chain (interactions along the main chain, all energy values in eV)

No. of band	MINDO/2				
	E_{MO} (type)	$E_{\min}(k_1 a_1)$	$E_{\max}(k_1 a_1)$	δE	
1	4.569 (σ)	4.957 (0)	5.232 (π)	0.265	
2	3.877 (σ)	2.930 (0)	3.964 (π)	1.034	
3	2.506 (σ)	2.216 (0)	2.912 (π)	0.696	
4	0.389 (π)	0.228 (π)	1.360 (0)	1.132	2.465
5	− 1.312 (σ)	− 0.231 (0)	2.214 (π)	2.465	
6	−11.102 (π)	−12.010 (π)	−11.125 (0)	0.885	10.108
7	−11.496 (σ)	−12.364 (π)	− 9.427 (0)	2.937	
8	−12.783 (σ)	−12.732 ($3\pi/4$)	−12.163 ($\pi/4$)	0.519	
9	−14.525 (π)	−16.811 (0)	−12.438 (π)	4.373	
10	−15.126 (σ)	−17.240 (π)	−12.789 (0)	4.451	
11	−17.632 (σ)	−19.535 (0)	−16.191 (π)	3.344	
12	−31.779 (σ)	−33.285 (π)	−29.861 (0)	3.424	
13	−38.725 (σ)	−43.356 (0)	−38.122 (π)	2.234	

polyformamide network (all energy values in eV, $R_{O\ H-N} = 2.66$ Å)

No. of band	MINDO/2				
	E_{MO} (type)	$E_{\min}(k_1 a_1, k_2 a_2)$	$E_{\max}(k_1 a_1, k_2 a_2)$	δE	
1	4.569 (σ)	5.940 (0, 0)	6.143 (π, 0)	0.203	
2	3.877 (σ)	3.155 (0, 0)	4.748 (π, $-\pi$)	1.593	
3	2.506 (σ)	3.007 (0, $-\pi/2$)	3.591 (π, $-\pi$)	0.584	
4	0.389 (π)	1.606 (0, 0)	2.522 (π, 0)	0.916	
5	− 1.312 (σ)	− 0.288 (0, 0)	1.327 ($\pi/2$, $\pi/2$)	1.615	
6	−11.102 (π)	−11.096 (π, $-\pi$)	− 9.117 (0, $-\pi$)	1.979	5.822
7	−11.496 (σ)	−11.750 (π, 0)	−11.019 ($\pi/2$, $\pi/2$)	0.731	
8	−12.783 (σ)	−13.235 ($\pi/2$, π)	−11.081 (0, 0)	2.154	
9	−14.525 (π)	−14.939 ($\pi/2$, 0)	−12.092 (0, 0)	2.847	
10	−15.126 (σ)	−16.961 (π, π)	−16.114 ($\pi/2$, π)	0.847	5.611
11	−17.632 (σ)	−21.725 (π, $-\pi$)	−16.373 (0, $-\pi$)	5.352	
12	−31.779 (σ)	−37.676 (0, $-\pi$)	−30.973 (π, $-\pi$)	6.703	16.761
13	−38.725 (σ)	−47.734 (0, 0)	−34.157 (0, $-\pi$)	13.577	

band in the case of the one-dimensional formamide chain (interactions along the main chain) and of the two-dimensional polyformamide network (see Tables 2 and 3).

In that one-dimensional polyformamide chain in which we have the interactions through the hydrogen bonds the σ bands are considerably broader than the π ones (see Table 1), while in the calculated two other model systems the widths of the two types of bands are about the same (see Tables 2 and 3).

The filled σ bands are rather broad already in the first model system (Table 1), and all filled bands and some of the empty ones are quite broad (widths of several eV's, in some cases over 10 eV) in the second and third model systems (Tables 2 and 3).

In connection with the obtained very broad σ bands it should be mentioned that this situation which was found also in other calculations [10, 11] contradicts to the usual picture of localized σ bonds. One could assume that this is the consequence of the different approximations applied in the CNDO/2 and MINDO/2 method, respectively. On the other hand André [20] has obtained similarly broad σ bands in his *ab initio* calculation of a polyene chain. Mathematically it is possible to find such a unitary transformation of the many-electron wave function of a periodic system which would produce localized σ electron wave functions (as it is usually done in the course of *ab initio* molecular calculations). Such a transformation would of course leave unchanged the total energy of the system, but the one-electron description would not be possible any longer.

Returning to the details of the band structures we can see from the Tables that while by the first model system we do not have overlapping bands, by the second and third model systems many of the filled bands (including the valence band) and the two lowest unfilled bands overlap in both approximations. In this way we obtain in some cases allowed regions of 10–22 eV widths (indicated by braces in Tables 2 and 3).

In all cases the highest filled molecular levels are π levels and the lowest unfilled ones σ levels. We can find the corresponding π and σ bands in the band structures though in the second and third models they overlap with other bands. In this way their widths become rather large in these systems (values between ~2.5 eV, and ~22 eV). On the other hand in the first model system the widths of the valence and conduction bands are between ~0.3 eV and 0.05 eV, respectively. It should be further noted that the conduction bands are positive in all models in the CNDO/2 approximation and their upper limits are positive in the second and third model systems also in the MINDO/2 approximation. Therefore the physical meaning of the virtual bands which fell into the ionization continuum is questionable.

The forbidden band widths between the valence and conduction bands are ~15.0 eV by all the three models in the CNDO/2 approximation and they are between 9.2–9.7 eV by the three different model systems in the MINDO/2 approximation (see Table 4).

In the case of the first model system (one-dimensional chain with interactions through the hydrogen bonds) we have used three different hydrogen bond distances, 2.66 Å, 2.75 Å, and 2.96 Å, respectively. As we can see from Table 1 increasing the distance from 2.66–2.75 Å causes only a slight decrease in the band widths. On the other hand increasing the hydrogen bond distance to 2.96 Å we have obtained generally a decrease of the band widths by a factor of two. For proteins the 2.66 and 2.75 Å distances are the usual ones. Since the change of the hydrogen bond distance from 2.66–2.75 Å did not change significantly the band structure, we have performed the calculation for the two-dimensional polyformamide network only by 2.66 Å.

By calculating the total electronic energy of a single formamide molecule and that of the two-dimensional periodic system we have found a delocalization energy per unit cell of ~25 eV in the CNDO/2 and of ~22 eV in the MINDO/2 approximation, respectively.

In the approximation of the electronic structure of periodic protein models as next step we intend to calculate the band structure of a simplified two-dimensional polyglycine model in which we shall not take into account the proper valence angles. In this way it will be enough to put one glycine molecule in the unit cell.

Acknowledgement. We should like to express our gratitude to Dr. A. Neszmélyi for putting to our disposal his fast matrix diagonalization program before publication. We are further indebted to Dr. G. Biczó for his critical remarks.

References

1. Evans, M. G., Gergely, J.: Biochim. biophysica Acta **3**, 188 (1949).
2. Szent-Györgyi, A.: Nature **148**, 157 (1941).
3. Coulson, C. A.: Personal communication.
4. Laki, K.: Studies Inst. Med. Chem. Univ. Szeged **2**, 43 (1942).
5. Suard, M., Berthier, G., Pullman, B.: Biochim. biophysica Acta **52**, 254 (1961).
6. Yomosa, S.: Biopolymer Symposia No. 1, 1 (1964).
7. Ladik, J.: Acta physica Acad. Sci. hung. **15**, 287 (1963); Nature **202**, 1208 (1964).
8. Suard-Sender, M.: J. Chim. physique **62**, 89 (1965).
9. Brillouin, L.: In: Horizons in biochemistry, p. 295, 1962.
10. Fujita, H., Imamura, I.: J. chem. Physics **53**, 4555 (1970).
11. Beveridge, D. L., Jano, I., Ladik, J.: J. chem. Physics.
12. Del Re, G., Ladik, J., Biczó, G.: Physic. Rev. **155**, 997 (1967).
13. Ladik, J., Biczó, G.: Acta chim. Acad. Sci. hung. **67**, 397 (1971).
14. Pople, J. A., Segal, G. A.: J. chem. Physics **44**, 3289 (1966).
15. Baird, N. C., Dewar, M. J. S.: J. chem. Physics **50**, 590 (1970).
16. Slater, J. C.: Quantum theory of atomic structure, Vol. I, p. 339–342. New York: McGraw-Hill Book Co. 1960.
17. Ohno, K.: Theoret. chim. Acta (Berl.) **2**, 219 (1964); Klopman, G.: J. Amer. chem. Soc. **87**, 3300 (1965).
18. Ladik, J., Appel, K : TN. 94. Quantum Chemistry Group, Uppsala University (1962); Ladik, J., Appel, K.: J. chem. Physics **40**, 2470 (1964).
19. Neszmélyi, A.: Annali dell'Instituto Superiore di Sanita (submitted).
20. André, J. M., Leroy, G.: Int. J. quant. Chemistry **5**, 557 (1971).

Prof. J. Ladik
Lehrstuhl für Theoretische Chemie
der Technischen Universität München
D-8000 München, Arcisstr. 21
Federal Republic of Germany

Theoret. chim. Acta (Berl.) 28, 37—51 (1972)
© by Springer-Verlag 1972

Der Elektronendichtequotient zweiatomiger Moleküle

I. Allgemeine Theorie und deren Anwendung auf das δ-Modell

W. A. Bingel und B. Klahn
Lehrstuhl für Theoretische Chemie der Universität Göttingen

Eingegangen am 1. August 1972

The Electron-Density Quotient of Diatomic Molecules

I. General Theory and Its Application to the δ-Function Model

The electron-density quotient (DQ = quotient of the electronic densities at the nuclei) of a diatomic molecule is discussed as a function of internuclear distance.

In part I of this paper a method for the calculation of the DQ using united-atom perturbation theory is given. For that purpose the λ-theory and the μ-theory developed by Byers-Brown is used.

In a model calculation the DQ is then calculated in two ways: firstly with the δ-function-model in its rigorous version, secondly by a perturbational approach to it. The R-expansions of the different calculations are compared with each other.

Es wird der Dichtequotient (DQ = Verhältnis der Elektronendichten an den Orten der Atomkerne) eines zweiatomigen Moleküls in Abhängigkeit vom Abstand R der Atomkerne untersucht.

Im Teil I dieser Arbeit wird gezeigt, wie man den DQ störungstheoretisch – ausgehend vom vereinigten Atom – ermitteln kann. Dazu wird die λ-Theorie und die Byers-Brownsche μ-Theorie verwendet.

Der DQ wird dann in einer Modellrechnung an Hand des δ-Modells exakt und störungstheoretisch berechnet. Die R-Entwicklungen der verschiedenen Rechnungen werden miteinander verglichen.

1. Einleitung und Problemstellung

Die meisten Autoren, die sich mit quantenchemischen Rechnungen an zweiatomigen Molekülen befassen, haben es sich zur Aufgabe gemacht, die Energiepotentialkurven eines Moleküls für verschiedene Zustände zu berechnen. Auch für die Bestimmung anderer Moleküleigenschaften, wie Dipol- und Übergangsmomente, sind Rechenmethoden angegeben worden [1]. Dagegen befaßt sich unseres Wissens keine der bisher publizierten Arbeiten mit dem Verhalten der *Elektronendichte an den Kernorten* eines zweiatomigen Moleküls.

Ist $\Psi(\boldsymbol{r}_1, \ldots, \boldsymbol{r}_N)$ die elektronische Wellenfunktion eines zweiatomigen Moleküls AB mit N Elektronen, so ist die Gesamtelektronendichte am Ort $\boldsymbol{r}_1$

$$\varrho(\boldsymbol{r}_1) = N \int |\Psi(\boldsymbol{r}_1, \ldots, \boldsymbol{r}_N)|^2 \, ds_1 \, d\tau_2 \ldots d\tau_N \,. \tag{1}$$

Dabei erstreckt sich die Integration in (1) über die Ortskoordinaten des 2-ten bis N-ten Elektrons und über alle Spinkoordinaten. Sie entfällt für Moleküle mit nur einem Elektron. Bezeichnen nun $\boldsymbol{r}_{\mathrm{A}}$ und $\boldsymbol{r}_{\mathrm{B}}$ die Orte der Atomkerne A und B des betrachteten Moleküls, so erhalten wir für die Elektronendichten an den Kernorten ϱ_{A} und ϱ_{B} nach (1)

$$\varrho_{\mathrm{A}} := \varrho(\boldsymbol{r}_1 = \boldsymbol{r}_{\mathrm{A}}) \,; \qquad \varrho_{\mathrm{B}} := \varrho(\boldsymbol{r}_1 = \boldsymbol{r}_{\mathrm{B}}) \,. \tag{2}$$

Wir wollen uns in dieser Arbeit nun nicht mit den Dichten ϱ_{A} und ϱ_{B} direkt sondern mit ihrem Verhältnis, dem *Dichtequotienten* $\varrho_{\mathrm{B}}/\varrho_{\mathrm{A}}$ *(DQ)* befassen, nach

(1) und (2) also mit dem Ausdruck

$$\frac{\varrho_B}{\varrho_A} = \frac{\{\int |\Psi(\boldsymbol{r}_1, \ldots, \boldsymbol{r}_N)|^2 ds_1 d\tau_2 \ldots d\tau_N\}_{\boldsymbol{r}_1 = \boldsymbol{r}_B}}{\{\int |\Psi(\boldsymbol{r}_1, \ldots, \boldsymbol{r}_N)|^2 ds_1 d\tau_2 \ldots d\tau_N\}_{\boldsymbol{r}_1 = \boldsymbol{r}_A}} . \tag{3}$$

Ist R der Abstand der Kerne A und B, d.h. $R = |\boldsymbol{r}_A - \boldsymbol{r}_B|$, so gilt

$$\lim_{R \to 0} (\varrho_B/\varrho_A) = 1 , \tag{4}$$

denn in der Grenze $R = 0$ befinden sich beide Kerne am gleichen Ort ($\boldsymbol{r}_A = \boldsymbol{r}_B$), so daß (4) aus (3) folgt.

Ferner erscheint es physikalisch einleuchtend, daß die Elektronendichte am Kern mit der größeren Kernladung den größeren Wert besitzt. Sind also Z_A und Z_B die Ladungen der beiden Atomkerne A und B und ist (was stets vorausgesetzt werden soll) $Z_A > Z_B$, so sollte $\varrho_A > \varrho_B$ gelten, für den DQ also

$$\varrho_B/\varrho_A < 1 \qquad (R \neq 0, Z_A > Z_B). \tag{5}$$

Bewiesen worden ist dies jedoch unseres Wissens bisher nicht. Es ist klar, daß im homonuklearen Fall ($Z_A = Z_B$) die Elektronendichten an den beiden Kernen gleich sind ($\varrho_A = \varrho_B$), so daß für den DQ

$$\varrho_B/\varrho_A \equiv 1 \qquad (\text{für alle } R \text{ und } Z_A = Z_B) \tag{6}$$

folgt. Daher brauchen wir den homonuklearen Fall in unserer Diskussion des DQ nicht weiter betrachten.

Der DQ hat weiterhin die Eigenschaft, daß er bei Vertauschung der Kernladungen Z_A und Z_B in seinen Kehrwert übergeht. Denn bei dieser Vertauschung geht offenbar ϱ_A in ϱ_B über und umgekehrt.

Um die genaue Abhängigkeit des DQ vom Kernabstand R und den Kernladungen Z_A, Z_B herauszufinden, ist es nun unerläßlich, die Wellenfunktion Ψ des Moleküls exakt oder genähert zu bestimmen. Dann erst kann man den DQ nach (3) berechnen.

Im allgemeinen kann die Wellenfunktion nur genähert bestimmt werden. Welches Näherungsverfahren dabei geeignet ist, hängt vom Bereich des Kernabstandes ab, der untersucht werden soll. Für $R = \infty$ etwa beschreiben wir das Molekül durch die Wellenfunktionen der *getrennten Atome* und erhalten so in einfacher Weise ϱ_A und ϱ_B als die Dichten der getrennten Atome an ihrem Kern. Um nun auch den Bereich großer bis mittlerer Kernabstände ($R < \infty$) zu erfassen, kann man eine Störungsrechnung durchführen, die in nullter Näherung gerade die getrennten Atome ($R = \infty$) beschreibt.

Für den Fall kleiner bis mittlerer Kernabstände dagegen empfiehlt sich die Verwendung einer Störungsrechnung, die vom anderen Extrem, dem *„vereinigten Atom"* (UA = United Atom), ausgeht. Dabei denkt man sich ein zweiatomiges Molekül aus einem einzigen Atom, dem UA, mit der Kernladung

$$Z = Z_A + Z_B \tag{7}$$

durch „Aufspalten" des Kerns entstanden. Man darf annehmen, daß solch eine Störungsrechnung für hinreichend kleine R zu brauchbaren Resultaten führt.

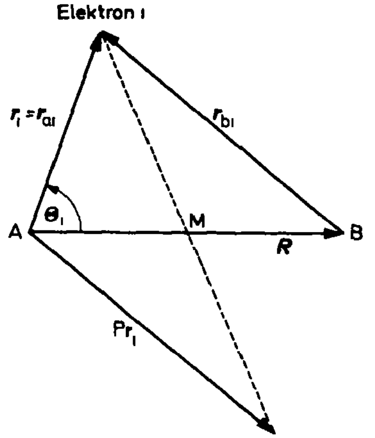

Fig. 1. Koordinatensystem für das zweiatomige Molekül AB

In dieser Arbeit (Teil I und II) soll vor allem der Fall kleiner Kernabstände behandelt werden. Wir gehen deshalb zunächst genauer darauf ein, wie die angedeutete UA-Störungstheorie sinnvoll durchzuführen ist. Dabei sollen zwei Methoden besprochen werden: die „λ-Theorie" und die von Byers-Brown [2] neu eingeführte „μ-Theorie".

2. Hamiltonoperator und Q-Symmetrie

Es sei AB ein zweiatomiges Molekül mit den Kernladungen Z_A, Z_B und N Elektronen; der Kern A befinde sich am Ort $\boldsymbol{r}_A = \boldsymbol{0}$, der Kern B am Ort $\boldsymbol{r}_B = \boldsymbol{R}$; $\boldsymbol{r}_i \equiv \boldsymbol{r}_{ai}$ und $\boldsymbol{r}_{bi}$ seien die Ortsvektoren (r_i, r_{bi} deren Beträge) des i-ten Elektrons vom Kern A bzw. B aus (vgl. Fig. 1) und r_{ij} der Abstand zwischen dem i-ten und j-ten Elektron.

Dann ist der nichtrelativistische elektronische Hamiltonoperator dieses Moleküls in atomaren Einheiten:

$$H = \sum_{i=1}^{N} \left(-\frac{1}{2} \Delta_i - Z_A/r_i - Z_B/r_{bi} \right) + \sum_{i<j} 1/r_{ij} \tag{8}$$

und der zu diesem Operator gehörige Energieeigenwert E und die Wellenfunktion Ψ sind Lösung der Schrödingergleichung

$$H\Psi = E\Psi. \tag{9}$$

Wir führen nun den Operator P ein, der in der noch zu besprechenden Byers-Brownschen μ-Theorie eine wesentliche Rolle spielt. Dieser Operator invertiert alle Elektronenkoordinaten am Molekülmittelpunkt M (vgl. Fig. 1), es gilt also für eine beliebige Funktion $f(\boldsymbol{r}_1, \ldots, \boldsymbol{r}_N)$

$$Pf(\boldsymbol{r}_1, \ldots, \boldsymbol{r}_N) = f(\boldsymbol{R} - \boldsymbol{r}_1, \ldots, \boldsymbol{R} - \boldsymbol{r}_N). \tag{10}$$

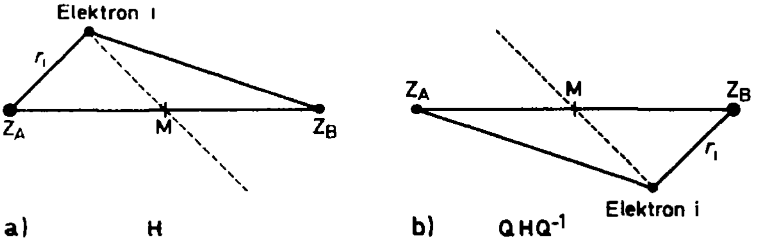

Fig. 2a Zweiatomiges Molekül ($Z_A > Z_B$) zum Hamiltonoperator H nach Gl. (8). b Zweiatomiges Molekül ($Z_A > Z_B$) zum Hamiltonoperator QHQ^{-1}

P ist ein hermitescher, unitärer Operator, und es gilt $P^2 = 1$, was mit (10) leicht einzusehen ist. Ferner sei I ein Operator, der die Kernladungen vertauscht, d.h. es ist

$$IZ_A = Z_B, IZ_B = Z_A . \tag{11}$$

Auch für den Operator I gilt die Beziehung $I^2 = 1$, denn zweimaliges Vertauschen der Kernladungen führt zum Ausgangsmolekül zurück.

Der Hamiltonoperator H ist für $Z_A \neq Z_B$ weder gegen Inversion der Elektronenkoordinaten am Molekülmittelpunkt noch gegen Vertauschung der Kernladungen invariant, wohl aber gegen beide Operationen *gleichzeitig*, d.h. gegen den Operator[1]

$$Q = PI = IP. \tag{12}$$

Es unterscheiden sich nämlich die Moleküle, die durch die Operatoren H (Fig. 2a) und durch QHQ^{-1} (Fig. 2b) beschrieben werden, lediglich durch ihre räumliche Orientierung, so daß zu beiden derselbe elektronische Hamiltonoperator

$$H = QHQ^{-1} \tag{13}$$

gehört. Wegen der Vertauschbarkeit der Operatoren H und Q [s. Gl. (13)] ist Ψ nun nicht nur Eigenfunktion von H [vgl. (9)], sondern auch von Q zum Eigenwert q:

$$Q\Psi = q\Psi . \tag{14}$$

Wegen $Q^2 = 1$ (was aus $P^2 = 1$ und $I^2 = 1$ folgt) hat q die Werte

$$q = \pm 1 . \tag{15}$$

Für das UA wird offenbar $Q = P$, so daß q die elektronische Parität des betrachteten UA-Zustandes bedeutet.

Die „Q-Symmetrie" der Wellenfunktion Ψ, charakterisiert durch Gl. (14), ist offenbar eine besondere Eigenschaft aller zweiatomigen Moleküle. Berechnet man Ψ störungstheoretisch, so ist es wünschenwert, daß die Q-Symmetrie *in jeder*

---

[1] Der Operator Q wird erstmalig von Wigner u. Witmer [3] verwendet im Zusammenhang mit Wellenfunktionen, die die Rotations-, Schwingungs- und elektronischen Zustände eines Moleküls beschreiben.

Ordnung der Störungstheorie erfüllt ist. Diese Bedingung wird von der Byers-Brownschen μ-Theorie erfüllt (s. S. 47). Wir erwarten deshalb, daß sich diese Theorie auch zur Berechnung des DQ besonders eignet.

3. λ- und μ-Theorie

Zur Durchführung einer UA-Störungstheorie ist zunächst der Hamiltonoperator H in einen ungestörten Operator H_0, der das UA beschreibt, und in einen Störoperator $\lambda V(\lambda$: Störungsparameter) aufzuteilen. Dabei soll sich das UA am Ort des Kernes mit der größeren Ladung, also am Ort des Kernes A, befinden. Mit dieser Festlegung folgen wir der Konvention von Byers-Brown [2].

Offenbar ist nun

$$H_0 := \sum_{i=1}^{N} \left(-\frac{1}{2} \Delta_i - Z/r_i \right) + \sum_{i<j} 1/r_{ij} \tag{16}$$

der Hamiltonoperator eines Atoms mit der Kernladung $Z = Z_A + Z_B$ und N Elektronen am Ort des Kernes A und damit der Hamiltonoperator des UA. Führen wir als Störungsoperator V und Parameter λ

$$V = Z \sum_{i=1}^{N} (1/r_i - 1/r_{bi}) \tag{17}$$

$$\lambda = Z_B/Z \tag{18}$$

ein, so läßt sich der Hamiltonoperator (8) in der Form

$$H = H_0 + \lambda V \tag{19}$$

schreiben.

Die physikalische Bedeutung der Zerlegung (19) kann man sich mit Hilfe von Fig. 3 klarmachen, wenn man sich den Störungsparameter λ von $\lambda = 0$ über $\lambda = Z_B/Z$ bis nach $\lambda = 1$ variiert denkt: Für $\lambda = 0$ ist die gesamte Kernladung Z des Moleküls bei A (s. Fig. 3 oben). Im Falle $\lambda = 1$ wird durch (19) das andere Extrem beschrieben, daß sich nämlich das UA und damit auch die gesamte Kernladung Z am Ort des Kernes B befindet (s. Fig. 3 unten). Zwischen diesen beiden Extremfällen liegt gerade das Molekül AB, das mit $\lambda = Z_B/Z$ durch die Zerlegung

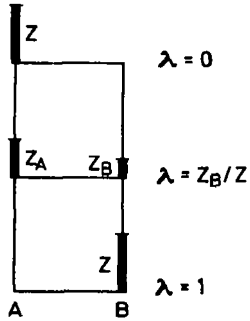

Fig. 3. Zeichnung zum Verständnis der Zerlegung des Hamiltonoperators nach Gl. (19)

Accession number
38966

(19) beschrieben wird. In diesem Fall hat der Kern A die Ladung Z_A und der Kern B die Ladung Z_B (s. Fig. 3 Mitte).

Zur Durchführung einer UA-Störungsrechnung ist der Energieeigenwert E und die Wellenfunktion Ψ nach dem Störungsparameter λ zu entwickeln:

$$E = E_0^{(\lambda)} + \lambda E_1^{(\lambda)} + \lambda^2 E_2^{(\lambda)} + 0(\lambda^3), \tag{20a}$$

$$\Psi = \Psi_0 + \lambda \Psi_1 + \lambda^2 \Psi_2 + 0(\lambda^3). \tag{20b}$$

Dabei berechnen sich die Störungsenergien und -funktionen $E_0^{(\lambda)}, E_1^{(\lambda)}, \ldots, \Psi_0, \Psi_1, \ldots$ nach den bekannten Gleichungen der Rayleigh-Schrödingerschen Störungstheorie (s. z.B. [4]). $E_0^{(\lambda)}$ und Ψ_0 sind gerade die Energie und die Wellenfunktion des UA.

Die hier beschriebene „λ-Theorie" – eine Bezeichnung, die auf Byers-Brown [2] zurückgeht – hat jedoch vor allem zwei Mängel:

1) Die λ-Entwicklung der Energie (20a) ist *nicht* symmetrisch in den Kernladungen, was auf den in Z_A und Z_B unsymmetrischen Störungsparameter λ zurückzuführen ist [s. Gl. (18)].

2) Die λ-Entwicklung der Wellenfunktion besitzt *keine* Q-Symmetrie, wenn man sie bei einer beliebigen Ordnung abbricht. Die Q-Symmetrie ist nicht einmal für das erste Glied der Entwicklung, nämlich die UA-Funktion Ψ_0, erfüllt. Denn wendet man den Operator $Q = PI$ auf die am Kern A zentrierte Funktion Ψ_0 an, so erhält man wegen des Operators P eine am Kern B zentrierte Funktion, so daß Ψ_0 nicht Eigenfunktion von Q sein kann.

Diese Mängel vermeidet man mit der μ-Theorie, die nun besprochen werden soll. Byers-Brown [2] führte eine *neue* Wellenfunktion ψ ein, aus der die exakte Wellenfunktion Ψ mit dem Transformationsoperator

$$\Lambda = 1 - \lambda + \lambda q P = Z^{-1}(Z_A + Z_B q P) \tag{21}$$

durch die Gleichung

$$\Psi = \Lambda \psi \tag{22}$$

gewonnen werden kann. Für die neue Wellenfunktion ψ läßt sich eine transformierte Schrödingergleichung angeben. Sie hat die Form (vgl. [2])

$$\mathscr{H} \psi = E \psi \tag{23}$$

wobei

$$\mathscr{H} = H_0 + \mu V(1 - qP) \tag{24}$$

und

$$\mu = \lambda(1 - \lambda) = Z_A Z_B / Z^2 \quad \text{ist.} \tag{25}$$

Obgleich $\mathscr{H}$ kein hermitescher Operator ist, sind seine Eigenwerte reell, denn $\mathscr{H}$ hat *dieselben* Eigenwerte wie der hermitesche Operator H.

Betrachten wir nun $V(1 - qP)$ als neuen Störungsoperator und μ als Störungsparameter, so erhalten wir als μ-Entwicklung von Energie und Wellenfunktion

$$E = E_0^{(\mu)} + \mu E_1^{(\mu)} + \mu^2 E_2^{(\mu)} + 0(\mu^3), \tag{26a}$$

$$\psi = \psi_0 + \mu \psi_1 + \mu^2 \psi_2 + 0(\mu^3). \tag{26b}$$

Für die Störungsenergien und -Funktionen gelten auch hier die Gleichungen der Rayleigh-Schrödingerschen Störungstheorie.

$E_0^{(\mu)}$ und ψ_0 sind als Eigenwert und -funktion von H_0 identisch mit den entsprechenden Größen der λ-Theorie, d.h. es ist $E_0^{(\mu)} = E_0^{(\lambda)}$ und $\psi_0 \equiv \Psi_0$. Man kann ferner zeigen, daß auch $E_1^{(\mu)} = E_1^{(\lambda)}$ ist. Wir brauchen deshalb bei diesen Größen zwischen λ- und μ-Theorie nicht zu unterscheiden und schreiben ϕ_0 statt $\psi_0 \equiv \Psi_0$, E_0 statt $E_0^{(\mu)} = E_0^{(\lambda)}$ und E_1 statt $E_1^{(\mu)} = E_1^{(\lambda)}$.

Besonders wichtig ist nun die Tatsache, daß die für die λ-Theorie angeführten Mängel für die μ-Theorie nicht bestehen:

1) Die μ-Entwicklung der Energie (26a) ist wegen des in Z_A und Z_B symmetrischen Störungsparameters μ [s. Gl. (25)] in den Kernladungen symmetrisch.

2) Ferner besitzt die störungstheoretisch berechnete Wellenfunktion $\Psi = A(\psi_0 + \mu\psi_1 + \cdots)$ die Q-Symmetrie, gleichgültig, nach welcher Ordnung die Störungsreihe (26b) abgebrochen wird (zum Beweis s. Byers-Brown [2]).

Wie zu erwarten, erweist sich die μ-Entwicklung (26a) der λ-Entwicklung (20a) bei numerischen Rechnungen als erheblich überlegen, wenn man die Störungsentwicklungen jeweils nach der ersten Ordnung abbricht (s. [2]). Wir werden sehen, daß diese Überlegenheit der μ-Theorie nicht nur bei der Berechnung der Energie sondern auch bei der Berechnung des DQ besteht.

4. Die Berechnung des DQ in λ- und μ-Theorie

Setzen wir die λ-Entwicklung von Ψ(20b) in die Gl. (3) für den DQ ein, so erhalten wir mit $\boldsymbol{r}_A = \mathbf{0}$ und $\boldsymbol{r}_B = \boldsymbol{R}$ (vgl. Fig. 1)

$$\frac{\varrho_B}{\varrho_A} = \frac{\{\int |\Psi_0 + \lambda\Psi_1 + 0(\lambda^2)|^2\, ds_1\, d\tau_2 \ldots d\tau_N\}_{\boldsymbol{r}_1 = \boldsymbol{R}}}{\{\int |\Psi_0 + \lambda\Psi_1 + 0(\lambda^2)|^2\, ds_1\, d\tau_2 \ldots d\tau_N\}_{\boldsymbol{r}_1 = \mathbf{0}}}\,. \tag{27}$$

Ebenso erhalten wir in der μ-Theorie mit (3), (22) und (26b)

$$\frac{\varrho_B}{\varrho_A} = \frac{\{\int |A(\psi_0 + \mu\psi_1 + 0(\mu^2))|^2\, ds_1\, d\tau_2 \ldots d\tau_N\}_{\boldsymbol{r}_1 = \boldsymbol{R}}}{\{\int |A(\psi_0 + \mu\psi_1 + 0(\mu^2))|^2\, ds_1\, d\tau_2 \ldots d\tau_N\}_{\boldsymbol{r}_1 = \mathbf{0}}}\,. \tag{28}$$

Brechen wir die λ- bzw. μ-Entwicklung in (27) bzw. (28) nach der nullten Näherung ab, verwenden wir also zur Berechnung des DQ nur die UA-Funktion $\phi_0 (\equiv \Psi_0 \equiv \psi_0)$, so nennen wir das Ergebnis den „*DQ in nullter Näherung*" und schreiben dafür $(\varrho_B/\varrho_A)_0$. Brechen wir die jeweilige Entwicklung erst nach der ersten Näherung ab, wird also auch die Störungsfunktion erster Ordnung (Ψ_1 bzw. ψ_1) bei der Berechnung des DQ berücksichtigt, so nennen wir das Ergebnis den „*DQ in erster Näherung*" und schreiben $(\varrho_B/\varrho_A)_1$.

Die Störungsfunktionen nullter und erster Ordnung bestimmen sich, wie schon bemerkt wurde, aus den Rayleigh-Schrödingerschen Störungsgleichungen. Diese lassen sich für λ- und μ-Theorie mit Hilfe des Parameters p so zusammenfassen:

$$(H_0 - E_0)\phi_0 = 0, \tag{29a}$$

$$E_1 = \langle\phi_0|V|\phi_0\rangle, \tag{29b}$$

$$(H_0 - E_0)\phi_1 = [E_1 - V(1 - pP)]\,\phi_0, \tag{29c}$$

$$E_2 = \langle\phi_0|V(1 - pP)|\phi_1\rangle - E_1\langle\phi_0|\phi_1\rangle \tag{29d}$$

wobei

$$\phi_0 \equiv \Psi_0 \equiv \psi_0, E_0 = E_0^{(\lambda)} = E_0^{(\mu)}, E_1 = E_1^{(\lambda)} = E_1^{(\mu)}.$$

Für $p = 0$(λ-Theorie) ist $\begin{cases} \phi_1 \equiv \Psi_1 \\ E_2 = E_2^{(\lambda)}. \end{cases}$ (30a)

Für $p = q$(μ-Theorie) ist $\begin{cases} \Phi_1 \equiv \psi_1 \\ E_2 = E_2^{(\mu)}. \end{cases}$ (30b)

Wir sind nunmehr in der Lage, den DQ störungstheoretisch zu berechnen, indem wir zunächst die Gl. (29a–c) lösen und dann den DQ nach (27) bzw. (28) berechnen.

5. Das δ-Modell

Es ist jedoch schon verhältnismäßig aufwendig, die Störungsgleichungen (29a–d) selbst für einfache Moleküle wie etwa HeH^+ oder HeH zu lösen. Exakt durchführbar ist eine solche Rechnung ohnehin nur für Moleküle mit nur *einem* Elektron wie z.B. HeH^{2+}. Deshalb ist es vorteilhaft, den DQ zunächst an Hand eines Modells, des *δ-Modells*, zu bestimmen. Das δ-Modell gestattet es nämlich, den DQ und seine R-Reihenentwicklung exakt anzugeben sowie auch die störungstheoretische Behandlung unserer Aufgabe [also die Lösung von (29a–d) und die Berechnung des DQ nach (27, (28)] exakt durchzuführen.

Das δ-Modell, das schon von Frost [5], Hund [6] und anderen Autoren diskutiert worden ist, wird durch den Hamiltonoperator

$$H^\delta = -\tfrac{1}{2} d^2/dx^2 - Z_A \delta(x - R/2) - Z_B \delta(x + R/2) \qquad (31)$$

beschrieben. Offenbar handelt es sich um ein lineares Modellsystem, das einem zweiatomigen Molekül mit einem Elektron entspricht [vgl. mit dem Hamiltonoperator (8)]. Dabei sind die Kernladungen Z_A und Z_B auf der x-Achse bei $x = R/2$ (Kern A) und bei $x = -R/2$ (Kern B) angeordnet (vgl. Fig. 4). An die Stelle der Coulomb-Potentiale sind δ-Funktionen getreten. Da der Mittelpunkt M dieses δ-Modells, anders als bei den Molekülen, im Nullpunkt des Koordinatensystems (d.h. der x-Achse) gewählt worden ist, bewirkt der unter (10) eingeführte Operator P eine Vorzeichenumkehr von x. Für eine beliebige Funktion $f(x)$ gilt somit

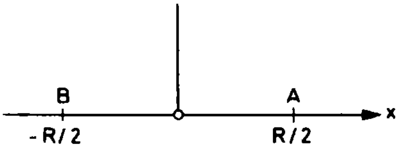

Fig. 4. Koordinatensystem für das δ-Modell

$$Pf(x) = f(-x). \qquad (32)$$

Die zum δ-Modell gehörige Wellenfunktion Ψ ist Lösung der Eigenwertgleichung $H^\delta \Psi = E\Psi$ und läßt sich exakt bestimmen. Als Lösung dieser Gleichung für E

und Ψ findet man (wobei $q = \pm 1$ der Eigenwert des Operators Q ist)

$$\Psi = \frac{1}{\sqrt{N_q}} \{ e^{-c_q|x-R/2|} + q e^{-c_q|x+R/2|} \}, \tag{33}$$

$$E = -c_q^2/2. \tag{34}$$

Der Energieparameter c_q ist Lösung der transzendenten Gleichung

$$\exp(-2c_q R) = (c_q - Z_A)(c_q - Z_B)/(Z_A Z_B) \tag{35}$$

und es gilt für γ_q und N_q

$$\gamma_q = \left(\frac{(c_q - Z_B) Z_A}{(c_q - Z_A) Z_B} \right)^{1/2} \tag{36}$$

$$N_q = \{ 1 + \gamma_q^2 + 2q\gamma_q (1 + c_q R) e^{-c_q R} \} / c_q. \tag{37}$$

N_q ist so gewählt, daß die Wellenfunktion auf 1 normiert ist, d.h. $\langle \Psi | \Psi \rangle = 1$.

Wie man mit den Gl. (33), (12), (11), (32), (36) und (37) leicht nachweist, besitzt die Wellenfunktion Ψ für das δ-Modell genau wie die Wellenfunktion eines Moleküls die Q-Symmetrie (14).

Ferner besitzt die Wellenfunktion des δ-Modells (33) an den beiden Kernen eine unstetige Ableitung, oder, wie man auch sagt, eine „Spitze" bzw. einen "cusp". Für solch einen "cusp" kann hier wie für Moleküle (s. [7]) eine "cusp"-Bedingung angegeben werden, die derjenigen für Moleküle formal sehr ähnlich ist. Dies ist ein weiterer Hinweis dafür, daß das δ-Modell für unsere Überlegungen ein geeignetes Modell ist.

Einen Überblick über den für alle exakten Rechnungen wesentlichen Energieparameter c_q kann man aufgrund von Gl. (35) gewinnen. Gl. (35) kann für jeden beliebigen aber festen Wert R nach c_q aufgelöst werden. Dies soll für zwei repräsentative Kernabstände R_1 und R_2 mit $R_1 < R_2$ durch ein graphisches Verfahren geschehen:

Man trägt die Funktionen $f_1(c,R) = \exp(-2cR)$ und

$$f_2(c) = (c - Z_A)(c - Z_B)/(Z_A Z_B)$$

mit dem Kernabstand R als Parameter in einem Diagramm über c auf. c_q ergibt sich wegen (35) dann als Schnittpunkt beider Kurven (vgl. Fig. 5). Nach Fig. 5 ergeben sich als Lösung von (35) entweder ein oder zwei Werte für c_q, je nachdem, ob R hinreichend klein ist (wie R_1) oder hinreichend groß (wie R_2). Dabei ist der größere der beiden c_q-Werte für *beliebige* Kernabstände R vorhanden; dieser Wert ist stets größer als Z_A und gehört zur Wellenfunktion Ψ mit $q = +1$.

Die zweite nur bei hinreichend großen Kernabständen existente Lösung c_q von (35) ist stets kleiner als Z_B und gehört zur Wellenfunktion $q = -1$. Es ist also

$$c_{-1} < Z_B < Z_A < c_{+1}. \tag{38}$$

Erst mit (38) ist die Gleichung (33) vollständig bestimmt.

Da nun die Wellenfunktion exakt bekannt ist, läßt sich auch der DQ exakt nach (3) bestimmen. Den Vektoren r_A und r_B in (3) entsprechen beim δ-Modell

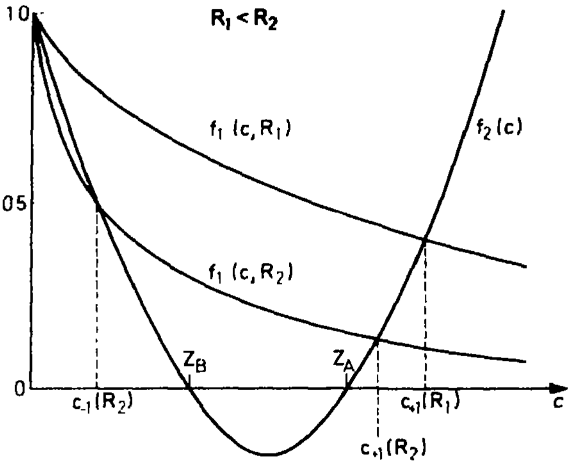

Fig. 5 Diagramm zur graphischen Bestimmung des Energieparameters c_q bei zwei verschiedenen Kernabständen R_1 und R_2 nach Gl. (35)

die Koordinaten $x = R/2$ und $x = -R/2$, so daß für den *DQ* folgt

$$\frac{\varrho_B}{\varrho_A} = \frac{\Psi^2(x = -R/2)}{\Psi^2(x = +R/2)}. \tag{39}$$

Setzen wir Ψ von Gl. (33) in (39) ein, so erhalten wir nach einfachen Umformungen unter Zuhilfenahme von (35) und (36)

$$\frac{\varrho_B}{\varrho_A} = \frac{(c_q - Z_A) Z_A}{(c_q - Z_B) Z_B}. \tag{40}$$

Damit läßt sich der *DQ* nun in Abhängigkeit vom Kernabstand numerisch praktisch beliebig genau bestimmen, indem man die transzendente Gl. (35) durch ein geeignetes Iterationsverfahren für c_q auflöst und das so bestimmte c_q in (40) einsetzt. Dies ist für den Fall $Z_A = 2$ und $Z_B = 1$ als Modell für das Molekül HeH^{2+} und für $q = +1$ geschehen. Das Ergebnis ist in Fig. 6 aufgetragen. Wie erwartet, ergibt sich eine Kurve, die für $R \to 0$ gegen 1 geht und deren Werte für $R > 0$ kleiner als 1 sind.

Für $R \to \infty$ geht die Kurve des *DQ* gegen 0. Dieses Verhalten ist auf Grund der Gl. (35) und (40) klar, denn offenbar wird (35) für $R \to \infty$ durch $c_{+1} = Z_A$ gelöst, so daß $\varrho_B/\varrho_A = 0$ nach Gl. (40) folgt. Die physikalische Bedeutung dieses Verhaltens liegt darin, daß sich das durch das δ-Modell beschriebene Teilchen für große R nur in der Nähe des Kernes A mit der größeren Ladung aufhält und die Ladungsdichte am Kern B daher gegen 0 geht.

Dieses Verhalten wird sich auch für Moleküle mit *einem* Elektron ergeben. Denn das eine Elektron kann sich für $R \to \infty$ ebenfalls nur in der Nähe *eines* Kernes aufhalten.

Es müssen nun noch einige Bemerkungen zu den beim δ-Modell verwendeten Einheiten gemacht werden: Offenbar ist der Hamiltonoperator des δ-Modells

H^δ [Gl. (31)] dimensionslos geschrieben. Man kann sich H^δ aus dem Operator

$$(H^\delta)' = -\hbar^2/(2m) \cdot d^2/dx^2 - Ze^2 [\delta(x - R/2) + \delta(x + R/2)]$$

durch Einführung atomarer Einheiten entstanden denken, wie das auch für den Hamiltonoperator eines Moleküls bekannt ist. Geht man nun bei Rechnungen an Molekülen vom dimensionslosen Hamiltonoperator aus, so erhält man bekanntlich alle berechneten Größen in atomaren Einheiten. Ebenso erhalten wir auch beim δ-Modell alle Größen in atomaren Einheiten, da wir vom dimensionalen Operator H^δ und nicht von $(H^\delta)'$ ausgehen.

6. Die *R*-Entwicklung der Energie und des *DQ* beim *δ*-Modell

Um das Verhalten der Energie und des DQ für kleine R herauszufinden, entwickeln wir beide Größen in eine Potenzreihe nach R. Dazu brauchen wir die R-Entwicklung von c_q. Da für kleine R nur die Lösung für $q = +1$ existiert, müssen wir uns auf c_{+1} beschränken.

Wie man an Hand von Gl. (35) sofort sieht, ist $c_{+1}(R = 0) = Z$, so daß $c_{+1}(R)$ die Entwicklung

$$c_{+1}(R) = Z + \sum_{n=1}^{\infty} a_n R^n \tag{41}$$

mit noch zu bestimmenden Koeffizienten a_n besitzt. Die Koeffizienten bestimmen wir, indem wir (35) links und rechts nach c_q entwickeln, die R-Entwicklung (41) für c_{+1} einsetzen und auf gleiche Potenzen von R abgleichen. Wir erhalten dann

$$c_{+1}(R) = Z\{1 - 2\mu ZR + 2\mu(ZR)^2 - \tfrac{4}{3}\mu(3\mu + 1)(ZR)^3 + 0(R^4)\}\,. \tag{42}$$

Setzen wir nun (42) in (34) bzw. (40) ein und entwickeln die entstehenden Ausdrücke wiederum nach R, so erhalten wir als exakte R-Reihenentwicklung der Energie und des DQ

$$E = -(Z^2/2) \cdot \{1 - 4\mu ZR + 4\mu(\mu + 1)(ZR)^2 - \tfrac{8}{3}\mu(6\mu + 1)(ZR)^3 + 0(R^4)\}, \tag{43}$$

$$\begin{aligned} \varrho_B/\varrho_A = {} & 1 - 2(Z_A - Z_B)R + 2(Z_A - Z_B)^2 R^2 \\ & - \tfrac{4}{3}(Z_A - Z_B)(Z_A^2 + Z_A Z_B + Z_B^2) R^3 + 0(R^4) \end{aligned} \tag{44}$$

und für den Spezialfall $Z_A = 2, Z_B = 1$ als Modell für HeH^{2+}

$$\varrho_B/\varrho_A = 1 - 2R + 2R^2 - \tfrac{28}{3} R^3 + 0(R^4)\,. \tag{45}$$

In der Entwicklung für die Energie tritt – anders als bei Molekülen (s. [8]) – ein in R lineares Glied auf. Man kann aber von einem so einfachen Modell auch nicht erwarten, daß alle Eigenschaften der Moleküle richtig beschrieben werden. Die Entwicklung (45) ist bis zum in R quadratischen Glied in Fig. 6 mit eingezeichnet. Man erkennt, daß die R-Entwicklung nur für sehr kleine R ($R < 0.2$) eine brauchbare Approximation des DQ liefert. Dies liegt wohl an der langsamen Konvergenz der Reihe (45); denn die Entwicklungskoeffizienten bilden dem Betrage nach eine wachsende Folge.

7. Störungstheoretische Bestimmung der Energie und des DQ für das δ-Modell

Wenn wir – was im Teil II dieser Arbeit geschehen soll – den DQ störungstheoretisch mit Hilfe von λ- und μ-Theorie für Moleküle berechnen wollen, müssen wir uns über die Qualität des angewandten Verfahrens im klaren sein. So ist etwa die Frage von besonderem Interesse, ob man mit der Kenntnis der UA-Funktion ϕ_0 auskommt, wenn man den Beginn der R-Entwicklung des DQ bestimmen möchte. Wir wollen diese Frage an Hand des δ-Modells untersuchen, und wir hoffen, daß sich das Ergebnis dieser Untersuchung auch auf Moleküle überträgt.

Zu diesem Zweck sind zunächst die Rayleigh-Schrödingerschen Störungsgleichungen (29a–d) für das δ-Modell zu lösen. Dem Hamiltonoperator H_0 des UA und dem Störungsoperator V entsprechen hier die Operatoren

$$H_0^\delta = -\frac{1}{2}\, d^2/dx^2 - Z\delta(x-R/2)\,, \tag{46}$$

$$V^\delta = Z[\delta(x-R/2) - \delta(x+R/2)]\,. \tag{47}$$

Dann gilt nämlich $H^\delta = H_0^\delta + \lambda V^\delta$ und für den Hamiltonoperator in der μ-Theorie, wie man zeigen kann, $\mathscr{H}^\delta = H_0^\delta + \mu V^\delta(1-qP)$. Die Störungsgleichungen für das δ-Modell schreiben sich daher in der Form [vgl. (29a–d)]

$$\left[-\frac{1}{2}\, d^2/dx^2 - Z\delta(x-R/2) - E_0\right]\phi_0 = 0\,, \tag{48a}$$

$$E_1 = \langle\phi_0|Z[\delta(x-R/2) - \delta(x+R/2)]\,|\phi_0\rangle\,, \tag{48b}$$

$$\begin{aligned}\left[-\frac{1}{2}\, d^2/dx^2 - Z\delta(x-R/2) - E_0\right]\phi_1 \\ = \{E_1 - Z[\delta(x-R/2) - \delta(x+R/2)]\,(1-pP)\}\,\phi_0\,,\end{aligned} \tag{48c}$$

$$E_2 = \langle\phi_0|Z[\delta(x-R/2) - \delta(x+R/2)]\,(1-pP)|\phi_1\rangle - E_1\langle\phi_0|\phi_1\rangle\,. \tag{48d}$$

Wie unter (30a–b) angegeben, erhalten wir aus (48a–d) für $p=0$ die Größen der λ- und für $p=q$ die der μ-Theorie. Als Lösung der Gl. (48a–d) finden wir

$$E_0 = -Z^2/2 \qquad \phi_0 = \sqrt{Z}\, e^{-Z|x-R/2|}\,, \tag{49a}$$

$$E_1 = Z^2(1-e^{-2ZR})\,, \tag{49b}$$

$$\begin{aligned}\phi_1 &= a\phi_0 + \\ &+\sqrt{Z}\begin{cases}(1-e^{-2ZR})e^{-Z(x-R/2)}(1/2+Zx) + b_1 e^{-Z(x-R/2)} & \text{für } x > R/2\\ (1-e^{-2ZR})e^{Z(x-R/2)}(1/2-Zx) + b_2 e^{-Z(x+R/2)} & \text{für } -R/2 < x < R/2\\ (1-e^{-2ZR})e^{Z(x-R/2)}(1/2-Zx) + b_2 e^{Z(x+R/2)} & \text{für } -R/2 > x\end{cases}\end{aligned} \tag{49c}$$

mit

$$\begin{aligned} b_1 &= e^{-2ZR} - ZR(1-e^{-2ZR}) - pe^{-ZR}\\ b_2 &= e^{-ZR} - p\end{aligned}$$

$$E_2 = Z^2(1-e^{-2ZR})\,\{p^2 - (1+e^{-2ZR})/2 - 2ZRe^{-2ZR}\}\,. \tag{49d}$$

Die Größe a in Gl. (49c) ist eine noch freie, vom Kernabstand abhängige Normierungskonstante. Wir wählen sie so, daß $\langle\phi_0|\phi_1\rangle = 0$ ist („intermediäre Normierung“).
Mit (20a), (26a) und (49a, b, d) können wir die Energie in zweiter störungstheoretischer Näherung nun für die λ- und die μ-Theorie hinschreiben:

$$E = Z^2 \begin{cases} -1/2 + \lambda(1-e^{-2ZR}) - \lambda^2(1-e^{-2ZR})[(1-e^{-2ZR})/2 + 2ZRe^{-2ZR}] \\ \qquad + 0(\lambda^3) \\ -1/2 + \mu(1-e^{-2ZR}) + \mu^2(1-e^{-2ZR})[1-(1+e^{-2ZR})/2 - 2ZRe^{-2ZR}] \\ \qquad + 0(\mu^3)\,. \end{cases} \tag{50}$$

Brechen wir die Entwicklung (50) nach dem in λ bzw. μ linearen Glied ab und entwickeln nach R, so ergibt sich

$$E = -\frac{Z^2}{2} \begin{cases} 1 \,\vdots\, -4\lambda ZR + 4\lambda(ZR)^2 + 0(R^3) & (\lambda\text{-Theorie}) \\ 1 \;-4\mu ZR \,\vdots\, + 4\mu(ZR)^2 + 0(R^3) & (\mu\text{-Theorie}) \\ 1 \;-4\mu ZR + 4\mu(\mu+1)(ZR)^2 + 0(R^3) & (\text{exakt})\,. \end{cases} \tag{51a}$$

Dabei ist die exakte R-Entwicklung von Gl. (43) übernommen. Brechen wir die Störungsentwicklung (50) erst nach dem in λ bzw. μ quadratischen Glied ab, so erhalten wir als R-Entwicklung der Energie

$$E = -\frac{Z^2}{2} \begin{cases} 1 - 4\mu ZR \,\vdots\, + 4\mu(ZR)^2 + 0(R^3) & (\lambda\text{-Theorie}) \\ 1 - 4\mu ZR \;\; + 4\mu(\mu+1)(ZR)^2 - \tfrac{8}{3}\mu(6\mu+1)(ZR)^3 \,\vdots\, + 0(R^4) & (\mu\text{-Theorie}) \\ 1 - 4\mu ZR \;\; + 4\mu(\mu+1)(ZR)^2 - \tfrac{8}{3}\mu(6\mu+1)(ZR)^3 \;\; + 0(R^4) & (\text{exakt})\,. \end{cases} \tag{51b}$$

Die gestrichelte Linie (- -) deutet jeweils an, bis zu welcher Potenz von R exakte und störungstheoretische Entwicklung übereinstimmen. Offenbar ist die μ-Theorie der λ-Theorie erheblich überlegen, was besonders in (51b) deutlich wird.

Die störungstheoretische Berechnung des DQ erfolgt nach (27) und (28). Die Integration in (27) und (28) entfällt hier, da es sich beim δ-Modell um ein Einteilchenmodell handelt, den Orten $\boldsymbol{r}_1 = \boldsymbol{R}$ bzw. $\boldsymbol{r}_1 = \boldsymbol{0}$ entsprechen hier, wie bereits oben erwähnt, die Koordinaten $x = -R/2$ und $x = R/2$. Setzen wir nun $\phi_0 \equiv \Psi_0 \equiv \psi_0$ von Gl. (49a) in (27) und (28) ein und vernachlässigen die Störungsfunktionen höherer Ordnung, so erhalten wir nach einfacher Rechnung für den DQ in nullter Näherung

$$\left(\frac{\varrho_{\mathrm{B}}}{\varrho_{\mathrm{A}}}\right)_0 = \begin{cases} e^{-2ZR} & \text{für die } \lambda\text{-Theorie} \\ \left(\dfrac{Z_{\mathrm{A}}e^{-ZR} + Z_{\mathrm{B}}}{Z_{\mathrm{A}} + Z_{\mathrm{B}}e^{-ZR}}\right)^2 & \text{für die } \mu\text{-Theorie.} \end{cases} \tag{52}$$

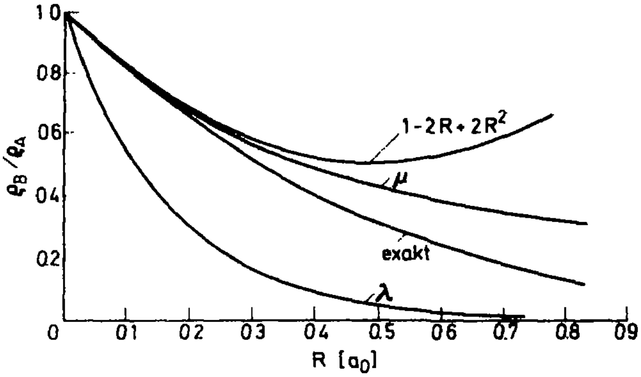

Fig. 6 Der DQ des ϱ-Modells als Funktion des Kernabstandes für $Z_A = 2$, $Z_B = 1$: „exakt" = exakte Kurve nach (40), „$1 - 2R + 2R^2$" = R-Entwicklung nach (45), „λ", „μ" = λ- und μ-Störungstheorie nullter Näherung

Der DQ von Gl. (52) ist in Fig. 6 für den Spezialfall $Z_A = 2$, $Z_B = 1$ als Modell für HeH^{2+} graphisch dargestellt („λ"- bzw. „μ"-Kurve). Für kleine Werte $R(\leqq 0.2)$ stellt der DQ nullter Näherung in der μ-Theorie schon eine recht brauchbare Approximation des exakten DQ dar. Die λ-Theorie dagegen ist offenbar wenig geeignet, das Verhalten des DQ zu beschreiben (vgl. Fig. 6). Diese Eigenschaften erkennen wir auch, wenn wir (52) nach R entwickeln und das Resultat mit der exakten R-Entwicklung des DQ (44) vergleichen:

$$(\varrho_B/\varrho_A)_0 = \begin{cases} 1 - 2ZR + 0(R^2) & (\lambda\text{-Theorie}) \\ 1 - 2(Z_A - Z_B)R + 2(Z_A - Z_B)^2 R^2 + 0(R^3) & (\mu\text{-Theorie}) \end{cases} \tag{53a}$$

$$(\varrho_B/\varrho_A)_{\text{exakt}} = 1 - 2(Z_A - Z_B)R + 2(Z_A - Z_B)^2 R^2 + 0(R^3) \qquad (\text{exakt}).$$

Berücksichtigen wir auch noch die Störungsfunktion erster Ordnung bei der Berechnung des DQ, setzen wir also (49a, c) unter Beachtung von (30a, b) in (27) und (28) ein, so erhalten wir den DQ erster Näherung für die λ- und μ-Theorie. Das Ergebnis dieser Rechnung ist in Fig. 7 wiederum für den Spezialfall $Z_A = 2$, $Z_B = 1$ im Vergleich mit dem exakten DQ und seiner R-Entwicklung (45) (bis hin zum in R quadratischen Glied) aufgetragen. Man sieht, daß der störungstheoretisch berechnete $DQ\,(\varrho_B/\varrho_A)_1$ eine bessere Approximation des exakten DQ darstellt als $(\varrho_B/\varrho_A)_0$ (vgl. Fig. 6), und daß auch hier die μ-Theorie der λ-Theorie überlegen ist. Dieses Verhalten ist wiederum auch aus der R-Entwicklung von $(\varrho_B/\varrho_A)_1$ abzulesen:

$$(\varrho_B/\varrho_A)_1 = \begin{cases} 1 - 2(Z_A - Z_B)R + 2(Z_A^2 - Z_A Z_B + 4Z_B^2)R^2 + 0(R^3) & (\lambda\text{-Theorie}) \\ 1 - 2(Z_A - Z_B)R + 2(Z_A - Z_B)^2 R^2 + 0(R^3) & (\mu\text{-Theorie}) \end{cases} \tag{53b}$$

$$(\varrho_B/\varrho_A)_{\text{exakt}} = 1 - 2(Z_A - Z_B)R + 2(Z_A - Z_B)^2 R^2 + 0(R^3) \qquad (\text{exakt}).$$

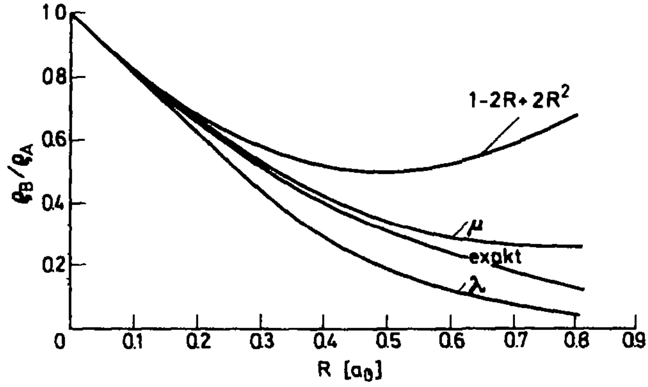

Fig. 7. Der *DQ* des δ-Modells als Funktion des Kernabstandes für $Z_A = 2$, $Z_B = 1$: „exakt" = exakte Kurve nach (40), „$1 - 2R + 2R^2$" = *R*-Entwicklung nach (45), „λ", „μ" = λ- und μ-Störungstheorie erster Näherung

Als weiteres besonders erfreuliches Resultat erhalten wir zudem, daß man mit der μ-Theorie nullter Näherung, also unter *alleiniger Kenntnis der* UA-*Funktion*, bereits die bis zum einschließlich in *R* quadratischen Glied richtige *R*-Entwicklung des *DQ* erhält.

Dieses Ergebnis läßt uns hoffen, daß auch bei Molekülen die Kenntnis der UA-Funktion ausreichend ist, um den Beginn der *R*-Entwicklung des *DQ* mittels μ-Theorie auszurechnen.

Diese Arbeit wurde unterstützt aus Mitteln der Deutschen Forschungsgemeinschaft im Rahmen des Schwerpunktprogramms „Theoretische Chemie".

Literatur

1. Bingel, W. A.: Z. Naturforsch. **12a**, 59 (1957).
2. Byers-Brown, W., Power, J. D.: Proc. Royal Soc. (London) **A317**, 545 (1970).
3. Wigner, E., Witmer, E. E.: Z. Physik **51**, 859 (1928).
4. Dalgarno, A.: Stationary perturbation theory, quantum theory, 1. elements, ed. by D. R. Bates, New York: Academic Press 1961.
5. Frost, A. A.: J. Chem. Physics **25**, 1150 (1956).
6. Hund, F.: Theorie des Aufbaues der Materie, S. 63ff. Stuttgart: Teubner 1961.
7. Bingel, W. A.: Z. Naturforsch. **18a**, 1249 (1963).
8. Bingel, W. A.: J. Chem. Physics **30**, 1250 (1959).

Prof. Dr. W. A. Bingel
Lehrstuhl für Theoretische Chemie
der Universität Göttingen
D-3400 Göttingen
Bürgerstr. 50a
Bundesrepublik Deutschland

Theoret. chim. Acta (Berl.) 28, 53—66 (1972)
© by Springer-Verlag 1972

Der Elektronendichtequotient zweiatomiger Moleküle

II. Anwendung der Theorie auf Moleküle und Entwicklung des Elektronendichtequotienten nach dem Kernabstand

B. Klahn und W. A. Bingel

Lehrstuhl für Theoretische Chemie der Universität Göttingen

Eingegangen am 1. August 1972

The Electron-Density Quotient of Diatomic Molecules

II. Application of the Theory to Molecules and Calculation of the Electron-Density Quotient as a Function of the Internuclear Distance

The electron-density quotient of diatomic molecules (DQ) is discussed as a function of the internuclear distance R:

The DQ of molecules with one electron is calculated both exactly and by a perturbational approach using λ- and μ-theory. An R-expansion of this DQ is derived.

The DQ of the molecules HeH^+, HeH and HeH^- are calculated numerically by a perturbational approach and by a SCF-calculation. An R-expansion of DQ is obtained, using these numerical results.

Finally, an R-expansion of the DQ is derived valid for all diatomic molecules. For this purpose Byers-Browns μ-theory was used with neglect of the electronic interaction and restriction to zero-order wave functions.

Es wird der Elektronendichtequotient zweiatomiger Moleküle (DQ) in Abhängigkeit vom Kernabstand R untersucht:

Für Moleküle mit einem Elektron wird der DQ exakt und störungstheoretisch mittels λ- und μ-Theorie berechnet und eine R-Entwicklung angegeben.

Für die Moleküle HeH^+, HeH und HeH^- wird der DQ durch numerische Verfahren störungstheoretisch bzw. durch eine SCF-Rechnung bestimmt und aus den Resultaten eine R-Entwicklung ermittelt.

Schließlich wird eine R-Entwicklung des DQ für beliebige zweiatomige Moleküle mittels der Byers-Brownschen μ-Theorie nullter Näherung unter Vernachlässigung der elektronischen Wechselwirkung hergeleitet. Das Resultat wird mit den durch numerische Rechnungen gewonnenen Ergebnissen verglichen.

1. Theorie

In Teil I dieser Arbeit [1] (im folgenden mit I zitiert) haben wir den Elektronendichtequotienten (DQ) zweiatomiger Moleküle eingeführt und gezeigt, wie man den DQ störungstheoretisch berechnen kann. Nachdem diese Störungstheorie dort lediglich für das δ-Modell durchgeführt worden ist, wollen wir den DQ nun auch für Moleküle berechnen.

Zunächst stellen wir jedoch noch einmal die für die Rechnungen grundlegenden Gleichungen zusammen:

Es sei AB ein zweiatomiges Molekül mit den Kernladungen Z_A und Z_B (wobei $Z_A > Z_B$ gelte) mit der Gesamtkernladung $Z = Z_A + Z_B$ und mit N Elektronen. Die Kerne mögen sich an den Orten $\boldsymbol{r}_A = \boldsymbol{0}$ und $\boldsymbol{r}_B = \boldsymbol{R}$ befinden (vgl. Fig. 1 von I), also einen Abstand $R = |\boldsymbol{R}|$ voneinander haben. $\Psi(\boldsymbol{r}_1, \ldots, \boldsymbol{r}_N)$ sei die zu diesem Molekül gehörige elektronische Wellenfunktion, wobei $\boldsymbol{r}_1, \ldots, \boldsymbol{r}_N$ die Ortsvektoren des 1-sten bis N-ten Elektrons vom Kern A aus seien. Dann verstehen wir unter dem *DQ* [vgl. I, Gl. (3)]

$$\frac{\varrho_{\mathrm{B}}}{\varrho_{\mathrm{A}}}=\frac{\{\int|\Psi(r_1,\ldots,r_N)|^2\,ds_1\,d\tau_2\ldots d\tau_N\}_{r_1=r_{\mathrm{B}}}}{\{\int|\Psi(r_1,\ldots,r_N)|^2\,ds_1\,d\tau_2\ldots d\tau_N\}_{r_1=r_{\mathrm{A}}}}. \tag{1}$$

Dabei wird über die Ortskoordinaten des 2-ten bis N-ten Elektrons und über alle Spinkoordinaten integriert.

Nun läßt sich der *DQ störungstheoretisch* berechnen, indem man die Wellenfunktion Ψ nach einem geeigneten Störungsparameter entwickelt und den *DQ* nach (1) bestimmt. Verwenden wir als nullte Näherung einer solchen Störungsentwicklung das zum Molekül gehörige „*vereinigte Atom*“ (UA), so erhalten wir die λ-Entwicklung ($\lambda=Z_{\mathrm{B}}/Z$) der Wellenfunktion Ψ, und der *DQ* schreibt sich nach (1) als [vgl. I, Gl. (27)]

$$\frac{\varrho_{\mathrm{B}}}{\varrho_{\mathrm{A}}}=\frac{\{\int|\Psi_0+\lambda\Psi_1+0(\lambda^2)|^2\,ds_1\,d\tau_2\ldots d\tau_N\}_{r_1=R}}{\{\int|\Psi_0+\lambda\Psi_1+0(\lambda^2)|^2\,ds_1\,d\tau_2\ldots d\tau_N\}_{r_1=0}}. \tag{2a}$$

Dabei ist Ψ_0 die UA-Funktion und Ψ_1 die Störungsfunktion erster Ordnung in der „λ-Theorie“.

Eine andere Möglichkeit zur störungstheoretischen Berechnung des *DQ* besteht darin, die Wellenfunktion Ψ mit dem Transformationsoperator[1] $A=1-\lambda+\lambda qP$ aus einer neuen von Byers-Brown [2] eingeführten Wellenfunktion ψ durch die Gleichung $\Psi=A\psi$ zu gewinnen. Auch für die Funktion ψ läßt sich eine Störungsrechnung durchführen, die in nullter Näherung vom UA ausgeht. Wie von Byers-Brown [2] bzw. in I gezeigt wird, entwickelt man die Wellenfunktion ψ dazu nach dem Störungsparameter $\mu=Z_{\mathrm{A}}Z_{\mathrm{B}}/Z^2$.

Für den *DQ* folgt dann aus (1) [vgl. I, Gl. (28)]

$$\frac{\varrho_{\mathrm{B}}}{\varrho_{\mathrm{A}}}=\frac{\{\int|A[\psi_0+\mu\psi_1+0(\mu^2)]|^2\,ds_1\,d\tau_2\ldots d\tau_N\}_{r_1=R}}{\{\int|A[\psi_0+\mu\psi_1+0(\mu^2)]|^2\,ds_1\,d\tau_2\ldots d\tau_N\}_{r_1=0}}. \tag{2b}$$

ψ_0 ist die UA-Funktion des Moleküls und daher mit Ψ_0 von Gl. (2a) identisch. Wir brauchen deshalb zwischen Ψ_0 und ψ_0 nicht zu unterscheiden und schreiben für beide Funktionen ϕ_0. Das ψ_1 in Gl. (2b) ist die Störungsfunktion erster Ordnung in der μ-Theorie und ist von Ψ_1 verschieden.

Die Funktionen ϕ_0, Ψ_1 und ψ_1 berechnen sich aus den Rayleigh-Schrödingerschen Störungsgleichungen, die in I in der Form [vgl. I (29a–c), (30a, b)]

$$(H_0-E_0)\phi_0=0, \tag{3a}$$

$$E_1=\langle\phi_0|V|\phi_0\rangle, \tag{3b}$$

$$(H_0-E_0)\phi_1=[E_1-V(1-pP)]\phi_0, \tag{3c}$$

$$\phi_1=\begin{cases}\Psi_1 & \text{für } p=0 \quad (\lambda\text{-Theorie})\\ \psi_1 & \text{für } p=q \quad (\mu\text{-Theorie})\end{cases} \tag{3d}$$

angegeben sind. Dabei ist H_0 der Hamiltonoperator des UA am Kern A [vgl. I, Gl. (16)], E_0 der Energieeigenwert von H_0 zur Eigenfunktion ϕ_0, E_1 die Störungsenergie erster Ordnung in λ- und μ-Theorie und V der unter I Gl. (17) angegebene

---

[1] Für die Bedeutung der Größe q und des Operators P siehe I, Gl. (10).

Störungsoperator. Mit Gl. (3c) läßt sich die Störungsfunktion erster Ordnung sowohl für die λ-Theorie ($p = 0$) als auch für die μ-Theorie ($p = q$) bestimmen.

Zur störungstheoretischen Berechnung des *DQ* sind also die Störungsgleichungen (3a–c) zu lösen und der *DQ* ist dann nach (2a, b) zu bestimmen. Wie schon in I festgelegt wurde, sprechen wir vom *DQ nullter Näherung* $(\varrho_B/\varrho_A)_0$, wenn wir die λ- bzw. μ-Entwicklung in (2a, b) nach der UA-Funktion abbrechen, und vom *DQ erster Näherung* $(\varrho_B/\varrho_A)_1$, wenn wir die Störungsentwicklungen jeweils nach der Funktion erster Ordnung abbrechen.

2. Der *DQ* für Einelektronenmoleküle

Wir wollen den *DQ* zunächst für Moleküle mit *einem* Elektron untersuchen. Bekanntlich ist die exakte Wellenfunktion für das Molekül HeH^{2+} von Bates u. Carson [3] in Form eines Produktes dreier Faktoren hergeleitet worden. Dabei hängt einer dieser Faktoren nur vom azimutalen Winkel und die beiden anderen von je einer elliptischen Koordinate ab. Mittels dieser exakten Wellenfunktion können wir den *DQ* nach (1) numerisch für verschiedene Kernabstände bestimmen. Die Ergebnisse dieser Rechnungen sind in Fig. 1 („exakte" Kurve) aufgetragen.

Wie zu erwarten war, erhalten wir für den *DQ* eine Kurve, die für $R \to 0$ gegen 1 geht, die für $R > 0$ stets kleinere Werte als 1 hat und die für $R \to \infty$ gegen 0 geht. Die beiden erstgenannten Eigenschaften sind aufgrund der Gl. (4) und (5) von I zu erwarten, die letztgenannte ist – wie bereits in I erläutert – darauf zurückzuführen, daß sich das eine Elektron für große *R* nur in der Nähe *eines* Kernes aufhalten kann; daher geht die Dichte am anderen Kern – hier am Kern B – gegen 0.

Nun ist jedoch einer der Faktoren der exakten Wellenfunktion in der Arbeit von Bates und Carson als eine Reihenentwicklung nach Kugelfunktionen angegeben, deren Entwicklungskoeffizienten sich aus einer Rekursionsformel ergeben. Daher stößt es, anders als beim δ-Modell, auf Schwierigkeiten, den im Prinzip bekannten exakten Ausdruck für den *DQ* nach dem Kernabstand *R* zu

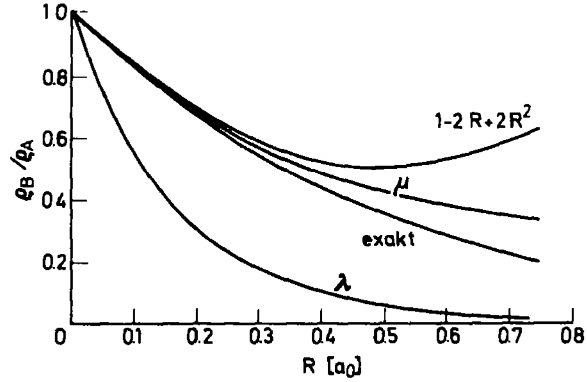

Fig. 1. Der *DQ* von HeH^{2+} als Funktion des Kernabstandes: „exakt" = exakte Kurve, „$1 - 2R + 2R^2$" = *R*-Entwicklung nach (13), „λ" bzw. „μ" = λ- bzw. μ-Störungstheorie nullter Näherung nach (12)

entwickeln. Wir wollen deshalb die R-Entwicklung aus störungstheoretischen Überlegungen gewinnen.

Dazu sind die Störungsgleichungen (3a–c) zu lösen, und der DQ ist nach (2a, b) zu berechnen. Der Operator des UA für beliebige Moleküle mit einem Elektron

$$H_0 = -\tfrac{1}{2}\Delta - Z/r \tag{4}$$

ist der Hamiltonoperator für wasserstoffähnliche Atome mit der Kernladung Z in atomaren Einheiten. Als Lösung der Störungsgleichung für E_0 und ϕ_0 (3a) erhalten wir daher Energie und Wellenfunktion eines wasserstoffähnlichen Atoms, im Grundzustand also (vgl. z.B. [4], S. 84)

$$E_0 = -Z^2/2\,; \qquad \phi_0 = (Z^3/\pi)^{1/2}\, e^{-Zr}\,. \tag{5a}$$

Für die Störungsenergie E_1 folgt dann durch Integration nach (3b)

$$E_1 = Z^2\{1 - 1/(ZR) + [1 + 1/(ZR)]\, e^{-2ZR}\}\,. \tag{5b}$$

Die Lösung von (3c) für die Störungsfunktion erster Ordnung ist von Power ([5], S. 102) explizit für den Fall $p=0$ (d.h. für die λ-Theorie) und für $Z=1$ angegeben worden und hat für $Z \geqq 1$ die Form

$$\Psi_1 = (Z^3/\pi)^{1/2}\, e^{-Zr} \cdot F(\xi,\eta) \tag{6}$$

wobei ξ und η elliptische Koordinaten sind:

$$\xi = (r + |R - r|)/R, \qquad \eta = (r - |R - r|)/R \tag{7}$$

$F(\xi,\eta)$ ist dabei durch die folgende Gleichung gegeben:

$$\begin{aligned} F(\xi,\eta) = {} & (E_1/Z^2)\,[(\xi+\eta)\cdot ZR/2 + ln(1+\xi)] \\ & + [1 + (1/ZR)]\,\{\Omega[-ZR(1-\eta)] - e^{-2ZR}\,\Omega[ZR(1+\eta)]\} \end{aligned} \tag{8}$$

mit

$$\Omega(x) = \sum_{n=1}^{\infty} \frac{x^n}{n \cdot n!}\,. \tag{9}$$

Wenn man auch die Störungsfunktion erster Ordnung für die μ-Theorie bestimmen möchte, so braucht die Gl. (3c) nicht erneut für $p=q$ gelöst zu werden. Denn zwischen den Funktionen Ψ_1 und ψ_1 besteht für $q=+1$ der Zusammenhang (vgl. [5], S. 31)

$$\psi_1 = \Psi_1 + S_{00}\,\phi_0 - P\phi_0 \tag{10}$$

mit

$$S_{00} = \langle\phi_0|P|\phi_0\rangle = [1 + ZR + (ZR)^2/3]\, e^{-ZR}\,. \tag{11}$$

Nach (10) erhalten wir daher mit (5a) und (6) für ψ_1:

$$\psi_1 = (Z^3/\pi)^{1/2}\,\{e^{-Zr}F(\xi,\eta) + S_{00}\,e^{-Zr} - e^{-Z|R-r|}\}\,. \tag{5c}$$

Wir berechnen nun den DQ in nullter Näherung für die λ- und μ-Theorie nach (2a, b). Nach einfacher Rechnung ergibt sich

$$\left(\frac{\varrho_B}{\varrho_A}\right)_0 = \begin{cases} e^{-2ZR} & \text{für die } \lambda\text{-Theorie} \\[2ex] \left(\dfrac{Z_A e^{-ZR} + Z_B}{Z_A + Z_B e^{-ZR}}\right)^2 & \text{für die } \mu\text{-Theorie}\,. \end{cases} \tag{12}$$

Das Ergebnis ist offenbar identisch mit der entsprechenden Rechnung am δ-Modell [vgl. I, Gl. (52)]. Daher bekommen wir auch *dieselbe* R-Entwicklung wie beim δ-Modell:

$$\left(\frac{\varrho_B}{\varrho_A}\right)_0 = \begin{cases} 1 - 2ZR + 0(R^2) & (\lambda\text{-Theorie}) \\ 1 - 2(Z_A - Z_B)R + 2(Z_A - Z_B)^2 R^2 + 0(R^3) & (\mu\text{-Theorie}). \end{cases} \tag{13}$$

Die Übereinstimmung mit den Resultaten für das δ-Modell läßt uns vermuten, daß die mittels der μ-Theorie gewonnene R-Entwicklung genau wie beim δ-Modell [vgl. I, Gl. (53a, b)] bereits bis zum in R quadratischen Glied einschließlich korrekt ist; d. h., diese Entwicklung wird durch die Berücksichtigung der Störungsfunktion ψ_1 nicht mehr verändert.

Um dies nachzuprüfen, berechnen wir den DQ erster Näherung, nunmehr jedoch nur in der μ-Theorie. Setzen wir (5a) und (5c) in (2b) ein, so erhalten wir unter Berücksichtigung von (7) als DQ erster Näherung der μ-Theorie:

$$(\varrho_B/\varrho_A)_1 = (Z_A\alpha + Z_B\beta)/(Z_A\beta + Z_B\alpha)$$

mit

$$\alpha = e^{-ZR} + \mu[e^{-ZR}F(1,1) + S_{00}e^{-ZR} - 1] \tag{14}$$

und

$$\beta = 1 + \mu[F(1,-1) + S_{00} - e^{-ZR}].$$

Setzen wir F und S_{00} gemäß (8) und (11) in (14) ein und entwickeln dann nach R, so folgt

$$(\varrho_B/\varrho_A)_1 = 1 - 2(Z_A - Z_B)R + 2(Z_A - Z_B)^2 R^2 + 0(R^3) \quad (\text{für die } \mu\text{-Theorie}). \tag{15}$$

Unsere Vermutung bestätigt sich also.

Strenggenommen müßte nun noch bewiesen werden, daß die Entwicklung (15) durch die Berücksichtigung der Störungsfunktionen höherer Ordnung, nämlich ψ_2, $\psi_3, \dots$ nicht mehr verändert wird; aber für eine „vernünftige" Störungstheorie sollte es nicht möglich sein, daß die Störungsfunktionen $\psi_2, \psi_3, \dots$ die Entwicklung (13) noch beeinflussen, wenn diese bereits von ψ_1 unverändert gelassen wird.

Zudem werden die Gl. (13) und (15) durch die numerische Berechnung des DQ aus der exakten Wellenfunktion für HeH^{2+} bestätigt: In Fig. 1 ist neben der Kurve für den exakten DQ auch die R-Entwicklung nach Gl. (15) eingezeichnet. Offensichtlich verhalten sich beide Kurven für $R \to 0$ gleich. Noch besser stimmen in Fig. 1 die Kurve des DQ nullter Näherung der μ-Theorie nach Gl. (12) – zu dessen Berechnung nur die Kenntnis der UA-Funktion nötig ist – und die exakte Kurve überein.

Die μ-Theorie ist demnach auch für die Berechnung des DQ bei Einelektronenmolekülen recht geeignet. Dies wird besonders deutlich im Vergleich mit der λ-Theorie: Der DQ nullter Näherung in der λ-Theorie nach Gl. (12), der in Fig. 1 graphisch dargestellt ist, verhält sich für kleine bis mittlere Kernabstände völlig falsch.

Wir sehen also, daß die Qualität von λ- und μ-Theorie für Einelektronenmoleküle genau wie beim δ-Modell ausfällt.

3. Numerische Berechnung des *DQ* für Moleküle mit mehreren Elektronen

Beim δ-Modell und bei Molekülen mit *einem* Elektron war es möglich, die Störungsgleichungen (3a-c) exakt zu lösen und dann eine R-Entwicklung des DQ anzugeben. Bei Molekülen mit mehr als einem Elektron entfällt diese Möglichkeit jedoch. Es lassen sich nicht einmal die Energie und die Wellenfunktion des UA exakt bestimmen. Wir sind daher auf numerische Näherungsrechnungen angewiesen.

Zur Berechnung des DQ sind also die Störungsgleichungen (3a–c) durch geeignete Verfahren bei verschiedenen Kernabständen zu lösen und der DQ dann in nullter und erster Näherung nach (2a, b) zu bestimmen. Der Umfang der hier durchgeführten Rechnungen machte es erforderlich, die einzelnen Aufgaben zu programmieren und die Programme auf einer elektronischen Rechenmaschine auszuführen.

Wir wollen nun den DQ für das Molekül HeH^+ – als Repräsentanten für alle Moleküle mit zwei Elektronen – berechnen. Die UA-Funktion ϕ_0 entwickeln wir nach natürlichen Orbitalen[2] χ_i (Abkürzung: NO)

$$\phi_0 = \sum_i \lambda_i \chi_i(\boldsymbol{r}_1)\chi_i(\boldsymbol{r}_2) \tag{16}$$

und lösen die Gl. (3a) für den Grundzustand des UA Li^+, indem wir die NO's und die Entwicklungskoeffizienten λ_i mit der Kutzelniggschen NO-Methode [7] berechnen.

Als Basisfunktionen verwenden wir bei dieser Rechnung gruppierte Gaussfunktionen mit einer von Huzinaga [8] für das Li-Atom optimisierten Basis; dabei werden s- und p-Funktionen berücksichtigt.

Für die Störungsfunktion erster Ordnung machen wir einen Ansatz der Form[3]

$$\phi_1 = \sum_{i,j} c_{ij}\varphi_i(\boldsymbol{r}_1)\varphi_j(\boldsymbol{r}_2). \tag{17}$$

Die Funktionen $\varphi_i(\boldsymbol{r})$ sind noch vorzugebende Basisfunktionen; wir rechnen wieder mit gruppierten Gaußfunktionen, die am Kern A zentriert sind, also mit *Einzentrenfunktionen*. Die Koeffizienten c_{ij} erhalten wir, indem wir die Differentialgleichung für ϕ_1 (3c) von links mit $\varphi_k(\boldsymbol{r}_1)\varphi_l(\boldsymbol{r}_2)$ multiplizieren und über $\boldsymbol{r}_1$ und $\boldsymbol{r}_2$ integrieren. Damit überführen wir (3c) auf ein lineares, inhomogenes algebraisches Gleichungssystem:

$$\begin{aligned}\sum_{i,j} c_{ij}\,&\langle\varphi_k(\boldsymbol{r}_1)\varphi_l(\boldsymbol{r}_2)|H_0 - E_0|\varphi_i(\boldsymbol{r}_1)\varphi_j(\boldsymbol{r}_2)\rangle\\ &= \langle\varphi_k(\boldsymbol{r}_1)\varphi_l(\boldsymbol{r}_2)|E_1 - V(1-pP)|\phi_0\rangle\,.\end{aligned} \tag{18}$$

Zur Lösung von Gl. (18) und der Bestimmung des DQ nach (2a) und (2b) war ein Rechenprogramm neu zu entwickeln. Die Resultate der mit diesem Programm durchgeführten Rechnungen, nämlich die Werte des DQ für verschiedene Kernabstände, sind in Fig. 2 in nullter Näherung und Fig. 3 in erster Näherung aufgetragen (λ- und μ-Kurve).

---

[2] Der Begriff „natürliches Orbital" geht auf Löwdin [6] zurück.

[3] Man kann sich den Ansatz (17) aus einer Entwicklung der Zweielektronenfunktion ϕ_1 nach zweireihigen Slaterdeterminanten entstanden denken. (17) ist gerade der Ortsanteil dieser Entwicklung.

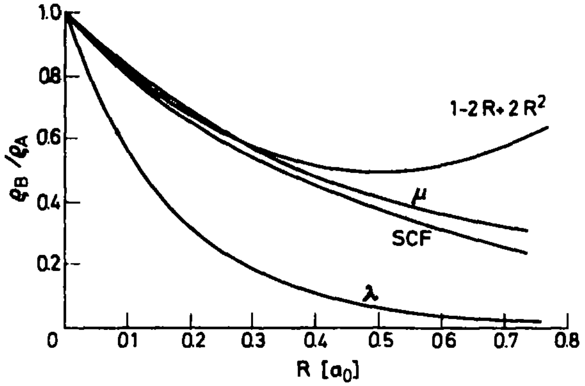

Fig. 2. Der DQ von HeH^+ als Funktion des Kernabstandes: „SCF“ = SCF-Kurve, „$1-2R+2R^2$“ = R-Entwicklung nach (32), „λ“ bzw. „μ“ = λ- bzw. μ-Störungstheorie nullter Näherung

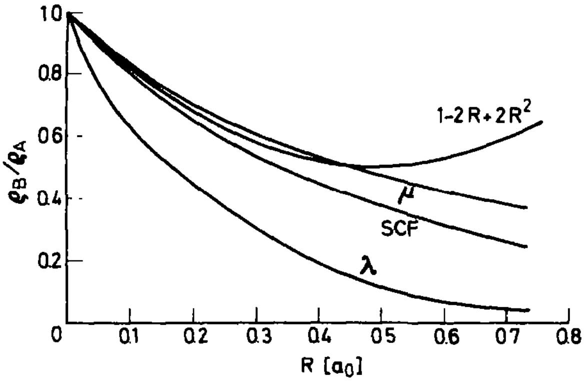

Fig. 3. Der DQ von HeH^+ als Funktion des Kernabstandes: „SCF“ = SCF-Kurve, „$1-2R+2R^2$“ = R-Entwicklung nach (32), „λ“ bzw. „μ“ = λ- bzw. μ-Störungstheorie erster Näherung

Da sich der DQ für HeH^+ nicht exakt berechnen läßt, wurde er zum Vergleich mit den störungstheoretisch ermittelten Werten auch mit einer Hartree-Fock-Wellenfunktion durch eine SCF-Rechnung bestimmt. Eine Basis aus gruppierten Gaußfunktionen haben wir dafür von Huzinaga [9] übernommen. Die so bestimmte SCF-Kurve ist ebenfalls in Fig. 2 und Fig. 3 eingetragen.

Ferner ist in Fig. 2 und Fig. 3 auch die unter Gl. (32) angegebene R-Entwicklung des DQ für HeH^+ eingezeichnet.

Als Repräsentanten der zweiatomigen Moleküle mit drei Elektronen betrachten wir das Molekül HeH. Für die UA-Funktion, d. h. für die Lösung von Gl. (3a), nehmen wir die Hartree-Fock-Wellenfunktion des Li-Atoms von Clementi [10]. Den mit dieser Funktion ϕ_0 nach (2a, b) berechneten DQ nullter Näherung haben wir in Fig. 4 aufgetragen. Die unter Gl. (32) angegebene R-Entwicklung ist für das Molekül HeH in Fig. 4 ebenfalls graphisch dargestellt.

Als Repräsentanten der zweiatomigen Moleküle mit vier Elektronen wählen wir das Anion HeH^- und bestimmen dessen DQ durch eine SCF-Rechnung.

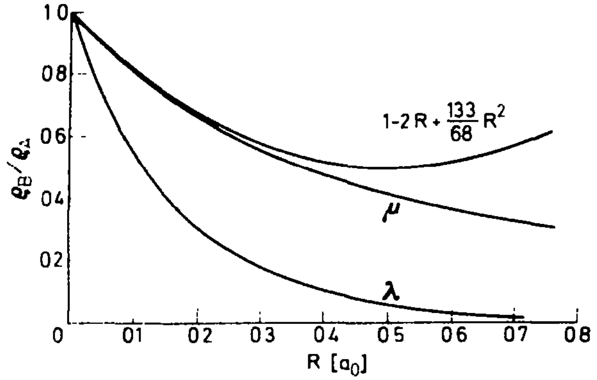

Fig. 4. Der *DQ* von HeH als Funktion des Kernabstandes: „1 − 2R + 133/68 R^2" = *R*-Entwicklung nach (32), „λ" bzw. „μ" = λ- bzw. μ-Störungstheorie nullter Näherung

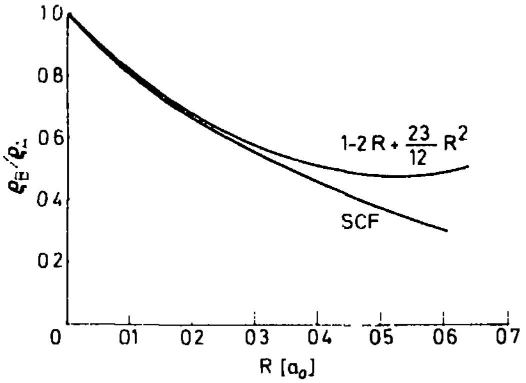

Fig. 5. Der *DQ* von HeH als Funktion des Kernabstandes: „SCF" − SCF-Kurve, „1 − 2*R* + 23/12R^2" = *R*-Entwicklung nach (32)

Dabei wird wieder dieselbe Basis von Huzinaga [9] wie bei der SCF-Rechnung für HeH$^+$ verwendet. Die zugehörige Kurve ist in Fig. 5 dargestellt und wird mit der unter (32) angegebenen *R*-Entwicklung des *DQ* verglichen.

4. Diskussion der Ergebnisse

Wie schon beim δ-Modell und bei Molekülen mit einem Elektron, so ersehen wir aus dem Vergleich von μ- und SCF-Kurve in Fig. 2 und Fig. 3, daß die μ-Theorie eine geeignete Methode zur Berechnung des *DQ* auch bei Molekülen mit zwei Elektronen ist, jedenfalls für kleine bis mittlere Kernabstände. Für diesen Bereich beschreibt die μ-Kurve das Verhalten des *DQ* nämlich relativ gut. Dagegen ist die λ-Theorie zur Berechnung des *DQ* offenbar wenig geeignet, denn die λ-Kurven (s. Fig. 2 und Fig. 3) haben selbst für kleine *R* völlig falsches Verhalten.

Auffallend ist noch, daß die μ-Theorie in erster Näherung des *DQ* etwas schlechtere Resultate liefert als in nullter Näherung (vgl. Fig. 2 und Fig. 3). Dies ist vermutlich auf die Einzentrigkeit der Basisentwicklung von ϕ_1 zurückzuführen und ist kein prinzipieller Defekt der μ-Theorie. Denn beim δ-Modell, wo ja ϕ_0 und ϕ_1 exakt bestimmt werden können (vgl. I), ist der *DQ* in erster Näherung besser als in nullter Näherung, wie es sein sollte (vgl. I, Fig. 6 und Fig. 7).

Für den *DQ* von HeH steht uns keine Vergleichsrechnung zur Verfügung; wir wollen aber dennoch annehmen, daß die oben diskutierten Eigenschaften der μ-Theorie auch hier gelten und die Kurve der μ-Theorie nullter Näherung also das richtige Verhalten für kleine R besitzt.

Als wesentliche Aussage entnehmen wir sodann den μ-Kurven der Figuren 1-4, daß sich der *DQ* für die Moleküle HeH^{2+}, HeH^{+} und HeH für kleine R wie

$$\varrho_\mathrm{B}/\varrho_\mathrm{A} = 1 - 2R + 0(R^2) \tag{19}$$

verhält, was an den jeweils mit eingezeichneten R-Entwicklungen abzulesen ist. Die Gl. (19) ist ein Spezialfall der allgemeineren – für Einelektronenmoleküle unter (13) bereits bewiesenen – Gleichung

$$\varrho_\mathrm{B}/\varrho_\mathrm{A} = 1 - 2(Z_\mathrm{A} - Z_\mathrm{B})R + 0(R^2) \tag{20}$$

In dieser Beziehung drückt sich für hinreichend kleine Kernabstände R die Tatsache aus, daß die Elektronendichte am Kern A, also am Kern mit der größeren Ladung, größer ist als am Kern B. Unsere Vermutung aus I Gl. (5), die wir dort durch die Ungleichung $\varrho_\mathrm{B}/\varrho_\mathrm{A} < 1$ formuliert haben, finden wir damit bestätigt.

5. Die *R*-Entwicklung des *DQ* bei Mehrelektronenmolekülen

Nachdem wir an Hand numerischer Rechnungen gesehen haben, daß für den *DQ* eine R-Entwicklung der Form (20) besteht, wollen wir diese Entwicklung nun durch *analytische* Überlegungen begründen. Dazu verwenden wir die μ-Theorie in nullter Näherung, denn diese hat sich sowohl beim δ-Modell als auch bei Molekülen mit ein und zwei Elektronen als geeignet erwiesen.

Für den *DQ* gilt in der μ-Theorie nach (2b) in nullter Näherung

$$\left(\frac{\varrho_\mathrm{B}}{\varrho_\mathrm{A}}\right)_0 = \frac{\{\int |\Lambda\phi_0|^2\, ds_1\, d\tau_2 \dots d\tau_N\}_{\boldsymbol{r}_1=\boldsymbol{R}}}{\{\int |\Lambda\phi_0|^2\, ds_1\, d\tau_2 \dots d\tau_N\}_{\boldsymbol{r}_1=\boldsymbol{0}}}\,, \tag{21}$$

wobei ϕ_0 eine Lösung von (3a) ist, also eine Wellenfunktion des UA. Setzen wir den Operator $\Lambda = 1 - \lambda + \lambda q P$ [vgl. I, Gl. (21)] in (21) ein, so folgt mit der Abkürzung $d\tau' = ds_1\, d\tau_2 \dots d\tau_N$

$$(\varrho_\mathrm{B}/\varrho_\mathrm{A})_0 = \varrho_0(\boldsymbol{r}_1 = \boldsymbol{R})/\varrho_0(\boldsymbol{r}_1 = \boldsymbol{0})$$

mit

$$\begin{aligned}\varrho_0(\boldsymbol{r}_1) := (1-\lambda)^2 \int \phi_0\phi_0^*\, d\tau' + \lambda(1-\lambda)q \int [\phi_0 P\phi_0^* + \phi_0^* P\phi_0]\, d\tau' \\ + \lambda^2 \int P\phi_0(P\phi_0^*)\, d\tau'\,.\end{aligned} \tag{22}$$

Die UA-Funktion für Mehrelektronenmoleküle läßt sich jedoch nicht exakt bestimmen. Um die Rechnung dennoch in einfacher Weise fortführen zu können, vernachlässigen wir die elektronische Wechselwirkung im Operator H_0. Eine Rechtfertigung für dieses Vorgehen werden wir an späterer Stelle geben.

Mit der Vernachlässigung zerfällt der Operator H_0 des UA in eine Summe von Einteilchenoperatoren für wasserstoffähnliche Atome der Kernladung Z, also in eine Summe von Operatoren der Form (4). Wir können ϕ_0 daher als antisymmetrisiertes Produkt von wasserstoffähnlichen Spinorbitalen $\psi_1, \ldots, \psi_N$[4], also als Slaterdeterminante schreiben:

$$\phi_0 = |\psi_1 \ldots \psi_N| \tag{23}$$

mit

$$\psi_i = \varphi_i \begin{cases} \alpha, & \text{für } m_{si} = 1/2 \\ \beta, & \text{für } m_{si} = -1/2 \end{cases} (i = 1, \ldots, N).$$

Dabei sind $\varphi_1, \ldots, \varphi_N$[4] die wasserstoffähnlichen Ortsfunktionen. Bekanntlich sind diese orthonormiert; daher sind auch die Spinorbitale ψ_i orthonormiert, so daß die für das Rechnen mit Slaterdeterminanten bekannte Gleichung (vgl. z.B. Kotani [12], S. 49)

$$\int \phi_0 \phi_0^* d\tau' = \frac{1}{N} \sum_{i=1}^{N} \varphi_i(\boldsymbol{r}_1) \varphi_i^*(\boldsymbol{r}_1) \tag{24a}$$

gilt. Daraus folgt sofort durch Koordinatentranslation

$$\int (P\phi_0)(P\phi_0)^* d\tau' = \frac{1}{N} \sum_{i=1}^{N} \varphi_i(\boldsymbol{R} - \boldsymbol{r}_1) \varphi_i^*(\boldsymbol{R} - \boldsymbol{r}_1). \tag{24b}$$

Nicht so unmittelbar einzusehen ist die Gleichung (Beweis: [13])

$$\begin{aligned} &\int [\phi_0 P \phi_0^* + \phi_0^* P \phi_0] d\tau' \\ &= \frac{1}{N} \sum_{i=1}^{N} (-1)^{\sum_{j \neq i} l_j} [\varphi_i(\boldsymbol{r}_1) \varphi_i^*(\boldsymbol{R} - \boldsymbol{r}_1) + \varphi_i^*(\boldsymbol{r}_1) \varphi_i(\boldsymbol{R} - \boldsymbol{r}_1)] + cR + 0(R^2). \end{aligned} \tag{24c}$$

Die Größen l_j $(j = 1, \ldots, N)$ in (24c) sind die Bahndrehimpulsquantenzahlen der Orbitalfunktionen φ_j; c ist eine bezüglich R konstante Größe, die von N und dem Besetzungszustand der Slaterdeterminante abhängt, deren genaue Kenntnis sich jedoch erübrigt.

Setzen wir nun die Gl. (24a–c) und $\lambda = Z_b/Z$ in (22) ein, so läßt sich der *DQ* mit der Abkürzung

$$\begin{aligned} f_i(Z_A, Z_B, R) = Z_A^2 |\varphi_i(\boldsymbol{R})|^2 + Z_A Z_B q (-1)^{\sum_{j \neq i} l_j} [\varphi_i^*(0) \varphi_i(\boldsymbol{R}) + \varphi_i^*(\boldsymbol{R}) \varphi_i(0)] \\ + Z_B^2 |\varphi_i(0)|^2 \end{aligned} \tag{25}$$

in der Form

$$\left(\frac{\varrho_B}{\varrho_A}\right)_0 = \frac{(1/Z^2) \sum_{i=1}^{N} f_i(Z_A, Z_B, R) + cR + 0(R^2)}{(1/Z^2) \sum_{i=1}^{N} f_i(Z_B, Z_A, R) + cR + 0(R^2)} \tag{26}$$

schreiben. Wir suchen nun die R-Entwicklung dieses Ausdrucks. Dazu bilden wir zunächst die R-Entwicklung von $f_i(Z_A, Z_B, R)$:

---

[4] Die Indices $1, \ldots, N$ von ψ (bzw. φ) stehen dabei für die Quantenzahlen n_i, l_i, m_i und m_{si} $(i = 1, \ldots, N)$.

Statt der abgekürzten Schreibweise φ_i für die wasserstoffähnlichen Funktionen notieren wir nun ausführlicher $\varphi_{n_i l_i m_i}(r,\theta,\phi)$, wobei r,θ,ϕ Kugelkoordinaten mit dem UA als Zentrum sind. Wir denken sie uns so gewählt, daß $\theta = 0$ einem Punkt auf der Kernverbindungslinie entspricht. Daher gilt:

$$\varphi_i(0) = \varphi_{n_i l_i m_i}(0,0,\phi)\,,$$

$$\varphi_i(R) = \varphi_{n_i l_i m_i}(R,0,\phi)\,.$$

Aus der expliziten Form der wasserstoffähnlichen Funktionen (s. z. B. [4], S. 84) kann man leicht herleiten:

$$\varphi_{nlm}(0,0,\phi) = (Z^3/\pi n^3)^{1/2}\,\delta_{l0}\,\delta_{m0}\,, \tag{27a}$$

$$\varphi_{n0m}(R,0,\phi) = (Z^3/\pi n^3)^{1/2}\,[1 - ZR + 0(R^2)]\,\delta_{m0}\,, \tag{27b}$$

$$\varphi_{nlm}(R,0,\phi) = 0(R^l) \quad \text{für} \quad l \geqq 1\,. \tag{27c}$$

Setzen wir (27a–c) in (25) ein, wobei die Fälle $l = 0$ und $l \geqq 1$ gesondert betrachtet werden, so erhalten wir schließlich

$$\begin{aligned} f_i(Z_A, Z_B, R) = (Z^3/\pi n_i^3)\,\Big\{&[Z_A + q(-1)^{\sum_j l_j} Z_B]^2 \\ &- 2Z_A Z R[Z_A + q(-1)^{\sum_j l_j} Z_B]\Big\}\,\delta_{l_i 0} + 0(R^2)\,. \end{aligned} \tag{28}$$

Nun müssen wir uns noch überlegen, ob $q = +1$ oder $q = -1$ ist [q = Eigenwert von Q, vgl. I, Gl. (14), (15)]. In I hatten wir gesehen, daß q die elektronische Parität des UA-Zustandes ist. Nun gilt aber für die Slaterdeterminante ϕ_0 bei $R \to 0$ wegen der elektronischen Parität der Orbitalfunktionen φ_i:

$$Q\phi_0 = P\phi_0 = (-1)^{\sum_j l_j}\,\phi_0\,. \tag{29}$$

Die Parität des UA-Zustandes ϕ_0 ist also $q = (-1)^{\sum_j l_j}$, so daß aus (28) folgt (wegen $q^2 = 1$)

$$f_i(Z_A, Z_B, R) = (Z^3/\pi n_i^3)\,\{(Z_A + Z_B)^2 - 2Z_A Z R(Z_A + Z_B)\}\,\delta_{l_i 0} + 0(R^2)\,,$$

was mit $Z = Z_A + Z_B$ in

$$f_i(Z_A, Z_B, R) = (Z^5/\pi n_i^3)\,(1 - 2Z_A R)\,\delta_{l_i 0} + 0(R^2) \tag{30}$$

übergeht. Setzen wir (30) in (26) ein, so ergibt sich für den DQ

$$\left(\frac{\varrho_B}{\varrho_A}\right)_0 = \frac{(1 - 2Z_A R) \sum\limits_{i=1}^{N} (Z^3 \delta_{l_i 0}/\pi n_i^3) + cR + 0(R^2)}{(1 - 2Z_B R) \sum\limits_{i=1}^{N} (Z^3 \delta_{l_i 0}/\pi n_i^3) + cR + 0(R^2)}$$

und als R-Entwicklung dieses Ausdrucks schließlich

$$(\varrho_B/\varrho_A)_0 = 1 - 2(Z_A - Z_B)\,R + 0(R^2)\,. \tag{31}$$

Wie wir sehen, hängt der Koeffizient des in R linearen Gliedes überhaupt nicht von den Größen n_i, l_i, m_i und c ab; (31) gilt somit für beliebige Besetzung der Slaterdeterminante (23) mit wasserstoffähnlichen Funktionen. Zudem haben wir mit (31) genau die gleiche R-Entwicklung des DQ erhalten wie durch die numerischen Rechnungen [vgl. Gl. (20)].

Die Übereinstimmung der R-Entwicklungen, die wir durch die numerischen Rechnungen und die soeben durchgeführten Betrachtungen gefunden haben, ist gerade die Rechtfertigung dafür, daß die elektronische Wechselwirkung vernachlässigt werden darf. Bei der numerischen Berechnung des DQ für HeH^+ wurde die Wechselwirkung nämlich mit der NO-Entwicklung (16) in nullter und mit Gl. (17) in erster Näherung berücksichtigt. Das Resultat (20) ist jedoch das *gleiche* wie bei Vernachlässigung der Wechselwirkung [Gl. (31)].

Wir können die R-Entwicklung des DQ mittels μ-Theorie nullter Näherung auch bis zum in R quadratischen Glied ausführen. Dazu ist das Integral (24c) explizit zu lösen. Ohne auf die zahlreichen Einzelheiten der Integralberechnungen und der Reihenentwicklungen einzugehen, geben wir das Ergebnis für Moleküle mit zwei, drei und vier Elektronen [zum Vergleich auch für solche mit nur einem Elektron nach Gl. (13)] im Grundzustand an:

$$
\begin{aligned}
(\varrho_B/\varrho_A)_0 &= 1 - 2(Z_A - Z_B)R \\
&\quad + 2(Z_A - Z_B)\,R^2 \cdot \begin{cases} Z_A - Z_B & \text{für ein Elektron} \\ Z_A - Z_B & \text{für zwei Elektronen} \\ Z_A - Z_B - Z/136 & \text{für drei Elektronen} \\ Z_A - Z_B - Z/72 & \text{für vier Elektronen} \end{cases} \\
&\quad + 0(R^3).
\end{aligned}
\tag{32}
$$

Die zu (32) gehörigen Kurven sind, wie schon oben erwähnt, in Fig. 1–5 jeweils für $Z_A = 2$, $Z_B = 1$ mit eingetragen. Vergleichen wir die Kurven von Fig. 2–5 untereinander, so stellen wir folgendes fest:

1) Die Kurve, die zur Gl. (32) für Moleküle mit zwei Elektronen gehört, verhält sich für kleine Kernabstände wie die unter Berücksichtigung der Wechselwirkung durch numerische Rechnungen gewonnenen Kurven der μ-Theorie nullter und erster Näherung (s. Fig. 2 und Fig. 3). Wir dürfen deshalb die Vernachlässigung der Wechselwirkung auch bei der Ableitung der Gl. (32) als gerechtfertigt betrachten.

2) Die zur R-Entwicklung für Moleküle mit vier Elektronen gehörige Kurve verhält sich für kleine Kernabstände annähernd wie die zum Vergleich eingezeichnete SCF-Kurve (s. Fig. 5).

Diese Tatsachen bestärken uns im Vertrauen auf die Zuverlässigkeit der Gl. (32). Außerdem scheint sich nun auch für Moleküle mit mehreren Elektronen zu bestätigen, daß man mit der μ-Theorie die richtige Entwicklung des DQ einschließich des in R quadratischen Gliedes erhält, wenn man *nur die* UA-*Funktion* ϕ_0 kennt. Dieser Sachverhalt ist uns bereits vom δ-Modell und von Einelektronenmolekülen her geläufig.

Ein wesentliches Resultat dieser Arbeit wollen wir nun aber noch besonders hervorheben:

Der Koeffizient des in R linearen Gliedes bei der Entwicklung des DQ nach dem Kernabstand, nämlich $-2(Z_A - Z_B)$ ist – jedenfalls im Rahmen der hier gemachten Näherungen (d.h. Vernachlässigung der Wechselwirkung und der ausschließlichen Verwendung der UA-Funktion zur Berechnung des DQ) – eine *universelle* Größe für alle zweiatomigen Moleküle [s. Gl. (31), (32)]. Dagegen hängen die Koeffizienten der höheren Potenzen von R vom speziellen Molekül und von seinem Anregungszustand ab.

6. Reihenentwicklung des DQ für große Kernabstände

Die bisher diskutierten R-Reihenentwicklungen des DQ können das Verhalten des DQ ihrer Natur nach nur für *kleine* R beschreiben. Um eine gute Beschreibung auch für *große* R zu erhalten, hat man nach einer geeigneten Funktion von R zu entwickeln.

So entwickelt z.B. Robinson [11] den in I diskutierten Energieparameter c_q des δ-Modells nach Potenzen von $\exp(-2Z_A R)$:

$$\begin{aligned} c_{+1} = {} & Z_A + [Z_A Z_B/(Z_A - Z_B)]\, e^{-2Z_A R} \\ & - [2R + 1/(Z_A - Z_B)]\,[Z_A Z_B/(Z_A - Z_B)]^2\, e^{-4Z_A R} \\ & + 0(e^{-6Z_A R}). \end{aligned}$$

Mit Gl. (40) von I folgt hieraus für den DQ

$$\begin{aligned} \frac{\varrho_B}{\varrho_A} = {} & \frac{Z_A^2}{(Z_A - Z_B)^2}\, e^{-2Z_A R} \left\{ 1 - 2\left(R + \frac{1}{Z_A - Z_B}\right) \frac{Z_A Z_B}{Z_A - Z_B}\, e^{-2Z_A R} \right. \\ & \left. + 0(e^{-4Z_A R}) \right\}. \end{aligned} \tag{33}$$

Es wäre zu untersuchen, ob sich für den DQ von Molekülen auch eine Entwicklung nach $\exp(-2Z_A R)$ finden läßt. Möglicherweise ergibt sich dafür eine *van der Waals-Entwicklung*, also eine solche nach Potenzen von $1/R$. Wir können jedoch darüber an dieser Stelle noch keine fundierten Aussagen machen.

Diese Arbeit wurde unterstützt aus Mitteln der Deutschen Forschungsgemeinschaft im Rahmen des Schwerpunktprogramms „Theoretische Chemie“.

Wir danken Herrn V. Dyczmons, der uns freundlicherweise das bei den numerischen Rechnungen benötigte SCF- und NO-Programm zur Verfügung stellte.

Alle numerischen Rechnungen wurden auf der Anlage UNIVAC 1108 der „Gesellschaft für wissenschaftliche Datenverarbeitung mbH Göttingen“ durchgeführt.

Literatur

1. Bingel, W.A., Klahn, B.: Theoret. chim. Acta (Berl.) **28**, 37 (1972).
2. Byers-Brown, W., Power, J.D.: Proc. Royal Soc. (London) **A317**, 545 (1970).
3. Bates, D.R., Carson, T.R.: Proc. Royal Soc. (London) **A234**, 207 (1956).
4. Eyring, H., Walter, J., Kimball, G.E.: Quantum Chemistry. New York: John Wiley & Sons, Inc., 1965.
5. Power, J.D.: Perturbation theory of short range atomic interactions. Theoretical Chemistry Institute, The University of Wisconsin, WIS-TCI-311 (1968).

6. Löwdin, P. O.: Physic. Rev. **97**, 1474 (1955).
7. Kutzelnigg, W.: Theoret. chim. Acta (Berl.) **1**, 327 (1963).
8. Huzinaga, S., Sakai, Y.: J. Chem. Physics **50**, 1371 (1969).
9. Huzinaga, S.: J. Chem. Physics **42**, 1293 (1965).
10. Clementi, E.: Tables of atomic functions, IBM J. Res. Devel. **9**, 2 (1965).
11. Robinson, P. D.: Proc. Physic. Soc. **78**, 537 (1961).
12. Kotani, M., Ohno, K., Kayama, K.: Handbuch der Physik 37/2 (1961).
13. Klahn, B.: Diplomarbeit, Lehrstuhl für Theoretische Chemie Göttingen (1972).

Prof. Dr. W. A. Bingel
Lehrstuhl für Theoretische Chemie
der Universität Göttingen
D-3400 Göttingen
Bürgerstr. 50a
Bundesrepublik Deutschland

Theoret. chim. Acta (Berl.) 28, 67—74 (1972)
© by Springer-Verlag 1972

SCF MO LCGO Studies on Hydrogen Bonding: The System $NH_3 \cdot H_2O$

Geerd H. F. Diercksen, Wolfgang P. Kraemer, and W. von Niessen
Max-Planck-Institut für Physik und Astrophysik, 8000 München 40, Germany

Received July 4, 1972

The energy hypersurface of the system $NH_3 \cdot H_2O$ is investigated for a number of different internuclear geometries. In the minimum energy structure involving a linear hydrogen bond, NH_3 acts as proton acceptor. The binding energy of the system is calculated to be 6.28 kcal/mole and the bond distance d(NO) to be 3.07 Å. The potential energy curve of the inversion of the hydrogenbonded NH_3 is computed and discussed.

Die Energiehyperflächen des $NH_3 \cdot H_2O$-Systems wurden für eine Anzahl von verschiedenen geometrischen Anordnungen untersucht. Im Falle der Struktur minimaler Energie wird eine lineare Wasserstoffbindung gebildet, NH_3 wirkt als Protonakzeptor. Die Berechnungen ergeben eine Bindungsenergie des Systems von 6,28 kcal/Mol und einen NO-Abstand von 3,07 Å. Außerdem wurde die Potentialkurve für die Inversion des über eine Wasserstoffbrücke gebundenen NH_3 berechnet und diskutiert.

The object of the present investigation is to study hydrogen bonding in the mixed ammonia-water dimer using an extended gaussian basis set, especially to get some information on the interaction in ammonia-water systems. It is well known from chemistry that ammonia is a stronger base (proton acceptor) than water. Therefore it is of particular interest to analyze the relative proton donor/acceptor strengths of the two molecular fragments in the hydrogen bonded system. No experimental results are available so far on the equilibrium geometry and on the hydrogen bonding energy of the mixed dimer and both semiempirical [1] and *ab initio* investigations [2] have been performed only recently. On the other hand, the inversion barrier of a single ammonia has been studied quite extensively experimentally [3] as well as theoretically [4]. As will be shown the ammonia-water dimer is relatively stable and it might well be possible to observe it in the vapour phase. In this connection it is of some interest to study the potential energy curve of the NH_3– inversion in the most stable geometrical structure of the system $NH_3 \cdot H_2O$.

The SCF wavefunctions and energies have been calculated using Roothaan's SCF MO LCGO method [5]. The calculations are carried out on an IBM 360/91 computer using the program system IBMOL/VERSION IV [6], modified by one of the authors (G.D.) [7], and by a test release of the program system MUNICH [8]. The molecular orbitals are expanded in a set of gaussian orbitals

$$\eta = x^l y^m z^n \exp(-\alpha r^2)$$

(unnormalized) which are contracted to reduce the number of linear parameters. The basis sets used in the present calculations consist of (11.7.1)-functions at the nitrogen and oxygen atoms, contracted to {5.4.1}-functions, and of (6.1)-functions at each hydrogen atom, contracted to {3.1}-functions [14]. The exponents α and the contraction coefficients are taken from the literature [9]. The exponents of the d-type polarization functions at the nitrogen and at the oxygen atom, and of the p-type polarization functions at the hydrogen atoms have been optimized by SCF-calculations on ammonia and water, resp., ($\alpha(d_N) = 0.75$, $\alpha(d_O) = 1.00$, $\alpha(p_H) = 0.75$).

The results obtained for the two subsystems ammonia and water using the basis sets described above are in good agreement with those of other extended basis set calculations [10, 4]. The data for the water molecule have been reported previously [11]. For the ammonia molecule in its experimental geometry (d(NH) = 1.91054 a.u., $\sphericalangle$ (HNH) = 106.7° [12]) the total SCF energy is computed to be $E^{SCF}(NH_3) = -56.21220$ a.u. The corresponding values for the theoretical equilibrium geometry are calculated to be (using a parabola approximation around the experimental geometry values with the increments $\Delta d = 0.1$ a.u., and $\Delta \sphericalangle = 5°$): d(NH) = 1.90 a.u., $\sphericalangle$ (HNH) = 107.2°, and $E^{SCF}(NH_3) = -56.21230$ a.u. For the planar geometry of ammonia ($\sphericalangle$ (HNH) = 120°) the total energy has been computed to be $E^{SCF}(NH_3) = -56.20279$ a.u. for a bond length of d(NH) = 1.91054 (exp. pyramidal), and to be $E^{SCF}(NH_3) = -56.20420$ a.u. for the theoretical equilibrium bond length of d(NH) = 1.87 a.u. (parabola approximation). From the SCF energies of the two theoretically determined equilibrium structures the height of the inversion barrier in the ammonia molecule is computed to be $E = 5.08$ kcal/mole [7]. From experimental measurements this energy barrier was found to be 5.81 kcal/mole [3]. In the most accurate single determinant SCF MO study on the NH_3 molecule reported so far [4], in which a more extended gaussian basis set has been used, the following geometrical parameters for the pyramidal structure have been obtained: d(NH) = 1.890 a.u. $\sphericalangle$ (HNH) = 107.2° giving an SCF energy of $E^{SCF}(NH_3)_{pyr} = -56.22191$ a.u., while for the planar structure with d(NH) = 1.860 a.u. an SCF energy of $E^{SCF}(NH_3)_{plan} = -56.21382$ a.u. has been calculated. The height of the NH_3-inversion barrier deduced from these energy values was found to be 5.08 kcal/mole, in agreement mit the theoretical value given above.

By a comparison of the results obtained for the monomers, H_2O and NH_3, with the corresponding experimental data it may be concluded that the basis set used in the present investigation provides a sufficient flexibility to calculate the equilibrium geometries and inversion barriers to a satisfactory accuracy also for the mixed dimer system.

The investigations have been restricted to two structures, both with linear hydrogen bonds between the molecular fragments NH_3 and H_2O, which are best characterized by their proton acceptor/donor properties: In structure A the NH_3 molecule acts as a proton acceptor and the H_2O molecule as a proton donor and in structure B the opposite is the case. The different geometrical configurations within the two main structures A and B of the mixed dimer discussed here will be described as follows: In all the three configurations A1, A2, A3 derived from structure A (Fig. 1) the nuclei H ... N ... H ... O ... H define a symmetry plane of the system, with the H-atoms at the two ends in "*trans*"-position. While the water molecule is always considered in its experimental geometry, the configurations A1, A2, and A3 differ in the various arrangements assumed for the NH_3

molecule: in structure A1 the ammonia molecule is treated in its experimental geometry, too, with the H-atoms pointing away from the water molecule. In structure A2, the ammonia molecule is considered in its planar geometry and the theoretical value is used for the bond distance d(NH), and finally in structure A3, the ammonia molecule is again treated in its experimental geometry, but this time with the H-atoms facing the water molecule. For the three geometries A1, A2, and A3 the bond distance d(NO) has been varied over a wide range.

In addition, geometrical configurations of structure A have been studied with intermediate angles ∢ (HNH). For all these angles the bond length d(NH) used is determined by linear interpolation between the values of the experimental pyramidal and the theoretical planar geometry of the ammonia molecule. For each angle two internuclear separations d(NO) have been studied: The minimum energy value d(NO) of structure A1, and a value determined by linear interpolation from the minimum energy values d(NO) of structures A1, A2, and A3, respectively. Similarly in the two geometrical configurations B1 and B2 derived from structure B (Fig. 2) the nuclei N ... H ... O ... H define the symmetry plane of the mixed

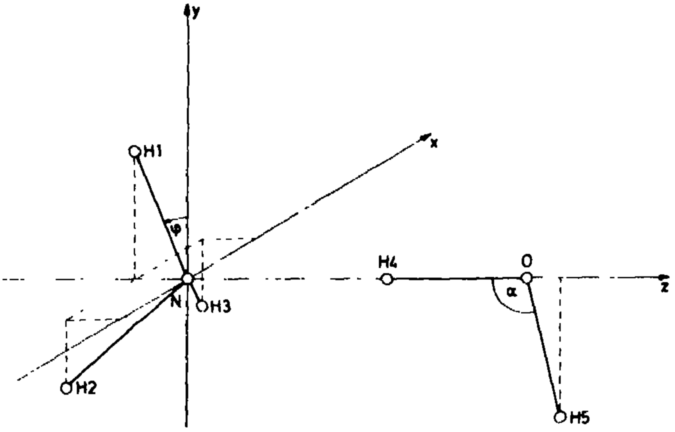

Fig. 1. Coordinate system for H_3N-HOH with NH_3 acting as proton acceptor (structure A)

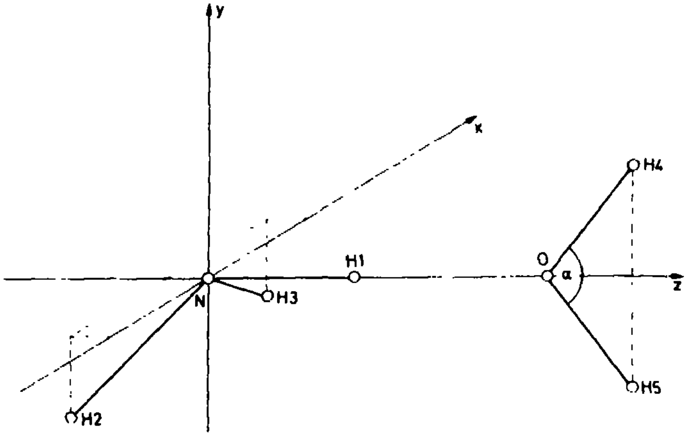

Fig. 2. Coordinate system for H_2NH-OH_2 with NH_3 acting as proton donor (structure B)

dimer, and in addition the hydrogen atoms not involved in hydrogen bonding and the associated nitrogen- and oxygen atom define two planes which are perpendicular to each other. In structure B1 the two subsystems ammonia and water are treated in their experimental geometry, while in structure B2 the ammonia molecule is considered in its planar geometry and the theoretical value

Table 1 Total SCF energies for the system NH_3 H_2O in different geometrical configurations (A) and (B)

	d(NO)	d(NH)	φ	E^{SCF}
Configuration (A), Fig. 1				
1(A1)	10.0	1.910537	22.13	−132.26587
2	8.0			−132.26837
3	6.5			−132.27264
4	6.0			−132.27397
5	5.75			−132.27418
6	5.5			−132.27372
7	5.0			−132.26863
8	4.5			−132.25061
9(A2)	6.75	1.87	0	−132.26134
10	6.25			−132.26210
11	5.75			132.26166
12	5.25			−132.25772
13(A3)	10.0	1.910537	−22.13	−132.26383
14	8.5			−132.26413
15	7.75			−132.26442
16	7.25			−132.26456
17	6.75			−132.26444
18	6.5			−132.26412
19	6.25			−132.26346
20	5.75			−132.26031
21	5.847	1.901378	17.13	−132.27300
22	6.083	1.87916	5	−132.26440
23	5.75			−132.26421
24	6.422		−5	132.26154
25	5.75			−132.26067
26	6.664	1.88832	−10	−132.26257
27	5.75			−132.26104
28	7.008	1.901378	17.13	−132.26468
29	5.75			−132.26182
30	7.492	1.919696	−27.13	−132.26097
Configuration (B), Fig. 2				
1(B1)	10.0	1.910537	–	−132.26505
2	8.0			−132.26616
3	6.75			−132.26756
4	6.25			−132.26788
5	6.0			−132.26767
6	5.0			−132.25673
7(B2)	6.5	1.87	–	−132.25970
8	6.25			−132.25991
9	6.0			−132.25990
10	5.75			−132.25948

All values in atomic units.

Table 2. Binding energies and equilibrium distances of some neutral hydrogen bonded molecules calculated using an [11s7p1d/6s1p] basis set

System	d(AB) [a.u.]	Binding energy [kcal/mole]	
H_3N HOH (A1)	5.797	6.28	
H_3N-HOH (A2) (NH_3 planar)	6.183	3.72[a]	
NH_3-HOH (A3) (NH_3 inverted pyramid)	7.23	0.23	
H_2NH-OH_2 (B1)	6.34	2.33	
H_2NH-OH_2 (B2) (NH_3 planar)	6.14	2.35[a]	
H_2O-HOH	5.67	4.83	[10]
HF-HF	5.50	4.5	[13]

[a] The binding energy refers to a water molecule in its experimental geometry and a *planar* NH_3 molecule at infinite separation.

has been used for the bond distance d(NH). For both structures B1 and B2 the variation of the bond length d(NO) has been studied over a wide range.

The total SCF-energies for all points on the hypersurface investigated are listed in Table 1. The binding energies for the more important structures of the mixed dimer $NH_3 \cdot H_2O$ and for some homomolecular dimers are compiled in Table 2. The potential energy curves for the variation of the distance d(NO) are displayed in Fig. 3 for the five structures described above.

It has been found by these investigations, that the three structures A1, B1, and A3 of the mixed dimer $NH_3 \cdot H_2O$ are all stable against dissociation into the molecular fragments NH_3 and H_2O. The minimum energy geometry is determined to be structure A1, with the ammonia molecule acting as the proton acceptor. The hydrogen bond energy (dimerisation energy) of this structure has been calculated to be $B = 6.28$ kcal/mol and the associated intersystem separation is computed to be $d(\mathrm{NO}) = 5.78$ a.u. Both values may be compared to those found in an earlier investigation using a somewhat smaller basis set: $B = 5.8$ kcal/mole, $d(\mathrm{NO}) = 5.896$ a.u. [2]. As it was expected from chemical experience, the structure B1 with the water molecule as the proton acceptor is less stable than A1. The binding energy obtained in this case is only about $B = 2.32$ kcal/mole (intersystem separation approximately $d(\mathrm{NO}) = 6.25$ a.u. ~ 3.31 Å). The corresponding results reported in the literature [2] are: $B = 2.3$ kcal/mole and $d(\mathrm{NO}) = 3.41$ Å.

For the homomolecular dimers of the constituting subsystems NH_3 and H_2O the following dimerisation energies have been computed: $B((H_2O)_2) = 4.83$ kcal/mole [10], and $B((NH_3)_2) = 2.71$ kcal/mole [2] (which might be slightly less accurate being calculated with a somewhat smaller basis set). From a comparison of these values it is concluded that in ammonia–water systems, mixed dimers of structure A1 or possibly higher mixed polymers should be predominant because of their greater hydrogen bonding energy compared to the homomolecular polymers. This would at least be expected to be true for water ammonia mixtures in the gas phase, where only smaller clusters occur as a result of the high thermal energy. The situation in solutions is apparently much more complex and no predictions can be made at the present stage for that case.

It can be seen from Fig. 3 that for equivalent geometries (pyramidal or planar) of the ammonia molecule the total energy of the mixed dimer is lower for structure

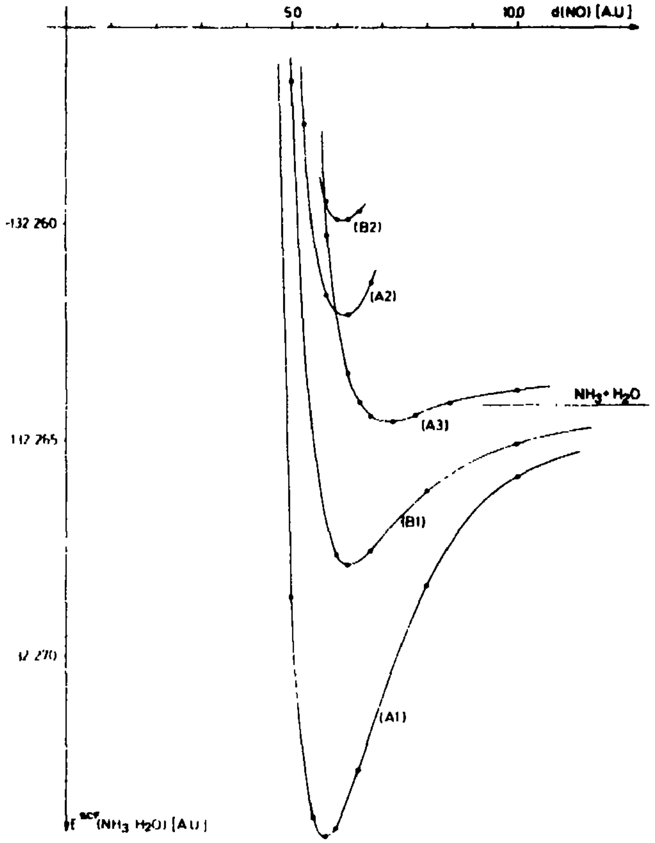

Fig. 3. Energy curves for a variation of the intersystem distance *d*(NO) for different structures of $NH_3 \cdot H_2O$; (A1): H_3N-HOH; (A2): H_3N HOH (NH_3 planar); (A3): NH_3 HOH (NH_3 inverted pyramid; (B1) H_2NH OH_2, (B2): H_2NH-OH_2 (NH_3 planar)

A than for structure B for all intersystem separations *d*(NO) investigated. This is well in accordance with the general chemical experience that ammonia is a stronger proton acceptor (base) than water. This result is supported by SCF-calculations on the protonated water and ammonia molecules: OH_3^+ and NH_4^+. The corresponding binding energies of the added proton are found to be quite different: $B(H_3O^+) = 173.05$ kcal/mole, $B(NH_4^+) = 215.84$ kcal/mole.

The potential energy curve of structure A3 is analyzed in some more detail: In this geometrical arrangement both subsystems ammonia and water are acting simultaniously as proton acceptor and donor. Because four hydrogen nuclei are "crowded" in a rather small region of space in this structure it was expected that the repulsion between the four hydrogen atoms might lead to an overall repulsion of the two subsystems for all intersystem separations *d*(NO). Therefore it was somewhat surprising to find that in a small region about an intersystem separation of *d*(NO = 7.23 a.u. the mixed dimer can stabilize even in this structure although with the rather small dimerisation energy of 0.23 kcal/mole. This result will change

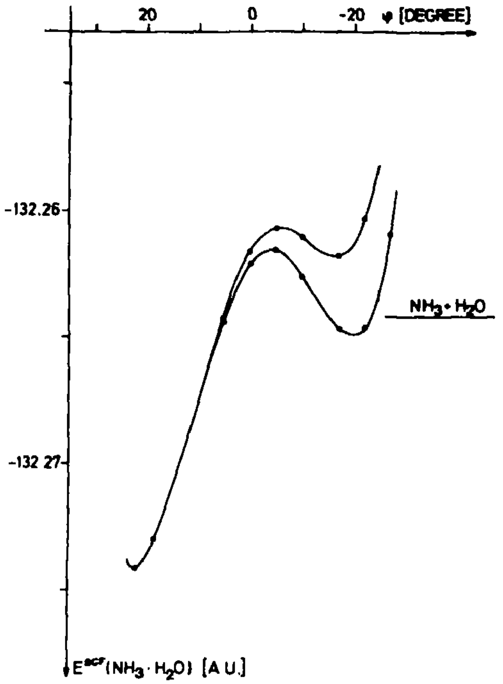

Fig. 4. Energy curve for the ammonia inversion (variation of the angle ∢ (HNH)) in structure A; upper curve d(NO) constant; lower curve d(NO) linearly interpolated

quantitatively if correlation energy is taken into account, but it is expected to be qualitatively correct because a rather flexible basis set is employed in the present calculations.

Two potential energy curves have been calculated for the inversion of a hydrogen bonded ammonia in the dimer $NH_3 \cdot H_2O$ in structure A and are shown in Fig. 4. The upper curve is calculated with a fixed NO-distance taken from the most stable structure A1 ($d(\mathrm{NO}) = 5.75$ a.u.), and the lower curve is calculated with (linearly) interpolated NO-distances, as described above. Unsymmetrical double minimum potentials have been obtained for this inversion. Both energy barriers are well above the energy of the infinitely separated subsystems by 2.2 kcal/mole and 1.6 kcal/mole, respectively. The same is true for the upper minimum of the upper energy curve which is unstable against a dissociation into the subsystems by 1.5 kcal/mole. Only the upper minimum of the lower potential energy curve seems to be stable against a dissociation into the subsystems with a very small binding energy of about $B = 0.4$ kcal/mole. The height of the barrier of the two potential energy curves with respect to the two minima has been calculated to be: 8.5 kcal/mole and 0.7 kcal/mole for the upper curve, and 7.9 kcal/mole and 2.0 kcal/mole for the lower curve, respectively. As a result of the perturbation caused by the attached water molecule and the resulting charge shift produced by the hydrogen bond formation it is not the geometrical configuration A2 (with a planar NH_3 fragment and $\varphi = 0$) which represents the maximum point of the inversion barrier. As can be seen in Fig. 4 both maxima are slightly shifted to negative φ-values (for a definition of φ see Fig. 1).

The experimental curve for the inversion is expected to be somewhat between the potential energy curves discussed above. Because of the high frequency of the inversion compared to the vibration of the two subsystems relative to each other, it is expected that the experimental curve is nearer to the upper theoretical curve. From the present results, without a more quantitative investigation of the individual vibrations, no definite prediction can be made on whether an inversion of a hydrogenbonded ammonia should be observable, or whether such an inversion leads instantly to a dissociation into the subsystems.

It is a pleasure to thank our technical staff for the careful preparation of the input for the programs and for its skillful assistance in running the computer.

References

1. Kollman, P. A., Allen, L. C.: J. Amer. chem. Soc. **92**, 753 (1970).
2. Kollman, P. A., Allen, L. C.: J. Amer. chem. Soc. **93**, 4991 (1971).
3. Swalen, J. D., Ibers, J. A.: J. chem. Physics **36**, 1914 (1962) (see this work for further references).
4. Rauk, A., Allen, L. C., Clementi, E.: J. chem. Physics **52** 4133 (1970) (see this work for further references)
5. Roothaan, C. C. J.: Rev. mod. Physics **23**, 69 (1951)
6. Veillard, A.: IBMOL/VERSION IV, Special IBM Technical Rept. San José, California: 1968.
7. Preuss, H., Diercksen, G.: Int. J. quant. Chemistry **1**, 605 (1967).
8. Diercksen, G. H. F., Kraemer, W. P.: MUNICH, Molecular Program System, Reference Manual, Special Technical Report. Max-Planck-Institut fur Physik und Astrophysik, München (to be published).
9. Salez, C., Veillard, A.: Theoret. chim. Acta (Berl.) **11**, 441 (1968).
10. Neuman, D., Moskowitz, J. W.: J. chem. Physics **49**, 2056 (1968)
11. Diercksen, G. H. F.: Chem. Physics Letters **4**, 373 (1969); Theoret. chim. Acta (Berl.) **21**, 335 (1971).
12. Diercksen, G. H. F. *et al.*: unpublished results.
13. Diercksen, G. H. F., Kraemer, W. P.: Chem. Physics Letters **6**, 419 (1970).
14. For a definition of the basis set notation used here, see: Moskowitz, J. W., Harrison, M. C.: J. chem. Physics **43**, 3550 (1965).

G. H. F. Diercksen
Max-Planck-Institut für Physik und Astrophysik
D-8000 München 40
Föhringer Ring 6
Federal Republic of Germany

Theoret. chim. Acta (Berl.) 28, 75–80 (1972)
© by Springer-Verlag 1972

Electronic Structures of Some Olefins and Their Radical Cations*

P. A. Clark**

Department of Chemistry, Vassar College, Poughkeepsie, New York and
Physikalisch-Chemisches Institut der Universität, CH-4056 Basel

Received April 17, 1972/August 17, 1972

CNDO/2 calculations of the electronic properties of the series of isomeric butenes and pentenes yield ionization potentials which reproduce the observed trends. These are interpreted in terms of the charge distribution effects of the alkyl groups.

CNDO/2 Rechnungen für die Butan- und Penten-Isomeren ergeben die richtigen Trends für die Ionisierungspotentiale. Sie werden im Zusammenhang mit der Änderung der Ladungsverteilung infolge Methylsubstitution diskutiert.

Des calculs CNDO/2 des propriétés électroniques des séries d'isomères du butène et du pentène fournissent des potentiels d'ionisation qui reproduisent les tendances observées. Les distributions de charge calculées pour les molécules sont utilisées pour interpréter les propriétés observées en termes d'effet du substituant alkyle.

Introduction

CNDO/2 calculations [1] have been carried out on the series of isomeric butenes and pentenes and their radical cations in order to investigate theoretically the effects of molecular structure on the electronic properties of these molecules. Semi-empirical calculations have been reported previously on the methyl-substituted ethylenes [2–4] but a study of the effects of larger alkyl groups on the olefinic properties had not been included. That the size of the alkyl group may itself be the determining influence on molecular properties has been demonstrated in the photoelectron spectra of alkyl halides [5] and the gas-phase acidities of alcohols and amines [6].

The present calculations use the parametrization of Pople and Segal [1] since these parameters have been chosen to yield charge distributions comparable to those of *ab initio* calculations and have been shown to reliably predict charge distribution effects in a wide variety of molecules [4]. The geometries used assume that all carbon atoms lie in a plane, with the exception of the iso-propyl group in 3-methyl-1-butene. Bond lengths and angles are as follows: $d(C=C = 1.33\,A$; $d(C-C) = 1.54\,A$; $d(C-H) = 1.10\,A$; olefins bond angles $= 120^\circ 54'$.

---

* Presented in part at the Eighth Theoretical Chemistry Symposium held at the Batelle Institute, Geneva, Switzerland; March 26–30, 1972.

** Inquiries should be adressed to the author at Vassar College.

Results and Discussion

Table 1 gives the calculated ionization potentials according to Koopmanns' theorem and also as the difference in total energies of the parent olefin and the radical cation, $\Delta E(M, M^+)$. Since the geometry is held fixed upon ionization, both values refer to the vertical IP. The experimental IP's are adiabatic photoionization values and would be expected to be different, generally, from the vertical ones (but see [7]); however, the trends observed upon alkyl substitution would probably not be affected, and the IP's calculated here correlate very well with the observed ones, as shown in Fig. 1.

Net charges for the olefins in their ground configurations are summarized in Table 1. The net π-electronic charge, $q^{\pi}_{C=C}$, is summed over the two doubly-bonded carbon atoms, as is the net total olefinic electronic charge, $q^{\text{total}}_{C=C}$. Σq_{alkyl} represents the sum over the net total charges of the alkyl groups. (Detailed net charges for some representative molecules are given in Fig. 2). Although $q^{\pi}_{C=C}$ becomes more negative as the number of alkyl groups increases, thus paralleling the decrease in IP as a function of the number of substituents, $q^{\pi}_{C=C}$ becomes less negative as the size of the alkyl group increase and thus cannot account for the decreasing IP as a function of substituent size. Conversely $q^{\text{total}}_{C=C}$ becomes more negative as the size of the alkyl group becomes larger, but becomes increasingly more positive as the number of alkyl substituents increases, and therefore also fails to account for the trends in IP.

The sum over the changes in the net charge of the alkyl groups upon ionization, $\Sigma \Delta q_{\text{alkyl}}$, is given for each olefin in Table 1 and is plotted versus observed IP in

Table 1. Ionization potentials, net charges, and change in net charges upon ionization.

	Ionization potential (eV)			Ground configuration			$\Sigma \Delta q_{\text{alkyl}}$
lefin	Koopmanns	$\Delta E(M, M^+)$	Exp.[a]	q^{π}_{C-C}	q^{total}_{C-C}	Σq_{alkyl}	on Ionizat
hylene	16.18	15.30	10.52	0.0000	−0.0530	–	–
opene	14.42	13.58	9.73	−0.0133	−0.0313	+0.0095	+0.2996
Butene	14.08	13.32	9.58	−0.0124	−0.0348	+0.0140	+0.3837
2-Butene	13.35	12.53	9.13	−0.0256	−0.0094	+0.0098	+0.4600
ins 2-Butene	13.24	12.32	9.13	−0.0226	−0.0102	−0.0008	+0.4928
Me Propene	13.57	12.51	9.23	−0.0270	−0.0168	+0.0124	+0.4482
Pentene	14.15	13.28	9.50	−0.0119	−0.0394	+0.0228	+0.3784
Me-1-Butene	14.07	13.18	9.51	−0.0259	−0.0428	+0.0214	+0.3896
Me-1-Butene	13.37	12.35	9.12	−0.0232	−0.0206	+0.0269	+0.4776
2-Pentene	13.21	12.39	9.11	−0.0250	−0.0132	+0.0170	+0.4903
ins 2-Pentene	13.10	12.18	9.06	−0.0219	−0.0139	+0.0031	+0.4928
Me-2-Butene	12.57	11.60	8.68	−0.0354	+0.0048	−0.0035	+0.5901
3-DiMe-2-Butene	11.95	10.93	8.30	−0.0442	+0.0202	−0.0200	+0.6836

[a] Bralsford, R., Harris, P. V., Price, W. C., Proc. Roy. Soc. (London) A **258**, 459 (1960); and Watanabe, K., Nakayama, T., Mottl, J.: J. Quant. Spectrsc. Radiat. Transfer **2**, 369 (1962); as quoted in Franklin, J. L. *et al.*: Ionization potentials, appearance potentials, and heats of formation of gaseous positive ions U. S. National Bureau of Standards 1969.

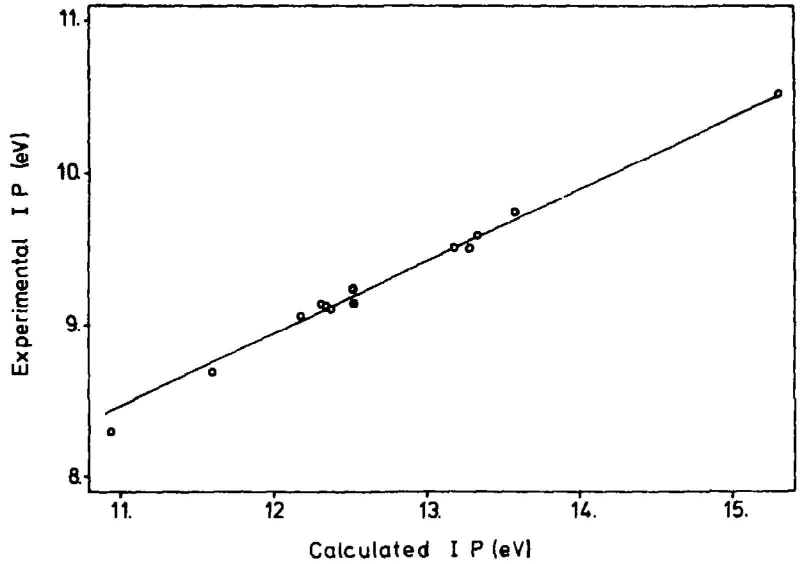

Fig. 1. Correlation between experimental and calculated ionization potentials, in electron volts

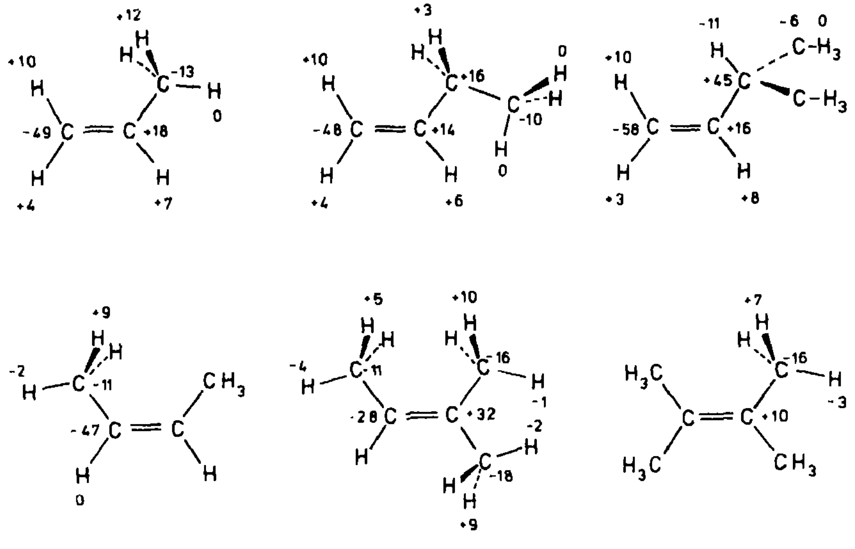

Fig. 2. Net charge densities, in units of 10^3 *e* , in (top:) propene, 1-butene, and 3-methyl-1-butene, (bottom:) *cis* 2-butene, 2-methyl-2-butene, and 2, 3-dimethyl-2-butene

Fig. 2. This shows the good, but not quite linear, correlation obtained between the decrease in the observed IP and the increase in $\Sigma\Delta q_{\text{alkyl}}$ upon ionization, which depends upon (1) the increase in the size of the alkyl substituent and (2) the increase in the number of alkyl substituents.

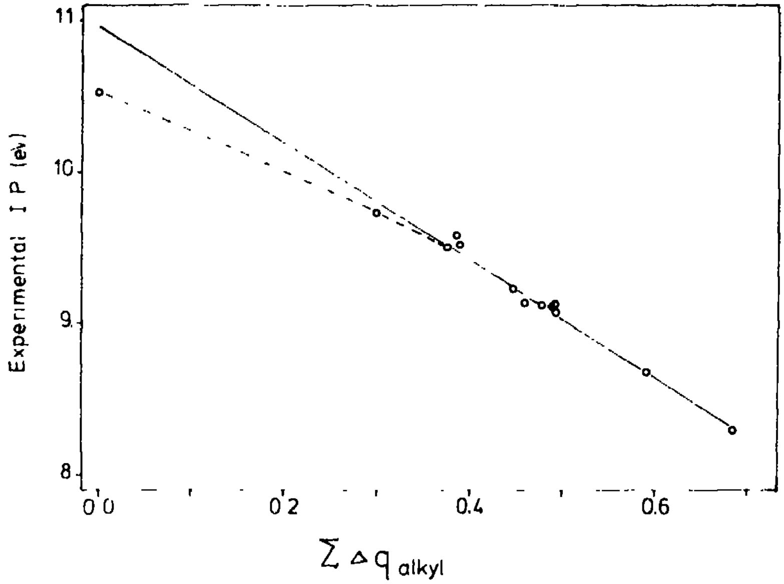

Fig. 3. Correlation between observed ionization potential (eV) and the change in the alkyl group charge density, $\Sigma \Delta q_{alkyl}$, upon ionization

Thus the observed trends in ionization potentials in these olefins may be explained on the basis of the relative ability of the alkyl substituents to donate charge to the positive hole left by the ionized electron, this ability increasing with size or complexity and also with number of alkyl groups. In discussing the effects of alkyl substituents on the gas-phase acidities of alcohols and amines and on the gas-phase basicities of amines, Brauman and Blair [6] have stated that the greater polarizability of the larger groups enhances their ability to stabilize a positive or negative charge in the molecule. However, Brogli and Heilbronner

Table 2. Extent of hyperconjugation as evidenced by the alkyl group contribution to the highest occupied π molecular orbital.

	Ground configuration			Radical cation		
	% H	% C	% Total	% H	% C	% Total
Propene	16.5	8.8	25.3	21.3	15.6	36.9
cis 2-Butene	22.8	9.2	32.0	26.4	14.2	40.6
2-Me-2-Butene	26.4	9.6	36.0	28.6	14.3	42.9
2,3-DiMe-2-Butene	30.0	9.1	39.1	31.1	13.0	44.1
1-Butene	27.7	13.7	41.4	45.4	28.6	74.0
1-Pentene[a]	26.3	12.7	39.0	28.8	26.2	55.0
3-Me-1-Butene	4.9	35.1	40.0	19.0	60.1	79.0

[a] Not the highest π but that containing a higher percentage of C = C character has been chosen.

have found in the photoelectron spectra of the alkyl halides that there is also an increasing conjugative effect with increasing alkyl group size [5].

That hyperconjugation plays a rôle in the stabilization of the radical cations may be seen from an inspection of the wavefunctions. The extent of hyperconjugation is indicated by the relative contribution of alkyl H and C atomic orbitals to the highest occupied π molecular orbital; this is given in Table 2 as % H, % C, and % total alkyl contribution for representative molecules and their radical cations. It is seen that the alkyl contribution increases with number of alkyl groups and also with size of the group, although the ethyl, n-propyl, and isopropyl groups have about the same extent of hyperconjugation in the parent olefins. As Mulliken has discussed, hyperconjugation increases in the cation [8]. n fact, the present calculations indicate that, in the cations with the larger substituents, the wavefunction for the singly-occupied π MO is considerably delocaized over the entire molecule. To what extent this is influenced by the assumed planarity of the alkyl chains, and by the strong interactions between π and σ MO's common to the CNDO method, is a serious question.

Baird [9] has reported hyperconjugation energies for propene, 1-butene, and 2-methylpropene calculated by the MINDO method and has found these energies to be an additive function of alkyl substitution. This additivity is not apparent in the CNDO/2 wavefunctions or in the charge distributions reported here. The present results do support the suggestion of Radom *et al.* [10] that C – C hyperconjugation may be more important than C–H hyperconjugation (compare 1-petene and 3-methyl-1-butene).

Although the correlation obtained here between ionization potential and charge distribution effects is good, the dependence of the quantities on the geometry used in the calculations is being investigated.

Charge distribution effects in alkyl-substituted fulvenes and their radical cations will be discussed in connection with the interpretation of the photoelecron spectra of these molecules [11].

Acknowledgements. I wish to thank Prof. H. D. Stidham of the University of Massachusetts for he hospitality of his laboratory extended during the time this work was begun. I am grateful to Prof. E. Heilbronner of the University of Basel for the opportunity of continuing this work in the stimulating atmosphere of his institute and for helpful discussions. I am indebted to Vassar College for a leave of absence during the academic year 1971/72.

References

1. Pople, J. A., Segal, G. A.: J. chem. Physics **44**, 3289 (1966).
2. Clark, P. A.: J. chem. Physics **48**, 4795 (1968).
3. Watson, F. H., Jr., Armstrong, A. T., McGlynn, S. P.: Theoret. chim. Acta (Berl.) **16**, 75 (1970)
4. Pople, J. A., Gordon, G.: J. Amer. chem. Soc. **89**, 4235 (1967).
5. Brogli, F., Heilbronner, E.: Helv. chim. Acta **54**, 1423 (1971).
6. Brauman, J. I., Blair, L. K.: J. Amer. chem. Soc. **92**, 5986 (1970); **93**, 3911, 4315 (1971).
7. The adiabatic and vertical IP's are identical in ethylene: Turner, D. W., Baker, C., Baker, A. D., Brundle, C. R.: Molecular photoelectron spectroscopy, p. 179. New York: Wiley Interscience 1970; and for *trans* 2-butene: Haselbach, E., Heilbronner, E.: Helv. chim. Acta **53**, 684 (1970). They may, however, be different in the olefins with the larger alkyl substituents.

8. Mulliken, R. S.: Rev. mod. Physics **14**, 265 (1942); Muller, N., Mulliken, R. S.: J. Amer. chem. Soc. **80**, 3489 (1958).
9. Baird, N. C.: Theoret. chim. Acta (Berl.) **16**, 239 (1970).
10. Radom, L., Pople, J. A., Buss, V., Schleyer, P. v. R.: J. Amer. chem. Soc. **92**, 6380 (1970).
11. Heilbronner, E., Brogli, F., Clark, P. A.: to be published

Dr. P. A. Clark
Department of Chemistry
Vassar College
Poughkeepsie, New York
USA

Theoret. chim. Acta (Berl.) 28, 81—84 (1972)
© by Springer-Verlag 1972

Isoelectronic Molecules

First- and Second-Order Properties and the Continuous Group $\boldsymbol{L}(l)$

Bernard J. Laurenzi

Department of Chemistry, State University of New York at Albany, Albany, New York 12222

Received July 20, 1972

The simple variation of the physical properties of isoelectronic molecules with nuclear charge and internuclear distance is shown to be the result of a symmetry property of their Hamiltonians and operators under the continuous group $L(l)$.

Es wird gezeigt, daß bei isoelektronischen Molekülen die Änderung der physikalischen Eigenschaften in Abhängigkeit von Kernladung und internuklearem Abstand aus einer Symmetrieeigenschaft ihrer Hamiltonoperatoren und Operatoren der kontinuierlichen Gruppe $L(l)$ resultieren.

1. Introduction

In a series of papers [1–3] we have shown that the NMR shielding constants of a sequence of isoelectronic atoms or molecules are rigorously interrelated in a simple way. This result is valid even in the presence of electron-electron repulsion [3]. Although we have used the NMR shielding constant as an example, the same could be said for many other properties.

More precisely, and by way of summary of the previous work, the first- and second-order properties defined as

$$\begin{aligned}\mathscr{P}_n^{(1)} &= \langle \Phi_n | A | \Phi_n \rangle\,,\\ \mathscr{P}_n^{(2)} &= \sum_{m \neq n} \langle \Phi_n | A | \Phi_m \rangle \langle \Phi_m | B | \Phi_n \rangle / (E_n - E_m)\,,\end{aligned} \tag{1}$$

in the case of homonuclear diatomic molecules have been shown to be given by

$$\begin{aligned}\mathscr{P}_n^{(1)} &= Z^{(\alpha' - \alpha)} g^{(1)}(ZR, z/Z)\,,\\ \mathscr{P}_n^{(2)} &= Z^{(\alpha' - \alpha + \beta' - \beta - 2)} g^{(2)}(ZR, z/Z)\,,\end{aligned} \tag{2}$$

respectively. In the equations above Φ_n is an eigenfunction of the electronic Schrödinger equation

$$H_e \Phi_n = (T_e + V)\, \Phi_n = E_n \Phi_n\,, \tag{3}$$

Where T_e is the total electronic kinetic energy and V is the total potential energy

$$V = -\sum_{k=1}^{N} \left\{ \frac{Z}{|\boldsymbol{r}_k - \boldsymbol{R}/2|} + \frac{Z}{|\boldsymbol{r}_k + \boldsymbol{R}/2|} \right\} + \sum_{k>j}^{N} \frac{z}{|\boldsymbol{r}_k - \boldsymbol{r}_j|}\,. \tag{4}$$

$\boldsymbol{A}$ and $\boldsymbol{B}$ are, respectively, appropriate homogeneous operators [2] of degree α and β in the position variables $\boldsymbol{r}$ and $\boldsymbol{R}$ and of degree α' and β' in the nuclear charges.

The functions $g^{(1)}$ and $g^{(2)}$ can in principle be determined from the boundary conditions [1]. Eqs. (2) make it clear that if we determine a property for one member of an isoelectronic sequence that all of them are determined; electron correlation having been taken care of in that one member-once and for all. Further, the equation is useful as a check on numerical calculations and gives assurance that one can interpolate between numerical results.

In obtaining Eqs. (2) the virial theorem [4] as well as the homogeniety of A and B were used. However, the results seemed to be of such a general and rigorous nature that it was felt that perhaps there was a more fundamental reason for their validity. This is indeed the case as we shall show below. We have found that Eqs. (2) arise as a result of the symmetry properties of the physical properties under the linear group $L(l)$ [5]. Indeed, one might say that isoelectronic atoms and molecules behave similarly because of the symmetry of their Hamiltonians and physical properties under $L(l)$. In view of the impact which the theory of symmetry is having in all branches of science we feel that it is worthwhile pointing out its underlying presence in the theory of isoelectronic species.

2. Theory

A. The Group $SL(2)$

For simplicity we will consider only one-electron, homonuclear diatomic molecules. More complicated cases can be treated using the same methods.

The set of operators $S(a)$ which transform the internuclear distance R and the nuclear charge Z according to

$$\begin{aligned} S(a)R &= aR, \\ &\qquad 0 < a < \infty \\ S(a)Z &= a^{-1}Z, \end{aligned} \tag{5}$$

is an example of a one-parameter (a) continuous Lie Group. In fact, it is the special linear group $SL(2)$ [5]. This is a simple, non-compact, Abelian group. The group elements corresponding to the identity and inverse are $S(1)$ and $S(a^{-1})$ respectively. We note also that the quantity ZR is invariant under the group.

A representation of the infinitesimal transformation (away from the identity) can be obtained as follows. We have for small δa

$$\begin{aligned} S(1+\delta a)R &= (1+\delta a)R, \\ S(1+\delta a)Z &= (1+\delta a)^{-1}Z = (1-\delta a)Z, \end{aligned} \tag{6}$$

which can be written as

$$\begin{aligned} S(1+\delta a)R &= \left(1+\delta a\left[R\frac{\partial}{\partial R} - Z\frac{\partial}{\partial Z}\right]\right)R, \\ S(1+\delta a)Z &= \left(1+\delta a\left[R\frac{\partial}{\partial R} - Z\frac{\partial}{\partial Z}\right]\right)Z. \end{aligned} \tag{7}$$

The operator in square brackets is called the generator of the infinitesimal transformation and will be denoted by $\mathscr{T}$.

In addition to the operators $S(a)$ we introduce a group of operators O_s which is isomorphic to S. These act on functions and in keeping with the usual conventions [6] we have

$$\begin{aligned} O_s f(R,Z) &= f(S^{-1}R, S^{-1}Z), \\ O_s(fg) &= (O_s f)(O_s g). \end{aligned} \tag{8}$$

It is not difficult to show that the generator of the infinitesimal transformation determines the form of the operators O_s and in fact it is [5]

$$O_s f(R,Z) = \exp(-[\ln a]\mathscr{T}) f(R,Z). \tag{9}$$

B. The Physical Properties

We begin by considering the effect of O_s on the electronic energy of a one-electron, homonuclear diatomic molecule. Or, more conveniently we consider the effect of O_s on E_n/Z^2. We have

$$O_s(E_n/Z^2) = \int (O_s\Phi_n)(O_s H_e/Z^2)(O_s\Phi_n)\,dr. \tag{10}$$

Since the electronic wave function has the general form [7] $\Phi_n = Z^{3/2}\,\Psi(ZR, Zr)$ it is clear that

$$O_s\Phi_n(Z,R,r) = a^{3/2}\,\Phi_n(Z,R,ar), \tag{11}$$

further, the result for the Hamiltonian is just

$$O_s[H_e(r)/Z^2] = [H_e(ar)/Z^2]. \tag{12}$$

As a consequence of these two equations Eq. (10) becomes

$$O_s(E_n/Z^2) = (E_n/Z^2). \tag{13}$$

The quantity (E_n/Z^2) is invariant under the group $SL(2)$. This alone establishes the fact that (E_n/Z^2) is a function of only the invariant quantity ZR. More formally one has

$$\exp(-[\ln a]\mathscr{T})(E_n/Z^2) = (E_n/Z^2). \tag{14}$$

However, in order for this equation to be valid for all values of a we must have

$$\mathscr{T}(E_n/Z^2) = 0, \tag{15}$$

which leads to

$$\left(R\frac{\partial}{\partial R} - Z\frac{\partial}{\partial Z}\right)E_n = -2E_n. \tag{16}$$

This partial differential equation for the electronic energy had been obtained in a previous paper [1]. There it was found that the general solution is

$$E_n(Z,R) = Z^2 E_n(ZR), \tag{17}$$

where $E_n(R)$ is the energy for the molecule H_2^+.

Next, we consider the first- and second-order properties whose operators are homogeneous functions of degree α in $\boldsymbol{r}$ and R and α' in Z, i.e.

$$\begin{aligned} A(a\boldsymbol{r},aR,Z) &= a^{\alpha}A(\boldsymbol{r},R,Z), \\ \text{and}\quad A(\boldsymbol{r},R,aZ) &= a^{\alpha'}A(\boldsymbol{r},R,Z). \end{aligned} \tag{18}$$

Using these equations we find that

$$O_s A(\boldsymbol{r},R,Z) = a^{(\alpha-\alpha')} A(a\boldsymbol{r},R,Z) \tag{19}$$

and so we are led to the result

$$O_s(\mathscr{H}_n^{(1)}/Z^{\alpha-\alpha'}) = (\mathscr{H}_n^{(1)}/Z^{\alpha-\alpha'}), \tag{20}$$

as before. The second-order properties go through in the same way.

In order to include the effect of electron-electron repulsion it is only necessary to consider the group $L(3)$ which is isomorphic to [8] $SL(2)$, i.e.

$$\begin{aligned} T(a)R &= aR, \\ T(a)Z &= a^{-1}Z, \\ T(a)z &= a^{-1}z. \end{aligned} \tag{21}$$

Here the generator ($\mathscr{L}$) is

$$\mathscr{L} = R\frac{\partial}{\partial R} - Z\frac{\partial}{\partial Z} - z\frac{\partial}{\partial z}. \tag{22}$$

With the help of functional operators O_T, together with the same reasoning which was used above we obtain Eqs. (2).

Having established a connection between Group Theory and the theory of isoelectronic systems it is hoped that this powerful and enormous field of mathematics will shed further light on the regularities observed in these systems as well as uncovering new ones.

References

1 Laurenzi, B. J. Theoret. chim. Acta (Berl.) **13**, 106 (1969)
2. Laurenzi, B. J., Saturno, A. F.: J. chem. Physics **53**, 579 (1970).
3 Saturno, A. F., Laurenzi, B. J.: J. chem. Physics **55**, 2255 (1971)
4. Laurenzi, B. J., Fitts, D. D.: J. chem. Physics **43**, 317 (1965).
5. Hamermesh, M.: Group Theory, Chapter 8. Mass: Addison-Wesley, 1962.
6 Ref. 5, p. 81.
7 In Ref. 3 we show that $(\mathscr{T} + \boldsymbol{r}\cdot\nabla)\Phi = (3/2)\Phi$. The general solution of this equation is $\Phi = Z^{3/2}\Psi(ZR, Z\boldsymbol{r})$ where Ψ is arbitrary.
8 Note that there are two invariants in this case, ZR and z/Z.

Dr. B. J. Laurenzi
Department of Chemistry
State University of New York at Albany
Albany, New York 12222, USA

Theoret. chim. Acta (Berl.) 28, 85–98 (1972)
© by Springer-Verlag 1972

Semi-Empirical Effective Pair Correlation Parameters and Correlation Energies of BH, CH, NH, OH, HF, N_2, and CH_4

H. Önder Pamuk

Teorik Kimya Bölümü, Orta-Doğu Teknik Üniversitesi, Ankara, Türkiye

Received June 20, 1972

A set of approximations ("EPCE-F2σ") is given for estimating the correlation energies of molecules. The approximations start from Sinanoğlu's pair correlations and his many-electron theory for ground states (MET). For application of this method, "effective pair correlation energies" must be known. In the present paper three sets of one-center effective pair correlation energies are obtained from the atomic pair correlation energies. A weighted average method is introduced for handling the non-transferable atomic correlation energies. For the corresponding two-center effective pair correlation energies several empirical expressions are given. Then using three sets of one-center effective pair correlation energies and for the two-center ones, the correlation energies of some diatomic hydrides, N_2 and CH_4 molecules are estimated. The results agree quite well with each other, with experimental values, and with those obtained by other methods.

Ein Näherungsverfahren („EPCE-F2σ") zur Abschätzung der Korrelationsenergie von Molekülen wird angegeben. Die Näherungen gehen von Sinanoglus Paarkorrelation und seiner Mehrelektronentheorie für Grundzustände (MET) aus. Zur Anwendung dieser Methode müssen „Effektive Paarkorrelationsenergien" bekannt sein. In der vorliegenden Veröffentlichung werden drei Sätze von solchen effektiven Paarkorrelationsenergien für ein Zentrum aus atomaren Paarkorrelationsenergien gewonnen. Zur Behandlung der nichtübertragbaren atomaren Korrelationsenergien wird eine Methode mit gewichteten Mittelwerten angewendet. Für die entsprechenden effektiven Paarkorrelationsenergien für zwei Zentren werden verschiedene semiempirische Ausdrücke angegeben. Mit je drei Sätzen von Werten für die genannten Energiewerte für ein Zentrum oder zwei Zentren werden die Korrelationsenergien für einige zweiatomige Hydride sowie die Moleküle N_2 and CH_4 abgeschätzt. Die Ergebnisse stimmen gut untereinander und mit experimentellen Werten sowie mit Werten aus anderen Verfahren überein.

Introduction

In a previous paper [1], Sinanoğlu and Pamuk have given a semi-empirical one and two center effective pair correlation method for estimating the correlation energies of π-electron systems. This method applied to planar π-systems, each center contributing one $2p\pi$-orbital or similarly to systems like a cluster of Hydrogen atoms with an s-orbital for each center. The method is based on Sinanoğlu's "Many-Electron Theory of Atoms and Molecules" (MET) for ground states and the breakdown of total correlation energy of such systems into $N(N-1)/2$, MO pair correlations introduced by him [2]. For doubly occupied ground states, Sinanoğlu has recently derived a LCAO-MET form of the theory, and from it a number of semi-empirical molecular correlation approximations. In the π-system paper [1], a more approximate form of these methods which applied strictly to π-systems on account of symmetry was used and was referred to as the MET-

EPCE-F2 method (EPCE = effective pair correlation energy) with the equation.

$$E^{\pi}_{\text{corr}} \underset{(\text{F2})}{\cong} \tfrac{1}{4} \sum_{p,q} P_{pp} P^{*}_{qq} \bar{\varepsilon}_{pq} \tag{1a}$$

where $P_{pq} = 2 \sum_{k} c^{k}_{p} c^{k*}_{q}$, the charge and bond order matrix and

$$\bar{\varepsilon}_{pq} \equiv \varepsilon_{p^{\alpha} q^{\beta}} + \varepsilon_{p^{\alpha} q^{\alpha}} \tag{1b}$$

referred to as (EPC). The "F2-approximation" involved the assumption

$$\varepsilon_{p^{\alpha} q^{\beta}} \cong 2\varepsilon_{p^{\alpha} q^{\alpha}} \tag{1c}$$

which led to the vanishing of the P_{pq} $(p \neq q)$ terms from Eq. (1a). The latter terms had not been noticed earlier and omitted as such by independent users of Eq. (1a) by Pamuk [4] and by Brown and Roby [5]. The $(\varepsilon_{pp}, \varepsilon_{pq})$-method had first been suggested by Sinanoğlu [6] by approximations analogous to ZDO on the MET equations, but without the further approximation, Eq. (1c).

In the present paper, we use the MET-EPCE-F2-method for non-π-molecules including $2s$, $2p_{x,y,z}$ orbitals, although this use implies many more approximations for sigma systems than the original π-case. These additional assumptions are discussed below. The use of an analog of Eq. (1a) for various molecules like diatomics, CH_4, etc. is not as rigorous as Sinanoğlu's new semi-empirical MO-MET-methods [3], nevertheless with the $\bar{\varepsilon}_{pq}$-average parameters evaluated and given in this paper, the results on total E_{corr}'s of many molecules are quite good.

The Use of MET-EPCE-F2 Method for Sigma Molecules

The approximations that lead to Eq. (1a) are not invariant under atomic coordinate transformations in non-π systems. Further in a general molecule of first row atoms with $2s$, $2p$ valence electrons there will be "cross pair correlations" as shown by the Sinanoğlu Non-Closed Shell correlation theory [2b]. In spite of these additional complexities we may use Eq. (1a) for sigma systems too in a more *ad hoc* way, assuming 1) the sum of all cross pairs are small or vanish, 2) the F2-approximation, Eq. (1c) is reasonable (certainly more than the full ZDO-like one of $\varepsilon^{\alpha\beta} \approx \varepsilon^{\alpha\alpha}$) in the P_{pq} $(p \neq q)$ only, 3) that the approximations hold in a given set of atomic coordinate frames only, as in the Brown-Roby approach [5], as contrasted by Pople's, to approximate MO-theory, and 4) that when actual MO's with non-zero overlaps are available, the P_{pp}'s of π-theory in Eq. (1a) become replaced by Mulliken *gross populations* [7], Q_{p_A}.

The last assumption is somewhat justified [4] if one uses the Mulliken Approximation (MULAP) for overlap charges, or if MO's can be expanded in a series in overlap integrals $S_{p_A q_B}$, although neither approximation is particularly effective in other than π-orbitals. With the usual gross populations we have for Eq. (1a),

$$E_{\text{corr}} \underset{\text{F2}\sigma}{\cong} \sum_{\text{A,B}} \sum_{p,q} \left(\sum_{k} \frac{Q^{k}_{p_A}}{N_k} \right) \left(\sum_{l} \frac{Q^{l}_{q_B}}{N_l} \right) \bar{\varepsilon}_{p_A q_B} \tag{1d}$$

where k, l are spinless MO's, and $N_k = N_l = 2$ for doubly occupied ground states.

To emphasize that the present method on σ-systems involves quite different approximations than the use of Eq. (1a) for π-systems, we shall refer to it, i.e. Eq. (1b) as the "EPCE-F2σ-method". We shall test the validity of the $\varepsilon_{\mu\mu}$, $\bar{\varepsilon}_{\mu\nu}$, AO-correlation parameters obtained below with application to diatomic hydrides as well as N_2 and CH_4.

Atomic Correlation Energies and their Use as One-Center Effective Pair Correlation Energies

In the theory of electron correlation in non-closed shells, i.e. Sinanoğlu's NCMET correlation energy is rigorously separated into three parts [2b]. (i) Internal correlation energy; (ii) Semi-internal correlation energy; (iii) All-external correlation energy. The corresponding correlations can be interpreted as virtual electrons come close to each other, they will interact and be virtually excited to other orbitals. The internal correlation energy is due to excitations within the H.F. (Hartree-Fock) sea. The semi-internal correlation energy is due to excitations in which an electron is excited to outside the H.F. sea and a second one is excited to a previously unoccupied one in the H.F. sea. The all external correlation energy is due to excitations to outside the H.F. sea. This is the only type which can occur in closed shell systems like Ne atom.

Because of the exclusion effect and the dependence of the pair correlation energies on the total H.F. potential, the internal and semi-internal correlation energies are strongly dependent on the total orbital angular momentum, L, total spin, S, the number of $2p$ electrons, and the charge of the nucleus, Z. (These are called environmental effects). The all-external Sinanoğlu pair correlation energies are independent of the overall L, and S values. These can be transferred from the atoms to their ions and vice-versa. They are only slightly dependent on Z. If we find the contribution of each pair to the internal and semi-internal correlation energies, then the atomic pair correlation energies can be expressed in two parts: a) Dynamical or transferable part which comes from the all external correlation energy; and b) Nondynamical or nontransferable part which comes from the internal and semi-internal correlation energies [8–12].

The ($1s$) electron-pair of atoms in molecules are not very different from those of free atoms. It can be assumed that the atoms in molecules contain two $1s$ electrons. But the number of the electrons on the other orbitals are rather different from those of free atoms. In general, the electron configuration of a first row atom in molecules can be taken as $1s^2 2s^n 2p^m$ where $0 \leqq n \leqq 2$ and $0 \leqq m \leqq 6$. This configuration does not correspond to a certain spectroscopic state but it can be approximated by taking a linear combination of several spectroscopic states [13]. Therefore, one center effective pair energies have to be found by taking the average values of the corresponding pair correlation energies of these states. However, the total correlation energy of a molecule is expressed in the (EPCE-F2σ)-method by Eq. (1d), where $Q^k_{p_A}$ is the partial gross atomic population on p^{th} AO of the A'th atom in the k'th MO; N_k is the number of the electrons in the k'th MO, and $\bar{\varepsilon}_{p_A q_B}$ is the effective pair correlation energy between the electrons on p'th AO of atom A and q'th AO of atom B. (The effective pair correlation energies are the sum of ($\alpha\alpha$) and ($\alpha\beta$) pair energies, Eq. (1b)). As we see in Eq. (1), the contribution of an effective pair correlation energy to the total correlation energy, is not its own value but the product

$$\left|\sum_k (Q^k_{p_A}/N_k)\right| \left|\sum_l (Q^l_{q_B}/N_l)\right| \bar{\varepsilon}_{p_A q_B} \,. \tag{2}$$

Hence, the electron populations partially take care of the electron promotion from the $2s$ orbital to $2p$ orbitals. Therefore, it seems that it is enough to take the average values of the pair energies coming from the spectroscopic states of $1s^2 2s^2 2p^n$ ($n = 0, \ldots, 6$) configurations.

For the above configurations the internal and semi-internal correlation energies are contributed by $2s \leftrightarrow 2s$ and $2s^2 \leftrightarrow 2p^m$ correlations, respectively. Thus, for a certain spectroscopic state, we may assume that (i) with the exception of $\bar{\varepsilon}_{2s^2}$ and $\bar{\varepsilon}_{2s\,2p}$, the nontransferable parts of all pair correlation energies are negligible; (ii) the internal correlation energy can be taken as the nontransferable part of the $\bar{\varepsilon}_{2s^2}$ effective pair correlation energy, (iii) the semi-internal correlation energy divided by the number of the $2p$ electrons can be taken as the nontransferable part of the $\bar{\varepsilon}_{2s\,2p}$ effective pair energies.

Since the transferable parts of the pair correlation energies are the same for all spectroscopic states of a certain atom, we do not need to find their average values. The average of the nontransferable parts can be found by giving appropriate weighting for multiplicity of the states coming from the ground state configurations $1s^2 2s^2 2p^n$ (for each n).

$$\bar{\varepsilon}_{p_A q_A}(\mathrm{ntr}) = \frac{\sum_i (2L_i+1)(2S_i+1)\,\bar{\varepsilon}^i_{p_A q_A}(\mathrm{ntr})}{\sum_i (2L_i+1)(2S_i+1)} \tag{3}$$

where $\bar{\varepsilon}_{p_A q_A}$ (ntr) is the average nontransferable part of the effective pair correlation energy $\bar{\varepsilon}_{p_A q_A}$ which is dependent on the number of $2p$ electrons; $\bar{\varepsilon}^i_{p_A q_A}$ (ntr) is the nontransferable part of the $\bar{\varepsilon}_{p_A q_A}$ in the i'th spectroscopic state; L_i and S_i are the total orbital angular momentum and the total spin of the same spectroscopic state; summations are taken over all states coming from the configuration $1s^2 2s^2 2p^n$. Finally we can assume that the nontransferable parts of $\bar{\varepsilon}_{2s^2}$ and $\bar{\varepsilon}_{2s\,2p}$ pair correlation energies change continuously and smoothly with the number of $2p$ electrons, n, of the atom in molecules. Hence we fit the polynomials

$$\bar{\varepsilon}_{2s^2}(\mathrm{ntr}) = an^2 + bn + c \tag{4}$$

and

$$\bar{\varepsilon}_{2s\,2p}(\mathrm{ntr}) = dn^2 + en + f \,. \tag{5}$$

The coefficients of these polynomials will be found in the next section. Eq. (5) is not applicable if $n \cong 0$.

One-Center Effective Pair Energies

Several approximations are involved in the determination of the two-center and nontransferable part of the one-center effective pair correlation energies. Therefore, the best atomic pair correlation energies may not give the best molecular correlation energies. This must be checked by numerical calculations. Consequently, it is better to try several sets of one-center effective pair correlation energies and choose the set which yields the value closest to the experimental correlation energies. Here, the experimental correlation energy of a molecule is defined as

$$E_{\text{corr}}^{\text{exp}} \equiv BE_{\text{H.F.}} - BE_{\text{exp}} + \sum_{\text{atoms}} E_{\text{corr}}(\text{atoms}) \tag{6}$$

where relativistic correction is neglected.

Set A. The transferable one-center effective pair correlation energies are listed in Table 1. The values of the $\bar{\varepsilon}_{1s^2}$(tr) and $\bar{\varepsilon}_{1s2s}$(tr) are from Ref. [15]. The transferable part of the $\bar{\varepsilon}_{2s^2}$ pair correlation energies are obtained from the dynamical $\bar{\varepsilon}_{2s^2}$ values for (N, ^4S) and (Ne, ^1S) which are from Ref. [8b]. It is assumed that they change linearly with the nuclear charge. The $\bar{\varepsilon}_{2s2p}$(tr), $\bar{\varepsilon}_{2p_x2p_y}$(tr) and $\bar{\varepsilon}_{2p_x^2}$(tr) for C, N, and O atoms are from Ref. [10a]; those for B and F atoms are found by extrapolation and may be less accurate than the other pair correlation energies.

The nontransferable parts of the $\bar{\varepsilon}_{2s^2}$ and $\bar{\varepsilon}_{2s2p}$ pair correlation energies are tabulated in Tables 2 and 3, respectively. They are determined as described in the

Table 1. Transferable one-center effective pair correlation energies in set *A* (in eV)

Pairs	B	C	N	O	F
$\bar{\varepsilon}_{1s^2}$	−1.219	−1.227	−1.233	−1.238	−1.241
$\bar{\varepsilon}_{1s2s}$	−0.112	−0.138	−0.156	−0.190	−0.220
$\bar{\varepsilon}_{1s2p}$	−0.1	−0.1	−0.1	−0.1	−0.1
$\bar{\varepsilon}_{2s^2}$	−0.03	−0.107	−0.166	−0.210	−0.244
$\bar{\varepsilon}_{2s2p}$	−0.30	−0.35	−0.41	−0.46	−0.52
$\bar{\varepsilon}_{2p_x2p_y}$	−0.98	−0.81	−0.63	−0.52	−0.46
$\bar{\varepsilon}_{2p_x^2}$	−1.11	−1.04	−0.97	−0.92	−0.90

[a] See text; note that $\bar{\varepsilon}_{pq} \equiv (\varepsilon_{p\alpha q\beta} + \varepsilon_{p\alpha q\alpha})$.

Table 2. Average $\bar{\varepsilon}_{2s}2$(ntr) correlation energies[a] in set *A*

n	0[b]	1	2	3	4
B	−1.417	−0.811	(−0.43)	-	—
C	−1.828	−1.109	−0.524	−0.177	—
N	−2.309	−1.329	−0.659	−0.273	−0.066
O	−2.554	−1.541	−0.775	−0.336	−0.090

[a] In electron volts; ($\bar{\varepsilon} \equiv \varepsilon(\alpha\beta) + \varepsilon(\alpha\alpha)$).
[b] $n = 0$ values are from Ref. [8].

Table 3. Average $\bar{\varepsilon}_{2s2p}$(ntr) correlation energies[a] in set *A*

n	1	2	3	4	5
B	−0.647	(−0.44)	-	—	
C	−0.760	−0.486	−0.272		—
N	−0.790	−0.541	−0.356	−0.183	−0.064
O	−0.800	−0.578	−0.393	−0.223	−0.100
F	(−0.81)	(−0.60)	(−0.42)	(−0.27)	(−0.13)

[a] In electron volts ($\bar{\varepsilon} \equiv \varepsilon(\alpha\beta) + \varepsilon(\alpha\alpha)$).

Table 4. Coefficients for the polynomials in Eqs. (4) and (5) for set A

Atom	a	b	c	d	e	f
B	−0.113	0.719	−1.417	0.0	0.207	−0.854
C	−0.119	0.942	−1.932	−0.030	0.364	−1.094
N	−0.090	0.836	−1.971	−0.018	0.275	−1.019
O	−0.097	0.924	−2.235	−0.017	0.273	−1.056
F				−0.005	0.185	−0.930

Table 5. Transferable one-center effective pair correlation Energies[a] in set B

Pairs	B	C	N	O	F
$\bar{\varepsilon}_{1s^2}$	−1.221	−1.240	−1.256	−1.261	−1.266
$\bar{\varepsilon}_{1s2s}$	−0.104	−0.090	−0.071	−0.082	−0.079
$\bar{\varepsilon}_{1s2p}$	−0.102	−0.102	−0.102	−0.102	−0.102
$\bar{\varepsilon}_{2s^2}$	−0.060	−0.102	−0.147	−0.190	−0.230
$\bar{\varepsilon}_{2s2p}$	0.421	−0.407	−0.420	−0.431	−0.446
$\bar{\varepsilon}_{2p_x2p_y}$	(−0.766)	−0.719	−0.661	−0.607	−0.572
$\bar{\varepsilon}_{2p_x^2}$	(−0.730)	−0.763	−0.781	−0.741	−0.729

[a] In electron volts. $\bar{\varepsilon}_{pq} \equiv \varepsilon_p\alpha_q\beta + \varepsilon_p\alpha_q\alpha$

Table 6. Average $\bar{\varepsilon}_{2s}2(ntr)$ correlation energies[a] in set B

n	0[b]	1	2	3	4
B	−1.417	−0.802	−0.292		-
C	−1.828	−1.088	−0.533	−0.187	
N	−2.309	−1.313	−0.679	−0.286	−0.073
O	−2.554	−1.522	−0.801	−0.352	−0.100

[a] In electron volts. $\bar{\varepsilon} \equiv \varepsilon(\alpha\beta) + \varepsilon(\alpha\alpha)$.

[b] $n = 0$ values are taken from Ref. [8].

Table 7. Average $\bar{\varepsilon}_{2s2p}(ntr)$ correlation energies[a] in set B

n	1	2	3	4	5
B	−0.586	−0.368	—		
C	−0.662	−0.481	−0.299	—	
N	−0.714	−0.535	−0.364	−0.202	—
O	−0.747	−0.568	−0.398	−0.247	−0.110
F	−0.771	−0.589	−0.421	−0.255	−0.125

[a] In electron volts $\bar{\varepsilon} \equiv \varepsilon(\alpha\beta) + \varepsilon(\alpha\alpha)$.

Table 8. Coefficients for the polynomials in Eqs. (4) and (5) for set B

Atom	a	b	c	d	e	f
B	−0.053	0.668	−1.417	0.0	0.218	−0.804
C	−0.100	0.847	−1.828	0.0	0.181	−0.843
N	−0.090	0.843	−2.005	−0.005	0.196	−0.906
O	−0.099	0.944	−2.293	−0.007	0.200	−0.935
F	--	---	—	−0.018	0.292	−1.135

previous section using the internal and semi-internal correlation energies for C, N, and O atoms given by Skutnik [10a] and by McKoy and Sinanoğlu [8b]. The values in parentheses are obtained by extrapolation.

Table 4 contains the coefficients for the polynomials in Eqs. (4), (5). The internal correlation energy is zero if there are 5 or more $2p$ electrons, because all space orbitals in the HF seas are occupied. The $2p$ population of the F atom in molecules is usually greater than 5. Therefore, the nontransferable parts of $\bar{\varepsilon}_{2s^2}$ pair energies for the F atom and its ions are not listed.

Set B. Recently Öksüz and Sinanoğlu have developed computer programs to obtain the internal and the semi-internal correlation energies of all states of the first row atoms and their ions [11], based on Sinanoğlu's Non-closed shell electron correlation and atomic structure theory [2b]. The experimental all-external energies are found from these values and from the experimental total correlation energies. The above workers have carried out two sets of least square analyses. In the first set they used the experimental all-external correlation energies for only the ground configuration $1s^2 2s^2 2p^n$ $(n = 1-6)$. In the second set, they included all states coming from the $1s^2 2s 2p^2$ and $1s^2 2s 2p^3$ as well as the ground configurations. In Table 5 the transferable pair energies obtained from the ground configurations alone are listed. The $\bar{\varepsilon}(2p_x 2p_y)$ and $\bar{\varepsilon}(2_{p_x^2})$ effective pair energies for the B atom are obtained by extrapolation.

The nontransferable parts of the $\bar{\varepsilon}_{2s^2}$ and the $\bar{\varepsilon}_{2s2p}$ are obtained from Eq. (3) using the internal and the semi-internal correlation energies which are from Refs. [8, 10b, 11]. They are tabulated in Tables 6 and 7. The coefficients of the polynomials in Eqs. (4), (5) are determined from these values and listed in Table 8.

Set C. The $\bar{\varepsilon}(2p_x^2)$ effective pair correlation energy in Set B is much smaller than the empirically found one-center or two-center effective pair correlation energies for the π-electron systems. This is due to the neglect of the non-transferable part of $\bar{\varepsilon}(2p_x^2)$ effective pair energy. The study of the one and two-center correlation energies for the Hydrogen molecule [14] and for π-electrons [1] has shown that the one-center pair correlation energies are slightly larger than the two-center effective pair energies at the equilibrium. Therefore, in this set, we disregard the calculated values of the $\bar{\varepsilon}(2p_x^2)$ atomic pair correlation energy of the carbon atom. Using only the $\bar{\varepsilon}(2p_x^2)$ pair energies for the N, O, and F atoms in the Set B we fit an equation:

$$\bar{\varepsilon}^{\mathrm{A}}_{(2p_x^2)} = -0.014 Z_{\mathrm{A}}^2 + 0.250 Z_{\mathrm{A}} - 1.845\ (\mathrm{e.V.}) \tag{7}$$

where Z_{A} is the nuclear charge of the atom A. Eq. (7) yields $\bar{\varepsilon}_{(2p_x^2)}(C) = -0.849$ eV and $\bar{\varepsilon}_{(2p_x^2)}(B) = -0.945$ eV. Other one-center effective pair energies in this set are the same as in Set B.

Two-Center Effective Pair Correlation Energies

Previously [1], for larger distances than the equilibrium bond length, we have assumed that the two-center effective pair energies can be represented by

$$\bar{\varepsilon}_{p_{\mathrm{A}} q_{\mathrm{B}}} = 0.5(\bar{\varepsilon}_{p_{\mathrm{A}} p_{\mathrm{A}}} + \bar{\varepsilon}_{q_{\mathrm{B}} q_{\mathrm{B}}}) f(R_{\mathrm{AB}}, p_{\mathrm{A}}, q_{\mathrm{B}}) . \tag{8}$$

where $\bar{\varepsilon}_{p_A p_A}$ and $\bar{\varepsilon}_{q_B q_B}$ are one-center pair correlation energies; $f(R_{AB}, p_A, q_B)$ is a function of the internuclear distance and the orbital exponents of the AO's p_A and q_B. Unfortunately, we do not have an exact expression for the function f. Therefore, we shall use empirical functions which can represent the ratio of the two-center effective pair correlation energy to the sum of the one-center effective pair energies for the H_2 molecule up to the $2R_e$ with an error less than ±0.05 eV. Thus we define the new function $F_{p_A q_B}$ as

$$F_{p_A q_B} = \bar{\varepsilon}_{p_A q_B}/(\bar{\varepsilon}_{p_A p_A} + \bar{\varepsilon}_{q_B q_B}) \,. \tag{9}$$

Fischer-Hjalmars gives the following relation between $F_{p_A q_B}$ and $F_{r_C s_D}$ [14]:

$$F_{p_A q_B} = k[S^2_{p_A q_B}/S^2_{r_C s_D}]\, F_{r_C s_D} \,, \tag{10}$$

where $S_{p_A q_B}$ and $S_{r_C s_D}$ overlap integrals and k is a scaling parameter. We found that $F_{p_A q_B}$ can be represented by

$$F^{(1)}_{p_A q_B} = (k_1 R_{AB} + 0.1)\, S^2_{p_A q_B} \,. \tag{11}$$

Since we shall introduce other approximate expressions, to indicate that this is the first approximation, we use (1) as a superscript. The two-center pair energies for the H_2 molecule taken from Ref. [14] and k_1 scaling parameters obtained from Eqs. (9) and (11) are listed in the third and the fourth columns of Table 9. The scaling parameter k_1 is approximately constant for distances smaller than 3 a.u.

Coulson has studied the change of the exponent of the H_2 molecule with the internuclear distance [16]. In Ref. [16] the exponents are given for internuclear distances different from those given in Table 9. The exponents given in this table are obtained by extrapolation. Of course, overlap integrals, $S_{p_A q_B}$, have different values if these exponents are used instead of the atomic value $\xi = 1$. Now the following expression is found to represent $F_{p_A q_B}$:

$$F^{(2)}_{p_A q_B} = (k_2 \varrho_{p_A q_B} + 0.08)\, S^2_{p_A q_B} \tag{12}$$

where

$$\varrho_{p_A q_B} = 0.5(\xi_{p_A} + \xi_{q_B})\, R_{AB} \,. \tag{13}$$

The scaling parameter k_2, given in the fifth column of Table 9, is also approximately constant up to $2R_e = 2.8$ a.u. If $k_1 = 0.5$ and $k_2 = 0.63$ are chosen as the best

Table 9. Two-center correlation energies for the H_2 molecule and parameters for approximate $F_{p_A q_B}$'s

R_{AB} (a.u.)	ξ[a]	ε^b_{pq} (eV)	k_1	k_2	k_3	k_4
1.2	1.240	−0.979	0.496	0.631	12.68	10.66
1.4	1.185	−0.964	0.491	0.631	12.81	10.44
1.6	1.140	−0.930	0.491	0.632	12.69	10.48
1.8	1.105	−0.880	0.494	0.632	12.96	10.61
2.0	1.075	−0.817	0.500	0.628	12.55	10.86
2.2	1.050	−0.741	0.503	0.619	12.27	10.63
2.6	1.005	−0.573	0.501	0.579	11.78	10.66
3.0	1.0	−0.397	0.471	0.535	10.91	10.91
3.5	1.0	−0.198	0.361	0.415	8.47	8.47
4.0	1.0	−0.035	0.090	0.137	2.53	2.53

[a] From Ref. [16]. — [b] From Ref. [14].

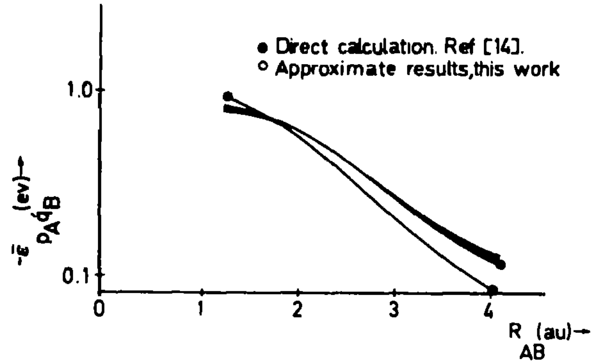

Fig. 1. Two-center correlation energy for the H_2 molecule

scaling parameters, naturally at large distances, the $\bar{\varepsilon}_{p_A q_B}$ effective pair energies obtained by these approximate expressions will be larger than the ones given in Table 9. However, the values of $\bar{\varepsilon}_{p_A q_B}$ effective pair energies at large distances are small and may be less accurate.

When these expressions are generalized to all two-center effective pair energies, Eq. (10) is automatically satisfied if 0.1 in Eq. (11) and 0.08 in Eq. (12) are neglected. However, Eqs. (11) and (12) predict $\bar{\varepsilon}_{p_A q_B} = 0$ if p_A and q_B are orthogonal orbitals. The correlation energy of electrons on such orbitals may be small but it is not necessarily zero. The use of charge overlap integrals

$$C_{p_A q_B} \equiv \langle \chi_{p_A}^2 \cdot \chi_{q_B}^2 \rangle \tag{14}$$

may give better results, where χ_p and χ_q are atomic orbitals. Therefore, we assume two more expressions for $F_{p_A q_B}$

$$F^{(3)}_{p_A q_B} = k_3 C_{p_A q_B} R_{AB}^2 \tag{15}$$

and

$$F^{(4)}_{p_A q_B} = k_4 C_{p_A q_B} \varrho^2_{p_A q_B} \, . \tag{16}$$

For the H_2 molecule k_3 and k_4 scaling parameters are calculated and listed in the last two columns of Table 9. The use of $k_3 = 12.5$ and $k_4 = 10.4$ yields also high values for $\bar{\varepsilon}_{p_A q_B}$ at large distances. The pair correlation energies obtained by these approximations are plotted versus internuclear distance in Fig. 1.

The best approach would be to determine as few parameters as possible. However, we have chosen three sets of one-center effective pair correlation energies and we have to determine three sets of corresponding two-center ones. If the internuclear axis is taken as the X-axis, we will denote an electron on the H atom by h, an electron on any first row atom by a, an electron on the $2p_y$ or on the $2p_z$ orbitals of the first row atoms by π, and an electron on other orbitals of the first row atoms by σ. The preliminary applications of the EPCE method have indicated that for each approximation of the two-center pair correlation energies we have to determine different scaling parameters at least for four types of pairs in order to obtain the correlation energies of N_2 and CH_4 comparable to the experimental values. These are $h-h$, $\pi-\pi$, $h-a$ and $\sigma-a$ type pairs. The parameters for $h-h$ type pairs have already been determined.

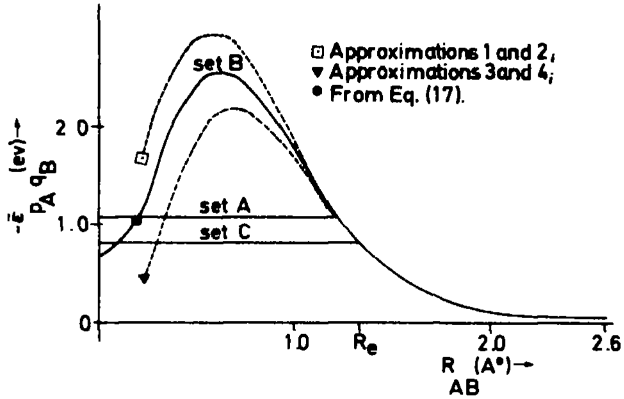

Fig. 2. Two-center correlation energy for $\pi-\pi$ type pairs

Table 10. Parameters for $F_{p_A q_A}$'s

Type of pair		k_1	k_2	k_3	k_4
	$h-h$	0.50	0.63	12.50	10.40
Set A	$h-a$	0.60	0.45	4.50	2.00
	$\sigma-a$	0.90	0.45	2.10	0.55
	$\pi-\pi$	2.34	1.49	23.60	8.93
Set B	$h-a$	0.77	0.54	5.46	2.51
	$\sigma-a$	1.15	0.54	2.62	0.49
	$\pi-\pi$	3.55	2.26	31.78	12.03
Set C	$h-a$	0.73	0.52	5.25	2.40
	$\sigma-a$	1.13	0.58	3.20	0.84
	$\pi-\pi$	2.87	1.86	29.41	11.14

The parameters for $\pi-\pi$ type pairs are determined from $\bar{\varepsilon}_{pq} = -0.794\,\text{eV}$ (the two-center effective pair correlation energies for the π electrons at the bond length of the benzene molecule), and from the one-center effective pair correlation energies of $\bar{\varepsilon}(2p_z^2)$ in each set. The necessary overlap and charge overlap integrals are calculated from the equations given in Appendices D and E of Ref. [17]. In the Sets A and C $F_{p_A q_B}$ is set equal to 0.5 for internuclear distances shorter than the distance where $F_{p_A q_B} \geq 0.5$. In the Set B, this condition is relaxed because the one-center effective pair energy, $\bar{\varepsilon}_{(2p_z 2)} = -0.763\,\text{eV}$, is smaller than the two-center one, $\bar{\varepsilon}_{pq} = -0.794\,\text{eV}$. The results for the $F_{p_A q_B}$'s are plotted in Fig. 2. The values of the scaling parameters are given in Table 10.

The parameters for $h-a$ type pairs are determined so that every approximation in each set will yield the value closest to the experimental correlation energy of the CH_4 molecule. The H.F. energy of CH_4 has been calculated by several workers [18–20]. The best value is $E_{\text{H.F.}} = -40.1983$ a.u. which yields the H.F. binding energy $BE_{\text{H.F.}} = 13.868\,\text{eV}$ [20]. The experimental binding energy of methane is $BE_{\text{H.F.}} = 18.175\,\text{eV}$ [21]. From Eq. (6) and $E_{\text{corr}}(^3P\,\text{C}) = -4.299\,\text{eV}$ [15], we find the experimental correlation energy for the CH_4 molecule $E_{\text{corr}}^{\text{exp}} = -8.61\,\text{eV}$. The electron populations are obtained from the wave function given by Pitzer [22]. The overlap and charge overlap integrals are computed using the equations given in Appendices D and E of Ref. [17]. The calculated parameters are listed in Table 10.

The parameters for the $\sigma - a$ type pairs are determined using the experimental correlation energy for the N_2 molecule. The H.F. energy of N_2 is $E_{\text{H.F.}} = -108.9956$ a.u. which yields the H.F. binding energy, $BE_{\text{H.F.}} = 5.27$ eV [23]. The experimental binding energy of the N_2 molecule is $BE_{\text{exp}} = 9.906$ eV [21]. Using $E_{\text{corr}}(^4S, \text{N}) = -5.115$ eV [15] and Eq. (6) we find $E^{\text{exp}}_{\text{corr}} = -14.87$ eV. Electron populations are from Ref. [24]. The overlap and the charge overlap integrals are again calculated using the equations in Appendices D and E of Ref. [17]. The resulting parameters are also listed in Table 10.

The trial calculations for small molecules have shown that any of the four approximations can predict the correlation energies of these molecules within the ± 0.5 eV range of the experimental values. However, the standard deviation is smallest if

$$F_{p_A q_B} = [3F^{(1)}_{p_A q_B} + F^{(2)}_{p_A q_B} + 3F^{(3)}_{p_A q_B} + F^{(4)}_{p_A q_B}]/8 \tag{17}$$

is used for the determination of the two-center effective pair energies.

For $F_{p_A q_B}$, Brown and Roby [25] have suggested the following expression

$$F_{p_A q_B} = 0.5/[k_1 S^{-1}_{p_A q_B} + 0.5 k_2 (\varepsilon_{p_A p_A} + \varepsilon_{q_B q_B}) R^6_{p_A q_B}] \tag{18}$$

with the following values $k_1 = 0.734424$, $k_2 = -0.257505\,(\text{Å})^{-6}\,(\text{eV})^{-1}$ and $\varepsilon_{p_A p_A} = \varepsilon_{q_B q_B} = 1.1430$ eV. Since the denominator in this expression becomes zero for $R_{p_A q_B} = 1.328$ Å, Eq. (18) cannot be used to estimate the ratio, given in Eq. (9), for any internuclear distance.

Preliminary Applications of the EPCE-F2σ Method

We have calculated the correlation energies of some diatomic hydrides, N_2 and CH_4 molecules to find out whether the one and two-center effective pair correlation energies yield acceptable values. The results are tabulated in Table 11. Experimental correlation energies obtained form the expression given in Eq. (6) are not the exact correlation energies. They contain the errors coming from the neglect of the relativistic effects, from the determination of the experimental binding energy, and from the H.F. calculations. Set *A*, Set *B*, and Set *C* are the results obtained by the EPCE method by using the effective pair correlation energy sets *A*, *B*, and *C* respectively. In these calculations two-center effective pair correlation energies are obtained from the expressions given in Eqs. (9) and (17). The "shrunk core" (S–C) and the "pair population method" (PPM) results are from Ref. [26]. With the exceptions of H.F. [27a], CH_4 [27b], and N^2 [28], the separated-ion (SI) values are calculated by us using the total correlation energies of atoms and ions [15]. Others [29, 30] have also calculated correlation energies of diatomic molecules by using the SI method. However, they give curves rather than the numbers, which makes comparison of them with the results of the EPCE method impossible.

In general correlation energies for diatomic molecules obtained by the EPCE method are in good agreement with those predicted by other methods and ex-

Table 11. Correlation energies of some small molecules (in eV)

Molecule		$E_{\text{cor}}^{\text{exp}}$	This work			S–C[d]	PPM[d]	SI[j]
			Set *A*	Set *B*	Set *C*			
BH^a	$^1\Sigma$	-4.20^c	-4.78	-4.81	-4.81	-4.86	-4.20	-4.34
CH^b	$^2\pi$	-5.48^c	-5.67	-5.69	-5.69	-5.98	-5.51	-5.67
NH^b	$^3\Sigma$	-6.82^c	-6.93	-6.97	-6.93	-7.02	-6.47	-6.99
OH^b	$^2\Pi$	-8.62^c	-8.51	-8.38	-8.60	-8.81	-8.47	-8.79
HF^b	$^1\Sigma$	-10.56^c	-10.56	-10.49	-10.12	-10.69	-10.37	-10.83^e
N_2^a	$^1\Sigma_g$	-14.96^f	-14.93	-15.02	-14.95	-13.44	-14.17	-15.19^g
CH_4^h		8.61	-8.60	-8.63	-8.64	—	-7.99	-9.28^i

[a] Wave functions are from Ref. [31].

[b] Wave functions are from Ref. [32].

[c] These values are from Ref. [29].

[d] These correlation energies are obtained by using E_{corr} of Ref. [26] and the atomic correlation energies of Ref [15]. SC – "Shrunk-Core" method; PPM = "Pair Populations Method" of Hollister and Sinanoğlu [26].)

[e] This value is from Ref. [27a].

[f] These are obtained from $E_{\text{corr}}^{\text{exp}}$ given in Ref. [26] and the atomic correlation energies of Ref. [15].

[g] This value is from Ref. [28].

[h] Wave function is from Ref. [22].

[i] This value is from Ref. [27b].

[j] Separated-Ions estimate by the writer.

perimental correlation energies. In the case of diatomic hydrides, the "shrunk core method" reduces to the united atom (UA) approach [33]. This approach overestimates the correlation energy of molecules. The SI value for the HF molecule is larger in absolute value than the S–C result. If the correlation energy of the F ion is obtained by extrapolation from the correlation energies of the 10-electron isoelectronic series, the resulting correlation energy in absolute value would be smaller than 10.69 eV, and not 10.83 eV as given in Ref. [27a]. The direct calculation of the correlation energy by the CI method gives -8.41 eV for the H.F. molecule, which is only 80% of the experimental correlation energy [34].

The agreement between the "EPCE-F2σ" results and the other values indicates that the effective pair correlation energies found here, can be used for all molecules. Another test for the weighted average method may be the calculation of the contribution of the $\bar{\varepsilon}_{2_s2}$ pair correlation energy of nitrogen atom in the N_2 molecule to the total correlation energy. This is calculated directly by a 2 × 2 CI and found to be approximately -0.3 eV per atom [26]. A rough estimation of this contribution was made by the PPM of Hollister and Sinanoğlu [12, 26]. We have calculated the $\bar{\varepsilon}_{(2_s2)}$ effective pair correlation energy for nitrogen atom in N_2 by using Eq. (4), the coefficients given in Table 4, and the electron populations given in Ref. [31]. The values of $\bar{\varepsilon}_{(2_s2)}$ are -0.368 eV in Set *A* and -0.389 eV in Set *B*, and *C*. The contributions of these to the molecular correlation energy are -0.279 eV in Set *A* and -0.295 in Sets *B* and *C*. Since these values are practically same as the 2 × 2 CI result, we expect to obtain better estimations by this method also for other atoms in molecules.

Conclusion

To estimate the correlation energy of a molecule by the present effective pair correlation energy method, (EPCE-F2σ), the effective pair correlations have to be known. While developing the method, it was assumed that these can be determined empirically. In this paper, three sets of effective pair correlation energies are given. The use of atomic pair correlation energies as one-center effective pair correlation energies is modified and the "Weighted Average" method is introduced. We expect that this method will help to obtain better correlation energies because its application, to the calculation of the contribution of pair correlation energy of the nitrogen atom in the N_2 molecule, yields comparable results with that obtained by 2×2 CI method.

For two-center effective pair correlation energies, several empirical expressions are given. However, the preliminary applications have indicated that a simple linear combination of them yields the best results. Using the one-center effective pair correlation energies and the final expression for the two-center effective pair correlation energies, the correlation energies of some diatomic hydrides, N_2 and CH_4 molecules are estimated. The results agree quite well with the experimental values. Therefore, it is expected the EPCE-F2σ method will predict even the correlation energies of large molecules (i.e. benzene, naphthalene etc.) with less than 10% error. The best of the three sets of effective pair correlation energies may be chosen after applying the (EPCE-F2σ) method to larger numbers of molecules.

References

1. Sinanoğlu, O., Pamuk, H. Ö.: Theoret. chim. Acta (Berl.), to be published.
2a. Sinanoğlu, O.: J. chem. Physics **33**, 1212 (1960).
2b. Sinanoğlu, I.: In: Atomic physics, Vol. I, p. 131. New York: Plenum Press 1969.
3. Sinanoğlu, O.: To be published.
4. Pamuk, H. Ö.: Ph.D. Thesis. Yale University (1968).
5. Brown and Roby. (See Ref. [25]).
6. Sinanoğlu, O.: Modern quantum chem., Ed. O. Sinanoglu. New York: Academic Press 1965.
7. Mulliken, R. S.: J. chem. Physics **23**, 1833, 1841, 23381 2343 (1955).
8a. Tuan, D. F., Sinanoğlu, O.: J. chem. Physics **41**, 2677 (1964).
8b. McKoy, V., Sinanoğlu, O.: J. chem. Physics **41**, 2689 (1964).
9. Silverstone, H. J., Sinanoğlu, O.: J. chem. Physics **44**, 1899, 3608 (1966).
10a. Skutnik, B. S.: Ph.D. Thesis. Yale University (1967).
10b. Skutnik, B. S., Öksüz, I., Sinanoğlu, O.: Int. quant. Chemistry **2**, 1 (1968).
11. Sinanoğlu, O., Öksüz, I.: Physic. Rev. Letters **21**, 507 (1968); Physic. Rev. **181**, 42 (1969).
12. Sinanoğlu, O.: Advances chem. Physics **14**, 237 (1969).
13. Moffit, W.: Proc. Roy. Soc. (London) A **210**, 224 (1951).
14. Fischer-Hjalmars, I.: In: Modern quantum chemistry, Ed. O. Sinanoğlu. New York: Acad. Press 1965.
15. Clementi, E.: J. chem. Physics **38**, 2248 (1963).
16. Coulson, C. A.: Trans. Faraday Soc. **33**, 1479 (1937).
17. Pamuk, H. Ö.: Ph.D. Thesis Yale University (1968); c.f. also Pamuk, H. Ö., Sinanoğlu, O.: Hacettepe Fen ve Müh. Dergisi, I, 42 (1971).
18. Krauss, M.: J. chem. Physics **38**, 564 (1963).
19. Woznick, B. J.: J. chem. Physics **40**, 2860 (1964).
20. Ritchie, C. D., King, H. F.: J. chem. Physics **47**, 564 (1967).

21. BE_{exp} is obtained from the data given by Lewis, G. N., Randall, M.: Thermodynamics, revised by Pitzer, K.S., Brewer, L.: New York: McGraw-Hill Book Co. Inc. 1961; Zero-Point corrections are based on Hertzberg, G.: Infrared and Raman Spectra. New York: D. Van Nostrand Co. 1945.
22. Pitzer, R.M.: J. chem. Physics **46**, 4871 (1967).
23. Cade, P.E., Sales, K.D., Wahl, A.C.: J. chem. Physics **44**, 1973 (1966).
24. Fraga, S., Ransil, B.: J. chem. Physics **34**, 727 (1961).
25. Brown, R.D., Roby, K.R.: Theoret. chim. Acta (Berl.) **16**, 291 (1970).
26. Hollister, C., Sinanoğlu, O.: J. Amer. chem. Soc. **88**, 13 (1966).
27a. Clementi, E.: J. chem. Physics **38**, 2780 (1963).
27b. Clementi, E.: J. chem. Physics **39**, 487 (1963).
28. Nesbet, R.K.: J. chem. Physics **40**, 3619 (1964).
29. Cade, P.E., Huo, W.M.: J. chem. Physics **47**, 614 (1967).
30. Allen, L.C.: In: Quantum theory of atoms, molecules, and the solid state, a tribute to J.C. Slater. Ed. P.O. Löwdin. New York: Acad. Press 1966.
31. Ransil, B.J.: Rev. mod. Physics **32**, 245 (1960).
32. Krauss, M.: J. chem. Physics **28**, 1021 (1958).
33. Stanton, R.E.: J. chem. Physics **36**, 1928 (1962).
34. Bender, C.F., Davidson, E.R.: J. chem. Physics **47**, 360 (1967).

Dr. H. Ö. Pamuk
Teorik Kimya Bölümü
Orta-Doğu Teknik
Üniversitesi
Ankara, Türkiye

Theoret. chim. Acta (Berl.) 28, 99 – 102 (1972)
© by Springer-Verlag 1972

Relatio

A Note on the Importance of Including Monoatomic Overlap Densities in the Calculation of CNDO/2 Charge Distributions

H. L. Hase, H. Meyer, and A. Schweig

Fachbereich Physikalische Chemie der Universität, D-3550 Marburg a.d. Lahn,
Biegenstraße 12, Germany

Received August 11, 1972

It is demonstrated that in the calculation of CNDO/2 charge density distributions the monoatomic overlap densities necessarily must be taken into account. Otherwise electron densities are obtained which are not invariant to molecular rotations and generally of wrong symmetry.

The valence electron density [1] of a closed shell molecule in the LCAO MO approximation is

$$\varrho = \sum_{\mu\nu} P_{\mu\nu} \phi_\mu \phi_\nu \tag{1}$$

where ϕ_μ and ϕ_ν are the valence basis AO's and $P_{\mu\nu}$ the elements of the density matrix. In the framework of the CNDO/2 method [1] (1) may be applied in two approximate forms both in accordance with the CNDO/2 normalization procedure: (i) by neglecting diatomic but retaining monoatomic overlap densities

$$\varrho = \varrho_{\mathrm{D}} + \varrho_{\mathrm{OD}}, \tag{2}$$

$$\varrho_{\mathrm{D}} = \sum_\mu P_{\mu\mu} \phi_\mu^2, \tag{2a}$$

$$\varrho_{\mathrm{OD}} = 2 \sum_A \sum_{\mu<\nu} P_{\mu\nu} \phi_\mu \phi_\nu \tag{2b}$$

where ϱ_{D} is due to the diagonal ($P_{\mu\mu}$) and ϱ_{OD} to the monoatomic off-diagonal ($P_{\mu\nu}$) matrix elements (overlap densities) and (ii) by neglecting both mono- and diatomic overlap densities

$$\varrho = \varrho_{\mathrm{D}} \tag{3}$$

In previous work [2–5] on CNDO/2 calculations of molecular multipole moments the inclusion of monoatomic overlap densities (application of (2)) was found essential for obtaining meaningfull results. However, in a recent paper [6] dealing with CNDO/2 and EH [7] charge densities Boyd applied (3) in the CNDO/2 case. In this communication we compare electron density maps of the hydrogen fluoride (HF) molecule obtained from (2) and (3). As the simple example shows the application of (3) is not allowed.

We assume the HF molecule lying in the xy plane of a Cartesian coordinate system: In case (a) with its bond axis parallel and in case (b) at an angle of 30° to the x-axis. Fig. 1 shows the density plots [8] for case (a) and Fig. 2 for case (b).

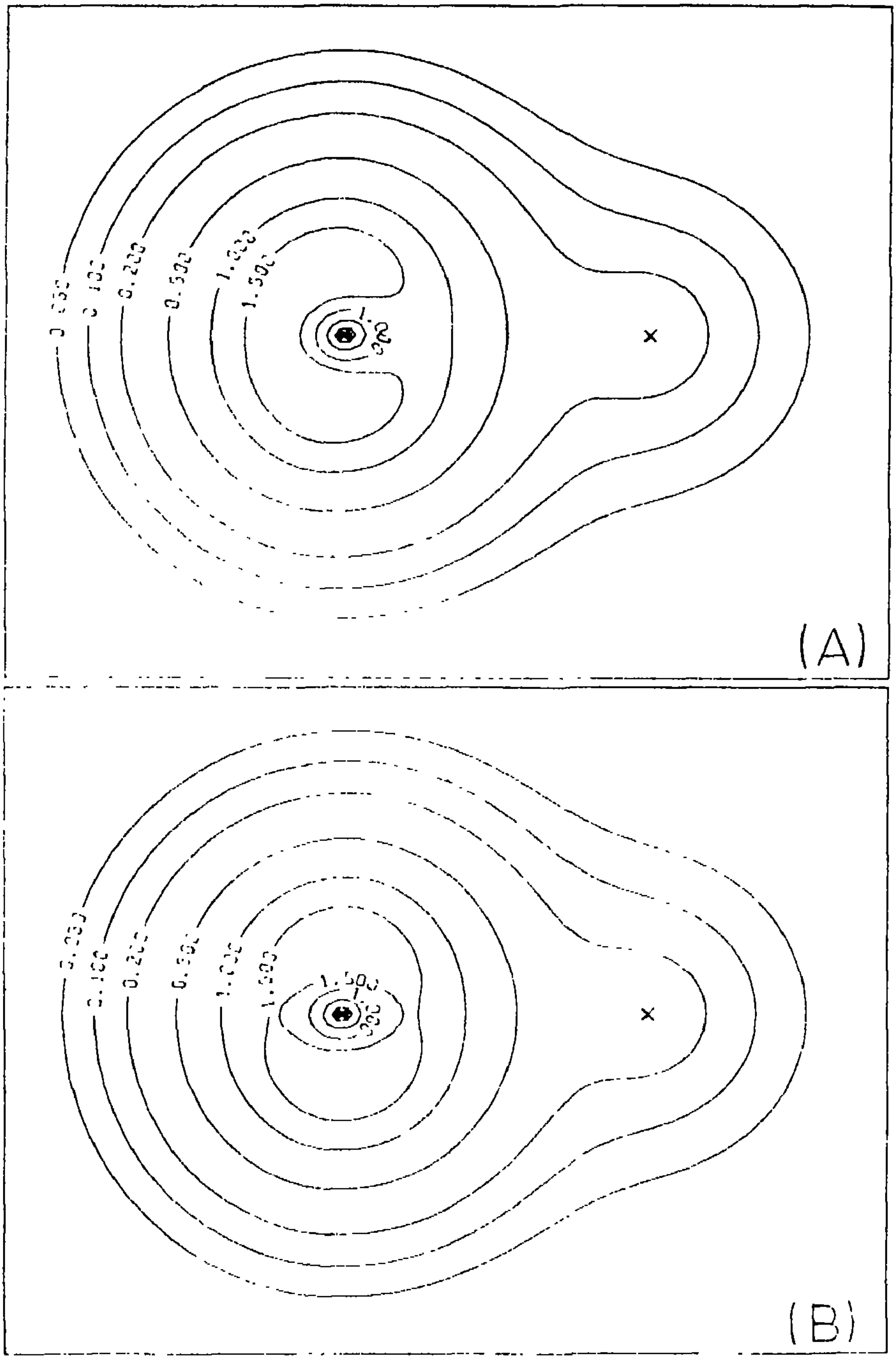

Fig. 1. Plots of the CNDO/2 densities [in a.u.] for the HF molecule lying with its molecular axis parallel to the x-axis (case (*a*) of the text). Map (A) was obtained from Eq. (2) (neglecting diatomic but retaining monatomic overlap densities) and map (B) from Eq. (3) (neglecting both mono- and diatomic overlap densities)

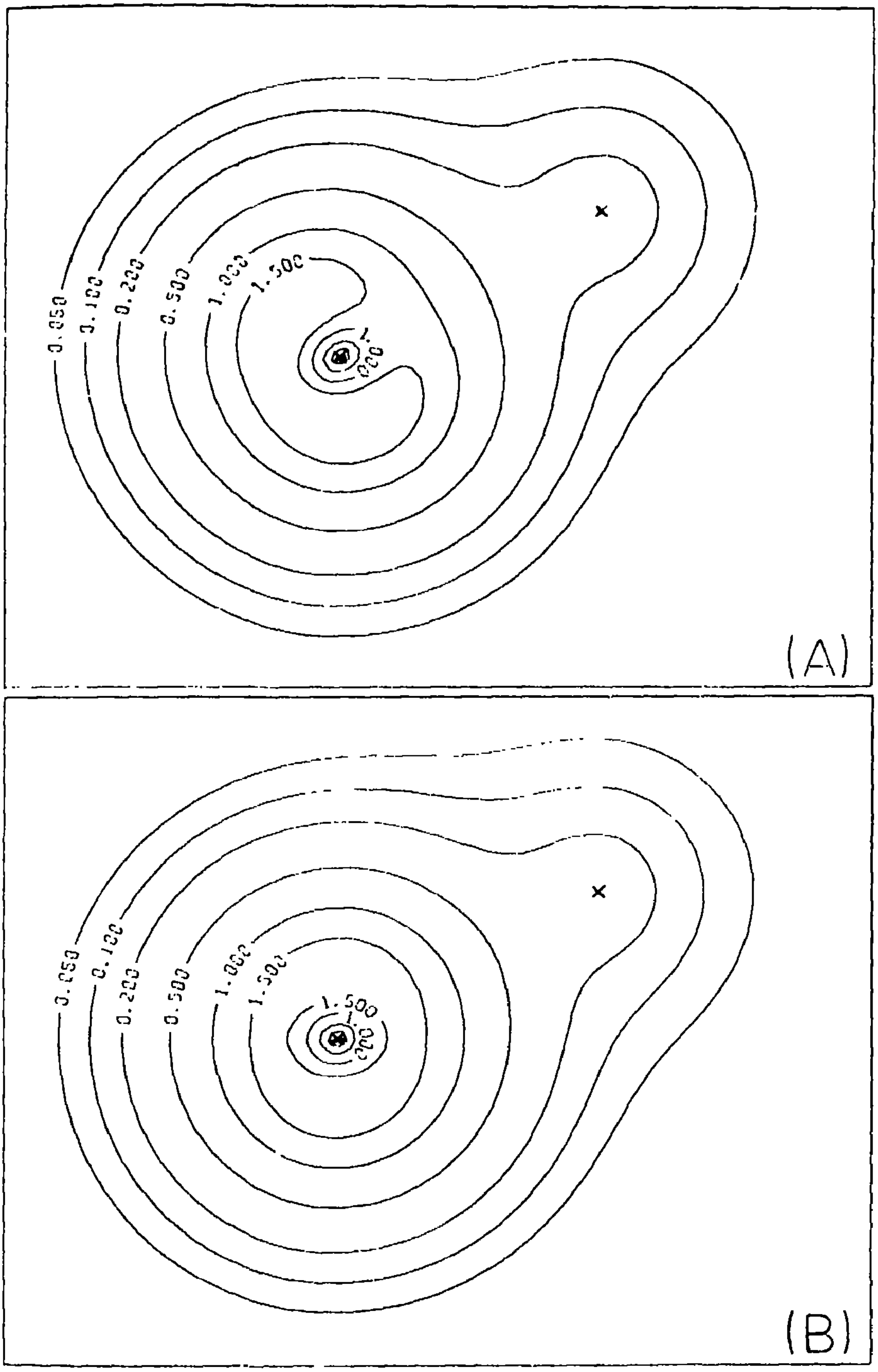

Fig. 2. Plots of the CNDO/2 densities [in a.u.] for the HF molecule lying at an angle of 30° to the x-axis (case (b) of the text). Maps (A) and (B) refer to the densities computed from Eqs. (2) and (3), respectively

As we see the density obtained from (3) is – opposite to the density obtained from (2) – not invariant to the molecular rotation and in the case (b) not symmetric to the molecular axis. Hence by neglecting monoatomic overlap densities wrong (physically unsound) CNDO/2 electron densities are produced.

Acknowledgements. This work was supported by the Deutsche Forschungsgemeinschaft and the Fonds der Chemischen Industrie.

References

1 Pople, J. A., Beveridge, D. L.: Approximate molecular orbital theory. New York: Mc. Graw-Hill, 1970
2 Santry, D. P., Segal, G. A.: J. chem. Physics **47**, 158 (1967).
3 Santry, D. P.: J. Amer. chem. Soc. **90**, 3309 (1968)
4 Meyer, H., Schweig, A.: Chem. Physics Letters **9**, 451 (1971).
5 Hase, H. L., Schweig, A.: Chem. Physics Letters **12**, 238 (1971).
6 Boyd, D. B.: Theoret. chim. Acta (Berl.) **23**, 383 (1972).
7 Hoffmann, R.: J. Amer. chem. Soc. **93**, 1064 (1971).
8 The density plots have been obtained with a CALCOMP-Plotter in conjunction with the TR 4 Computer of the Zentrale Rechenanlage der Philipps-Universität, Marburg/Lahn. For the method for computing and plotting contour lines, see: Hahn, H., Radloff, J.: Elektron. Rechenanl. **14**, 128 (1972)

Prof. Dr. A. Schweig
Fachbereich Physikalische Chemie
der Universität
D-3550 Marburg/Lahn
Biegenstr. 12
Federal Republic of Germany

Theoret. chim. Acta (Berl.) 28, 103—110 (1973)
© by Springer-Verlag 1973

Commentationes

Ab initio Calculations of Small Hydrides Including Electron Correlation

VIII. Equilibrium Geometry and Harmonic Force Constants of BH_3

M. Gelus

Laboratoire de chimie générale, Université scientifique et médicale de Grenoble

W. Kutzelnigg

Institut für Physikalische Chemie und Elektrochemie der Universität Karlsruhe

Received August 16, 1972

The harmonic force constants and vibration frequencies of BH_3 (which is not directly accessible to experimental studies) are calculated both in SCF approximation and including correlation in the IEPA-PNO scheme, using a Gaussian basis set. The results are compared with those of related molecules like BH and BH_2.

Die harmonischen Kraftkonstanten und Schwingungsfrequenzen des BH_3 (das experimentellen Untersuchungen nicht unmittelbar zugänglich ist) werden sowohl in der SCF-Näherung als auch unter Einschluß der Elektronenkorrelation in der IEPA-PNO-Näherung mit einer Basis von Gaußfunktionen berechnet. Die Ergebnisse werden mit denen verwandter Moleküle wie BH und BH_2 verglichen.

Les constantes de force et frequences de vibration harmoniques de la molecule BH_3 (qui est inaccessible a des etudes experimentales directes) sont calculées dans le cadre des methodes SCF et IEPA-PNO utilisant une base d'orbitales Gaussiennes. On compare les resultats avec ceux obtenus recemment pour des molecules comme BH et BH_2.

1. Introduction

BH_3 is, like BeH_2 [1], one of the simplest "normal" molecules, yet information from experiment about the properties of BH_3 (like of BeH_2) are virtually nonexistent. The reason for this lack of information is probably that whenever BH_3 is formed in a chemical reaction it readily dimerizes to B_2H_6 (like BeH_2 polymerizes). The experimental values of the dimerization energy of BH_3 is rather uncertain [2], but theoretical calculations [3] suggest that it is close 35 kcal/mol.

In a previous note [3] (see also [4]) we have already reported our results concerning the binding energy of BH_3 with respect to B + 3H. To get more knowledge of this molecule we decided to compute its harmonic force constants and vibration frequencies and to study to which extent they are influenced by electron correlation [5].

In the literature one finds two references to the vibration frequencies of BH_3. Shepp and Bauer [6] proposed an estimate of the normal frequencies of BH_3 based on an assumed geometry of BH_3, on data of compounds such as BH_3CO, on Badger's rule [7] and on an extrapolation in the series BBr_3, BCl_3, BF_3. The vibration frequencies given in the same paper are partially inconsistent with the force constants.

Morrey *et al.* [8] have studied the thermolysis of B_2H_6 by means of IR spectroscopy and found some absorption frequencies that they tentatively assigned to BH_3. The values of the two references [6, 8] do not agree at all.

2. Method

The computational method used is the same as in our previous studies [3–5], the IEPA-PNO method (IEPA = independent electron pair approximation, PNO = pair natural orbitals), the first step of which is always a conventional molecular Hartree-Fock-calculation. Then the canonical Hartree-Fock orbitals are transformed to localized ones and the pair correlation energies both for two electrons in the same orbital (intrapair correlation energy ε_{ii}) and for two electrons in different localized orbitals (interpair correlation energy ε_{ij}) are calculated independently. The sum of these pair correlation energies is regarded as an approximation to the total correlation energy. In this study we have not calculated the contributions to the correlation energy that involve the K-shell, since previous calculations (e.g. [5]) indicate that they remain invariant upon changes in geometry.

For BH_3 in D_{3h} or C_{3v} geometry there is only one type of localized valence-shell orbital, corresponding to one BH bond, and hence only one intrapair and one interpair correlation energy has to be calculated. In the case of an in-plane deformation the BH-bonds are no longer equivalent and several different intrapair and interpair correlation contribution have to be considered. Since the effect of correlation is small anyway we renounced on this extra labour and computed the in-plane deformation in Hartree-Fock approximation only.

The basis set of gaussian lobes is essentially the same as used in our study of B_2H_6 [3]. It consists of a 9s, 2p-Huzinaga basis with the contractions (5, 1, 1, 1, 1) and (2, 1) for boron and a 5s-Hoyland basis with the contraction (4, 1) for hydrogen. In each of three directions (x, y, z) on each hydrogen atom a p-group with $\eta = 0.65$ was added.

This basis is rather small, but supposed to be sufficient for the present purpose.

3. Potential Field and Force Constants

We first calculated the energy of BH_3 in D_{3h} geometry and varied the BH bond length (Table 1). The minimum was found for $R_0 = 2.248\,a_0 = 1.190$ Å in Hartree-Fock-approximation and for $R_0 = 2.253\,a_0 = 1.192$ Å if one includes

Table 1. Energy of BH_3 in D_{3h} geometry as function of the BH bond distance

R(in a_0)	2.05	2.15	2.25	2.35	2.45
$-E_{HF}$	26.36353	26.37779	26.38206	26.37813	26.36792
$-\varepsilon_{ii}$	0.02806	0.02802	0.02828	0.02836	0.02860
$-\varepsilon_{ij}$	0.00804	0.00794	0.00787	0.00784	0.00783
$-E$	26.47183	26.48567	26.49051	26.4867	26.47721

Table 2. Energy of BH_3 for $R = 2.25\ a_0$ as a function of the in plane – deformation of one BH bond

α	0^0	5^0	10^0
$-E_{HF}$	26.38206	26.38131	26.37908

Table 3. Energy of BH_3 for $R = 2.25\ a_0$ as a function of a simultaneous out-of-plane deformation of the three BH bonds (keeping C_{3v} symmetry)

γ	0°	5°	10°	15°
$-E_{HF}$	26.38206	26.37911	26.37016	26.35522
$-\varepsilon_{ii}$	0.02828	0.2826	0.02843	0.02872
$-\varepsilon_{ij}$	0.00787	0.00789	0.00799	0.00817
$-E$	26.49051	26.48756	26.47942	26.46588

correlation. Keeping R fixed at 2.25 a_0 we have then studied both an in-plane deformation (Table 2) and an out-of plane deformation (Table 3). In either case the minimum of the energy was found for the planar molecule with trigonal symmetry, i.e. BH_3 has in fact the symmetry group D_{3h}.

The potential hypersurface V of a planar AX_3 – molecule of this type can, in the neighbourhood of its equilibrium geometry, up to terms of 2nd order in the internal displacement coordinates be expressed as

$$\begin{aligned}2V = {} & 2E_0 + f_r(r_1^2 + r_2^2 + r_3^2) + 2f_{rr'}(r_1r_2 + r_2r_3 + r_1r_3)\\ & + f_\alpha R_0^2(\alpha_{12}^2 + \alpha_{23}^2 + \alpha_{13}^2) + 2f_{r\alpha} \cdot R_0(r_1 \cdot \alpha_{12}\\ & + r_2\alpha_{12} + r_2\alpha_{23} + r_3\alpha_{23} + r_3\alpha_{13} + r_1\alpha_{13})\\ & + 2f_{r\alpha'} \cdot R_0(r_1\alpha_{23} + r_2\alpha_{13} + r_3\alpha_{12})\\ & + 2f_{\alpha\alpha'} \cdot R_0^2(\alpha_{12}\alpha_{13} + \alpha_{12}\alpha_{23} + \alpha_{13}\alpha_{23})\\ & + f_\gamma \cdot R_0^2(\gamma_1^2 + \gamma_2^2 + \gamma_3^2) + 2f_{\gamma\gamma'}R_0^2(\gamma_1\gamma_2 + \gamma_2\gamma_3 + \gamma_1\gamma_3)\,.\end{aligned}$$

Here R_0 is the equilibrium BH-bond distance, r_i means the change in the length of the bond between B and the i-th H atom, the α_{ij} refer to in-plane deformation and γ_i to the out-of-plane deformation of the i-th BH-bond with respect to the original molecular plane. Due to reasons of symmetry (D_{3h}) and redudancy $\left(\sum_{i<j} \alpha_{ij} = 0\right)$ the different coefficients are not independent, but the following relations hold

$$f_\alpha = -2f_{\alpha\alpha'}$$
$$f_{r\alpha'} = -2f_{r\alpha}$$
$$f_\gamma = f_{\gamma\gamma'}\,.$$

An alternative expression of $2V$ is in terms of the symmetry-coordinates S_i

$$2V = 2E_0 + F_1 S_1^2 + F_2 S_2^2 + F_3(S_3^2 + S_3'^2) + 2F_{34}(S_3 S_4 + S_3' S_4') + F_4(S_4^2 + S_4'^2)$$

with

$$S_1(A') = \frac{1}{\sqrt{3}}(r_1 + r_2 + r_3),$$

$$S_2(A'') = \frac{1}{\sqrt{3}} R_0(\gamma_1 + \gamma_2 + \gamma_3),$$

$$S_3(E') = \frac{1}{\sqrt{2}}(r_1 - r_2),$$

$$S_3'(E') = \frac{1}{\sqrt{6}}(r_1 + r_2 - 2r_3),$$

$$S_4(E') = \frac{1}{\sqrt{2}} R_0(\alpha_{13} - \alpha_{23}),$$

$$S_4'(E') = \frac{1}{\sqrt{6}} R_0(2\alpha_{12} - \alpha_{13} - \alpha_{23}).$$

The force constants F_i for symmetry coordinates are related to the f_i for internal coordinates through

$$F_1 = f_r + 2f_{rr'},$$

$$F_2 = 3f_\gamma,$$

$$F_3 = f_r - f_{rr'},$$

$$F_{34} = 3f_{r\alpha},$$

$$F_4 = \tfrac{3}{2} f_\alpha.$$

The F_i constitute the elements of the Wilson F-matrix [9], in terms of symmetry coordinates, the corresponding G-matrix [9] elements are

$$G_1 = \frac{1}{m_H},$$

$$G_2 = \frac{1}{R_0^2}\left(\frac{1}{m_H} + \frac{3}{m_B}\right),$$

$$G_3 = \frac{1}{m_H} + \frac{3}{2m_B},$$

$$G_{34} = -\frac{3\sqrt{3}}{2R_0 \cdot m_B},$$

$$G_4 = \frac{3}{R_0^2}\left(\frac{1}{m_H} + \frac{3}{2m_B}\right).$$

S_1 and S_2 are automatically normal coordinates of A' and A'' symmetry respectively. The corresponding force constants F_1 and F_2 are obtained directly from the dependence of $2V$ on either of their symmetry coordinates (Tables 1 and 3).

The vibration frequencies ν_1 and ν_2 are given as

$$2\pi\nu_1^2 = \frac{F_1}{m_H},$$

$$2\pi\nu_2^2 = F_2\left(\frac{1}{m_H} + \frac{3}{m_B}\right).$$

The vibration frequencies ν_3 and ν_4 of E' symmetry are obtained from the eigenvalues $\lambda_i = 2\pi\nu_i^2$ of the product matrix

$$\begin{pmatrix} F_3 & F_{34} \\ F_{34} & F_4 \end{pmatrix} \cdot \begin{pmatrix} G_3 & G_{34} \\ G_{34} & G_4 \end{pmatrix}.$$

In order to calculate ν_3 and ν_4 one ought to compute first F_3, F_{34} and F_4 or alternatively f_r, $f_{rr'}$, $f_{r\alpha}$ and f_α. Previous calculations on BeH_2 [1] and BH_2 [10] indicated that the off-diagonal stretching force constants of molecules of this kind are very small in absolute value, namely

In SCF-approximation	With correlation	
$f_{rr'} = -0.04$ mdyn/Å	$= +0.12$ mdyn/Å	for BeH_2
$= +0.12$ mdyn/Å	-0.14 mdyn/Å	for BH_2 $(X\,^2A_1)$
$= -0.03$ mdyn/Å	-0.11 mdyn/Å	for BH_2 $(A\,^2B_1)$

compared to $f_r \approx 4$ mdyn/Å. We do not think that the calculated values of $f_{rr'}$ (note the occurence of a change in sign with inclusion of correlation) are really significient (i.e. beyond the error limits of the calculations) so that we decided to put $f_{rr'} = 0$ and consequently $F_3 = f_r = F_1$. Previous calculations [10] also suggest that $f_{r\alpha}$ should be very small

$$\begin{aligned} f_{r\alpha} &= 0.041 \text{ mdyn/Å} \quad \text{in SCF-approximation} \quad \text{for } BH_2(X\,^2A_1) \\ &= 0.054 \text{ mdyn/Å} \quad \text{with correlation} \quad \text{for } BH_2(X\,^2A_1). \end{aligned}$$

So we decided to put $f_{r\alpha} = 0$ as well. We calculated f_α from the dependence of the energy of BH_3 upon in-plane deformation of one BH-bond. The assumption $f_{rr'} = f_{r\alpha} = 0$, which seems to be well justified for BH_3 is, of course, known as the simple valence force field approximation. In order to be conform with the notation [12] of the valence force field model we introduce the force constants

$$\tilde{f}_\alpha = \tfrac{3}{2} f_\alpha \quad \text{and} \quad \tilde{f}_\gamma = 3 f_\gamma$$

rather than f_α and f_γ. For ν_3 and ν_4 one then obtains the wellknown [17] expressions

$$2\pi(\nu_3^2 + \nu_4^2) = \left(\frac{1}{m_H} + \frac{3}{2m_B}\right)(f_r + 3\tilde{f}_\alpha),$$

$$4\pi^2\nu_3^2\nu_4^2 = 3\left(\frac{1}{m_H^2} + \frac{3}{m_H m_B}\right) f_r \cdot \tilde{f}_\alpha.$$

In our calculation the approximation that consists in neglecting $f_{rr'}$ and $f_{r\alpha}$ has an effect only on the vibration frequencies of the E' species, the A' and A'' frequencies would not be altered if we introduced $f_{rr'}$ and $f_{r\alpha}$ explicitly.

For comparison with experiment, anharmonicity effects have, of course, to be dealt with as well.

4. Discussions of the Results

The calculated equilibrium distances and harmonic force constants of BH_3 (both in SCF approximation and with correlation) are tabulated and compared with previous estimates [6, 8] in Table 4.

The effect of correlation is very small. As it has been observed in other cases [10, 11] correlation increases the bond length slightly and diminishes somewhat the stretching force constant.

A direct comparison of our computed values with their experimental counterparts is not possible (even if they were precisely known) since our calculations refer to harmonic force constants and vibration frequencies, whereas the values deduced from observed spectra contain implicitly anharmonicity effects. Generally "anharmonic" force constants of XH-bonds are about 10% smaller than the corresponding harmonic ones, so our "harmonic" value of 4.1 mdyn/Å would be consistent with an "anharmonic" force constant of about 3.7 mdyn/Å which is in sufficient agreement with the value of 3.5 mdyn/Å generally assumed [12] for the stretching force constant of a terminal bond in B_2H_6.

If one has to choose between the two previous estimates [6, 8] our results would rather support the values of Morrey *et al.* [8].

Rather interesting is the comparison (Table 5) of BH_3 with BH [5], BH_2^+ [13] and BH_2 [11] for which quite reliable calculations are available (even if one has to bear in mind that the basis sets for the different molecules were of different quality). The decrease in bond length on going from BH to BH_2^+ can to a first approximation be understood in terms of hybridisation. The hybrid-AO of boron in BH is nearly a pure p-AO, in both BH_2 ($X\,^2A_1$) and in BH_3 it is roughly

Table 4. Harmonic force constants and vibration frequencies for $^{11}BH_3$

	R_0	f_r	$\tilde f_\alpha$	$\tilde f_\gamma$	$\nu_1(A')$	$\nu_2(A'')$	$\nu_3(E')$	$\nu_4(E')$
	in a_0	in mdyn/Å				in cm^{-1}		
Hartree Fock	2.248	4.26	0.30	0.80	2680	1310	2860	1300
With correlation	2.253	4.10	–	0.75	2620	1270	2810	1300
Ref. [6][a]	2.19	3.38	0.13	0.30	2384	801	(2976)	(1735)
Ref. [8]	–	3.41	0.25	1.13	2400	1560	2560	1190
		±0.78	±0.04	±0.04	± 300	± 50	± 100	± 10

[a] The frequencies in parentheses are inconsistent with the force constants given by the same authors.

Table 5. Comparison of the harmonic force constants in different boron hydrides (the first entry is always without, the second with correlation)

	R_0	f_r	$\tilde{f}_\alpha$	$\tilde{f}_\gamma$
	(in a_0)	in mdyn/Å		
BH	2.311; 2.316	3.33; 3.19	–	
$BH_2(X^2A_1)$	2.234; 2.276	3.96; 3.70	0.32; 0.27	–
BH_3	2.248; 2.253	4.26; 4.10	0.30;	0.80; 0.75
$BH_2(A^2B_1)$	2.196; 2.223	4.65; 4.57	0.28; 0.25	
BH_2^+	; 2.221	; 4.17	; 0.27	

sp^2 and in both BH_2 ($A\,{}^2B_1$) and BH_2^+ it is sp. In the order $p \rightarrow sp^3 \rightarrow sp^2 \rightarrow sp$ the bond strength is known to increase which implies a decrease in bond length and an increase in the force constant. In fact the stretching force constants behave in the expected way. The bending force constants are almost the same for BH_3 and the lowest state of BH_2 ($X\,{}^2A_1$, with an equilibrium angle of 129°). The force constant (~ 0.8 mdyn/Å) for an out-of plane deformation in BH_3 is rather large.

It is hard to give error estimates for the calculated values. There are too many sources for possible errors. The neglect of $f_{rr'}$ and $f_{r\alpha}$ is probably the least harmful. More serious is the limatation of the basis set. There is some evidence that with small basis sets, configurations of high symmetry are represented more poorly than those of lower symmetry. So extension of the basis may lower the energy more strongly for the equilibrium than for distorted geometry and hence increase the force constants for angular deformation. Another source of error is the fact that IEPA is only an approximation and that the deviations from additivity of the pair correlation energies may depend on geometry. This point has recently been stressed by Meyer [14]. A really refined calculation of the vibrational spectrum should also consider the cubic and quartic terms in the potential and their influence on the vibration frequencies. We do not think that (except for diatomic molecules) the present state of numerical quantum chemistry is such as to encourage one to do the extra labour.

5. The Zero-Point Energy

The original motive for this study was the need for a reliable value of the zero point of BH_3 to calculate the dimerization energy to B_2H_6 [3]. From the harmonic vibration frequencies we obtain 17.3 kcal/mole which is very close to the value of 18 kcal/mole estimated by us [3] on more heuristic grounds.

Acknowledgement. The work reported here has been sponsored in part by Deutsche Forschungsgemeinschaft and by Fonds der Chemie.

Most of the computations were performed at the IBM 360/75 of C.I.R.C.E. (Orsay) with grants given by CNRS to the laboratoire de chimie generale in Grenoble. Some computation was carried out at the UNIVAC 1108 of the University of Karlsruhe.

The authors are grateful to R. Ahlrichs and V. Staemmler for contributions and comments.

References

1. Ahlrichs, R., Kutzelnigg, W.: Theoret. chim. Acta (Berl.) **10**, 377 (1968).
2. Johnson, H. D., Shore, S. G.: Fortschr. Chem. Forsch. **15**, 87 (1970).
3. Gelus, M., Ahlrichs, R., Staemmler, V., Kutzelnigg, W.: Chem. Physics Letters **7**, 503 (1970).
4. Jungen, M., Ahlrichs, R.: Theoret. chim. Acta (Berl.) **17**, 348 (1970).
5. Gelus, M., Ahlrichs, R., Staemmler, V., Kutzelnigg, W.: Theoret. chim. Acta (Berl.) **21**, 63 (1971).
6. Shepp, A., Bauer, S. H.: J. Amer. chem. Soc. **76**, 265 (1954).
7. Badger, R. M.: J. chem. Physics **2**, 128 (1934).
8. Morrey, J. R., Johnson, A. B., Fu, Y., Mill, G. R.: Advances chem. Ser. **32**, 157 (1961).
9. Wilson, E. B., Decius, J. C., Cross, P. C.: Molecular vibrations. New York: Mc Graw Hill 1955.
10. Staemmler, V., Jungen, M.: Chem. Physics Letters **16**, 187 (1972).
11. Herzberg, G.: Molecular spectra and molecular structure, Vol. II: Infrared and raman spectra of polyatomic molecules. Princeton: van Nostrand 1945.
12. Venkateswarlu, K., Thiruganasambandam, D.: Proc. Indian Acad. Sci. A **48**, 344 (1958).
13. Jungen, M.: Chem. Physics Letters **5**, 241 (1970).
14. Meyer, W.: J. chem. Physics: in press.

Dr. W. Kutzelnigg
Institut für Physikalische Chemie
und Elektrochemie der Universität Karlsruhe
D-7500 Karlsruhe
Kaiserstr. 12
Federal Republic of Germany

Theoret. chim. Acta (Berl.) 28, 111–120 (1973)
© by Springer-Verlag 1973

An Application of RPA Theory to Conjugated Systems in the Excited States

Kazuo Kitaura and Kichisuke Nishimoto

Department of Chemistry, Osaka City University, Sumiyoshi-Ku, Osaka, Japan

Received May 19, 1972

RPA theory has been applied to the calculations of the electronic spectra of some conjugated systems, considering only π-electrons explicitly. Electron repulsion integrals have been calculated using Slater AO's with appropriate orbital exponents. The present calculation shows that the correlation effect between π-electrons is rather small for the lowest $\pi-\pi^*$ transitions. Good results have been obtained, when we calculate the electron repulsion integrals using orbital exponents evaluated by Slater rule. "Effective" electron interaction in the excited states has been discussed, using the calculated results. The calculated oscillator strengths were considerably improved by RPA.

Die RPA wurde auf die Berechnung der UV-Spektren des π-Elektronensystems konjugierter Moleküle angewendet, wobei die Coulombintegrale für Slaterorbitale mit Exponenten gemäß der Slaterregeln ermittelt wurden. Es zeigt sich, daß die Korrelationseffekte für die tieferen Übergänge ziemlich gering sind und daß sich insbesondere die Oszillatorenstärken sehr gut ergeben. Schließlich wurden eine effektive Elektronenwechselwirkung in angeregten Zuständen diskutiert.

La théorie RPA fondée sur l'équation du mouvement a été appliquée à des calculs de la structure électronique et des spectres de systèmes conjugués en ne considérant explicitement que les électrons π. Les intégrales de répulsion électronique ont été calculées en utilisant des OA de Slater avec des exposants orbitaux appropriés. Nos calculs montrent que les effets de corrélation entre électrons π sont plutot faibles pour les plus basses transitions π - π^*. De bons résultats ont été obtenus en calculant les intégrales de répulsion électronique en utilisant les exposants orbitaux évalués par la règle de Slater. L'interaction électronique «effective» dans les états excités est discutée sur la base des résultats obtenus.

1. Introduction

Electron correlation must be very important in many electron systems. It is well known in many body technique [1] that electron correlation can be treated by RPA (random phase approximation) and ladder approximation methods. For high density electron systems, such as atoms and molecules, we can, however, neglect ladder diagrams [1]. In order to clarify the electron correlation, Gutfreund and Little [2, 3] calculated the screened potential in the π-electron systems by means of RPA method. Their theory leads to some interesting results. However, their theory includes an ambiguity in the calculation of effective interaction between excited configurations. In this paper, we use another RPA formula, which was recently derived by Dunning and McKoy [4] from the equations of motion method for the non-empirical calculation of excited molecules[1]. The RPA is a low-order approximation to the equations of motion, however it calculates directly the excitation energies. This method is applied to the calculations of the electronic spectra of benzene, benzene-N-heterocycles, and naphthalene, using ZDO (zero differential overlap) approximation. In the present method, only the correlation effect of π-electrons on the $\pi - \pi^*$ transitions is considered. Namely, the ground state electronic structure of the molecule is assumed to be unchanged.

---

[1] The same RPA equation was derived by McLachlan and Ball from the time-dependent Hartree-Fock theory [Rev. mod. Physics 36, 844 (1964)].

2. Method

RPA equation can be derived from either of the following theories;

1. Time-dependent Hartree-Fock theory
2. The particle-hole Green's function method
3. Equations of motion method.

Starting from the equations of motion, a RPA equation was derived by the following manner [4]; the total Hamiltonian may be written as, in atomic units,

$$\begin{aligned} \boldsymbol{H} &= \sum_i \left[(-1/2)\,\Delta_i - \left(\sum_\alpha Z_\alpha/r_{\alpha i}\right)\right] + (1/2)\sum_i\sum_j (1/r_{ij}) \\ &= \sum_i H_i + (1/2)\sum_i\sum_j v_{ij}\,. \end{aligned} \tag{1}$$

In the Hartree-Fock approximation, we replace the electron interaction term by an effective one particle potential V_i. Therefore, Eq. (1) can be expressed as,

$$\boldsymbol{H} = \sum_i (\boldsymbol{H}_i + V_i) + \sum_i \left((1/2)\sum_j v_{ij} - V_i\right). \tag{2}$$

SCF MO is the eigenfunction of the following Hartree-Fock equation

$$(\boldsymbol{H} + V)|i\rangle = \varepsilon_i|i\rangle\,. \tag{3}$$

In the notation of second quantization, Eq. (2) is represented by

$$\boldsymbol{H} = \sum_i \varepsilon_i \boldsymbol{a}_i^+ \boldsymbol{a}_i + (1/2)\sum_{ijkl} V_{ijkl}\boldsymbol{a}_j^+ \boldsymbol{a}_i^+ \boldsymbol{a}_k \boldsymbol{a}_l - \sum_{jk\beta}(V_{\beta j\beta k} - V_{\beta jk\beta})\,\boldsymbol{a}_j^+ \boldsymbol{a}_k\,. \tag{4}$$

The operators $\boldsymbol{a}_i^+$ and $\boldsymbol{a}_i$ are the creation and annihilation operators. The integral V_{ijkl} is defined by

$$V_{ijkl} = \int \psi_i^*(1)\,\psi_j^*(2)\,(1/r_{12})\,\psi_k(1)\,\psi_l(2)\,d\tau\,.$$

The ψ_i denotes the molecular spin orbital. In this equation and the ones to follow, we denote by the subscripts

$\alpha,\beta,\gamma,\delta$ ... single particle states occupied in the Hartree-Fock ground state (i.e., hole states)

m,n,p,q ... single particle states unoccupied in the Hartree-Fock ground state (i.e., particle states)

i,j,k,l ... any states (either particle or hole).

Let us define an excitation operator $A^+(E)$. This operator generates an excited state $|E\rangle$, of the Hamiltonian $\boldsymbol{H}$, with excitation energy ΔE, when it operates on the ground state $|0\rangle$, i.e.,

$$A^+(E)\,|0\rangle = |E\rangle\,. \tag{5}$$

The problem is to solve the following equation of motion

$$[H, A^+(E)]\,|0\rangle = \Delta E\, A^+(E)\,|0\rangle\,. \tag{6}$$

Using the commutation rules for a_i^+, a_i, Eq. (6) can be easily rewritten as

$$(E-E_0)\,\langle 0|\,[A(E), a_m^+ a_\alpha]\,|0\rangle - \langle 0|\,\{A(E), [H, a_m^+ a_\alpha]\}\,|0\rangle = 0 \tag{7}$$

$$\begin{aligned}[H, a_m^+ a_\alpha] = {} & (\varepsilon_m - \varepsilon_\alpha + V_{m\alpha\alpha m} - V_{m\alpha m\alpha})\, a_m^+ a_\alpha \\ & + \sum_{(n\beta)}{}' (V_{\alpha nm\beta} - V_{\alpha n\beta m})\, a_m^+ a_\beta + \sum_{(n\beta)} (V_{\alpha\beta mn} - V_{\alpha\beta nm})\, a_\beta^+ a_m\,.\end{aligned} \tag{8}$$

In RPA theory, we must consider de-excitation processes, $a_\alpha^+ a_m$, in addition to the usual singly excitation processes, $a_m^+ a_\alpha$. This means that RPA theory takes the doubly excited configurations included in the true ground state into consideration. Therefore, a better approximation to excitation operator, $S^+(E)$, would be

$$S^+(E) = \sum_{(m\alpha)} [g(m\alpha{:}E)\, a_m^+ a_\alpha - h(m\alpha{:}E)\, a_\alpha^+ a_m]\,. \tag{9}$$

Using Eq. (9), Eq. (7) becomes

$$(E-E_0)\,\langle 0|\,[S(E), a_m^+ a_\alpha]\,|0\rangle - \langle 0|\,\{S(E), [H, a_m^+ a_\alpha]\}\,|0\rangle = 0\,. \tag{10}$$

Using the commutators for a_i^+, a_i we get the set of equations from which the eigenfunctions for excited states and the corresponding excitation energies can be obtained,

$$\begin{aligned}(\varepsilon_m - \varepsilon_\alpha + V_{m\alpha\alpha m} - V_{m\alpha m\alpha} - (E-E_0)]\, g(m\alpha) & \\ + \sum_{(n\beta)}{}' (V_{\alpha nm\beta} - V_{\alpha n\beta m})\, g(n\beta) + \sum_{(n\beta)} (V_{\alpha\beta mn} - V_{\alpha\beta nm})\, h(n\beta) = 0\,, &\end{aligned} \tag{11}$$

where $g(m\alpha)$ and $h(n\beta)$ are the coefficients to be determined. In the present calculation, ZDO (zero differential overlap) approximation is used.

For the RPA, the transition moment is

$$^1D_{\mathrm{RPA}} = -\sqrt{2}\,\Sigma(g(m\alpha) + h(m\alpha))\, d_{m\alpha}\,,$$

where

$$d_{m\alpha} = \int \psi_m^*(1)\, r\, \psi_\alpha(1)\, d\tau\,.$$

The oscillator strength f is defined by

$$f = 0.0875 \times \Delta E \times |D|^2\,, \tag{12}$$

where ΔE is the calculated excitation energy in unit of eV.

For the evaluation of electron repulsion integrals, many approximations have been proposed [5]. In the present study, we would like to elucidate the correlation effect between π-electrons by RPA. For this purpose, it may be better to calculate the electron repulsion integral,

$$\gamma_{\mu\nu} = \int \varphi_\mu^2(1)\,(1/r_{12})\,\varphi_\nu^2(2)\, d\tau\,,$$

where φ_μ is the $2p\pi$ AO associated with μ-th atom, by the theoretical procedure than the semi-empirical estimation. Thus, we calculate $\gamma_{\mu\nu}$ using Slater AO's [6] with appropriate orbital exponents, ζ.

ζ's are estimated by the following three ways;

Case 1. ζ is calculated by the Slater rule [6], i.e., 1.625 for carbon and 1.95 for nitrogen.

Case 2. For one center integral $\gamma_{\mu\mu}$, ζ_μ is estimated as to reproduce the value of Pariser-Parr approximation [7],

$$\gamma_{\mu\mu} = I_\mu - A_\mu .$$

For the calculation of two center $\gamma_{\mu\nu}$'s, the values of ζ's are assumed to be same with the Case 1. It will be able to take some part of correlation effect by semi-empirical or empirical estimations of basic integrals over AO's into consideration. Pariser and Parr [7] estimated the $\gamma_{\mu\mu}$'s semi-empirically, and the two center $\gamma_{\mu\nu}$'s in the range of distance of $2.8\,A \geqq r > 0A$ by a empirical quadratic equation. In order to examine the effect of electron correlation in atoms on the molecular electronic spectra, we calculate one center $\gamma_{\mu\mu}$'s by semi-empirical procedure by this case.

Case 3. ζ's are estimated by Pariser-Parr approximation. They can be obtained by a relation

$$\zeta_\mu = \frac{(I_\mu - A_\mu)\,(\text{in eV})}{10.648} .$$

Calculated ζ's are 1.045 for carbon and 1.159 for nitrogen, respectively. Slater rule was proposed for the semi-quantitative explanation of atomic spectra [6]. There is no valence state in a free atom. Therefore, it will be, to a first approximation, able to assign same value of ζ for *ns* and *np* AO's. In a molecule, each atoms would be in an appropriate hybridization state, so that ζ for a $2p\pi$AO may differ from that for a σ-type AO. When we assume that we can estimate a proper ζ for $2p\pi$AO by Pariser-Parr approximation, it is reasonable to use such ζ's for the calculation of all $\gamma_{\mu\nu}$'s.

For the valence state energies, we used the experimental values given by Hinze and Jaffe [8]. That is, $2p\pi$ ionization potentials are 11.16 eV for carbon and 14.12 eV for nitrogen, respectively. The values of valence state electron affinities are 0.03 eV for carbon and 1.78 eV for nitrogen, respectively.

For a simplicity, all of two center core integrals,

$$\beta_{\mu\nu} = \int \varphi_\mu(1)\, H_{\text{core}}\, \varphi_\nu(1)\, d\tau ,$$

and bond distances are assumed to be -2.4 eV and 1.4 Å.

The procedure of calculation is as follows; Firstly, we calculate SCF MO's by conventional Hartree-Fock scheme using ZDO approximation. Secondly, we construct all possible singly excited configurations. The excited state of molecule can be expressed by the linear combinations of these configurations. So that, we must diagonalize the configuration interaction matrix of *m* order and then obtain the excited state energies and state functions by this procedure. In the Tables, we denote this type calculation by SECI (singly excited configuration interaction). Thirdly, we may perform the RPA calculation considering the same number of de-excitation processes. Therefore, RPA matrix to be solved in the present calculation should be $2m \times 2m$ in dimension.

RPA matrix is usually not Hermite, so that the coefficients in Eq. (11), $g(m\alpha)$ and $h(m\alpha)$'s, have to be normalized differently, by the following relation,

$$\Sigma[g(m\alpha;E)\,g(m\alpha;E')-h(m\alpha;E)\,h(m\alpha;E')]=\pm\delta_{EE'}, \qquad (13)$$

where $g(m\alpha;E)$ and $h(m\alpha;E)$ mean the coefficients associated with an excited state $|E\rangle$.

3. Results and Discussion

One of the most important problems in the calculation of electronic spectra of a molecule is the estimation of electron repulsion integrals. In Table 1, $\gamma_{\mu\nu}$'s calculated by various approximations are summarized. It is interesting to note that the values of $\gamma_{\mu\nu}$'s of Case 3 are rather close to those of Pariser's, except only γ_{12}.

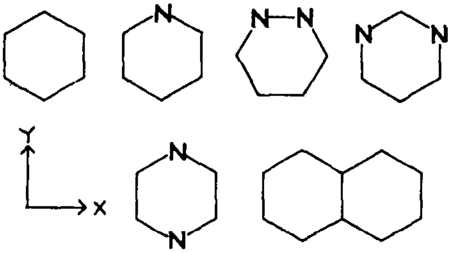

Fig. 1. Molecular frameworks

Table 1. Calculated electron repulsion integrals for benzene (in eV)

Distance (in Å)	Case 1	Case 2	Case 3	Pariser[a]	Nishimoto-Mataga[b]
0	17.277	(11.13)	(11.13)	10.959	(11.13)
1.4	9.040	9.040	7.770	6.895	5.345
2.425	5.655	5.655	5.332	5.682	3.872
2.8	4.953	4.953	4.730	4.978	3.517

[a] Ref. [9].
[b] Ref. [10].

Electronic Spectra

Calculated results for singlet $\pi-\pi^*$ transitions are summarized in Tables 2, 3, and 4. As seen from these Tables, RPA theory based on Case 1 calculates excellent results of transition energies from the ground state to the two lowest excited states of benzene and benzene-N-heterocycles. Furthermore, the calculated oscillator strength is remarkably improved by RPA method. Namely, usual SECI theory calculates almost of twice value compared with observed ones, whereas RPA theory calculates the oscillator strengths very close to experimental values. This great deduction of oscillator strength by RPA is due to a contribution of de-excitation processes which correspond to the de-excitation of the doubly excited components of the true ground state.

Table 2 Transition energies (ΔE in eV) and intensities (f) of benzene[a]

State	Case 1		Case 2		Case 3		Obs.	Ref.
	SECI	RPA	SECI	RPA	SECI	RPA		
$^1B_{2u}$	5.13(0)	4.84(0)	5.13(0)	4.84(0)	5.01(0)	4.86(0)	4.9 (–)	[11]
$^1B_{1u}$	6.16(0)	6.10(0)	3.51(0)	2.82(0)	4.82(0)	4.77(0)	6.07(.1)	[12]
	13.42(0)	13.36(0)	12.96(0)	12.96(0)	12.14(0)	12.14(0)		
$^1E_{1u}$	9.11(3.125)	8.03(1.450)	8.08(2.771)	7.38(1.548)	7.48(2.567)	6.99(1.537)	6.95	[12]
$^1E_{2g}$	10.04(0)	9.63(0)	7.98(0)	7.94(0)	8.31(0)	8.23(0)		
	10.26(0)	10.25(0)	10.26(0)	10.25(0)	9.43(0)	9.43(0)		

[a] The oscillator strengths are given in brackets.

Table 3. Transition energies (ΔE in eV) and intensities (f) of benzene N-heterocycles

State	Case 1		Case 2		Case 3		Obs.	Ref
	SECI	RPA	SECI	RPA	SECI	RPA		
				Pyridine				
$^1B_2$	5.14(0.005)	4.85(0.004)	5.26(0.067)	5.05(0.059)	4.94(0.072)	4.80(0.063)	4.9 (–)	[11]
	9.13(1.552)	8.05(0.719)	8.03(0.449)	7.70(0.618)	7.53(1.135)	7.11(0.689)	7.22 (–)	[12]
	10.01(0)	9.63(0)	8.37(0.650)	8.20(0.084)	8.36(0.002)	8.28(0.001)		
	10.32(0.004)	10.29(0.001)	10.59(0.008)	10.58(0.009)	9.48(0.018)	9.47(0.010)		
$^1A_1$	6.32(0.005)	6.24(0.004)	4.33(0.002)	3.96(0.002)	5.15(0.002)	5.12(0.002)	6.17(0.2)	[12]
	9.25(1.465)	8.15(0.709)	7.96(0.922)	7.51(0.741)	7.46(1.206)	7.01(0.754)	7.22(–)	[12]
	10.31(0.054)	9.89(0.010)	8.48(0.301)	8.37(0.049)	8.47(0.042)	8.37(0.011)		
	10.50(0.066)	10.34(0)	10.81(0.002)	10.80(0)	9.58(0.002)	9.57(0.001)		
	13.53(0.002)	13.45(0)	13.25(0)	13.25(0)	12.23(0)	12.23(0)		
				Pyridazine				
$^1A_1$	5.15(0.004)	4.85(0.004)	5.03(0.060)	4.73(0.050)	4.94(0.055)	4.78(0.049)	5.00(–)	[11]
	9.38(1.451)	8.22(0.704)	8.07(0.296)	7.60(0.655)	7.64(1.169)	7.16(0.699)	7.32(0.5)	[13]
	10.19(0.044)	9.78(0.008)	8.43(1.024)	8.13(0.041)	8.50(0.029)	8.41(0.005)		
	10.48(0.119)	10.36(0.005)	10.57(0.025)	10.55(0.008)	9.69(0.039)	9.66(0.014)		
$^1B_2$	6.45(0.004)	6.36(0.004)	3.65(0)	3.05(0)	5.03(0)	5.00(0)	6.39(0.1)	[13]
	9.18(1.500)	8.08(0.711)	7.91(0.705)	7.35(0.703)	7.39(1.212)	6.91(0.745)	7.32(0.5)	[13]
	10.35(0.034)	10.02(0.007)	8.28(0.652)	8.09(0.042)	8.43(0.040)	8.33(0.010)		
	10.63(0.047)	10.35(0.002)	10.26(0.018)	10.25(0.006)	9.44(0.017)	9.43(0.008)		
	13.66(0.002)	13.56(0)	13.36(0)	13.36(0)	12.45(0)	12.45(0)		
				Pyrimidine				
$^1B_2$	5.15(0.005)	4.86(0.004)	5.73(0.083)	5.60(0.074)	5.09(0.076)	4.96(0.067)	5.16(–)	[11]
	9.30(1.413)	8.21(0.701)	8.34(0.813)	8.05(0.624)	7.71(1.089)	7.32(0.686)	7.40(0.5)	[13]
	10.38(0.041)	10.03(0.016)	8.93(0.133)	8.87(0.040)	8.62(0.036)	8.54(0.009)		
	10.71(0.142)	10.41(0)	11.57(0)	11.57(0.001)	9.91(0)	9.91(0)		
$^1A_1$	6.52(0.006)	6.42(0.006)	5.47(0.006)	5.30(0.006)	5.41(0.005)	5.39(0.005)	6.42(0.16)	[13]
	9.22(1.522)	8.11(0.712)	8.25(0.870)	7.97(0.671)	7.51(1.117)	7.12(0.724)	7.40(0.5)	
	10.17(0.030)	9.76(0.003)	8.60(0.072)	8.56(0.019)	8.45(0.003)	8.38(0.001)		
	10.41(0.003)	10.34(0.001)	11.03(0.008)	11.03(0.010)	9.61(0.015)	9.60(0.012)		
	13.61(0.001)	13.52(0)	13.47(0.001)	13.47(0.001)	12.34(0)	12.34(0)		

Table 3 (Continued)

Case 1		Case 2		Case 3		Obs.	Ref.
SECI	RPA	SECI	RPA	SECI	RPA		
			Pyrazine				
5.13(0.020)	4.82(0.018)	4.84(0.219)	4.50(0.165)	4.71(0.217)	4.50(0.172)	4.77(–)	[11]
9.20(1.557)	8.10(0.707)	8.73(1.168)	8.11(0.581)	7.98(1.063)	7.56(0.595)	7.65(0.5)	[13]
6.47(0.021)	6.37(0.020)	3.73(0.003)	3.16(0.003)	5.10(0.010)	5.07(0.010)	6.33(0.145)	[13]
9.59(1.593)	8.34(0.695)	8.28(1.350)	7.57(0.733)	7.66(1.240)	7.17(0.744)	7.65(0.5)	[13]
13.62(0.006)	13.53(0)	13.26(0)	13.26(0)	12.32(0)	12.31(0)		
9.92(0)	9.58(0)	7.81(0)	7.78(0)	8.13(0)	8.06(0)		
10.44(0)	10.37(0)	10.62(0)	10.61(0)	9.76(0)	9.75(0)		
10.29(0)	10.01(0)	8.09(0)	8.04(0)	8.32(0)	8.24(0)		
10.84(0)	10.53(0)	10.89(0)	10.89(0)	10.01(0)	9.99(0)		

Table 4. Transition energies and intensities of naphthalene

Case 1		Case 2		Case 3		Obs.	Ref.
SECI	RPA	SECI	RPA	SECI	RPA		
4.39(0)	4.07(0)	4.39(0)	4.07(0)	4.28(0)	4.10(0)	3.97(0.002)	[14]
7.45(2.538)	6.73(1.350)	6.87(2.563)	6.34(1.447)	6.45(2.370)	6.04(1.445)	5.63(1.70)	[14]
9.81(0)	9.52(0.065)	8.18(0.002)	8.09(0.001)	8.23(0.044)	8.15(0.021)		
10.04(0.314)	9.80(0)	9.81(0)	9.80(0)	9.03(0)	9.03(0)		
11.07(0)	11.06(0)	11.07(0)	11.06(0)	10.10(0)	10.09(0)		
11.87(0.039)	11.87(0.017)	11.86(0.023)	11.86(0.014)	10.78(0.029)	10.77(0.019)		
5.00(0.100)	4.87(0.099)	2.91(0.050)	1.76(0.034)	4.00(0.107)	3.87(0.097)	4.51(0.18)	[14]
7.73(0.523)	7.19(0.437)	7.02(0.664)	6.51(0.480)	6.61(0.676)	6.26(0.469)	6.51(0.21)	[14]
9.64(1.518)	9.16(0.610)	8.50(0.559)	8.38(0.423)	8.43(1.032)	8.25(0.591)	7.44(0.8)	[15]
10.79(0.243)	10.30(0.005)	9.35(0.832)	9.07(0.201)	9.13(0.178)	9.00(0.020)		
11.10(0)	11.10(0)	11.10(0)	11.10(0)	10.27(0)	10.27(0)		
12.56(0.034)	12.52(0.006)	12.23(0.044)	12.21(0.012)	11.41(0.022)	11.40(0.007)		
15.95(0.002)	15.93(0.002)	15.80(0.001)	15.80(0.001)	14.56(0.002)	14.55(0.002)		
6.38(0)	6.25(0)	6.38(0)	6.25(0)	6.13(0)	6.06(0)		
8.85(0)	8.66(0)	7.25(0)	7.16(0)	7.50(0)	7.37(0)		
8.88(0)	8.84(0)	8.85(0)	8.30(0)	8.12(0)	7.84(0)		
10.15(0)	8.97(0)	8.92(0)	8.84(0)	8.24(0)	8.11(0)		
12.17(0)	12.03(0)	11.60(0)	11.58(0)	10.89(0)	10.87(0)		
13.01(0)	13.01(0)	13.01(0)	13.01(0)	11.92(0)	11.92(0)		
6.97(0)	6.71(0)	4.71(0)	4.58(0)	5.45(0)	5.40(0)		
7.35(0)	7.35(0)	7.35(0)	7.35(0)	6.72(0)	6.71(0)		
9.30(0)	8.84(0)	8.18(0)	7.90(0)	8.88(0)	7.71(0)		
9.81(0)	9.80(0)	9.81(0)	9.80(0)	9.05(0)	9.04(0)		
13.23(0)	13.16(0)	12.87(0)	12.87(0)	12.02(0)	12.01(0)		
15.20(0)	15.20(0)	15.20(0)	15.20(0)	13.85(0)	13.85(0)		

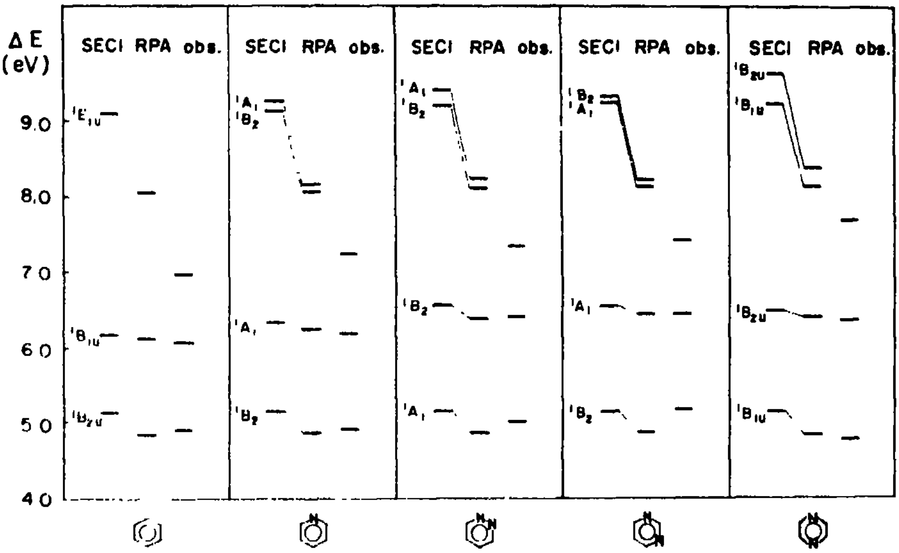

Fig. 2. Energy levels of benzene and benzene N-heterocycles (Case 1)

In the calculation of Case 2, we obtained extremely unsatisfactory results of the transition energies from the ground state to the second lowest excited states, which are polarized to the direction of molecular y axis. The reason for this may be ascribed to the fact that transition energy of $^1B_{1u}$ species is mainly determined by a difference of $(\gamma_{11} - \gamma_{12})$ (see Eq. (14)). In Case 2, $\gamma_{11} - \gamma_{12}$ is extremely small compared with other two cases.

RPA theory of Case 3 calculates rather good results for the energies of the first and third lowest excited states. However, the results for second lowest excited states are unsatisfactory.

It will be meaningful to estimate effective interactions between π-electrons in tions is generally large, whereas that of the second transitions is rather small.

Correlation Effect and "Effective" $\gamma_{\mu\nu}$'s

It will be meaningful to estimate effective interactions between π-electrons in the excited states. When we consider only four lowest singly excited configurations (4CI) in benzene, the transition energies can be expressed as follows in ZDO approximation;

$$\begin{aligned} \Delta E(^1B_{2u}) &= -2\beta + (1/6)(\gamma_{12} - 3\gamma_{13} + 2\gamma_{14}) \\ \Delta E(^1B_{1u}) &= -2\beta + (1/6)(2\gamma_{11} - 5\gamma_{12} + 7\gamma_{13} - 4\gamma_{14}) \qquad (14) \\ \Delta E(^1E_{1u}) &= -2\beta + (1/6)(\gamma_{11} + 4\gamma_{12} - 4\gamma_{13} - \gamma_{14}) \,. \end{aligned}$$

In the RPA calculation, we have to consider the corresponding four de-excitation processes. The calculated results based on 4CI using $\gamma_{\mu\nu}$'s of Case 1 are given in Table 5. In this paper, we assume the transition energies of benzene calculated

Table 5. Transition energies and intensities of benzene (2)

State	Case 1	
	4CI	RPA
$^1B_{1u}$	5.130(0)	4.843(0)
$^1B_{2u}$	6.322(0)	6.320(0)
$^1E_{1u}$	9.111(3.125)	8.026(1.450)

by RPA theory can be given by the same equations with Eq. (14) and define the corresponding $\gamma_{\mu\nu}$'s as "effective" electron repulsion integrals, $\gamma_{\mu\nu}^{\text{eff}}$'s. Then, we can easily obtain, from Table 5,

$$\gamma_{11}^{\text{eff}} - \gamma_{12}^{\text{eff}} = 6.040\,\text{eV}$$

$$\gamma_{12}^{\text{eff}} - \gamma_{13}^{\text{eff}} = 2.445\,\text{eV}$$

$$\gamma_{13}^{\text{eff}} - \gamma_{14}^{\text{eff}} = 1.093\,\text{eV}.$$

When we assign 4.953 eV for the value of γ_{14}^{eff}, we obtain

$$\gamma_{11}^{\text{eff}} = 14.531(17.277)\,\text{eV}$$

$$\gamma_{12}^{\text{eff}} = 8.491(\ 9.040)\,\text{eV}$$

$$\gamma_{13}^{\text{eff}} = 6.046(\ 5.655)\,\text{eV}$$

where, for a comparison, the corresponding theoretical values are given in the brackets. That is, γ_{11} and γ_{12} are respectively decreased by 2.75 eV and 0.55 eV, whereas that of γ_{13} is increased by 0.39 eV by correlation effect at the low lying excited states. This fact indicates that there is a rather complicated many body interactions, such as induced polarization in electron cloud suggested in the previous paper [16]. The excited singlet states involve large amounts of ionic structures, in terminology of valence bond theory. Therefore, an effect of electron correlation on γ_{11} should be quite large. This may be a reason why γ_{11}^{eff} is decreased remarkably at the excited states.

In order to make further improvement of the present calculation, it should be considered the following problems; 1. The effect of $\sigma - \pi$ interactions on $\gamma_{\mu\nu}$'s must be taken into account. 2. Two center core integral $\beta_{\mu\nu}$ should be varied with the change in the interatomic distance. 3. $\gamma_{\mu\nu}$'s should be calculated using the interatomic distances in the equilibrium positions in each molecules. In the next papers, we will study the above mentioned problems.

Acknowledgement. We are grateful to the Computer Center of University of Kyoto for providing machine time.

References

1. Mattuck, R. G.: A guide to Feynman diagrams in the many body problems. New York: MacGraw-Hill
2. Gutfreund, H., Little, W. A.: Physic. Rev. 183, 68 (1969).
3. Gutfreund, H., Little, W. A.: J. chem. Physics 50, 4468, 4478 (1969).
4. Dunning, H. T., McKoy, V.: J. chem. Physics 47, 1735 (1967).
5. Parr, R. G.: The quantum theory of molecular electronic structure. New York: W. A. Benjamin 1963.

6. Slater, J. C.: Physic. Rev. **36**, 51 (1930).
7. Pariser, R., Parr, R. G.: J. chem. Physic. **21**, 767 (1953).
8. Hinze, J., Jaffe, H. H.: J. Amer. chem. Soc. **84**, 540 (1962).
9. Pariser, R.: J. chem. Physics **24**, 324 (1956).
10. Nishimoto, K., Mataga, N.: Z. physik. Chem. (Frankfurt) **12**, 335 (1957).
11. Halverson, F., Hirt, R. C.: J. chem. Physics **19**, 711 (1951).
12. El-Sayed, M. A.: J. chem. Physics **36**, 552 (1962).
13. Parkin, J. E., Innes, K. K.: J. molecular Spectroscopy **15**, 407 (1965).
14. Murrell, J. N.: The theory of the electronic spectra of organic molecules. London: Methuen 1963.
15. Mann, D. E., Platt, J. R., Klevens, H. B.: J. chem. Physics **17**, 481 (1949).
16. Nishimoto, K.: Theoret. chim. Acta (Berl.) **7**, 207 (1967).

Prof. Dr. K. Nishimoto
Department of Chemistry
Osaka City University
Sumiyoshi-ku, Osaka
Japan

Theoret. chim. Acta (Berl.) 28, 121—140 (1973)
© by Springer-Verlag 1973

Wellenfunktionen und Terme des Systems Atom/zweiatomiges Molekül bei großen intermolekularen Abständen

E. E. Nikitin und S. Ja. Umanskij

Institut für chemische Physik, Akademie der Wissenschaften, Moskau, UdSSR

Eingegangen am 4. April 1972

Wave-Functions and Terms of the System Atom/Diatomic Molecule in the Case of Large Intermolecular Distances

Wavefunctions of the system atom/homonuclear diatomic molecule are constructed, and their symmetry behaviour is examined; both atom and molecule can be degenerate with respect to spin and orbital. The classification of the states of the triatomic system with large atom-molecule distances is analogous to that of diatomic molecules consisting of different atoms, and is based on the approximate symmetry of the effective Hamiltonian of the system. H_{eff} contains spin-orbit, Coulomb, dispersion, and exchange interactions. General expressions for the matrix elements of H_{eff} are obtained. The matrix elements of the exchange interaction are calculated with the aid of a one centre approximation for a molecule with two equal nuclei.

Wellenfunktionen des Systems Atom/homonukleares zweiatomiges Molekül werden konstruiert und ihr Symmetrieverhalten wird untersucht; dabei sind Atom und Molekül beide bahn- und spinentartet. Die erhaltene Klassifizierung der Zustände des dreiatomigen Systems bei großen Atom-Molekül-Abständen ist der für zweiatomige Moleküle aus verschiedenen Atomen analog und basiert auf der Näherungssymmetrie des eingeführten effektiven Hamilton-Operators des Systems. H_{eff} enthält Spin-Bahn-, Coulomb-, Dispersions- und Austauschwechselwirkung. Man erhält allgemeine Ausdrücke für die Matrixelemente von H_{eff}. Die Matrixelemente der Austauschwechselwirkung werden mit Hilfe einer Einzentrennäherung für das Molekül aus zwei gleichen Kernen berechnet.

1. Einleitung

Die Berechnung der Potentialflächen von Atomsystemen ist unumgänglich für die Deutung der Molekülspektren sowie der Mechanismen für Energie- und Teilchenaustausch bei Molekülstößen. Obwohl *a priori*-Rechnungen viel Information über adiabatische Potentiale einfacher Systeme liefern (s. z. B. die Übersicht von Krauss [1]), werden in Spektroskopie und Stoßtheorie noch häufig grobe Modellansätze verwendet, die manchmal qualitativ nicht mit den Resultaten der *a priori*-Rechnungen übereinstimmen (z. B. das Modell der Paarpotentiale für Atom + zweiatomiges Molekül). Die Lage ist noch unbefriedigender, wenn entartete Molekülzustände vorliegen, so daß bei der Annäherung der Moleküle aus einem Energiezustand mehrere Potentialflächen entstehen.

Das allgemeine Problem vereinfacht sich etwas, wenn man sich auf so große Molekülzustände beschränkt, daß die Molekülwechselwirkung kleiner ist als die elektronische Anregungsenergie der isolierten Moleküle. Diese Einschränkung erlaubt jedoch noch, die Prozesse der Umwandlung von Rotations- und Schwingungsenergie in Translationsenergie zu betrachten oder Quasiresonanzübertragung von Elektronenenergie. Ein gleichartiges Herangehen an die Berechnung der Wechselwirkung zweier Atome wurde von uns [2] formuliert und durch eine asymptotische Methode zur Berechnung der Austauschintegrale ergänzt [3–6]; es erlaubt die näherungsweise Berechnung der Beiträge der ersten und zweiten störungstheoretischen Ordnung, und damit die Bestimmung der relativen Lage der Elektronenterme zweiatomiger Moleküle bei großen Kernabständen. Daß die asymptotische Methode der Termberechnung für das H_2-Molekül in einem weiten Bereich brauchbar ist, ist wohlbekannt, s. z. B. [5]. Kürzlich gelang der Vergleich der asymptotischen Methode mit Resultaten von *a priori*-Rechnungen für die Termsysteme, die bei der Annäherung von $\mathrm{Li}^*(1s^2 2p)$ und $\mathrm{Li}(1s^2 2s)$ sowie von $\mathrm{O}(1s^2 2s^2 2p^4)$ und $\mathrm{O}(1s^2 2s^2 2p^4)$ entstehen [7].

Die befriedigende Genauigkeit des asymptotischen Verfahrens in diesen Fällen, sowie die Ergebnisse für den Querschnitt von Intramultiplettaustausch bei Atomstößen [8–12], die mit der asymptotischen Abschätzung der Austauschwechselwirkung erhalten wurden, veranlaßten uns, das angegebene Verfahren für die Termberechnung des Systems Atom/zweiatomiges Molekül zu verallgemeinern. Da die Klassifizierung der Zustände nach Symmetrierassen in dieser Methode wesentlich ist, haben wir uns auf Moleküle mit gleichen Kernen beschränkt.

Die Arbeit ist wie folgt aufgebaut: Zuerst wird die Aufgabe allgemein formuliert und das Symmetrieverhalten des antimetrierten Produkts der Wellenfunktionen von freiem Atom und Molekül untersucht. Dann wird ein effektiver Hamiltonoperator der Wechselwirkung bei großen Abständen in einer beschränkten Funktionsbasis aufgebaut und das Einzentrenmodell des homodinuklearen Moleküls diskutiert. Im nächsten Abschnitt wird der Beitrag der Spin-Bahn-, Quadrupol-Quadrupol-, Dispersions- und Austauschwechselwirkung zu den Energiematrixelementen behandelt. Wir verwenden atomare Einheiten: $e = \hbar = m = 1$.

2. Formulierung der Aufgabe

Wir betrachten nach dem Stoß ein Atom und ein Molekül, die bis zum Stoß durch Wellenfunktionen $|k_2\rangle_b$ bzw. $|k_1\rangle_a$ beschrieben werden, wo k_2 und k_1 Sätze von Quantenzahlen sind. Uns interessiert die Wahrscheinlichkeit dafür, daß nach dem Stoß Molekül und Atom in Zustände mit den Quantenzahlen k_1^* und k_2^* übergehen. Wenn die Resonanzdefekte $\Delta\varepsilon$ bei den uns interessierenden Prozessen und die Energien der Relativbewegung ε_{trans} viel kleiner sind als die charakteristische Energie der Elektronenanregung im isolierten Atom und Molekül (z. B. die Termaufspaltung in Atomen mit einem Elektron, meist von einigen eV), dann werden die Übergänge gewöhnlich bei großen Molekülabständen geschehen, wo $\varepsilon_w \simeq \Delta\varepsilon$ (ε_w ist die Wechselwirkungsenergie zwischen Atom und Molekül). In diesem Fall kann man hoffen, daß Linearkombinationen der Form $\hat{A}|k_1\rangle_a|k_2\rangle_b$ befriedigende Näherungen für die adiabatischen Wellenfunktionen von Atom und Molekül in Wechselwirkung bei den für uns wesentlichen Abständen sind. $|k_1\rangle_a$ und $|k_2\rangle_b$ sind die Wellenfunktionen des isolierten Moleküls bzw. Atoms, die zur Gruppe der Molekül- bzw. Atomzustände gehören, zwischen denen die zu untersuchenden Übergänge geschehen[1]; wo n_a und n_b die Elektronenzahlen von Molekül und Atom sind, P der Permutationsoperator für die Elektronen und $\delta_P = 1$ für gerade, $= -1$ für ungerade Permutation.

---

[1] $\hat{A} = [(n_a + n_b)!/n_a!\,n_b!]^{-1/2} \sum_P \delta_P P$.

Diese Näherung ist eine direkte Verallgemeinerung des Heitler-Rumer-Verfahrens [13] zur Berechnung der Wechselwirkung zweier kugelsymmetrischer Moleküle unter der Voraussetzung, daß die intramolekularen Elektronenkorrelationsenergien viel größer sind als die Wechselwirkung zwischen den Molekülen.

Die Bestimmung der Wechselwirkung für den Fall, daß zur oben angegebenen Gruppe eine große Zahl von Zuständen des getrennten Atoms und Moleküls gehören, geschieht in zwei Teilen.

Zuerst müssen zur Vereinfachung der Säkulargleichungen und der Termidentifizierung aus den antimetrischen Produkten der Atom- und Molekülwellenfunktionen Linearkombinationen gebildet werden, die zu irreduziblen Darstellungen der Symmetriegruppe des Gesamt-Hamiltonoperators gehören. Dann ist ein Verfahren zur Berechnung der Matrixelemente des Hamiltonoperators mit diesen Funktionen auszuarbeiten.

3. Die Wellenfunktion des Systems Atom + Molekül an zwei gleichen Atomen

Bei Vernachlässigung der Spin-Bahn-Wechselwirkung ist das direkte Produkt $E = P \times R_S \times G$, wo P die Permutationsgruppe aller Elektronen ist, R_S die Drehgruppe im Spinraum und G die Symmetriegruppe des Systems im Ortsraum. Die Hinzunahme der Spin-Bahn-Wechselwirkung reduziert die Symmetrie auf die Gruppe E, die das direkte Produkt von P mit G ist, wobei die Operationen aus G gleichzeitig auf die Spin- und Ortsvariablen wirken.

Im allgemeinen Fall ist die Punktgruppe des dreiatomigen Systems C_s und enthält die identische Operation und die Spiegelung in der Ebene der drei Atome. Die entsprechende adiabatische Quantenzahl beim Fehlen von Kramers-Entartung ist der Charakter der Spiegelung der Gesamtelektronenwellenfunktion an dieser Ebene. Speziell können einen wesentlichen Beitrag zur Wahrscheinlichkeit nichtelastischer Übergänge Konfigurationen beitragen, deren Symmetrie nahe bei C_{2v} (gleichschenkliges Dreieck) oder $C_{\infty v}$ (linear) liegt. Die adiabatischen Quantenzahlen (irreduzible Darstellungen und Charaktere) für die Symmetrien C_s und C_{2v} sind in Tab. 1 angegeben, mit folgender Bezeichnung der Symmetrieoperationen: σ_v, Spiegelung an der Atomebene, C_2, Rotation um π um die Achse, die in dieser Ebene durch den Schwerpunkt geht, $\sigma_{v'}$, Spiegelung an der Ebene, die diese Achse enthält und senkrecht zu σ_v steht.

Bei großen Abständen Atom–Molekül ist, wie weiter unten gezeigt wird, der Hamiltonoperator näherungsweise (wir nennen ihn axial) diagonal zur Quantenzahl M_L- der Projektion des Atombahnmoments auf die Achse, die den Schwerpunkt des Moleküls mit dem Atom verbindet. Diese Näherungssymmetrie erlaubt die Einführung einer für weitere Anwendungen bequemen Klassifizierung der Terme des dreiatomigen Systems für große Atom-Molekül-Abstände.

Im folgenden nehmen wir an, daß die Spin-Bahn-Wechselwirkung im Atom und Molekül stets viel kleiner ist als die Wechselwirkung zwischen ihnen; wir konstruieren eine Basis, analog „*a*" in [2]. Die Wellenfunktion des isolierten Moleküls bezeichnen wir mit $|\Gamma \tilde{\Lambda} S_1 M_{S_1}\rangle$, wo Γ eine irreduzible Darstellung der Gruppe $D_{\infty h}$ des Moleküls aus zwei gleichen Atomen ist (Λ_{w1} bei $\Lambda = |\tilde{\Lambda}| \neq 0$, Σ^{σ}_{w1} bei $\Lambda = 0$, wo w_1 die Parität, σ der Charakter einer Spiegelung längs der Molekülachse ist, s. [2]), $\tilde{\Lambda}$ die Projektion des Molekülbahndrehimpulses auf

Tabelle 1. Adiabatische Quantenzahlen (irreduzible Darstellungen und Charaktere) bei dreiatomigen Systemen. Bei linearer Anordnung ist die adiabatische Klassifizierung die des Moleküls mit zwei verschiedenen Atomen (s. z. B. [2])

Gruppe C_{2v}					
Eindeutige Darstellungen	E		C_2	σ_v	$\sigma_{v'}$
A_1	1		1	1	1
B_1	1		−1	1	−1
A_2	1		1	−1	−1
B_2	1		−1	−1	1
Doppeldarstellungen	E	Q	C_2, C_2Q	σ_v, σ_vQ	$\sigma_{v'}, \sigma_{v'}Q$
$E''\begin{pmatrix}\gamma\\\beta\end{pmatrix}$	2	−2	0	0	0

Gruppe C_s			
Eindeutige Darstellungen	E	σ_1	
A'	1	1	
A''	1	−1	
Doppeldarstellungen	E	Q	$\sigma_1, \sigma_1 Q$
$E''\begin{pmatrix}\gamma\\\beta\end{pmatrix}$	2	−2	0

seine Achse, S_1 die Gesamtspinquantenzahl des Moleküls, M_{S_1} ihre Projektion auf den Radiusvektor $\boldsymbol{R}$ vom Molekülschwerpunkt zum Atom. Die Atomwellenfunktion wird mit $|S_2Lw_2\gamma M_{S_2}M_L\rangle$ bezeichnet, wo S_2 und L die Quantenzahlen des Gesamtspins und Bahndrehimpulses sind, M_{S_2} und M_L ihre Projektionen auf $\boldsymbol{R}$, w_2 die Parität, γ eine zusätzliche Quantenzahl.

Da die Elemente der Gruppen P, R_S und G kommutieren, können sie einzeln angewandt werden. Das Verhalten gegen die Gruppe P ist schon bestimmt, da wir antimetrische Produkte nehmen. Das Verhalten gegen die Gruppe R_S folgt einfach aus dem Zusammensetzen der Spinmomente von Atom und Molekül, die in unserem Fall bestimmte Werte haben. Eine Funktion $|SM_SM_L\Gamma\tilde{\Lambda}L\rangle$ mit Eigenwerten des Gesamtspins S und seiner $\boldsymbol{R}$-Projektion M_S ist also

$$|SM_SM_L\Gamma\tilde{\Lambda}L\rangle = \hat{A}\sum_{M_{S_1}M_{S_2}}\begin{bmatrix}S_1 & S_2 & S\\ M_{S_1} & M_{S_2} & M_S\end{bmatrix}|\Gamma\tilde{\Lambda}S_1M_{S_1}\rangle \times |S_2Lw_2\gamma M_{S_2}M_L\rangle\,. \tag{1}$$

$\begin{bmatrix}S_1 & S_2 & S\\ M_{S_1} & M_{S_2} & M_S\end{bmatrix}$ ist ein Clebsch-Gordan-Koeffizient.

Infolge der Diagonalität der Wechselwirkung bezüglich der Quantenzahlen M_L und der Invarianz des ganzen Systems gegen Spiegelung an der Atomebene kombinieren die Linearkombinationen (für $\Lambda \neq 0$)

$$|SM_SM_L\Lambda w_1L\pm\rangle = \frac{1}{\sqrt{2}}(|SM_SM_L\Lambda w_1\tilde{\Lambda}L\rangle \pm |SM_SM_L\Lambda w_1 - \tilde{\Lambda}L\rangle) \tag{2}$$

in der Axialnäherung nicht miteinander. Somit haben wir in dieser Näherung zwei Funktionensätze, deren jeder nach der Gruppe $C_{\infty v}$ zu klassifizieren ist; das rechtfertigt den Namen der Näherung. Ist das Molekül in einem $\Sigma^{\sigma}_{w_1}$-Zustand, kann die Funktion $|S M_S M_L \Sigma^{\sigma}_{w_1} L\rangle$ selbst nach dieser Gruppe klassifiziert werden.

Zur Berechnung der Abweichung von der Axialnäherung muß man den Zusammenhang der eingeführten Linearkombinationen mit den Basisfunktionen der wahren Symmetriegruppe des dreiatomigen Systems bestimmen. Für C_{2v} und C_s ergeben sich bei $\Lambda \neq 0$ die Basisfunktionen:

$$|S M_S M_L \Lambda_{w_1} L A \pm\rangle = \frac{1}{\sqrt{2}}(|S M_S M_L \Lambda_{w_1} L+\rangle \pm |S M_S - M_L \Lambda_{w_1} L+\rangle) \tag{3}$$

$$|S M_S M_L \Lambda_{w_1} L B \pm\rangle = \frac{1}{\sqrt{2}}(|S M_S M_L \Lambda_{w_1} L-\rangle \pm |S M_S - M_L \Lambda_{w_1} L-\rangle)\,. \tag{4}$$

Bei $\Lambda = 0$ haben folgende Funktionen das richtige Symmetrieverhalten gegen diese Gruppen:

$$|S M_S M_L \Sigma^{\sigma}_{w_1} L \pm\rangle = \frac{1}{\sqrt{2}}(|S M_S M_L \Sigma^{\sigma}_{w_1} L\rangle \pm |S M_S - M_L \Sigma^{\sigma}_{w_1} L\rangle)\,. \tag{5}$$

Die Charaktere der Funktionen (3)–(5) zu den verschiedenen Operationen der Gruppen C_s und C_{2v} sind in Tab. 2 angegeben. Dabei wird vorausgesetzt, daß die Wellenfunktionen des zweiatomigen Moleküls so festgelegt sind, daß

$$\hat{\sigma}_v |\Lambda_{w_1} \tilde{\Lambda} S_1 M_S\rangle = |\Lambda_{w_1} - \tilde{\Lambda} S_1 M_{S_1}\rangle\,.$$

Bei Einschluß der Spin-Bahn-Wechselwirkung wirken die Symmetrieoperationen der Gruppen C_s und C_{2v} auch auf die Spinvariablen. Bei halbzahligem Spin treten Doppeldarstellungen der Gruppen C_{2v} und C_s auf, und die Funktionen (3)–(5) sind schon Basisfunktionen dieser Doppeldarstellungen. Bei ganzzahligem Spin gehen bei den Operationen aus C_{2v} und C_s die Funktionen

$$|S \pm N\rangle = \frac{1}{\sqrt{2}}(|S M_S N\rangle \pm |S - M_S N\rangle) \tag{6}$$

in sich über, wo $|S M_S N\rangle$ eine der Funktionen (3)–(5) ist. Die Charaktere $\chi_\pm$ der Funktionen (6) bezüglich Symmetrietransformationen ergeben sich aus den Charakteren χ_N der Funktionen (3)–(5) wie folgt,

$$\chi_\pm(C_2) = (-1)^{M_S}\chi_N(C_2);\ \chi_\pm(\sigma_v) = \pm(-1)^{S-M_S}\chi_N(\sigma_v);\ \chi_\pm(\sigma'_v) = \pm(-1)^{S}\chi_N(\sigma'_v)\,. \tag{7}$$

Für die lineare Atomanordnung werden die richtigen Linearkombinationen mit und ohne Spin-Bahn-Wechselwirkung aus den Funktionen $|S M_S M_L \Gamma \tilde{\Lambda} L\rangle$ analog

Tabelle 2. Charaktere der Transformationen der Wellenfunktionen (3)–(5)

$\|S M_S M_L \Lambda_{w_1} L A +\rangle$	$w_1(-1)^{M_L}$	$w_2(-1)^{L-M_L}$	$w_1 w_2(-1)^{L+\Lambda}$
$\|S M_S M_L \Lambda_{w_1} L A -\rangle$	$w_1(-1)^{M_L}$	$-w_2(-1)^{L-M_L}$	$-w_1 w_2(-1)^{L+\Lambda}$
$\|S M_S M_L \Lambda_{w_1} L B +\rangle$	$-w_1(-1)^{M_L}$	$-w_2(-1)^{L-M_L}$	$w_1 w_2(-1)^{L+\Lambda}$
$\|S M_S M_L \Lambda_{w_1} L B -\rangle$	$-w_1(-1)^{M_L}$	$w_2(-1)^{L-M_L}$	$-w_1 w_2(-1)^{L+\Lambda}$
$\|S M_S M_L \Sigma^{\sigma}_{w_1} L +\rangle$	$\sigma w_1(-1)^{M_L}$	$\sigma w_2(-1)^{L-M_L}$	$w_1 w_2(-1)^{L}$
$\|S M_S M_L \Sigma^{\sigma}_{w_1} L -\rangle$	$\sigma w_1(-1)^{M_L}$	$-\sigma w_2(-1)^{L-M_L}$	$-w_1 w_2(-1)^{L}$
	C_2	σ_v	$\sigma_{v'}$

dem in [2] untersuchten Molekül aus 2 verschiedenen Atomen konstruiert; wir werden darauf nicht weiter eingehen.

4. Wechselwirkungsmatrix für große Abstände Atom-Molekül

Ableitung des effektiven Hamiltonoperators

Weiter oben wurde eine verallgemeinerte Heitler-Rumer-Näherung eingeführt, in der angenommen wird, daß man beim Berechnen der Potentialflächen bei Abständen, für die bei langsamen Stößen inelastische Übergänge mit einem kleinen Resonanzdefekt verlaufen, den Basissatz auf Zustände der offenen Kanäle beschränken kann (weiter unten werden wir das den Satz O nennen). Diese Annahme ist so zu verstehen, daß man einen effektiven Hamiltonoperator H_{eff} bestimmen kann, so daß die ganze Energie des Systems bei den uns interessierenden Abständen sich aus der Säkulargleichung ergibt:

$$\det\langle k_1\, k_2|\hat{H}_{\mathrm{eff}} - E|k_1'\, k_2'\rangle = 0\,,$$

wo $|k_1\, k_2\rangle = |k_1\rangle_a|k_2\rangle_b$ eine Funktion des Satzes O ist.

$\hat{H}_{\mathrm{eff}}$ berücksichtigt den Einfluß der Antimetrierung und schließt den Beitrag von Zuständen ein, die im Satz O nicht enthalten sind. Der Aufbau von $\hat{H}_{\mathrm{eff}}$ ist analog der Ableitung des Spin-Hamilton-Operators in der Theorie des Ferromagnetismus mit direktem Austausch. Wir konstruieren $\hat{H}_{\mathrm{eff}}$ für den allgemeinen Fall der Wechselwirkung zwischen zwei Molekülen a und b mit vielen Elektronen gemäß dem Gedanken von Herring [14, 15] ([15] enthält eine Bibliographie zur Ableitung des Spin-Hamilton-Operators). In nullter Näherung wird angenommen, daß die Spin-Bahn-Wechselwirkung fehlt. Das erlaubt die Einführung von Quantenzahlen $S_1, M_{S_1}, S_2, M_{S_2}$ für die Gesamtspins der Moleküle a und b und ihre Projektionen auf die intermolekulare Achse, und die Bestimmung der Funktionen

$$|S M_S S_1\, k_1\, S_2 k_2\rangle = \sum_{M_{S_1} M_{S_2}} \begin{vmatrix} S_1 & S_2 & S \\ M_{S_1} & M_{S_2} & M_S \end{vmatrix} |S_1\, k_1\, M_{S_1}\rangle_a |S_2 k_2 M_{S_2}\rangle_b\,, \tag{8}$$

die zu Werten S des Gesamtspins und M_S der Projektionen gehören (k_1 und k_2 bedeuten die Sätze aller übrigen Quantenzahlen der Moleküle a und b).

Betrachten wir zwei hypothetische wechselwirkende Moleküle a und b, deren zu einem Molekül gehörende Elektronen $1_a \ldots n_a$ bzw. $1_b \ldots n_b$ ununterscheidbar sind, aber intermolekular unterscheidbar. Der Hamiltonoperator dieses Systems ist $\hat{H} = \hat{H}_a + \hat{H}_b + \hat{V}_{ab}$, wo $\hat{H}_a$ und $\hat{H}_b$ die nichtrelativistischen H-Operatoren der Moleküle a und b in adiabatischer Näherung sind und von den Elektronenkoordinaten $1_a \ldots n_a$ bzw. $1_b \ldots n_b$ abhängen; $\hat{V}_{ab}$ ist der Operator der intermolekularen elektrostatischen Wechselwirkung. Herring gab in [14] gewichtige Argumente dafür an, daß man aus den exakten Wellenfunktionen $|\Psi\rangle$ dieses hypothetischen Systems Linearkombinationen $|S M_S S_1\, k_1\, S_2\, k_2\, e\rangle$ bilden kann, die folgende Eigenschaften haben:

1. Sie entsprechen der Lokalisierung der Elektronen $1_a \ldots n_a$ am Molekül a, $1_b \ldots n_b$ am Molekül b und sind antimetrisch für jedes Molekül;

2. Für $|\boldsymbol{r}_{i_{a,b}}| \to \infty$, wo $|\boldsymbol{r}_{i_{a,b}}|$ der Abstand des Elektrons $i_{a,b}$ von seinem Molekül ist, wird $\big||S M_S S_1\, k_1\, S_2\, k_2\, e\rangle\big| \sim e^{-\alpha_{a,b}|\boldsymbol{r}_{i_{a,b}}|}$ mit $\alpha_{a,b} = \sqrt{2 I_{a,b}}$ und $I_{a,b}$ = Ionisierungsenergie des Moleküls a bzw. b;

3. Sie haben Symmetrieeigenschaften ganz analog den Funktionen $|SM_S S_1 k_1 S_2 k_2\rangle$;

4. Bei Molekülabständen $R \to \infty$ geht $|SM_S S_1 k_1 S_2 k_2 e\rangle \to |SM_S S_1 k_1 S_2 k_2\rangle$.

Die antimetrierten Funktionen $\hat{A}|SM_S S_1 k_1 S_2 k_2 e\rangle$ beschreiben erlaubte physikalische Zustände; und die exakte Gleichung für Systemterme, die zu bestimmten Werten des Gesamtspins und bei $R \to \infty$ in Terme des Satzes O übergehen, wird

$$\det \langle SM_S S_1 k_1 S_2 k_2 e|\hat{H} - E|\hat{A} SM_S S'_1 k'_1 S'_2 k'_2 e\rangle = 0 \,. \tag{9}$$

Zur Lösung der Gl. (9) braucht man erstens ein Näherungsverfahren für die Funktionen $|SM_S S_1 k_1 S_2 k_2 e\rangle$, zweitens die in (9) auftretenden Matrixelemente mit diesen Näherungsfunktionen. Bei ziemlich großen Molekülabständen sind die Funktionen $|SM_S S_1 k_1 S_2 k_2\rangle$ eine gute Näherung für $|SM_S S_1 k_1 S_2 k_2 e\rangle$. Aber diese der Heitler-London-Näherung für H_2-Molekül analoge Näherung ist unbefriedigend, weil sie die Verzerrung der Wellenfunktionen durch die Korrelation der Elektronen der verschiedenen Moleküle nicht berücksichtigt. Diesen Verzerrungen entsprechen jedoch störungstheoretisch Energieglieder höherer Ordnung, die bei großem R von gleicher Größenordnung sind wie der Beitrag erster Ordnung, und erstens die Dispersionswechselwirkung und zweitens den richtigen asymptotischen Verlauf der Austauschwechselwirkung bedingen [3, 14]. Während bei der Berechnung der Dispersionswechselwirkung die Verzerrung der Wellenfunktionen der Moleküle a und b in den Bereichen wesentlich ist, wo sie groß sind, so ist zur Bestimmung der Austauschwechselwirkung der Einfluß der Elektronenkorrelation in den exponentiellen „Schwänzen" der Funktionen der Einzelmoleküle im intermolekularen Bereich wichtig. Dieser Umstand erlaubt im folgenden die wichtige Annahme, daß der Korrelationseffekt der Austauschwechselwirkung unabhängig von der Dispersionswechselwirkung berechnet werden kann (wir werden diese Annahme 4a nennen). Außerdem führen wir Annahme 4b ein, wonach bei den betrachteten Abständen Glieder der Ordnung ε_{W_w}, k^2 vernachlässigbar sind, wo k das Überlappungsintegral von an verschiedenen Molekülen lokalisierten Orbitalen ist. Diese Annahme umfaßt die weitere, daß man von $\hat{A}$ bei großen Abständen nur die Elektronenpermutation in den Molekülen und einzelne Permutationen zwischen den Molekülen braucht; außerdem kann die Nichtorthogonalität bei der Normierung der Wellenfunktionen vernachlässigt werden.

Mit 4a und 4b und Beschränkung auf Störung zweiter Ordnung für die Coulomb-Wechselwirkung kann man die Matrixelemente zu (9) schreiben

$$\langle SM_S S_1 k_1 S_2 k_2|\hat{H}_a + \hat{H}_b + \hat{V}_{ab} + \hat{V}_{ab2} + \hat{V}_{Aust} - E|SM_S S'_1 k'_1 S'_2 k'_2\rangle \,. \tag{10}$$

Hier ist $\hat{V}_{ab2}$ der Operator der Coulomb-Wechselwirkung bis zur zweiten Ordnung, der weiter unten bestimmt wird, und

$$\begin{aligned} &\langle SM_S S_1 k_1 S_2 k_2|\hat{V}_{Aust}|SM_S S'_1 k'_1 S'_2 k'_2\rangle \\ &= -n_a n_b \langle SM_S S_1 k_1 S_2 k_2 e|(\hat{H} - E)\, P^{\sigma}_{1_a 1_b}\, P^{\chi}_{1_a 1_b}|SM_S S'_1 k'_1 S'_2 k'_2 e\rangle \,, \end{aligned} \tag{11}$$

wo $P^{\sigma}_{1_a 1_b}$ der Spinaustauschoperator ist und $P^{\chi}_{1_a 1_b}$ der Operator für die Ortskoordinaten der Elektronen 1a und 1b ist. Für (11) wurde die Eigenschaft 1 der

Funktionen $|SM_SS_1k_1S_2k_2e\rangle$ benutzt. Nach [15] und bei Vernachlässigung von Gliedern der Ordnung ε_{W_w}, k^2 entsprechend 4b, erhält man für die Matrixelemente $\hat{V}_{\mathrm{Aust}}$ bequeme berechenbare Ausdrücke mit Überlappungsintegralen, die nicht mehr von E abhängen:

$$\begin{aligned}\langle SM_SS_1k_1S_2k_2|\hat{V}_{\mathrm{Aust}}|SM_SS'_1k'_1S'_2k'_2\rangle &= \tfrac{1}{4}n_a n_b \int d\sigma_{1_a}\ldots d\sigma_{N_b}\int_\Sigma d\Sigma \\ &\times\{(\Psi^{SS_1S_2e*}_{M_Sk_1k_2}\nabla_{3(n_a+n_b)m}P^{\sigma}_{1_a1_b}P^{\chi}_{1_a1_b}\Psi^{SS'_1S'_2e}_{M_Sk'_1k'_2}+\Psi^{SS'_1S'_2e}_{M_Sk'_1k'_2}\nabla_{3(n_a+n_b)m} \\ &\times P^{\sigma*}_{1_a1_b}P^{\chi*}_{1_a1_b}\Psi^{SS_1S_2e*}_{M_Sk_1k_2})-([P^{\sigma*}_{1_a1_b}P^{\chi*}_{1_a1_b}\Psi^{SS_1S_2e}_{M_Sk_1k_2}]\nabla_{3(n_a+n_b)m}\Psi^{SS'_1S'_2e}_{M_Sk_1k_2} \\ &+[P^{\sigma}_{1_a1_b}P^{\chi}_{1_a1_b}\Psi^{SS'_1S'_2e}_{M_Sk'_1k'_2}]\nabla_{3(n_a+n_b)m}\Psi^{SS_1S_2e}_{M_Sk_1k_2})\}\,.\end{aligned} \tag{12}$$

In Formel (12) steht die Integration über Spin- und Ortsvariable und die Bezeichnung $\Psi^{SS_1S_2e}_{M_Sk_1k_2}$ für die Funktion $|SM_SS_1k_1S_2k_2e\rangle$.

Die Überlappung Σ wird durch $z_{1_a}=z_{1_b}$ bestimmt (s. Fig. 1), wenn anfangs die Koordinatensysteme mitten zwischen den Molekülzentren a und b liegen und die z-Achse längs des Basisvektors $\boldsymbol{R}$ zwischen diesen Zentren liegt. $\nabla_{3(n_a+n_b)m}$ ist der $3(n_a+n_b)$-fache Gradient in der Normalen zur Überlappung Σ.

Die Spinbahnkopplung ist unter der Annahme nach [16, 17] leicht mitzunehmen, daß sie sich von der in den freien Molekülen nur wenig unterscheidet, d. h. $\hat{V}_{s.o} = \hat{V}_{s.o.a}+\hat{V}_{s.o.b}$, wo $\hat{V}_{s.o.a}$ und $\hat{V}_{s.o.b}$ die Operatoren der Spin-Bahn-Wechselwirkung in den isolierten Molekülen a und b sind. Außerdem folgt aus Annahme 4b, daß die Glieder $\hat{V}_{s.o.}k^2$ wegfallen, so daß bei den uns interessierenden Abständen die Spin-Bahn-Wechselwirkungsenergie meist von gleicher Größenordnung wie die intermolekulare Wechselwirkungsenergie ist.

Somit haben wir den folgenden Ausdruck für $\hat{H}_{\mathrm{eff}}$:

$$\hat{H}_{\mathrm{eff}}=\hat{H}_a+\hat{H}_b+\hat{V}_{s.o.a}+\hat{V}_{s.o.b}+\hat{V}_{ab}+\hat{V}_{ab2}+\hat{V}_{\mathrm{Aust}}\,, \tag{13}$$

wobei die Bedeutung der verschiedenen Glieder aus den Formeln (10) bis (12) folgt.

Im konkreten Fall der Kopplung eines Atoms mit einem Molekül aus zwei gleichen Atomen berechnet man die Matrixelemente H_{eff} bequem in einem Koordinatensystem k_1, dessen z_1-Achse längs $\boldsymbol{R}$ liegt, die y_1-Achse senkrecht auf der Ebene $\varrho\boldsymbol{R}$, wo ϱ der Radiusvektor zwischen den Atomen im Molekül ist.

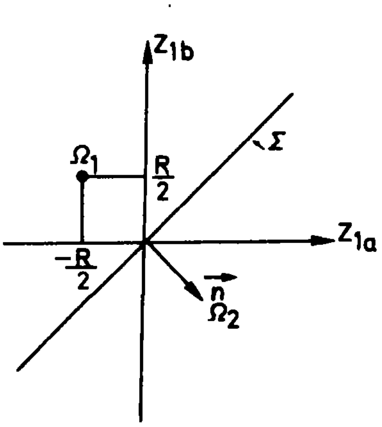

Fig. 1

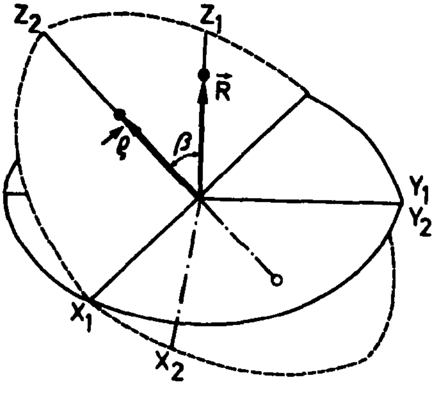

Fig. 2

Andererseits werden die Matrixelemente verschiedener auf das Molekül bezogener Operatoren, wie der Operator des Quadrupolmoments, des Spins, usw. im Koordinatensystem k_2 berechnet, dessen z_2-Achse in der Molekülachse liegt. k_2 erhält man aus k_1 durch Drehen um den Winkel β zwischen $\boldsymbol{R}$ und $\boldsymbol{\varrho}$ um die y_1-Achse (s. Fig. 2). Die entsprechenden Drehmatrizen zur Beschreibung der Transformation der Wellenfunktionen mit bestimmtem Drehimpuls j

$$D^j_{m'm}(\beta) = \langle jm'|e^{-iJ_y\beta}|jm\rangle$$

werden z. B. im Buch von Edmonds [18] angegeben.

Die Matrix des in $\hat{H}_{\text{eff}}$ enthaltenen Operators ($\hat{H}_a + \hat{H}_b$) ist im Funktionensatz O diagonal; ihre Diagonalelemente sind die Summe der Energien von isoliertem Atom und Molekül, die man dem Experiment entnehmen kann. Doch zur Berechnung der Matrixelemente des Wechselwirkungsanteils von $\hat{H}_{\text{eff}}$ braucht man explizite Ausdrücke für die Wellenfunktionen des freien Atoms und Moleküls. Wir werden aus einfachen Modellen für das Vielelektronenatom und homodiatomare Molekül Ausdrücke für verschiedene Matrixelemente herleiten.

Atomare und molekulare Wellenfunktionen

Wir interessieren uns für Atom-Molekül-Wechselwirkungen bei Abständen, die wesentlich größer sind als ihre gaskinetischen Dimensionen. Bei diesen Abständen kommt der Hauptanteil der Wechselwirkungsenergie von den obersten Valenzelektronenschalen. Deshalb werden wir nur die Koordinaten der Valenzelektronen in die Wellenfunktionen von freiem Atom und Molekül einführen; die Elektronen der inneren Schalen ergeben für sie ein effektives Feld, das unabhängig von der Atom-Molekül-Kopplung ist. Wir bemerken, daß die Wechselwirkung der Elektronen der inneren abgeschlossenen Schalen von Atom und Molekül keinen großen Einfluß auf die Wahrscheinlichkeit nichtelastischer Prozesse hat, die bei großen Abständen ablaufen; so hat man häufig eine hohe Symmetrie und erhält ein additives Glied zu allen Termen, die aus Satz O entstehen, ohne Termaufspaltungen. Die Wellenfunktionen der Valenzschalen nähern wir durch Linearkombinationen von Determinanten aus Einelektronenspinbahnfunktionen an, die zu einer Konfiguration gehören.

Das Atommodell und die entsprechenden genäherten Wellenfunktionen fi unsere Rechnungen sind ausführlich in [2] behandelt. Für ein Atom mit p-Valen schale, das wir in dieser Arbeit betrachten werden, sind die Wellenfunktionen

$$\begin{aligned}|S_2 L p^n M_{S_2} M_L\rangle = \sum_{S'L'} G^{S_2L}_{S'L'} \sum_{M_{S'}m_S} \sum_{M_{L'}m} \begin{bmatrix} S' & 1/2 & S_2 \\ M_{S'} & m_S & M_{S_2}\end{bmatrix} \\ \times \begin{bmatrix} L' & 1 & L \\ M_{L'} & m & M_L\end{bmatrix} |S' L' p^{n-1} M_{S'} M_{L'}\rangle\, \varphi^{1\alpha}_{\bar{n}m}(r_1)\, \chi^{1/2}_{m_S}(\sigma_1)\,.\end{aligned} \qquad (1$$

Hier ist n die Zahl der Valenzelektronen, $G^{S_2L}_{S'L'}$ sind in [19, 20] tabellierte Koeff zienten, $|S'L'p^{n-1}M_{S'}M_{L'}\rangle$ antimetrische Wellenfunktionen zur Konfiguratio p^{n-1},

$$\varphi^{1\alpha}_{\bar{n}m}(r_1) = Y^1_m(\vartheta_1, \varphi_1)\, \varphi^{1\alpha}_{\bar{n}}(r_1)$$

ist das Atomorbital des ersten Elektrons, ($Y^1_m(\vartheta_1, \varphi_1)$ ist eine Kugelfunktion, $\bar{n}$ d Hauptquantenzahl), $\chi^{1/2}_{m_s}(\sigma_1)$ ist die Spinfunktion des ersten Elektrons. Die Summ in (14) läuft über alle Terme der Konfiguration p^{n-1}. Bei $r \to \infty$ hat die radia Wellenfunktion $\varphi^{1\alpha}_{\bar{n}}(r_1)$ die Asymptote $A r_1^{\frac{1}{\alpha}-1} e^{-\alpha r}$, wo $\alpha = \sqrt{2I}$ mit der Ion sierungsenergie I.

Wir gehen jetzt genauer auf die Wellenfunktionen des homodiatomare Moleküls in Born-Oppenheimer-Näherung ein. In dieser Näherung hängen al Eigenschaften des Moleküls: Gesamtelektronenenergie, Multipolmomente, vert kale Ionisierungsenergie I_b [2] parametrisch vom Kernabstand ϱ ab.

Die ϱ-Abhängigkeit von Multipolmomenten und I_b ist sehr interessant für di Berechnung von Elektronenschwingungsübergängen bei Atom-Molekül-Stöße [21]. Wir werden diese Abhängigkeit hier nicht untersuchen.

Wir nehmen an, daß im homodiatomaren Molekül das äußere Elektron sic im selbstkonsistenten Hartree-Fock-Feld der übrigen Elektronen und der Kern bewegt, das die Symmetrie $D_{\infty h}$ hat und von der Wechselwirkung mit dem en fernten Atom nicht verändert wird. Die Einelektronenzustände werden nac „a“ von Hund [2] klassifiziert.

Die Einelektronenmolekülorbitale $\varphi^{\gamma\alpha}_{\lambda}(r)$, wo γ der Satz von Quantenzahle des Einelektronenzustands, λ die Projektion des Bahnmoments auf die Molekü achse, $\alpha = \sqrt{2I_b}$ ist, werden häufig aus dem Matrixverfahren von Hartree-Foc erhalten, wobei $\varphi^{\gamma\alpha}_{\lambda}(r)$ sich als Linearkombination einiger Basisfunktionen ergib Im einfachsten Fall wird $\varphi^{\gamma\alpha}_{\lambda}(r)$ als Linearkombination eines beschränkte Satzes von Atomorbitalen dargestellt (MO-LCAO-Methode); bei einer kleine Zahl von Atomorbitalen ergeben sich die Koeffizienten oft eindeutig aus d Symmetrie.

Wir führen ein Koordinatensystem mit Ursprung genau zwischen den Kerne auf der Molekülachse z ein und entsprechende Kugelkoordinaten r, ϑ, φ. Da Potential $V(r)$, in dem sich das Valenzelektron bewegt, kann nach Legendre Polynomen $P_k(\cos\vartheta)$ entwickelt werden:

$$V(r) = \sum_{k=0}^{\infty} V_k(r)\, P_k(\cos\vartheta)\,. \qquad (1$$

---

[2] Die vertikale Ionisierungsenergie I_b ist die Differenz der Elektronenenergien von Molekül ur Ion bei festem ϱ.

Wegen der Inversionsinvarianz des Systems fallen in (15) alle Glieder mit ungeradem k weg. Wegen der hohen Symmetrie des untersuchten Systems spielt in der Summe (15) das kugelsymmetrische Glied $V_0(r)$ die Hauptrolle. Daher kann man hoffen, daß bei der Entwicklung von $\varphi_\lambda^{\gamma\alpha}(\boldsymbol{r})$ nach Kugelfunktionen

$$\varphi_\lambda^{\gamma\alpha}(\boldsymbol{r}) = \sum_{l=|\lambda|}^{\infty} \varphi_l^{\gamma\alpha}(r)\, Y_\lambda^l(\vartheta, \varphi) \tag{16}$$

das erste nichtverschwindende Glied den Hauptbeitrag liefert. Dieser Umstand wird bei Rechnungen an zweiatomigen Molekülen viel benutzt, die auf der Näherung des „vereinigten" Atoms fußen [22]. Die Reinheit der Quantenzahl $l = 0$ bei $ns\sigma$-Termen des H_2-Moleküls wurde von Chen [23] gründlich untersucht. Er fand, daß der Anteil von Funktionen mit anderen l-Werten bei $\varrho \leqq 3$ a. E. einige Prozent nicht übersteigt. Für $r \to \infty$ folgt aus genauen Rechnungen von Bates *et al.* [24], daß man für Terme anderer Typen die gleiche Situation hat. Nach dem Obengesagten und unter Beachtung der Grobheit anderer Näherungen in dieser Arbeit halten wir es für zweckmäßig, uns im Ausdruck (16) auf das erste nichtverschwindende Glied zu beschränken, das qualitativ die richtige Winkelverteilung der Elektronendichte liefert.

Wenn wir analog zum Atom (s. [2]) annehmen, daß für $r_1 \to \infty$ die Außenelektronen des Moleküls durch eine Wellenfunktion des Grundzustands des entsprechenden Ions beschrieben werden und im Molekülinneren die Hartree-Fock-Näherung benutzt wird, wird die Asymptote $\varphi_\lambda^{\gamma\alpha}(\boldsymbol{r}_1)$ für $r_1 \to \infty$

$$\varphi_\lambda^{\gamma\alpha}(\boldsymbol{r}_1)_{r_1 \to \infty} \to A_\lambda^\gamma(\vartheta_1, \varphi_1)\, r_1^{\frac{1}{\alpha}-1}\; e^{-\alpha r_1}. \tag{17}$$

In der in dieser Arbeit benutzten Einzentrennäherung ist

$$A_\lambda^\gamma(\vartheta_1, \varphi_1) = A\, Y_\lambda^l(\vartheta_1, \varphi_1), \tag{18}$$

wo l das erste nichtverschwindende Glied in der Entwicklung (16) bezeichnet. Die Konstante A bestimmt man durch Zusammensetzen der Funktion (17) mit dem Hartree-Fock-Orbital oder einem Näherungsausdruck dafür an der Molekülgrenze.

Sind in der höchsten Molekülschale mehrere Elektronen (bis zu 2 in σ_w^+-Schalen, bis zu 4 in λ_w), so gibt man die antimetrische Wellenfunktion bequem, wie bei den Atomen, so an, daß die Koordinaten des ersten Elektrons abgetrennt werden. Das ergibt eine zu (14) analoge Formel

$$\begin{aligned} |\Gamma\tilde{\Lambda}SM_S(\lambda_w)^n\rangle = {} & \sum_{S'\Gamma'} G_{S'\Gamma'}^{SI} \sum_{M_{S'}m_s} \sum_{\tilde{\Lambda}'\tilde{\lambda}} \begin{bmatrix} S' & 1/2 & S \\ M_{S'} & m_s & M_S \end{bmatrix} \\ & \times \begin{bmatrix} \Gamma' & \lambda_w & \Gamma \\ \tilde{\Lambda}' & \tilde{\lambda} & \tilde{\Lambda} \end{bmatrix} |\Gamma'\tilde{\Lambda}'S'M_{S'}(\lambda_w)^{n-1}\rangle\, \varphi_\lambda^{\lambda w\alpha}(\boldsymbol{r}_1)\, \chi_{m_s}^{1/2}(\sigma_1), \end{aligned} \tag{19}$$

wo $|\Gamma'\tilde{\Lambda}'S'M_{S'}(\lambda_w)^{n-1}\rangle$ antimetrische Wellenfunktionen zur Konfiguration $(\lambda_w)^{n-1}$ sind, $\varphi_\lambda^{\lambda w\alpha} \cdot \chi_{m_s}^{1/2}$ die Spin-Bahn-Molekülfunktion des ersten Elektrons ist, $\begin{bmatrix} \Gamma' & \lambda_w & \Gamma \\ \tilde{\Lambda}' & \tilde{\lambda} & \tilde{\Lambda} \end{bmatrix}$ Clebsch-Gordon-Koeffizienten der Gruppe $D_{\infty h}$ und $G_{S'\Gamma'}^{SI}$ genealogische

Tabelle 3. Genealogische Koeffizienten $G^{S\Gamma}_{S'\Gamma'}$ für die Konfigurationen $(\lambda_w)^2$ und $(\lambda_w)^3$

$(\lambda_w)^2$ \ λ_w	Λ_w
${}^1\Sigma_g^+$	1
${}^1(2\lambda)_g$	1
${}^3\Sigma_g$	1

$(\lambda_w)^3$ \ $(\lambda_w)^2$	${}^1\Sigma_g^+$	${}^1(2\lambda)_g$	${}^3\Sigma_g^-$
Λ_w	$\frac{1}{\sqrt{6}}$	$-\frac{1}{\sqrt{3}}$	$\frac{1}{\sqrt{2}}$

Koeffizienten sind. Die Clebsch-Gordon-Koeffizienten erhält man bekanntlich [25] aus der Gleichung

$$|\Gamma\tilde{\Lambda}\rangle = \sum_{\tilde{\Lambda}_1\tilde{\Lambda}_2} \begin{vmatrix} \Gamma_1 & \Gamma_2 & \Gamma \\ \tilde{\Lambda}_1 & \tilde{\Lambda}_2 & \tilde{\Lambda} \end{vmatrix} |\Gamma_1\tilde{\Lambda}_1\rangle|\Gamma_2\tilde{\Lambda}_2\rangle,$$

wo $|\Gamma\tilde{\Lambda}\rangle$ Basisfunktionen der irreduziblen Darstellungen sind, in die das direkte Produkt der Darstellungen Γ_1 und Γ_2 mit den Basisfunktionen $|\Gamma_1\tilde{\Lambda}_1\rangle$ und $|\Gamma_2\tilde{\Lambda}_2\rangle$ zerfällt. Die Funktionen $|\Gamma\tilde{\Lambda}\rangle$ kann man nach folgenden offensichtlichen Regeln für das direkte Produkt erhalten:

1. $\Gamma_1 = \Lambda_{1w_1}, \Gamma_2 = \Lambda_{2w_2}, \Lambda_1 > \Lambda_2 > 0$. Das direkte Produkt zerfällt in zwei nichtverschwindende Darstellungen: $\Gamma_+ = (\Lambda_1 + \Lambda_2)_{w_1 \cdot w_2}$ mit Basisfunktionen $|\Gamma_+\tilde{\Lambda}\rangle = |\Gamma_1\tilde{\Lambda}_1\rangle \cdot |\Gamma_2\tilde{\Lambda}_2\rangle\,\delta_{\tilde{\Lambda},\tilde{\Lambda}_1+\tilde{\Lambda}_2}$ und $\Gamma_- = (\Lambda_1 - \Lambda_2)_{w_1 \cdot w_2}$ mit Basisfunktionen $|\Gamma_-\tilde{\Lambda}\rangle = |\Gamma_1\tilde{\Lambda}_1\rangle \cdot |\Gamma_2\tilde{\Lambda}_2\rangle\,\delta_{\tilde{\Lambda},\tilde{\Lambda}_1+\tilde{\Lambda}_2}$.

2. $\Gamma_1 = \Lambda_{w_1}, \Gamma_2 = \Lambda_{w_2}, \Lambda > 0$. Das direkte Produkt zerfällt in drei nichtverschwindende Darstellungen: $(2\Lambda)_{w_1 \cdot w_2}$ mit Basisfunktionen

$$|(2\Lambda)_{w_1 \cdot w_2}\tilde{\Lambda}\rangle = |\Gamma_1\tilde{\Lambda}_1\rangle|\Gamma_2\tilde{\Lambda}_2\rangle\,\delta_{\tilde{\Lambda},\tilde{\Lambda}_1+\tilde{\Lambda}_2};$$

$\Sigma^{\pm}_{w_1 \cdot w_2}$ mit Basisfunktionen

$$|\Sigma^{\pm}_{w_1 \cdot w_2}\rangle = \frac{1}{\sqrt{2}}(1 \pm \hat{\sigma}_v)|\Gamma_1\tilde{\Lambda}_1\rangle|\Gamma_2\tilde{\Lambda}_2\rangle\,\delta_{\tilde{\Lambda}_1,-\tilde{\Lambda}_2},$$

wo $\hat{\sigma}_v$ der Operator der Spiegelungen an einer die Molekülachse enthaltenden Ebene ist.

3. $\Gamma_1 = \Sigma^{\pm}_{w_1}, \Gamma_2$ beliebig. Das direkte Produkt liefert eine nichtverschwindende Darstellung, und die entsprechenden Basisfunktionen sind $|\Sigma^{\pm}_{w_1}\rangle|\Gamma_2\Lambda_2\rangle$.

Die genealogischen Koeffizienten $G^{S\Gamma}_{S'\Gamma'}$ für die Konfigurationen $(\lambda_w)^n$ können leicht nach [19] berechnet werden und sind in Tab. 3 angegeben.

Wir gehen nun zur Berechnung der Matrixelemente verschiedener Glieder von H_{eff} nach Formel (13) über.

Spin-Bahn-Wechselwirkung

Weiter oben machten wir die Annahme $\hat{V}_{\mathrm{s.o.}} = \hat{V}_{\mathrm{s.o.a}} + \hat{V}_{\mathrm{s.o.b}}$. In unserem Fall ist $\hat{V}_{\mathrm{s.o.a}} = A_a\hat{L}_{z_2a}\hat{S}_{z_2a}$, wo A_a die Spin-Bahn-Kopplungskonstante im Molekül ist; L_{z_2a} und S_{z_2a} sind die Operatoren der Projektionen von Gesamtbahn- bzw. Spinmoment des Moleküls auf seine Achse (die z_2-Achse im oben angegebenen k_2-Koordinatensystem), und $\hat{V}_{\mathrm{s.o.b}} = A_b\boldsymbol{L}_b\boldsymbol{S}_b$, wo A_b die Spin-Bahn-Kopplungskonstante im Atom ist; $\boldsymbol{S}_b$ und $\boldsymbol{L}_b$ sind die Gesamtspin- bzw. Bahnmomentoperatoren des Atoms. Der Ausdruck für die Matrixelemente von $\hat{V}_{\mathrm{s.o.b}}$ für die Funktionen (1) fällt mit dem entsprechenden Ausdruck in [2] zusammen. Hier leiten wir den Ausdruck für die Matrixelemente von $\hat{V}_{\mathrm{s.o.a}}$ ab.

Die Wellenfunktionen (1), für die wir die Matrixelemente berechnen müssen, entsprechen der Spinquantisierung von Atom und Molekül nach der z_1-Achse. Daher müssen wir zur Berechnung der Matrixelemente $\hat{S}_{z_2\mathrm{a}} \equiv \hat{S}^1_{02\mathrm{a}}$ durch die sphärischen Komponenten $\hat{S}^1_{q1\mathrm{a}}$ des Vektoroperators des Molekülspins $\hat{\boldsymbol{S}}_\mathrm{a}$ im Koordinatensystem k_1 ausdrücken. Dieser Ausdruck ist

$$\hat{S}^1_{02\mathrm{a}} = \sum_q D^1_{q0}(\beta)\, \hat{S}^1_{q1\mathrm{a}} \, . \tag{20}$$

Mit (20) erhält man leicht folgenden Ausdruck für ein Matrixelement $\hat{V}_{\mathrm{s.o.a}}$ in den Funktionen (1):

$$\begin{aligned} \langle S M_S M_L \Lambda_{w_1} \tilde{\Lambda} L | \hat{V}_{\mathrm{s.o.a}} | S' M'_S M'_L \Lambda'_{w_1} \tilde{\Lambda}' L' \rangle &= \delta_{\tilde{\Lambda}\tilde{\Lambda}'} \delta_{LL'} \delta_{M_L M_{L'}} \\ &\times (-1)^{S_1+S_2+S'+1} A_\mathrm{a} \tilde{\Lambda} D^1_{M_S - M_{S'};o}(\tilde{\beta}) \left[(2S'+1)(2S_1+1)(S_1+1)S_1\right]^{1/2} \\ &\times \begin{bmatrix} S' & 1 & S \\ M'_S & M_S - M'_S & M_S \end{bmatrix} \begin{Bmatrix} S_1 & S & S_2 \\ S' & S_1 & 1 \end{Bmatrix} \delta_{S_1 S'_1} \delta_{S_2 S'_2} \delta_{\Lambda_{w_1} \Lambda'_{w_1}} \, , \end{aligned} \tag{21}$$

wo $\begin{Bmatrix} S_1 & S & S_2 \\ S' & S_1 & 1 \end{Bmatrix}$ ein $6j$-Symbol ist, s. z. B. [18].

Die Coulomb-Wechselwirkung in erster störungstheoretischer Näherung

Bei großen Molekülabständen kann der Coulomb-Operator $\hat{V}_{\mathrm{ab}}$ nach Multipolen entwickelt und auf wenige Glieder beschränkt werden. Die allgemeine Entwicklung in irreduziblen Tensoroperatoren wurde von Rose [26] erhalten. Im k_1-Koordinatensystem wird die Rose-Entwicklung besonders einfach

$$\hat{V}_{\mathrm{ab}} = \sum_{\chi_1=0}^{\infty} \sum_{\chi_2=0}^{\infty} R^{-(\chi_1+\chi_2+1)} \sum_q \frac{(-1)^{\chi_2}(\chi_1+\chi_2)!\, \hat{Q}^{\chi_1}_{q\mathrm{a}} \hat{Q}^{\chi_2}_{q\mathrm{b}}}{[(\chi_1+q)!(\chi_1-q)!(\chi_2+q)!(\chi_2-q)!]^{1/2}} \, , \tag{22}$$

wo $\hat{Q}^{\chi_1}_{q\mathrm{a}}, \hat{Q}^{\chi_2}_{q\mathrm{b}}$ die sphärischen Komponenten der Multipolmomentoperatoren vom Rang χ_1 bzw. χ_2 für die Moleküle a bzw. b sind. Man erhält sie wie folgt:

$$\hat{Q}^\chi_q = \sum_i e_i r_i^\chi \sqrt{\frac{4\pi}{2\chi+1}} \cdot Y^\chi_q(\vartheta_i, \varphi_i) = \sum_i \hat{Q}^\chi_q(r_i, \vartheta_i, \varphi_i) \, . \tag{23}$$

Hier ist e_i die Ladung des i-ten Molekülteils, $r_i, \vartheta_i, \varphi_i$ sind die Kugelkoordinaten dieses Teils in einem zu k_1 parallelen System, dessen Ursprung im Molekülzentrum liegt. Diese Definition der Multipolmomente steht auch in [20]. Für unser System sind am wichtigsten die Dipol-Dipol- und Quadrupol-Quadrupol-Wechselwirkungen. Die entsprechenden Operatoren sind

$$\hat{V}_{\mathrm{ab\,dip.}} = -\frac{2}{R^3} \sum_q \frac{1}{(1-q)!(1+q)!} \hat{Q}^1_{q\mathrm{a}} \hat{Q}^1_{-q\mathrm{b}} \, , \tag{24}$$

$$\hat{V}_{\mathrm{ab\,quadr.}} = \frac{24}{R^5} \sum_q \frac{1}{(2-q)!(2+q)!} \hat{Q}^2_{q\mathrm{a}} \hat{Q}^2_{-q\mathrm{b}} \, . \tag{25}$$

Für ein Atom mit $L \neq 0$ und einem homodiatomaren Molekül erhält man in erster störungstheoretischer Näherung eine Quadrupol-Quadrupol-Wechselwirkung.

In unserem Modell ergibt sich das Quadrupolmoment des Atoms aus den gemittelten Abstandsquadraten der äußersten Elektronen. Der theoretische Wert des Molekülquadrupolmoments ist sehr empfindlich gegen Näherungen in den Wellenfunktionen. Daher gibt es keine einfachen Abschätzungsmethoden wie beim Atom. Für $\Lambda \neq 1$ ist die Größe

$$Q = \langle \Gamma \tilde{\Lambda} \gamma | \hat{Q}_0^2 | \Gamma \tilde{\Lambda} \gamma \rangle = \langle \Gamma - \tilde{\Lambda} \gamma | \hat{Q}_0^2 | \Gamma - \tilde{\Lambda} \gamma \rangle \tag{26}$$

wesentlich, wo $\hat{Q}_0^2$ im k_2-System angegeben wird. In [27] sind theoretische und experimentelle Q-Werte für die Gleichgewichtsabstände ϱ_0 zahlreicher Moleküle im Elektronengrundzustand angegeben. Experimentelle und theoretische Quadrupolmomente angeregter Elektronenzustände fehlen praktisch in der Literatur. Vernachlässigt man die Änderung der Elektronendichte und des Gleichgewichtsabstands beim Übergang zu angeregten Zuständen, so zeigt die Hartree-Fock-Näherung leicht, daß der Q-Wert für alle drei aus der Konfiguration $(\lambda_w)^2$ hervorgehenden Terme gleich ist. Daher kann für die Wechselwirkung eines Moleküls in irgendeinem der zu $(\lambda_w)^2$ gehörenden Zustände mit einem Atom der Q-Wert für den Grundzustand verwendet werden. Für $\Lambda = 1$ ist das Matrixelement $\langle \Pi_w 1 \gamma | \hat{Q}_2^2 | \Pi_w^{-1} \gamma \rangle$ nicht gleich 0. Diesen Fall werden wir nicht behandeln.

Die Operatoren $\hat{Q}_{qn}^2$ des Molekülquadrupolmoments aus (25) im k_1-Koordinatensystem hängen mit $\hat{Q}_{q2n}^2$ im k_2-System wie folgt zusammen:

$$\hat{Q}_{qn}^2 = \sum_q D_{qq'}^{2*}(\beta)\, \hat{Q}_{q'2n}^2 . \tag{27}$$

Einen Beitrag zu Matrixelementen $\hat{V}_{\text{ab quadr}}$ der Funktionen (1) bei $\Lambda \neq 1$ gibt nur das Glied mit $q' = 0$ in (27). Mit [18]

$$D_{m0}^l(\beta) = \left(\frac{4\pi}{2l+1} \right)^{1/2} Y_m^{l*}(\beta, 0) \tag{28}$$

haben wir folgenden Ausdruck für die Matrixelemente $\hat{V}_{\text{ab quadr.}}$:

$$\begin{aligned} \langle S M_S M_L \Lambda_{w_1} \tilde{\Lambda} L | \hat{V}_{\text{ab quadr.}} | S' M_S' M_L' \Lambda_{w_1} \tilde{\Lambda}' L' \rangle &= \delta_{\tilde{\Lambda}\tilde{\Lambda}'}\, \delta_{SS'}\, \delta_{M_S M_S'} \\ &\times \delta_{S_1 S_1'}\, \delta_{S_2 S_2'}\, \frac{4\gamma}{R^5} \left[\frac{\pi}{5(2L+1)} \right]^{1/2} \frac{\left| \begin{matrix} L' & 2 & L \\ M_L' & M_L - M_L' & M_L \end{matrix} \right|}{(2 - M_L + M_L')!(2 + M_L - M_L')!} \\ &\times Q_n \langle S_2 L \gamma_2 \| \hat{Q}_l^2 \| S_2 L' \gamma_2' \rangle\, Y_{M_L' - M_L}^2(\beta, 0) , \end{aligned} \tag{29}$$

wo $\langle S_2 L \gamma_2 \| \hat{Q}_l^2 \| S_2 L' \gamma_2' \rangle$ Matrixelemente des Atomquadrupolmoments sind, die nach [2] durch $\langle r^2 \rangle$ ausgedrückt werden.

Dispersionswechselwirkung

Mit dem Satz O der Zustände der isolierten Atome und Moleküle liefert $V_{\text{ab disp.}}$ einen Beitrag der Ordnung $1/R^6$ zur Wechselwirkungsmatrix in zweiter störungstheoretischer Ordnung. Dieser Beitrag wird Dispersionswechselwirkung genannt. Wir nehmen an, daß die Termaufspaltung der Basis 0 klein ist gegen die Energie der Elektronenkorrelation in den isolierten Molekülen. Daher kann man in den Energieausdrücken zweiter störungstheoretischer Ordnung diese Aufspaltungen weglassen und $E_{k1} = E_{01}$, $E_{k2} = E_{02}$ annehmen, wo E_{01} und E_{02} tiefe Niveaus von Atom und Molekül sind, die zum Satz O gehören. Wir verwenden mit Mavroyannis und Stephen [28] die Formel

$$\frac{1}{a+b} = \frac{2}{\pi} \int_0^\infty \frac{ab}{(a^2+\omega^2)(b^2+\omega^2)}\, d\omega \tag{30}$$

und schreiben die Matrixelemente $\hat{V}_{\mathrm{ab\,disp.}} = \hat{V}_{\mathrm{ab\,disp.\,2}}$

$$\begin{aligned} \langle S M_S S_1 k_1 S_2 k_2 | \hat{V}_{\mathrm{ab\,disp.}} | S' M_S' S_1' k_1' S_2' k_2' \rangle &= \delta_{SS'} \delta_{M_S M_S'} \delta_{S_1 S_1'} \\ &\times \delta_{S_2 S_2'} \cdot \left(-\frac{1}{R^6}\right) \sum_{qq'} \frac{1}{(1-q)!(1+q)!(1-q')!(1+q')!} \frac{2}{\pi} \int_0^\infty \langle S_1 k_1 | \hat{\alpha}^{11}_{qq'a}(\omega) | S_1' k_1' \rangle \\ &\times \langle S_2 k_2 | \hat{\alpha}^{11}_{-q-q'}(\omega) | S_2' k_2' \rangle\, d\omega\,, \end{aligned} \tag{31}$$

wo

$$\langle Sk | \hat{\alpha}^{11}_{qq'}(\omega) | Sk' \rangle = 2 \sum_{n \neq k,k'} \frac{(E_{Sn} - E_0) \langle S_n | \hat{Q}^1_q | S_n \rangle \langle S_n | \hat{Q}^1_{q'} | S_{k'} \rangle}{(E_{Sn} - E_0)^2 + \omega^2} \tag{32}$$

die dynamische Dipolarisierbarkeit bei der imaginären Frequenz $i\omega$ ist. Somit führt das Zweizentrenproblem der Dispersionswechselwirkung Atom-Molekül auf die dynamischen Polarisierbarkeiten der isolierten Partner. Der Operator $\hat{\alpha}^{11}_{qq'}(\omega)$ in Formel (32) ergibt sich bei rotierenden Koordinatensystemen als direktes Produkt zweier irreduzibler Tensoroperatoren vom Rang 1. Für das weitere ist die Einführung irreduzibler Tensoroperatoren bequem:

$$\hat{\alpha}^{\chi}_{\mu}(\omega) = \sum_{\mu_1 \mu_2} \begin{bmatrix} 1 & 1 & \chi \\ \mu_1 & \mu_2 & \mu \end{bmatrix} \hat{\alpha}^{11}_{\mu_1 \mu_2}(\omega)\,. \tag{33}$$

Allgemein ergibt sich die Polarisierbarkeit des Atoms in einen entarteten Zustand, der bei Weglassen der Spin-Bahn-Kopplung durch Quantenzahlen S, L und γ charakterisiert ist, aus Matrixelementen $\langle SL\gamma \| \hat{\alpha}^{\chi}(\omega) \| SL\gamma \rangle$. Mit der Formel für die Summe dreier Clebsch-Gordon-Koeffizienten [18]

$$\begin{aligned} &\sum_{m_1, m_2, m_3} \begin{bmatrix} j_1 & j_2 & j_{12} \\ m_1 & m_2 & m_{12} \end{bmatrix} \begin{bmatrix} j_3 & j_2 & j_{32} \\ m_3 & m_2 & m_{32} \end{bmatrix} \begin{bmatrix} j_{32} & j_1 & j \\ m_{32} & m_1 & m \end{bmatrix} \\ &= [(2_{j_{12}}+1)(2_{j_{32}}+1)]^{1/2} (-1)^{2J} \begin{Bmatrix} j_1 & j_2 & j_{12} \\ j_3 & j & j_{32} \end{Bmatrix} \begin{bmatrix} j_{12} & j_3 & j \\ m_{12} & m_3 & m \end{bmatrix} \end{aligned} \tag{34}$$

erhalten wir folgenden Ausdruck für die irreduziblen Matrixelemente

$$\begin{aligned} \langle SL\gamma \| \hat{\alpha}^{\chi}(\omega) \| SL\gamma \rangle &= (2\chi+1)^{\frac{1}{2}} (-1)^{L+\chi} \sum_{L'\gamma'} \frac{E_{SL'\gamma'} - E_{SL\gamma}}{(E_{SL'\gamma'} - E_{SL\gamma})^2 + \omega^2} \\ &\times (-1)^{L'} \begin{Bmatrix} L' & 1 & L \\ \chi & L & 1 \end{Bmatrix} |SL\gamma \| \hat{Q}^1 \| SL'\gamma' \rangle|^2\,. \end{aligned} \tag{35}$$

Dabei ist

$$\langle SL\gamma \| \hat{\alpha}^0(\omega) \| SL\gamma \rangle = -\sqrt{3(2L+1)}\, \alpha(SL\gamma)\,, \tag{36}$$

wo

$$\alpha(SL\gamma) = \sum_{M_S M_L} \frac{1}{(2S+1)(2L+1)} \langle SL\gamma M_S M_L | \hat{\alpha}^{11}_{00}(\omega) | SL\gamma M_S M_L \rangle ,$$

die über alle entarteten Zustände gemittelte Atompolarisierbarkeit in einem elektrischen Feld längs der z-Achse ist. Für Atomzustände mit $L=0$ ist nur das Matrixelement $\langle 0S\gamma \| \hat{\alpha}^0(\omega) \| 0S\gamma \rangle$ von 0 verschieden.

Beim homodiatomaren Molekül müssen wir vom Koordinatensystem k_1, in dem wir bisher alle Formeln geschrieben haben, zum System k_2 übergehen. Dabei ist

$$\hat{\alpha}^{\chi}_{\mu}(\omega) = \sum_{\mu'} D^{\chi *}_{\mu\mu'}(\beta)\, \hat{\alpha}^{\chi}_{\mu' 2}(\omega) . \tag{37}$$

Man zeigt leicht mit Hilfe der Invarianz der Rotation um die Molekülachse und der Beziehung $\hat{T}^{\gamma +}_q = (-1)^q \hat{T}^{\chi}_{-q}$ (hermitescher Operator), daß bei $\Lambda \neq 1$ nur die Matrixelemente $\hat{\alpha}^0_{02}(\omega)$ und $\hat{\alpha}^2_{02}(\omega)$ ungleich 0 sind. Die Matrixelemente dieser Operatoren erhält man wie folgt aus den Polarisierbarkeiten $\alpha_{\|}(\omega)$ und $\alpha_{\perp}(\omega)$:

$$\langle \Gamma \tilde{\Lambda} S M_S | \hat{\alpha}^0_{0L}(\omega) | \Gamma \tilde{\Lambda} S M_S \rangle = -\frac{1}{\sqrt{3}} (\alpha_{\|}(\omega) + 2\alpha_{\perp}(\omega)) , \tag{38}$$

$$\langle \Gamma \tilde{\Lambda} S M_S | \hat{\alpha}^2_{02}(\omega) | \Gamma \tilde{\Lambda} S M_S \rangle = \sqrt{\frac{2}{3}} (\alpha_{\|}(\omega) - \alpha_{\perp}(\omega)) . \tag{39}$$

Die dynamische Polarisierbarkeit ist für eine Reihe von Atomen mit kugelsymmetrischen Zuständen nach der Variationsmethode [29- 31] streng berechnet worden, für das O-Atom mit der Vielteilchen-Störungstheorie [32–33].

Kürzlich erschien eine Arbeit [34], in der die dynamische Polarisierbarkeit einiger einfacher Atome von oben und unten abgeschätzt wurde.

Eine vereinfachte Abschätzung von $\langle k | \hat{\alpha}^{\chi}_{\mu}(\omega) | k' \rangle$ ergibt sich beim Ersatz von $(E_{Sn} - E_0)$ in (32) durch eine mittlere Störungsenergie ΔE. In dieser Näherung ist

$$\langle k | \hat{\alpha}^{\chi}_{\mu}(\omega) | k' \rangle = \frac{\Delta E}{(\Delta E)^2 + \omega^2}\, 2 \langle k | \hat{\Phi}^{\chi}_{\mu} | k' \rangle \tag{40}$$

mit

$$\hat{\Phi}^{\chi}_{\mu} = \sum_{\mu_1 \mu_2} \begin{bmatrix} 1 & 1 & \chi \\ \mu_1 & \mu_2 & \mu \end{bmatrix} \hat{Q}^1_{\mu_1} \hat{Q}^1_{\mu_2} . \tag{41}$$

Notieren wir $\hat{\Phi}^1_{\mu} \equiv 0$. Berechnet man die statische Polarisierbarkeit in gleicher Näherung, so kann man $\langle k | \hat{\alpha}^{\chi}_{\mu}(\omega) | k' \rangle$ für $\chi \neq 1$ in der Form

$$\langle k | \hat{\alpha}^{\chi}_{\mu}(\omega) | k' \rangle = \frac{(\Delta E)^2}{(\Delta E)^2 + \omega^2} \langle k | \hat{\alpha}^{\chi}_{\mu}(0) | k' \rangle \tag{42}$$

schreiben. Bei $\chi = 1$ ist der Übergang von (40) nach (41) nicht durchführbar, da $\langle k | \hat{\alpha}^1_{\mu}(\omega) | k' \rangle \equiv 0$ in der gewählten Näherung. ΔE entspricht größenordnungsmäßig der Energie der ersten Resonanzanregung. London [35] schlug vor, ΔE gleich der Ionisierungsenergie des Moleküls zu setzen. Mavroyannis und Stephan [28] untersuchten ein kugelsymmetrisches Atom, setzten $\alpha(\omega)$ als $a(b+\omega^2)^{-1}$ an und erhielten unter der Bedingung, daß der Ausdruck für $\omega \to 0$ und $\omega \to \infty$

gegen die richtigen Grenzen geht, daß $\Delta E = \sqrt{\frac{n}{\tilde{\alpha}}}$, wo α die statische Atompolarisierbarkeit und n die Elektronenzahl im Atom ist. Der Vergleich mit experimentellen Daten und strengen Rechnungen zeigt, daß man bei Vielelektronenatomen die besten Ergebnisse erhält, wenn n gleich der Zahl der Elektronen ist, deren Übergänge das Atomspektrum bis zur Ionisierung ergeben (gewöhnlich die Elektronen der höchsten Schale). Diese Näherung wurde zuerst von Slater und Kirkwood erhalten [36]. Für ein Atom in einem bahnentarteten Zustand ist die Formel (40) zur Abschätzung der Dispersionswechselwirkung bequemer. Zur Berechnung der Matrixelemente $\hat{\Phi}^{\chi}_{\mu}$ benutzen wir das in [2] beschriebene Atommodell. Dabei sind in $\hat{Q}^{1}_{\mu}$ nur die Koordinaten der Valenzelektronen einzusetzen. Ein äquivalentes Verfahren benutzten Callaway und Bauer [37] zur Berechnung der Dispersionswechselwirkung eines bahnentarteten Atoms mit einem kugelsymmetrischen. Dieses Modell entspricht der Slater-Kirkwood-Näherung darin, daß die Atompolarisierbarkeit durch die Valenzelektronen bestimmt wird. Haben wir eine Valenzschale $(\tilde{n}l)^{\varkappa}$, so geben Glieder der Form $\hat{Q}^{1}_{\mu_1}(r_i, \vartheta_i, \varphi_i)\,\hat{Q}^{1}_{\mu_2}(r_j, \vartheta_j, \varphi_j)$ für $i \neq j$ keinen Beitrag zum Matrixelement $\hat{\Phi}^{\chi}_{\mu}$, weil $\hat{Q}^{1}_{\mu}(r, \vartheta, \varphi)$ ein ungerader Operator ist. Daher errechnen sich die Matrixelemente des Operators zu

$$\begin{aligned} \hat{\Phi}'^{\chi}_{\mu} &= \sum_{i=1}^{n} \sum_{\mu_1\mu_2} \begin{bmatrix} 1 & 1 & \chi \\ \mu_1 & \mu_2 & \mu \end{bmatrix} \hat{Q}^{1}_{\mu_1}(r_i, \vartheta_i, \varphi_i)\,\hat{Q}^{2}_{\mu_2}(r_i, \vartheta_i, \varphi_i) \\ &= -\begin{bmatrix} 1 & 1 & \chi \\ 0 & 0 & 0 \end{bmatrix} \sum_{i=1}^{n} r_i^{2-\chi}\,\hat{Q}^{\chi}_{\mu}(r_i, \vartheta_i, \varphi_i). \end{aligned} \tag{43}$$

In (43) setzten wir die Elektronenladung -1 und die bekannte Formel für das Produkt zweier Kugelfunktionen ein

$$Y^{l_1}_{m_1}(\vartheta,\varphi)\cdot Y^{l_2}_{m_2}(\vartheta,\varphi) = \sum_{l} \sqrt{\frac{(2l_1+1)(2l_2+1)}{4\pi(2l+1)}} \begin{bmatrix} l_1 & l_2 & l \\ m_1 & m_2 & m_1+m_2 \end{bmatrix} \begin{bmatrix} l_1 & l_2 & l \\ 0 & 0 & 0 \end{bmatrix} Y^{l}_{m_1+m_2}(\vartheta,\varphi). \tag{44}$$

Für die Matrixelemente $\hat{\alpha}^{\chi}_{\mu}(\omega)$ haben wir mit dieser Näherung

$$\langle SL(\tilde{n}l)^{\varkappa} \| \hat{\alpha}^{0}(\omega) \| SL(\tilde{n}l)^{\varkappa} \rangle = -2n\langle r^2 \rangle \sqrt{\frac{2L+1}{3}}\, \frac{\Delta E}{(\Delta E)^2 + \omega^2}, \tag{45}$$

$$\langle SL(\tilde{n}l)^{\varkappa} \| \hat{\alpha}^{2}(\omega) \| SL(\tilde{n}l)^{\varkappa} \rangle = -2\sqrt{\frac{2}{3}}\, \langle SL(\tilde{n}l)^{\varkappa} \| \hat{Q}^{2} \| SL(\tilde{n}l)^{\varkappa} \rangle \times \frac{\Delta E}{(\Delta E)^2 + \omega^2}. \tag{46}$$

Mit Hilfe der Symmetrieeigenschaften der Clebsch-Gordon-Koeffizienten zeigt man leicht, daß die Dispersionswechselwirkung von Atom und homodiatomarem Molekül bei $\Lambda \neq 1$ allgemein durch 4 Parameter bestimmt wird: ε(00), ε(22), ε(02) und ε(20), wo

$$\varepsilon(\chi_1\chi_2) = \frac{2}{\pi} \int_0^{\infty} d\omega \langle \Gamma\tilde{\Lambda}S_1 M_{S_1} | \hat{\alpha}^{\chi_1}_{02a}(\omega) | \Gamma\tilde{\Lambda}S_1 M_{S_1} \rangle \langle S_2 L_2 \gamma_2 \| \hat{\alpha}^{\chi_2}_{b}(\omega) \| S_2 L_2 \gamma_2 \rangle. \tag{47}$$

Die Ausdrücke für die Matrixelemente von $\hat{V}_{\text{ab disp.}}$ sind

$$\langle S M_S M_L \Gamma \tilde{\Lambda} L | \hat{V}_{\text{ab disp.}} | S M_S M_L' \Gamma \tilde{\Lambda}' L \rangle = -\delta_{\tilde{\Lambda}\tilde{\Lambda}'} \frac{1}{R^6} \sum_{\chi_1 \chi_2} \sum_{qq'} \varepsilon(\chi_1 \chi_2) \times \begin{bmatrix} 1 & 1 & \chi_1 \\ q & q' & q+q' \end{bmatrix}$$
$$\times \begin{bmatrix} 1 & 1 & \chi_2 \\ -q & -q' & -q-q' \end{bmatrix} \begin{bmatrix} L & \chi_2 & L \\ M_L & -q-q' & M_L' \end{bmatrix} [(1+q)!(1-q)!(1-q')!(1+q')]^{-1}$$
$$\times \sqrt{\frac{4\pi}{(2\chi_1+1)(2L+1)}}\, Y^{\chi_1}_{M_L - M_L'}(\beta, 0)\,. \tag{48}$$

Austauschwechselwirkung

Zur Berechnung der Matrixelemente von $\hat{V}_{\text{Aust.}}$ nach Formel (12) braucht man die Funktionen $\Psi^{SS_1S_2e}_{Msk_1k_2}$, die die Elektronenkorrelation in Atom und Molekül berücksichtigen. Entsprechend der Annahme 4 ziehen wir nur Einelektronenpermutationen zwischen Atom und Molekül in Betracht und berechnen den Einfluß ihrer Korrelation auf die entsprechenden Einelektronenschwänze der Atom- und Molekülwellenfunktionen (in (12) konkret für die Permutation der Elektronen 1a und 1b). Nach Annahme 4a kann man in dem Bereich des Konfigurationenraums, der dem Aufenthalt der Elektronen bei ihrem Molekül bzw. Atom entspricht, $\Psi^{SS_1S_2e}_{Msk_1k_2} \simeq \Psi^{SS_1S_2}_{Msk_1k_2}$ setzen. Mit den Ausdrücken (14) und (19) für die Wellenfunktionen von Atom und Molekül wird $\Psi^{SS_1S_2}_{Msk_1k_2}$ zum Produkt $\varphi^{\lambda w\alpha_a}_{\lambda}(\boldsymbol{r}_{1a}) \cdot \varphi^{1\alpha_b}_{nm_2}(\boldsymbol{r}_{1b})$. Die Molekülorbitale $\varphi^{\lambda w\alpha_a}_{\lambda}(\boldsymbol{r})$ setzen wir in Einzentrennäherung an. Die axiale Symmetrie des zweiatomigen Moleküls wirkt sich in dieser Näherung so aus, daß wir erstens die Kugelfunktionen nach der Molekülachse quanteln und zweitens in (19) nur zweifache Entartung der Niveaus zu gegebenem λ_w zulassen. Beim Übergang zur Quantisierung nach der z_1-Achse des k_1-Koordinatensystems haben wir

$$\varphi^{\lambda w\alpha_a}_{\lambda} = \sum_{m_1} D^{l}_{m_1\lambda}(\tilde{\beta})\, \varphi^{\lambda w\alpha_a}_{m_1}\,, \tag{49}$$

wo die $\varphi^{\lambda w\alpha_a}_{m_1}$ der Quantisierung nach z_1 entsprechen und die Beziehung von l zur Symmetrie der Einelektronenmolekülorbitale oben erklärt wurde. So geht $\Psi^{SS_1S_2}_{Msk_1k_2}$ in die Funktionen $\varphi^{\lambda w\alpha_a}_{m_1}(\boldsymbol{r}_{1a})\, \varphi^{1\alpha_b}_{\tilde{n}m_2}(\boldsymbol{r}_{1b})$ über. Da $\Psi^{SS_1S_2e}_{Msk_1k_2}$ die Korrelation der Elektronen 1a und 1b im Gebiet zwischen Atom und Molekül berücksichtigt, erhält man aus $\Psi^{SS_1S_2}_{Msk_1k_2}$ für $\varphi^{\lambda w\alpha_a}_{m_1} \cdot \varphi^{1\alpha_b}_{\tilde{n}m_2}$ noch $\varphi^{\lambda w\alpha_a 1\alpha_b}_{m_1\tilde{n}m_2}(\boldsymbol{r}_{1a}, \boldsymbol{r}_{1b})$, was nicht mehr ein Produkt von Funktionen ist, die allein von $\boldsymbol{r}_{1a}$ bzw. $\boldsymbol{r}_{1b}$ abhängen. Die Funktion $\varphi^{\lambda w\alpha_a 1\alpha_b}_{m_1\tilde{n}m_2}$ ist durch die exakte Lösung des Problems zweier gekoppelter Elektronen im Feld der Atom- und Molekülrümpfe zu bestimmen. Dabei setzt man mit demselben Fehler, den die Einzentrennäherung bringt, dieses Feld im Bereich der z_1-Achse, woher der Hauptbeitrag zum Austauschintegral kommt, axialsymmetrisch an. Daher sind die Funktionen $\varphi^{\lambda w\alpha_a 1\alpha_b}_{m_1\tilde{n}m_2}(\boldsymbol{r}_{1a}, \boldsymbol{r}_{1b})$ gleich den entsprechenden Funktionen, die in [6] für die Wechselwirkung zweier Atome bei großen Abständen erhalten wurden. Damit erhält man aus Formel (12) leicht folgenden Ausdruck für die Matrixelemente $V_{\text{Aust.}}$:

$$\begin{aligned}
&\langle S M_S M_L \Gamma \tilde{\Lambda} L | \hat{V}_{\text{Aust.}} | S' M_S' M_L' \Gamma' \tilde{\Lambda}' L' \rangle = \delta_{SS'} \delta_{M_S M_S'} n_{\mathrm{a}} n_{\mathrm{b}} \\
&\times \sum_{S_2'' L''} \sum_{S_1'' \Gamma''} G^{S_1 \Gamma}_{S_1'' \Gamma''} G^{S_1' \Gamma'}_{S_1'' \Gamma''} G^{S_2 L}_{S_2'' L''} G^{S_2' L'}_{S_2'' L''} (-1)^{S_2 + S_2' - 2S_2''} \\
&\times [(2S_1+1)(2S_2+1)(2S_1'+1)(2S_2'+1)]^{1/2} \begin{Bmatrix} S_1'' & \frac{1}{2} & S_1 \\ \frac{1}{2} & S_2'' & S_2 \\ S_1' & S_2' & S \end{Bmatrix} \\
&\times \sum_{M_L'' m_2 m_2'} \sum_{m_1' m_1} \sum_{\lambda'' \tilde{\lambda} \lambda'} \begin{bmatrix} L'' & 1 & L \\ M_L'' & m_2 & M_L \end{bmatrix} \begin{bmatrix} L'' & 1 & L' \\ M_L'' & m_2' & M_L' \end{bmatrix} \\
&\times \begin{bmatrix} \Gamma'' & \lambda_w & \Gamma \\ \tilde{\Lambda}'' & \tilde{\lambda} & \tilde{\Lambda} \end{bmatrix} \begin{bmatrix} \Gamma'' & \lambda_w & \Gamma' \\ \tilde{\Lambda}'' & \tilde{\lambda}' & \tilde{\Lambda}' \end{bmatrix} D^{l*}_{m_1 \tilde{\lambda}}(\beta) D^{l}_{m_1' \tilde{\lambda}'}(\beta) \\
&\times \langle l \alpha_{\mathrm{a}} m_1 ; \tilde{n} p \alpha_{\mathrm{b}} m_2 | J | l \alpha_{\mathrm{a}}' m_1' ; \tilde{n} p \alpha_{\mathrm{b}}' m_2' \rangle ,
\end{aligned} \tag{50}$$

wo $\begin{Bmatrix} S_1'' & \frac{1}{2} & S_1 \\ \frac{1}{2} & S_2'' & S_2 \\ S_1 & S_2' & S \end{Bmatrix}$, 9$j$-Symbole sind und $\langle l \alpha_{\mathrm{a}} m_1 ; \tilde{n} p \alpha_{\mathrm{b}} m_2 | J | l \alpha_{\mathrm{a}}' m_1' ; \tilde{n} p \alpha_{\mathrm{b}}' m_2' \rangle$ Zweielektronenaustauschintegrale, die für $l = 0, 1$ in [6] bestimmt worden sind.

Daraus folgt, daß die Integrale $\langle l \alpha_{\mathrm{a}} 0; \tilde{n} p \alpha_{\mathrm{b}} 0 | J | l \alpha_{\mathrm{a}}' 0; \tilde{n} p \alpha_{\mathrm{b}}' 0 \rangle$ (in der Quantenchemie σ-Integrale genannt) wesentlich größer sind als die übrigen. Setzt man in (50) nur diese Integrale ein, so werden die Matrixelemente $\hat{V}_{\text{Aust.}}$ diagonal bezüglich der Quantenzahlen M_L, und wir erhalten die oben erwähnte Axialnäherung. In dieser Näherung erhält man leicht, mit den Symmetrieeigenschaften der Rotationsmatrizen $D^l_{mm'}(\beta)$ und den Koeffizientenwerten von $\begin{bmatrix} \Gamma'' & \lambda_w & \Gamma \\ \Lambda'' & \tilde{\lambda} & \tilde{\Lambda} \end{bmatrix}$ und $G^{S\Gamma}_{S''\Gamma''}$, folgenden Ausdruck für die Matrixelemente $\hat{V}_{\text{Aust.}}$:

$$\begin{aligned}
&\langle S M_S M_L \Lambda_w \tilde{\Lambda} L | \hat{V}_{\text{Aust.}} | S M_S M_L \Lambda_w \tilde{\Lambda}' L' \rangle \\
&= \langle S M_S M_L \Lambda_w - \tilde{\Lambda} L | \hat{V}_{\text{Aust.}} | S M_S M_L \Lambda_w - \tilde{\Lambda}' L' \rangle , \\
&\langle S M_S M_L \Sigma_w^+ L | \hat{V}_{\text{Aust.}} | S M_S M_L \Sigma_w^- L' \rangle = 0 , \\
&\langle S M_S M_L \Sigma_w^\pm L | \hat{V}_{\text{Aust.}} | S M_S M_L \Lambda_w \tilde{\Lambda} L' \rangle \\
&= \pm \langle S M_S M_L \Sigma_w^\pm L | \hat{V}_{\text{Aust.}} | S M_S M_L \Lambda_w - \tilde{\Lambda} L' \rangle .
\end{aligned} \tag{51}$$

5. Schlußfolgerung

Die hier beschriebene Methode zur Termberechnung für ein dreiatomiges System ist nur bei hinreichend großen Abständen R zwischen Atom und zweiatomigem Molekül brauchbar, wo die Elektronenfunktionen des Systems genau genug durch eine Heitler-Rumer-Struktur darstellbar sind. Bei Verkleinerung von R sind Wechselwirkungen der Strukturen zu beachten; die Methode kann für diesen Fall verallgemeinert werden, verliert jedoch dabei die Einfachheit der Austauschintegralberechnung. Bei noch kleinerem R wird die Wechselwirkung der Strukturen so stark, daß in nullter Näherung die Methode der Molekülzustände (MO) ohne Konfigurationswechselwirkung zweckmäßig ist. Der Übergang zwischen beiden Methoden kann nur durch Lösen der Säkulargleichungen mit Konfigurations- und Strukturwechselwirkung verfolgt werden. Solche Arbeiten sind recht selten, und wir weisen nur auf eine hin [38], in der die Energieflächen für H_2 ($^1\Sigma_g^+$)+O(^3P); O(^1D) berechnet wurden. Die dort formulierte Einzentrennäherung ergibt, daß die Austauschwechselwirkung für alle Zustände, die aus $^1\Sigma_g^+ + {}^3P$ und $^1\Sigma_g^+ + {}^1D$ hervorgehen, zur Abstoßung von H_2 und O führt. Der Vergleich mit den Resultaten von [38] zeigt, daß die Wechselwirkung dieses Typs beim Kopplungsterm $^1A_1$ schon bei $R > 5$ a. E. auftritt, entsprechend einer Wechselwirkungsenergie unter 0,05 a. E. Diese Zahlen verdeutlichen den Anwendungsbereich der angegebenen Methode, wobei in diesem Bereich die Genauigkeit die der MO-Methode mit Konfigurationswechselwirkung übertrifft.

Literatur

1. Krauss, M.: Compendium of *ab initio* calculations of molecular energies and properties. NBS Technical Note, 438 (1967).
2. Nikitin, E. E., Umanskij, S. Ja.: Theoret. chim. Acta (Berl.) **13**, 91 (1969).
3. Gorkow, L. P., Pitajewskij, L. P.: D.A.N. UdSSR **151**, 822 (1963).
4. Herring, C., Flicker, M.: Physic. Rev. **134** A, 362 (1964).
5. Smirnow, B. M., Čibisow, M. I.: J. exp. theoret. Physics **48**, 940 (1965).
6. Umanskij, S. Ja., Voronin, A. I.: Theoret. chim. Acta (Berl.) **12**, 166(1968).
7. Resnikow, A. I., Umanskij, S. Ja.: Theoret. exp. Chem. **7**, 585 (1971).
8. Dashevskaya, E. D., Voronin, A. I., Nikitin, E. E.: Canad. J. Physics **47**, 1237 (1969).
9. Dashevskaya, E. D., Voronin, A. I., Nikitin, E. E.: Canad. J. Physics **47**, 981 (1969).
10. Voronin, A. I., Gordeew, E. P., Umanskij, S. Ja.: Astron. Journ. **48**, 275 (1971).
11. Nikitin, E. E., Reznikov, A. I.: Chem. Physics Letters **8**, 161 (1971).
12. Nikitin, E. E., Zembekov, A. A.: Chem. Physics Letters **9**, 213 (1971).
13. Heitler, W., Rumer, J.: Z. Physik **68**, 12 (1929).
14. Herring, C.: Rev. mod. Physics **34**, 631 (1962).
15. Herring, C.: Magnetism., Vol. 2 B, p. 2, 1966.
16. Nikitin, E. E.: Opt. i Spektr. **10**, 443 (1961).
17. Fontana, P. R.: Physic. Rev. **125**, 1597 (1961).
18. Edmonds, A. R.: Angular momentum in quantum mechanics. Princeton 1957.
19. Racah, G.: Physic. Rev. **63**, 367 (1943).
20. Sobelman, I. I.: Einführung in die Theorie der Atomspektren. Moskau 1963.
21. Nikitin, E. E., Umanskij, S. Ja.: D.A.N. UdSSR **196**, 145 (1971).
22. Bishop, D. M.: Advances in quantum chemistry, Vol. 3, p. 1, 1967.
23. Chen, Tien Chi: J. chem. Physics **29**, 347 (1958).
24. Bates, D. R., Ledsham, R., Stewart, A. L.: Philos. Trans. Roy. Soc. **246**, 215 (1953).
25. Hamermesh, M.: Gruppentheorie. Moskau 1966.
26. Rose, M. E.: J. math. Physics **37**, 2153 (1958).
27. Stogrin, D. E., Stogrin, A. P.: Molecular Physics **11**, 371 (1966).
28. Mavroyannis, C., Stephen, M. J.: Molecular Physics **5**, 629 (1962).
29. Chan, Y. M., Dalgarno, A.: Molecular Physics **9**, 349 (1965).
30. Chan, Y. M., Dalgarno, A.: Molecular Physics **9**, 525 (1965).
31. Dalgarno, A.: Advances in chemical physics, Vol. 12, p. 143, 1968.
32. Kelly, H. P.: Physic. Rev. **144**, 39 (1966).
33. Kelly, H. P.: Physic. Lett. **29** A, 30 (1969).
34. Langhoff, P. W., Gordon, R. G., Karplus, M.: J. chem. Physics **55**, 2126 (1971).
35. London, F.: Z. physik. Chem. B **11**, 222 (1930).
36. Slater, J. C., Kirkwood, J. G.: Physic. Rev. **37**, 682 (1931).
37. Callaway, J., Bauer, E.: Physic. Rev. A **140**, 1072 (1965).
38. Jangi, R. A., Badez, R. F. W.: J. chem. Physics **55**, 5369 (1971).

Professor Dr. E. E. Nikitin
Institute of Chemical Physics
Academy of Sciences
Vorobyevskoye chaussée 2–6
Moscow, V-334
UdSSR

Theoret. chim. Acta (Berl.) 28, 141—149 (1973)
© by Springer-Verlag 1973

Die Elektronenstruktur von Steroidhormonen

2. Die Nebennierenrindenhormone

H. Repmann

Lehrstuhl für Spezielle Physikalische Chemie, Technische Universität Berlin

Eingegangen am 18. August 1972

The Electronic Structure of Steroid Hormones

2. The Adrenal Cortex Hormones

Extended Hückel calculations have been carried out on the adrenal cortex hormones cortisol, cortisone, corticosterone, aldosterone and on the synthetic compounds prednisone and dexamethasone. Total energies, orbital energies, the results of Mulliken population analyses (gross charges, overlap populations, frontier electron densities), and dipole moments are presented and discussed.

Es werden erweiterte Hückel-Rechnungen an den Nebennierenrindenhormonen Cortisol, Cortison, Corticosteron, Aldosteron und an den zwei synthetischen Verbindungen Prednison und Dexamethason durchgeführt. Die Gesamtenergie, die Einelektronenenergien, die Ergebnisse der Mullikenschen Populationsanalysen (Nettoatomladungen, Überlappungspopulationen, Außenelektronenladungen) und die Dipolmomente werden mitgeteilt und diskutiert.

1. Einleitung

Im ersten Teil dieser Arbeit [1] wurde über erweiterte Hückel-Rechnungen an Sexualhormonen berichtet. In dem vorliegenden zweiten Teil werden die Ergebnisse der Untersuchungen an den Nebennierenrindenhormonen (Corticoiden) Cortisol, Cortison, Corticosteron, Aldosteron und an den zwei von den Hormonen abgeleiteten synthetischen Verbindungen Prednison und Dexamethason (Fig. 1) mitgeteilt.

Das Cortisol, ferner das mit diesem im Körper im Redoxgleichgewicht stehende Cortison und das Corticosteron besitzen vorwiegend glucocorticoide Wirkung, das heißt, sie fördern die Neubildung von Glykogen in der Leber und wirken auf den Proteinstoffwechsel abbauend. Das Aldosteron gilt als das wichtigste Mineralcorticoid. Es begünstigt den Eintritt von Natriumionen in die Zelle und fördert den Austritt von Kaliumionen aus der Zelle. Glucocorticoide und mineralcorticoide Wirkung lassen sich jedoch nicht scharf voneinander abgrenzen. Die Nebennierenrindenhormone besitzen außerdem stark entzündungshemmende Eigenschaften. Die synthetischen Verbindungen Prednison und Dexamethason übertreffen in dieser Hinsicht die natürlichen Hormone um das 10- bis 100fache, beeinflussen dagegen den Mineralstoffwechsel verhältnismäßig wenig [2].

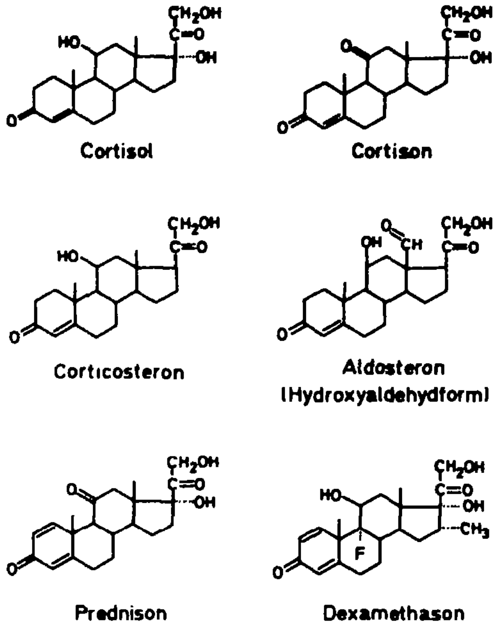

Cortisol Cortison

Corticosteron Aldosteron (Hydroxyaldehydform)

Prednison Dexamethason

Fig. 1

2. Methode

Zur Untersuchung der Elektronenstruktur der genannten Verbindungen werden hier nur EHMO-Rechnungen durchgeführt. Auf eine Ermittlung der Atomladungen nach der „Del Re–HMO"-Methode wird verzichtet, denn einerseits haben die Untersuchungen an den Sexualhormonen [1] ergeben, daß zwar die nach der EHMO-Methode berechneten Atomladungen im Mittel um einen Faktor von etwa 3 größer sind als die nach der „Del Re HMO"-Methode berechneten, daß jedoch der Gang näherungsweise übereinstimmt (linearer Korrelationskoeffizient 0,98), andererseits sind inzwischen von Carbó u. Pardillos [3] „Del Re–HMO"-Rechnungen für einige Corticoide durchgeführt worden. Die für die EHMO-Rechnungen verwendeten Parameterwerte sind bereits in [1] Tab. 1 angegeben. Hier sind lediglich die für das Fluor benutzten Parameter zu ergänzen: Slater-Exponent 2,600; Coulomb-Integrale $H_{ii}(2s) = -43{,}00$ eV, $H_{ii}(2p) = -20{,}88$ eV.

3. Molekülgeometrien

Die Koordinaten der Kohlenstoffatome der untersuchten Moleküle (ausgenommen die der Atome C-1 und C-2 von Prednison und die der Atome C-1, C-2 und C-22 [Kohlenstoffatom der Methylgruppe an C-16] von Dexamethason, die berechnet werden) werden der von Cooper und Norton [4] durchgeführten Röntgenstrukturanalyse des 12α-Brom-11β-Hydroxyprogesterons entnommen, desgleichen die Koordinaten der Sauerstoffatome an den Kohlenstoffatomen

C-3 und C-20. Für die Berechnung des 11-Carbonylsauerstoffs von Cortison und Prednison wird ein Bindungsabstand von 1,23 Å [5] gewählt und angenommen, daß das Sauerstoffatom in der Ebene durch die Atome C-9, C-11, C-12 und auf der Winkelhalbierenden des Winkels C-9–C-11–C-12 liegt. Die Lage des Sauerstoffatoms der 11β-Hydroxygruppe von Cortisol, Corticosteron, Aldosteron (Hydroxyaldehydform) und Dexamethason wird unter Zugrundelegung eines C–O-Abstandes von 1,43 Å [5] und unter Voraussetzung angenähert tetraedrischer Struktur der Bindungen am Kohlenstoffatom C-11 berechnet. Entsprechend wird bei der Berechnung der Sauerstoffkoordinaten der 17α-Hydroxygruppe von Cortisol, Prednison und Dexamethason verfahren. Bei der Berechnung der Koordinaten des Carbonylsauerstoffs am C-18 des Aldosterons wird vorausgesetzt, daß das Sauerstoffatom in der Ebene durch die Atome C-14, C-13, C-18 liegt, der C–O-Abstand 1,23 Å und der Winkel C-13–C-18–O-18 122° beträgt. Die Lage des Sauerstoffatoms der Hydroxygruppe am C-21 bezüglich der Atome C-17 und O-20 wird in Fig. 2(a) veranschaulicht. Für das Cortisol wird außerdem eine Rechnung durchgeführt, bei der das Sauerstoffatom O-21 in der Ebene durch C-17, C-20, O-20 liegt (s. Fig. 2(b)). Der Bindungsabstand C–F beim Dexamethason wird zu 1,38 Å gewählt. Die Koordinaten der Wasserstoffatome werden wie in [1] mit Hilfe eines Teilprogrammes des X-Ray-Programmsystems berechnet, wobei für die C–H-Abstände ein Wert von 1,095 Å, für die O-H-Abstände ein Wert von 0,96 Å verwendet wird.

4. Ergebnisse und Diskussion

4.1. Gesamtenergie

Die Gesamtenergie, berechnet als Summe der mit den Besetzungszahlen multiplizierten Einelektronenenergien [6, 7], ist in der ersten Spalte der Tab. 1 für die untersuchten Moleküle aufgeführt. Sie kann zur Bestimmung der stabilsten Konformation oder Konfiguration eines Moleküls herangezogen werden. Cortisol I (so werde die in Fig. 2(a) veranschaulichte Konformation des Cortisols bezeichnet, bei der das Sauerstoffatom O-21 etwa 90° aus der Ebene durch O-20, C-20 und C-21 herausgedreht ist) erweist sich 1,08 eV stabiler als das Cortisol II (so werde die in Fig 2(b) veranschaulichte Konformation des Cortisols bezeichnet, bei der die Atome O-20, C-20, C-21 und O-21 koplanar angeord-

Tabelle 1

Molekül	$-E_{\text{ges}}$ [eV]	$-E_{\text{TUMO}}$ [eV]	$-E_{\text{HBMO}}$ [eV]	$E_{\text{TUMO}} - E_{\text{HBMO}}$ [eV]
Cortisol (I)	2722	9,46	11,76	2,30
Cortisol (II)	2721	9,41	11,75	2,34
Cortison	2691	9,46	11,78	2,32
Corticosteron	2574	9,42	11,76	2,34
Aldosteron	2690	9,68	11,77	2,09
Prednison	2658	9,69	11,80	2,11
Dexamethason	2972	9,69	11,75	2,06

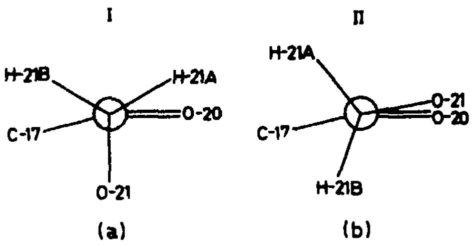

Fig 2. Konformationen in der Seitenkette von Cortisol. Newman-Projektionen in Richtung C-21, C-20

net sind). Die Röntgenstrukturanalyse des 4-Chlor-Cortisons von Duax *u. Mitarb.* [8, 9] zeigt, daß das Hydroxysauerstoffatom O-21 im Kristall 7° aus der Ebene durch O-20, C-20 und C-21 herausgedreht ist. Die Atomanordnung in der C-17-Seitenkette entspricht also im Kristall eher der Konformation II des Cortisols als der Konformation I. Nach der Rechnung ist die Konformation I stabiler. Das kann, abgesehen von dem Näherungscharakter des Rechenverfahrens, auf das Vorhandensein von intermolekularen Wasserstoffbindungen im Kristall gegenüber dem freien Molekül zurückzuführen sein. Kier [10] gibt auf Grund von erweiterten Hückel-Rechnungen eine koplanare Anordnung der Atome C-20, O-20, C-21 und O-21 an. Bei diesen Untersuchungen werden jedoch nur der Ring *D* mit der C-17-Seitenkette in die Rechnungen einbezogen. Wegen der größeren Stabilität des Cortisols I im Rahmen der hier benutzten Rechenmethode wird die bei diesem vorliegende Konformation für alle hier untersuchten Moleküle zugrunde gelegt.

4.2. Einelektronenenergien. Elektronen-Donator-Akzeptor-Eigenschaften

In Tab. 1 sind neben der Gesamtenergie des Moleküls die Energie des tiefsten unbesetzten (TUMO), die Energie des höchsten besetzten (HBMO) Molekülorbitals und die Energiedifferenz zwischen beiden Orbitalen aufgeführt. Bereits bei der Untersuchung der Elektronenstruktur der Sexualhormone [1] hat sich gezeigt, daß diese sich hinsichtlich der Energie des höchsten besetzten Molekülorbitals und somit hinsichtlich der Elektronen-Donatoreigenschaften nur wenig unterscheiden (vgl. Fig. 2 in [1]). Das Gleiche gilt auch für die hier untersuchten Nebennierenrindenhormone. Die tiefliegenden unbesetzten Molekülorbitale lassen sich den ungesättigten Teilen der Moleküle zuordnen, da in die Molekülfunktion eines solchen unbesetzten Molekülzustandes wesentlich nur die Atomfunktionen derjenigen Atome eingehen, die an Doppelbindungen beteiligt sind und deren nächste und teilweise zweitnächste Nachbarn (vgl. auch die virtuellen Außenelektronenladungen in Fig. 3c, d). In Tab. 2 sind die Energien der tiefliegenden unbesetzten Molekülorbitale eingetragen und es wird die Zuordnung dieser tiefliegenden unbesetzten Molekülorbitale zu bestimmten Teilen des betreffenden Moleküls angegeben. Die beiden tiefstliegenden Molekülorbitale sind jeweils der C-20-Carbonylgruppe bzw. den ungesättigten Teilen im Ring *A* mit dem Sauerstoffatom O-3 zugeordnet. Die Elektronen-Akzeptoreigenschaften der Corticoide sind demnach hauptsächlich durch diese Gruppen bestimmt. Aufgrund dieser tiefliegenden Akzeptor-Molekülorbitale sollte die Elektronenaffinität der

Tabelle 2. Energien der tiefliegenden unbesetzten Molekülorbitale (in eV)

Cortisol I	Cortisol II	Cortison	Corticosteron	Aldosteron	Prednison	Dexamethason
					−5,13(*k*)	−5,13(*k*)
−6,11(*e*)	−6,11(*e*)	−6,11(*e*)	−6,11(*e*)	−6,11(*e*)	−7,74(*k*)	−7,74(*k*)
	−8,61(*f*)	−8,93(*g*)	−9,30(*f*)	−9,16(*i*)	−8,94(*g*)	
−9,41(*e*)	−9,41(*e*)	−9,42(*e*)	−9,42(*e*)	−9,41(*e*)	−9 45(*f*)	−9,45(*f*)
−9,46(*f*)		−9,46(*f*)		−9 68(*i*)	−9,69(*k*)	−9,69(*k*)

Symbol	Zugeordnetes Bindungssystem
e	O=C(3)–C(4)=C(5)
f	C(20)=O
g	C(11)=O
i	O=C(18)–C(13)–C(17)–C(20)=O
k	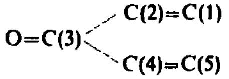 $O{=}C(3)\genfrac{}{}{0pt}{}{\diagup C(2){=}C(1)}{\diagdown C(4){=}C(5)}$

Corticoide größer als die der Androgene und viel größer als die der Östrogene sein. Dieses qualitative Ergebnis wird durch die Elektronenabsorptionsmessungen an Steroiden von Lovelock *u. Mitarb.* [11] bestätigt. Wird ausgehend von der Annahme, daß die absorbierten Elektronen die tiefstliegenden unbesetzten Molekülorbitale besetzen, für sechs Moleküle, für die sowohl Rechnungen als auch Messungen vorliegen, eine mehrfach lineare Regressionsanalyse durchgeführt, indem die Energien der zwei tiefstliegenden unbesetzten Molekülorbitale mit dem Absorptionskoeffizienten für thermische Elektronen korreliert werden, so ergibt sich mit den in Tab. 3 zusammengestellten Daten ein mehrfacher Korrelationskoeffizient von 0,84.

Die Rechnungen für Cortisol I und II zeigen, daß die energetische Lage des Molekülorbitals *f* der C-20-Ketogruppe (vgl. Tab. 2) von der Lage der Hydroxygruppe an C-21 abhängig ist. Beim Cortisol II liegt dieses Molekülorbital um 0,85 eV höher als bei dem hinsichtlich der Gesamtenergie stabileren Cortisol I.

Tabelle 3

Molekül	$-E_{1^*}$[a]	$-E_{2^*}$[a]	Elektronenabsorptionskoeffizient *A* nach [11][b]
Östron	8,85	8,04	0.03
Testosteron	9,41	6,11	8,4
19-Nortestosteron	9,40	6,10	9,1
Androstendion	9,52	8,80	23,5
Progesteron	9,41	8,53	22,2
Cortison	9,46	9,42	63,5

[a] Die Indizes 1*, 2* usw. beziehen sich auf das tiefste (TUMO), das zweittiefste usw. unbesetzte Molekülorbital. (Die Indizes 1, 2, usw. bezeichnen das höchste (HBMO), zweithöchste usw. besetzte Molekülorbital).

[b] Die angegebenen Werte gelten für Elektronen thermischer Energie. Der Elektronenabsorptionskoeffizient des Chlorbenzols ist als Einheit gewählt worden.

Die Regressionsfunktion lautet: $A = -44{,}2\,E_{1^*} - 10{,}5\,E_{2^*} - 474{,}4$.

Die energetisch höhere Lage dieses Molekülorbitals bedingt eine Verringerung der Elektronenakzeptorfähigkeit der C-20-Ketogruppe. Die Elektronen-Akzeptoreigenschaften können sich also allein schon durch Konformationsunterschiede beachtlich ändern. Die Elektronenakzeptorfähigkeit der C-20-Ketogruppe ist bei vorgegebener Konformation außerdem abhängig von der Anzahl benachbarter Hydroxygruppen. Das Progesteron besitzt keine benachbarte Hydroxygruppe. Sein der C-20-Ketogruppe zugeordnetes Molekülorbital liegt bei −8,53 eV (vgl. Fig. 2 in [1]). Beim Corticosteron, das eine Hydroxygruppe an C-21 trägt, liegt dieses Molekülorbital bei −9,30 eV, beim Cortisol, Prednison und Dexamethason, die je eine Hydroxygruppe an C-17 und C-21 besitzen, bei −9,46 bzw. −9,45 eV. Die Elektronen-Akzeptorfähigkeit der C-20-Carbonylgruppe wird demnach durch die benachbarten Hydroxygruppen vergrößert.

Vermutlich kommt den Elektronen-Akzeptoreigenschaften für den molekularen Wirkungsmechanismus der Nebennierenrindenhormone eine besondere Bedeutung zu.

4.3. *Ladungsverteilungen und Dipolmomente*

Die Ergebnisse der Mullikenschen Populationsanalysen [12] sind für das Cortisol (I) in den Fig. 3 und 4 dargestellt[1]. In Fig. 3a sind die Nettoatomladungen $Q(k)$ (in [12] als "gross charge on atom k" bezeichnet) und in Fig. 4 die Überlappungspopulationen $n(k, l)$ (in [12] als "total overlap population between atoms k and l" bezeichnet) angegeben. Nach Fukui [13] können für den intramolekularen

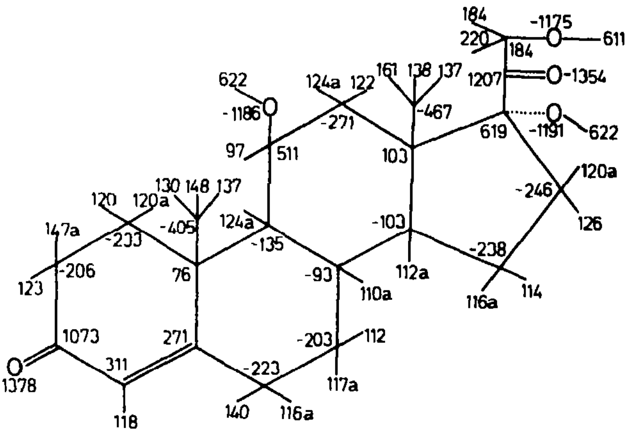

Fig. 3a

Fig. 3. a Cortisol I. Nettoatomladungen (× 10^{-3} at. E.). b Cortisol I. Außenelektronenladungen des höchsten besetzten Molekülorbitals (× (−1) 10^{-3} at. E.). c Cortisol I. Virtuelle Außenelektronenladungen des tiefsten (mit zwei virtuellen Elektronen besetzten) „unbesetzten" Molekülorbitals (× (−1) 10^{-3} at. E.). d Cortisol I. Virtuelle Außenelektronenladungen des zweittiefsten (mit zwei vituellen Elektronen besetzten) „unbesetzten" Molekülorbitals (× (−1) 10^{-3} at. E.)

---

[1] Tabellen mit den Ergebnissen der Mullikenschen Populationsanalysen für die übrigen Moleküle können vom Autor angefordert werden.

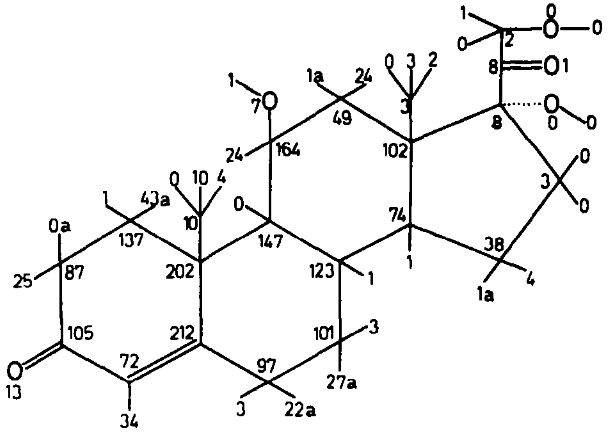

Fig. 3b

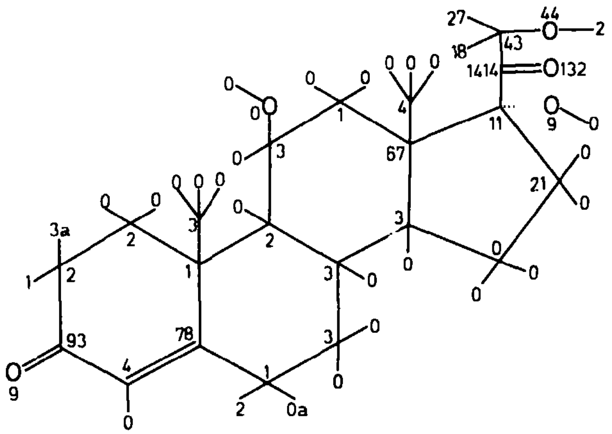

Fig. 3c

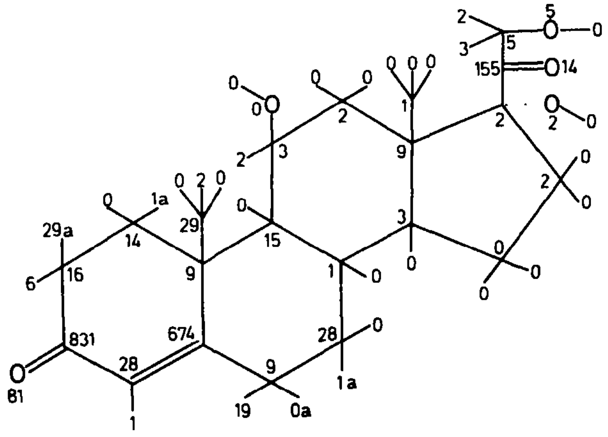

Fig. 3d

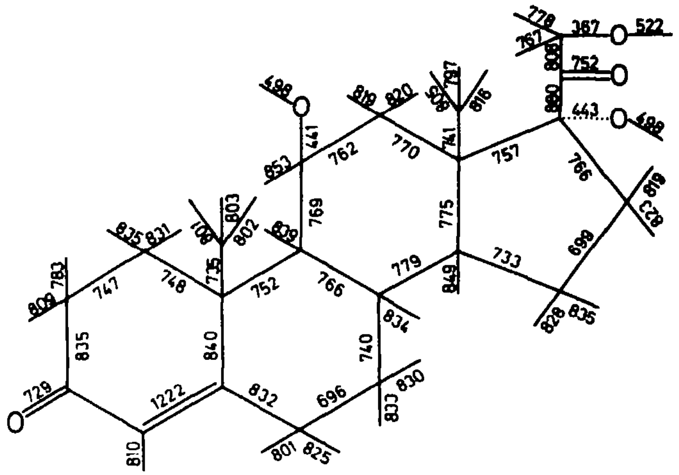

Fig. 4. Cortisol I. Überlappungspopulationen (× (− 1) 10^{-3} at. E.)

Vergleich der Reaktivität bestimmter Atome die Außenelektronenladungen herangezogen werden. Daher sind in Fig. 3b auch die Außenelektronenladungen des höchsten besetzten Molekülorbitals $N(1;k)$ (in [12] als "subtotal gross population in molecular orbital 1 on atom k" bezeichnet; bezüglich der hier durchgeführten Numerierung der Molekülorbitale vgl. Anmerkung a) zu Tab. 3) und in Fig. 3c, d die virtuellen Außenelektronenladungen $N(1^*;k)$, $N(2^*;k)$ der zwei tiefsten (jeweils mit zwei virtuellen Elektronen besetzten) „unbesetzten" Molekülorbitale aufgeführt. Die starke Lokalisierung der tiefsten unbesetzten Molekülorbitale, auf die bereits in Abschnitt 4.2 hingewiesen wurde, zeigt sich bei den virtuellen Außenelektronenladungen darin, daß sich diese hauptsächlich an solchen Atomen lokalisieren, die an Doppelbindungen beteiligt sind.

Die nach der Punktladungsnäherung berechneten Dipolmomente sind in Tab. 4 zusammengestellt. Leider konnten für die hier untersuchten Moleküle in der Literatur keine gemessenen Dipolmomente gefunden werden, so daß auf einen Vergleich zwischen Rechnung und Beobachtung verzichtet werden muß. Aus dem Vergleich der gemessenen und berechneten Dipolmomente einiger im ersten Teil dieser Arbeit untersuchter Moleküle und der Moleküle Cyclopentanol, Cyclohexanol, Cyclopentanon und Cyclohehexanon ergibt sich, daß die

Tabelle 4. Dipolmomente

Molekül	μ[D]	μ/3,08[D]
Cortisol (I)	9,64	3,13
Cortisol (II)	7,25	2,35
Cortison	10,34	3,36
Corticosteron	7,50	2,44
Aldosteron	4,85	1,57
Prednison	12,06	3,92
Dexamethason	14,54	4,72

nach der EHMO-Methode berechneten Dipolmomente im Mittel um den Faktor 3,08 zu groß sind.

In Tab. 4 sind daher auch die um den Faktor 1/3,08 verkleinerten Dipolmomente angegeben. Cortisol (I) und (II) (vgl. Fig. 2) unterscheiden sich erwartungsgemäß hinsichtlich ihres Dipolmomentes. Lägen Meßwerte für das Dipolmoment des Cortisols (in einem unpolaren Lösungsmittel) vor, so wäre es vermutlich möglich zu entscheiden, welche der beiden Konformationen beim freien Molekül tatsächlich vorliegt.

Ich danke dem Personal der Abteilung „Informatik Rechnerbetrieb" des Fachbereiches Kybernetik der Technischen Universität Berlin für die Durchführung der Rechnungen auf der IBM 360/67.

Literatur

1. Repmann, H.: Theoret. chim Acta (Berl.) **17**, 396 (1970).
2. Siehe Lehrbücher der Biochemie, z. B. Buddecke, E.: Grundriß der Biochemie. Berlin: Walter de Gruyter 1970.
3. Carbó, R., Pardillos, M.: Afinidad **27**, 513 (1970).
4. Cooper, A., Norton, D. A.: Acta crystallogr. B **24**, 811 (1968).
5. Tables of interatomic distances and configuration in molecules and ions. Special publication No. 11. London: The Chemical Society 1958.
6. Moore, E. B., Jr., Cook, W. C., Row, A. R. M.: Extended Hückel theory calculations (EXTHUC). Program 64, Quantum Chemistry Program Exchange.
7. Hoffmann, R.: J. chem. Physics **39**, 1397 (1963) Appendix.
8. Duax, W. L., Cooper, A., Norton, D. A.: Acta crystallogr. B **27**, 1 (1971).
9. Cooper, A., Duax, W. L.: J. pharm. Sci. **58**, 1159 (1969).
10. Kier, L. B.: J. med. Chem. **11**, 915 (1968).
11. Lovelock, J. E., Simmonds, P. G., Vandenheuvel, W. J. A.: Nature **197**, 249 (1963).
12. Mulliken, R. S.: J. chem. Physics **23**, 1833 (1955).
13. Fukui, K.: Fortschr. chem. Forsch. **15**, 1 (1970).

Dr. H. Repmann
Lehrstuhl für Spezielle Physikalische Chemie
D-1000 Berlin 12,
Straße d. 17. Juni 135
Bundesrepublik Deutschland

Theoret. chim. Acta (Berl.) 28, 151—160 (1973)
© by Springer-Verlag 1973

Photodecomposition of Ketene to Form Methylene

Harold Basch
Department of Chemistry, Bar Ilan University, Ramat Gan, Israel

Received September 13, 1972

Correlation curves for a least motion departure path of methylene in the photocomposition of ketene are interpreted in terms of least energy paths. It is concluded that the first excited triplet state of ketene can probably form $^3CH_2(^3B_2)$ and $^1CH_2(^1A_1)$ relatively rapidly and the first excited singlet state can give $^3CH_2(^3B_2)$ easily in a near least motion path. However, the formation of $^1CH_2(^1A_1)$ from the first excited singlet state of ketene by a near-least motion path appears to be highly improbable.

Die Korrelationskurven des Reaktionswegs mit dem geringsten anfänglichen Bewegungsaufwand des Methylens, das durch Photozersetzung des Ketens gebildet wird, werden mit Hilfe des Reaktionswegs geringster Energie interpretiert. Es wird gefolgert, daß sich aus dem ersten angeregten Triplettzustand des Ketens wahrscheinlich relativ schnell $^3CH_2(^3B_2)$ und $^1CH_2(^1A_1)$ bilden können und daß die Bildung von $^3CH_2(^3B_1)$ aus dem ersten angeregten Singulettzustand auf einem Weg, der näherungsweise dem eingangs genannten entspricht, erfolgt. Die Bildung von $^1CH_2(^1A_1)$ nach diesem Reaktionsweg ist dagegen sehr unwahrscheinlich.

Introduction

Although the chemical reactions of methylene (CH_2) in both its ground triplet ($^3CH_2$) and lowest energy singlet ($^1CH_2$) electronic[2] states are under extensive study, both experimentally and theoretically, very little is yet known about the intrinsic mechanism of the photodecomposition process by which methylene is initially generated from, for example, ketene. A knowledge of the mechanism of this reaction, as given by the potential energy surface governing the motion of the species involved, could lead to the resolution of such important but experimentally difficult questions as what are the initial kinetic and internal energies of the methylene and their primary photon energy dependencies. The lack of information about the specific vibrational level or even electronic state in which the methylene is initially formed in the photolysis experiment clearly clouds any conclusions or analysis based on subsequent methylene reactions.

Methylene is obtained in the photolysis of ketene up to the highest wavelength possible (~ 3660Å) thermodynamically consistent with the known energetics of the over-all $CH_2CO = CH_2 + CO$ reaction [1]. However, the reaction apparently requires an activation energy [2, 3]. Quantum yields for photodissociation are found to be much less than unity and variable with temperature pressure and wavelength (for $\lambda \geqq 3130$Å). These characteristics, especially the pressure dependence, indicate that the ketene excited electronic state or states populated in the photolysis process is (are) long-lived. It has also been established that at all but the highest wavelengths singlet methylene is obtained in higher yield than triplet methylene, although both are obtained above 2600Å [4]. Interestingly enough, the recombination reaction ($CO + CH_2$ to make ketene) is much faster with $^3CH_2$ than with $^1CH_2$ [4, 5]. A complicating factor in describing the photodissociation reaction mechanism is the recent series of ^{14}C experiments [5, 6]. In the reaction of methylene containing radioactive ^{14}C with CO the product ^{14}CO is found with $^1CH_2$ but not with $^3CH_2$ as the initial methylene reactant. Conversly, the photolysis of selectively labelled ketene ($^{14}CH_2CO$) produces ^{14}CO in significant percentage yield that increases with time and decreased pressure. Any proposed mechanism for the $CH_2CO = CH_2 + CO$ system should be consistent with the known properties of the process as well, of course, as with the ultraviolet spectroscopy of ketene itself.

The electronic spectrum of ketene has been reported and discussed several times with very little agreement about its assignment [7–9]. According to Laufer and Keller [9] the gas phase absorption spectrum in the 4700–2600Å range consists of diffuse bands superimposed on a broad continuum and peaking at about 3.75 eV; the total system representing a single electronic transition. This last conclusion differs with all previous opinions on the number of distinct electronic states appearing in this wavelength region. The diffuseness presumably arises from predissociation of the vibronic levels leading to the dissociation into CH_2 and CO fragments. The transition is characteristically weak [7] and with intensity similar to the electric dipole forbidden $^1A_2(n, \pi^*)$ transition in formaldehyde. The vibrational mode of the band progressions has been identified as the in-plane bending mode of the skeletal C–C–O fragment. Thus presumably in its equilibrium geometry this state is strongly in-plane bent. The next absorption systems begins at about 2130Å and consists of a series of 4 sharp bands of decreasing intensity with an average energy separation of about 1040 cm^{-1} [8].

An assignment of the long wavelength transition as well as identification of the electronic states important in the photolysis process requires an enumeration and description of the molecular orbitals (MO s) of ketene and their correlation with the combined orbital description of CH_2 and CO. In C_{2v} symmetry with the molecule in the xz plane the ground electronic structure of ketene in primarily $\ldots 7a_1^2\ 2b_1^2\ 2b_2^2$ (b_2 transforms as the coordinate y) where the convention of listing only the highest occupied MO of a given representation has been adopted. The simplest possible path for the photodissociation process is for CH_2 and CO to separate along the linear $C-C=O$ axis, preserving C_{2v} symmetry at all separations. We call this path the least motion departure (or approach) path and any deviation from this path obtained by a modest angular (in plane or out of plane) motion of the CO relative to planar CH_2 (including radial displacement of the fragments and reorientation of the carbonyl, for example) a near-least motion path.

Qualitative Considerations

For the least motion path it is possible to draw the schematic correlation diagram shown in Table 1. Here the familiar low-lying electronic states of methylene [10–12] combined with the ground state electronic configuration of CO($^1\Sigma^+$) on the right hand side are connected to the corresponding electronic states of normal ketene on the left side. The energy ordering of the ketene states is obtained by the usual considerations; ground ($^1A_1$) state lowest, singly excited triplet ($^3B_2$)

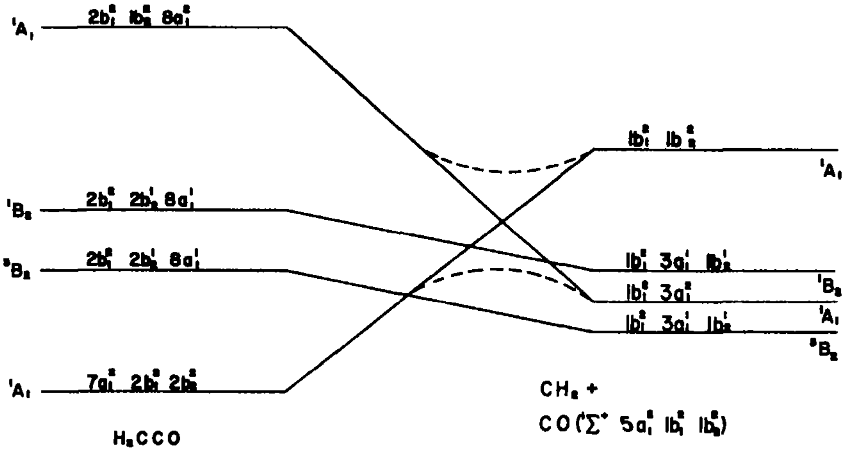
$^1A_1$ $2b_1^2$ $1b_2^2$ $8a_1^2$
$^1B_2$ $2b_1^2$ $2b_2^1$ $8a_1^1$
$^3B_2$ $2b_1^2$ $2b_2^1$ $8a_1^1$
$^1A_1$ $7a_1^2$ $2b_1^2$ $2b_2^2$
H_2CCO
$1b_1^2$ $1b_2^2$ $^1A_1$
$1b_1^2$ $3a_1^1$ $1b_2^1$ $^1B_2$
$1b_1^2$ $3a_1^2$ $^1A_1$
$1b_1^2$ $3a_1^1$ $1b_2^1$ $^3B_2$
CH_2 +
$CO(^1\Sigma^+$ $5a_1^2$ $1b_1^2$ $1b_2^2)$

Fig. 1. Schematic state correlation diagram for the least motion path in $H_2CCO = CH_2 + CO$

state next, corresponding singlet ($^1B_2$) next, and doubly excited singlet ($^1A_1$) state highest in energy. Although the energy ordering of the methylene states are well established, the total energy spread between the $^3B_2$ and upper $^1A_1$ states is not known precisely but certainly does not exceed 4eV [10, 11]. The $^1CH_2$ state referred to previously is to be identified with the lower $^1A_1$ CH_2 state and $^3CH_2$ with the $^3B_2$ state of Fig. 1.

The simple correlation diagram in Fig. 1, although strictly relevant only to the least motion path and is, as we will see, incomplete since it omits certain very relevant states, is informative. The non-identification of the ground ($^1A_1$) state electronic configuration of ketene with the combined fragments lowest energy $^1A_1$ state electronic configuration leads to an avoided crossing of these curves at intermediate separations due to configuration interaction (dashed lines). This in return predicts the presence of a barrier to chemical reaction in forming ketene from $CH_2(^1A_1)$ and $CO(^1\Sigma^+)$ by a least motion approach. In the terminology of Hoffmann and Woodward [13] the path is "forbidden" and the concerted reaction will probably proceed (if at all) by some other path in which the barrier is, at least, much reduced, if not completely absent. Based on the previous work of Hoffmann and co-workers [14] a reasonable guess at the most favourable path can be made. The least energy path is expected to involve an initially perpendicular attack of CO on the methylene plane where the carbonyl carbon lone pair is approaching the empty $1b_2$ MO of the methylene carbon.

In any event the ground $^1A_1$ state of ketene does connect with the lowest energy $^1A_1$ state of combined $^1CH_2 + CO$, contrary to previous descriptions, [4, 10, 15] and $^1A_1$ is the lowest energy singlet electronic state along the least energy path. This in turn requires that the formation of $^1CH_2$ from the excited singlet electronic state of ketene, as presumably happens in the photolysis experiment, must involve the close overlap and coupling of the vibronic levels of this latter photolysis state and the ground $^1A_1$ state in a low energy region; their direct connection being precluded even in the absence of symmetry elements.

Calculations on the low-lying electronic states of ketene has consistently predicted [7, 8, 15] the lowest energy state to be of A_2 symmetry arising out of a $2b_2 \rightarrow 3b_1$ one electron transition. In Fig. 1 no states of A_2 symmetry appear. Since the b_2 and b_1 representations in C_{2v} symmetry correlate with the π_x and π_y of the carbonyl $C_{\infty v}$ local symmetry the terminating state of this transition in ketene will correlate with one of the excited states of the free CO molecule which begin at ~ 6eV above its ground state. Thus the $^{3,1}A_2$ states which presumably lie immediately above the ground state of ketene connect to combined fragment states higher in energy than in all the $CH_2 + CO(^1\Sigma^+)$ states shown in Fig. 1.

Of course, if the band system observed in the long wavelength region of the ketene spectrum is identified with the calculated A_2 state then the longest wavelength transitions are to a strongly in-plane bent geometric conformer of that state. The lower symmetry of the bent geometry will allow configuration mixing with the like-spin B_2 states of Fig. 1 (to give A'' states in C_s symmetry).

This is important since, as it appears from Fig. 1, the relative ordering of the lowest A_2 and B_2 states inverts on going from normal ketene to the dissociated $CH_2 + CO$ fragments and thus would be expected to cross in the least motion path symmetry (C_{2v}). The resultant avoided crossing in the lower symmetry (C_s) allows a direct connection between the $^3A_2$ state of normal ketene and the $^3CH_2 + CO(^1\Sigma^+)$ combined fragment ground states with a barrier for dissociation. Again, the magnitude of this barrier is departure geometry dependent and in the least energy path for this state possibly wholly absent.

Results

In order to obtain more quantitative information about the behavior of all these states as a function of $CH_2 - CO$ separation *ab initio* single and multi configuration self consistent field (SCF) calculations were carried out in an extended basis set of contracted gaussian orbitals. The geometry of the CH_2 and CO fragments were frozen at their normal ketene values [11] and calculations carried out at $C - C$ distances (R) identified by their difference from the normal ketene value; *i.e.* $\Delta R = 0, 2, 4,$ and 10 a.u. The basis set was taken as Dunning's 4^s, 2^p contraction [17] of Huzinaga's (9^s, 5^p) C and O atom gaussian sets [18]. The carbon atom basis sets were each augmented by a single two component orbital of s-type with analytical form, 0.690445(0.01918) + 0.3296448(0.009401) to mimic a 3*s* atomic orbital. Here the exponents are in parenthesis preceded by the respective gaussian function expansion coefficient and both were chosen based on previous work [19–22]. The need for extravalent basis orbitals of this type is demonstrated for the B_2 states. For the hydrogen atom Huzinaga's 4^s set was scaled by a factor of $(1.2)^2$ and the smallest exponent member split off to form a separate basis function, as previously [21]. The final basis set is thus 36 functions contracted from 84 gaussians.

Open shell single configuration SCF calculations were carried out on the lowest energy $^{1,3}B_2$ and $^{1,3}A_2$ electronic states of ketene. The former states arise out of the $2b_2 \rightarrow 8a_1$ one electron transition from the ketene ground state electronic configuration. Since the $^{1,3}A_2$ states arising out of the $2b_2 \rightarrow 3b_1$ excitation correlate with the excited electronic states of the CO molecule at large interfragment separations the single configuration wave functions valid for these states in normal ketene are not proper space eigenfunction for the corresponding CO states due to the neglect of averaging over degenerate π_x and π_y orbital occupancies. Therefore, single configuration SCF results were obtained only at $\Delta R = 0$ and 2 a.u. for the A_2 states. This situation can be treated correctly and automatically by a configuration interaction approach of the open shell states at all R; in which case the proper degeneracies would appear naturally at large R.

The single configuration SCF computer programs used in this study have been described previously [20]. Essentially the orthogonality constrained method described by Segal [23] is used to solve the SCF equations. Careful checking revealed no initial input dependence of any SCF result reported here.

For the $^1A_1$ states of ketene at all R multi configuration SCF calculations were carried out using all 6 possible configurations arising from the distribution of 2 spin-paired sets of electrons among 4 orbitals ($7a_1$, $2b_2$, $8a_1$, and $3b_2$). Both configuration and basis orbital expansion coefficients were simultaneously optimized in the usual variational procedure [24, 25]. The Fock-type equations for the orbitals are similar to those described in detail previously and the equations were solved for in the same orthogonality constrained manner [24]. This particular set of configurations were chosen based on a consideration of Fig. 1 and a previous such study on ethylene [24]. An additionally important consideration was the expectation that in using a more restricted number of configurations the orbital nature of the $8a_1$ MO would be strongly dependent on the choice of configurations. Essentially, the problem revolves about the point that the occupancies of the $2b_2$ and $8a_1$ MO's are strong functions of R as shown in Fig. 1. It follows then that the $8a_1$ MO that properly correlates the $2b_2$ orbital will probably look very different from the $8a_1$ MO necessary to correlate the $7a_1$ orbital. There are thus two "$8a_1$" MO's and we have here allowed the variational procedure to find and use the more important of the two.

The resulting state energies are displayed in Table 1 and drawn in Fig. 2. The fine details of these curves cannot, of course, be determined precisely from the widely separated values of interfragment separation (ΔR) appearing in Table 1. The curves of Fig. 2 are thus semi-schematic. Based on the arguments to be subsequently presented it is not believed that more precise curves for the least motion path would alter any conclusions presented here.

Table 1. Energies of various states of ketene as a function of C–C bond distance[a]

State	$^1A_1$	$^1A_1$[b]	$^3A_2$	$^1A_2$	$^3B_2$	$^1B_2$
$\Delta R = 0$	−151.6967 (−151.6721)[c]	−150.9368	−151.5574	−151.5500	−151.4676	−151.4615
$\Delta R = 2$	−151.5110	−151.4401	−151.3996	−151.3991	−151.5682	−151.4978
$\Delta R = 4$	−151.5544	−151.4297			−151.5926	−151.5200
$\Delta R = 10$	−151.5585	−151.4291			−151.5937	−151.5215

[a] Tabulated as R, the deviation of the C–C bond distance from the ketene equilibrium geometry value (in a. u.).

[b] Second lowest energy solution for the 6 configuration MC–SCF.

[c] Single configuration SCF energy.

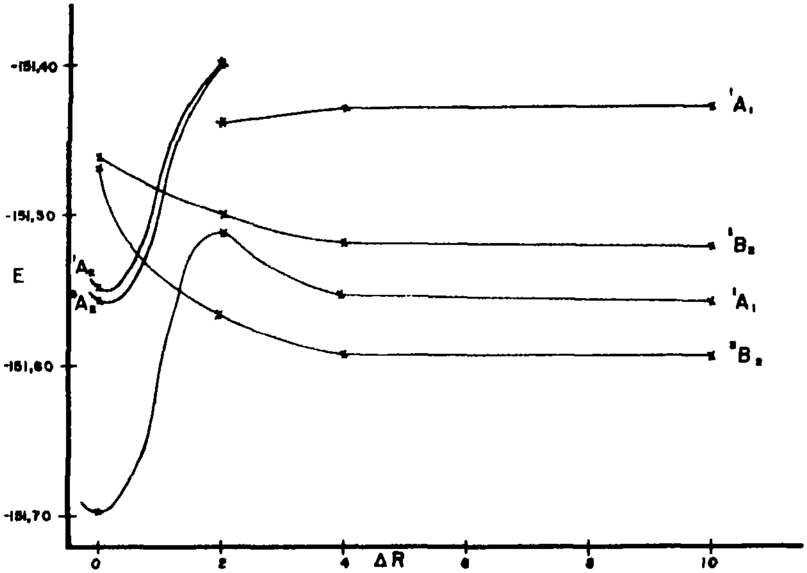

Fig. 2. Calculated state correlation diagram for the least motion path in $H_2CCO = CH_2 + CO$

Table 2. Orbital character of the valence molecular orbitals of ketene

$7a_1$	CO
$8a_1$	CH_2
$3b_1$	CO
$2b_2$	CH_2
$3b_2$	CO

The orbital character of the various relevant MO's as the interfragment separation becomes large is shown in Table 2. There are no differences among the multi or single configuration SCF results with regard to the orbital character of these MO's. The $2b_2 \rightarrow 3b_1 (^{3,1}A_2)$ upper states are here seen to have the character of charge transfer states, $CH_2 \rightarrow CO$. However, probably at intermediate interfragment separations a CO→CO transition of this symmetry will drop lower in energy than the "charge transfer" state. This further justifies not taking the $^{1,3}A_2$ state calculations beyond $\Delta R = 2$ a.u. in the single configuration SCF formalism.

The $2b_2 \rightarrow 8a_1 (^{3,1}B_2)$ states are here calculated to have substantial Rydberg character at the equilibrium ketene geometry, becoming pure valence as R increases. The relevant Rydberg basis orbital is centered primarily on the methylene carbon with almost no contribution from the carbonyl carbon Rydberg basis orbital. Price and co-workers [26] have identified several members of a Rydberg series in the electronic spectrum of ketene leading to an (adiabatic) ionization energy of 9.60 eV. This value of the first ionization potential is confirmed by the photoelectron spectroscopy (PES) study of Baker and Turner [27]. The quantum defect of $\delta \sim 1.07$ assigned by Price *et al.* [26] can be used to calculate an (adiabatic) energy of 5.95 eV for the $n = 3$ member of the series from the Rydberg formula. This compares with the calculated (vertical) $^1A_1 \rightarrow {}^1B_2$ excitation energy of 6.40 eV from Table 1. The band system observed by McGlynn and co-workers [8] with an (adiabatic) energy of 5.82 eV has the form of a Rydberg series (several sharp bands of decreasing intensity) and is similar to the first band system in the PES [27] where an interval of $\sim 1020\,\mathrm{cm}^{-1}$ has also been observed and identified as a $C-C=O$ stretch mode. A strong similarity in the intensity and vibrational frequency distributions between a Rydberg band system and the corresponding ionization process in the PES has been noted [28]. A measurement of the optical absorption spectrum at 2150–1950Å in condensed phase would establish the upper state orbital nature of the absorption in this region [29]. Such a drastic change in orbital character as a function of internuclear separation is not unknown; Mulliken has recently discussed several such cases [30].

Del Bene [15] has calculated that a $^3A_1$ state should lie just above the $^{1,3}A_2$ states but presumably still below the $^{1,3}B_2$ states. The equilibrium geometry for the $^3A_1$ state is calculated to be out-of-plane bent with an elongated $C-C$ bond (1.54Å) relative to that in normal ketene ($\sim$1.32Å). This state arises essentially out of a $2b_2 \rightarrow 3b_2$ one electron transition and from Table 2 is thus seen to correlate with a $CO\,^3(\pi \rightarrow \pi^*)$ transition which begin at 6 eV in normal CO. This state can therefore not play on important role in the long wavelength photochemistry of ketene.

Discussion

The photodissociation reaction can now be discussed based on Fig. 2 and considerations previously outlined. The objective is to consider the feasibility of a near least motion path for the long wavelength photodissociation reaction. Again it should be emphasized that the curves in Fig. 2 are not precise even for the least-motion path and that, in any event, they will certainly be modified for their respective least energy paths. In the photolysis experiment at long wavelength ketene is apparently excited exclusively into the $^1A_2$ state which lies very close to and is interspersed with the vibronic levels of the $^3A_2$ state. There are several reasons for adopting this point of view. Firstly, no sensitized biacetyl emmission is observed using light between 2800 and 3660Å [31]. Then there is the cogent analysis of Laufer and Keller [9]. It is also quite reasonable to assume that where a singlet and triplet state are so close-lying the greater probability consistently resides in the singlet being preferentially populated for a given wavelength energy excitation in the range in which the 2 states overlap.

As a function of interfragment separation the rising $^{3,1}A_2$ curves are seen to cross the rapidly descending $^3B_2$ state, as expected. Geometry and configuration optimization would presumably moderate the climb rate of the A_2 states such that, all factors considered, the crossing in the least energy path would take place at lower relative energy for the $^1A_2$ state than shown while the avoided crossing of $^3A_2$ with $^3B_2$ (in the C_s geometry of an in-plane bent structure) will put the lower branch state at even lower energy. Formation of $^3CH_2$ from the $^3A_2$ state of ketene is thus seen to be favorable in a near least motion path with perhaps a small barrier to photodissociation. A more detailed analysis must await a greater knowledge of the potential surface for the following reasons. The lowest energy $^3A_2$ vibronic levels presumably correspond to the in-plane bent equiblibrum geometry for this state. For these vibronic levels the barrier to photodissociation would be expected to be highest except that the more distorted the system is away from C_{2v} symmetry presumably the greater the interaction between $^3A_2$ and $^3B_2$ and hence (relatively speaking) the greater the tendency to the lower the barrier through configuration interaction.

The behavior of the $^1A_2$ and $^3B_2$ curves follows the same qualitative considerations for a near-least motion least energy path as for the $^3A_2$, $^3B_2$ pair with the additional need for intersystem crossing. Since an intersystem crossing is necessary for any mechanism that produces $^3B_2$ methylene from $^1A_2$ ketene its need cannot prejudice any given mechanism. With this in mind the near-least motion path looks reasonably favorable as the means of producing $^3CH_2$ from $^1A_2$ ketene. Of course, in long wavelength photolysis producing initially $^1A_2$ ketene there will be a higher barrier to overcome than starting with $^3A_2$ ketene.

The crossing of the $^1A_1$ and $^3B_2$ curves at intermediate interfragment separations means that initial excitation to the A_2 state of ketene could also be followed by the production of $^1CH_2$ depending on spin-orbit coupling strength, height of the barrier along the $^1A_1$ path, and $^1A_1 - {}^3B_2$ energy gap in CH_2 itself. This process could take place even at long wavelengths if the smoothing out of the barrier in the energy optimized path for the $^1A_1$ state allows the $^3B_2$ state to cross $^1A_1$ at lower energies than shown in Fig. 2. This is not definite, however, since the optimized geometry for $^3B_2$ is in-plane bent whereas the lowest energy path for $^1A_1$ is expected to be out-of-plane bent. Again it is a question of competing factors and there could be a number of no symmetry geometric conformers with similar probabilities for $^3B_2 \rightarrow {}^1A_1$ cross over.

The production of $^1A_1$ methylene ($^1CH_2$) from $^1A_2$ ketene at energies above the $^1A_1$ barrier does not at all appear feasible by a near-least motion departure, according to Fig. 2, even taking into account geometric relaxation. As pointed out [4] the close overlap and hence coupling between vibronic levels of $^1A_2$ and $^3A_2$ states should make the intersystem crossing rate between them particularly high. However, since precursor $^3A_2$ ketene is not observed as shown, for example, by the absence of an O_2 perturbation effect on the ketene spectrum [9] this mechanism cannot contribute significantly to the production of $^3CH_2$ and certainly not $^1CH_2$. The problem with the direct production of ground state $^1A_1$ methylene from $^1A_2$ ketene in a least motion path is that the $^1A_2$ and $^1A_1$ curves don't approach each other and hence their vibronic levels cannot couple which is required in order to obtain a transition rate between them. Of course, an in-plane bent near least motion path will lower the $^1A_2$ energy curves while possibly raising the $^1A_1$ energy which is expected to be out-of-plane bent in it's least energy path. Nonetheless, the gap in Table 1 and Fig. 2 appears rather too large to be bridged by any simple distortion of the least-motion path. The geometry optimized curves of Del Bene (Fig. 4) [15], when corrected for the proper behavior of the $^1A_1$ state, constitute important evidence in this regard.

Neither can the $^1B_2$ state play an important intermediary role here. The $^1A_1 \rightarrow {}^1B_2$ transition is electric dipole allowed in ketene and should be observed.

Although SCF calculations on singlet states can be difficult to interpret [20, 21] triplet states do not seem to present any such problem. Here the (vertical) $^3B_2$ state is calculated to fall at 5.58 eV above the single configuration SCF $^1A_1$ state (Table 1). It is difficult to imagine a spectroscopic triplet state lying below the calculated SCF state in the basis set used here. This fixes the corresponding spectroscopic $^1B_2$ state in the neighborhood of 6 eV in ketene. In methylene the $^1B_2 - {}^1A_1$ adiabatic energy difference is known experimentally [11] to be 0.88 eV. Although the geometry dependence of the $^1B_2$ state is not known it's very different orbital character from the $^1A_2$ state suggests that interaction between them will be small in geometric conformers in which such interaction is symmetry allowed. The $^1B_2$ curve is thus expected to always be above $^1A_1$.

For wavelengths around and below the dissociation energy to form $^1CH_2$ it is necessary to explore to what extent the lower vibronic levels of $^1A_2$ overlap and couple with the upper orbitational levels of the ground $^1A_1$ state in ketene. Absorption to $^1A_2$ begins at 2.65 eV [19] whereas $\Delta H^0_{f298^0}$ for $H_2CCO(^1A_1) = CH_2(^3B_2) + CO(^1\Sigma^+)$ is put at ~3.52 eV with the formation of $CH_2(^1A_1)$ at least 0.1 eV higher in energy [1]. Even according to Dixon and Kirby [7] who place the lowest absorption to the $^1A_2$ state at 3.22 eV such overlap exists [4]. The number of overlapping levels clearly depends on the height of the barrier to formation of $^1A_1$ but not necessarily along its least energy path where the barrier height is expected to be smallest. It would appear that the barrier is necessary in order to effect the stronger bound state-bound state coupling as opposed to bound-continium coupling which is not efficient for photodissociation processes in the absence of a curve crossing [32]. Clearly we must have more information about the multidimensional potential surface for these states in the neighborhood of the equilibrium geometry. Generally, however, it appears that for a near-least motion path at long wavelengths ($\lambda > 3300$ Å) the possibility at least exists for $^1A_2$ coupling with quasi-bound vibrational levels of the ground $^1A_1$ state above the dissociation energy to $^1CH_2$ with tunneling to the dissociated singlet products.

The photolytically generated $^1A_2$ state of ketene at long wavelength is thus seen to have two available channels in a near least motion path. To form $^3CH_2$ involves a spin-orbit coupling induced intersystem crossing to the $^3B_2$ state in the neighborhood of the intersection point of the two curves. Below the crossing point the probability to form $^3CH_2$ presumably decreases. The formation of $^1CH_2$ appears to be feasible only in the direction that a barrier to the thermal decomposition of ketene (to singlet products) exists. Under these circumstances it can be expected that the $^1A_2$ state will in general be relatively long-lived due to the absence of a rapid near-least motion relaxation path.

Rowland and co-workers [5, 6] have recently suggested that the ketene photodissociation reaction to form $^1CH_2$ goes through a 3 membered ring oxirene intermediate. The theoretical evidence presented here suggests that $^1CH_2$ will not be readily obtained in a near-least motion path. Since the ketene $^1A_2$ state is expected to be relatively longlived rearrangement of normal ketene to a ring structure before dissociation is a possibility. The question of the least energy path for the rearrangement process remains to be answered.

Acknowledgements. This work was supported by the U. S. National Bureau of Standards under grant number 1-35962.

References

1. Carr, R. W., Eder, T. W., Topor, M. G.: J. chem. Physics **53**, 4716 (1970).
2. Ho, S. Y., Noyes, W. A.: J. Amer. chem. Soc. **89**, 5091 (1967).
3. Strachan, A. N., Thornton, D. E.: Canad. J. Chem. **46**, 2353 (1968).
4. DeGraff, B. A., Kistiakowsky, G. B.: J. physic. Chem. **71**, 3984 (1967).
5. Montague, D. C., Rowland, F. S.: J. Amer. chem. Soc. **93**, 5381 (1971).
6. Russell, R. L., Rowland, F. S.: J. Amer. chem. Soc. **92**, 7508 (1970).
7. Dixon, R. N., Kirby, G. H.: Trans. Faraday Soc. **62**, 1406 (1966).
8. Rabalais, J. W., McDonald, J. M., Scherr, V., McGlynn, S. P.: Chem. Reviews **71**, 73 (1971).
9. Laufer, A. H., Keller, R. A.: J. Amer. chem. Soc. **93**, 61 (1971).
10. Chu, S. Y., Sui, A. K. Q., Hayes, E. F.: J. Amer. chem. Soc. **94**, 2969 (1972).
11. Hertzberg, G.: Electronic spectra of Polyatomic molecules. Princeton: Van Nostrand 1967.
12. O'Neal, S. V., Schaefer III, H. F., Bender, C. F.: J. chem. Physics **55**, 163 (1971); Del Bene, J. E.: Chem. Physics Letters **9**, 68 (1971).
13. Hoffmann, R., Woodward, R. B.: Accounts Chem. Res. **1**, 17 (1968).
14. Dobson, R. C., Hayes, D. M., Hoffmann, R.: J. Amer. chem. Soc. **93**, 6188 (1971); Hoffmann, R.: J. Amer. chem. Soc. **90**, 1475 (1968); Hoffmann, R., Gleiter, R., Mallory, F. B.: J. Amer. chem. Soc. **92**, 1460 (1970).
15. Del Bene, J.: J. Amer. chem. Soc. **94**, 3713 (1972).
16. Nesbet, R. K.: J. chem. Physics **43**, 4403 (1965).
17. Dunning, T. H.: J. chem. Physics **53**, 2823 (1970).
18. Huzinaga, S.: J. chem. Physics **42**, 1293 (1965).
19. Basch, H., McKoy, V.: J. chem. Physics **53**, 1628 (1970).
20. Basch, H.: Molecular Physics **23**, 683 (1972).
21. Basch, H., Robin, M. B., Kuebler, N. A.: J. chem. Physics **47**, 1201 (1967).
22. Dunning, T. H., Hunt, W. J., Goddard III, W. A.: Chem. Physics Letters **4**, 146 (1969).
23. Segal, G.: J. chem. Physics **53**, 360 (1970).
24. Basch, H.: J. chem. Physics **55**, 1700 (1971).
25. Das, G., Wahl, A. C.: J. chem. Physics **44**, 87 (1966).
26. Price, W. C., Teegan, J. P., Walsh, A. D.: J. chem. Soc. **1951**, 920.
27. Baker, C., Turner, D. W.: Chem. Comm **1969**, 481.
28. Basch, H., Robin, M. B., Kiebler, N. A., Baker, C., Turner, D. W.: J. chem. Physics **51**, 52 (1969).
29. Robin, M. B., Kuebler, N. A.: J. molecular Spectroscopy **33**, 274 (1970); Miron, E., Raz, B., Jortner, J.: J. chem. Physics **56**, 5265 (1972).
30. Mulliken, R. S.: Chem. Physics Letters **14**, 137, 141 (1972).
31. Grossman, M., Semelick, G. P., Unger, I.: Canad. J. Chem. **47**, 3079 (1969).
32. Gebelein, H., Jortner, J.: Theoret. chim. Acta (Berl.) **25**, 143 (1972).

Prof. Harold Basch
Department of Chemistry
Bar Ilan University
Ramat Can
Israel

Theoret. chim. Acta (Berl.) 28, 161--168 (1973)
© by Springer-Verlag 1973

Hydrogen Bond Studies

66*. *Ab initio* Studies of the Conformation of the Oxonium Ion in Solids

Jan Almlöf

Institute of Chemistry, University of Uppsala, Box 531, S-751 21 Uppsala, Sweden

Ulf Wahlgren

Institute of Theoretical Physics, University of Stockholm,
Vanadisvägen 9, S-113 46 Stockholm, Sweden

Received February 3, 1972/August 28, 1972

The oxonium ion, H_3O^+, has been studied with the MO-LCAO method in order to determine its equilibrium geometry. The main purpose has been to study effects of the external electrostatic forces exerted on the ion situated in crystals whose structures are experimentally known. Calculations have also been performed on the free ion, where the energy minimum is found for a non-planar conformation with H-O-H angles of 116.6° and O-H distances of 0.96 Å. The effect of an external field is essentially to lengthen the O-H distances and decrease the H-O-H angles in order to form approximately linear hydrogen bonds.

Die Gleichgewichtsgeometrie des Oxoniumions H_3O^+ wurde mit Hilfe der MO-LCAO Methode bestimmt. In erster Linie sind die Effekte, die von externen elektrostatischen Kräften auf das Ion in Kristallen mit bekannter Struktur ausgeübt werden, untersucht worden. Es wurden aber auch Rechnungen für das freie Ion durchgeführt, wobei die minimale Energie im Falle der nicht planaren Konformation mit H-O-H Winkeln von 116,6° und einem O-H-Abstand von 0,96 Å erhalten wurde. Der Effekt eines externen Feldes besteht hauptsächlich in einer Verlängerung der O-H Bindung und einer Verringerung des H-O-H-Winkels, so daß näherungsweise lineare Wasserstoffbindungen gebildet werden.

Introduction

The properties of the oxonium ion have long attracted great interest, both from a theoretical and experimental standpoint. A number of X-ray investigations have therefore been performed on crystal structures containing this ion. Unfortunately, this method gives very poorly resolved hydrogen atom positions. Experimental difficulties have hitherto prevented the use of the neutron diffraction technique which is a more powerful tool in that context. Hence, not even the geometry of the oxonium ion has yet been established accurately. In all crystals studied so far, however, the H_3O^+ ion is pyramidally surrounded by three electronegative atoms at short distances. This is usually taken as evidence for short and hence approximately linear hydrogen bonds, indicating a pyramidal geometry for the oxonium ion. A non-planar conformation for the free ion was also suggested by Joshi [1], who performed a non-empirical MO-LCAO calculation with an all-electron one-centre wavefunction. In this case an H-O-H angle of 111° was obtained for the equilibrium geometry.

---

* Part 65 will appear in Acta Cryst. in the near future.

In contrast, Grahn [2,3] found a planar geometry both from MO and from VB calculations, and the same result was reported by Moskowitz and Harrison [4] and by Kollman and Allen [5] after much more elaborate calculations. The potentials for symmetric bending in these cases were very shallow, however. In the calculations presented below, the energy minimum was found with a non-planar geometry for the free ion, but, since the inversion barrier found is only 0.3 kcal/mole^{-1}, there is no fundamental difference between our results and the previous ones. They all indicate, in fact, that the energy difference between a planar and a pyramidal geometry of the free ion is too small to make any safe conclusion to be drawn as to the conformation of the ion in solids.

The calculations reported below were therefore undertaken in an attempt to study the oxonium ion when subjected to force fields created by a real crystal environment.

Method and Calculations

The molecular calculations were carried out using the MO LCAO method, allowing an external electrostatic field to be taken into account when appropriate. A local modification of the program IBMOL IV [6] was used to perform these calculations. The MO's were expanded into a set of basis functions, each consisting of a linear combination of single Gaussians. The basis set used contained four *s*- and two *p*-type contracted functions centred on an oxygen, and two *s*- and one *p*-type function on each hydrogen. Thus, a total of 25 contracted basis functions were employed. The orbital exponents and contraction coefficients are given in Table 1.

When an ion is situated in an ionic crystal, it is assumed that the predominant effects on its properties can be attributed to the electrostatic influence from surrounding ions. As this is a long-range effect, the electrostatic potential from the whole crystal ought to be taken into account in the calculations. (Indeed, test calculations have shown that the electrostatic forces on an ion in a crystal cannot be satisfactorily described by including only a small number of neighbouring atoms). This potential can easily be evaluated following a method proposed by Ewald [9] and further developed by Bertaut [10], a brief description of which is given in the Appendix.

The ion was studied in four different surroundings: in solid hydrochloric acid monohydrate [11] and in the three non-equivalent positions in solid sulfuric acid dihydrate [12]. For each surrounding, the potential was evaluated at a large number of points within the van der Waals surface of the ion in its approximate equilibrium position. The surroundings of the ion were then approximately described by 45 suitably placed point charges, the values of which were determined by a least-squares fit to the calculated potential values. In order to obtain the best fit the positions of the point charges were also varied. However, point charges were always placed at the sites of the three hydrogen-bonded acceptor atoms around the H_3O^+ ion.

Using this approach, the inclusion of external electrostatic forces in the Hartree-Fock scheme is a trivial matter, since these point charges will contribute to the one-electron part of the Fock-operator in exactly the same way as they would if they were atomic nuclei.

The total energy of the ion was calculated with 12–14 conformations in each environment, as well as for the free ion. The equilibrium geometry for each case was obtained by fitting an analytic expression to these energy values and determining its minimum. The energy expressions used were of the form

$$A\cdot[1-\exp\{-\beta(r-r_0)\}]^2+p(r,\theta),$$

where the first term is simply a Morse function, p is a polynomial of second degree in r and θ, r denotes the O–H distance and θ the H–O–H angle.

The Ewald method applied for the potential calculation requires a description of the crystal structure in terms of point charges. This was no problem in the case of the sulfate and chloride ions, where the atomic positions are experimentally known. The sulfur and oxygen atoms in the sulfate ion were assigned formal charges of +1.34 and −0.835 from previous ab initio calculations [13]. The same strategy could obviously not be used for the oxonium ions, since only the positions of the oxygen atoms were known from experiments.

Instead, the orientation of each oxonium ion was systematically varied with the oxygen atom fixed in its experimentally determined position. For each orientation the classical electrostatic energy of the crystal was calculated, using a method described by Baur [14]. The geometry and charge distribution used for the H_3O^+ ion in these calculations were chosen from the calculations made on the free ion. These properties were not quite the same as those obtained in the final calculations. However, these slight variations turned out to have little effect on the final result.

The conformation of the H_3O^+ ion was restricted to obey C_{3v} symmetry in all calculations, although, in the case of sulfuric acid dihydrate the surroundings did not possess perfect threefold symmetry. This restriction was not considered to be a serious drawback, since the deviations were quite small and would not affect the general picture of the effect of a crystal environment.

Results and Discussion

As mentioned earlier, previous calculations using similar methods have indicated a planar conformation for the H_3O^+ ion. The calculations made by Kollman and Allen were slightly better than ours energywise (−76.316 a.u., compared to −76.222 a.u. in the present work). However, the geometry was not fully optimized in their calculation, and a similar strategy would have resulted in a planar conformation in our case also. Moskowitz and Harrison made a more careful search of the energy surface. Their basis set was quite small, however ($E_{\min} = -75.846$ a.u.), and especially the lack of polarization functions on hydrogen may be responsible for the discrepancy between their results and ours.

The calculated total energies for the different conformations and environments are shown in Table 2. A comparison with equivalent calculations on the water molecule [15] gives a proton affinity for the water molecule of 189 kcal · mole^{-1}. The experimental value for the proton affinity is 182 ± 7 kcal · mole^{-1} [16].

The equilibrium geometries in the five different environments are shown in Table 3. The equilibrium O–H distance of 0.944 Å. agrees well with the value 0.958 Å. found by Kollman and Allen. The application of an external field results

Table 1. Orbital exponents (α) and contraction coefficients (c). The constants for oxygen were selected from the work of Roos and Siegbahn [7]. The s exponents and coefficients for hydrogen are those given by Huzinaga [8], and scaled by a factor 1.25. The contraction of primitive Gaussians is shown with brackets

		α	c
Oxygen	s	2714.89	0.007355
		415.725	0.054884
		91.9805	0.266058
		24.4515	0.761744
		7.22296	1.0
		1.06314	1.0
		0.322679	1.0
	p	7.75579	0.232222
		1.62336	0.863870
		0.36503	1.0
Hydrogen	s	16.7019	0.032828
		2.51663	0.231208
		0.567196	0.817238
		0.154146	1.0
	p	0.8	1.0

Table 2. Total energies and geometries for the H_3O^+ ion. d denotes the distance between the oxygen atom and the plane of the three hydrogen atoms, a is the projection of the H-O vector onto this plane. I, II and III denote the three independent oxonium ions in $H_2SO_4 \cdot 2H_2O$ in order corresponding to O(7), O(8) and O(9) in Ref. [12]. An asterisk* denotes the minimum energy for the environment under consideration

d	a	Free ion	$HCl \cdot H_2O$	I	II	III
0.0	1.85	−76.22062	−76.51992	−76.49454	−76.38835	−76.55127
0.1	1.80	0.22225	0.52495	0.49925	0.39505	0.54012
0.2	1.75	0.22009	0.52417	0.50092	0.39830	0.53540
0.2	1.80	0.22223	--	–	–	–
0.2	1.85	0.22023	--	–	–	–
0.3	1.65	–	--	0.48913	0.38719	0.52628
0.5	1.70	0.21992	0.52939	0.51164	0.41252	0.55479
0.5	1.75	0.22179	0.53395	0.51331	0.41484	0.56081
0.5	1.80	0.21981	0.53481	0.51112	0.41329	0.56323
0.5	1.85	–	0.53257	0.50364	0.40010	0.55416
0.7	1.65	–	0.52613	0.51563	0.41672	0.55786
0.7	1.75	–	0.53108	0.51424	0.41727	0.56613
0.8	1.70	0.21627	0.52574	0.51472	0.41716	0.56276
1.0	1.65	–	–	0.50496	0.40594	0.56022
1.0	1.75	–	0.53108	0.49397	0.39713	0.54717
0.351	1.780	0.22245*	–	–	–	–
0.496	1.788	0.22067	0.53490*	–	–	–
0.709	1.688	0.21701	–	0.51660*	–	–
0.708	1.700	0.21702	–	–	0.41874*	–
0.676	1.776	0.21436	–	–	–	0.56653*

Table 3. Equilibrium geometries for the oxonium ion. α_{exp} denotes the mean value of the three experimentally determined X ... O ... X angles around each ion. The notations I, II and III are the same as in Table 2

		r_{O-H}(Å)	α_{H-O-H}	α_{exp}
Free ion		0.96	117°	–
$HCl\cdot H_2O$		0.98	113°	110°
$H_2SO_4\cdot 2H_2O$	I	0.97	106°	109°
	II	0.98	106°	105°
	III	1.00	108°	108°

Table 4. Atomic formal charges for the oxonium ion. Column A gives the charges for the equilibrium geometry as in the crystal. The charges in B were calculated using the same geometries, but without an external field. The notations I, II and III are the same as in Table

		A		B	
		q_O	q_H	q_O	q_H
Free ion				+0.015	+0.328
$HCl\cdot H_2O$		−0.074	+0.358	−0.014	+0.338
$H_2SO_4\cdot 2H_2O$	I	+0.050	+0.275 +0.336 +0.339	+0.095	+0.302
	II	+0.006	+0.303 +0.341 +0.350	+0.077	+0.308
	III	−0.154	+0.378 +0.386 +0.390	−0.027	+0.342

in relatively small increases in the O–H distances (0.01–0.04 Å). In contrast, there are considerable changes in the H–O–H angles, tending to make the O–H ... X arrangement approximately linear. The magnitudes of these changes correspond to displacements of the protons of 0.08–0.20 Å. These distortions of the molecular geometry are much greater than those observed in the solid state for similar molecules such as NH_3 or H_2O. It is therefore tempting to assume that the angles in H_3O^+ are usually easily distorted. However, the vibrational force constants for H_2O and NH_3 indicate that some 0.1 kcal/mole^{-1}/degree^{-1} are required to distort the angles in these molecules. This compares well with the inversion barrier of 0.3 kcal/mole^{-1} and the equilibrium angle of 116.6° in H_3O^+. The above assumption is therefore unjustified, and the large distortions must instead be attributed to H_3O^+ carrying a positive charge. This will result in an ability to form much stronger hydrogen bonds than in the case of a neutral molecule. The H–O–H angles obtained agree fairly well with the averaged X ... O ... X angles, as obtained from experiment (cf. Table 3).

It follows from the population analysis, that there are two main sources of charge redistribution within the ion (cf. Table 4). Firstly, there is a considerable change in charge distribution due to the alterations of the geometry only. This can be seen from Table 4 by comparing the populations in column B for different geometries. A lengthening of the O–H distance results in an electron flow towards oxygen, whereas a decrease in the H–O–H angle will have the opposite effect. Secondly, the application of an external field will bring about an increase of negative charge at the oxygen atom. This is to be expected since it will increase the dipole moment of the ion and make the interaction with the field more energetically favourable. As these effects are of the same order of magnitude, it is not possible to obtain accurate information about the charge distribution unless the geometry of the ion is properly optimized, as in the case of $HCl \cdot H_2O$. In $H_2SO_4 \cdot 2H_2O$, the restrictions mentioned above (C_{3v} symmetry) will render the values of the charges obtained somewhat unreliable. However, the most spectacular effect of introducing an external field is not the charge redistribution but rather the large changes in geometry.

The decrease in H–O–H angles obviously expresses the tendency to form as short –H ... X hydrogen bond contacts as possible, as does the lengthening of the O–H distances. There is no experimental evidence for these changes but similar effects are known for other cases of hydrogen bonding (i.e. H_2O_2 in $Na_2C_2O_4 \cdot H_2O_2$ and in $Li_2C_2O_4 \cdot H_2O_2$ [17, 18]).

Appendix

Provided that the crystal can be described as an assembly of point charges, the electrostatic potential at a point not identical to an atom site can be written as

$$\mathrm{P}(\boldsymbol{r}) = \sum_{i,l} \frac{Q_i}{|\boldsymbol{r} - \boldsymbol{r}_i - \boldsymbol{t}_l|}.$$

The summations over i and l are to be taken over all atoms i in a unit cell and over all unit cells l, respectively. Q_i and $\boldsymbol{r}_i$ are the charge and position of atom i, and $\boldsymbol{t}_l$ denotes a lattice translation in direct space. In practice, it is found that this sum is very slowly convergent or even divergent, and it must therefore be rewritten according to Ewald [9] to make the evaluation possible.

Consider the function

$$F(\boldsymbol{r},\varrho) = \frac{2}{\sqrt{\pi}} \sum_l \exp\{-\varrho^2(\boldsymbol{r} - \boldsymbol{t}_l)^2\} \tag{1}$$

F is periodic in space and can be expanded in a Fourier series:

$$F(\boldsymbol{r},\varrho) = \sum_{\boldsymbol{k}} F_{\boldsymbol{k}} \exp(2\pi i\, \boldsymbol{k} \cdot \boldsymbol{r}), \tag{2}$$

where

$$\begin{aligned} F_{\boldsymbol{k}} &= \frac{2}{\sqrt{\pi}\, V} \int \sum_l \exp\{-\varrho^2(\boldsymbol{r} - \boldsymbol{t}_l)^2 - 2\pi i \boldsymbol{k} \cdot \boldsymbol{r}\}\, d\tau \\ &= \frac{2}{\sqrt{\pi}\, V} \sum_l \int \exp(-\varrho^2 r^2 - 2\pi\, i \boldsymbol{k} \cdot \boldsymbol{r})\, d\tau = \frac{2\pi}{v \varrho^3} \exp(-\pi^2 k^2/\varrho^2). \end{aligned} \tag{3}$$

V and v denote the volumes of the whole crystal and of one unit cell, respectively.

(1), (2) and (3) give

$$\frac{2}{\sqrt{\pi}}\sum_{l}\exp\{-\varrho^2(\boldsymbol{r}-\boldsymbol{t}_l)^2\}=\frac{2\pi}{v\varrho^3}\sum_{\boldsymbol{k}}\exp(-\pi^2k^2/\varrho^2+2\pi i\boldsymbol{k}\cdot\boldsymbol{r}). \tag{4}$$

Consider the identity

$$\frac{1}{|\boldsymbol{r}-\boldsymbol{t}_l|}=\frac{2}{\sqrt{\pi}}\int_0^\infty\exp\{-\varrho^2(\boldsymbol{r}-\boldsymbol{t}_l)^2\}\,d\varrho\,.$$

If this equation is summed over all l and the integration is split at some arbitrary point χ, Eq. (4) can be used to give

$$\begin{aligned}\sum_{l}\frac{1}{|\boldsymbol{r}-\boldsymbol{t}_l|}&=\frac{2\pi}{v}\sum_{\boldsymbol{k}}\int_0^{\chi}\frac{1}{\varrho^3}\exp(-\pi^2k^2/\varrho^2+2\pi i\boldsymbol{k}\cdot\boldsymbol{r})\,d\varrho\\&+\frac{2}{\sqrt{\pi}}\sum_{l}\int_{\chi}^{\infty}\exp\{-\varrho^2(\boldsymbol{r}-\boldsymbol{t}_l)^2\}d\varrho=\frac{1}{\pi v}\sum_{\boldsymbol{k}}\frac{1}{k^2}\exp(-\pi^2k^2/\chi^2+2\pi i\boldsymbol{k}\cdot\boldsymbol{r})\\&+\sum_{l}\frac{1}{|\boldsymbol{r}-\boldsymbol{t}_l|}\operatorname{erfc}(\chi|\boldsymbol{r}-\boldsymbol{t}_l|)\,.\end{aligned}$$

Finally, substituting $\boldsymbol{r}-\boldsymbol{r}_i$ for $\boldsymbol{r}$, multiplying by Q_i and summing over i:

$$\begin{aligned}\sum_{i,l}\frac{Q_i}{|\boldsymbol{r}-\boldsymbol{r}_i-\boldsymbol{t}_l|}&=\sum_{i,l}\frac{Q_i}{|\boldsymbol{r}-\boldsymbol{r}_i-\boldsymbol{t}_l|}\operatorname{erfc}(\chi|\boldsymbol{r}-\boldsymbol{r}_i-\boldsymbol{t}_l|)\\&+\frac{1}{\pi v}\sum_{\boldsymbol{k}}A_{\boldsymbol{k}}\exp(-\pi^2k^2/\chi^2+2\pi i\boldsymbol{k}\cdot\boldsymbol{r})/k^2,\end{aligned}$$

where $A_{\boldsymbol{k}}=\sum_{j}Q_j\exp(-2\pi i\boldsymbol{k}\cdot\boldsymbol{r}_j)$, sometimes termed the electrostatic structure factor. Given a suitable choice of χ, both series are rapidly convergent.

Acknowledgements. The authors wish to thank Dr. J.-O. Lundgren for providing the preliminary electrostatic calculations. We are also indebted to Prof. I. Olovsson and Dr. B. Roos for their kind support. This work has been supported by grants from the Swedish Board for Technical Development and the Swedish Natural Science Research Council.

References

1. Joshi, B. D.: J. chem. Physics **47**, 2793 (1967).
2. Grahn, R.: Ark. Fysik **19**, 147 (1961).
3. Grahn, R.: Ark. Fysik **21**, 1 (1962).
4. Moskowitz, J. W., Harrison, M. C.: J. chem. Physics **43**, 3550 (1965).
5. Kollman, P. A., Allen, L. C.: J. Amer. chem. Soc. **92**, 6101 (1970).
6. Veillard, A.: IBMOL Version 4, Special IBM Technical Report. San José 1968.
7. Roos, B., Siegbahn, P.: Theoret. chim. Acta (Berl.) **17**, 209 (1970).
8. Huzinaga, S.: J. chem. Physics **42**, 1293 (1965).
9. Ewald, P. P.: Ann. Physik **64**, 253 (1921).
10. Bertaut, F.: J. Physique Radium **13**, 499 (1952).
11. Yoon, Y. K., Carpenter, G. B.: Acta crystallogr. **12**, 17 (1959).

12. Taesler, I., Olovsson, I.: J. chem. Physics **51**, 4213 (1969).
13. Gelius, U., Roos, B., Siegbahn, P.: Theoret. chim. Acta (Berl.) **23**, 59 (1971).
14. Baur, W. H.: Acta crystallogr. **19**, 909 (1965).
15. Almlöf, J., Lindgren, J., Tegenfeldt, J.: J. molecular Structure (in press).
16 De Pas, M., Leventhal, J. J., Friedman, L.: J. chem. Physics **51**, 3748 (1969).
17. Pedersen, B. F., Pedersen, B.: Acta chem. scand. **18**, 1454 (1964).
18. Pedersen, B. F.: Acta chem. scand. **23**, 1871 (1969).

Dr. J. Almlöf
Institute of Chemistry
University of Uppsala
Box 531, S-75121 Uppsala
Sweden

Theoret. chim. Acta (Berl.) 28, 169—177 (1973)
© by Springer-Verlag 1973

A Comparative Study of Approximate SCF MO Treatments of Hydrides*

A. Gołębiewski, J. Mrozek and R. Nalewajski
Department of Theoretical Chemistry, Jagiellonian University, Cracow, Poland

Received May 8, 1972

A comparative study of approximate and exact *ab initio* treatments of H_2O, NH_3 and CH_4 has been carried out. Three approximate schemes based on the NDDO approach are introduced. The results compare well with best results obtained by other authors.

Die angenäherte und exakte *ab initio* Behandlung von H_2O, NH_3 and CH_4 wird verglichen. Drei Verfahren, die auf die NDDO-Näherung zurückgehen, werden eingeführt. Die Resultate sind von vergleichbarer Qualität wie die besten Ergebnisse anderer Autoren.

1. Introduction

In the early stage of quantum chemistry a basic method of treatment of polyatomic molecules was that of the simple LCAO MO method with an effective one-electronic Hamiltonian. With the rapid development of computers interest has rapidly shifted towards more complex semiempirical schemes. At present most common approaches are the CNDO, INDO, MC ZDO, MINDO, NDDO and related methods [1–7]. Unfortunately, despite the considerable number of apparently successful applications, all these methods are lacking in rigour. The S-expansion technique of the $S^{-1/2}$ matrix which was used in an attempt to justify these methods has failed to do so [7–10].

While semi-empiricism has been having these difficulties there has been remarkable progress in the development of non-empirical (*ab initio*) methods. Numerical approximations of integrals have been worked out which reduce the necessary computer time and the required storage capacity significantly. Hence we anticipate that approximate non-empirical schemes are going to replace the oversimplified semiempirical ones. Finding a simple and satisfactory approach of this kind is certainly one of the principle goals of the present day quantum chemistry.

The purpose of this work is to analyze the applicability of three partially new approximate treatments based on the NDDO scheme and the Gaussian lobe function expansion. The analysis has been carried out for three molecules, H_2O, NH_3 and CH_4. For these cases a rather large body of comparative material is available.

---

* The work was partly supported by the Institute of Low Temperatures of the Polish Academy of Sciences, Wrocław.

2. Notation

In what follows we have adopted an abbreviated notation for the various schemes:

1) The notation for the theoretical framework is the standard one, i.e. SCF, CI, MC SCF. If not stated differently the standard SCF scheme is always implied.

2) The types of the basis functions are denoted by S – for STO's, by H – for approximate or exact Hartree-Fock atomic orbitals, by C – for a formal contracted set of any type of functions, by G – for single Cartesian Gaussian functions, by L – for single Gaussian lobe functions and by F – for floating spherical Gaussian functions; a symmetrical orthogonalization of the whole basis is denoted by a wavy bar, e.g. $\tilde{S}$, $\tilde{H}$ or $\tilde{C}$.

3) The degree of the zero differential overlap is symbolized in a standard way (CNDO, INDO, MC ZDO, NDDO, etc.) [1–7].

Additionally we use throughout the paper the following two symbols: NMTC – for a method Neglecting More than Two-Center integrals and FS – for a Full Scheme method, with no ZDO-type approximations at all.

4) The dimensions of the contracted and of the uncontracted sets strongly influence the computer time and the required storage capacity. Let us assume that independently of the parent atom the uncontracted set consists of altogether N_s s-type functions, N_p p-type and N_d d-type ones. Let us similarly assume that we have altogether n_s s-type contractions, n_p p-type ones and n_d d-type ones. We shall use the notation (n_s, n_p, n_d X; N_s, N_p, N_d Y) where X stands for S, H, C or F and the symbol Y stands for G, L or F. If a still more detailed specification is required we shall use the notation of contractions in accordance with Johansen's work [11].

5) Except in the FS approach many molecular integrals are neglected at first and evaluated approximately afterwards. Depending on the approximation we shall put:

/R for the Ruedenberg approximation of the remaining many-center integrals [12],

/M – for the Mulliken formula [13] and

/N_s', N_p', N_d' Z where Z = G, L or F – in the case of calculation of the remaining integrals with a smaller basis set of uncontracted functions. If the smaller uncontracted set is contained in the original one (truncation of the set) we shall put Z = Y. Otherwise we put Z = Y′.

3. Details of the Approach

The calculations to be reported are based on the following four schemes:

$$\mathrm{FS}(n_s, n_p\,\mathrm{C};\ N_s, N_p\,\mathrm{L}), \quad \text{equivalent to} \quad \mathrm{FS}(n_s, n_p\,\mathrm{H};\ N_s, N_p\,\mathrm{L}), \tag{1}$$

$$\mathrm{NDDO}(n_s, n_p\,\mathrm{C};\ N_s, N_p\,\mathrm{L})/N_s', N_p'\,\mathrm{L}, \tag{2}$$

$$\mathrm{NDDO}(n_s, n_p\,\mathrm{H};\ N_s, N_p\,\mathrm{L})/R, \tag{3}$$

$$\mathrm{NDDO}(n_s, n_p\,\mathrm{C};\ N_s, N_p\,\mathrm{L})/R. \tag{4}$$

We use Whitten's expansion of Hartree-Fock atomic orbitals of oxygen, nitrogen and carbon into Gaussian lobe functions [14]. In Johansen's notation it has the general form $\langle X|3,3,4;5\rangle$. To distinguish them from atomic orbitals the three Whitten type contracted sets of "*s*-type" are denoted in what follows by $1S$, $2S$ and $3S$. The larger expansion of the $1s$ orbital of a hydrogen atom, $\langle \mathrm{H}|3\rangle$, and the smaller one, $\langle \mathrm{H}|2\rangle$ were those given by Veillard *et al.* [15]. The smaller uncontracted set for oxygen, nitrogen and carbon atoms was obtained by truncation. Let $f_s = \Sigma\, c_{js} g_j$ be a typical form of a contracted set function where $|c_{1s}| \geqq |c_{2s}| \geqq \cdots \geqq |c_{Ks}|$. Then, in the truncated form, $f_s \approx N_s(c_{1s}g_1 + c_{2s}g_2)$ where N_s is a renormalization constant.

The geometry of H_2O was taken over from Neumann and Moskowitz [16]: $R_{\mathrm{OH}} = 1.80$ a.u. and $\sphericalangle = 105°$. It differs only slightly from the experimental one. In the remaining two cases the approximate equilibrium parameters were taken as: $R_{\mathrm{NH}} = 1.91$ a.u., $\sphericalangle = 106.7°$ and $R_{\mathrm{CH}} = 2.05$ a.u., $\sphericalangle = 109°28'$. In calculating the inversion barrier of NH_3 the bond lengths were kept constant.

The framework of Roothaan's SCF theory for closed shell systems, the details of the NDDO approach and the description of the Ruedenberg approximation for many-center integrals are described elsewhere [17, 1, 6, 12]. Probably the only explanation required is for the Ruedenberg approximation in terms of non-orthogonal contracted sets; it is to be noted that the original approximation is based on orthogonal atomic orbitals.

Let f_{A} be a row vector of non-orthogonal (in general) contracted sets of atom A and let f_{B} have a similar meaning for atom B. In the case of a sufficiently large basis we can write that $f_{\mathrm{A}} \approx f_{\mathrm{B}} C_{\mathrm{AB}}$ and $f_{\mathrm{B}} \approx f_{\mathrm{A}} C_{\mathrm{BA}}$. It follows that $S_{\mathrm{BA}} \approx S_{\mathrm{BB}} C_{\mathrm{AB}}$ and $S_{\mathrm{AB}} \approx S_{\mathrm{AA}} C_{\mathrm{BA}}$, where $S_{\mathrm{BA}} = \int f_{\mathrm{B}}^{+} f_{\mathrm{A}}\, dV$, $S_{\mathrm{BB}} = \int f_{\mathrm{B}}^{+} f_{\mathrm{B}}\, dV$, $S_{\mathrm{AB}} = S_{\mathrm{BA}}^{+}$ and $S_{\mathrm{AA}} = \int f_{\mathrm{A}}^{+} f_{\mathrm{A}}\, dV$. Therefore

$$f_{\mathrm{A}} \approx f_{\mathrm{B}} S_{\mathrm{BB}}^{-1} S_{\mathrm{BA}}\,, \tag{5}$$

$$f_{\mathrm{B}} \approx f_{\mathrm{A}} S_{\mathrm{AA}}^{-1} S_{\mathrm{AB}}\,. \tag{6}$$

Considering the product $f_{\mathrm{A}}^{+} f_{\mathrm{B}}$ we can expand either f_{A} or f_{B}, or take the average product of both these expansions. We come in this way to a generalization of the Ruedenberg formula,

$$f_{\mathrm{A}}^{+} f_{\mathrm{B}} \approx \tfrac{1}{2}(f_{\mathrm{A}}^{+} f_{\mathrm{A}} S_{\mathrm{AA}}^{-1} S_{\mathrm{AB}} + S_{\mathrm{AB}} S_{\mathrm{BB}}^{-1} f_{\mathrm{B}}^{+} f_{\mathrm{B}})\,. \tag{7}$$

In general the expansion is restricted to orbitals (contracted sets) of occupied shells. In such a case the accuracy of this approximation is not very high. If the nonorthogonality of contracted sets of atom A and similarly of atom B is not large then with an accuracy comparable to that of expansion (7) we can write that

$$f_{\mathrm{A}}^{+} f_{\mathrm{B}} \approx \tfrac{1}{2}(f_{\mathrm{A}}^{+} f_{\mathrm{A}} S_{\mathrm{AB}} + S_{\mathrm{AB}} f_{\mathrm{B}}^{+} f_{\mathrm{B}})\,. \tag{8}$$

This is the approximation which is the basis of the NDDO modified scheme denoted by NDDO(n_s, n_p C; N_s, N_p L)/R.

Ruttink [18] has shown that the Ruedenberg approximation leads to results which are invariant under rotations of the local axes and which are independent of the choice of hybrid orbitals. The familiar Mulliken approximation does not exhibit such a property [18]. Therefore we have not investigated the Mulliken approximation in any greater detail.

The program for methods (1)-(4) was written in Algol 60 and is available on request. The calculations were performed on the ODRA 1204 computer at the University Computer Center. Also a FORTRAN IV version is now being prepared for use with a larger computer.

When passing from Cartesian Gaussian functions to Gaussian lobe functions the number of basic integrals increases very rapidly. For example the one center integral $(d_{xy}d_{xz}|d_{xy}d_{xz})$ is reducible to 256 integrals over branch functions. However, taking into account all equivalences one can reduce the number of basic integrals. In the particular case the reduction is by a factor of 20. In our program the equivalence of integrals is treated automatically.

4. Results

In Tables 1 3 we compare the results of the full scheme method (1) and the NDDO mixed basis approach (2) with representative results of other authors. Comparisons are made for the total energy, the orbital energies, the ionization potentials via the Koopmans theorem and, to a lesser extent, for the binding energy.

As seen in the tables, despite the significantly smaller number of variation parameters, the full scheme approach FS(...C; ...L) yields results of a comparable quality to those obtained by Roos and Siegbahn. The results obtained for the ammonia molecule are also comparable to those obtained by Kaldor and Shavitt who used Slater type orbitals.

Our results with the NDDO(...C; ...L)/...L approximation compare rather well with the FS results of other authors. In none of the considered cases is the calculated total energy below the Hartree-Fock limit. The calculated total energy is however sometimes slightly below the appropriate FS value (Table 1).

In a non-approximate SCF treatment the ionization potentials estimated via the Koopmans theorem are usually too high when compared to experiment.

Table 1. Comparison of SCF results for H_2O

uantity	Neumann, Moskowitz [16]	Roos, Siegbahn [19]	Johansen [11]		Present work	
	FS(9, 15, 10C; 18, 21, 10G)	FS(8, 6C; 15, 9G)	FS(4, 3C; 23, 21G)	NDDO(4, 3C; 23, 21G)/8, 6G′	FS(5, 3C; 16, 15L)	NDDO(5, 3 16, 15L)/10,
otal energy	−76.044	−75.875	−75.808	−75.663	−75.891	−75.955
inding energy	0.235	—	—	—	0.100	0.164
rbital energy						
a_1	−20.550	−20.550	−20.42	−20.47	−20.514	−20.171
a_1	− 1.347	− 1.347	− 1.28	− 1.17	− 1.359	− 1.394
b_2	− 0.714	− 0.694	− 0.66	− 0.66	− 0.697	− 0.578
a_1	− 0.577	− 0.544	− 0.55	− 0.55	− 0.569	− 0.491
b_1	− 0.503	− 0.486	− 0.52	− 0.52	− 0.529	− 0.424

Experimental total energy = −76.485 [20]; Hartree-Fock limit = −76.093 [21], −76.06 [31]; Experimental binding energy = 0.370, 0.349 [21]; Ionization potentials: $I_1 = 0.463$, $I_2 = 0.533$, $I_3 = 0.595$ [22].

Table 2. Comparison of SCF results for NH_3

Quantity	Rauk, Allen, Clementi [23][a]	Roos, Siegbahn [19]	Kaldor, Shavitt [24]	Present work	
	FS(20, 24, 12C; 37, 42, 12G)	FS(10, 6C; 19, 9G)	FS(5, 3S; 5, 3S)	FS(6, 3C; 19, 15L)	NDDO(6,. 19, 15L)/12
Total energy	−56.222	−56.093	−56.006	−56.041	−55.917
Binding energy	—	—	0.241	0.153	0.129
Inversion barrier	0.008	—	0.017	− 0.00046	− 0.052
Orbital energy					
$1a_1$	−15.535	−15.535	−15.540	−15.583	−15.168
$2a_1$	− 1.148	− 1.142	− 1.102	− 1.174	− 1.170
$1e$	− 0.635	− 0.615	− 0.583	− 0.645	− 0.464
$3a_1$	− 0.428	− 0.407	− 0.369	− 0.471	− 0.346

Experimental total energy = −56.605 [20]; Hartree-Fock limit = −56.222 [25], −56.227 [26]; Experimental binding energy = 0.474 [24]; Experimental inversion barrier = 0.0092 [27]; Ionization potentials: $I_1 = 0.379$ [28], 0.404 [29]; $I_2 = 0.562$ [30], 0.625 [29].

[a] Optimized geometry.

Table 3. Comparison of SCF results for CH_4

Quantity	Ritchie, King [31]	Klessinger [32]		Present work	
	FS(21, 27C; 25, 27G)	FS(6, 3S; 20, 9G)	FS(6, 3S; 18, 9G)	FS(7, 3C; 22, 15L)	NDDO(7, 3C; 22, 15L)/14, 6L
Total energy	−40.198	−40.001	−39.812	−40.033	−39.909
Binding energy	—	0.424	0.432	0.352	0.228
Orbital energy					
$1a_1$	−11.222	−11.389	−11.308	−11.385	−10.088
$2a_1$	− 0.930	− 0.972	− 0.971	− 1.010	− 1.041
$1t_2$	− 0.535	− 0.576	− 0.576	− 0.607	− 0.425

Experimental total energy = −40.526 [20]; Hartree-Fock limit = −40.23 [31]; Experimental binding energy = 0.625 [34], 0.668 [31]; Ionization potentials: $I_1 = 0.500$, $I_2 = 0.849$, $I_3 = 10.617$ [33].

The same conclusion is obviously true with our FS approach. The mixed basis scheme (2), on the other hand, yields results which almost in every case are too low. The average values resulting from these two methods compare surprisingly well with experiment:

	I_{average}	I_{exp}	$I_{\text{best SCF}}$
H_2O	0.476	0.463	0.503
	0.530	0.533	0.577
	0.637	0.595	0.714
NH_3	0.408	0.379; 0.404	0.428
	0.554	0.562; 0.625	0.635
CH_4	0.516	0.500	0.535
	1.025	0.849	0.930
	10.736	10.617	11.222

It is to be noticed that the results of best exact SCF calculations are in general worse.

The inversion barrier of the ammonia molecule is almost a classic problem in quantum chemistry. Many SCF calculations have been performed in order to evaluate its magnitude [23–25, 35, 36]. It has been shown at the SCF level, with non-varied bond lengths that to obtain a correct sign of the barrier a large extended basis set is required [23, 25]. Good agreement with experiment obtained with a small basis set should be considered accidental. Kaldor and Shavitt, for example, obtained a less satisfactory value of the total energy than we in our FS approach. Yet their prediction of the barrier was qualitatively correct while ours was not. We would like to point out, however, that we tried to estimate the barrier also with the smaller of the two considered sets i.e. the truncated one. The barrier of this FS(6, 3C; 12, 6L) calculation was in still better agreement with experiment: 0.0106. Let us recall that even the extended calculations of Body, McClure and Clementi yielded a negative barrier (−0.000436) the value of which, by the way, is almost exactly the same as that following from our FS(6, 3C; 19, 15L) treatment (−0.000457). The barrier to inversion is thus a very subtle effect and we believe it should not be treated by approximate SCF methods.

The idea of a mixed basis scheme is not entirely new. The closest approach is that developed by McWeeny, Hollis, Cook and Palmieri [37, 38] and the NDDO(...C; ...G)/...G′ scheme elaborated by Johansen [11]. We shall discuss the latter work only as the results obtained in the former one were relatively poor. Johansen used Cartesian Gaussian functions and two optimized independently uncontracted sets. Thus, in principle, her approach should be more accurate than ours. In practice it is not precisely so (Table 1) despite the use of a much larger uncontracted set.

Another somewhat related work is that published by Brown, Burden and Hart [39]. It is based on Gaussian lobe functions. Similarly to Johansen they optimized the smaller basis set. However, their ZDO assumption was less restrictive; their NMTC scheme should be in principle more accurate than any one based on the NDDO method. However, the number of integrals to be calculated exactly is in their case several times larger than in the NDDO case and increases for larger molecules very rapidly. A comparison of some of their results with ours is given in Table 6.

In Table 6 we compare the expansion coefficients of molecular orbitals for H_2O, for two related SCF schemes: FS(5, 3C; 16, 15L) and NDDO(5, 3C; 16, 15L)/10, 6L. It follows from the table that except for the lowest state the reproduction of the coefficients by the mixed basis scheme is not satisfactory. Exactly the same result was found for NH_3 and CH_4. The total electron density is not expected to differ greatly but the contours of orbitals may differ significantly.

The applicability of the two suggested NDDO(...)/R schemes is analysed in Table 5. The pure NDDO scheme, perhaps accidentally, gives a good estimate of the highest occupied level. The estimation of the total energy, however, is very poor. Such a large error in a non-empirical scheme does not help in under-

Table 4. Comparison of expansion coefficients of molecular orbitals of H_2O for two related SCF schemes: FS(5, 3C; 16, 15L) and NDDO(5, 3C; 16, 15L)/10, 6L. Coefficients of the second scheme are given in brackets

Orbital	O 1S	O 2S	O 3S	O $2p_x$	O $2p_y$	O $2p_z$	H_1 $1s$
$1a_1$	0.0511	0.0066	0.9792	0.0021	—	—	−0.0011
	(0.0514)	(0.0017)	(0.9800)	(0.0007)	—	—	(0.0018)
$2a_1$	−0.0103	0.8663	−0.2279	0.1640	—	—	0.1188
	(−0.0084)	(0.6361)	(−0.1927)	(0.0799)	—	—	(0.2850)
$1b_2$	—	—	—	—	0.6569	—	0.4120
	—	—	—	—	(0.9393)	—	(0.0876)
$3a_1$	−0.0042	0.4651	−0.0879	0.8456	—	—	−0.1908
	(−0.0012)	(0.0625)	(−0.0294)	(1.0328)	—	—	(+0.1197)
$1b_1$	—	—	—	—	—	1.0 (1.0)	—

Table 5. Applicability of the Ruedenberg approximation and the mixed basis scheme in the SCF MO calculations for ammonia molecule

antity	NDDO(5, 3H; 19, 15L)	NDDO(5, 3H; 19, 15L)/*R*	NDDO(6, 3C; 19, 15L)/*R*	NDDO(6, 3C; 19, 15L)/12, 6L	FS(6, 3C; 19, 15L FS(5, 3H; 19, 15L
tal energy	−79.649	−55.448	−55.880	−55.917	−56.041
bital energies					
1	−16.478	−14.760	−15.116	−15.168	−15.583
1	− 8.219	− 0.855	− 1.017	− 1.170	− 1.173
	− 2.580	− 0.271	− 0.366	− 0.464	− 0.645
1	− 0.451	− 0.140	− 0.246	− 0.346	− 0.471

[a] Within quoted decimal numbers the results of these two calculations are the same.

Table 6. On applicability of simplified SCF treatments of hydrides

Method	Authors	− Total energy		
		H_2O	NH_3	CH_4
Hartree-Fock limit	see Tables 1–3	76.093	56.222 56.227	40.173 40.198
Minimal STObasis with an approximate estimation of integrals	Body [42]	75.723	55.872	40.078
Double Gaussian modification of the FSGO model	Rouse, Frost [43]	72.792	53.814	38.485
Small Gaussian expansion of the minimal STO basis				
FS(*n* + 2, 3S; 3*n* + 8, 9G)	Klessinger [32]	75.571	55.907	40.001
FS(*n* + 2, 3S; 3*n* + 6, 9G)	Hehre *et al.* [44]	—	—	39.715
NDDO(*n* + 2, 3Š; *n* + 2, 3S)/*R*	Brown *et al.* [41]	75.387	55.590	—
NDDO(4, 3C; 23, 21G)/8, 6G′	Johansen [11]	75.663	—	—
NMTC(*n* + 3, 3C; 5*n* + 10, 15L)/3*n* + 5, 9L′	Brown *et al.* [39]	75.959	56.088	40.101
NDDO(6, 3C; 19, 15L)/*R*	present work	—	55.880	—
NDDO(5, 3H; 19, 15L)/*R*	present work	—	55.448	—
NDDO(*n* + 3, 3C; 3*n* + 10, 15L)/2*n* + 6, 6L	present work	75.955	55.917	39.909

standing the success of appropriate semiempirical schemes. Comparing the results of the three approximate schemes

NDDO(...C; ...L)/...L
NDDO(...H; ...L)/*R*
NDDO(...C; ...L)/*R*

with those which follow from the appropriate FS approach one finds that the mixed basis scheme is definitely the best. Noteworthy is that the Ruedenberg approximation when applied to slightly non-orthogonal contracted sets yielded better results than in the standard case.

Let us also note that the more or less typical case, NDDO(...H; ...L)/*R*, has so far not been investigated. The closest attempts at this are the NDDO(...$\tilde{S}$; ...S)/*R* and NDDO(...S; ...S)/*R* schemes proposed by Brown *et al.* [40, 41].

5. A Comparative Study of Simplified SCF Treatments

In Table 6 we compare the total energy of H_2O, NH_3 and CH_4 as obtained in various approximate SCF treatments found in the literature. According to the table the result closest to the Hartree-Fock limit is obtained using the NMTC(...C; ...L)/...L′ method of Brown, Burden and Hart. Not far behind are the results of our NDDO(...C; ...L)/...L scheme. Optimizing the smaller set and increasing the dimension of the uncontracted set (at least to that used by Brown *et al.*) would certainly give still better results. Therefore, in our opinion, the more laborious NMTC scheme is not superior to the NDDO one.

Results obtained with other approximate treatments are usually worse. Only the small Gaussian expansion method on a minimal STO basis, as worked out by Klessinger [32] or Hehre, Stewart and Pople [44], is of comparable quality.

Acknowledgement. The authors are grateful to Prof. H. S. Taylor for valuable comments on the manuscript.

References

1. Pople, J. A., Santry, D. P., Segal, G. A.: J. chem. Physics **43** S, 129 (1965).
2. Pople, J. A., Segal, G. A.: J. chem. Physics **44**, 3289 (1966).
3. Pople, J. A., Beveridge, D. L., Dobosh, P. A.: J. chem. Physics **47**, 2026 (1967).
4. Dewar, M. J. S., Haselbach, E. J.: J. Amer. chem. Soc. **92**, 590 (1970).
5. Bodor, N., Dewar, M. J. S., Harget, A., Haselbach, E.: J. Amer. chem. Soc. **92**, 3584 (1970).
6. Brown, R. D., Roby, K. R.: Theoret. chim. Acta (Berl.) **16**, 175 (1970); **16**, 194 (1970).
7. Brown, R. D., James, B. H., O'Dwyer, M. F.: Theoret. chim. Acta (Berl.) **17**, 264 (1970).
8. Dahl, J. P.: Acta chem. scand. **21**, 1244 (1967).
9. Fischer-Hjalmars, I.: Advances in quant. Chemistry **2**, 25 (1965).
10. Gray, N. A. B., Stone, A. J.: Theoret. chim. Acta (Berl.) **18**, 389 (1970).
11. Johansen, H.: Theoret. chim. Acta (Berl.) **21**, 9 (1971).
12. Ruedenberg, K. J.: J. chem. Physics **19**, 1433 (1951).
13. Mulliken, R. S.: J. Chim. physique **46**, 497 (1949).
14. Whitten, J. L.: J. chem. Physics **44**, 359 (1966).
15. Veillard, A.: IBMOL: Computation of wave-functions for molecules of general geometry, Version 4. San Jose: IBM Research Laboratory.

16. Neumann, D., Moskowitz, J. W.: J. chem. Physics **49**, 2056 (1968).
17. Roothaan, C. C. J.: Rev. mod. Physics **23**, 69 (1951).
18. Ruttink, P. J. A.: Theoret. chim. Acta (Berl.) **6**, 83 (1966).
19. Roos, B., Siegbahn, P.: Theoret. chim. Acta (Berl.) **17**, 199 (1970).
20. Hopkinson, A. C., Holbrook, N. K., Yates, K., Czismadia, I. G.: J. chem. Physics **49**, 3596 (1968), and ref. therein.
21. Ref. [16] and ref. therein.
22. Allen, L. C., Karo, A. M.: Rev. mod. Physics **32**, 275 (1960).
23. Rauk, A., Allen, L. C., Clementi, E.: J. chem. Physics **52**, 4133 (1970).
24. Kaldor, U., Shavitt, I.: J. chem. Physics **45**, 888 (1966).
25. Body, R. G., McClure, D. S., Clementi, E.: J. chem. Physics **49**, 4916 (1968).
26. Snyder, L. C.: J. chem. Physics **46**, 3602 (1967).
27. Swalen, J. D., Ibers, J. A.: J. chem. Physics **36**, 1914 (1962).
28. Kiser, R. W., Gallegos, J.: J. physic. Chem. **66**, 947 (1962).
29. Sun, H., Weissler, G. L.: J. chem. Physics **23**, 1160 (1955).
30. McDowell, C. A.: J. chem. Physics **24**, 618 (1956).
31. Ritchie, C. D., King, H. F.: J. chem. Physics **49**, 2056 (1968).
32. Klessinger, M.: Theoret. chim. Acta (Berl.) **15**, 353 (1969).
33. Hamrin, K., Johansson, G., Gelius, H., Fahlmann, A., Nordling, C., Siegbahn, K.: Chem. Physics Letters **1**, 613 (1968).
34. Kraus, M.: J. chem. Physics **38**, 564 (1963).
35. Pipano, A., Gilman, R. R., Bender, C. F., Shavitt, I.: Chem. Physics Letters **4**, 583 (1970).
36. Pipano, A., Gilman, R. R., Shavitt, I.: Chem. Physics Letters **5**, 285 (1970).
37. Cook, D. B., Hollis, P. C., McWeeny, R.: Molecular Physics **13**, 553 (1967).
38. Cook, D. B., Palmieri, P.: Molecular Physics **17**, 271 (1969).
39. Brown, R. D., Burden, F. R., Hart, B. T.: Theoret. chim. Acta (Berl.) **22**, 214 (1971).
40. Brown, R. D., Burden, F. R., Williams, G. R.: Theoret. chim. Acta (Berl.) **18**, 98 (1970).
41. Brown, R. D., Burden, F. R., Williams, G. R., Phillips, L. F.: Theoret. chim. Acta (Berl.) **21**, 205 (1971).
42. Body, R. G.: Theoret. chim. Acta (Berl.) **18**, 107 (1970).
43. Rouse, R. A., Frost, A. A.: J. chem. Physics **50**, 1705 (1969).
44. Hehre, W. J., Stewart, R. F., Pople, J. A.: J. chem. Physics **51**, 2657 (1969).

Professor A. Gołębiewski
Department of Theoretical Chemistry
Jagiellonian University
Krupnicza 41, Kraków, Poland

Theoret. chim. Acta (Berl.) 28, 179–191 (1973)
© by Springer-Verlag 1973

Unrestricted Hartree Fock Perturbation Theory

B. L. Burrows
Mathematics Department, North Staffordshire Polytechnic, Stafford, England

Received April 20, 1972

The coupled and uncoupled Hartree Fock perturbation theories are generalised using unrestricted Hartree Fock theory. The variational approach to coupled theory is discussed and various corrections to the uncoupled theory are considered. Trial calculations are carried out to obtain atom-atom polarizabilities for Allyl and the first excited triplet state of *cis*-Butadiene, and to obtain estimates of spin and charge densities for various heterocyclics.

Die gekoppelte and die ungekoppelte Hartree-Fock Störungstheorie werden mit Hilfe der uneingeschränkten Hartree-Fock-Theorie verallgemeinert. Das Variationsverfahren für die gekoppelte Theorie wird diskutiert und verschiedene Korrekturen für die ungekoppelte Theorie werden untersucht. Es werden Testrechnungen durchgeführt, um die Atom-Atom-Polarisierbarkeiten des Allylradikals und des ersten angeregten Tripletzustandes von *cis*-Butadien, und um die Spin- und Ladungsdichten verschiedener Heterozyklen abzuschätzen.

1. Introduction

For many years there has been considerable interest in perturbation theoretic treatments of molecules (see Refs. [1–10]). Almost all of these have been restricted to the ground state, or the excited states, of the most common type of molecule that is those molecules with an even number of electrons. For these molecules the ground state wavefunction is a singlet and may be approximated by a single determinant of $2m$ functions of space and spin coordinates (spin orbitals) where $2m$ is the number of electrons. The purpose of this paper is to extend these calculations to calculations applied to molecules with an odd number of electrons, and to triplet excited states of molecules with an even number of electrons, using unrestricted Hartree-Fock perturbation theory. That is to say the zero order approximation for the perturbation theory is taken to be the unrestricted Hartree-Fock single determinant. This function is a determinant of spin orbitals v_i^0 which are products of a space function u_i^0 and a spin function α or β. The single determinant is constrained to be an eigenfunction of $\hat{S}_z$ and this is done by assuming that p spin orbitals are associated with α spin and q with β spin so that

$$\frac{1}{2}(p-q)=M \tag{1}$$

where M is the chosen eigenvalue of $\hat{S}_z$. For a molecule with an even number of electrons, if we choose $M=1$ the single determinant is an approximation to the wavefunction for the first triplet excited state so that unrestricted perturbation theory becomes an excited state perturbation theory. A full discussion of the

It is easy to see that if we define

$$P_{uv}^k = \sum_{i=1}^{p} \sum_{j=0}^{k} a_{iu}^{k-j} a_{iv}^{*j} \tag{19}$$

and

$$Q_{uv}^k = \sum_{i=1}^{q} \sum_{j=0}^{k} b_{iu}^{k-j} b_{iv}^{*j} \tag{20}$$

then we may express $F_{rs}^{\alpha_k}$ and $F_{rs}^{\beta_k}$ in the form

$$F_{rs}^{\alpha_k} = h_{rs}\delta_{k0} + z_{rs}\delta_{k1} + \sum_{uv}^{m} P_{uv}^k([rv|su] - [rv|us]) + \sum_{uv}^{m} Q_{uv}^k[rv|su] \tag{21}$$

and

$$F_{rs}^{\beta_k} = h_{rs}\delta_{k0} + z_{rs}\delta_{k1} + \sum_{uv}^{m} P_{uv}^k[rv|su] + \sum_{uv}^{m} Q_{uv}^k([rv|su] - [rv|us]) \tag{22}$$

where

$$h_{rs} = \int \omega_r^*(1)h(1)\omega_s(1)d\tau\,, \tag{23}$$

$$z_{rs} = = \int \omega_r^*(1)z(1)\omega_s(1)d\tau \tag{24}$$

and

$$[rv|us] = \int \omega_r^*(1)\omega_v^*(2)\frac{1}{r_{12}}\omega_u(1)\omega_s(2)d\tau\,. \tag{25}$$

The additional conditions that the orbitals remain orthonormal are given by the following set of equations:

$$\sum_{rs}^{m} \sum_{j=0}^{k} b_{ir}^{*j} b_{ls}^{k-j} S_{rs} = \delta_{k0}\delta_{il}\,, \tag{26}$$

$$\sum_{rs}^{m} \sum_{j=0}^{k} a_{ir}^{*j} a_{ls}^{k-j} S_{rs} = \delta_{k0}\delta_{il}\,. \tag{27}$$

The first and second order changes in the total energy of the molecule are given by

$$E_1 = \sum_{rs}^{m} (P_{sr}^0 + Q_{sr}^0)\, z_{rs} \tag{28}$$

$$2E_2 = \sum_{rs}^{m} (P_{sr}^1 + Q_{sr}^1)\, z_{rs}\,. \tag{29}$$

For a pi-electron system the Pariser-Parr-Pople schemes enables F^{α_k} to be considerably simplified:

$$F_{rs}^{\alpha_k} = h_{rs}\delta_{k0} + z_{rs}\delta_{k1} + \delta_{rs}\Big(\sum_{v}^{m} (P_{vv}^k + Q_{vv}^k)\gamma_{rv}\Big) - \frac{1}{2} P_{rs}^k \gamma_{rs} \tag{30}$$

where γ_{rs} is the electron repulsion integral and the functions $\{\omega_r\}$ are orthonormal so that $S_{rs} = \delta_{rs}$. Expressions for $F^{\beta k}$ are similar in form with P_{uv}^k and Q_{uv}^k interchanged.

3. Variational Principle

It is possible to calculate the first order coupled wavefunction making use of a variational principle. This is sometimes to be prefered to the more conventional perturbation method where Eqs. (12) and (13) are solved iteratively. The variational procedure for the coupled functions was developed by Langhoff, Karplus and Hurst [3]. In order to examine this procedure as applied to unrestricted perturbation theory we will use a result established by Epstein and Johnson [6]. Consider any single determinant approximation to the perturbed system $\hat{\Psi}$ such that

$$\hat{\Psi} = \sum_{k=0}^{\infty} \lambda^k \hat{\psi}_k \tag{31}$$

and $\hat{\psi}_0 = \Psi_0$ the Hartree-Fock wavefunction for the unperturbed system. Let Ψ^c be the coupled single determinant approximation to the perturbed system so that

$$\Psi^c = \sum_{k=0}^{\infty} \lambda^k \psi_k^c . \tag{32}$$

As Ψ^c is the best single determinant for the perturbed system we have the following inequality:

$$E\,(\text{exact}) \leqq \frac{\langle \Psi^c | \mathscr{H} + \lambda W | \Psi^c \rangle}{\langle \Psi^c | \Psi^c \rangle} \leqq \frac{\langle \hat{\Psi} | \mathscr{H} + \lambda W | \hat{\Psi} \rangle}{\langle \hat{\Psi} | \hat{\Psi} \rangle} . \tag{33}$$

This may be written as

$$E\,(\text{exact}) \leqq \sum_{k=0}^{\infty} E_k^c \lambda^k \leqq \sum_{k=0}^{\infty} \hat{E}_k \lambda^k . \tag{34}$$

Now by Brillouin's theorem

$$\langle \hat{\psi}_1 | \mathscr{H} | \Psi_0 \rangle + \langle \Psi_0 | \mathscr{H} | \hat{\psi}_1 \rangle = 0 \tag{35}$$

so that

$$E_0^c + \lambda E_1^c = \hat{E}_0 + \lambda \hat{E}_1 . \tag{36}$$

Consequently we may cancel these terms in (34) and obtain the following inequality

$$\sum_{k=2}^{\infty} E_k^c \lambda^k \leqq \sum_{k=2}^{\infty} \hat{E}_k \lambda^k \tag{37}$$

for all values of λ in the range [0, 1]. If we consider the limit as $\lambda \to 0$ we see that

$$E_2^c \leqq \hat{E}_2 \tag{38}$$

which is the result of Epstein and Johnson. Now if we assume all wavefunctions are real

$$\begin{aligned} \hat{E}_2 = {} & 2E_0 \langle \Psi_0 | \hat{\psi}_2 \rangle + \langle \hat{\psi}_1 | \hat{H}_0 | \hat{\psi}_1 \rangle + 2 \langle \Psi_0 | W | \hat{\psi}_1 \rangle \\ & + \left\langle \hat{\Psi} \left| \sum_{i<j} \frac{1}{r_{ij}} - \sum_i \left(G^{\alpha 0}(i) | \alpha \rangle \langle \alpha | + G^{\beta 0}(i) | \beta \rangle \langle \beta | \right) - C^0 \right| \hat{\Psi} \right\rangle_2 \end{aligned} \tag{39}$$

where

$$E_0 = \sum_{i=1}^{p} E_{\alpha_i}^0 + \sum_{i=1}^{q} E_{\beta_i}^0 + C^0 . \tag{40}$$

The single determinant $\hat{\Psi}$ may be written in the form of Eq. (2) that is

$$\hat{\Psi} = (n!)^{-\frac{1}{2}} \det \{ \hat{\psi}_1(1) \alpha(1) \ldots \hat{\phi}_1(p+1) \beta(p+1) \ldots \hat{\phi}_q(p+q) \beta(p+q) \} \tag{41}$$

where

$$\hat{\psi}_i = \sum_{k=0}^{\infty} \hat{\psi}_i^k \lambda^k \tag{42}$$

$$\hat{\phi}_i = \sum_{k=0}^{\infty} \hat{\phi}_i^k \lambda^k , \tag{43}$$

and without loss of generality the sets of functions $\{\hat{\psi}_i\}$ and $\{\hat{\phi}_i\}$ are chosen separately orthonormal. Expressing $\hat{\Psi}$ in this way it is easy to verify that

$$\begin{aligned}\hat{E}_2 = & \sum_{i=1}^{p} \langle \hat{\psi}_i^1(1) | F^{\alpha o}(1) - E_{\alpha_i}^0 | \hat{\psi}_i^1(1) \rangle \\ & + \sum_{i=1}^{q} \langle \hat{\phi}_i^1(1) | F^{\beta o}(1) - E_{\beta_i}^0 | \hat{\phi}_i^1(1) \rangle + 2 \sum_{i=1}^{p} \langle \hat{\psi}_i^1(1) | z(1) | \psi_i^0(1) \rangle \\ & + 2 \sum_{i=1}^{q} \langle \hat{\phi}_i^1(1) | z(1) | \phi_i^0(1) \rangle + \sum_{i=1}^{p} \sum_{j=1}^{p} (2[\hat{\psi}_i^1 \hat{\psi}_j^1 | \psi_i^0 \psi_j^0] \\ & - [\hat{\psi}_i^1 \hat{\psi}_j^1 | \psi_j^0 \psi_i^0] - [\hat{\psi}_i^1 \psi_j^0 | \hat{\psi}_j^1 \psi_i^0]) + \sum_{i=1}^{q} \sum_{j=1}^{q} (2[\hat{\phi}_i^1 \hat{\phi}_j^1 | \phi_i^0 \phi_j^0] \\ & - [\hat{\phi}_i^1 \hat{\phi}_j^1 | \phi_j^0 \phi_i^0] - [\hat{\phi}_i^1 \phi_j^0 | \hat{\phi}_j^1 \phi_i^0]) + \sum_{i=1}^{p} \sum_{j=1}^{q} 4[\hat{\psi}_i^1 \hat{\phi}_j^1 | \psi_i^0 \phi_j^0] \,.\end{aligned} \tag{44}$$

We note that $\hat{E}_2$ depends only on zero and first order orbitals. Also since $\hat{E}_2$ is always greater or equal to the coupled second order energy E_2^c and idential with E_2^c when $\hat{\Psi} = \Psi^c$ we may calculate the first order orbitals $\{\psi_i^{c1}\}$ and $\{\phi_i^{c1}\}$ by minimising (44) with respect to variations in $\{\hat{\psi}_i^1\}$ and $\{\hat{\phi}_i^1\}$ subject to the conditions:

$$\langle \hat{\phi}_i^1 | \phi_j^0 \rangle + \langle \phi_i^0 | \hat{\phi}_j^1 \rangle = 0 \,, \tag{45}$$

$$\langle \hat{\psi}_i^1 | \psi_j^0 \rangle + \langle \psi_i^0 | \hat{\psi}_j^1 \rangle = 0 \,. \tag{46}$$

4. Uncoupled Perturbation Theory

The complexity of the equations of coupled perturbation theory has led to considerable interest in the simpler uncoupled perturbation theory. In his original paper Dalgarno [2] showed that it is possible to correct the energies obtained from the simpler uncoupled theory; this theory is discussed in the next section. The zero order equation is identical with that of coupled theory (Eqs. (5) and (6)).

If we now perturb the system by a sum of one electron operators $\lambda W = \lambda \sum_i z(i)$ as in Section 2 we obtain the perturbation equations

$$(\hat{H}_0 - E_0)\, \Psi_k = (E_1 - W)\, \Psi_{k-1} + \sum_{i=2}^{k} E_i\, \Psi_{k-i} \delta_{k_1} \tag{47}$$

for $k \geqq 1$. These equations differ from those of coupled theory in that they neglect the change of the self consistent terms due to the perturbation. Expanding the orbitals $\{\psi_i\}$ and $\{\phi_i\}$ in terms of a basis set $\{\omega_r\}$ as in Section 2 we obtain the equations:

$$\sum_{s=1}^{m} (F_{rs}^{\alpha_0} - E_{\alpha_i}^0 S_{rs})\, a_{is}^k = \sum_{s=1}^{m} \left((E_{\alpha_i}^1 S_{rs} - z_{rs})\, a_{is}^{k-1} + \delta_{k_1} \sum_{j=2}^{k} E_{\alpha i}^j S_{rs} a_{is}^{k-j} \right) \tag{48}$$

$$\sum_{s=1}^{m} (F_{rs}^{\beta_0} - E_{\beta_i}^0 S_{rs})\, b_{is}^k = \sum_{s=1}^{m} \left((E_{\beta_i}^1 S_{rs} - z_{rs})\, b_{is}^{k-1} + \delta_{k_1} \sum_{j=2}^{k} E_{\beta_i}^j S_{rs} b_{is}^{k-j} \right) \tag{49}$$

for all orders $k \geqq 1$. The first and second order energies are given by

$$E_1 = \langle \Psi_0 | W | \Psi_0 \rangle = \sum_{rs} (P^0_{sr} + Q^0_{sr}) z_{rs} \tag{50}$$

$$E_2 = \langle \Psi_1 | W | \Psi_0 \rangle = \frac{1}{2} \sum_{rs} (P^1_{sr} + Q^1_{sr}) z_{rs} \tag{51}$$

where the charge and bond order matrices of the k^{th} order are defined analogously to Eqs. (19) and (20).

5. Corrections

Uncoupled theory usually gives poor energies compared with coupled theory. It has been found, however that it is possible to correct the uncoupled results so that their accuracy is comparable. This was first introduced by Dalgarno [2] and has been developed by Tuan *et al.* [1] and Amos and Musher [8]. In order to correct the uncoupled energies we define V such that

$$V = \mathscr{H} - \hat{H}_0 \,. \tag{52}$$

Suppose we have solved the uncoupled equations to infinite order so that we obtain the uncoupled wavefunctions and energy defined as follows:

$$\Psi^0 = \sum_{k=0}^{\infty} \lambda^k \Psi_k \,, \tag{53}$$

$$E^0 = \sum_{k=0}^{\infty} \lambda^k E_k \,. \tag{54}$$

Let

$$\hat{H} = \hat{H}_0 + \lambda W \tag{55}$$

then

$$\hat{H} \Psi^0 = E^0 \Psi^0 \,. \tag{56}$$

Consider the perturbation equation

$$(\hat{H} + \mu V)\left(\sum_{k=0}^{\infty} \mu^k \Psi^k\right) = \left(\sum_{k=0}^{\infty} \mu^k \Psi^k\right)\left(\sum_{j=0}^{\infty} \mu^j E^j\right) \tag{57}$$

then the first order correction to the energy is given by

$$E^1 = \langle \Psi^0 | V | \Psi^0 \rangle \,. \tag{58}$$

If we assume that the wavefunctions are real and expand in powers of we can obtain corrections for the first and second order uncoupled energies:

$$E^1_1 = 0 \tag{59}$$

$$\begin{aligned} E^1_2 = {} & \sum_{i=1}^{p} \sum_{j=1}^{p} (2[\psi^1_i \psi^1_j | \psi^0_i \psi^0_j] - [\psi^1_i \psi^1_j | \psi^0_j \psi^0_i] - [\psi^1_i \psi^0_j | \psi^1_j \psi^0_i]) \\ & + \sum_{i=1}^{q} \sum_{j=1}^{q} (2[\phi^1_i \phi^1_j | \phi^0_i \phi^0_j] - [\phi^1_i \phi^1_j | \phi^0_j \phi^0_i] - [\phi^1_i \phi^0_j | \phi^1_j \phi^0_i]) \\ & + 4 \sum_{i=1}^{p} \sum_{j=1}^{q} [\psi^1_i \phi^1_j | \psi^0_i \phi^0_j] \,. \end{aligned} \tag{60}$$

In the case of coupled theory we define $\hat{H}$ such that

$$\hat{H} = \hat{H}_0 + \lambda W + \sum_{k=0}^{\infty} \left(\sum_i (G^{\alpha k}(i) | \alpha \rangle \langle \alpha | + G^{\beta k}(i) | \beta \rangle \langle \beta |) + C^k \right) \tag{61}$$

where the C^k are chosen so that to all orders of λ

$$\langle \Psi^0 | \mathscr{H} + \lambda W | \Psi^0 \rangle = \langle \Psi^0 | \hat{H} | \Psi^0 \rangle . \tag{62}$$

If we define V so that

$$V = \mathscr{H} - \hat{H} + \lambda W \tag{63}$$

and proceed with the double perturbation procedure as in the uncoupled case we obtain

$$E^1 = \langle \Psi^0 | V | \Psi^0 \rangle = 0 . \tag{64}$$

This result is usually summarised by stating that coupled theory is correct to first order although as V is a different operator in the uncoupled case, this is perhaps not a fair comparison.

One of the most significant differences between the single determinant approximation for a molecule with an even number of electrons and one with an odd number is that the former is an eigenfunction of $\hat{S}^2$ whereas the latter is not. The single determinant for an odd number of electrons may be expanded in pure spin states. To obtain a better approximation to the ground state wavefunction Amos and Hall have suggested the use of an annihilator of the largest unwanted component spin state [18]. If the ground state is an eigenfunction of $\hat{S}^2$ with eigenvalue s then the annihilator of the next component A_{s+1} is given by

$$A_{s+1} = \hat{S}^2 - (s+1)(s+2) . \tag{65}$$

The operator $\hat{S}^2$ can be taken as

$$\hat{S}^2 = \frac{1}{2}(p+q) + \frac{1}{4}(p-q)^2 + \sum_{i\alpha j\beta} P^{\delta}_{i_\alpha j_\beta} \tag{66}$$

where $P^{\delta}_{i_\alpha j_\beta}$ exchanges the spin function associated with the i^{th} orbital with α spin and the j^{th} orbital with β spin so that for example

$$P^{\delta}_{i_\alpha j_\beta} \Psi_0 = -(n!)^{\frac{1}{2}} \det \{ \psi_1^0(1)\alpha(1) \ldots \phi_j^0(i)\alpha(i) \ldots \psi_i^0(j)\beta(j) \ldots \phi_q^0(p+q)\beta(p+q) \} . \tag{67}$$

In both coupled and uncoupled theory we may correct the single determinant wavefunction by annihilating the highest unwanted spin component perturbatively. To do this we will use Amos-Musher perturbation theory [11]. As before we assume that we have solved the coupled or uncoupled equations to infinite order. The theory will be developed in terms of the operator $\hat{H}$ which has been defined earlier and which is different depending on whether we are using coupled or uncoupled theory. In either case we have

$$\hat{H} \Psi^0 = E^0 \Psi^0 \tag{68}$$

where Ψ^0 and E^0 are defined by Eqs. (53) and (54). Define

$$V = \mathscr{H} - \hat{H} + \lambda W . \tag{69}$$

From (68) we have

$$A_{s+1}\hat{H}\Psi^0 = E^0 A_{s+1}\Psi^0 . \tag{70}$$

Consider the perturbation equations

$$\begin{aligned} A_{s+1}(\hat{H}+\mu V)\Psi^0 + (\hat{H}+\mu V)\left(\sum_{k=1}^{\infty}\mu^k\Psi^k\right) \\ = \left(A_{s+1}\Psi^0 + \sum_{k=1}^{\infty}\mu^k\Psi^k\right)\left(\sum_{k=0}^{\infty}\mu^k E^k\right). \end{aligned} \tag{71}$$

From these we obtain

$$E^1 = \langle\Psi^0|A_{s+1}V|\Psi^0\rangle/\langle\Psi^0|A_{s+1}|\Psi^0\rangle \tag{72}$$

Expanding in powers of λ where

$$\langle\Psi^0|A_{s+1}V|\Psi^0\rangle = \sum_{k=0}^{\infty}\lambda^k Y^k , \tag{73}$$

$$\langle\Psi^0|A_{s+1}|\Psi^0\rangle = \sum_{k=0}^{\infty}\lambda^k X^k \tag{74}$$

and

$$E^1 = \sum_{k=0}^{\infty} E^1_k \lambda^k \tag{75}$$

we may obtain terms through first order in μ and k^{th} order in λ.

6. Results and Discussion

Trial calculations have been carried out on a number of alternants. The perturbations used were point perturbations of the form

$$z_{rs} = \delta_{ru}\delta_{su} \qquad \text{for some } u . \tag{76}$$

In Table 1 the second order energies obtained by the various methods that have been outlined in the previous sections are listed. The term correction 1 refers to the ordinary correction discussed in Section 5 whereas correction 2 is taken to mean correction by Amos-Musher perturbation theory. The geometric approximation, first introduced by Musher and Schulman [7] (see also references [12, 13]), has also been used and the results are given in Table 1.

The perturbation theory developed is suitable for the treatment of aza substituted benzene ions. We assume that the Nitrogen atoms may be represented by a change in the one electron operators so that

$$\begin{aligned} z_{rs} &= v\delta_{rs} \quad \text{if } r \text{ is a Nitrogen site} \\ &= 0 \quad \text{otherwise}. \end{aligned} \tag{77}$$

The value of the parameter v has been discussed by Amos and in this work his parameter will be used namely $v = -1.73$ eV [14].

Table 1

Molecule	Allyl		*Cis*-butadiene triplet	
Perturbation at atom	1	2	1	2
Uncoupled E	−0.024	−0.032	−0.017	−0.039
Uncoupled E + Correction 1	−0.033	−0.043	−0.023	−0.052
Geometric approx	−0.039	−0.048	−0.026	−0.058
Uncoupled E + Correction 2	−0.034	−0.043	−0.022	−0.052
Coupled E	−0.039	−0.048	−0.029	−0.058
Coupled E + Correction 2	−0.034	−0.045	−0.030	−0.058

Table 2

Molecule	Atom	UBS	UAS	CBS	CAS
Pyridazine 2/3 substituted	2	0.320	0.288	0.347	0.317
	4	0.123	−0.053	−0.109	−0.043
	5	0.302	0.264	0.262	0.227
Pyrimidine 2/6 substituted	6	0.273	0.237	0.174	0.160
	1	0.125	−0.055	−0.039	−0.015
	3	0.352	0.316	0.451	0.399
	4	−0.126	−0.056	−0.209	−0.093
Pyridine 1 substituted	1	0.394	0.356	0.330	0.306
	2	0.060	0.076	0.160	0.136
	3	0.023	0.045	−0.053	0.007
	4	0.440	0.400	0.457	0.413
Pyrazine − 1/4 substituted	1	0.402	0.366	0.364	0.338
	2	0.049	0.067	0.068	0.082
Pyridine + 1 substituted	1	−0.121	−0.025	−0.095	−0.020
	2	0.313	0.265	0.289	0.245
	3	0.313	0.264	0.335	0.279
	4	−0.130	−0.028	−0.155	−0.033
Pyrazine + 1/4 substituted	1	−0.126	−0.026	−0.129	−0.029
	2	0.313	0.263	0.314	0.262
Pyrimidine + 2/6 substituted	6	0.031	0.061	0.052	0.062
	1	0.383	0.322	0.259	0.211
	3	0.050	0.076	0.050	0.078
	4	0.457	0.409	0.537	0.507
Pyridazine + 2/3 substituted	2	0.059	0.081	0.078	0.094
	4	0.418	0.362	0.403	0.353
	5	0.023	0.057	0.019	0.055

UBS	Uncoupled spin densities before annihilation.
UAS	Uncoupled spin densities after annihilation.
CBS	Coupled spin densities before annihilation.
CAS	Coupled spin densities.

Table 3

Molecule	Atom	UBC	UAC	CBC	CAC
Pyrazine –	1	1.388	1.412	1.437	1.439
1/4 substituted	2	1.056	1.057	1.032	1.032
Pyridine –	1	1.407	1.411	1.494	1.492
1	2	1.066	1.066	1.025	1.021
substituted	3	1.085	1.083	1.101	1.101
	4	1.292	1.294	1.254	1.256
Pyrimidine –	6	1.342	1.342	1.442	1.440
2/6	1	0.897	0.897	0.810	0.812
substituted	3	1.204	1.202	1.134	1.134
	4	1.010	1.011	1.037	1.037
Pyridazine –	2	1.332	1.332	1.363	1.363
2/3	4	0.959	0.961	0.937	0.939
substituted	5	1.210	1.208	1.200	1.198
Pyrimidine +	6	1.044	1.046	1.135	1.137
2/6	1	0.629	0.627	0.546	0.544
substituted	3	0.808	0.810	0.743	0.743
	4	0.668	0.664	0.698	0.696
Pyridazine +	2	0.958	0.960	0.984	0.980
2/3	4	0.652	0.648	0.630	0.626
substituted	5	0.890	0.892	0.886	0.890
Pyridine +	1	1.122	1.122	1.192	1.192
1	2	0.699	0.701	0.656	0.656
substituted	3	0.755	0.757	0.769	0.771
	4	0.971	0.967	0.958	0.956
Pyrazine +	1	1.101	1.101	1.156	1.156
1/4 substituted	2	0.700	0.700	0.672	0.672

UBC	Uncoupled charge densities before annihilation.
UAC	Uncoupled charge densities after annihilation.
CBC	Coupled charge densities before annihilation.
CAC	Coupled charge densities after annihilation.

If we define

$$\bar{P}_{rs} = P^0_{rs} + P^1_{rs} + P^2_{rs} \tag{78}$$

and

$$\bar{Q}_{rs} = Q^0_{rs} + Q^1_{rs} + Q^2_{rs} \tag{79}$$

then approximations to the spin and charge densities at atom r are given by

$$\bar{P}_{rr} - \bar{Q}_{rr} \tag{80}$$

and

$$\bar{P}_{rr} + \bar{Q}_{rr} \tag{81}$$

respectively. These are calculated for various aza substituted benzene ions and the results are given in Tables 2 and 3. Approximations are also given to the spin and charge densities after the highest unwanted spin components has been annihilated. The theory of this has been developed by Snyder and Amos [15]. The approximations to the spin and charge densities are of the form

$$\bar{R}_{rr} - \bar{S}_{rr} \tag{82}$$

and

$$\bar{R}_{rr} + \bar{S}_{rr} \tag{83}$$

where

$$\bar{R}_{rs} = \bar{P}_{rs} + (\underline{\bar{P}}\,\underline{\bar{Q}}\,\underline{\bar{P}}_{rs} - \tfrac{1}{2}\underline{\bar{P}}\,\underline{\bar{Q}}_{rs} - \tfrac{1}{2}\underline{\bar{Q}}\,\underline{\bar{P}}_{rs})2/\chi\,, \tag{84}$$

$$\bar{S}_{rs} = \bar{Q}_{rs} + (\underline{\bar{Q}}\,\underline{\bar{P}}\,\underline{\bar{Q}}_{rs} - \tfrac{1}{2}\underline{\bar{Q}}\,\underline{\bar{P}}_{rs} - \tfrac{1}{2}\underline{\bar{P}}\,\underline{\bar{Q}}_{rs})2/\chi \tag{85}$$

and

$$\chi = \tfrac{1}{2}(p+q) + \tfrac{1}{4}(p-q)^2 - (s+1)(s+2) - \sum_{rs} \bar{P}_{sr}\bar{Q}_{rs}\,. \tag{86}$$

As the ground state wavefunctions of the benzene ions are degenerate it is necessary to choose the correct zero order wavefunction for the perturbation. It is possible to choose the two degenerate wavefunctions for the benzene anion (or the cation) so that one of the functions is symmetric with respect to reflection about a plane perpendicular to the molecular plane through atoms 1 and 4 (numbering sequentually from any atom) and the other antisymmetric. This choice imposes a constraint on the Hartree-Fock solution. As $G^{\alpha o}$ and $G^{\beta o}$ depend on the spin orbitals the numerical procedure used was an iterative procedure. If the initial approximation is chosen symmetric (antisymmetric) then at each stage of the iteration the wavefunction will be symmetric (antisymmetric). Wavefunctions obtained this way are not actually energetically equivalent (see Amos and Snyder [16]). However this procedure enables a zero order wavefunction of the correct symmetry to be obtained. For a discussion of which zero order function to choose for a particular aza substitution see Ref. [17].

On examination of Table 1 we see that the results for the geometric approximation are very close to those for coupled theory. This is in line with previous calculations using the geometric approximation [7, 12, 13]. The corrections for the pure spin state (correction 2) may be seen to be smaller than the differences between the uncoupled and coupled theory results.

From Tables 2 and 3 it may be seen that although the correction of Snyder and Amos has only a small effect on the coupled and uncoupled charge densities it has a significant effect on the spin densities. Thus it appears that for charge density calculations the annihilation of the highest unwanted spin state may be unnecessary. For spin density calculations, which involve differences between quantities, and are consequently of a different order of magnitude to the charge densities, it may be necessary to carry out the perturbative calculations to higher orders or to annihilate other unwanted spin states. However the spin densities so obtained are usually related to experimental results using one of several empirical formulae. Considering the inaccuracies inherent in these formulae the accuracy obtained in the calculations presented here is probably sufficient for comparison with experiment.

Acknowledgements. I would like to express my appreciation to Dr. A. T. Amos for much helpful advice during the course of this work and to the S.R.C. for the provision of maintenance grant.

References

1. Tuan, D. Fu-Tai, Epstein, S., Hirschfelder, J. O.: J. chem. Physics **44**, 433 (1966).
2. Dalgarno, A.: Proc. Royal Soc. (London) A **251**, 282 (1959).
3. Langhoff, P. W., Karplus, M., Hurst, R. P.: J. chem. Physics **44**, 505 (1966).
4. Hall, G. G., Amos, A. T.: Theoret. chim. Acta (Berl.) **5**, 148 (1966).
5. Musher, J. I.: J. chem. Physics **46**, 369 (1967).
6. Epstein, S. T., Johnson, R. E.; J. chem. Physics **47**, 2275 (1967).

7. Schulman, J. M., Musher, J. I.: J. chem. Physics **49**, 4845 (1968).
8. Amos, A. T., Musher, J. I.: Molecular Physics **13**, 509 (1967).
9. Pople, J. A., Scholfield, P.: Proc. Royal Soc. (London) A **233**, 233, 241 (1951).
10. Pople, J. A., Nesbet, R. K.: J. chem. Physics **22**, 571 (1954).
11. Amos, A. T., Musher, J. I.: Chem. Physics Letters **1**, 149 (1967).
12. Amos, A. T.: J. chem. Physics **52**, 603 (1970).
13. Tuan, D.: Chem. Physics Letters **7**, 115 (1970).
14. Amos, A. T.: Theoret. chim. Acta (Berl.) **5**, 148 (1966).
15. Amos, A. T., Snyder, L. C.: J. chem. Physics **41**, 1773 (1964).
16. Snyder, L. C., Amos, A. T.: J. chem. Physics **42**, 3670 (1965).
17. Burrows, B. L.: J. chem. Physics (1971).
18. Amos, A. T., Hall, G. G.: Proc. Royal Soc. (London) A **263**, 483 (1961).
19. Amos, A. T.: Molecular Physics **5**, 91 (1962).

Dr. B. L. Burrows
Mathematics Department
North Staffordshire Polytechnic
Stafford, England

Theoret. chim. Acta (Berl.) 28, 193–199 (1973)
© by Springer-Verlag 1973

The Electronic Structure of the Oxygen Double-Bridged $\mu\mu'$-Dioxo-bis (Oxodichloroaquo) Dimolybdate (V)-Ion by SCCC MO Method

Leszek Natkaniec, Mikołaj F. Rudolf, and Bogusława Jeżowska-Trzebiatowska
Institute of Chemistry, University of Wrocław, Wrocław, Poland

Received May 31, 1972

Results of SCCC MO calculations for the dimeric oxygen double-bridged $[Mo_2O_4Cl_4(H_2O)_2]^{2-}$ ion are reported. On the basis of these results the previously reported spectra and magnetic properties may be explained. The strong direct molybdenum – molybdenum interaction in the $Mo_2O_4^{2+}$ core was proved to exist.

Die Ergebnisse von SCCC MO-Rechnungen für das zweikernige Ion $[Mo_2O_4Cl_4(H_2O)_2]^{2-}$ mit zweifacher Sauerstoffbrücke werden mitgeteilt. Danach können die früher angeführten magnetischen und spektralen Eigenschaften dieses Ions verstanden werden. Die Existenz starker unmittelbarer Molybdän-Molybdän Wechselwirkungen innerhalb des $Mo_2O_4^{2+}$ Kerns wird nachgewiesen.

Résultats de calculs SCCCMO pour l'ion dimère $Mo_2O_4Cl_4(H_2O)_2^{2-}$. Sur la base de ces résultats les propriétés spectrales et magnétiques précédemment obtenues peuvent être expliquées. L'existence d'une forte interaction directe molybdène-molybdène dans le coeur $Mo_2O_4^{2+}$ est clairement démontrée.

Introduction

Theoretical and experimental investigations of both-monomeric and polymeric oxocomplexes of *d*-electronic elements are since many years the subjects to intensive studies. The problem of binuclear systems with single oxygen bridges, such as Cr – O – Cr, Fe – O – Fe, Re – O – Re, Ru – O – Ru and Mo – O – Mo, have been considered and led to the elaboration of the theory of linear oxygen bridge-bonding [1–4]. Theoretical calculations performed with regard to all interatomic interactions for the $Re_2OCl_{10}^{4-}$ ion indicated the specific features of electronic structure of two paramagnetic ions bonded by an anion, and showed also the influence of ligands coordinated on such a nuclei.

Studies on the chemistry of quinquevalent molybdenum proved, that in the $MoOCl_5^{2-}$ and $MoOBr_5^{2-}$ ions hydrolysis reactions, the bi- and tetranuclear oxomolybdates (V) are formed, in which the molybdenum atoms are bonded by double oxygen bridges [5]. The results of studies on spectral (UV, IR) and magnetic properties of synthetized polymeric oxomolybdates (V) not only confirmed the existence of the dimeric cores of the

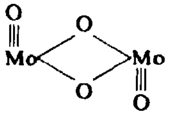

type in those complexes, but indicated also their specific electronic structure. The interatomic interactions within such cores were recognized (magnetic moment reduction to 0.3–0.5 BM) [6, 7].

In spite of attempts to theoretical interpretation of the electronic structure of copper (II) acetate dihydrate, made with simplified methods, the satisfactory and reliable interpretation was reported by Bersuker [8] who considered in the SCCC MO approximation the complete atomic arrangement, the ligand – ligand and metal – metal interactions.

In the present work the results of the electronic structure calculations of the $[Mo_2O_4Cl_4(H_2O)_2]^{2-}$ ion, carried out by the SCCC MO method [9], are reported.

The Calculation and Results

Since the X-Ray structure of the $\mu\mu'$-dioxo-bis (oxodichloroaquo) dimolybdate (V) ion has not been determined yet, its geometrical configuration and bond lengths were determined indirectly, using the known X-Ray data for mono- and binuclear oxomolybdates (V) [10–15]. The structure of the complex is shown on Fig. 1. The symmetry of the complex ion was assumed to be C_{2h} and all the angles in the bridge core were assumed to be equal to 90°. For the diatomic overlap integrals calculations, the Mo–O_t, Mo–O_b, Mo–Cl and Mo–H_2O bond lengths were assumed to be equal to: 1.67, 1.90, 2.63 and 2.27 Å respectively. On Fig. 2 the coordinate system of the $[Mo_2O_4Cl_4(H_2O)_2]^{2-}$ ion is presented. At the calculations the 4*d*, 5*s* and 5*p* molybdenum valence orbitals, *ns* and *np* valence orbitals of oxygen and chlorine atoms and one σ-orbital (sp^3 hybrid) for each water molecule were taken into account in the function basis. Therefore the complete function basis contained 52 orbitals from all the atoms in the molecule.

The analytical expressions of orbitals were taken for Mo^{1+} as reported by Basch [16], for Cl^0 as reported by Freeman [17] and for O^0 as reported by Ballhausen [18]. The diagonal matrix elements for molybdenum were approxi-

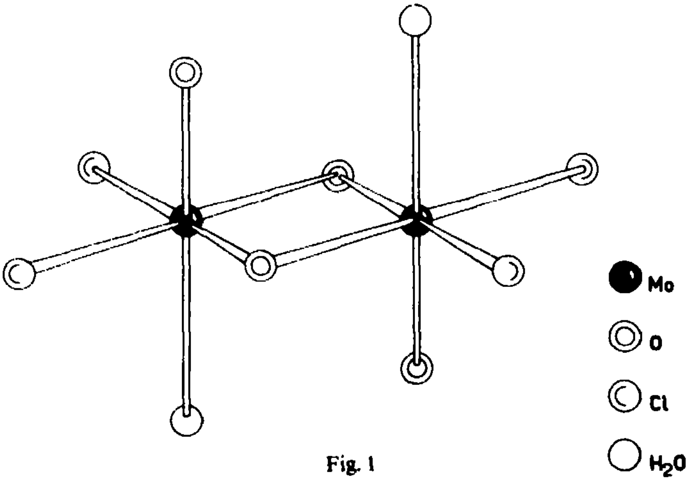

Fig. 1

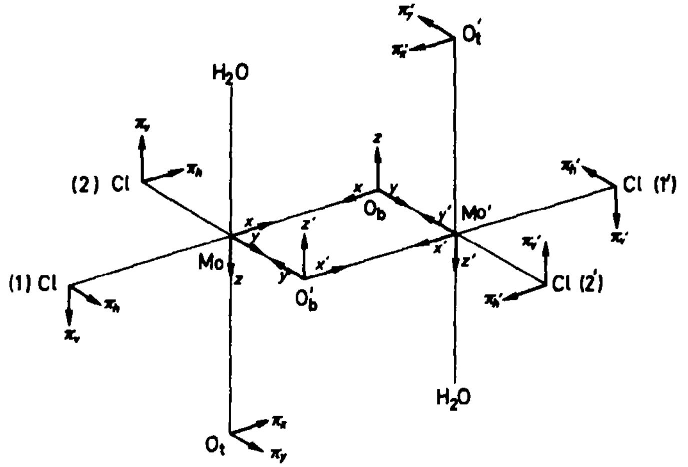

Fig. 2

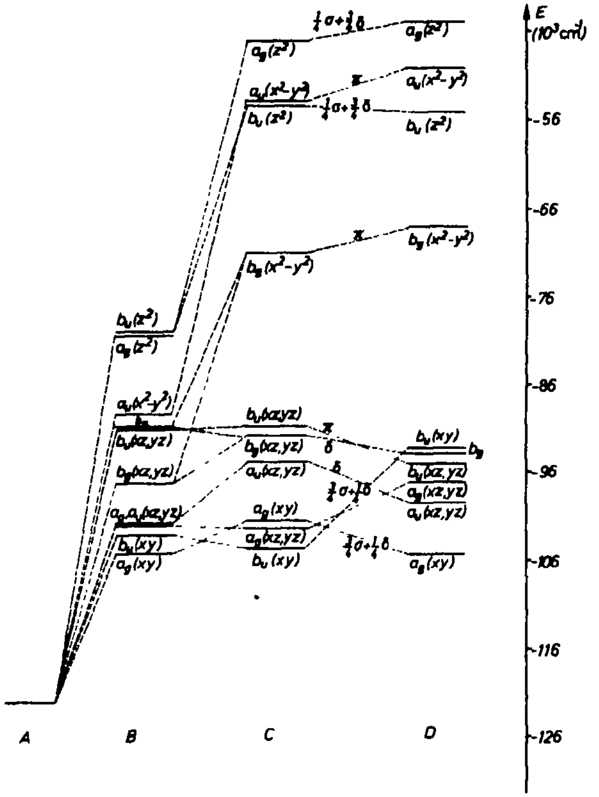

Fig. 3. *A* Molybdenum *d*-Valence orbitals; *B* *A* + MO–O_t, Cl, H_2O interaction; *C* *B* + MO–O_b interaction; *D* *C* + MO–MO interaction

Table 1. Energies and symmetries of molecular orbitals of the $[Mo_2O_4Cl_4(H_2O)_2]^{2-}$ ion

Energy	Symmetry	Contribution of molybdenum and ligands orbitals						
$[10^3 \cdot cm^{-1}]$								
-276.1	$1a_g$	s_{O_b}	(0.487)	s_{O_t}	(0.448)			
-264.3	$1b_u$	s_{O_t}	(0.968)					
-262.8	$1a_u$	s_{O_b}	(0.958)					
-259.1	$2a_g$	s_{O_t}	(0.480)	s_{O_b}	(0.432)			
-208.5	$3a_g$	s_{Cl}	(0.914)					
207.1	$2b_u$	s_{Cl}	(0.976)					
-205.2	$2a_u$	s_{Cl}	(0.943)					
-204.2	$1b_g$	s_{Cl}	(0.963)					
160.6	$3b_u$	σ_{H_2O}	(0.488)	d_{xz}	(0.145)	$p_{z_{O_b}}$	(0.122)	
-158.7	$4a_g$	σ_{H_2O}	(0.583)					
-151.0	$5a_g$	$p_{x_{O_b}}$	(0.410)	d_{xy}	(0.343)			
-150.8	$4b_u$	d_{xz}	(0.229)	$p_{\sigma_{O_t}}$	(0.220)	σ_{H_2O}	(0.192)	π_x (0.132
150.7	$2b_g$	d_{xz}	(0.348)	π_x	(0.290)	$p_{z_{O_b}}$	(0.286)	
-143.8	$5b_u$	$p_{x_{O_b}}$	(0.423)	$p_{\sigma_{Cl}}$	(0.139)	d_{xy}	(0.119)	
-141.4	$6a_g$	$p_{\sigma_{O_t}}$	(0.705)					
139.6	$3a_u$	π_x	(0.505)	d_{xz}	(0.309)			
139.3	$6b_u$	$p_{\sigma_{O_t}}$	(0.584)					
-136.4	$3b_g$	$p_{x_{O_b}}$	(0.661)	$d_{x^2-y^2}$	(0.252)			
-136.1	$4a_u$	$p_{x_{O_b}}$	(0.415)	$d_{x^2-y^2}$	(0.228)	$p_{\sigma_{Cl}}$	(0.202)	
135.4	$7a_g$	$p_{\sigma_{Cl}}$	(0.360)	π_x	(0.286)			
127.4	$4b_g$	$p_{\sigma_{Cl}}$	(0.543)	$d_{x^2-y^2}$	(0.148)			
-127.0	$7b_u$	$p_{\sigma_{Cl}}$	(0.539)	π_h	(0.135)			
-125.8	$8a_g$	$p_{\sigma_{Cl}}$	(0.384)	π_x	(0.229)	d_{xz}	(0.191)	
119.8	$5a_u$	$p_{\sigma_{Cl}}$	(0.428)	$p_{x_{O_b}}$	(0.396)			
-118.3	$5b_g$	π_x	(0.286)	$p_{z_{O_b}}$	(0.250)	$p_{\sigma_{Cl}}$	(0.177)	π_v (0.149
-117.0	$8b_u$	$p_{z_{O_b}}$	(0.485)	π_x	(0.178)			
-116.9	$9a_g$	π_h	(0.473)	$p_{x_{O_b}}$	(0.261)	d_{xy}	(0.207)	
-110.4	$9b_u$	π_h	(0.473)	π_x	(0.324)			
109.7	$10a_g$	π_v	(0.862)					
-108.2	$10b_u$	π_v	(0.466)	π_h	(0.200)			
-108.2	$6a_u$	π_x	(0.849)					
-106.2	$7a_u$	π_h	(0.982)					
105.5	$6b_g$	π_h	(0.952)					
-105.2	$11a_g$	π_h	(0.471)	d_{xy}	(0.367)	$p_{x_{O_b}}$	(0.138)	
-102.2	$7b_g$	π_v	(0.620)	d_{xz}	(0.150)	π_x	(0.137)	
-99.3	$8a_u$	d_{xz}	(0.532)	π_x	(0.319)			
-97.1	$12a_g$	d_{xz}	(0.684)	π_x	(0.225)			
-94.8	$11b_u$	d_{xz}	(0.490)	π_x	(0.269)	$p_{z_{O_b}}$	(0.144)	
-93.7	$8b_g$	d_{xz}	(0.430)	$p_{z_{O_b}}$	(0.269)	π_x	(0.148)	π_v (0.133
-93.1	$12b_u$	d_{xy}	(0.701)	$p_{x_{O_b}}$	(0.203)			
-68.0	$9b_g$	$d_{x^2-y^2}$	(0.551)	$p_{\sigma_{Cl}}$	(0.217)	$p_{x_{O_b}}$	(0.193)	
-54.9	$13b_u$	d_{z^2}	(0.521)	$p_{z_{Mo}}$	(0.124)	σ_{H_2O}	(0.123)	
-50.1	$9a_u$	$d_{x^2-y^2}$	(0.541)	$p_{\sigma_{Cl}}$	(0.196)	$p_{x_{O_b}}$	(0.118)	
-44.8	$13a_g$	d_{z^2}	(0.475)	$p_{z_{Mo}}$	(0.190)			
12.8	$14b_u$	s_{Mo}	(0.501)	$p_{z_{Mo}}$	(0.250)	$p_{x_{Mo}}$	(0.196)	
18.2	$10b_g$	$p_{x_{Mo}}$	(0.953)					
30.5	$14a_g$	$p_{z_{Mo}}$	(0.354)	$p_{x_{O_b}}$	(0.305)			
67.0	$10a_u$	$p_{x_{Mo}}$	(0.892)					
74.7	$15b_u$	$p_{x_{Mo}}$	(0.833)	s_{Mo}	(0.120)			
79.8	$15a_g$	$p_{x_{Mo}}$	(0.757)					
134.8	$16b_u$	$p_{z_{Mo}}$	(0.575)	s_{Mo}	(0.326)			
168.2	$16a_g$	s_{Mo}	(0.488)	$p_{z_{Mo}}$	(0.382)			

mated with negative values of VOIP similarly as reported by Gołębiewski [19]. For ligands it was assumed, that the H_{ii}'s are independent on charge and are equal to the negative values of VOIP for the neutral ligands. The non-diagonal matrix elements were approximated as given by Cusachs [20]. The calculations were carried out employing the Mulliken population analysis [21] until the charge and configuration selfconsistence were obtained [22]. The results of these calculations are presented in Table 1 and shown on Fig. 3.

Discussion

To examine the influence of different types of interactions on the MO ordering, the calculations of the electronic structure of the $\mu\mu'$-dioxo-bis (oxodichloroaquo) dimolybdate (V) ion were carried out stepwise starting with the model of simple molybdenum-non-bridging ligand interactions (Fig. 3 B). If one considers this type of interactions only, the molybdenum d-orbitals are splitted into two groups: the first one being strongly antibonding with respect to the molybdenum-ligand σ-interaction, originating from octahedral e_g orbitals and the second group of orbitals originating from octahedral t_{2g} orbitals. For this approximation the following energetic ordering of orbitals was obtained (Fig. 3 B)

$$a_g, b_u(d_{z^2}) \gg a_u, b_g(d_{x^2-y^2}) > a_g, a_u, b_g, b_u(d_{xz}, d_{yz}) > a_g, b_u(d_{xy}).$$

That the both nuclei are bonded by the bridging oxygen atoms results in the energy increase of antibonding orbitals $a_g, b_u(d_{z^2})$ and $a_u, b_g(d_{x^2-y^2})$ (Fig. 3 C). The changes in energy of π-orbitals are small and their direction can not be explicitly justified.

The metal-metal interaction has the peculiar character (Fig. 3 D). In the group of σ-MO's it has mainly the character of π–π or δ–δ interactions and is not the cause of essential changes in energy. In the group of π–MO's essential changes in the energetic ordering of MO's due to the metal-metal interaction are observed. Under the influence of that interaction, first of all of the σ-type, the $a_g(d_{xy})$ and $b_u(d_{xy})$ orbitals became the bonding and antibonding ones, respectively. Since the $a_g(d_{xy})$ orbital is occupied by two electrons, the metal-metal interaction through d_{xy} orbitals is in that case the factor leading to an additional stabilization of the complex and deciding on the molybdenum-molybdenum bond order. Taking the foregoing analysis into account it should be stated, that the ligands have the strongest influence on energetic splitting of d-orbitals of molybdenum. The metal-metal interaction is less important, except of the σ-type interaction.

To analyze the character of particular bonds in the examined compound the bond orders, overlap populations and gross atomic populations were calculated. The bond order definition and population analysis, both given by Mulliken were applied [21]. In Table 2 some of the obtained results are presented. The electron overlap populations are calculated per one ligand atom. Hence they comprise the total electron density in the overlap area between one ligand and two molybdenum atoms. For nonbridging ligands they are practically reduced to the overlap populations between one ligand and one molybdenum atom.

Table 2. Overlap populations for individual bonds in the $[Mo_2O_4Cl_4(H_2O)_2]^{2-}$ ion

Bond symmetry	Mo–Mo[a]	Mo–Mo[b]	Mo–O_b	Mo–O_t	Mo–Cl	Mo–O_{H_2O}
A_g	0.0373	0.0464	0.0182	0.1049	0.0616	0.0774
B_u	0.0047	−0.0184	0.0576	0.0863	0.0135	0.0712
A_u	0.0078	0.0055	0.0187	0.0617	0.0504	
B_g	−0.0090	−0.0077	0.0577	0.0324	0.0265	
Total O. P.	0.0408	0.0258	0.1522	0.2853	0.1520	0.1486

[a] Only *d*-orbitals considered.

[b] All *s*, *p* and *d*-valence orbitals of molybdenum are considered.

Metal-Metal Bond. The largest contribution have the a_g orbitals (Table 2), and first of all the $a_g(d_{xy})$ orbital. It is the result of the large value of the overlap integral between d_{xy} orbitals, corresponding mainly to the σ-type interaction and of the presence of two electrons on the $a_g(d_{xy})$ molybdenum orbital.

Molybdenum-Oxygen (Terminal) Bond. The subtotal overlap populations decrease in the ordering:

$$a_g > b_u > a_u > b_g .$$

It is clear because in the representations a_g and b_u there appear the d_{z^2} and p_z molybdenum orbitals which cause the strong bonding with the O_t atoms. The d_{xz}, d_{yz} orbitals of b_g and b_u symmetries and p_z molybdenum orbitals of b_u symmetry are very much involved in the π-bonding with the bridge-oxygen atoms. Therefore their contributions in the Mo–O_t π-bonding are smaller if compared with orbitals a_g and a_u. The more it is clear if one compare the contributions of a_g and b_u orbitals in the total overlap populations for Mo–O_t and Mo–H_2O bonds. In the later case these contributions are comparable, because the water molecule is only a σ-bonding ligand.

Molybdenum-Oxygen (Bridge) Bonds. The b_u and b_g orbitals have the largest contribution, while the a_g and a_u orbitals exhibit a remarkably lower bonding effect. It is caused by the contribution in molecular orbitals b_u and b_g of $p_{z_{O_b}}$ orbitals which forms with the d_{xz}, d_{yz} orbitals of molybdenum (for symmetry b_u also with p_z molybdenum orbitals) the strongly bonding π-MO's in the plane perpendicular to the bridge ring. Moreover, the interaction of p-orbitals of molybdenum and of the bridge-oxygen atoms is much stronger for the b_g symmetry than for the a_u one (overlap integral values amounts 0.430 and 0.084 respectively). On the other hand the $d_\pi - p_\pi$ interaction in the bridge plane gives the stronger bonding effect for b_u symmetry than for the a_g one, because two electrons are located on the $a_g(d_{xy})$ orbital, which is antibonding with respect of that interaction.

Molybdenum-Chlorine Bonds. The strongest bonding effects give the a_g and a_u orbitals. Also in that case it is due to the stronger π-interaction between d_{xz} orbitals of molybdenum and π_v orbitals of chlorine. The p_x and p_y orbitals of molybdenum of a_u symmetry could combine with σ- and π_h orbitals of chlorine rather than $b_g(p_x, p_y)$ orbitals because the latter ones are already very much involved in the bonding with bridge oxygen atoms.

Results of theoretical calculations are in agreement with experimental data previously obtained by us [5–7]. Complexes of the $[Mo_2O_4Cl_4(H_2O)_2]^{2-}$ type exhibit only a small, practically temperature independent paramagnetism of the magnitude of $300 \cdot 10^{-6}\,\text{cm}^3/\text{mole}$. On the highest occupied energy level $a_g(d_{xy})$ two paired electrons are located. The energy distance between this orbital and the next one of higher energy amounts $6000\,\text{cm}^{-1}$. Therefore any contribution of excited triplet states e.g. $a_g(d_{xy})^1\, a_u(d_{xz})^1\, {}^3A_u$ leading to a temperature dependent paramagnetism must be neglected.

Acknowledgements. This research was supported by a grant from the Polish Academy of Sciences.

References

1. Dunitz, I. D., Orgel, L. E.: J. chem. Soc. **1953**, 2594.
2. Jeżowska-Trzebiatowska, B., Kozłowski, H., Natkaniec, L.: Bull. Acad. polon. Sci., Sér. Sci. chim. **19**, 115 (1971).
3. Jeżowska-Trzebiatowska, B.: Pure Appl. Chem. **27**, 89 (1971).
4. Schmidtke, H. H.: Theor. chim. Acta (Berl.) **20**, 92 (1971).
5. Jeżowska-Trzebiatowska, B., Rudolf, M. F.: Roczniki Chem. **41**, 453 (1967; **42**, 1221 (1968).
6. Jeżowska-Trzebiatowska, B., Rudolf, M. F.: Bull. Acad. polon. Sci., Sér. Sci. chim. **17**, 419 (1969).
7. Jeżowska-Trzebiatowska, B., Rudolf, M. F.: Roczniki Chem. **44**, 745, 1031 (1970).
8. Bersuker, I. B., Titova, Yu. G.: Theoret. Exper. Chim. **6**, 469 (1970).
9. Ballhausen, C. J., Gray, H. B.: Molecular orbital theory. New York: Benjamin 1964.
10. Głowiak, T.: Dissertation, Wrocław 1967.
11. Atovmian, L., Dyachenko, O. A., Lobkovskii, E. B.: private information.
12. Scane, I. G.: Acta crystallogr. **23**, 85 (1967).
13. Cotton, F. A., Morehouse, S. M.: Inorg. Chemistry **4**, 1377 (1966).
14. Knox, J. R., Prout, C. K.: Acta Crystallogr. B **25**, 1857 (1969).
15. Delbaere, L. T. J., Prout, C. K.: Chem. Comm. **1971**, 162.
16. Basch, H., Gray, H. B.: Theoret. chim. Acta (Berl.) **4**, 367 (1966).
17. Freeman, A. J., Watson, R. E.: Physics Rev. **123**, 521 (1961).
18. Ballhausen, C. J., Gray, H. B.: Inorg. Chemistry **1**, 111 (1962).
19. Gołębiewski, A., Kowalski, H.: Theoret. chim. Acta (Berl.) **12**, 293 (1968).
20. Cusachs, L. C.: J. chem. Physics **43**, 157 (1965).
21. Mulliken, R. S.: J. chem. Physics **23**, 1833, 1844 (1955).
22. Basch, H., Viste, A., Gray, H. B.: J. chem. Physics **44**, 10 (1966).

Prof. Dr. B. Jeżowska-Trzebiatowska
Institute of Chemistry
University of Wrocław
Wrocław, Poland

Theoret. chim. Acta (Berl.) 28, 201–207 (1973)
© by Springer-Verlag 1973

Optimized Extended Hückel Theory for Calculating the Ionization Potentials and Dissociation Energies of Hydrocarbons

J. L. Chenot

Université de Paris, Faculté des Sciences, Paris, France

Received June 2, 1972

The EH method is modified by introducing new parameters so as to obtain better agreement between theoretical calculations and experimental values concerning ionization potentials and dissociation energies.

Die EH Methode wurde durch Einführung neuer Parameter so geändert, daß bessere Übereinstimmung von theoretischen Berechnungen und experimentellen Werten für Ionisationspotentiale und Dissoziationsenergien erreicht wird.

La méthode EH est modifiée par l'introduction de nouveaux paramètres destinés à obtenir un meilleur accord entre les calculs théoriques et les valeurs expérimentales des potentiels d'ionisation et des énergies de dissociation.

Introduction

Among the theoretical methods available in quantum chemistry for describing molecular electronic structure, it is surprising to see that the oldest one is continuing to attract many authors. This success can mainly be attributed to its great simplicity. Despite the rapid development of electronic digital computers, theoretical *ab-initio* or even semi-empirical SCF methods are very long and costly for analyzing fairly large molecules.

Since the original research by Hückel [1] his method has undergone a great many changes. The main stages in this evolution are as follows: introduction of overlaps and addition of σ bonds [2] (EH), exact calculation of kinetic energy [3] (KEH), using formal charges to calculate diagonal elements in the Hamiltonian [4 5] (IEH). Unfortunately, this last method requires several iterations, and trouble with the convergence often greatly increases calculation time. So in this respect this method is not very different from semi-empirical ones such as CNDO or MINDO. On the other hand, kinetic energy can be taken into consideration more or less satisfactorily without being exactly calculated [7]. At the same time, EH calculations provide quite good correlations with experimental values, even when the absolute values are way off. This is what led us to modify the somewhat arbitrary parameters introduced in EH calculations. In this article we describe how a set of parameters is determined from experimental values relating to small molecules.

Parameters of the Optimized Extended Hückel Theory

The formulation and standard approximations of EH have already been described in detail elsewhere [6], and so we are concerned solely with the notations. Molecular orbitals are LCAOs

$$\Psi_j = \sum_{p=1}^{n} C_{jp}\Phi_p \qquad j = 1, \ldots, n .$$

The matrix equation to be solved may be written

$$(H - \varepsilon S)\,C = 0$$

in which H is the Hamiltonian matrix

S is the overlap matrix,

ε is the diagonal matrix of the molecular-orbital energy with coefficients in the C matrix.

This equation may be solved by the standard Lowdin method, but we preferred Cholesky's decomposition of S [8]. The S matrix was calculated exactly by using QCPE's OVLAP subroutine for Slater type atomic orbitals.

For standard EH calculations the diagonal elements of the H matrix are taken minus the VOIP

$$H_{ii} = -\mathrm{VOIP}(\Phi_i) . \tag{1}$$

As in Ref. [6] this approximation may be justified by comparison with SCF calculations. We assume that H_{ii} is in some way a mean value of the corresponding F_{ij}. But with what is now known we cannot ascertain whether-VOIP(Φ_i) is a good mean value. So we are led to write

$$H_{ii}^{\mathrm{A}} = \alpha(A, s \text{ or } p)$$

in which α is a parameter to be determined for each atom and each type of atomic orbital by model calculation.

For the off-diagonal terms of the H matrix, several formulas have been proposed:

$$H_{ij} = \tfrac{1}{2} K S_{ij}(H_{ii} + H_{jj}) \qquad [2] ,$$
$$H_{ij} = -K S_{ij}\sqrt{H_{ii} \times H_{jj}} \qquad [4] ,$$
$$H_{ij} = S_{ij}(1 - 0.5|S_{ij}|)(H_{ii} + H_{jj}) \qquad [5] ,$$
$$H_{ij} = S_{ij}(a + bS_{ij})(H_{ii} + H_{jj}) \qquad [9] .$$

So we tried out the following formulas:

$$H_{ij}^{\mathrm{AB}} = a(\mathrm{A}, \mathrm{B}, |)\, S_{ij}(H_{ii}^{\mathrm{A}} + H_{jj}^{\mathrm{B}}) , \tag{I}$$
$$H_{ij}^{\mathrm{AB}} = S_{ij}(1 + b(\mathrm{A}, \mathrm{B}, |)\, S_{ij})(H_{ii}^{\mathrm{A}} + H_{jj}^{\mathrm{B}}) , \tag{II}$$
$$H_{ij}^{\mathrm{AB}} = S_{ij}(a(\mathrm{A}, \mathrm{B}, |) + b(\mathrm{A}, \mathrm{B}, |)\, S_{ij})(H_{ii}^{\mathrm{A}} + H_{jj}^{\mathrm{B}}) . \tag{III}$$

Parameters a and b were calculated for each pair of atoms and for $| = \sigma$ or π bonds. The above three types of calculations are hereunder referred to as Methods I, II, and III. Formulas I, II and III must be written according to the

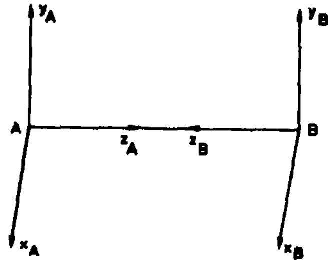

Fig. 1

coordinate system drawn in Fig. 1 in order to preserve their non-variance with respect to the molecular coordinate system.

Solving system (1) gives n eigenvalues, ε_i. For a $2p$ electron system, Koopman's theorem enables us to determine the molecular ionization potentials

$$-\varepsilon_p, -\varepsilon_{p-1}, \ldots, \varepsilon_1 .$$

Hoffman (2) has shown that

$$E_\varepsilon = -2 \sum_{i=1}^{p} \varepsilon_i$$

is a satisfactory approximation of dissociation energy D, except for one constant. For a better scaling we can create the formula

$$D = E_\varepsilon - \sum_{A} \left(\sum_{i \in A} \mathrm{VOIP}_i(A) \right) .$$

The VOIP is used for occupied atomic orbitals in the ground state. This formula can be rewritten in a more condensed form:

$$D = E_\varepsilon - \sum_{A} e(A) . \qquad (2)$$

For more precise calculating (SCF formulation)

$$D = E_\varepsilon + \frac{1}{2} \sum_{i,j} P_{ij} G_{ij} - \sum_{A<B} \frac{Q_A Q_B}{r_{AB}} - \sum_{A} e'(A) \qquad (3)$$

with $e'(A)$ being the energy required to take all valence electrons away from atom A. In order to use Eq. (2) we must assume

$$\frac{1}{2} \sum_{i,j} P_{ij} G_{ij} + \sum_{A} (e(A) - e'(A)) - \sum_{A<B} \frac{Q_A Q_B}{r_{AB}} \# 0 . \qquad (4)$$

In order to find the best $e(A)$ parameters for Eq. (4), calculations were made with reference to the experimental dissociation energies of small molecules.

Determining Parameters

The different parameters (α, a, b, e) were determined by the direct minimization of the function

$$F = \frac{1}{m} \sum_{i=1}^{m} Q_i^2 \left(\frac{Y_i^{\mathrm{ex}} - Y_i^{\mathrm{calc}}}{Y_i^{\mathrm{ex}}} \right)^2$$

Table 1

	Y[a]	Exp. val.	Method I		Method II		Method III	
			Q_i	Calc. val.	Q_i	Calc. val.	Q_i	Calc. val.
CH_4	IP	12.98	100	13.41	100	13.24	100	12.80
	D	394	100	405.4	100	407	100	394.2
C_2H_6	IP	11.51	100	11.76	100	11.59	100	11.52
	IP'	19.18	20	16.71	20	16.8	20	19.10
	D	674.6	100	659.9	100	657.7	100	680.9
C_2H_4	IP	10.48	100	10.63	100	10.77	100	10.63
	IP'	12.50	20	12.93	20	12.46	20	12.14
	IP''	14.39	20	14.11	20	14.22	20	14.30
	IP'''	19.13	20	16.12	20	16.11	20	18.12
	D	537.7	100	520.3	100	528.5	100	533.6
C_2H_2	IP	11.41	100	10.85	100	10.91	100	11.31
	IP'	16.41	20	16.17	20	15.79	20	17.00
	D	391.8	100	398.5	100	393.1	100	391.4
H_2	$\frac{1}{re}\frac{\partial D}{\partial r}(re)$	0.0	0		0	–	100	0.001
	IP	15.427	100	15.22	100	15.38	100	15.54
	D	103.3	100	103.6	100	103.3	100	103.1
C_2	$\frac{1}{re}\frac{\partial D}{\partial r}(re)$	0.0	0	-	0	—	100	0.009
	D	143.2	100	143.5	100	153.8	100	143.3
CH	$\frac{1}{re}\frac{\partial D}{\partial r}(re)$	0.0	0	—	0		100	0.022
	D	80.0	100	80.0	100	79.8	100	80.0
Mean diff.			# 2.3		# 2.0		# 0.7	

---

[a] IP = ionization potential.

Table 2[a]

		I	II	III
H	$\alpha(1s)$	−0.4463	−0.4307	−0.3853
	e	−0.4768	−0.4827	−0.4892
C	$\alpha(2s)$	−0.5103	−0.4900	−0.6324
	$\alpha(2p)$	−0.3456	−0.3402	−0.3126
	e	−1.7459	−1.7098	−1.9318
H–H	$a(\sigma)$	0.8146	1.0	1.4228
	$b(\sigma)$	0.0	−0.1670	−0.5080
C–C	$a(\sigma)$	0.8874	1.0	2.0287
	$a(\pi)$	0.8052	1.0	0.7854
	$b(\sigma)$	0.0	−0.2844	−2.4838
	$b(\pi)$	0.0	−0.4299	1.1070
C–H	$a(\sigma)$	0.8798	1.0	1.3101
	$b(\sigma)$	0.0	−0.1282	−0.4261

---

[a] α and e are given in atomic units.

in which Y_i^{ex} and Y_i^{calc} are, respectively, the experimental and calculated values of the ionization potentials and the dissociation energies for Methods I and II together with the

$$\varrho_i^2\, 2\left(\frac{\partial D}{\partial r}(r_e)\right)^2$$

amounts for the diatomic molecules in Method III, with ϱ_i being weighting factors. Optimization was done using the subroutine RSMOD [10] until a precision of 10^{-4} was reached for each variable. Table 1 gives the experimental values and the corresponding calculated values after optimization, together with the ϱ_i factors. The mean deviation (MD) is the quantity $\sqrt{F}$. Ionization potentials (in eV) were found in Ref. [11] and [12], and bond lengths and angles in international tables [14]. Table 2 lists all the parameters required, along with their numerical values after optimization (α and e are in atomic units).

Findings and Discussion

The parameters determined in this way were first used to calculate the ionization energies (Table 3) and dissociation energies (Table 4) for 31 hydro-

Table 3

	Exp.	*C*	I	II	III
CH_4	12.99	13.77	13.41	13.24	12.80
C_2H_6	11.49	12.69	11.75	11.59	11.52
C_3H_8	11.07	12.19	11.40	11.10	10.69
n-C_4H_{10}	10.50	11.73	11.05	10.67	9.97
i-C_4H_{10}	10.78	12.02	11.28	10.92	10.40
C_2H_4	10.48	12.32	10.63	10.77	10.63
C_3H_6	9.84	11.81	10.46	10.47	10.22
$CH_2{=}C(CH_3)_2$	9.35	11.66	10.37	10.53	10.05
C_3H_4	10.16	11.84	10.47	10.48	10.16
cis 1.3 C_4H_6	9.29	11.58	10.17	10.12	10.07
trans 1.3 C_4H_6	9.27	11.64	10.21	10.17	10.09
C_2H_2	11.41	12.44	10.85	10.91	11.31
$HC{\equiv}CCH_3$	10.36	11.97	10.68	10.63	10.82
$CH_3C{\equiv}CCH_3$	9.85	11.50	10.50	10.32	10.34
$HC{\equiv}CCH{=}CH_2$	9.9	11.71	10.30	10.24	10.32
$HC{\equiv}C{-}C{\equiv}CH$	10.2	11.76	10.39	10.30	10.63
C_6H_6	9.25	11.64	10.35	10.38	9.99
$C_6H_5CH_3$	9.20	11.50	10.24	10.19	9.52
o-$C_6H_4(CH_3)_2$	8.96	11.35	10.18	10.09	9.14
m-$C_6H_4(CH_3)_2$	9.01	11.44	10.20	10.13	9.29
p-$C_6H_4(CH_3)_2$	8.86	11.29	10.13	10.00	9.25
$C_{10}H_8$	8.26	11.07	9.86	9.73	8.67
cyclo C_3H_6	10.53	12.04	10.87	10.74	10.76
cyclo C_4H_8	10.53	11.53	10.88	10.38	10.02
cyclo C_5H_{10}	10.92	11.75	11.28	10.78	10.26
cyclo C_6H_{12}	9.79	11.39	10.99	10.48	9.76
CH_3	9.84	11.09	9.66	9.50	8.84
C_2H_5	8.80	10.47	9.40	9.09	8.24
n-C_3H_7	8.69	10.34	9.29	8.96	7.92
sec-C_3H_7	7.90	10.10	9.18	8.77	7.82
C_2H_3	9.35	10.68	9.52	9.21	8.28

Table 4

	Exp.	*C*	I	II	III
CH_4	394	242.2	405.3	407	394.2
C_2H_6	674.6	380.7	659.7	657.7	680.9
C_3H_8	954.3	511.9	915.3	908.8	962.6
n-C_4H_{10}	1234.7	623.1	1174.7	1160.7	1240.9
i-C_4H_{10}	1236.7	635.5	1174.3	1162.2	1242.3
C_2H_4	537.7	285.5	520.1	528.5	533.8
C_3H_6	820.4	423.7	776.5	780.9	818.1
$CH_2{=}C(CH_3)_2$	1091.4	564.0	1034.4	1034.3	1092.4
C_3H_4	675.2	344.9	636.0	647.2	651.4
cis 1 3 C_4H_6	969.8	472.9	892.7	903.0	947.4
trans 1.3 C_4H_6	967.5	478.9	897.0	908.9	959.8
C_2H_2	391.8	135.4	398.3	393.1	391.4
$HC{\equiv}CCH_3$	676.8	359.1	644.6	647.8	696.6
$CH_3C{\equiv}CCH_3$	951.0	497.4	902.0	897.9	950.0
$HC{\equiv}CCH{=}CH_2$		410.2	767.1	777.1	844.6
$HC{\equiv}C{-}C{\equiv}CH$		339.8	641.7	648	699.6
C_6H_6	1318.1	574.2	1146.1	1151.0	1188.2
$C_6H_5CH_3$	1582.7	709.0	1402.9	1402.6	1458.3
o-$C_6H_4(CH_3)_2$	1861.9	842.7	1658.9	1652.8	1721.9
m-$C_6H_4(CH_3)_2$	1862.1	843.9	1659.8	1654.2	1728.5
p-$C_6H_4(CH_3)_2$	1861.9	843.4	1659.7	1653.9	1728.0
$C_{10}H_8$		828.7	1763.6	1756.7	1780.0
cyclo C_3H_6	812.6	412.5	778.5	785.7	870.6
cyclo C_4H_8		538.1	1029.3	1019.8	1171.3
cyclo C_5H_{10}	1374.9	639.2	1286.4	1259.1	1392.6
cyclo C_6H_{12}	1680.0	792.1	1543.0	1516.2	1691.4
CH_3	293 (*b*)	164.7	291.7	295.3	284.6
C_2H_5	584 (*b*)	311.1	547.9	549.5	577.7
n-C_3H_7	≃ 859 (*b*)	444.4	805.5	803.2	861.2
sec-C_3H_7	≃ 859 (*b*)	446.8	805.0	802.3	861.2
C_2H_3	≃ 430 (*b*)	217.2	400.9	409.7	416.3

carbons and hydrocarbon radicals. This enabled us to compare our three methods with the standard EH theory using standard parameters [15] and Cusachs's approximation [5] (hereunder referred to as *C*). For the ionization potentials we found the following root mean squares:

C	1.82 eV,
I	0.76 eV,
II	0.68 eV,
III	0.53 eV.

Less agreement was found for conjugated diolefins and aromatics.

Dissociation energy calculations were not so satisfactory. However, Methods I, II and III give much better results than Method *C* which is about 50% off. With Method III we found a root mean square of 12.5 kcal, excepting cyclic hydrocarbons.

The method we have outlined in this article can be generalized and applied to series of compounds that are wider than hydrocarbons, as would seem to be proved by preliminary research. However, less agreement can be predicted for more polar molecules (e.g. containing chlorine or fluorine) where the approximation of uniform electron density is unsatisfactory.

Acknowledgement. The author gratefully thanks Pr. R. Daudel for helpfull discussions, and C. Bléjean for programming assistance.

References

1. Hückel, E.: Z. Physik **60**, 423 (1930).
2. Hoffmann, R.: J. chem. Physics **39**, 1397 (1963).
3. Newton, M. D., *et al.*: J.A.C.S. **88**, 2353 (1966).
4. Viste, A., Gray, H. B.: Inorg. Chemistry **3**, 1113 (1964).
5. Cusachs, L. C., Reynolds, J. W.: J. chem. Physics **43**, 5160 (1965).
6. Blyholder, G., Coulson, C. A.: Theoret. chim. Acta (Berl.) **10**, 316 (1968).
7. Cusachs, L. C.: J. chem. Physics **43**, 5157 (1965).
8. Wilkinson, J. H.: The algebrai eigenvalue problem 1964.
9. Ferreira, R.: Theoret. chim. Acta (Berl.) **3**, 147 (1965).
10. Vigne, J.: Etude et mise en oeuvre d'algorithmes de recherches d'un extemum d'une fonction de plusieurs variables, thesis (1969).
11. Al-Joboury, M. I., Turner, D. W.: J.C.S. 4434 (1964).
12. Vedeneyer, V. I., *et al.*: Bond energies, ionization potentials and electron affinities, ed. Coudon E. Arnold 1962.
13. Rossini: Selected values of properties of hydrocarbons 1947.
14. Interactomic Distances. London: The chemical society 1958.
15. Basch, H., *et al.*: Theoret. chim. Acta (Berl.) **3**, 458 (1965).

J. L. Chenot
Institut Français du Pétrole
1, Av. de Bois Préau
F-92502 Rueil-Malmaison, France

Theoret. chim. Acta (Berl.) 28, 209—212 (1973)
© by Springer-Verlag 1973

Relatio

Electronic Structure of BF_3-Benzaldehyde

Eduardo A. Castro and O. M. Sorarrain
Facultad de C. Exactas, Dpto. de Fisica, La Plata, CC N°67, Argentina

Received May 18, 1972

Two different models were assumed for BF_3-benzaldehyde: a charge transfer complex and a $\sigma - \sigma$ one. The CNDO/2 and the Mulliken's population analysis were used. From the given numerical results we clearly conclude a $\sigma - \sigma$ model. An electronic migration from benzaldehyde to BF_3 and other results of the population analysis are also discussed.

Introduction

Two structures have been given for the boron trifluoride-benzaldehyde complex: a) charge transfer complex [1] and b) complex of $\sigma - \sigma$ type [2]. The purpose of the present paper is to find the B–O of equilibrium, to study the electronic structure of the complex for the equilibrium distance and to discuss the changes in electronic charges for both components in the complex, respect to the lonely ones. We have used the CNDO/2 approximation [3] as method of calculation, with a Mulliken's population analysis [4].

Method of Calculation and Model Employed

We used a standard programme [5]. The internuclear distances were taken as shows Table 1.

In order to make the conformational analysis we took the BF_3 molecule with a planar configuration [6–10] at a distance of 20Å (distance B–O in the x axe) and then we were changing that distance up to 10Å. This planar configuration was assumed perpendicular to the plane of the benzaldehyde molecule. From 10Å we continued with the variation of the B–O distance, meanwhile we have changed the spatial configuration of the BF_3 molecule from a planar to a tetrahedral one [11–13]; simultaneously the B–F distance was modified up to the tetrahedral equilibrium one.

Table 1. Internuclear distances (see Fig. 1)

Atoms	r(Å)
C–O	1.24
B–F(s)	1.30
$s = 16, 17, 18$	
C(1)–C(2)	1.48
C(p)–C($p+1$)	1.39
$p = 1, \ldots, 6$	
C–H	1.08

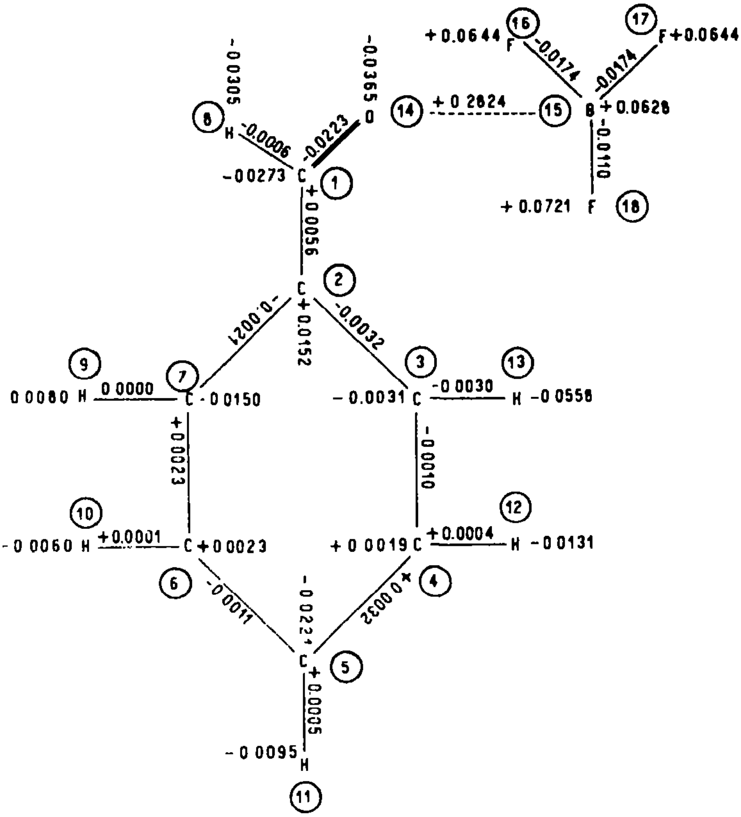

Fig 1

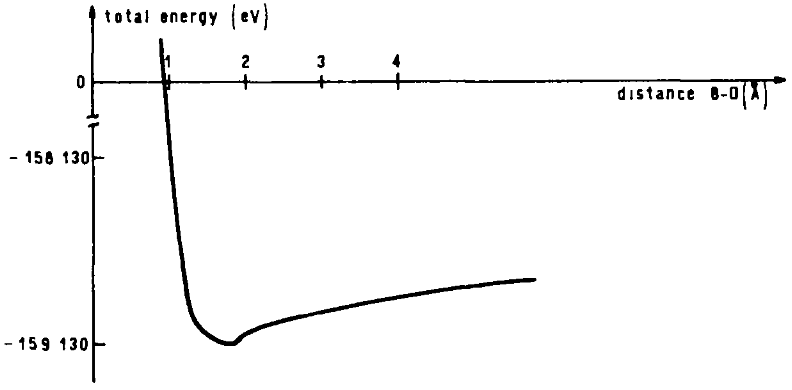

Total energy as a function of B-O distance

Fig. 2

Numerical Results and Discussion

A) Conformational Analysis

As a criterion for the equilibrium molecular geometry we have taken the absolute minimum for the total energy of the system [14]. In Fig. 2 we give the total energy as a function of the B–O distance; an absolute minimum occurs at 1.8Å, then it is not possible to have a charge transfer complex [15].

In similar compounds, but with a less voluminous substituent, the equilibrium distance between B and O was found to be about 1.5Å [12]. In the actual case the difference in 0.3Å may be due to a steric hindrance between H(13) and F(18) (see Fig. 1).

B) Population Analysis

The F(16) and F(17) are not in the same molecular plane than the remaining elements, so it is not possible to divide their bonds with B in σ and π types. For the other F, B and C atoms we have orbitals of π type. The atomic orbitals in the molecular plane (px and py) have a non-zero overlapping with the $2s$ orbitals of the neighborhood elements, then they give a contribution to σ molecular orbitals.

In Fig. 1 the numerical results are given at the equilibrium distance (differences in electron and overlap populations between the total values for the complex and for the isolated molecules BF_3 and benzaldehyde). We took a tetrahedrical structure for the free BF_3, which is ficticius, but adequate for comparative purposes.

From the numerical results we can see that there are not appreciable variations for the C atoms, except in C(1). For the remaining elements there are weak changes (increase of positive charge) for the H atoms, and remarkable ones for the O, B and F (a decrease for O and an increase for the B and F of negative charge). Then, there is an electronic transfer from benzaldehyde to BF_3 which is in agreement with the experimental results about the pseudo-substituent CHO : BF_3 [2]. For the B–O bond we notice there is an appreciable overlap population at the equilibrium distance. It is due to a lowering in the populations of another bonds such as B–F and mainly C(1)-O, as we can see in Fig. 1. The C-H populations remain practically constant, for the C-C ones only a small change is observed. Then, there are important contributions from C(1) and O to the B–O bond and we can see also contributions from the H atoms for the increased negative changes in the F atoms.

Finally we can say that the B–O bond formation in the benzaldehyde–BF_3 complex imply a whole transference of negative charges from the benzaldehyde to the BF_3 molecule, being the principal donors the C(1), O and H atoms. From this bond formation all the overlap populations in the C–C and C-H bonds remain practically constant, being the C(1)-O and the B-F populations those that change appreciably.

References

1. Taillandier, M., Liquier, J., Taillandier.: J. molecular Structure **2**, 437 (1968).
2. Rabinovitz, M., Grinvald, A.: Tetrahedron Letters **7**, 641 (1971).
3. Pople, J. A., Segal, G. A.: J. chem. Physics **44**, 3289 (1966).

4. Mulliken, R.S.: J. chem. Physics **23**, 1833, 1841 (1955).
5. Available from the Quantum Chemistry Program Exchange. Bloomington (Indiana): Indiana University.
6. Bailey, C.R., Hale, J.B., Thompson, J.W.: J. chem. Physics **5**, 274 (1937).
7. Braune, H., Pinnow, P.: Z. physik. Chem. B **35**, 239 (1937).
8. Goldfinger, P.: Naturw. **17**, 387 (1929).
9. Levy, H.A., Brockway, L.O.: J. Amer. chem. Soc. **59**, 2085 (1937).
10. Ruff, O., Ebert, F., Menzel, W.: Z. anorg. allg. Chem. **197**, 273 (1931).
11. Bauer, S.H., Finlay, G.R., Laubengayer, A.W.: J. Amer. chem. Soc. **65**, 889 (1943).
12. Bauer, S.H., Finlay, G.R., Laubengayer, A.W.: J. Amer. chem. Soc. **67**, 339 (1945).
13. Laubengayer, A.W., Finlay, G.R.: J. Amer. chem. Soc. **65**, 884 (1943).
14. Pople, J.A., Beveridge, D.L.: Approximate molecular orbital theory, p. 85–86. New York: Mc. Graw-Hill Book Company 1970.
15. Suzuki, H.: Electronic absorption spectra and geometry of organic molecules, p. 104. New York: Academic Press 1967.

Dr. Eduardo A. Castro
Facultad de Ciencias Exactas
Departamento de Fisica
La Plata, CC N°67
Argentina

Theoret. chim. Acta (Berl.) 28, 213—222 (1973)
© by Springer-Verlag 1973

Commentationes

The Influence of Polarization Functions on Molecular Orbital Hydrogenation Energies

P. C. Hariharan and J. A. Pople

Department of Chemistry, Carnegie-Mellon University, Pittsburgh, Pennsylvania 15213

Received September 25, 1972

Polarization functions are added in two steps to a split-valence extended gaussian basis set: *d*-type gaussians on the first row atoms C, N, O and F and *p*-type gaussians on hydrogen. The same *d*-exponent of 0.8 is found to be satisfactory for these four atoms and the hydrogen *p*-exponent of 1.1 is adequate in their hydrides. The energy lowering due to *d* functions is found to depend on the local symmetry around the heavy atom. For the particular basis used, the energy lowerings due to *d* functions for various environments around the heavy atom are tabulated. These bases are then applied to a set of molecules containing up to two heavy atoms to obtain their LCAO-MO-SCF energies. The mean absolute deviation between theory and experiment (where available) for heats of hydrogenation of closed shell species with two non-hydrogen atoms is 4 kcal/mole for the basis set with full polarization. Estimates of hydrogenation energy errors at the Hartree-Fock limit, based on available calculations, are given.

Polarisationsfunktionen werden in zwei Schritten einer Basis von Gauß-Orbitalen hinzugefügt: *d*-Gauß-Funktionen für die Atome C, N, O und F und *p*-Gaußfunktionen für H. In allen Fällen ist ein *d*-Exponent von 0.8 bzw. ein *p*-Exponent von 1.1 bei den Hydriden befriedigend. Dabei hängt die Energieerniedrigung, die tabelliert wiedergegeben wird, von der lokalen Symmetrie am schweren Kern ab. Mit dieser Basis wird dann die LCAO-MO-SCF-Energie für Moleküle mit 2 schweren Atomen berechnet. Die mittlere absolute Abweichung zwischen Theorie und Experiment für Hydrierungswärmen von solchen Molekülen (mit abgeschlossener Schale) ist 4 kcal/Mol bei Einschluß aller Polarisationsfunktionen. Der Schätzwert für Hydrierungswärmen in der Hartree-Fock-Grenze wird ebenfalls angegeben.

1. Introduction

Although it has long been recognized that single-determinant molecular orbital theory does not give good bond dissociation energies because of neglect of electron correlation, there remains the possibility that it is more effective in predicting the energies of reactions involving only closed shell species, where correlation corrections may largely cancel. This hypothesis was put forward by Snyder [1]. One important class of reactions of this type is hydrogenations of organic molecules to products containing only one non-hydrogen atom (methane, ammonia, water, etc.). The energies of such reactions relate the strength of bonds between heavy atoms to bonds involving hydrogen. The validity of such a hypothesis is important since an adequate theory of hydrogenation energies would permit evaluation of the total energy of larger molecules, the energies of the hydrogenation products being well known.

Ideally, molecular orbital calculations should be carried out with a large enough basis for the Hartree-Fock limit to be reached. In practice, however, this is only possible for a number of rather small systems. Consequently, attention has been devoted to reaction energies using a more limited basis set, requiring that the same basis be used for reactants and products. Here it is hoped that some of the errors due to the limitation of basis set will also cancel to some extent. An extensive study of this sort was first carried out by Snyder and Basch [2], who examined a number of reactions using a contracted gaussian basis of the "split-shell" or "double zeta" type – that is with two basis functions per atomic orbital (ten functions for carbon, nitrogen etc. and two for hydrogen). They found moderate agreement with experiment for heats of hydrogenation, the theoretical values being mostly too negative. Further work with a rather simpler "split valence shell" basis (4-31*G*) gave similar results [3, 4].

All the systematic molecular orbital studies of hydrogenation energies to date have used only *s*- and *p*-type atomic functions in the basis. For a limited number of the molecules involved, more extensive basis sets including polarization functions (*d*-type on heavy atoms and *p*-type on hydrogen) have been used in individual calculations so that Snyder and Basch [2] were able to make some observations about the difference between errors with their "double-zeta" basis and errors at the Hartree-Fock limit. However, nobody has yet attempted a systematic study of hydrogenation energies at a uniform level with a basis including polarization functions. Such a study is presented here for a set of molecules involving atoms H, C, O, N and F with two non-hydrogen atoms. The aims are (1) to find whether addition of polarization functions gives overall improved agreement with experimental hydrogenation energies, and (2) to make a comparative study of the consequent total energy lowering as a function of atom and type of chemical environment.

2. Method and Procedure

The molecules considered in this paper are those containing H, C, N, O and F which can be represented by a classical valence structure without formal charges and which contain up to two heavy atoms. Standard model geometry [4, 5] is used throughout (see footnote [a] to Table 2). Carbon monoxide is added to the list with a bondlength of 1.13 Å. The standard model is used partly because experimental geometries are incompletely known and partly so that the results can be fitted in with a systematic study of larger molecules. Various studies not reported in detail here indicate that hydrogenation energies calculated at experimental geometries are generally within 1 kcal/mole of the standard geometry values.

Molecular orbital methods are standard using the Roothaan equations [6] (with the appropriate unrestricted generalization [7] for the triplet ground state of O_2). We begin with already published results using the 4-31*G* basis set [4, 8]. This has an *s* inner shell function which is a linear combination of four *s*-type gaussians and a valence shell (*s* and *p*) represented by inner (three-gaussian) and outer (one-gaussian) parts. For hydrogen, similar (31) *s*-type functions are used. This basis has the special feature that gaussian *s* and *p* exponents are shared in the valence shell for computational efficiency.

The 4-31G basis is improved in three successive steps. To begin with, it is replaced by 6-31G which differs by improvement of the inner shell function [9]. This is found to lower total energies substantially, but should not lead to large changes in chemical properties such as reaction energies. Nevertheless, it is desirable to test this before adding polarization functions.

The next step is the addition of a set of single (uncontracted) d-gaussian functions to the 6-31G set for heavy atoms, the hydrogen functions being unmodified. The additional six (unnormalized) functions are

$$(x^2, y^2, z^2, xy, yz, zx) \exp(-\alpha_d r^2).$$

These are equivalent to the five pure d-type functions

$$(3z^2 - r^2, xz, yz, xy, x^2 - y^2) \exp(-\alpha_d r^2)$$

together with the further s-type function $r^2 \exp(-\alpha_d r^2)$. We have retained all six functions rather than just the five pure-d functions, since the appropriate integrals can be evaluated more directly.

The addition of the d-functions would be most economically carried out if the exponent α_d were chosen to be identical to that in the outer s and p functions of 6-31G. This is because the integral evaluation program actually treats all ten functions s, p and d together. However, this turns out to be somewhat ineffective since the outer s and p functions are very diffuse and the d-type polarization functions do not interact strongly with the inner valence shell functions.

It is next necessary to select some standard values for the d-gaussian exponent α_d. To do this, energy-optimized values were first obtained for the six molecules listed in Table 1 by minimizing the total energy. The results are reasonably consistent with some comparable previous studies. For methane, Rothenberg and Schaefer [10] found $\alpha_d = 0.74$ for d-functions added to a double-zeta type basis. For ammonia, Kari and Csizmadia [11] obtain 0.75. Dunning [12] has given values of 0.75 for water and 0.98 for the nitrogen molecule. Diercksen [13] obtained 1.0 for water. Hankins, Moskowitz and Stillinger [16] found an optimum exponent of 0.897 for water. These results suggest that the optimum value of α_d does not depend strongly on the underlying sp basis provided extended basis sets are used.

The results of Table 1 suggest that α_d has some dependence on chemical environment (as with pairs NH_3, N_2 and CH_4, C_2H_2) but, on the other hand,

Table 1. Total energies (hartrees) and optimum d-type exponents α_d

Molecule	Optimum α_d	Energy 6-31 G	 6-31 $G + d$ functions
CH_4	0.73	− 40.18038	− 40.19518
NH_3	0.75	− 56.16320	− 56.18381
H_2O	0.74	− 75.98508	− 76.00994
HF	0.84	− 99.98348	−100.00287
N_2	0.92	−108.86762	−108.94336
C_2H_2	0.83	− 76.79261	− 76.81737

there is little evidence of significant change along the atomic series C, N, O, F. On the basis of the optimum values given here, we select $\alpha_d = 0.8$ as the standard value for all the heavy atoms C, N, O and F. We adopt this value in all subsequent calculations.

The next step is to extend the basis further by adding *p*-polarization functions

$$(x, y, z) \times \exp(-\alpha_p r^2)$$

on the hydrogen atoms and find optimum values for α_p. This has been done by first fixing $\alpha_d = 0.8$ and minimizing the energy for α_p. No attempt has been made to find the minimum by varying both parameters. This procedure has been carried out only for CH_4 and HF. For CH_4, the optimum value of α_p is found to be 1.2, leading to a total energy of −40.20162 hartrees. Rothenberg and Schaefer [10] found $\alpha_p = 1.08$ in a comparable study. For HF, the optimum value is 1.0 giving an energy of −100.01124 hartrees. On the basis of these results, a choice of an average value of $\alpha_p = 1.1$ seems appropriate. This will be adopted as standard in subsequent calculations.

3. Results and Discussion

We have now introduced two extensions of the 6-31*G* basis. In the first (which we refer to as 6-31*G**), there are six extra uncontracted *d*-type gaussian functions on heavy atoms. The second, more elaborate, set (6-31*G***) also has three *p*-type gaussian functions on each hydrogen atom. All three of these bases have been applied to the complete set of molecules under investigation. The total energies are listed in Table 2.

In the following discussion, we shall attempt to make some comparisons with results at the Hartree-Fock limit even though these are not well established for many molecules. The final column of Table 2 gives a set of estimates of the energy at this limit for molecules which have been studied with more extensive bases than any used here. These figures are slightly below the best calculated energies in most cases and necessarily rather tentative.

Energies of hydrogenation reactions (ΔE) are easily derived from the results in Table 2. The theoretical values of ΔE for the 4-31*G*, 6-31*G* and the full polarization set 6-31*G*** are listed in Table 3. The corresponding estimates at the Hartree-Fock limit are also given for C_2H_2, HCN, CO, N_2 and F_2. Again, these values are subject to considerable uncertainty and may have an error of ±5 kcal/mole. The final column of Table 3 lists experimental values corrected for temperature effects and zero-point motion. For some of the molecules these may also be subject to an uncertainty of several kilocalories.

The theoretical results are clearly poorest for O_2 which is reasonable, since this molecule has a triplet ground state and hydrogenation involves a change in the number of unpaired electrons. If O_2 is omitted from the list, we may test the relative success of the basis sets by evaluating the mean absolute deviation between theory and experiment when the latter is available. This gives 6.8, 7.1 and 4.0 kcal/mole for 4-31*G*, 6-31*G* and 6-31*G*** respectively. We deduce that improvement of inner shell orbitals causes little change in theoretical hydrogenation energies but that addition of polarization functions leads to a marked overall improvement. If we consider the available results for single hydrogenations (addition of only one molecule of hydrogen), the mean deviation is reduced to 3.1 kcal/mole for the basis with full polarization functions.

Before analyzing these results in more detail, it is useful to present the energy lowerings due to *d*-function inclusion (6-31*G*→6-31*G**) for various valence environments of the heavy atoms. These are given for symmetrical molecules in Table 4 and show a number of interesting features. The energy lowerings are

Table 2

Total energies (hartrees) with standard polarization functions and estimated Hartree-Fock limits

Molecule[a]	6-31 *G*	6-31 *G**	6-31 *G***	Limit[c]
H_2	− 1.12676	− 1.12676	− 1.13129	− 1.1336
CH_4	− 40.18038	− 40.19506	− 40.20159	− 40.225
NH_3	− 56.16320	− 56.18374	− 56.19499	− 56.225
OH_2	− 75.98508	− 76.00987	− 76.02255	− 76.065
FH	− 99.98343	−100.00281	−100.01122	−100.071
$HC{\equiv}CH$	− 76.79261	− 76.81732	− 76.82138	− 76.860
$H_2C{=}CH_2$	− 78.00317	− 78.03037	− 78.03754	
$H_3C{-}CH_3$	− 79.19651	− 79.22774	− 79.23724	
$HC{\equiv}N$	− 92.82763	− 92.87317	− 92.87515	− 92.920
$H_2C{=}NH$	− 93.97527	− 94.02105	− 94.02824	
$H_3C{-}NH_2$	− 95.16717	− 95.20819	− 95.22200	
$C^-{\equiv}O^+$	−112.66722	−112.73718	−112.73718	−112.791
$H_2C{=}O$	−113.80789	−113.86370	−113.86711	
$H_3C{-}OH$	−114.98682	−115.03387	−115.04501	
$H_3C{-}F$	−138.99200	−139.03445	−139.03961	
$N{\equiv}N$	−108.86762	−108.94234	−108.94234	−108.997
$HN{=}NH$	−109.92792	−109.99123	−109.99768	
$H_2N{-}NH_2$	−111.11852	−111.16733	−111.18147	
$HN{=}O$	−129.71179	−129.78123	−129.78426	
$H_2N{-}OH$	−130.92160	−130.97505	−130.98818	
$H_2N{-}F$	−154.90449	−154.95130	−154.95897	
$O{=}O$[b]	−149.54546	−149.61440	−149.61440	
$HO{-}OH$	−150.70287	−150.75299	−150.76540	
$HO{-}F$	−174.68169	−174.72327	−174.72980	
$F{-}F$	−198.64605	−198.67290	−198.67290	−198.770

[a] Bond lengths and angles as specified in Ref. [5]. $r(C^-{\equiv}O^+) = 1.13$ Å. Other conformational information: Staggered bonds for single bonds to carbon, $HN{=}NH$ *trans*, $H_2N{-}NH_2$ with 90° dihedral angle between nitrogen lone pair directions, $H_2N{-}OH$ with nitrogen lone pair *cis* to OH, $HO{-}OH$ with 90° dihedral angle.

[b] Lowest triplet state energies.

[c] Estimated Hartree-Fock limits based on the following references or calculations reported therein: H_2, Kolos, W., Roothaan, C. C. J.: Rev. mod. Physics 32, 219 (1960); CH_4, Ref. [10]; NH_3, Ref. [14]; OH_2, Neumann, D., Moskowitz, J. W.: J. chem. Physics 49, 2056 (1968); FH, Cade, P. E., Huo, W. M.: J. chem. Physics 47, 614 (1967); $HC{\equiv}CH$ and $HC{\equiv}N$, McLean, A. D., Yoshimine, M.: Tables of linear molecule wave functions (IBM Corporation, 1967); $C^-{\equiv}O^+$, Huo, W. M.: J. chem. Physics 43, 624 (1965); $N{\equiv}N$, Cade, P. E., Sales, K. D., Wahl, A. C.: J. chem. Physics 44, 1973 (1966); $F{-}F$, Ref. [15].

Table 3. Complete hydrogenation energies ΔE (kcal/mole)

Reaction	Calculated 4-31 G[a]	6-31 G	6-31G^{**}	Limit[b]	Exp.[c]
$HC\equiv CH + 3H_2 \rightarrow 2CH_4$	−117.8	−117.9	−117.9	−119	−105.4
$H_2C=CH_2 + 2H_2 \rightarrow 2CH_4$	− 65.9	− 65.3	− 64.7		− 57.2
$H_3C-CH_3 + H_2 \rightarrow 2CH_4$	− 23.5	− 23.5	− 21.7		− 18.1
$HC\equiv N + 3H_2 \rightarrow CH_4 + NH_3$	− 83.4	− 85.1	− 80.0	− 81	− 76.8
$H_2C=NH + 2H_2 \rightarrow CH_4 + NH_3$	− 72.1	− 72.0	− 66.4		
$H_3C-NH_2 + H_2 \rightarrow CH_4 + NH_3$	− 30.9	− 31.2	− 27.2		− 25.7
$^-C\equiv O^+ + 3H_2 \rightarrow CH_4 + H_2O$	− 72.4	− 74.0	− 58.4	− 64	− 63.9
$H_2C=O + 2H_2 \rightarrow CH_4 + H_2O$	− 64.3	− 65.3	− 59.3		− 57.3
$H_3C-OH + H_2 \rightarrow CH_4 + H_2O$	− 32.0	− 32.6	− 30.0		− 30.3
$H_3C-F + H_2 \rightarrow CH_4 + HF$	− 27.4	− 28.3	− 26.3		− 29.5
$N\equiv N + 3H_2 \rightarrow 2NH_3$	− 47.3	− 49.3	− 33.7	− 33	− 37.7
$HN=NH + 2H_2 \rightarrow 2NH_3$	− 90.7	− 91.0	− 81.4		− 83.5
$H_2N-NH_2 + H_2 \rightarrow 2NH_3$	− 50.4	− 50.9	− 48.5		− 50.0
$HN=O + 2H_2 \rightarrow NH_3 + H_2O$	−114.2	−114.8	−107.1		−102.9
$H_2N-OH + H_2 \rightarrow NH_3 + H_2O$	− 62.0	− 62.7	− 61.5		
$H_2N-F + H_2 \rightarrow NH_3 + HF$	− 71.2	− 72.4	− 72.8		
$O=O + 2H_2 \rightarrow 2H_2O$	−107.1	−107.4	−105.5		−125.1
$HO-OH + H_2 \rightarrow 2H_2O$	− 86.3	− 88.2	− 93.1		− 86.8
$HO-F + H_2 \rightarrow H_2O + HF$	− 98.2	−100.4	−108.4		
$F-F + H_2 \rightarrow 2HF$	−118.9	−121.8	−137.0	−149	−133.8

[a] From Ref. [5] except for carbon monoxide which is based on E(4-31 G) = − 112.55234 hartrees for a bondlength of 1.13 Å.

[b] Based on estimated Hartree-Fock limiting energies listed in Tab. 2.

[c] Heats of hydrogenation at 0 K corrected for zero-point vibrations. See Ref. [4] for details.

Table 4 Energy lowerings per atom (kcal/mole) due to addition of d-functions

Atom	Molecule	Energy lowering
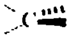	CH_4	9.2
	C_2H_6	9.8
C=	C_2H_4	8.5
C≡	C_2H_2	7.8
	NH_3	12.9
	N_2H_4	15.3
N=	N_2H_2	19.9
N≡	N_2	23.4
	H_2O	15.6
	H_2O_2	15.7
O=	O_2	22.1
F—	HF	12.2
	F_2	8.4

generally smallest for carbon. Comparing various types of carbon, it is found that the lowering is greatest for saturated tetrahedral carbon. This is a slightly surprising result in view of the high symmetry involved. It may perhaps be rationalized by noting that tetrahedral symmetry does not include an inversion operation and does, therefore, permit mixing of d-functions into those molecular orbitals which already include the valence *p*-functions. The carbon atoms in acetylene, on the other hand, have an approximate local center of inversion, in the sense that there are bonds in opposite directions. Mixing between *d* and *p* functions may well be reduced under these circumstances. $s-d$ mixing may occur, but this may be less effective because the *s*-type orbitals are more tightly bound. The trigonal carbon in ethylene is apparently intermediate between acetylene and ethane.

For nitrogen and oxygen atoms, the energy lowerings are larger. This can perhaps be attributed to greater anisotropy and non-uniformity of the charge distribution within the atom, leading to stronger polarization effects. Unlike the carbon series, the effect is greatest for the atom with unsaturated valency. Triply-bonded nitrogen and doubly-bonded oxygen have no pseudo-center of symmetry and *d*-polarization is large. The doubly-bonded oxygen value obtained from O_2 is not, of course, a suitable general model, but the strong *d*-lowering in formaldehyde (35.0 kcal/mole) suggests that the carbonyl oxygen contribution is of the order of 26 kcal/mole.

Table 5 gives a corresponding set of energy lowerings due to the addition of *p*-functions on hydrogen subsequent to *d*-function inclusion ($6\text{-}31G^* \rightarrow 6\text{-}31G^{**}$). These are smallest for H—H and C—H bonds but increase sharply in going to more polar bonds. This can be attributed partly to additional polarization effects in the σ-bond, but another contributing factor in a molecule such as HF is delocalization of π-electron onto hydrogen if $p\pi$ functions are available there.

We now return to the discussion of the hydrogenation energies shown in Table 3. The results for the hydrocarbons show little change due to the addition of polarization functions, all hydrogenation energies being too negative. Using the $6\text{-}31G^{**}$ basis, the results for acetylene give $\Delta E_{\text{th}} - \Delta E_{\text{exp}} = -12.5$ kcal/mole which is the poorest result for all the singlet-state molecules. The fact that no improvement is achieved by addition of polarization functions suggests that an error of this order may remain at the Hartree-Fock limit. The estimate based on more accurate calculations lends support to this. All of the one-step hydrogenation energies for the C_2 hydrocarbons are also too negative, $6\text{-}31G^{**}$ values for $\Delta E_{\text{th}} - \Delta E_{\text{exp}}$ being -5.1, -3.8 and -3.6 kcal/mole for acetylene, ethylene and ethane respectively.

Table 5. Energy lowering per hydrogen atom (kcal/mole) due to addition of *p*-functions

Bond	Molecule	Energy lowering
H—H	H_2	1.4
C—H	CH_4	1.0
	C_2H_6	1.0
	C_2H_4	1.1
	C_2H_2	1.3
N—H	NH_3	2.4
	N_2H_4	2.2
	N_2H_2	2.0
O—H	H_2O	4.0
	H_2O_2	3.9
F—H	FH	5.3

The behavior of the three N_2 compounds is quite different. With the *sp* bases (4-31*G* and 6-31*G*), the theoretical hydrogenation energy of N_2 is too negative. Snyder and Basch [2] also found this. However, addition of polarization functions changes this sharply and the final (6-31*G***) result gives $\Delta E_{th} - \Delta E_{exp} = +4$ kcal/mole. The estimated Hartree-Fock limit, noted by Rauk, Allen and Clementi [14] is close to this. Inspection of Table 4 shows that the large change in ΔE_{th} due to inclusion of polarization functions is primarily due to the large extra *d*-lowering for the N_2 molecule, partly offset by extra hydrogen *p*-lowering for hydrogens in NH bonds. The other N_2 compounds diimide and hydrazine show similar changes of rather smaller magnitude.

We have already noted that the theoretical hydrogenation energy of the oxygen molecule is too positive, which is consistent with a smaller correlation correction for a triplet-state. For the remaining symmetrical single bonds in hydrogen peroxide and the fluorine molecule, the theoretical hydrogenation energies are too negative. In the case of F_2, an even more negative value of -149 kcal/mole is obtained if the estimated Hartree-Fock energies are used. This gives $\Delta E_{th} - \Delta E_{exp} = -15$ kcal/mole, a discrepancy already noted by Snyder and Basch [2]. It is evident that for this molecule, a significant change in ΔE_{th} occurs as the best of our basis sets is extended to the Hartree-Fock limit. This may well be due to the limitation of using only four primitive *p*-gaussians in the valence shell of fluorine since Snyder and Basch (using a basis with five primitive *p*-gaussians but without polarization functions) obtain a better result than 6-31*G*. It should also be noted that the fluorine molecule is somewhat exceptional in that no binding relative to separate fluorine atoms is obtained at the Hartree-Fock limit [15].

For the unsymmetrical molecules with two heavy atoms, the results of Table 3 are generally intermediate between those of the corresponding symmetrical systems. Thus, we have already noted that C_2 molecules give $\Delta E_{th} - \Delta E_{exp}$ too negative and N_2 molecules slightly too positive. For CN compounds, the corresponding values are slightly too negative. In the case of hydrogen cyanide, the value of $\Delta E_{th} - \Delta E_{exp}$ is about -4 kcal/mole with 6-31*G*** and with the estimated Hartree-Fock values. Among the other molecules, we may note that the value of ΔE_{th} for carbon monoxide changes sharply on addition of polarization functions. This is similar to the result for the isoelectronic molecule N_2.

Another related class of formal reactions that may be investigated in a similar way is the separation of multiple bonds into single bonds. For example, the reaction

$$H_2C=CH_2 + 2CH_4 \rightarrow 2H_3C-CH_3$$

is one in which the two "parts" of the CC double bond of ethylene are separated into CC single bonds in separate ethane molecules, the number of CH bonds remaining constant. It is the bond separation reaction [3] for ethylene, treated as a member of the cycloalkane series $(CH_2)_n$. The energy of the reaction is also the amount by which the double bond is stronger than two single bonds. The theoretical values for the energies of these reactions using the 6-31*G*, 6-31*G** and 6-31*G*** bases are compared with experimental data in Table 6. It is evident that addition of polarization functions improves the results leading to

Table 6. Energies of multiple bond separation reactions (kcal/mole)

Reaction	Calculated 6-31G	Calculated 6-31G*	Calculated 6-31G**	Experimental
$HC\equiv CH + 4CH_4 \rightarrow 3H_3C{-}CH_3$	− 47.3	− 53.8	− 52.7	− 51.1
$H_2C{=}CH_2 + 2CH_4 \rightarrow 2H_3C{-}CH_3$	− 18.3	− 22.0	− 21.2	− 21.0
$HC\equiv N + 2CH_4 + 2NH_3 \rightarrow 3H_3C{-}NH_2$	+ 8.3	+ 3.9	+ 1.4	+ 0.3
$H_2C{=}O + CH_4 + OH_2 \rightarrow 2H_3C{-}OH$	− 0.2	+ 0.6	+ 0.8	+ 3.3
$N\equiv N + 4NH_3 \rightarrow 3H_2N{-}NH_2$	+ 103.4	+ 110.0	+ 111.6	+ 112.3
$HN{=}NH + 2NH_3 \rightarrow 2H_2N{-}NH_2$	+ 10.8	+ 15.1	+ 15.5	+ 16.5

Table 7. Hydrogenation energy errors $\Delta E_{th} - \Delta E_{exp}$ with the 6-31G** basis (kcal/mole)

	Single bonds				Double bonds			Triple bonds	
	C	N	O	F	C	N	O	C	N
C	−3.6	−1.5	+0.3	+3.2	−7.5		− 2.0	−12.5	−3.2
N		+1.5				+2.1	+ 4.1		+4.0
O			−6.3				+19.6*		
F				−3.2					

* Triplet state

Table 8. Estimated hydrogenation energy errors $\Delta E_{th} - \Delta E_{exp}$ at the Hartree-Fock limit (kcal/mole)

	Single bonds				Double bonds			Triple bonds	
	C	N	O	F	C	N	O	C	N
C	−4	−1	−2	− 3	−8	−2	−4	− 12	−3
N		+1	−2	− 5		+2	−4		+3
O			−6	−10					
F				−15					

excellent agreement with experiment for both 6-31G* and 6-31G**. (Close correspondence between 6-31G* and 6-31G** results is expected since all hydrogens remain bonded to the same type of other atom in these reactions).

The success of the comparison with experiment displayed in Table 6 suggests that the energies of these reactions would continue to be given well at the Hartree-Fock limit. If this is so, it would follow that the correlation contribution to the energy of a double (or triple) bond would be close to two (or three) times the correlation contribution to the corresponding single bond.

Next, it is useful to summarize the differences between theoretical and experimental hydrogenation energies in chart form so that trends are apparent. Table 7 does this for the 6-31G** basis. It may be noted that the values for double and triple bonds are roughly two and three times those for single bonds. This reflects the successful comparison in Table 6. Finally, we may make an attempt to estimate the residual error in all the theoretical hydrogenation energies at the Hartree-Fock limit. Table 8 displays such an estimate based on the discussion in this paper. The numbers are arrived at in the following steps.

(1) Values for double and triple bonds are taken to be respectively twice and thrice those for single bonds in accordance with the hypothesis put forward above.

(2) Available evidence suggests that the 6-31G^{**} values for CC, CN and NN bonds are close to the Hartree-Fock limit.

(3) For the FF bond in the fluorine molecule, the Hartree-Fock value of about −15 kcal/mole is 12 kcal/mole more negative than the 6-31G^{**} result. It is therefore suggested that the value for the C–F bond in methyl fluoride should be reduced by 6 kcal/mole, giving −3 kcal/mole as the estimated limiting error.

(4) Values for the remaining bonds are interpolated roughly to give the complete table.

It should be emphasized that the numbers given in Table 8 are only tentative and may have to be modified in the light of future studies with larger basis sets. However, they do sum up our present assessment of the performance of Hartree-Fock theory in predicting hydrogenation energies.

Acknowledgement. We are grateful to Dr. R. Ditchfield of Bell Telephone Laboratories for test output from POLYATOM and for some discussions. The invaluable expertise of Mr. David Rodgers, Chief Engineer, Computation Center, Carnegie-Mellon University, at both the hardware and software aspects of the UNIVAC 1108 considerably lightened the task of programming.

This research was supported in part by the National Science Foundation under Grant GP 25617

References

1. Snyder, L. C.: J. chem. Physics **46**, 3602 (1967); Thermochemistry and the electronic structure of molecules. Houston, Texas: The Robert A. Welch Foundation Research Bulletin No. 29 August 1971.
2. Snyder, L. C., Basch, H.: J. Amer. chem. Soc. **91**, 2189 (1969).
3. Hehre, W. J., Ditchfield, R., Radom, L., Pople, J. A.: J. Amer. chem. Soc. **92**, 4796 (1970).
4. Radom, L., Hehre, W. J., Pople, J. A.: J. Amer. chem. Soc. **93**, 289 (1971).
5. Pople, J. A., Gordon, M. S.: J. Amer. chem. Soc. **89**, 4253 (1967).
6. Roothaan, C. C. J.: Rev. mod. Physics **23**, 69 (1951).
7. Pople, J. A., Nesbet, R. K.: J. chem. Physics **22**, 571 (1954).
8. Ditchfield, R., Hehre, W. J., Pople, J. A.: J. chem. Physics **54**, 724 (1971).
9. Hehre, W. J., Ditchfield, R., Pople, J. A.: J. chem. Physics **56**, 2257 (1972).
10. Rothenberg, S., Schaefer III, H. F.: J. chem. Physics **54**, 2764 (1971).
11. Kari, R. E., Csizmadia, I. G.: J. chem. Physics **56**, 4337 (1972).
12. Dunning, Jr., T. H.: J. chem. Physics **55**, 3958 (1971).
13. Diercksen, G. H. F.: Theoret. chim. Acta (Berl.) **21**, 335 (1971).
14. Rauk, A., Allen, L. C., Clementi, E.: J. chem. Physics **52**, 4133 (1970).
15. Wahl, A. C.: J. chem. Physics **41**, 2600 (1964).
16. Hankins, E. D., Moscowitz, J. W., Stillinger, F. H.: J. chem. Physics **53**, 4544 (1970).

Professor J. A. Pople
Department of Chemistry
Carnegie - Mellon University
Pittsburgh, Pennsylvania 15213
USA

Theoret. chim. Acta (Berl.) 28, 223–233 (1973)
© by Springer-Verlag 1973

The Electronic Structure of Bicyclo [2.1.1] hexane

J. M. Lehn* and G. Wipff

Chemistry Department, Harvard University, Cambridge, Mass. 02138, USA and
Institut de Chimie, Université Louis Pasteur, 4, Rue Blaise Pascal, 67-Strasbourg, France**

Received July 3, 1972

Non empirical SCF-LCAO-MO calculations have been performed on bicyclo [2.1.1] hexane using a molecule optimized minimal basis set of gaussian functions. The electronic structure, the nature of the molecular orbitals and of the bonds are analyzed. The most notable results lie in the strong interaction between the two bridgehead sites and between two of the CH bonds of the methylene bridges. Interactions between fragment orbitals are considered. The relations with the molecular properties are discussed, especially with respect to molecular strain.

Nichtempirische SCF-LCAO-MO-Rechnungen wurden für das Bicyclo [2.1.1]-Hexan durchgeführt, wobei ein minimaler am Äthylen optimierter Basissatz von Gaußfunktionen verwendet wurde. Die Elektronenstruktur sowie die Art der Molekülorbitale und der Bindungen wird untersucht. Als bemerkenswerte Resultate erscheinen die starke Wechselwirkung zwischen den beiden Brückenkopf-Gruppen sowie zwischen den beiden CH-Bindungen der Methylenbrücken. Die Wechselwirkungen zwischen den Orbitalen von Molekülbruchstücken werden untersucht. Die Beziehungen zu den molekularen Eigenschaften werden diskutiert, insbesondere im Hinblick auf molekulare Ringspannung.

Une étude théorique *ab initio* SCF-LCAO-MO du bicyclo [2.1.1] hexane a été effectuée en utilisant une base minimale de fonctions gaussiennes optimisée sur une molécule. La structure électronique, la nature des orbitales moléculaires et des liaisons ont été analysées. Le résultat le plus marquant est l'existence d'une forte interaction entre les deux sites en tête de pont et aussi entre deux des liaisons C-H des ponts méthylène. Par ailleurs on peut mettre en évidence des interactions entre «orbitales de fragments». Les relations entre structure électronique et propriétés moléculaires (spécialement la tension de cycle) sont discutées.

1. Introduction

Strained polycyclic molecules may be expected to present special bonding relationships, in line with their specific molecular properties.

The electronic structure of bicyclo [1.1.0] butane [1–3] and of bicyclo [1.1.1] pentane [3–5] has been investigated recently by means of non-empirical SCF-LCAO-MO calculations. Several other saturated polycyclic systems have also been analyzed within the same theoretical framework (cubane, *syn*- and *anti*-tricyclooctanes, bicyclo [2.1.0] pentane, spiropentane, [3]). These calculations revealed many pecularities in the electronic structures of these systems.

Extending our studies of strained molecules aimed at providing a theoretical description of the concept of molecular "strain", we present here a non-empirical study of bicyclo [2.1.1] hexane, I, whose chemistry has been actively investigated over the last years [6].

---

* Present Address: Université Louis Pasteur, Strasbourg.

** Equipe de Recherche Associée au C.N.R.S. N° 265.

Two semi-empirical calculations of this system have also been performe recently [7], as well as a study of its thermal isomerization [8].

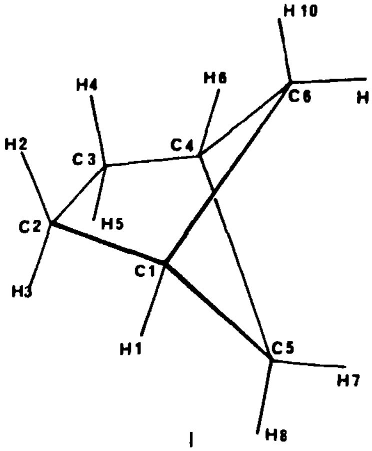

I

2. Results

2.1. Method of Computation – Basis Set

The computations have been performed using the general program IBMO [9].

The basis set employed was a molecule optimized minimal basis set c gaussian type functions (GTF's) containing 5*s* and 2*p* GTF's on carbon an 2*s* GTF's on hydrogen contracted into 2*s* and 1*p* on carbon and 1*s* on hydroger (5.2/2; 2.1/1) basis set.

This basis set has been obtained by starting with the atomic (5.2) set derive for carbon by Whitman and Hornback [10], keeping the same exponents an contraction coefficients for the four inner *s* functions on carbon and optimizin the exponent of the outer *s* function and the exponents and contraction coefficient of the *p* functions. The exponents and the contraction coefficients of the hydrogc *s* functions have been taken from the work of Huzinaga [11], but the scalin factor of these *s* functions has been optimized. The optimization has been per formed by minimizing the total energy of the ethylene molecule at the e. perimental geometry [3]. The exponents, contraction coefficients and scalin factor obtained in this way form the basis set employed in the present as we as in previous calculations [3, 5, 12].

The results are:

Exponents (contraction coefficients):

Carbon

s 381.0(0.0236); 59.18(0.1521); 13.79(0.4654); 3.833(0.4953); 0.3816(1.0),

p 1.413(1.0); 0.3058(1.9241).

Hydrogen (scaling factor = 1.35)

s 1.83216(0.27441); 0.2771(0.82123).

The total energies of methane, D_{3d} ethane and ethylene obtained with the atomic and the optimized basis sets are respectively: -39.9176 and -39.9468 a.u. for methane, -78.7136 and -78.7704 for ethane, -77.5017 and -77.5482 for ethylene. C–C bond length optimization in ethane [3] and cyclooctatetraene [12] yields slightly larger values (by three hundredth of an angström or less) than the experimental length.

2.2. *Results*

The geometry of the bicyclo [2.1.1] hexane molecule has been taken from the most recent electron diffraction study [13]. These geometrical parameters differ from those obtained in an earlier investigation [14]. However it is very unlikely that the changes involved would alter significantly the electronic structure of the molecule.

The total energy calculated for bicyclo [2.1.1] hexane is equal to -270.5968 a.u., with $V_{nn} = 329.0299$, $V_{ee} = 416.5634$, $T = 232.3466$ and $V_{ne} = -1248.5367$ a.u. The orbital energies and the overlap populations are given in Table 1. The first six molecular orbitals (MO's) are 1*s* MO's of energy -11.263 ($1A_1$ and $1B_2$ at C_5 and C_6), -11.262 ($2A_1$ and $1B_1$, at C_2 and C_3), -11.261 a.u. ($3A_1$ and $2B_1$ at C_1 and C_4).

Fig. 1 represents MO diagrams drawn approximatively to scale; it includes the lowest unoccupied MO.

The calculated ionization potential and dipole moment are respectively 8.56 eV and 0.167 D (along the z axis with the positive end at z positive).

3. Discussion

3.1. *Electronic Structure of Bicyclo* [2.1.1] *Hexane*

The population analyses given in Table 1 and the MO diagrams of Fig. 1 provide a detailed description of the electronic structure of bicyclo [2.1.1.] hexane.

The present discussion will therefore bear primilary on the special features present in this system (characteristic MO's; interaction patterns, nature of the bonds) and on their possible significance with respect to the molecular properties.

Nature of the Molecular Orbitals

The first six MO's are of C 1*s* type and will not be further discussed. It is noteworth that the seventeen remaining MO's may be grouped in two ways[1]:

a) one may distinguish C–C and C–H MO's; it is found that except for the highest occupied MO (HOMO), which is of C–H type, the C–H MO's are sandwiched between a group of low lying and a group of high lying C–C MO's;

b) one may also group together the MO's describing primarily the C–CH_2–CH_2–C fragment and those contributing mainly to the cyclobutane fragment; they may be either of C–C or of C–H type within each set. Some MO's are delocalized over the whole system; some also may be clearly recognized as

---

[1] It should be stressed that none of the MO's is exclusively of a given type. They are more or less delocalized and this classification refers to the principal character of a given MO.

Table 1. Bicyclo [2.1.1] hexane: Overlap populations

Molecular orbitals			Centers									
N°	Symmetry	Energy	C_1C_2	C_2C_3	C_1C_5	C_1H_1	C_2H_2	C_5H_7	C_5H_8	C_1C_4	C_5C_6	Total[a]
7	$4A_1$	−1.190	0.071	0.060	0.108	0.017	0.014	0.014	0.029	0.042	0.057	0.909
8	$5A_1$	−0.973	0.024	0.216	0.045	0.0	0.080	0.025	0.010	0.010	0.033	0.877
9	$3B_1$	−0.922	0.138	−0.002	0.043	0.099	0.042	0.0	0.0	−0.018	0.006	0.800
10	$2B_2$	−0.883	0.007	0.002	0.056	0.0	0.002	0.118	0.159	0.005	−0.016	0.791
11	$4B_1$	−0.718	0.011	0.002	0.042	0.072	0.123	0.0	0.0	−0.006	0.008	0.830
12	$6A_1$	−0.710	0.050	0.043	0.007	0.123	0.008	0.139	0.054	−0.003	0.0	0.832
13	$7A_1$	−0.652	0.027	0.022	0.032	0.188	0.010	0.090	0.009	0.042	0.024	0.884
14	$3B_2$	−0.615	0.010	0.084	0.0	0.0	0.119	0.100	−0.001	0.0	−0.007	0.771
15	$8A_1$	−0.582	0.031	0.034	0.055	0.0	0.025	0.0	0.164	0.010	0.095	0.849
16	$1A_2$	−0.507	0.059	−0.083	0.053	0.0	0.134	0.0	0.0	−0.012	−0.015	0.756
17	$4B_2$	−0.480	−0.019	0.030	0.030	0.0	0.054	0.176	0.085	0.004	−0.057	0.797
18	$5B_1$	−0.465	0.028	−0.008	0.070	0.215	0.0	0.0	0.0	−0.183	0.024	0.599
19	$9A_1$	−0.451	−0.016	0.394	0.006	0.016	0.040	0.050	0.051	0.003	0.018	0.801
20	$10A_1$	−0.400	0.141	0.132	−0.046	0.047	0.003	0.062	0.079	0.026	0.017	0.659
21	$2A_2$	−0.397	−0.058	−0.046	0.118	0.0	0.091	0.0	0.0	−0.021	−0.042	0.611
22	$6B_1$	−0.396	0.261	−0.119	0.023	0.004	0.039	0.0	0.0	−0.033	0.009	0.635
23	$5B_2$	−0.313	0.004	0.001	0.070	0.0	0.0	0.0	0.125	0.027	−0.338	0.228
24	$11A_1$	+0.427	−0.507	0.206	0.114	0.0	−0.036	−0.154	−0.410	0.107	0.089	−1.428
Total (MO 1 to 23)			0.768	0.759	0.715	0.781	0.784	0.774	0.763	−0.106	−0.184	

[a] Including overlap populations between non-bonded centers.

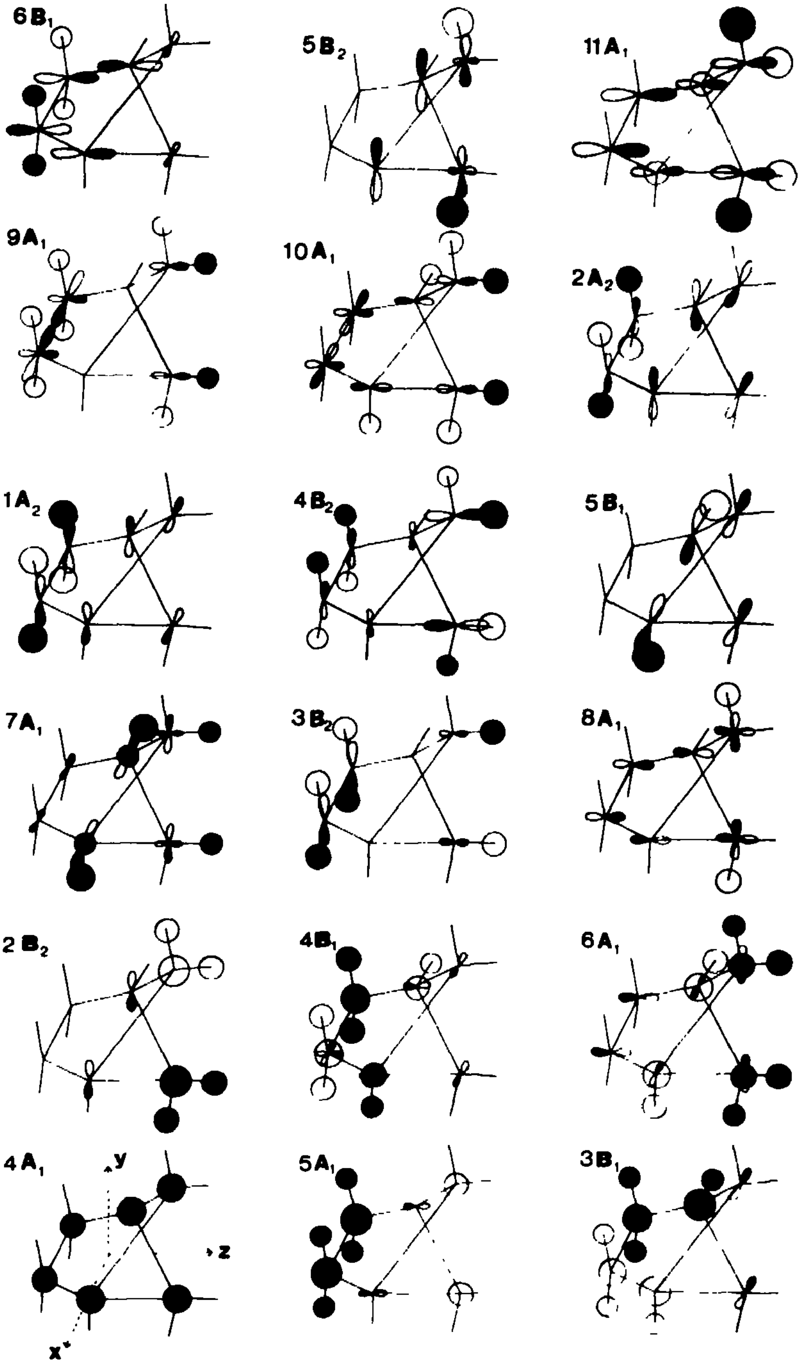

Fig. 1. Schematic representation of the molecular orbitals of bicyclo [2.1.1] hexane (see energies in Table 1)

combinations of fragment orbitals (FO's) resulting from the interaction between the orbitals of the ethylene and cyclobutane fragments.

We shall discuss in turn the C–C MO's, the C–H MO's and the interactions between fragment MO's.

1) C–C Type Molecular Orbitals

There are alltogether seven MO's of dominant C–C type. Three of them ($4A_1$, $5A_1$, $3B_1$, 7–9) form a group of low lying MO's containing mainly C 2*s* atomic orbitals (AO's). The four others ($9A_1$, $10A_1$, $2A_2$, $6B_1$, 19–22) are high lying MO's using exclusively C 2*p* AO's to complete the description of the C–C framework. Two low lying ($5A_1$, $3B_1$) and two high lying ($9A_1$, $6B_1$) MO's describe primarily the central ($5A_1$, $9A_1$) and lateral ($3B_1$, $6B_1$) C–C bonds of the ethylene fragment. $10A_1$ is delocalized over the whole molecule and contributes to all three C–C bonds of the ethylene bridge. The two remaining MO's, $4A_1$ and $2A_2$, lie predominantly on the C–C bonds of the cyclobutane moiety. In particular, $2A_2$ is reminiscent of the b_{1g} external Walsh orbital of cyclobutane [16, 17].

2) C–H Type Molecular Orbitals

It may be noted at the start that some C–H MO's may be clearly recognized as combinations of semi-localized methylene group orbitals of either σ or π type [15] (Fig. 2).

a) Among the ten C–H MO's, four are primarily localized on the CH_2 groups. $2B_2$ and $4B_1$ are antisymmetric combinations of σ type CH_2 group orbitals; $2B_2$ combines the two methylene groups of the one carbone bridges and $4B_1$ mixes those of the ethylene bridge. They both contain mainly *s* type AO's at the CH_2 sites. $3B_2$ and $1A_2$ are respectively the symmetric (*S*) and antisymmetric (*A*) combinations of the π type CH_2 orbitals of the methylene groups in the ethylene fragment.

b) MO $6A_1$ describes both the bridgehead and the *exo* C_5–H_7, C_6–H_9 C–H bonds. $4B_2$ is mainly localized on these last bonds but contributes also to the C–H bonds in the ethylene bridges. $6A_1$ and $4B_2$ contain respectively the *S* and *A* combinations of the C_5–H_7 and C_6–H_9 bonds.

c) Among the remaining four MO's, $7A_1$ and $5B_1$ describe mainly the bridgehead C–H bonds. They are respectively the *S* and *A* combinations of these two bonds. The large splitting of these two levels (ca. 5.1 eV) is due to the relatively short $C_1 \ldots C_4$ distance (2.10 Å) which leads to a marked interaction between the two bridgeheads. An even larger splitting (6.7 eV) has been found between the corresponding bridgehead levels in bicyclo [1.1.1] pentane where the distance between the bridgeheads is even shorter [5].

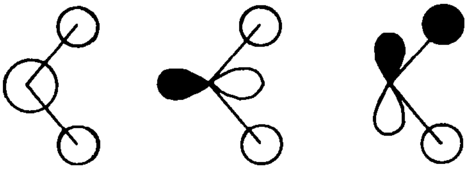

Fig. 2 Methylene group orbitals

d) The two remaining MO's $8A_1$ and $5B_2$ may be considered respectively as the S and A combinations of the two *endo* C–H bonds, C_5–H_8 and C_6–H_{10}. The splitting of these two levels amounts to 7.6 eV, i.e. it is even larger than the splitting of the bridgehead levels in bicyclo [1.1.1] pentane although the $C_5 \ldots C_6$ distance is larger (2.06 Å) than the bridgehead distance is the latter molecule (1.845 Å). $5B_2$ also contributes to the cyclobutane C–C bonds in a manner analogous to the e_u type external Walsh orbital of cyclobutane [15–17] (see also below).

Figs. 3 and 4 show some selected MO electron density diagrams.

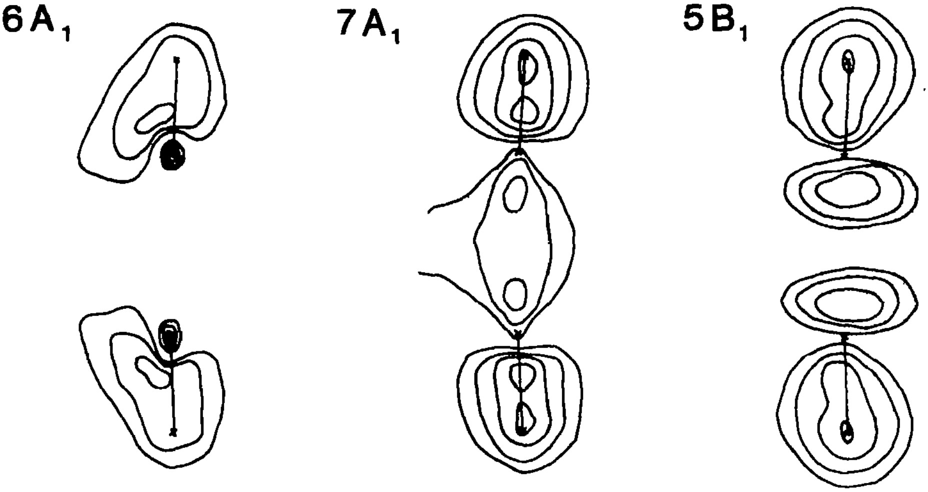

Fig. 3. Electron density diagrams of the three MO's describing the bridgehead C–H bonds of bicyclo [2.1.1] hexane

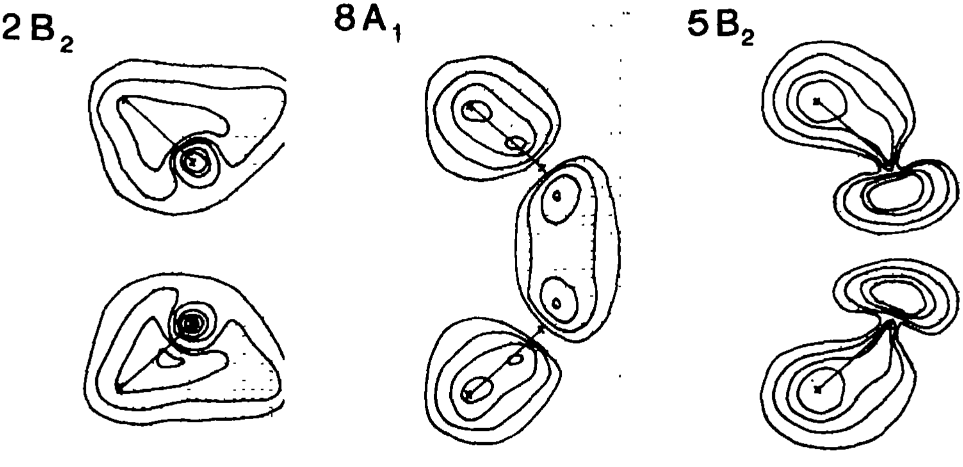

Fig. 4. Electron density diagrams of the three MO's describing the *endo* C_5–H_8 and C_6–H_{10} bonds of bicyclo [2.1.1] hexane

3) Interactions between Fragment Orbitals

Among the MO's of bicyclo [2.1.1] hexane, some result more clearly than others from the interaction between FO's localized on the ethylene and cyclobutane fragments of the molecule. We shall now analyze how some MO's are constructed. The *A* combination of the π type group orbitals belonging to two methylene groups in the ethylene bridge lead to a FO: $[\pi(CH_2)_a - \pi(CH_2)_b]$ which may interact with the b_{1g} type Walsh FO of cyclobutane. Since the CH_2 orbitals are expected to be lower in energy than the cyclobutane Walsh orbital (by analogy with the respective energies of C–H MO's and C–C MO's in cyclobutane itself), the lower lying CH_2–CH_2 FO will mix in the Walsh FO in a bonding manner and the higher lying Walsh FO will mix in the CH_2–CH_2 FO in an antibonding manner [18]. The resulting MO's correspond to $1A_2$ and $2A_2$ respectively. The interaction pattern is illustrated in Fig. 5. An additional slight admixture of the unoccupied a_{2g} Walsh orbital of cyclobutane [15–17] is also observed.

Another example is found in MO's $3B_2$ and $4B_2$ which contain respectively the *S* and *A* combinations of the π FO's built on the CH_2–CH_2 bridge on one side and on the two methylene bridges on the other side. The resulting MO's are of the type:

$$3B_2\colon\ [\pi(CH_2)_a + \pi(CH_2)_b] + [C_5H_7 - C_6H_9]\,,$$

$$4B_2\colon\ [\pi(CH_2)_a + \pi(CH_2)_b] - [C_5H_7 - C_6H_9]\,.$$

However in the one carbon bridges the C_5 H_7 and C_6 H_9 bonds contribute to these MO's much more than the C_5 H_8 and C_6 H_{10} bonds. It may be noted that in these two MO's the CH_2–CH_2 group enters by its FO built on the *S* combination of the individual $\pi(CH_2)$ group orbitals.

One also notices that $3B_1$ and $4B_1$ are respectively the *S* and *A* combinations of the two *A* FO's built from the ethylene groups CH_2 on one side and from the bridgehead CH bonds on the other side.

Nature of the Bonds

A general study of various strained molecules has shown that the characteristic features of strained bonds are, in terms of electronic structures: low C–C overlap population (OP), high *p* character, "bent bond" electron distribution; in addition the MO's describing strained bonds have generally relative high energies and form the top occupied MO's of the system.

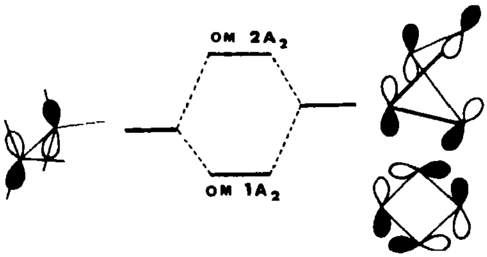

Fig. 5. Interaction diagram between the antisymmetric C–H type fragmant orbital of the ethylene bridge and the b_{1g} Walsh type fragment orbital of the cyclobutane moiety of bicyclo [2.1.1] hexane

Table 1 clearly shows that indeed, the cyclobutane C–C bonds which are expected to be more strained than the C–C bonds of the two carbon bridge also have lower OP. How quantitatively total overlap population may serve as a measure of "strain" in a bond remains to be seen. Nevertheless, there seems to be a noticeable correlation between these two terms in a variety of systems [3]. Computations performed with the same basis set yield the following C–C OP's [3]: 0.75 for ethane, 0.72 for cyclobutane, 0.71 for bicyclo [1.1.1] pentane, 0.65 for cyclopropane. In bicyclo [1.1.0] butane, the low OP of the central C–C bond has been noted by several authors [2–4]; indeed the OP's of the central and lateral bonds are respectively 0.48 and 0.68 [3], the former being even lower than in cyclopropane. It thus is seen that in bicyclo [2.1.1] hexane the ethylene bridge is unstrained and the C–C bonds in the cyclobutane fragment are comparable to those of cyclobutane itself.

Localization of the delocalized SCF MO's using the procedure of Foster and Boys [19] yield the following hybridizations of the carbon orbitals involved in the localized MO's:

$$sp^{2.50}-sp^{2.60} \text{ for } C_1\text{–}C_2,\ sp^{2.65} \text{ for } C_2\text{–}C_3,\ sp^{3.10}-sp^{2.05} \text{ for } C_1\text{–}C_5.$$

On the same basis one obtains $sp^{2.50}$, $sp^{2.80}$ and $sp^{3.90}$ for ethane, cyclobutane and cyclopropane respectively. Thus the carbon sites in the ethylene bridge are more strained than in ethane but less than in cyclobutane in agreement with the small C_1–C_2–C_3 angle of 102.1° [14] (C–C–C angle = 87.8° in cyclobutane [20]). The high p character in the C_1 orbitals used in the cyclobutane bonds is also in line with the very small C_5–C_1–C_6 angle of 78°2 [13]. But the low p character found for the C_5 center is rather surprising in view of a C_1–C_5–C_4 angle of 89.4° [13]; this result is difficult to rationalize at the present stage.

The above discussion seems to indicate that overlap population and orbital hybridization may be used for describing "*strain*" in C–C *bonds* and at C *centers* respectively. However it will be necessary to analyze in detail other strained systems [3] in order to test the generality of these results.

Finally, coming to the orbital energies of the C–C MO's, it is seen that they are indeed high lying; however, the HOMO is of C–H type.

This is due to the strong interaction between the C_5–H_8 and C_6–H_{10} bonds which leads to a large level splitting and places the A combination of these two bonds (HOMO, $5B_2$) well *above* the top C–C MO's[2].

The same feature was found for bicyclo [1.1.1] pentane, where the A combination of the bridgehead C–H bonds is the HOMO. In the present case, the interaction between the bridgeheads themselves is much weaker so that the corresponding MO's ($7A_1$ and $5B_1$) remain both below the top C–C MO's.

With respect to the non-bonded OP's between $C_1 \ldots C_4$ and $C_5 \ldots C_6$ it is seen that the antibonding character found arises from the A C–H combinations (MO's $5B_1$ and $5B_2$ respectively).

---

[2] We have found that in tricyclo [3.3.0.0] octane the HOMO (symmetry $2B_1$; energy: −0.368 a.u.) describes the cyclobutane ring and is strongly antibonding for the other C–C bonds. The A combination of the C–H bonds is appreciably lower in energy.

3.2. Electronic Structure and Properties

The most striking electronic features which might confer characteristic properties to the bicyclo [2.1.1] hexane molecule, lie in the interaction between the bridgeheads and, especially, in the stereospecific interaction between the C_5–H_8 and C_6–H_{10} bonds.

It is found that the bridgehead bromide of bicyclo [2.1.1] hexane solvolyses 10^7 times faster than 1-bromobicyclo [2.2.1] heptane, which is less strained [22]. Furthermore *endo*-5-bicyclo [2.1.1] hexyl tosylate (-OTs in the H_8 position) undergoes acetolysis at a rate 10^8 faster than its *exo* isomer, and at a rate 10^3 faster than cyclobutyl tosylate itself [23].

Although the exact nature of the transition state is not known, the striking rate accelerations observed may be connected with the stereospecific transannular interactions found here in the parent hydrocarbon; these interactions should stabilize the developping carbocation in the solvolysis process. Furthermore, one expects the cross-ring interaction to be stronger in *I* (C_5, C_6 interaction) than in cyclobutane itself, since *I* contains a much more puckered cyclobutane ring, thus enhancing the rate of solvolysis, in addition to other effects (like C–C participation) which may also operate.

Semi-empirical calculations have shown that a stereospecific cross-ring interaction exists in cyclobutane cations, which may explain the higher reactivity of an equatorial leaving group as compared to the axial isomer [24].

The high solvolytic reactivity of bridgehead derivatives of bicyclo [1.1.1] pentane is also in agreement with the strong bridgehead interaction present in the parent molecule [5]. In addition, it has been found that the overlap population between the bridgehead carbons goes from antibonding in bicyclo [1.1.1] pentane to non-bonding in its bridgehead cation [5]. It is probable that similar stabilization effects operate in the cationic species derived from leaving groups at C_1 and *endo* at C_5 in bicyclo [2.1.1] hexane.

It also appears that the rate of solvolysis of bicyclo [2.1.1] hexyl-2-tosylate is appreciably higher than one would expect on the basis of purely geometrical (small C_1 C_2–C_3 angle) considerations [25, 26]. Conjugation of the cyclobutane fragment Walsh orbital with the developping cation empty orbital at C_2 (bisected conformation of cyclobutylcarbinyl cation [17]) should indeed lead to a rate enhancement[3].

In view of the structural[4] and reactional[5] analogies between bicyclo [2.1.1] hexane and bicyclo [3.1.1] heptane, it is probable that the latter molecule presents electronic features similar to those of *I*, in particular its HOMO is probably also the antisymmetric combination of the two *endo* C–H bonds at C_5 and C_6.

The large *s* character of the bridgehead C–H bond ($sp^{2.20}$) as compared to ethane ($sp^{3.00}$) and cyclobutane ($sp^{2.85}$) C–H bonds also accounts for the decreased basicity and increased acidity of the bridgehead amine and carboxylic acid respectively [22]. Furthermore, one would expect a large $^{13}C_1$–H_1 nuclear spin-spin coupling constant; no experimental value has yet been reported, but a correlation between *s* character and ^{13}C–H coupling constants [3] leads to a value of about 160–165 Hz for this coupling.

---

[3] Conjugation of the cyclobutane system with the π systems of bicyclo [2.1.1]-2-hexanone [27] and of bicyclo [2.1.1]-2-hexene [28, 29] may explain the unusual UV spectra of these molecules (see also [17]).

[4] The C_6, C_7 distance in bicyclo [3.1.1] heptane is 2.1 Å [30].

[5] The *endo*-6-bicyclo [3.1.1] heptyl tosylate undergoes acetolysis 10^6 times faster than its *exo* isomer [31].

Finally, in analogy with the case of bicyclo [1.1.1] pentane [4, 5], the large long range coupling between the two *endo* hydrogens H_8 and H_{10} (7 Hz; [32]) may be related to the cross-ring interaction described above.

For the same reason the existence of a significant long range coupling between the bridgehead protons is also to be expected.

References

1. Newton, M. D., Schulman, J. M.: J. Amer. chem. Soc. **94**, 767 (1972).
2. Whitman, D. R., Chiang, J. F.: J. Amer. chem. Soc. **94**, 1126 (1972).
3. Wipff, G.: Thèse de 3e Cycle, Université Louis Pasteur, Strasbourg (1971).
4. Newton, M. D., Schulman, J. M.: J. Amer. chem. Soc. **94**, 773 (1972).
5. Lehn, J. M., Wipff, G.: Chem. Physics Letters **15**, 450 (1972).
6. Meinwald, J., Meinwald, Y. C.: Advances in alicyclic Chemistry **1**, 1 (1966), ed. by Hart and G. J. Karabatsos. New York: Academic Press.

7a. Yonezawa, T., Shimizu, K., Morimoto, H., Kato, H.: Nippon Kagaku Zasshi **90**, 142 (1969).
7b. Dallinga, G., Ros, P.: Recueil Trav. chim. **87**, 906 (1968).

8. Favini, G., Zuccarello, F.: Gazz. chim. ital. **98**, 1417 (1968).
9. Veillard, A.: IBMOL Version 4, Special IBM Technical Report, San Jose, California (1968).
10. Whitman, D. R., Hornback, C. J.: J. chem. Physics **51**, 398 (1969).
11. Huzinaga, S.: J. chem. Physics **42**, 1293 (1965).
12. Wipff, G., Wahlgren, U., Kochanski, E., Lehn, J. M.: Chem. Physics Letters **11**, 350 (1971).
13. Chiang, J. F.: J. Amer. chem. Soc. **93**, 5044 (1971).
14. Dallinga, G., Toneman, L. H.: Recueil Trav. chim. **86**, 171 (1967).
15. Salem, L., Wright, J. S.: J. Amer. chem. Soc. **91**, 5947 (1969).
16. Wright, J. S., Salem, L.: J. Amer. chem. Soc. **94**, 322 (1972).
17. Hoffmann, R., Davidson, R. B.: J. Amer. chem. Soc. **93**, 5699 (1971).
18. Hoffmann, R.: Accounts Chem. Research **4**, 1 (1971).
19. Foster, J. M., Boys, S. F.: Rev. mod. Physics **32**, 300 (1960).
20. Skancke, P. N.: Thesis, Oslo (1960).
21. Lehn, J. M., Wipff, G.: Work in progress.
22. Wiberg, K. B., Lowry, B. R.: J. Amer. chem. Soc. **85**, 3188 (1963).
23. Wiberg, K. B., Fenoglio, R. A., Williams, V. Z., Jr., Ubersax, R. W.: J. Amer. chem. Soc. **92**, 568 (1970).
24. Wiberg, K. B.: Tetrahedron **24**, 1083 (1968).
25. Meinwald, J., Gassman, P. G.: J. Amer. chem. Soc. **85**, 57 (1963).
26. Meinwald, J., Shelton, J. C., Buchanan, G. L., Courtin, A.: J. org. Chem. **33**, 99 (1968).
27. Bond, F. T., Jones, H. L., Scerbo, L.: Tetrahedron Letters 4685 (1965).
28. Meinwald, J., Uno, F.: J. Amer. chem. Soc. **90**, 800 (1968).
29. Robin, M. B., Basch, H., Kuebler, N. A., Kaplan, B. E., Meinwald, J.: J. chem. Physics **48**, 5037 (1968).
30. Dallinga, G., Toneman, L. H.: Recueil Trav. chim. **88**, 185 (1969).
31. Wiberg, K. B., Hess, B. A., Jr.: J. Amer. chem. Soc. **89**, 3015 (1967).
32. Meinwald, J., Lewis, A.: J. Amer. chem. Soc. **83**, 2769 (1961).

Prof. Dr. J. M. Lehn
Institut de Chimie
Université de Louis Pasteur
1, rue Blaise Pascal
F-67008 Strasbourg, France

Theoret. chim. Acta (Berl.) 28, 235–239 (1973)
© by Springer-Verlag 1973

On Asymptotic Calculation of the Exchange Interaction

E. A. Andreev

Institute of Chemical Physics, Academy of Sciences, Moscow

Received May 30, 1972

The asymptotic calculation of the exchange interaction between two atoms with the same ionization potentials is carried out. It is established that the second term (of relative order $R^{-1/2}$) of the asymptotic series becomes zero. The dependence of the atom-molecule exchange interaction on vibrational coordinates is also discussed.

Die Austauschwechselwirkung zwischen zwei Atomen mit gleichem Ionisationspotential wird asymptotisch berechnet. Es wird gezeigt, daß der zweite Term (von der relativen Ordnung $R^{-1/2}$) der asymptotischen Reihe verschwindet. Die Abhängigkeit der Atom-Molekül-Austauschwechselwirkung von den Schwingungskoordinaten wird ebenfalls diskutiert.

The total interaction between atoms and molecules at large distances consists of multipole and exchange terms. General expression for multipole interaction are well known (see, for example, Ref. [1]). As for exchange interaction, Gor'kov and Pitaevsky [2] and Herring and Flicker [3] considered the hydrogen molecule and showed that the Heitler-London approximation is inadequate at large interatomic distances R. They introduced the asymptotic method of calculation of the splitting between the lowest singlet and triplet states (due to exchange interaction) of the H_2 molecule. We shall discuss the conditions of validity of this method and also the results of later works.

Consider two one-electron atoms whose nuclei are at the points $+a$ and $-a$ of the z-axis. Let the atoms have the same ionization potentials, equal to $\alpha^2/2$[1]. The asymptotic behaviour of the electron wave functions is given by Ref. [4] as

$$\psi^0_\pm = A_\pm \, |\vec{r} \mp \vec{a}|^{\frac{1}{\alpha}} \quad \exp(-\alpha \, |\vec{r} \mp \vec{a}|) \,. \tag{1}$$

We shall calculate the first two terms of the asymptotic series for the splitting between the singlet and triplet states, described respectively by the wave functions $\psi_s(\vec{r}_1, \vec{r}_2)$ and $\psi_t(\vec{r}_1, \vec{r}_2)$. We have

$$H \psi_{s,t} = E_{s,t} \psi_{s,t} \tag{2}$$

where (when $|z_1|$ and $|z_2| \sim a$, and ϱ_1 and $\varrho_2 \sim \sqrt{a}$, z and ϱ-cylindrical coordinates, $a \to \infty$; see also Ref. [2])

$$H \simeq -\frac{1}{2}\Delta_1 - \frac{1}{2}\Delta_2 - \frac{1}{|\vec{r}_1 + \vec{a}|} - \frac{1}{|\vec{r}_2 + \vec{a}|} - \frac{1}{|\vec{r}_1 - \vec{a}|} - \frac{1}{|\vec{r}_2 - \vec{a}|} + \frac{1}{r_{12}} + \frac{1}{2a} \tag{3}$$

---

[1] Atomic units are used.

Let

$$\psi_1 = \frac{\psi_s + \psi_t}{\sqrt{2}}; \quad \psi_2 = \frac{\psi_s - \psi_t}{\sqrt{2}}; \quad \psi_2(\vec{r}_1, \vec{r}_2) = \psi_1(\vec{r}_2, \vec{r}_1) \tag{4}$$

where, for instance, ψ_1 corresponds to the state when the first electron is localized at the atom "$-a$", and the second one – at the atom "$+a$". Then [2]

$$\Delta E = E_t - E_s = -4 \oint_s \psi_2 \frac{\partial}{\partial z_1} \psi_1 ds \tag{5}$$

where S is the surface $z_1 = z_2$.

Consider firstly the hamiltonian

$$\tilde{H} = H - \frac{1}{r_{12}}. \tag{6}$$

The corresponding localized wave functions $\tilde{\psi}_1$ and $\tilde{\psi}_2$ do not strongly differ from atomic ones and can be determined by analogy with Ref. [5] and [2]

$$\tilde{\psi}_1(\vec{r}_1, \vec{r}_2) = f_1 \psi^0(\vec{r}_1 + \vec{a})\, \psi^0_+(\vec{r}_2 - \vec{a}) \equiv f_1 \psi^0_1, \tag{7}$$

$$\tilde{\psi}_2(\vec{r}_1, \vec{r}_2) = f_2 \psi^0(\vec{r}_2 + \vec{a})\, \psi^0_+(\vec{r}_1 - \vec{a}) \equiv f_2 \psi^0_2, \tag{8}$$

$$f_1 = \left| \frac{2a(2a - |z_1 + z_2|)}{(a - z_1)(a + z_2)} \right|^{1/\alpha} \exp\left(- \frac{2a + z_1 - z_2 - |z_1 + z_2|}{4\alpha a} \right), \tag{9}$$

$$f_2(\vec{r}_1, \vec{r}_2) = f_1(\vec{r}_2, \vec{r}_1). \tag{10}$$

The following terms of asymptotic series for f_1 and f_2 have the relative order $1/R$.

The main contribution to the integral (5) comes from the region $\alpha(|\vec{r} - \vec{a}| + |\vec{r} + \vec{a}| - 2a) \sim 1$ – an oblong ellipsoid of revolution in the coordinate space of each electron. In this region

$$\psi^0_-(1)\, \psi^0_+(2) \simeq A_- A_+ [(a + z_1)(a - z_2)]^{\frac{1}{\alpha} - 1} \cdot \exp\left\{ -\alpha \left[2a + z_1 - z_2 + \frac{\varrho_1^2}{2(a + z_1)} + \frac{\varrho_2^2}{2(a - z_2)} \right] \right\} \tag{11}$$

Let $\vec{\varrho}_{12} = \vec{\varrho}_1 - \vec{\varrho}_2, \vec{\varrho} = \vec{\varrho}_1 + \vec{\varrho}_2, z_{12} = z_1 - z_2$ and

$$\psi_1 = \chi_1 \tilde{\psi}_1; \quad \psi_2 = \chi_2 \tilde{\psi}_2; \quad \chi_2(\vec{r}_1, \vec{r}_2) = \chi_1(\vec{r}_2, \vec{r}_1) \tag{12}$$

We have the following equation for χ_1

$$\left(- \Delta_{12} - 2 \frac{\nabla_{12} \tilde{\psi}_1}{\tilde{\psi}_1} \nabla_{12} + \frac{1}{r_{12}} \right) \chi_1 = 0 \tag{13}$$

or

$$(H_1+H_2)\chi_1=0\,; \qquad H_2=H'+H'', \tag{14}$$

$$H_1=2\alpha\frac{\partial}{\partial z_{12}}+\frac{1}{r_{12}}, \tag{15}$$

$$H'=-\Delta_{12}, \tag{16}$$

$$H''=2\alpha\left[\frac{\varrho_{12}+\varrho\cos\varphi}{4(a+z_1)}+\frac{\varrho_{12}-\varrho\cos\varphi}{4(a-z_2)}\right]\frac{\partial}{\partial\varrho_{12}}, \tag{17}$$

where φ is the angle between $\vec{\varrho}$ and $\vec{\varrho}_{12}$.

The first approximation for χ_1 is obtained by solving the equation $H_1\chi=0$. To obtain the second approximation (whose relative order is $R^{-1/2}$ [3]) we must take into account H_2. Note that we neglected the derivates $\partial/\partial\varrho$, as the first term χ of χ_1 does not depend on ϱ [2].

If we put $\chi_1=\chi+\varkappa$, then we obtain

$$H_1\varkappa=-(H'+H'')\chi \tag{18}$$

– a linear differential equation for $\varkappa$. Therefore

$$\varkappa=\varkappa'+\varkappa'' \tag{19}$$

where

$$H_1\varkappa'=-H'\chi\,; \qquad H_1\varkappa''=-H''\chi \tag{20}$$

Take firstly into account the terms H_1 and H' of the total hamiltonian. Then we find $\varkappa'$ and (at the same time) obtain the correct behaviour of χ_1 when $r_{12}\to 0$.

$$\Delta_{12}\chi'-2\alpha\frac{\partial\chi'}{\partial z_{12}}-\frac{1}{r_{12}}\chi'=0\,; \qquad \chi'=\chi+\varkappa' \tag{21}$$

This equation can be solved by introducing parabolic coordinates (then the variables are separated), but one can use the analogy of the problem of scattering in the Coulomb field [5] with wave number $k=i\alpha$. A solution, satisfying the boundary conditions ($\chi_1\to 1$ when $z_1\to -a$ or $z_2\to a$) has the following form

$$\chi'=\frac{\Gamma(1+1/2\alpha)}{[4\alpha(a-|z|)]^{1/2\alpha}}\,\Phi\left(-\frac{1}{2\alpha},1,-\alpha(r_{12}-z_{12})\right); \qquad z=\frac{z_1+z_2}{2} \tag{22}$$

where Φ is a confluent hypergeometric function. The first term of expansion (22) (when $|z_{1,2}|\sim a$, $\varrho_{1,2}\sim\sqrt{a}$, $a\to\infty$) gives the result obtained in Ref. [2, 3] and the second term gives $\varkappa'$.

Consider now the terms H_1 and H'' together. One can obtain by analogy with Ref. [3]

$$\chi''=\exp\left(-\frac{1}{\alpha}S_1\right); \qquad \chi''=\chi+\varkappa'' \tag{23}$$

The expression for S_1 is very unwieldy (see Ref. [3]). The expansion of S_1 in series gives

$$\chi''=\left[\frac{r_{12}-z_{12}}{4(a-|z|)}\right]^{1/2\alpha}\left[1-\frac{a\varrho_{12}^2-z\varrho_{12}\varrho\cos\varphi}{4\alpha(a^2-z^2)(r_{12}-z_{12})}+\cdots\right]. \tag{24}$$

On the surface $S(z_{12}=0)$

$$\chi_1 \simeq \left[\frac{\varrho_{12}}{4(a-|z|)}\right]^{1/2\alpha}\left[1+\frac{1}{4\alpha^3\varrho_{12}}-\frac{a\varrho_{12}-z\varrho\cos\varphi}{4\alpha(a^2-z^2)}\right]. \tag{25}$$

So we have

$$\Delta E = 8\int_0^a dz \iint d\vec{\varrho}_1 d\vec{\varrho}_2 f_1 f_2 \chi_2 \psi_2^0 \left(\chi_1 \frac{\partial\psi_1^0}{\partial z_1}+\psi_1^0\frac{\partial\chi_1}{\partial z_1}\right)_{z_1=-z_2=z}. \tag{26}$$

By integrating (26) over $\vec{\varrho}_1, \vec{\varrho}_2$, (or $\vec{\varrho}, \vec{\varrho}_{12}$) one finds that contributions from the terms corresponding to $\varkappa$ and $\partial\chi/\partial z_1$ are cancelled (note these terms have the order $(\alpha^3 a)^{-1/2}$ relative to the first term). The final expression for ΔE is

$$\Delta E = A^2 A_+^2 R^{\frac{7}{2\alpha}-1} e^{-2\alpha R}\frac{4\pi^2\Gamma\left(\frac{1}{2\alpha}\right)}{2^{1/\alpha}\alpha^{2+1/\alpha}} I(\alpha)[1+0(1/R)] \tag{27}$$

where the function

$$I(\alpha)=\int_0^1 (1+x)^{\frac{1}{2\alpha}}(1-x)^{\frac{3}{2\alpha}} e^{\frac{x-1}{\alpha}}\,dx \tag{28}$$

is given in Table 1.

Table 1.

α	I
0.1	1.17_{10}
0.2	2.35_{10}
0.4	3.78_{10}
0.6	0.101
0.8	0.168
1.0	0.231
1.2	0.287

Equation (27) is valid if the following conditions are satisfied: $R\alpha^2/2 \gg 1$ (then the behaviour of wave functions is determined by the exponential term); $2R\alpha^3 \gg 1$ (then only the first term of the asymptotic expansion of wave function need be retained); as has been shown above, the analogous parameter is used for the asymptotic expansion of the exchange interaction. In particular for the case of two H atoms we have now the condition $R \gg 1$ (instead of the previous one: $\sqrt{R} \gg 1$, which has been obtained in Ref. [3]). Note that the values of the splitting between singlet (E_s) and triplet (E_t) states of H_2 obtained by variational numerical calculations [6] and by the asymptotic method ($E_t - E_s \simeq 1.65 \cdot R^{5/2}\exp(-2\cdot R)$) are not considerably different from each other even at rather small interatomic distances (25% at $R=3$).

Attempts to obtain the asymptotic expressions for the exchange interaction between two atoms with different ionization potentials have been made by Smirnov and Chibisov [7], and Uwansky and Voronin [8], and the procedure analogous to [2] has been used. But one can show that the results of [7, 8] do not give an exact asymptotic expansion. The point is that the main contribution to the exchange integral (let $\alpha_1 < \alpha_2$) comes from the region $\sim 1/(\alpha_2 - \alpha_1)$ near the second atom (in the case $\alpha_1 = \alpha_2$ it comes from the whole region $\sim R$ between the atoms). So the expansion parameter would not depend on R and not tend to zero when $R \to \infty$.

But if α_1 and α_2 are close to each other then for a variety of practical calculations one can use the formulas from [7] and [8] for $\sigma - \sigma$ exchange integrals. The criterion of their validity is that the quantity $q = (\alpha_2 - \alpha_1) \cdot R < 1$. Then it follows from the results of Ref. [7, 8] that an additional term $ch(q \cdot x)$ appears under the integral (28) (where $\alpha = (\alpha_1 + \alpha_2)/2$). But within the accuracy of the given procedure this term can be neglected thus considerably simplifying the analysis of the exchange interaction.

Consider now the interaction between an atom and a molecule, and let the corresponding α_a and α_m be close to each other. The interaction potential at large distances usually is written in the following form (see e.g. the review [9])

$$U(R,x) = C \exp[-\beta(R - \lambda x)] \tag{29}$$

where x is the vibrational coordinate, C and λ are the parameters of the problem and (in accordance with the given theory) $\beta = \alpha_a + \alpha_m(x)$. Then the perturbation (to first order in x; see Ref. [9]) $V(R,x) = x \cdot \partial U(x=0)/\partial x$ which causes vibration transitions is

$$V = x \cdot C \exp(-\beta R)\left[\beta\lambda - R\frac{\partial\alpha_m(0)}{\partial x}\right]. \tag{30}$$

The usual approach [9] does not take into account the dependence of β on vibrational coordinate x.

I thank Dr. E. E. Nikitin and Dr. M. Ja. Ovchinnikova for the discussion of this work.

References

1. Hirschfelder, J. O., Curtiss, C. F., Bird, R. B.: Molecular theory of gases and liquids. New York: Wiley 1954.
2. Gor'kov, L. P., Pitaevsky, L. P.: Dokl. Acad. Nauk USSR, **151**, 822 (1963), in Russian.
3. Herring, C., Flicker, M.: Physic. Rev. A **134**, 362 (1963).
4. Petrashen, M. I., Abarenkov, I. V.: Vestnik LGU **5**, 141 (1954), in Russian.
5. Landau, L. D., Lifshitz, E. M.: Quantum mechanics. Moscow: Fismatgiz 1963, in Russian.
6. Kolos, W., Wolniewicz, L. J.: J. chem. Physics **43**, 2429 (1965).
7. Smirnov, B. M., Chibisov, M. I.: JETF **48**, 939 (1965), in Russian.
8. Umansky, S. Ja., Voronin, A. I.: Theoret. chim. Acta (Berl.) **12**, 166 (1968).
9. Takayanagi, K.: Progr. theoret. Physics Suppl., **25**, 1 (1963)

Dr. E. A. Andreev
Institute of Chemical Physics
Academy of Sciences
Moscow, USSR

Theoret. chim. Acta (Berl.) 28, 241—265 (1973)
© by Springer-Verlag 1973

Electronic Structure of the Nickel Tetracyanonickelate $Ni(CN)_4^{2-}$ and Nickel Carbonyl $Ni(CO)_4$. An *ab-initio* LCAO–MO–SCF Calculation

J. Demuynck and A. Veillard

Institut de Chimie, Université Louis Pasteur, BP 296/R 8, F-67 Strasbourg, France

Received September 5, 1972

The electronic structure of the $Ni(CN)_4^{2-}$ ion in its ground and first excited states and of the $Ni(CO)_4$ molecule in its ground state have been investigated through an LCAO-MO-SCF calculation with a gaussian basis set (12, 8, 5/8, 4) contracted to a [5, 4, 2/3, 2 (C)/2, 1 (N or O)] set. The sequence of ionization potentials (I.P.) computed for $Ni(CO)_4$ from the Koopmans' theorem is in agreement with previous assignments for the experimental spectrum. On the contrary, Koopmans' theorem turns out to be not valid for the $Ni(CN)_4^{2-}$ ion, that is the sequence of I.P. computed as the difference of the total energy for this ion and the mononegative ion is different from the sequence of orbital energies for $Ni(CN)_4^{2-}$. The computed I.P. turn to be rather sensitive to the electrostatic potential of the crystal represented through a set of point charges. The Ni atom in $Ni(CO)_4$ bears a small positive charge of 0.24*e*, as a result of π back-bonding to the ligands. Charge transfer upon coordination and the nature of the ligand-metal bonding is compared in these two complexes through the results of a population analysis and a description in terms of localized orbitals. Separate SCF calculations have been performed for the lowest excited states of $Ni(CN)_4^{2-}$. Although $\pi \rightarrow \pi^*$ transitions would be expected as the lowest ones on the basis of orbital energy values, the lowest computed transitions correspond to $d \rightarrow d$ excitations, in agreement with previous assignments for the experimental spectrum. This is traced to the role of Coulomb and exchange terms in the computed transition energies together with the importance of electronic relaxation upon excitation.

Mit Hilfe einer LCAO-MO-SCF Rechnung unter Verwendung eines Gauß-Basissatzes (12, 8, 5/8, 4), der zu einem [5, 4, 2/3, 2 (C)/2, 1 (N oder O)] Satz kontrahiert wurde, wurden Untersuchungen über die Elektronenstruktur des $[Ni(CN)_4]^{-2}$-Ions im Grundzustand und in den ersten angeregten Zuständen und des $Ni(CO)_4$-Moleküls im Grundzustand durchgeführt. Die mit dem Koopmanschen Theorem berechnete Reihenfolge der Ionisationspotentiale des $Ni(CO)_4$ stimmt mit früheren Zuordnungen zum experimentell erhaltenen Spektrum überein.

Für $[Ni(CN)_4]^{-2}$ gilt dieses Theorem dagegen nicht, das heißt, die Reihenfolge der I.P., die als Differenz der Gesamtenergie dieses Ions und des einfach negativen Ions bestimmt werden, unterscheidet sich von der Reihenfolge der Orbitalenergien von $[Ni(CN)_4]^{2-}$.

Die berechneten I.P. sind in hohem Maße von dem elektrostatischen Potential des Kristalls, der durch einen Satz von Punktladungen dargestellt wird, abhängig. Aufgrund der π-Rückbindung zu den Liganden trägt das Nickelatom in $Ni(CO)_4$ eine geringe positive Ladung (0,24*e*). "Charge Transfer" durch Koordination und Natur der Ligand-Metall-Bindung werden in beiden Komplexen anhand der Resultate einer Populationsanalyse und mit Hilfe von lokalisierten Orbitalen verglichen. Für den niedrigsten angeregten Zustand von $[Ni(CN)_4]^{2-}$ wurden gesonderte SCF Rechnungen durchgeführt. Obwohl aufgrund der Orbitalenergien $\pi \rightarrow \pi^*$ Übergänge die niedrigste Energie haben sollten, ergeben die Rechnungen in Übereinstimmung mit dem Experiment $d \rightarrow d$ Anregungen. Diese Tatsache wird auf Coulomb- und Austauschterme in den berechneten Übergangsenergien und den Einfluß der Elektronenrelaxation bei der Anregung zurückgeführt.

La structure électronique de l'ion $Ni(CN)_4^{2}$ dans l'état fondamental et dans les premiers états excités ainsi que celle de la molécule $Ni(CO)_4$ dans l'état fondamental ont été étudiées par la méthode LCAO-MO-SCF avec une base de fonctions gaussiennes (12, 8, 5/8, 4) contractée en [5, 4, 2/3, 2 (C)/2, 1 (N ou O)]. La séquence des potentiels d'ionisation calculée pour $Ni(CO)_4$ d'après le théorème de Koopmans est en accord avec celle proposée antérieurement pour l'interprétation du spectre expérimental. Par contre le théorème de Koopmans ne parait pas valable pour l'ion $Ni(CN)_4^{2-}$. En effet, la sequence des potentiels d'ionisation calculés comme la différence des énergies de cet ion et de l'ion $Ni(CN)_4$ est différente de la séquence des énergies d'orbitale pour $Ni(CN)_4^{2-}$. Les valeurs calculées pour les potentiels d'ionisation de cet ion sont très sensibles à l'effet du potentiel électrostatique du cristal, représenté par un ensemble de charges ponctuelles. L'atome de Ni dans $Ni(CO)_4$ porte une charge positive de $0{,}24e$, conséquence du transfert en retour π vers les ligands. L'importance du transfert de charge au cours de la coordination et la nature de la liaison métal-ligand sont comparées dans ces deux complexes à partir des résultats de l'analyse de population et d'une description en termes d'orbitales localisées. Les états excités les plus bas de $Ni(CN)_4^{2}$ ont donné lieu à des calculs SCF distincts. Bien que les plus hautes orbitales occupées et les plus basses orbitales virtuelles dans l'état fondamental de $Ni(CN)_4^{2}$ soient des orbitales π et π^* des ligands, les transitions calculées les plus basses correspondent aux excitations $d \rightarrow d$. Ceci est lié au rôle joué par les termes coulombiens et d'échange dans les énergies d'excitation ainsi qu'à l'importance de la relaxation électronique au cours de l'excitation.

Introduction

Transition metal complexes may be classified into σ complexes and π complexes [1]. In the σ complexes, coordination of the ligand to the metal atom is insured through a σ lone pair of the ligand group[1]. In the π complexes, coordination is achieved through the π electrons of the ligand, like in the ferrocene molecule or in the silver-ethylene complex. Ligands which coordinate through their σ electrons may be further classified according to their acceptor ability with respect to donation from the metal atom (or backbonding). This property is associated with the presence of empty π orbitals (which are sometimes π^* antibonding orbitals) on the ligand. For instance, while the chlorine ion Cl^- has no acceptor ability as long as one does not introduce 3*d* and higher orbitals of the chlorine atom, the cyanide and carbonyl ligands CN^- and CO have empty π^* orbitals and are susceptible of π back-bonding from the metal atom.

We present here a study of the coordination in the two complexes nickel tetracyanonickelate $Ni(CN)_4^{2-}$ and nickel carbonyl $Ni(CO)_4$. Studies of the coordination of the ligand Cl^- in the tetrachlorocuprate complex $CuCl_4^{2-}$ and of π coordination in the ferrocene and nickel bis-(π-allyl) molecules will be reported later [2]. The choice of the $Ni(CN)_4^{2-}$ and $Ni(CO)_4$ complexes is based on a number of reasons. Both the cyanide ion and the carbonyl molecule are susceptible of π back-bonding, however to a different extent. The cyanide ion is considered as a good σ electron donor and a poor π electron acceptor while the carbonyl ligand should be a poorer σ donor and a better π acceptor [3]. Both complexes are representative of two important types of structures, corresponding respectively to the square-planar arrangement (D_{4h} symmetry) and to the tetrahedral arrangement (T_d symmetry). Both have been the subject of a fairly extensive experimental work in relation with the electronic structure in the ground and excited states. The photoelectron spectrum has been reported for both complexes [4–6]. The experimental absorption spectrum of the $Ni(CN)_4^{2-}$ ion has been investigated by many authors [7–13].

---

[1] We assume that the ligand is a linear or planar molecule, hence the possible classification into σ and π orbitals; however it is usually extended to molecules of any geometry like for instance the phosphines PR_3.

Many theoretical studies, either qualitative or semi-empirical, have been reported previously for these two complexes. Qualitative energy level schemes have been put forward for the $Ni(CN)_4^{2-}$ ion mostly in connection with the interpretation of the electronic spectrum. Although they may differ in small details like the relative ordering of the filled $3d$ orbitals, most of these schemes rely on the assumption that each molecular orbital of the complex may be correlated with a metal $3d$ orbital or with a ligand σ or π orbital and have agreed on the following sequence of energy levels in the complex [9, 13, 14]

$$\pi(\mathrm{CN}^-) < \sigma(\mathrm{CN}^-) < 3d_{z^2}, 3d_{xz}, 3d_{yz}, 3d_{xy} \ll 3d_{x^2-y^2} < \pi^*(\mathrm{CN}^-).$$

However, on the basis of an extended Hückel calculation, Piepho *et al.* have suggested that the $3d_{x^2-y^2}$ level lie above some $\pi^*(\mathrm{CN}^-)$ levels [13]. Sometimes ago, one of us (A.V.), on the basis of a Wolsberg-Helmholz type calculation with partial inclusion of the Coulomb repulsion, concluded that the π levels of the cyanide ligands should be above the $3d$ levels in the complex [15].

Semi-empirical calculations have been reported for the $Ni(CO)_4$ complex [16–17]. Nieuwpoort performed a non-empirical calculation for this molecule but had to rely on various approximations for the evaluation of the three- and four-center integrals [18]. Most calculations have agreed that the highest occupied orbitals are the $2e$ and $9t_2$ orbitals which correspond to the splitting of the metal $3d$ orbitals under the tetrahedral ligand field. However Nieuwpoort calculation gives the highest filled orbital to be $2e$ followed by $9t_2$, whilst this order is reversed in other calculations. Both calculations by Nieuwpoort [18] and Hillier [17] give a formal negative charge on the Ni atom close to one electron. When this work was completed [19], Hillier has reported a non-empirical calculation with a basis of contracted Gaussian type functions [20]. The order of the highest filled orbitals is $9t_2$ followed by $2e$ and the population analysis now indicates a small positive charge on the nickel atom.

Computations

The present calculations are of the SCF-LCAO-MO type using a basis set of Gaussian functions. For the Ni atom, a $12s$, $8p$, $5d$ Gaussian basis set is built by starting from a $12s$, $6p$, $4d$ set with its exponents optimized for the ground state of Ni0 [21]. The lowest two exponents for the s functions (which may be considered as describing the $4s$ atomic orbital) are set equal to 0.32 and 0.08 (the lowest two exponents optimized for the atom correspond to a $4s$ atomic orbital which is too diffuse for the molecular wavefunction). This basis set is incremented with two p functions of exponents 0.32 and 0.08 in order to describe the $4p$ atomic orbital and one additional $3d$ function of exponent 0.2 (this allows the atomic $3d$ function to expand upon formation of the complex). A $8s$, $4p$ basis set was used for the atoms of the ligands [22]. These atomic sets are contracted to a $5s$, $4p$, $2d$ set for the Ni atom, a $3s$, $2p$ set for the C atom and a $2s$, $1p$ set for the N and O atoms. Within some limitations, emphasis has been put on a better description of the valence shells. For this reason, the valence shells $3d$, $4s$ and $4p$ of Ni, $2s$ and $2p$ of C are described by two contracted functions, while only one contracted function is used for the inner shells. However, due to some limitations on the total number of contracted functions, only one contracted function has been used for each orbital of the N and O atoms. Although this may introduce a slight lack of balance between the two atoms of the ligands, this should not alter the description of the ligand-metal bond.

The interatomic distances were taken as

$$\mathrm{Ni-C} = 1.86\ \text{Å} \quad \mathrm{C-N} = 1.15\ \text{Å} \quad \text{in } \mathrm{Ni(CN)_4^{2-}}\ (D_{4h})\ [23]\,,$$

$$\mathrm{Ni-C} = 1.84\ \text{Å} \quad \mathrm{C-O} = 1.15\ \text{Å} \quad \text{in } \mathrm{Ni(CO)_4}\ (T_d)\ [24]\,.$$

The choice of the coordinate axis and the numbering of the atoms are the ones given in Fig. 1 and 2.

Open-shell calculations for the ionized and excited states of the $\mathrm{Ni(CN)_4^{2-}}$ ion have been performed in the Restricted Hartree-Fock formalism as given by Roothaan [25]. The corresponding vector coupling coefficients for the various states may be found in Ref. [26].

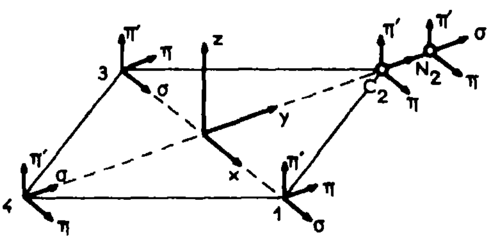

Fig. 1. Choice of the coordinate axis and numbering of the atoms for $\mathrm{Ni(CN)_4^{2-}}$

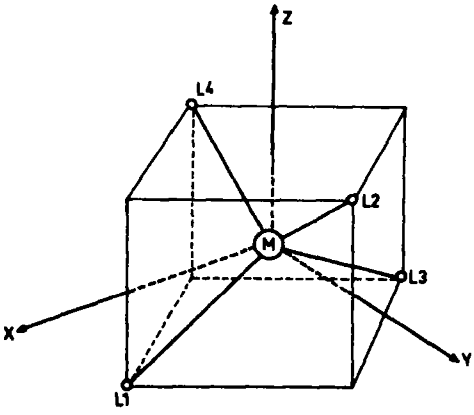

Fig. 2. Choice of the coordinate axis for $\mathrm{Ni(CO)_4}$

Table 1. Total energy (in a.u.)

	This calculation	Previous calculation
Ni^{2+} ($3d^8\ {}^3F$)	-1502.975	$-1506.028^{a,b}$
Ni^0 ($3d^{10}\ {}^1S$)	-1503.614	
CN^-	$-\ 92.138$	$-\ 92.323^{a,c}$
CO	$-\ 112.550$	$-\ 112.789^{a,d}$
$Ni(CN)_4^{2-}$	-1872.496	
$Ni(CO)_4$	-1953.949	

[a] Value close to the Hartree-Fock limit.
[b] Ref. [27].
[c] Ref. [28].
[d] Ref. [29].

Results and Discussion

The Ground State of $Ni(CN)_4^{2-}$ *and* $Ni(CO)_4$

Preliminary results for the ground state of the $Ni(CN)_4^{2-}$ ion have been previously reported [19] and will not be repeated here.

Total Energy and Binding Energy

The total energy computed is reported in Table 1 together with the values for the metal atom, the ion and the ligands. The energy values for the ligands CN^- and CO may be compared with previous estimates of -92.323 and -112.789 a.u., which are probably close to the Hartree-Fock limit.

A binding energy of 608 kcal/mole is computed for the $Ni(CN)_4^{2-}$ ion with respect to the ion Ni^{2+} and the ligands CN^-. However it should be realized that most of this computed binding energy corresponds to the electrostatic energy associated with the ion-ion interaction. For this reason it is not possible to compare the computed value with the experimental estimate of -43 kcal/mole for solvated ions [30].

For the nickelcarbonyl molecule, the computed binding energy of 86 kcal/mole may be compared to the experimental value of 140 kcal/mole in the gaz phase [31].

Orbital Energies and Ionization Potentials

The sequence of orbital energies for the $Ni(CN)_4^{2-}$ ion has already been reported [19]. One important result was that this sequence may be represented as

$$3d \sim \sigma(CN^-) < \pi(CN^-)$$

and is different from the one which has been commonly assumed

$$\pi(CN^-) < \sigma(CN^-) < 3d\,.$$

According to Koopmans' theorem [32], the ionization potential associated with the removal of one electron from a given orbital of a closed-shell system is

Table 2. Orbital energies and overlap populations for the ground state of Ni(CO)$_4$

Orbital	Orbital energy (in a.u.)[a]	Overlap population Ni–C	C–O	Nature
$9t_2$	– 0.395	–0.061	–0.073	$3d_{x^2-y^2,xz,yz}$
$2e$	– 0.471	0.007	–0.004	$3d_{xy}, 3d_{z^2}$
$8t_2$	– 0.644	0.225	–0.108	5σ
$1t_1$	– 0.653		0.294	π
$7t_2$	– 0.662	0.007	0.292	π
$1e$	– 0.665	0.009	0.196	π
$8a_1$	– 0.693	0.019	–0.025	5σ
$6t_2$	– 0.793	–0.043	0.234	4σ
$7a_1$	- 0.809	–0.117	0.062	4σ
$6a_1$	1.530	0.001	0.124	3σ
$5t_2$	1.530	0.004	0.372	3σ
$4t_2$	3.103	0.017		$3p_{x,y,z}$
$5a_1$	- 4.482	–0.017		$3s$
$4a_1$	11.419 (– 11.396)			2σ
$3t_2$	– 11.419 (11.396)			2σ
$3a_1$	- 20.657 (– 20.632)			1σ
$2t_2$	- 20.657 (- 20.632)			1σ
$1t_2$	32.615 (32.288)			$2p_{x,y,z}$
$2a_1$	36.802 (– 36.472)			$2s$
$1a_1$	304.746 (304.438)			$1s$

[a] The values between parenthesis refer to the free metal or to the ligand.

merely the opposite of the corresponding orbital energy. Before we discuss the validity of Koopmans' theorem for the Ni(CN)_4^{2} ion and the influence of the crystal lattice upon the computed ionization potentials, we will first discuss the orbital energies associated with the molecular orbitals of Ni(CO)$_4$.

The orbital energies of Ni(CO)$_4$ are given in Table 2. The sequence of the highest orbital energies

$$8a_1(\sigma_L) < 1e(\pi_L) \sim 7t_2(\pi_L) \sim 1t_1(\pi_L) \sim 8t_2(\sigma_L) < 2e(d_M) < 9t_2(d_M)$$

(with the subscripts M and L standing for metal and ligand) is similar to the one reported by Hillier [20] except for an interversion of the $1e$ and $7t_2$ levels which are nearly degenerate. The experimental ionization potentials are compared in Table 3 with the values computed according to Koopmans' theorem. Our calculation supports the assignment proposed previously for the first three ionization potentials (I.P.) corresponding to the $9t_2$, $2e$ and $8t_2$ orbitals. However a few words of caution appear necessary. Five orbitals, from $8t_2$ to $8a_1$, have their orbital energy in a range of 0.05 a.u. (1.4 eV). That the third experimental I.P. corresponds to the $8t_2$ orbital seems to be supported by the photoelectron spectrum of Ni(PF$_3$)$_4$ [33]. Through a comparison of the I.P. for this complex and the free ligand, Hillier has established that the I.P. associated with an orbital which is chiefly a ligand lone pair (then corresponding to the $8t_2$ orbital of Ni(CO)$_4$) is lower than the I.P. for molecular orbitals which are mostly fluorine $2p$ orbitals (then corresponding to the $1t_1$, $7t_2$ and $1e$ orbitals of Ni(CO)$_4$). However, any assignment beyond the $8t_2$ orbital based on Koop-

Table 3. Computed and experimental ionization potentials in $Ni(CO)_4$ (in eV)

This calculation		Previous calculation[a]		Experimental[b]	
$-\varepsilon_i$	Assignment	$-\varepsilon_i$	Assignment		Assignment
10.75	$9t_2$	11.67	$9t_2$	8.8	t_2
12.82	$2e$	13.50	$2e$	9.7	e
17.52	$8t_2$	18.47	$8t_2$	14.8	t_2
17.77 − 18.09	$1t_1, 1e, 7t_2$	18.67 − 18.96	$1t_1, 1e, 7t_2$		
18.86	$8a_1$	19.59	$8a_1$	18.2	a_1

[a] Ref. [2].
[b] Ref. [5] and [6].

mans' theorem may be considered as dubious given the approximations involved: neglect of the electronic relaxation upon ionization and of the change in correlation energy between the molecule and the ion. We will discuss in detail (cf. below) the importance of the electronic relaxation during ionization for the $Ni(CN)_4^{2-}$ ion. These approximations, together with the limitation in the basis set used, will also explain the difference between the computed and experimental values of the I.P., which is never less than 2 eV. The basis set seems to play a major role with this respect, since there is a significant improvement, of about 1 eV, between our computed values and the ones of Ref. [20].

Some information may be derived from the change in orbital energy when going from the metal and the ligands to the complex. The corresponding values for the metal and the ligands are also given in Table 2. For the inner-shells of the Ni atom, the orbital energies are lowered by 0.3 a.u. upon complexation. This stabilization is indicative of an electron transfer from the metal to the ligand (cf. the population analysis below). One would then expect an increase of the electron density on the C atom and a corresponding destabilization of the 1*s* orbital. Unexpectedly one finds a very slight stabilization of these orbitals (by 0.023 a.u. = 0.62 eV), which we have been unable to explain. Barber *et al.* have reported a computed chemical shift of 0.3 eV for the carbon and 0.4 eV for the oxygen 1*s* orbitals in qualitative agreement with an experimental destabilization of respectively 2.2 and 1.4 eV compared to free CO [34]. Slightly different experimental values, corresponding to a shift of respectively 1.7 and 0.3 eV to lower binding energy, have been reported by Clark and Adams [35].

The good agreement between the sequence of orbital energies and the experimental I.P. for $Ni(CO)_4$ indicates that Koopmans' theorem is probably valid for this molecule. This may not be true for the $Ni(CN)_4^{2-}$ ion. A somewhat similar situation has been encountered for the ferrocene molecule, with the highest occupied orbitals being π ligand orbitals rather than metal 3*d* orbitals [36]. However, it has been shown that Koopmans' theorem is not valid for this molecule and that the lowest ionization potentials computed as the difference of the energy for the molecule and the ion are associated with orbitals which have a 3*d* orbital character, in good agreement with the experimental evidence [36]. For this reason we have decided to investigate further the problem of the ionization potentials of the ion $Ni(CN)_4^{2-}$ by computing separately the energy of the mononegative species $Ni(CN)_4^-$.

Calculations have been carried out for the electronic states of $Ni(CN)_4^-$ corresponding to removal of one electron from the orbitals $8e_u(\pi_L)$, $1a_{2g}(\pi_L)$, $9a_{1g}(3d_{z^2})$, $1e_g(3d_{xz}, 3d_{yz})$ and $1b_{2g}(3d_{xy})$ of $Ni(CN)_4^{2-}$. The geometry for $Ni(CN)_4^-$ in its various electronic states has been kept the same as the one used for $Ni(CN)_4^{2-}$, hence the computed ionization energies may be compared to vertical I.P. The corresponding energies are reported in Table 4, together with the I.P. according to Koopmans' theorem and the I.P. computed as the difference of the energy for the two species. The main conclusion, similar to the one reached for ferrocene, is that it is not possible to rely on Koopmans' theorem to establish the sequence of I.P. The lowest ionization energies, when computed as the difference of the energy for the two species, correspond to removal of one electron from the metal 3*d* orbitals and not from the π ligand orbitals. In fact, Koopmans' theorem turn to be approximately valid for the π ligand orbitals (for instance the orbital energy of the $8e_u$ orbital, 0.121 a.u., is not very different from the I.P. of 0.113 a.u. computed as the difference of the energy values) but not for the metal 3*d* orbitals (compare for instance the energy orbital of $+0.182$ a.u. for the $9a_{1g}$ orbital and the computed I.P. of -0.033 a.u.). The computed I.P. corresponding to the removal of one electron from the $9a_{1g}$ and $1e_g$ orbitals is negative, namely the $Ni(CN)_4^-$ ion in its $^2A_{1g}$ and ^2E_g electronic states is computed to be more stable than the $Ni(CN)_4^{2-}$ ion in its ground state. This increased stability associated with the removal of one negative charge from the dinegative ion is merely an artefact due to the neglect of the surrounding crystal, which exerts a stabilizing effect on the negative ion through the corresponding positive charge. We have carried out additional calculations which try to account for the electrostatic potential of the crystal. The crystal has been represented in the SCF calculation by a set of point charges occupying the positions of the atomic nuclei within a sphere of a given radius. In a first set of calculations (hereafter called Lattice I), the radius of the sphere was taken as 4.8 Å and the point charges were the ones which result from the population analysis for the free ion [19]. The positions of the atomic nuclei in the crystal have been derived from the structure of $K_2Ni(CN)_4$ [43]. In a second set of calculations (called Lattice II), the radius of the sphere was increased to 6.2 Å and the point charges used were taken as the ones given by the population analysis corresponding to the Lattice I calculation.

The corresponding results are also reported in Table 4. Inclusion of the crystal potential results in a stabilization of both the orbital energies and the I.P. It also stabilizes the $Ni(CN)_4^{2-}$ ion compared to the $Ni(CN)_4^-$ ion. As a result, I.P. computed as the difference of the energy for both ions turn now to be positive and much larger. The lowest I.P. corresponds to the removal of an electron from orbitals which have mainly a metal 3*d* character and the corresponding sequence, which seems to be independent of the inclusion of crystal effects, is

$$\text{I.P.}(9a_{1g}) < \text{I.P.}(1e_g) < \text{I.P.}(1b_{2g}).$$

On the contrary, the magnitude of the computed I.P. turns to be extremely sensitive to the inclusion of the crystal effect and the convergence of the computed

Table 4. Computed ionization energies of $Ni(CN)_4^{2-}$

Species	Configuration	State	Free ion		Lattice I		Lattice II	
			Energy[a]	Computed I.P.[a]	Energy[a]	Computed I.P.[a]	Energy[a]	Computed I.P.[a]
$Ni(CN)_4^{2-}$		$^1A_{1g}$	−1872.496		−1873.263		−1874.799	
$Ni(CN)_4^-$	$8e_u^3$	^2E_u	−1872.383	+0.113[b] (0.121)[c]	−1872.616	+0.647[b] (0.656)[c]	−1874.245	0.544[b] (0.568)[c]
	$1a_{2g}^1$	$^2A_{2g}$	−1872.380	+0.116 (0.123)	−1872.612	+0.651 (0.658)	−1874.238	0.561 (0.568)
	$1b_{2u}^1$	$^2B_{2u}$			−1872.606	+0.657 (0.662)		(0.575)
	$3a_{2u}^1$	$^2A_{2u}$			−1872.586	+0.677 (0.683)		(0.596)
	$9a_{1g}^1$	$^2A_{1g}$	−1872.529	−0.033 (0.182)	−1872.787	+0.476 (0.695)	−1874.408	0.391 (0.611)
	$5b_{1g}^1$	$^2B_{1g}$			−1872.595	+0.668 (0.702)		(0.618)
	$1e_g^3$	^2E_g	−1872.509	−0.013 (0.267)	−1872.762	+0.500 (0.778)	−1874.385	0.414 (0.692)
	$1b_{2g}^1$	$^2B_{2g}$	−1872.470	+0.026 (0.335)	−1872.719	+0.544 (0.850)	−1874.343	0.456 (0.764)

[a] Values in a.u.

[b] I.P. computed as the difference of the energy value for the two species.

[c] I.P. computed according to Koopmans' theorem.

Table 5. Population analysis for the highest molecular orbitals of $Ni(CO)_4$

	Ni									C_1				O_1				Character
	s	x	y	z	x^2-y^2	xy	xz	yz	z^2	s	x	y	z	s	x	y	z	
$9t_2$		0.17	0.17	0.17	1.30		1.30	1.30		0.17	0.05	0.01	0.04		0.03	0.05	0.04	d_{Ni}
$2e$						1.83			1.83						0.01	0.04	0.03	d_{Ni}
$8t_2$		0.04	0.04	0.04	0.47		0.47	0.47		0.52	0.29		0.15		0.11		0.06	5σ
$1t_1$											0.06	0.20	0.12		0.18	0.59	0.35	π
$7t_2$					0.01		0.01	0.01			0.08	0.21	0.15		0.19	0.49	0.37	π
$1e$						0.07			0.07		0.05	0.15	0.10		0.11	0.33	0.23	π
$8a_1$	0.10									0.17	0.11		0.06	0.01	0.09		0.04	5σ
$6t_2$		−0.02	−0.02	−0.02	0.02		0.02	0.02		0.28	0.07		0.03	0.30	0.55		0.27	4σ
$7a_1$	−0.13									0.17	0.05		0.02	0.09	0.13		0.07	4σ
$6a_1$										0.05	0.03		0.02	0.35	0.03		0.02	3σ
$5t_2$		0.01	0.01	0.01	0.01		0.01	0.01		0.17	0.10		0.05	1.04	0.10		0.05	3σ

values with the number of point charges included in the calculation seems to be slow. The experimental photoelectron spectrum of $Ni(CN)_4^{2-}$ shows a peak around 9.0 eV which corresponds probably to the 3*d* orbitals, followed by a broad absorption region in the range 11–14 eV corresponding probably to the ligand π orbitals [4].

Two major conclusions may be drawn from the above results. The first one is that Koopmans' theorem is not always valid. The rigorous and sometimes only satisfactory way of estimating I.P. is to compute separately the energy associated with the two species. This appears to be especially true whenever the orbital energies associated with the ligand π orbitals are higher than the ones associated with the metal 3*d* orbitals, as it occurs for both the $Ni(CN)_4^{2-}$ ion and for the ferrocene molecule [36]. In these two cases, the sequence of I.P. computed as the difference of the energy for the two species is different from the sequence of I.P. according to Koopmans' theorem (i.e. from the sequence of orbital energies). The other conclusion is that the crystal potential has to be taken into account for the calculation of the I.P. of an ionic species.

The Wavefunction and Electron Density Associated with the Ground State of $Ni(CN)_4^{2-}$ *and* $Ni(CO)_4$

The wavefunction for the $Ni(CN)_4^{2}$ ion in terms of symmetry adapted orbitals has been previously reported and discussed briefly [19]. We will not report the wavefunction of the $Ni(CO)_4$ molecule but rather give in Table 5 the results of a population analysis [37] for the highest molecular orbitals. For the sake of comparison, the population analysis for the free ligand CO is given in Table 6. The orbitals $5t_2$ to $1t_1$ are nearly pure ligand orbitals. The orbital $8t_2$ is a bonding combination (with an overlap population of 0.225) of the lone pair orbital 5σ of the C atom with the 3*d* metal orbitals, with 26% of metal orbital. The $9t_2$ orbital is the corresponding antibonding combination (with an overlap population of −0.061), with 74% of metal orbital. The 2*e* orbital is a nearly pure metal 3*d* orbital with no metal-carbon bonding character.

The electron transfer corresponding to the formation of the metal-ligand bond may be discussed in terms of gross atomic and orbital populations. These are reported in Table 7 for the $Ni(CO)_4$ and CO molecules. We will refer to the Ni atom in its $3d^{10}\,{}^1S$ state, this is a common and convenient assumption [38]. The Ni atom in the complex bears a formal positive charge of 0.24*e*. This is the result of a loss of 0.77*e* from the *d* orbitals (0.57*e* for the *d* functions belonging to the t_2 representation and 0.20*e* for the ones belonging to the *e* representation) with a gain of 0.57*e* in the 4*p* orbitals (mostly through the $8t_2$ and $9t_2$ orbitals). The population associated with the 4*s* orbital is close to zero, this is in agreement with the result reported by Hillier [20]. The configuration obtained for the Ni atom $4s^{-0.02}\,4p^{0.57}\,3d^{9.23}$ is close to the one given by Hillier $4s^{0.04}\,4p^{0.35}\,3d^{9.22}$. The largest change in the populations of the ligand CO upon formation of the complex is the decrease in the population of the 2*s* orbital of the C atom, from 1.67*e* to 1.53*e*. This is a consequence of the sharing of the lone pair of the C atom, namely the 5σ orbital which is built

Table 6. Population analysis for the ligand CO

Orbital	Overlap population C O	C				O			
		s	*x*	*y*	*z*	*s*	*x*	*y*	*z*
5σ	−0.295	1.17	0.46		0.23		0.10		0.05
1π	0.748		0.16	0.49	0.33		0.50	1.51	1.01
4σ	0.260	0.26	0.07		0.03	0.43	0.81		0.40
3σ	0.510	0.23	0.12		0.06	1.39	0.13		0.06
Total	1.223	1.66	0.81	0.49	0.65	1.82	1.54	1.51	1.52

Table 7. Gross atomic and orbital populations for $Ni(CO)_4$ and CO

	$Ni(CO)_4$			CO	
	Ni	C_1	O_1	C	O
4*s*/2*s*	−0.02	1.53	1.79	1.67	1.81
$4p_x/2p_x$	0.19	0.88	1.53	0.81	1.54
$4p_y/2p_y$	0.19	0.57	1.51	0.49	1.51
$4p_z/2p_z$	0.19	0.72	1.52	0.65	1.52
$3d_{x^2-y^2}$	1.81				
$3d_{xy}$	1.90				
$3d_{xz}$	1.81				
$3d_{yz}$	1.81				
$3d_{z^2}$	1.90				
Formal charge	+0.24	+0.29	−0.35	+0.37	−0.37

mostly from the 2*s* orbital of the C atom. This decrease in the 2*s* population is more than balanced by an increase in the 2*p* populations of the C atom, as a result of the π backbonding from the Ni atom to the ligand. It is observed that there is little change in the populations on the O atom[2].

---

[2] The electronic structure of $Ni(CO)_4$ has been investigated recently by the SCF-Xα-SW method [46]. The results are at variance with ours with respect to the interpretation of the bonding. In agreement with our calculation, the highest occupied level is $9t_2$ followed by the $2e$ level, both corresponding principally to Ni 3*d*-like orbitals. The levels immediately below are

$$7a_1(5\sigma) < 6t_2(4\sigma) < 8a_1(4\sigma) < 7t_2(5\sigma) < 1e(1\pi) < 8t_2(4\sigma) < 1t_1(1\pi).$$

The $8t_2$, $8a_1$ and $6t_2$ levels are described as almost exclusively CO 4σ orbitals. This interpretation is certainly erroneous for either the $8t_2$ or the $6t_2$ level, one of these levels, probably the $8t_2$, has to be a CO 1π orbital. The stability of the molecule is attributed to the $7a_1$ and $7t_2$ orbitals which are described as strong covalent admixtures of Ni 4*s*-like and 3*d*-like partial waves with the 5σ carbon "lone-pair" orbitals of the CO ligands. This is at variance with our conclusion that the Ni 4*s* orbital does not participate to the bonding in $Ni(CO)_4$. Finally it is stated without much proof that there is no evidence for any significant metal-to-ligand π back-donation, which is also at variance with our conclusions. π back-bonding is evidenced in our calculation through the formal positive charge of the Ni atom and through the decrease in the formal positive charge of the C atom compared to CO (which results from an increase in the populations of the 2*p* orbitals). This π back-bonding seems to be the result of an intricate process at the molecular orbital level. The 2*e* molecular orbital shows no contribution of the carbon 2*p* orbitals but rather one from the oxygen 2*p* orbitals. Through the $7t_2$ and $1e$ molecular orbitals, there is a small electronic transfer from the oxygen 2*p* orbitals to the carbon 2*p* orbitals, compared to the electron distribution in the free CO. The whole process is equivalent to a transfer from the $3d_\pi$ orbitals of the Ni atom to the carbon 2*p* orbitals.

A comparison of the populations associated with the two complexes $Ni(CN)_4^{2-}$ (see Table 3 of Ref. [19]) and $Ni(CO)_4$, and of the charge transfer upon formation of these complexes, point to some significant similitudes and differences:

- in both complexes the metal atom bear a formal positive charge but, as expected, this one remains larger for the NiII of $Ni(CN)_4^{2-}$ than for the Ni^0 of $Ni(CO)_4$;
- in $Ni(CN)_4^{2-}$ the NiII ($3d^8$) gains d electrons while the Ni^0 ($3d^{10}$) of $Ni(CO)_4$ can only loose d electrons[3];
- the population of the $4s$ orbital is important in $Ni(CN)_4^{2-}$ but is close to zero in $Ni(CO)_4$. On the contrary the population of the $4p$ orbitals is larger in $Ni(CO)_4$, with the three orbitals equally populated while only the $4p_x$ and $4p_y$ orbitals are appreciably populated in $Ni(CN)_4^{2-}$;
- the above results are not incompatible with the "old" concepts of dsp^2 and sp^3 hybridizations respectively, although the $4s$ orbital does not seem to participate to the bonding in $Ni(CO)_4$;
- while the cyanide ion behaves only as a σ-donor, the carbonyl molecule acts simultaneously as a σ-donor and a π-acceptor;
- the σ charge-transfer is much smaller for the CO molecule than for the CN^- ion (compare for instance the variation of the $2s$ orbital population of the C atom from CN^- to $Ni(CN)_4^{2-}$ and from CO to $Ni(CO)_4$).

A more familiar picture of the bonding may be obtained in terms of localized bonds. These have been derived from the canonical SCF orbitals through a unitary transformation according to the localization criterion proposed by Boys [39]. We have reported in Tables 8 and 9 some characteristics of the localized orbitals corresponding to the lone pairs and bonds of the complexes and the free ligands. Most significant is the change in the coordinates of the center of gravity for the electronic distribution (hereafter called "charge center") of the localized orbitals upon formation of the complex. Electron density

Table 8. Localized orbitals of $Ni(CO)_4$ and CO

Localized	Coordinates of the charge center[a, b, c]			Overlap population[b]	
orbital	x	y	z	Ni–C	C–O
Ni–C[d]	2.126 (2.200)	−0.016 (0.000)	−1.503 (−1.556)	0.066	−0.164 (−0.248)
C–O	3.816 (3.845)	0.020 (0.234)	−3.317 (−3.264)	−0.022	0.454 (0.442)
C–O	4.238 (4.114)	−0.448 (−0.503)	−2.709 (−2.884)	−0.022	0.457 (0.442)
C–O	4.259 (4.347)	0.429 (0.269)	−2.681 (−2.553)	−0.022	0.457 (0.442)
O:	5.073 (5.079)	0.000 (0.000)	−3.586 (−3.591)	−0.030	0.204 (0.149)

[a] In a.u.

[b] The numbers in parenthesis refer to the free ligand CO.

[c] The coordinates of the nuclei are:
Ni 0., 0., 0. C 2.839, 0., −2.008 O 4.613, 0., −3.262.

[d] C: for the free ligand CO.

---

[3] If one would consider the Ni atom in its ground state $3d^8 4s^2$, one would conclude that it gains d electrons, but one should introduce a loss of two electrons from the $4s$ orbitals.

Table 9. Localized orbitals of $Ni(CN)_4^{2-}$ and CN^-

Localized orbital	Coordinates of the charge center[a, b, c]			Overlap population[b]	
	x	y	z	Ni–C	C–N
Ni–C[d]	2.478 (2.640)	0.000 (0.000)	0.003 (0.000)	0.489	−0.151 (−0.307)
C–N	4.729 (4.779)	−0.006 (−0.015)	−0.584 (−0.588)	−0.011	0.581 (0.570)
C–N	4.780 (4.779)	−0.505 (−0.502)	0.298 (0.307)	−0.015	0.580 (0.570)
C–N	4.782 (4.779)	0.511 (0.517)	0.286 (0.281)	−0.015	0.580 (0.570)
N:	6.370 (6.383)	0.000 (0.000)	−0.003 (0.000)	−0.117	0.331 (0.208)

[a] In a.u.

[b] The numbers in parenthesis refer to the free ligand CN^-

[c] The coordinates of the nuclei are:
Ni 0., 0., 0. C 3.515, 0., 0. N 5.688, 0., 0.

[d] C: for the free ligand CN^-.

contours for the localized orbital corresponding to the σ metal-ligand bond are given in Figs. 3 and 4. The difference in the coordination of the ligand to the metal for the two complexes is apparent both from Figs. 3 and 4 and from Tables 8 and 9. From the figures, one may see that the $3d_{x^2-y^2}$ orbital participates to the bonding in $Ni(CN)_4^{2-}$, while clearly there is less participation of a $3d$ orbital to the σ bonding in $Ni(CO)_4$. There is also a difference in the degree of coordination and bonding. The Ni–C overlap population for the localized orbital is 0.489 in $Ni(CN)_4^{2-}$ and only 0.066 in $Ni(CO)_4$. Upon coordination, there is a shift in the position of the "charge center" for the lone pair of the

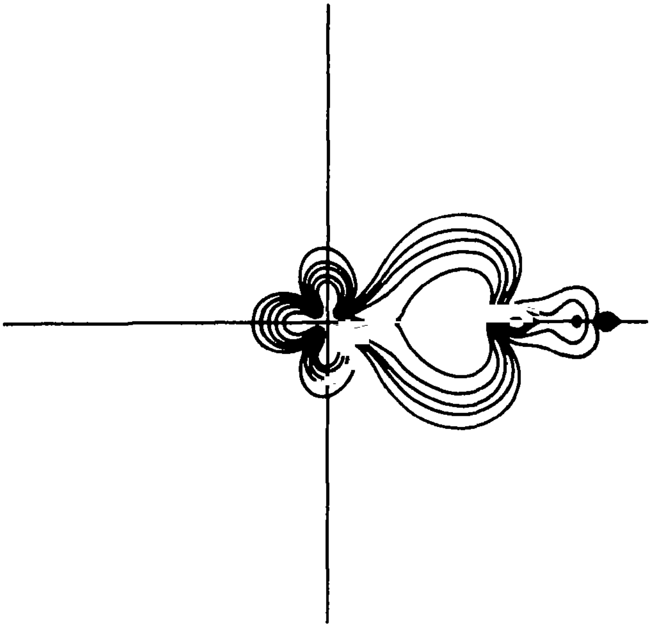

Fig. 3. Electron density contours for the Ni-C localized orbital in $Ni(CN)_4^{2-}$

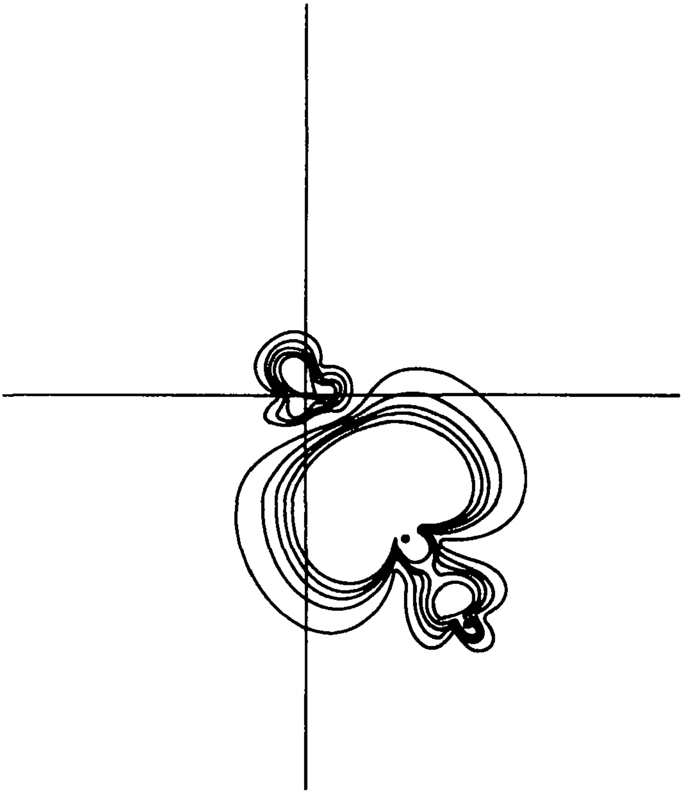

Fig. 4 Electron density contours for the Ni-C localized orbital in $Ni(CO)_4$

C atom. This shift amounts to 0.162 a.u. in $Ni(CN)_4^{2-}$ and to only 0.090 a.u. in $Ni(CO)_4$. Although the charge center corresponding to the lone pair of the C atom is appreciably shifted during the formation of the complex, at least for $Ni(CN)_4^{2-}$, it still remains in the complex relatively close to the C atom (the charge center is at 2.478 a.u. from the Ni atom and at 1.037 a.u. from the C atom in $Ni(CN)_4^{2-}$): this has been previously considered as a characteristics of the dative bond [40].

The effect of the coordination on the binding of the CO and CN^- ligands has been discussed by several authors. It has been pointed out that the 5σ orbital is antibonding in both ligands, so that removal of electron density from this orbital should result in σ-bond strengthening [47]. From CNDO calculations for a series of XCO molecules, the CO σ bond order was found to increase very slightly and the CO π bond order to decrease (except for HCO^+), with the π decrease considerably larger than the σ increase in some instances [48]. Similar conclusions were reached for the CN^- ligand, with the σ bond order increasing only slightly and the π bond order very much reduced when the substituent was a backbonding atom.

From Tables 2 and 6, it is found that the CO total overlap raises from 1.223 for the free ligand to 1.358 in $Ni(CO)_4$. There is a similar increase for the CN^- ligand, from 1.592 for the free ion to 1.889 in $Ni(CN)_4^{2-}$. The σ overlap population raises for both ligands, mostly as the result of an increase in the overlap population of the 5σ orbital (the value of -0.295 for the free CO should be compared to the sum of the overlap populations for the $8a_1$ and $8t_2$ orbitals in $Ni(CO)_4$, which is -0.133), together with a small increase for the 4σ orbital and a small decrease for the 3σ orbital (see Tables 2 and 6). In $Ni(CN)_4^{2-}$, where the σ and π contributions are exactly separable, there is a small decrease in the π overlap population of 0.939 compared to the value of 1.054 for the free ligand. The changes in the σ electron distribution of the ligands appear as important, if not more, as the ones in the π electron distribution.

Excited States and Electronic Transitions in $Ni(CN)_4^{2-}$

We report in this section some results relative to the excited states of $Ni(CN)_4^{2-}$. The purpose of this work was not to compute accurate (i.e. within one thousand cm^{-1}) values of the transition energies for this ion, but rather to provide with a *semi-quantitative model* of the sequence of excited states. This was prompted by the results obtained for the ground state of the ion, with the π ligand orbitals lying higher than the occupied d orbitals of the metal. At first such a result would conflict with the usual assignment of the lowest transitions as $d-d$ or ligand field transitions [8]. This study was also started with a number of questions in mind:

– what is the relationship between the sequence of occupied and virtual orbitals obtained for the ground state and the sequence of electronic transitions? In many semi-empirical calculations which do not introduce *explicitly* the electron repulsion, excitation energy may be written as the difference of the orbital energies for the two orbitals i and j involved in the excitation

$$\Delta E_{i\to j} = \varepsilon_j - \varepsilon_i .$$

Conversely, a sequence of energy levels has been sometimes advanced for the ground state of the molecule or ion on the basis that it does account for the sequence of electronic transitions [14];

– such an hypothesis may be valid as long as the transition energy $\Delta E_{i\to j}$ parallel $\varepsilon_j - \varepsilon_i$. However, the rigorous way to calculate $\Delta E_{i\to j}$ is to achieve a separate minimization of the ground state and excited state energies E_i and E_j, with the transition energy given as the difference

$$\Delta E_{i\to j} = E_j - E_i . \tag{I}$$

An equally common approximation is the use of virtual orbitals from the ground state calculation to describe the excited states. Then the excitation energy may be written as [41]

$$\left.\begin{aligned} {}^1E(i\to j) &= \varepsilon_j - \varepsilon_i - J_{ij} + 2K_{ij} \\ {}^3E(i\to j) &= \varepsilon_j - \varepsilon_i - J_{ij} \end{aligned}\right\} . \tag{II}$$

Table 10. Highest occupied and lowest empty orbitals of $Ni(CN)_4^{2-}$ (from the ground state calculation)

Orbital	Orbital energy[a]	Nature
$3e_g$	0.589	π^*
$6b_{1g}$	0.587	$d_{x^2-y^2}$
$9e_u$	0.576	$4p_x, 4p_y$
$10a_{1g}$	0.550	$4s$
$3b_{2g}$	0.527	π^*
$4a_{2u}$	0.402	π^*
$8e_u$	−0.121	π
$1a_{2g}$	−0.123	π
$2e_g$	−0.132	π
$1b_{2u}$	−0.136	π
$2b_{2g}$	−0.156	π
$3a_{2u}$	−0.160	π
$9a_{1g}$	−0.182	d_{z^2}
$5b_{1g}$	−0.182	5σ
$7e_u$	−0.195	5σ
$8a_{1g}$	−0.231	4σ
$4b_{1g}$	−0.263	4σ
$1e_g$	−0.267	$d_{xz,yz}$
$6e_u$	−0.278	4σ
$1b_{2g}$	−0.335	d_{xy}

[a] In a.u.

How good is the approximation of building the excited wavefunction from virtual orbitals? Then how much important is the term J_{ij} or $J_{ij} - 2K_{ij}$ compared to the difference of orbital energies?

The sequence of orbital energies for the highest occupied and lowest empty ("virtual") orbitals, as given by the ground state calculation [19], is indicated in Table 10. Each excited state corresponding to a single excitation from one occupied to one empty orbital of Table 10 has been the subject of an independant SCF calculation in the RHF scheme. Separate SCF calculations have been performed for the singlet and triplet states. Excitations involving two orbitals belonging to the same irreducible representation (like the $8e_u \rightarrow 9e_u$ or $5b_{1g} \rightarrow 6b_{1g}$) have not been considered [25]. We have assumed for each excited state the same geometry as the one used for the ground state (cf. below).

The computed transitions energies are reported in Table 11. Excitations above 70000 cm^{-1} are not reported in this table. It is immediately apparent that the sequence of transition energies has no relationship with the sequence of orbital energies. On the basis of orbital energies, one would expect as lowest energy transitions the ones corresponding to the excitations $8e_u \rightarrow 4a_{2u}$, $1a_{2g} \rightarrow 4a_{2u}$, $8e_u \rightarrow 3b_{2g}$ which may be classified as $\pi \rightarrow \pi^*$ transitions. It turns out from Table 11 that the *lowest transitions correspond to $d \rightarrow d$ excitations* from the $9a_{1g}$, $1e_g$ and $1b_{2g}$ orbitals to the $6b_{1g}$ orbital. Further confirmation of the lack of relationship between orbital energies and excitation energies is provided by the fact that the sequence of energy transitions corresponding to the excitation from a given orbital X to the lowest empty orbitals ($4a_{2u}$, $3b_{2g}$, $10a_{1g}$, $9e_u$, $6b_{1g}$) always satisfy[4]

$$E(X \to 6b_{1g}) < E(X \to 4a_{2u}) < E(X \to 3b_{2g}) < E(X \to 10a_{1g}) < E(X \to 9e_u)$$

despite the fact that the $6b_{1g}$ orbital has the highest orbital energy. Conversely, if one considers the sequence of energy transitions corresponding to the excitation from the highest occupied orbitals (from $1b_{2g}$ to $8e_u$) to a given empty orbital X, it is found that (consider for instance the case $X = 4a_{2u}$)

$$E(9a_{1g} \to X) < E(1e_g \to X) < E(1b_{2g} \to X) < E(8e_u \to X)$$

despite the fact that the $9a_{1g}$, $1e_g$ and $1b_{2g}$ are not the highest occupied orbitals. A more careful analysis shows that the sequence of orbital energies may parallel the sequence of transition energies as long as the comparison deals with orbitals of the same nature (for instance the three $3d$ orbitals $1b_{2g}$, $1e_g$ and $9a_{1g}$, or the ligand π orbitals from $3a_{2u}$ to $8e_u$), but breaks down when it involves both the metal $3d$ and the ligand orbitals.

Table 11. Computed transition energies (in cm^{-1}) in $Ni(CN)_4^{2-}$

Transition	Excited state[a]	Transition energy	Nature of the transition
$9a_{1g} \to 6b_{1g}$	$^1B_{1g}$	20600	$d_{z^2} \to d_{x^2-y^2}$
	$^3B_{1g}$	4000	
$1e_g \to 6b_{1g}$	^1E_g	21900	$d_{xz}, d_{yz} \to d_{x^2-y^2}$
	^3E_g	7700	
$1b_{2g} \to 6b_{1g}$	$^1A_{2g}$	22500	$d_{xy} \to d_{x^2-y^2}$
	$^3A_{2g}$	14700	
$9a_{1g} \to 4a_{2u}$	$\underline{^1A_{2u}}$	33900	$d_{z^2} \to \pi^*$
	$^3A_{2u}$	30300	
$1e_g \to 4a_{2u}$	$\underline{^1E_u}$	37900	$d_{xz}, d_{yz} \to \pi^*$
	^3E_u	36000	
$1b_{2g} \to 4a_{2u}$	$^1B_{1u}$	46900	$d_{xy} \to \pi^*$
	$^3B_{1u}$	46700	
$9a_{1g} \to 3b_{2g}$	$^1B_{2g}$	58500	$d_{z^2} \to \pi^*$
$1e_g \to 3b_{2g}$	^1E_g	62300	$d_{xz}, d_{yz} \to \pi^*$
	^3E_g	61700	
$8e_u \to 6b_{1g}$	$\underline{^1E_u}$	68600	$\pi \to d_{x^2-y^2}$
	^3E_u	66000	
$1a_{2g} \to 6b_{1g}$	$^1B_{2g}$	69700	$\pi \to d_{x^2-y^2}$

[a] Excited states corresponding to allowed transitions from the ground state are underlined.

---

[4] The full set of computed transition energies, including excitations above 70000 cm^{-1}, may be found in Ref. [26].

Table 12. Transition energies computed as the difference of the energy for the two states and estimated from orbital energies, Coulomb and exchange integrals

Transition $i \to j$	$\varepsilon_j - \varepsilon_i$ [a]	J_{ij} [a]	K_{ij} [a]	Transition energy [b, c]	Transition energy [b, d]
$1a_{2g} \to 4a_{2u}$	0.525	0.185	0.001	75170	71700
$9a_{1g} \to 4a_{2u}$	0.584	0.248	0.015	80330	33900
$1a_{2g} \to 3b_{2g}$	0.650	0.226	0.034	108000	106000
$9a_{1g} \to 3b_{2g}$	0.709	0.247	0.005	103600	58500
$1a_{2u} \to 6b_{1g}$	0.710	0.209	0.002	111000	69700
$9a_{1g} \to 6b_{1g}$	0.769	0.529	0.023	62770	20600

[a] In a.u.

[b] In cm^{-1}

[c] Computed according to ${}^1E(i \to j) = \varepsilon_j - \varepsilon_i - J_{ij} + 2K_{ij}$.

[d] Computed as the difference of the energy for the two states.

The reason for these inversions is to be found both in the fact that the excitation energy cannot be written as a difference of orbital energies (after assuming that the excited state may be represented through the occupied and virtual orbitals of the ground state) and in the fact that these occupied and virtual orbitals obtained for the ground state cannot provide a satisfactory description of the excited state. To investigate the relative importance of both effects, we have reported in Table 12, for a set of transitions, the values of $\varepsilon_j - \varepsilon_i$, of $\Delta E_{i \to j}$ computed as the difference of the energies for the ground state and the excited state, and of $\Delta E_{i \to j}$ as given by formula II (with the approximation that ε_i and ε_j are the orbital energies from the ground state calculation and that the integrals K_{ij} and J_{ij} are computed for the ground state orbitals). If one considers first the sequence of excitation energies as given by formula II and the difference of orbital energies $\varepsilon_j - \varepsilon_i$ (columns 5 and 2 of Table 12) they parallel approximately for five transitions out of six and the reason is that J_{ij} remain approximately constant, in a range 0.18–0.25 a.u., for these five excitations. However, the $d-d$ excitation $9a_{1g} \to 6b_{1g}$ which is the highest in energy if one considers the difference of orbital energies, is the lowest according to formula II. The reason is that the corresponding Coulomb integral J_{ij} raises to 0.53 a.u. for this excitation. This points to the importance of the Coulomb integral J_{ij} in the determination of the excitation energies. A similar conclusion has been previously reached by Basch *et al.* for the hypothetical compound NiF_4^{2-} [42]. Moreover, a comparison of the excitation energies as given by formula II and by the difference of the energies for the ground and excited states (Columns 5 and 6 of Table 12) indicate that the use of formula II (with integrals computed from the ground state wavefunction) may be a poor approximation. Whenever the transition $i \to j$ involves one metal $3d$ orbital as i or j, formula II may be in error by as much as 45000 cm^{-1}. From Table 12, it is apparent that formula II provides a satisfactory approximation only when both i and j are ligand orbitals. It has already been shown for the ferrocene molecule [36] that there is an important electronic relaxation upon ionization of an electron from a metal $3d$ orbital and that, on the contrary, there is little electronic rearrangement when the ionization

Table 13. A comparison of some "occupied" molecular orbitals ϕ_i from the ground state calculation and from some excited state calculations

Orbital	Nature of the excitation	LCAO coefficients[a,b]
From the ground state calculation		
$1a_{2g}$		$0.32\ 2p_C^1 + 0.22\ 2p_C^2 + 0.71\ 2p_N$
$9a_{1g}$		$0.36\ 4s_{Ni}^2 - 0.23\ 2p_C^1 + 0.42\ 2p_N + 0.72\ 3d_{z^2}^1$
From the excited state calculation		
$1a_{2g}$	$1a_{2g} \to 4a_{2u}$	$0.32\ 2p_C^1 + 0.22\ 2p_C^2 + 0.71\ 2p_N$
$1a_{2g}$	$1a_{2g} \to 3b_{2g}$	$0.31\ 2p_C^1 + 0.24\ 2p_C^2 + 0.70\ 2p_N$
$1a_{2g}$	$1a_{2g} \to 6b_{1g}$	$0.30\ 2p_C^1 + 0.21\ 2p_C^2 + 0.73\ 2p_N$
$9a_{1g}$	$9a_{1g} \to 6b_{1g}$	$0.95\ 3d_{z^2}^1$
$9a_{1g}$	$9a_{1g} \to 3b_{2g}$	$0.98\ 3d_{z^2}^1$
$9a_{1g}$	$9a_{1g} \to 4a_{2u}$	$0.99\ 3d_{z^2}^1$

[a] Only coefficients greater than 0.2 are reported.

[b] The notations $2p_C^1$, $2p_C^2$, $3d^1$, etc. ... refer to split orbitals.

Table 14. A comparison of some "excited" molecular orbitals ϕ_j from the ground state calculation and from some excited state calculations

Orbital	Nature of the excitation	LCAO coefficients[a,b,c]
From the ground state calculation ("virtual" orbitals)		
$6b_{1g}$		$-1.24\ 2s_C^2 + 0.26\ 2s_N + 0.23\ 2p_C^1 + 0.38\ 2p_C^2 - 0.28\ 2p_N + 0.85\ 3d^1 + 0.53\ 3d_{x^2-y^2}^2$
$9e_u$		$-1.73\ 2s_C^2 - 0.23\ 2s_N + 2.12\ 4p_{x,y}^2 + 0.60\ 2p_{1C}^2 + 0.22\ 2p_{2C}^1 - 0.54\ 2p_{2N}$
$10a_{1g}$		$-0.69\ 4s^1 + 4.46\ 4s^2 - 3.02\ 2s_C^2 - 0.40\ 2s_N + 1.88\ 2p_C^2 - 0.61\ 3d_{z^2}^2$
$3b_{2g}$		$-0.29\ 2p_C^1 - 0.58\ 2p_C^2 + 0.82\ 2p_N + 0.25\ 3d_{xy}^1$
$4a_{2u}$		$-0.94\ 4p_z^2 + 0.52\ 2p_N$
From the excited state calculation		
$6b_{1g}$	$1a_{2g} \to 6b_{1g}$	$-0.49\ 2s_C^2 + 0.99\ 3d_{x^2-y^2}^1$
$9e_u$	$5b_{1g} \to 9e_u$	$-1.39\ 2s_C^2 + 1.63\ 4p_{x,y}^2 + 0.46\ 2p_{1C}^2 + 0.30\ 2p_{2C}^1 + 0.23\ 2p_{2C}^2 - 0.68\ 2p_{2N}$
$10a_1$	$1e_g \to 10a_{1g}$	$-0.64\ 4s^1 + 4.01\ 4s^2 - 2.70\ 2s_C^2 - 0.28\ 2s_N + 1.55\ 2p_C^1 - 0.40\ 3d_{z^2}^2$
$3b_{2g}$	$1a_{2g} \to 3b_{2g}$	$-0.31\ 2p_C^1 - 0.55\ 2p_C^2 + 0.75\ 2p_N + 0.28\ 3d_{xy}^1 - 0.25\ 3d_{xy}^2$
$4a_{2u}$	$1a_{2g} \to 4a_{2u}$	$-0.86\ 4p_z^2 + 0.52\ 2p_N$

[a] Only coefficients greater than 0.2 are reported.

[b] The notations $2s_C^1$, $2s_C^2$, $2p_C^1$, etc. ... refer to split orbitals.

[c] The notations $2p_{1C}$, $2p_{2C}$, etc. ... refer to orbitals centered on the carbon atoms C_1 and C_2 (Fig. 1).

involves an electron from a ligand orbital. A similar conclusion may be reached relative both to the importance of the electronic relaxation upon excitation (change in the "occupied" orbital ϕ_i) and to the significance of "virtual" orbitals compared to the orbitals optimized for each excited state (change in ϕ_j). We have reported in Tables 13 and 14 the expressions for some orbitals ϕ_i and ϕ_j

Table 15. Transitions and assignments in $Ni(CN)_4^{2-}$, according to Refs. [8] and [10]

Energy[a]	Extinction coefficient ε	Assignment
22400	2	${}^1A_{1g} \to {}^1A_{2g}$ $d_{xy} \to d_{x^2-y^2}$
23000	50	$\to {}^1B_{1g}$ $d_{z^2} \to d_{x^2-y^2}$
27000	100	$\to {}^1E_g$ $d_{xz,yz} \to d_{x^2-y^2}$
32300	700	$\to {}^1B_{1u}$ $d_{xy} \to \pi^*$
35200	4200	$\to {}^1A_{2u}$ $d_{z^2} \to \pi^*$
37600	10600	$\to {}^1E_u$ $d_{xz,yz} \to \pi^*$

[a] In cm^{-1}.

both from the ground state calculation and from some excited state calculation. An orbital ϕ_i like the $1a_{2g}$ orbital, which is a ligand π orbital, remains nearly unchanged when its occupation number changes from 2 to 1. On the contrary, an orbital ϕ_i like the $9a_{1g}$ orbital, which is a rather diffuse metal $3d$ orbital in the ground state, is strongly affected upon excitation and becomes a nearly pure $3d$ orbital. If we turn now to the ϕ_j orbital (Table 14), the difference between the virtual orbital and the corresponding orbital optimized for the excited state is more pronounced for the $6b_{1g}$ orbital (which appears to be less diffuse when optimized for the excited state) than for the other orbitals. Again the $6b_{1g}$ orbital is predominantly a metal $3d$ orbital.

So far, we have not discussed the relationship between the computed excitation energies and the experimental absorption spectrum. The experimental spectrum of $Ni(CN)_4^{2-}$ has been studied by many authors. We shall refer mostly to the work of Ballhausen and coll. [8] and to the work of Piepho and coll. [13]. On the basis of the polarized spectra of crystals in conjunction with ligand-field theory, Ballhausen has proposed the assignments given in Table 15. This has been confirmed by Stephens on the basis of the magnetic circular dichroïsm spectrum [12]. It has been shown later that the introduction of spin-orbit coupling does not change basically the interpretation of the spectrum [13].

The experimental spectrum shows three weak bands in the range 22000–27000 cm^{-1}, which have been interpreted as symmetry-forbidden $d-d$ (or "ligand-field") transitions [8]. The corresponding singlet excitations are computed (Table 11) as the lowest energy excitations, in the range 20000 to 22500 cm^{-1}. The next three bands of the experimental spectrum, in the range 32000–37600 cm^{-1}, have been considered as charge-transfer excitations from a $3d$ orbital (b_{2g}, a_{1g}, e_g) to the ligand antibonding orbital $4a_{2u}$. The computed energies corresponding to these excitations fall in the range 33900–46900 cm^{-1} and come next to the $d-d$ excitations. We might consider this agreement, which is semiquantitative, as satisfactory, especially when one is reminded of the rather severe limitations of this type of calculation: use of a limited basis set and neglect of the change in correlation energy[5].

---

[5] The assumption that the excited state retains the geometry of the ground state is not an approximation as long as the reported experimental energies correspond to vertical transitions. According to Ballhausen *et al.*, $Ni(CN)_4^{2-}$ should remain square planar in the ${}^1A_{2g}$ state but should distort in the ${}^1E_g$ and ${}^1B_{1g}$ state [8].

However, there is some disagreement between the assignment given for the experimental spectrum (Table 15) and the sequence of computed excitations (Table 11). According to the assignment of the experimental spectrum, the sequence for both the $d-d$ and $d-\pi^*$ excitations is

$$(b_{2g}\rightarrow X)<(a_{1g}\rightarrow X)<(e_g\rightarrow X)$$

where X stands for b_{1g} or a_{2u}. The sequence of computed excitations is different

$$(a_{1g}\rightarrow X)<(e_g\rightarrow X)<(b_{2g}\rightarrow X).$$

However, this disagreement may be not so severe. In fact, the band which has been assigned to the $b_{2g}\rightarrow b_{1g}$ excitation is observed at 22400 cm^{-1} only in the barium tetracyanonickelate. For other salts, this band would appear at highest frequencies and would be covered by the more intense charge-transfer bands [10]. In fact, according to Ballhausen *et al.*, this transition is expected to occur around 30000 cm^{-1} [8]. Then, the experimental sequence of excitations would be

$$(a_{1g}\rightarrow b_{1g})<(e_g\rightarrow b_{1g})<(b_{2g}\rightarrow b_{1g})$$

in agreement with the computed sequence of Table 11. The assignment of the charge-transfer bands above 30000 cm^{-1} is probably more difficult. Stephens *et al.*, on the basis of magnetic circular dichroïsm (MCD) measurements, have established the excited state order $^1A_{2u}<{}^1E_u$, in agreement with the computed energies of Table 11 [12]. Piepho *et al.*, also on the basis of the MCD spectrum, assign the band around 32300 cm^{-1} as a composite $^1B_{1u}+{}^3A_{2u}$ (due to explicit consideration of spin-orbit coupling) [13]. Their justification for assuming that this band arises partially from the $^1A_{1g}\rightarrow{}^1B_{1u}$ transition is that its intensity seems too large to result from an $^1A_{1g}\rightarrow{}^3A_{2u}$ transition alone. However, the possibility of a sequence of excited states

$$^1A_{2u}<{}^1E_u<{}^1B_{1u}$$

does not appear to have been ruled out definitely.

There is little indication in the literature, if any, on the triplet electronic states. The $d\rightarrow d$ transitions to a triplet state are predicted at 4000, 7700 and 14700 cm^{-1} [6]. Two very weak bands have been reported by Ballhausen *et al.* at 5600 and 7000 cm^{-1} but do not correspond to electronic transitions. Weak absorptions at 20000 cm^{-1} have also been assigned as spin-forbidden transitions [8]. For the $3d\rightarrow\pi^*$ excitations, the triplet state is found to be about 200–3600 cm^{-1} below the singlet state. In the energy level scheme proposed by Piepho *et al.* in the absence of spin-orbit coupling, the corresponding triplet states lie some 2500–3500 cm^{-1} below the singlet states [13].

We have reported in Table 16 the results of a population analysis for some excited states. For the three $d\rightarrow d$ transitions, there is a nearly constant increase in the formal charge of the Ni atom compared to the ground state. This is due to the fact that, when one $3d$ electron is excited into the $d_{x^2-y^2}$ orbital, the ease of σ-coordination of the ligands to the metal through the $d_{x^2-y^2}$ orbital is decreased.

---

[6] The reason for the large difference between the energies of the singlet and triplet states $^1B_{1g}$ and $^3B_{1g}$ is to be found in the large value of K_{ij} (see Table 12).

Table 16. Population analysis for the ground state and some excited states of $Ni(CN)_4^{2-}$

	Ground state	$^1B_{1g}$ $d_{z^2} \to d_{x^2-y^2}$	^1E_g $d_{xz,yz} \to d_{x^2-y^2}$	$^1A_{2g}$ $d_{xy} \to d_{x^2-y^2}$	^1E_g $d_{xz,yz} \to \pi^*$	^1E_u $\pi \to d_{x^2-y^2}$
Ni 4*s*	0.41	0.35	0.39	0.40	0.43	0.43
$4p_x$	0.17	0.19	0.18	0.17	0.23	0.12
$4p_y$	0.17	0.19	0.18	0.17	0.23	0.12
$4p_z$	0.04	0.05	0.05	0.04	0.06	0.02
$3d_{x^2-y^2}$	0.91	1.58	1.58	1.59	1.36	1.30
$3d_{xy}$	1.95	1.95	1.95	0.98	2.15	1.92
$3d_{xz}$, $3d_{yz}$	1.97	1.97	1.48	1.97	1.49	1.95
$3d_{z^2}$	1.96	1.01	1.98	1.98	1.97	1.92
q^a	+0.46	+0.74	+0.73	+0.72	+0.60	+0.27
C 2*s*	1.26	1.31	1.31	1.31	1.16	1.35
$2p\sigma^b$	1.14	1.16	1.16	1.16	1.10	1.13
$2p\pi$	0.84	0.83	0.83	0.85	0.92	0.79
$2p\pi'$	0.91	0.92	0.92	0.90	0.90	0.84
q^a	−0.14	−0.22	−0.22	−0.22	−0.18	−0.11
N 2*s*	1.66	1.66	1.66	1.66	1.66	1.67
$2p\sigma$	1.53	1.54	1.54	1.54	1.52	1.53
$2p\pi$	1.18	1.19	1.19	1.16	1.30	1.09
$2p\pi'$	1.10	1.08	1.08	1.10	1.00	1.18
q^a	−0.47	−0.47	−0.47	−0.47	−0.47	−0.46

[a] Formal charge.

[b] The orbitals $2p\sigma$, $2p\pi$, $2p\pi'$ are defined in Fig. 1.

Compared to the ground-state, the population of the $3d$ orbital from where the electron is excited is decreased by about one electron (one-half for the degenerate d_{xz} and d_{yz} orbitals). In a charge-transfer transition of the type $d_{xz,yz} \to \pi^*$, the change in the formal charge of the Ni atom is small (from +0.46 to +0.60). This is due to the fact that the π charge transfer from the metal to the ligand induces an increased σ charge transfer from the ligand to the metal, as it may be seen from the population of the $3d_{x^2-y^2}$, $4p_x$ and $4p_y$ orbitals. Excitations which are classified as ligand to metal charge transfer ($\pi \to d_{x^2-y^2}$) appear to have only a limited effect on the formal charge of the metal atom, since only a fraction of an electron is transferred from the ligand into the $d_{x^2-y^2}$ orbital.

Conclusion

We have used the LCAO-MO-SCF method to investigate the electronic structure of the $Ni(CN)_4^{2-}$ ion and of the $Ni(CO)_4$ molecule, with a medium size basis set of Gaussian orbitals. The sequence of orbital energies for the highest occupied orbitals is predicted to be

$$3d \sim \sigma(CN^-) < \pi(CN^-)$$

for the $Ni(CN)_4^{2-}$ ion and

$$8a_1(\sigma_L) < 1e(\pi_L) \sim 7t_2(\pi_L) \sim 1t_1(\pi_L) \sim 8t_2(\sigma_L) < 2e(d_M) < 9t_2(d_M)$$

for the $Ni(CO)_4$ molecule. For this molecule, our sequence is different from the one obtained by Nieuwpoort [18] which puts the $2e$ orbital as the highest filled orbital, but in agreement with the recent calculation of Hillier [20] and with previous assignment of the experimental spectrum [6]. We may infer that Koopmans' theorem is probably true for this molecule. If the same would be true for the $Ni(CN)_4^{2-}$, the lowest I.P. would be associated with the removal of an electron from orbitals which are predominantly ligand π orbitals. Separate calculations for various electronic states of the mononegative ion $Ni(CN)_4^-$ have indicated that the lowest ionization energies should correspond to removal of one electron from the metal $3d$ orbitals and not from the π ligand orbitals. Reasonable values of the corresponding I.P. can be achieved only when the electrostatic potential of the crystal is accounted for. A somewhat similar situation is found in the calculation of the lowest electronic transitions of $Ni(CN)_4^{2-}$. Since the highest occupied and lowest virtual orbitals for this ion are π and π^* ligand orbitals, $\pi \to \pi^*$ transitions would be expected as the lowest ones on the basis of orbital energy values. Separate SCF calculations indicate that the lowest computed transitions are associated with $d \to d$ excitations. The disagreement between the sequence of computed transitions and the one expected on the basis of orbital energies may be traced to the role of Coulomb and exchange integrals in the computed transition energies together with the importance of electronic relaxation upon excitation. These conclusions are probably rather general when, in the sequence of orbital energy, some ligand orbitals are found above the metal $3d$ orbitals. This situation, with similar results, has been found

---

[7] In the sequence of orbital energy, ligand orbitals have been equally found above the doubly occupied metal $3d$ orbitals in NiF_4^{2-} [42], CuF_4^{2-} [44], $NiCl_4^{2-}$ [45].

also in the ferrocene molecule [36] and the $CuCl_4^{2-}$ ion [2]. It is probably rather general when the ligand is either a negative ion like in $Ni(CN)_4^{2-}$ or $CuCl_4^{2-}$ [7] or a neutral molecule with an extended π-electron system like in ferrocene. On the contrary, one may expect that the highest occupied orbitals will have a character of metal 3*d* orbitals when the ligand is a neutral molecule with a limited π system, like in $Ni(CO)_4$. One major consequence is that it does not seem possible any more to discuss the electronic spectrum of this type of complexes on the basis of a molecular orbital scheme or conversely to derive an orbital scheme from the assigned transitions, as it has been currently assumed [14, 9].

Our results are in agreement with the chemical evidence that the cyanide ion is a better σ-donor and a poorer π-acceptor than the carbonyl ligand, with a negligible π back-bonding in $Ni(CN)_4^{2-}$ and a weak σ bonding in $Ni(CO)_4$. While both previous calculations by Nieuwpoort [18] and Hillier [17] gave a formal negative charge on the Ni atom close to one electron in $Ni(CO)_4$, we find that the Ni atom bears a small positive charge as the result of a limited σ charge transfer opposed by π backbonding.

Acknowledgements. We are grateful to the CNRS for a generous donation of computer time at the Centres de Calcul de Strasbourg-Cronenbourg et d'Orsay (C.I.R.C.E.). It is a pleasure to acknowledge the assistance given by the staffs of these Computation Centers. We thank Dr. W. C. Nieuwpoort for a helpful discussion and Dr. K. Jørgensen who kindly made available the photoelectron spectrum of $Ni(CN)_4^{2-}$.

References

1. See for instance: Cotton, F. A., Wilkinson, G.: Advanced inorganic chemistry, p. 719. New-York: Interscience Publishers 1968.
2. Demuynck, J., Coutiere, M.-M., Veillard, A.: to be published.
3. Griffith, W. P.: Quart. Rev. **16**, 188 (1962).
4. Jørgensen, K.: private communication.
5. Lloyd, D. R., Schlag, E. W.: Inorg. Chemistry **8**, 2544 (1969).
6. Green, J. C., King, D. L., Eland, J. H. D.: Chem. Comm. 1121 (1970).
7. Kida, S., Fujita, J., Nakamoto, K., Tsuchida, R.: Bull. chem. Soc. Japan **31**, 79 (1958).
8. Ballhausen, C. J., Bjerrum, N., Dingle, R., Eriks, K., Hare, C. R.: Inorg. Chemistry **4**, 514 (1965).
9. Mason, R., Gray, H. B.: J. Amer. chem. Soc. **90**, 5721 (1968)
10. Dahl, J. P., Dingle, R., Vala, M. T.: Acta chem. scand. **23**, 47 (1969).
11. Haines, R. A., Smith, A. A.: Can. J. Chem. **46**, 1444 (1968).
12. Stephens, P. J., McCaffery, A. J., Schatz, P. N.: Inorg. Chemistry **7**, 1923 (1968).
13. Piepho, S. B., Schatz, P. N., McCaffery, A. J.: J. Amer. chem. Soc. **91**, 5994 (1969).
14. Gray, H. B., Ballhausen, C. J.: J. Amer. chem. Soc. **85**, 260 (1963)
15. Millie, P., Veillard, A.: J. Chim. physique **20** (1965).
16. Schreiner, A. F., Brown, T. L.: J. Amer. chem. Soc. **90**, 3368 (1958).
17. Hillier, I. H.: J. chem. Physics **52**, 1948 (1970).
18. Nieuwpoort, W. C.: Philips Res. Rept. Suppl. No. 6, 1 (1965).
19. Demuynck, J., Veillard, A., Vinot, G.: Chem. Physics Letters **10**, 522 (1971).
20. Hillier, I. H., Saunders, V. R.: Chem. Comm. 642 (1971).
21. Roos, B., Veillard, A., Vinot, G.: Theoret. chim. Acta (Berl.) **20**, 1 (1971).
22. Whitman, D. R., Hornback, C. J.: J. chem. Physics **51**, 398 (1969).
23. Holt, E. M., Watson, K. J.: Acta chem. scand. **23**, 14 (1969).
24. Ladell, J., Post, B., Faukuchen, I.: Acta crystallogr. **5**, 795 (1952).
25. Roothaan, C. C. J.: Rev. mod. Physics **32**, 179 (1960).
26. Demuynck, J.: Thèse de Doctorat d'Etat. Strasbourg, 1972.
27. Clementi, E.: Atomic energy tables. Supplement to IBM J. of Res. Develop. **9**, 1 (1965).

28. Bonaccorsi, R., Petrongolo, C., Scrocco, E., Tomasi, J.: Chem. Physics Letters **3**, 473 (1969).
29. McLean, A. D., Yoshimine, M.: Tables of linear molecule wave functions, Supplement to IBM J. of Res. Develop., 1967.
30. Christensen, J. J., Izatt, R. M., Hale, J. D., Pack, R. T., Watt, G. D.: Inorg. Chemistry **2**, 337 (1963).
31. Fischer, A. K., Cotton, F. A., Wilkinson, G.: J. Amer. chem. Soc. **81**, 800 (1959).
32. Koopmans, T.: Physica **1**, 104 (1933).
33. Hillier, I. H., Saunders, V. R., Ware, M. J., Bassett, P. J., Lloyd, D. R., Lynaugh, N.: Chem. Comm. 1316 (1970).
34. Barber, M., Connor, J. A., Hillier, I. H., Saunders, V. R.: Chem. Comm. 682 (1971).
35. Clark, D. T., Adams, D. B.: Chem. Comm. 740 (1971).
36. Coutiere, M.-M., Demuynck, J., Veillard, A.: Theoret. chim. Acta (Berl.) **27**, 281 (1972).
37. Mulliken, R. S.: J. chem. Physics **23**, 1833 (1955).
38. Mulliken, R. S.: Molecular complexes, p. 281. London: Wiley Interscience 1969.
39. Boys, S. F.: Rev. mod. Physics **32**, 296 (1960).
40. Millie, P., Berthier, G.: In: La nature et les propriétés des liaisons de coordination, p. 31. Paris: Editions du Centre National de la Recherche Scientifique, 1970.
41. Roothaan, C. C. J.: Rev. mod. Physics **23**, 69 (1951).
42. Basch, H., Hollister, C., Moskowitz, J. W.: In: Sigma molecular orbital theory, p. 449; O. Sinanoglu and W. Kenneth, Ed. New Haven: Yale University Press 1970.
43. Vannerberg, N. G.: Acta chem. scand. **18**, 2385 (1964).
44. Tossell, J. A., Lipscomb, W. N.: J. Amer. chem. Soc. **94**, 1505 (1972).
45. Dedieu, A., Veillard, A.: unpublished results.
46. Johnson, K., Wahlgren, U.: Int. J. quant. Chemistry, in press.
47. Dekock, R. L., Sarapu, A. C., Fenske, R. F.: Inorg. Chemistry **10**, 38 (1971).
48. Purcell, K. F.: J. Amer. chem. Soc. **91**, 3487 (1969).

Dr. A. Veillard
Institut de Chimie
Université Louis Pasteur
BP 296/R 8
F-67 Strasbourg, France

Note added in proof. The reported binding energy of 86 kcal/mole for the nickelcarbonyl molecule is with respect to $Ni^0(3d^{10}\ ^1S)$. A full account of the results of Ref. [20] has been given by Hillier and Saunders (Mol. Physics **22**, 1025 (1971)).

Theoret. chim. Acta (Berl.) 28, 267--282 (1973)
© by Springer-Verlag 1973

Vibronic and Spin-Orbit Splitting in Spectra of Systems Exhibiting Jahn-Teller-Effect

Peter Habitz and Wilhelm Hans Eugen Schwarz
Lehrstuhl für Theoretische Chemie der Universität, Wegelerstr. 12, 53 Bonn, Germany

Received October 6, 1972

Simple two- and three-dimensional models have been used to investigate the vibronic states of molecules exhibiting Jahn-Teller-Effect. According to the topology of the adiabatic potential surface, two cases have to be distinguished, which may (A) or may not (B) be treated in the Born-Oppenheimer approximation. In the latter case B strong Jahn-Teller coupling leads to a splitting of an $A \rightarrow E$ absorption line into three peaks instead of the usual two ones. This additional splitting originates from transitions into the first and second metastable level of the upper potential well. However, the vibronic splitting will often be smeared out by coupling of the Jahn-Teller effect to a distortion of a Jahn-Teller inactive vibration. The effective spin-orbit splitting of an absorption band with unresolved vibrational structure is larger than in the case of vanishing Jahn-Teller coupling, contrary to the spin-orbit splitting of single vibronic levels. An experimental example of this effect is discussed. In Jahn-Teller case B it may be interpreted as a superposition of the vibronic and the spin-orbit splitting effects.

Mittels einfacher zwei- und dreidimensionaler Modelle wurden die vibronischen Zustände von Molekülen untersucht, die einen Jahn-Teller-Effekt zeigen. Entsprechend der Topologie der adiabatischen Potentialfläche sind zwei Fälle A und B zu unterscheiden, die im Rahmen der Born-Oppenheimer-Näherung behandelt werden können bzw. wo dies nicht möglich ist. Im letzteren Falle B führt eine sehr starke Jahn-Teller-Kopplung zur Aufspaltung einer $A \rightarrow E$ Absorptionslinie in drei statt wie üblich in zwei Peaks. Diese zusätzliche Aufspaltung rührt her von Übergängen in die ersten beiden metastabilen Resonanzzustände der oberen Potentialmulde. In vielen Fällen wird mit einer Jahn-Teller-Kopplung der asymmetrischen Schwingung eine Verschiebung der Gleichgewichtslage einer Jahn-Teller inaktiven Schwingung einherlaufen: Die vibronischen Aufspaltungen sollten daher durch Schwingungsverbreiterung teilweise verschmiert sein. Während die Spin-Bahn-Aufspaltung einzelner vibronischer Niveaus durch Jahn-Teller-Kopplung verringert wird, wird die effektive Spin-Bahn-Aufspaltung einer Absorptionslinie mit nichtaufgelöster Schwingungsstruktur vergrößert. Ein experimentelles Beispiel für diesen Effekt wird diskutiert. Im Jahn-Teller-Fall B kann er als Überlagerung der vibronischen und der Spin-Bahn-Aufspaltung interpretiert werden.

1. Introduction

Let us consider a molecule with a degenerate electronic state in the Born-Oppenheimer approximation. Under a symmetry-breaking distortion, the degenerate electronic state will usually split. According to Jahn and Teller [1–3] there exists at least one nontotally symmetric vibrational coordinate, x, for a non-linear molecule M, where the splitting is linear in x. If M is stable against dissociation, the corresponding adiabatic potential curves may be approximated by

$$V(x) = k/2(x \pm R_0)^2 .$$

Now let us consider a second symmetry coordinate y, one which will result in vibrational bands of appreciable intensity. We have to distinguish between

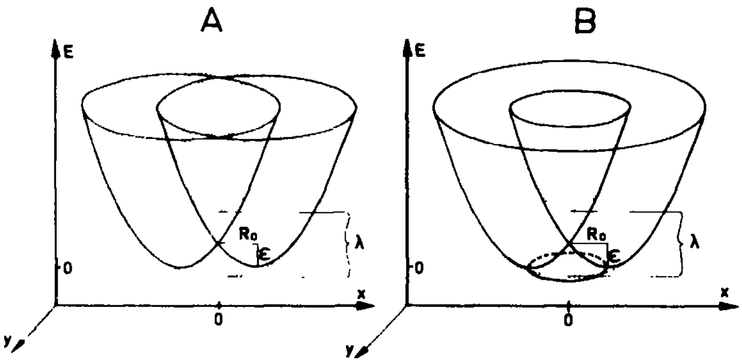

Fig. 1. Potential energy as a function of two symmetry coordinates. Case A: x is Jahn-Teller active, y inactive (two intersecting paraboloids). Case B: both x and y are Jahn-Teller active (only one surface, the Jahn-Teller cone). Dotted lines: an additional spin-orbit coupling leads to two separate adiabatic potential surfaces in both cases

Table 1. Classification of Jahn-Teller effect

Non-linear symmetries with degenerate representations	Degenerate electronic state	Jahn-Teller active symmetry coordinates	Relevant symmetry coordinates	Topology of the corresponding adiabatic potential energy surface
Tetragonal	E	b_1, b_2	one b, one a_1	A
			b_1 and b_2	B
Trigonal, pentagonal, hexagonal	E	e	e	B
Cubic	E	e	e	B
	T	e, t	e	A
			t	B

two possibilities: A) the y-coordinate is Jahn-Teller inactive or B) it is active. These cases A and B differ by the topology of the potential surface as is shown in Fig. 1. Examples of the two cases are given in Table 1. E.g. case A is approximately realized by a doubly degenerate electronic state of a tetragonal molecule, if only vibrations of species a_1 and b_2 are of relevance for the phenomenon to be discussed, i.e. the optical absorption spectrum. The main difference between the two cases is, that the adiabatic surfaces A may be considered as diabatic surfaces, too, whereas this is not possible with the adiabatic surface B. Correspondingly the nuclear motion in case A may be calculated within the Born-Oppenheimer approximation, whereas in case B one has to use at least the diabatic two-state approximation [4], as has been done in the classical works of Longuet-Higgins *et al.* and Ballhausen [5].

2. Calculational Model

In this way we have calculated vibronic energy levels and wave functions. Some details are given in Appendix A, see also Ref. [6]. The following simple adiabatic potential surfaces have been used:

Case A: the two surfaces V_1 and V_2 depend on a one-fold degenerate J.T. active coordinate x and an inactive coordinate, which is now denoted by z, with harmonic force constants k and k_z, respectively:

$$V_{1,2}(x, z) = \frac{k}{2}(x \pm R_0)^2 + \frac{k_z}{2}(z - Z_0)^2 .$$

Case B: the two branches V_+ and V_- depend on two J. T. active coordinates x and y. In order to investigate the effect of an J. T. inactive mode in this case, too, we introduce a third coordinate z. However, for simplification we assume x, y to be degenerate (J. T. active e mode);

$$V_\pm(x, y, z) = \frac{k}{2}(\sqrt{x^2 + y^2} \pm R_0)^2 + \frac{k_z}{2}(z - Z_0)^2 .$$

Case A and this special case B may be looked at as limiting cases of a general case B with $k_x \neq k_y$ and $R_x \neq R_y$: then case A means $R_x = R_0$, $R_y = 0$ and case B $k_x = k_y$, $R_x = R_y$.

The Jahn-Teller energy ε, the difference between the potential minimum and the energy of the symmetric configuration (see Fig. 1), is given in both cases by

$$\varepsilon = \frac{k}{2} R_0^2 .$$

Furthermore, we want to investigate the influence of an additional spin-orbit interaction in an eletronic doublet state. The corresponding matrix element between the two adiabatic electronic states ψ_+, ψ_- constituing the ^2E may be approximated by

$$\langle \psi_+ | H_{\mathrm{so}} | \psi_- \rangle = i \frac{\lambda}{2} .$$

Then the adiabatic potential energies are

$$U_\pm(x, z) = \frac{k}{2}(x^2 + R_0^2) \pm \sqrt{(k R_0 x)^2 + \frac{\lambda^2}{4}} + \frac{k_z}{2}(z - Z_0)^2$$

for case A, and

$$U_\pm(x, y, z) = \frac{k}{2}(r^2 + R_0)^2 \pm \sqrt{(k R_0 r)^2 + \frac{\lambda^2}{4}} + \frac{k_z}{2}(z - Z_0)^2$$

for case B, where we have introduced $r^2 = x^2 + y^2$.

In both cases, these are two separate non-intersecting surfaces (see Fig. 1).

3. Line Shapes of Electronic $A \rightarrow E$ Transitions for Case B

In this paragraph we will discuss the line shape of an $^2A \rightarrow {}^2E$ absorption spectrum at low temperatures. In this case the initial state is the lowest vibrational state of the electronic state A with an assumed potential curve

$$V_A(x, y, z) = \frac{k'}{2}(x^2 + y^2) + \frac{k'_z}{2} z^2 .$$

Usually the force constants of the initial and the final state will be somewhat different. However, as we need the lowest vibrational function only for the calculation of Franck-Condon factors, the results will not change significantly, if we use $k' = k$, and $k'_z = k_z$ instead, for computational reasons. The line shapes are calculated with an inherent line width of $2\omega_0$ for each vibronic component ($\omega_0 = \sqrt{k/M}$, M = reduced mass), so that the vibrational structure of the spectrum is smeared out.

Vibronic Splittings

At first we discuss the case $\lambda = Z_0 = 0$. Results for several values of the Jahn-Teller parameter ε are displayed in Fig. 2. We see, that the band shapes exhibit a more and more pronounced splitting, as the Jahn-Teller coupling increases. The two main peaks of this well known vibronic splitting of the absorption bands, may be interpreted as originating from transitions into the lower and upper

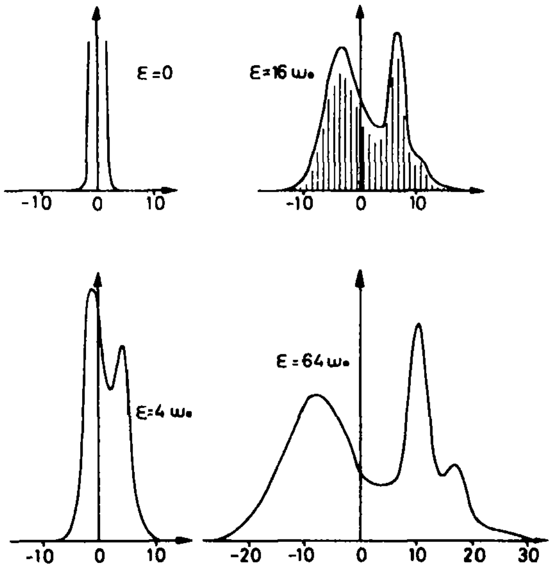

Fig. 2. Line shape of an electronic $A \rightarrow E$ transition at 0° K, calculated from $E \times e$ vibronic states. Natural line width $= 2\omega_0$. Jahn-Teller energy $\varepsilon = 0, 4, 16$ and $64\,\omega_0$. (For $\varepsilon = 16\,\omega_0$ single vibronic transition intensities are shown, too.)

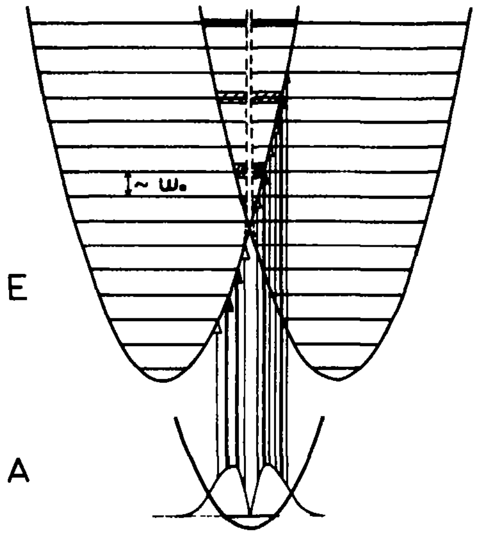

Fig. 3. $A \rightarrow E$ transitions in the configuration-coordinate model. —— adiabatic potential curves, - - effective potential including the pseudocentrifugal term $\frac{1}{4Mr^2}$. —— vibronic levels, ▨ resonances in the inner potential well

well of the potential surface (see Fig. 3). A simple semiclassical model [2, 9] predicts two bands of equal shape centered at $E = 0$ and yields

$$\Delta E_{\text{vib}} = \sqrt{4\varepsilon\omega_0}$$

for the distance of the two maxima. Augmenting the adiabatic potential surface by a pseudocentrifugal term [2, 9] (see Fig. 3), the refined semiclassical model even yields the shift of the two bands to higher energies and a smaller width of the upper peak (see Fig. 2).

Furthermore we see from Fig. 2 that an increasing Jahn-Teller coupling leads to a further splitting of the absorption line shape. A third peak is fully developed at $\varepsilon = 64\,\omega_0$, on the right side of which we see an additional shoulder. Although neither the simple nor the refined semiclassical model is able to explain this phenomenon, we are nevertheless convinced that it is not merely an artifact of our calculational procedure: the basis sets of the numerical quantummechanical calculations have been expanded until the line shape did not change any more. Furthermore the results are reproducible with double precision arithmetic.

In order to investigate this new phenomenon, we will at first analyse the wave functions of the vibronic states. In the approximation used [5, 6] the vibronic wave functions are usually written as

$$\Psi = \psi_1(\xi)\cdot\chi_1(r, \phi) + \psi_2(\xi)\cdot\chi_2(r, \phi)$$

where ψ_1, ψ_2 are the two degenerate diabatic electronic wave functions depending on the electronic coordinates ξ only, and χ_1, χ_2 are the nuclear wave functions

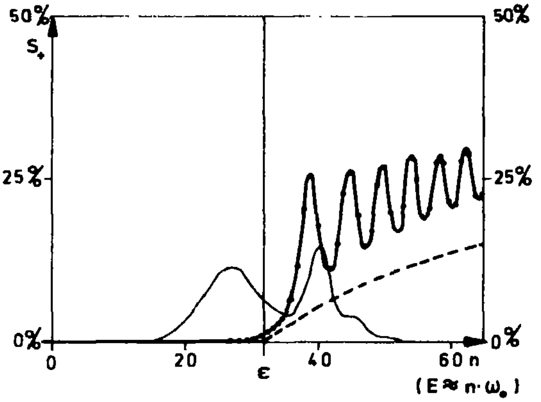

Fig 4. Integrated density of vibronic $E \times e$ states associated with the upper part of the adiabatic potential surface versus vibronic main quantum number n ($\varepsilon = 32\,\omega_0$, $\lambda = 0$, $m = 0$). —— quantum mechanical result, - - - - classical approximation. absorption line shape of an $A \to E$ transition

depending on $r = \sqrt{x^2 + y^2}$ and $\phi = \operatorname{arc\,tg} y/x$. Ψ may be transformed into[1]

$$\Psi = e^{i(m+\frac{1}{2})\phi} \cdot [\psi_+(\xi, \phi) \cdot \chi_+(r) + i\psi_-(\xi, \phi) \cdot \chi_-(r)]$$

where ψ_+, ψ_- are the adiabatic electronic wave functions corresponding to the upper and lower part of the adiabatic energy surface, and where the ψ's and χ's are real. From the normalization integral

$$1 = \langle \Psi | \Psi \rangle = \langle \psi_+ | \psi_+ \rangle \langle \chi_+ | \chi_+ \rangle + \langle \psi_- | \psi_- \rangle \langle \chi_- | \chi_- \rangle = S_+ + S_- \ .$$

one may calculate the percentages of the vibronic states, S_+ and S_-, associated with the upper and lower parts of the surface, respectively. The integrals needed are given in appendix A.

The result for $\varepsilon = 32\,\omega_0$ is shown in Fig. 4.

For energy values below ε, the system is nearly entirely on the lower part of the surface, for $E \gg \varepsilon$: $S_+ \to \frac{1}{2}$. This behaviour is to be expected from the classical model: the maximum probability is near the turning points, which are given by $r_t = R_0 \cdot \left(\sqrt{\frac{E}{\varepsilon}} \pm 1\right)$. If we approximate S_+/S by the ratio of lengths of the lines of turning points in the x-y-plane, we obtain

$$S_+ = \begin{cases} 0 & \text{for} \quad E < \varepsilon \\ \frac{1}{2}\left(1 - \sqrt{\frac{\varepsilon}{E}}\right) & \text{for} \quad E > \varepsilon \end{cases}$$

which is plotted, too, in Fig. 4. (Refined classical models – e.g. using $1/p_\pm$ with $p_\pm = \sqrt{2M(E - U_\pm)}$ for the probability distribution function – do not lead to better quantitative agreement with the quantum mechanical result.)

---

[1] Only states with $m = 0$ may be reached by optical transitions from the vibrational groundstate of A [5].

However, contrary to the classical model, the quantum mechanical model shows pronounced oscillations of S_+ for $E > \varepsilon$. According to the Franck-Condon principle these should also show up in the line shape and explain the appearance of a third peak for large ε values. In Fig. 2, $\varepsilon = 64\,\omega_0$, and Fig. 4 ($\varepsilon = 32\,\omega_0$), we can even observe a further shoulder on the high energy side of the spectrum.

The maxima in the S_+-curve should correspond to metastable resonances in the upper potential well (see Fig. 3). As the well is very narrow (for $\varepsilon \gg \omega_0$) and extremely anharmonic, we expect that the energy spacings between the lowest levels are much larger than ω_0 and decrease with increasing quantum number. Furthermore, as the lowest states have their density maxima near the origin, they will lead to large Franck-Condon factors. Therefore, one might expect, that on the tail of the main progression (beginning at $E = \omega_0$, with rather harmonic spacings ω_0 and intensity maximum somewhat below $E = \varepsilon$) there is superimposed a second anharmonic progression with large spacings, with the first and most intense line somewhat above $E = \varepsilon$.

However, as the lowest states of the upper potential well are located near the branching point of the potential surface, they will show a large probability of changing over to the lower potential well. In other words, those states of the upper well, which give rise to strong transitions, will most strongly interact with the quasicontinuum of the broad lower well. Therefore we obtain only one single progression as shown for $\varepsilon = 16\,\omega_0$ in Fig. 2. This corresponds to the fact, that even for the second and third maximum, the probability of the final state to be on the inner part of the potential surface, is much smaller than 50% as is shown in Fig. 4.

Nevertheless, as the higher maxima in the absorption band are associated with the resonances in the upper well, their energy values E_n should be calculable from the quasiclassical quantisation rule:

$$\int_0^{r_t(E_n)} \sqrt{2M(E_n - (1 + r/R_0)^2)}\,dr = n\pi, \qquad n = 1, 2, 3 \ldots \tag{2}$$

Here we have omitted the pseudocentrifugal term of the potential in order to solve the integral in closed form, but have retained the restriction of the integration variable to positive values. Eq. (2) has been solved approximately in Appendix B. From there we obtain

$$\boxed{\Delta E \approx 1.65 \sqrt[3]{\varepsilon\omega_0^2}}$$

for the energy gap between the first two resonance states, which compares favourably well with the quantum mechanically calculated splitting between the second and third peaks of the spectra. The energy distance to the next maximum is somewhat smaller (see Fig. 4) and comes out to be $\Delta E \approx 1.39 \sqrt[3]{\varepsilon\omega_0^2}$.

From this discussion it is evident, that the additional vibronic splitting of the band shape is not an artifact of our simple model potential and should show up, too, in the case of more realistic ones, including higher order terms in the J. T. coupling, spin-orbit interaction and unharmonicity of the zero-order energy.

Effective Spin-Orbit Splitting

We now investigate the case where the spin-orbit coupling constant no longer vanishes. As is well known [7] and is evident from the adiabatic energy surfaces (see Fig. 1) the Jahn-Teller effect is suppressed by strong spin-orbit interaction. Similarly, a strong Jahn-Teller coupling quenches the spin-orbit coupling. The physical importance of this phenomenon was established by Ham [8] and is since then called the Ham-effect. The Ham-effect shows up e.g. in the reduced spin-orbit splitting of vibronic levels, if the Jahn-Teller coupling is switched on; this may be seen in a recent calculation of one of the authors (Figs. 3, 4 of

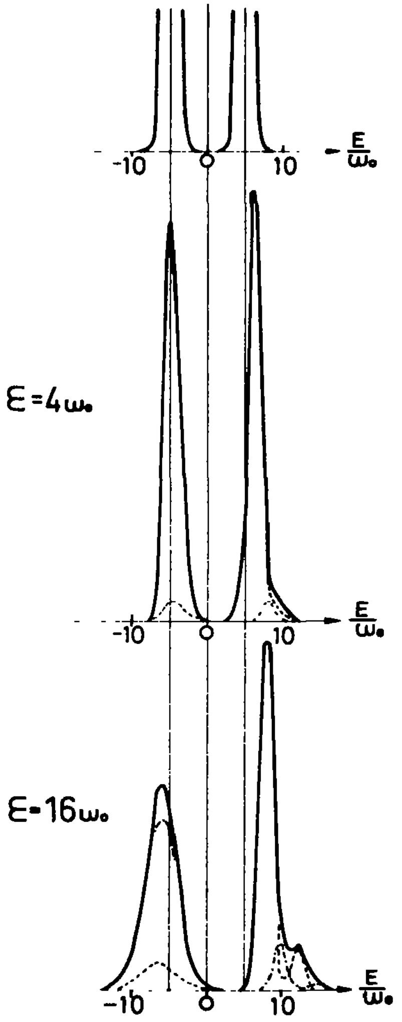

Fig. 5. Line shape of an electronic $^2A \to {}^2E$ transition at 0° K, calculated from $E \times e$ vibronic states. Natural line width $= 2\,\omega_0$, Jahn-Teller energy $\varepsilon = 0, 4, 16\,\omega_0$; spin-orbit splitting $\lambda = 10\,\omega_0$. The broken curves correspond to the intensities of the two spin-components

Ref. [6]). Contrary to this, we see from Fig. 5 that the effective spin-orbit splitting of a non-resolved vibrational band system becomes larger, if an additional Jahn-Teller coupling increases (see, too, Fig. 4 of Ref. [6]).

We have applied the simple semiclassical model to the case of nonvanishing spin-orbit coupling. One rather easily obtains for the peak distance

$$\Delta E_{\mathrm{vib+so}} = \mathrm{Max}\{\lambda; \sqrt{4\varepsilon\omega_0}\}$$

This obviously does not correspond to our quantum-mechanical result (Fig. 5), which can phenomenologically be described rather well by the equation

$$\boxed{\Delta E_{\mathrm{vib+so}} = \sqrt{4\varepsilon\omega_0 + \lambda^2}} \tag{1}$$

This corresponds to a superposition of both the vibronic and spin-orbit splitting as two independent effects.

We also used the refined semiclassical model. However, it seems not to be possible to get a closed formula for the splitting, and the equations must be solved numerically. The results are in good agreement with the quantum-mechanical result as well as with the empirical Eq. (1).

Jahn-Teller Coupling and Vibrational Broadening

Finally we consider the case $Z_0 \neq 0$. We give a preliminary remark about the order of magnitude of Z_0: Let us describe the potential energy by some Valence Force Field model. In many cases, the J.T. active vibration is of the streching type or at least includes a marked bond stretching. Now, if the bond stretching parameters (i.e. bond lengths and valence force constants) will change upon electronic excitation to the degenerate E state, the parameters of all the stretching normal vibrations, including the a_{1g} mode, will change simultaneously.

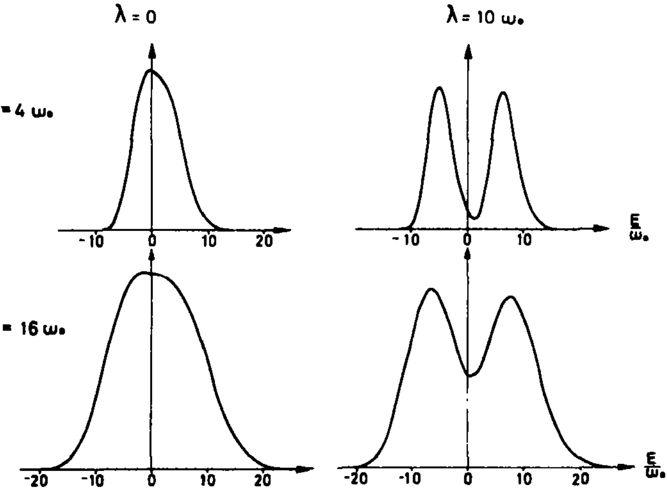

Fig. 6. Line shape of an electronic $^2A \rightarrow {}^2E$ transition at 0° K; $E \times e$ Jahn-Teller coupling (Jahn-Teller energy $= 4, 16\,\omega_0$) and a corresponding vibrational broadening by an a-mode; natural line width $2\,\omega_0$: spin-orbit splitting 0 and $10\,\omega_0$. Compare Fig. 2

(A special example is discussed in Chapter 5.) Therefore, the vibronic structure in the absorption line shape, caused by a strong dynamical J. T. effect in the upper state, will usually be smoothed by strong vibrational broadening due to the a_{1g} mode. As the additional splitting of the absorption line is much weaker than the main vibronic splitting we expect that the former one will usually be suppressed. Furthermore, at nonzero temperature hot bands will contribute, too, in this direction.

Line shapes for the case, where $k = k_z$ and $R_0 = Z_0$, are plotted in Fig. 6. Even the main vibronic splitting is smeared out, and we only obtain an asymmetric band with a shoulder on the high-energy side. Such line-shapes are experimentally realized e.g. in the spectra of many Ti^{3+} L_6-complexes [10], whereas in other cases (see e.g. Refs. [11]) line shapes are obtained which are intermediate between those of Figs. 2 and 6. No experimental spectra are known to us which are identical with those calculated without allowance for vibrational broadening by an a mode. Especially the only experimental hint for a third peak is supposed to be an artifact [11a]. Finally we remark that irrespective of an additional vibrational broadening the line-shape remains asymmetric and the effective splitting (that is the peak distance of two gaussians, into which the spectrum may be decomposed) is empirically given by the relation (1).

4. Line Shapes of Electronic $A \rightarrow E$ Transitions for Jahn-Teller Coupling Case A

In Fig. 7 we have drawn absorption line shapes of electronic $A \rightarrow E$ transitions with Jahn-Teller case A vibronic coupling. In the case of zero spin-orbit interaction we only observe vibrational broadening of the bands, but no asymmetry and no vibronic splitting as in case B.

As mentioned before, the adiabatic potential surfaces for case A and B are topologically equivalent, if we take a spin-orbit coupling into account. Therefore we except some similarity of case B band shapes and case A band shapes if $\lambda \neq 0$. And indeed, as is seen on the left side of Fig. 7, both phenomena are exhibited by the calculated ${}^2A \rightarrow {}^2E$ band shapes: a) the additional vibronic structure and b) the enhancement of the effective spin-orbit splitting by vibronic coupling. However, these vibronic effects only show up if there is strong spin-orbit interaction. And they are rather strongly suppressed by an additional a_{1g} vibrational broadening (see rhs. of Fig. 7). If R_0 and Z_0 are of comparable magnitude any asymmetry is no longer observable.

As for case B, the simple semiclassical model is not capable of reproducing the quantum mechanically calculated vibronic effects even qualitatively. On the other hand the refined semiclassical model predicts band shapes in rough agreement with Fig. 7. But we did not succeed in obtaining closed formulae for the splitting. Therefore we only give an empirical formula, which is fitted to the quantum mechanical results and reproduces them within $0.1\,\omega_0$ for parameter values in the range of $\lambda < 20\,\omega_0$ and $\varepsilon < 64\,\omega_0$:

$$\boxed{\Delta E_{\mathrm{so+vib}} = \sqrt{\lambda^2 + \omega_0 \cdot \sqrt[3]{20\,\lambda\varepsilon^2}}}$$

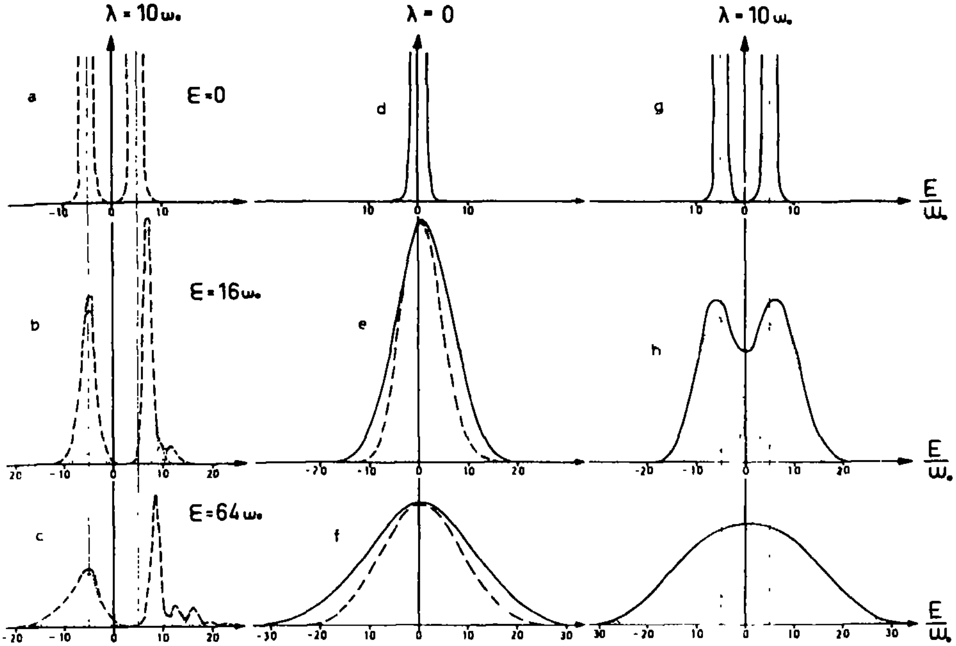

Fig. 7. Line shape of an electronic $^2A \rightarrow {}^2E$ transition at 0° K. $E \times b$ Jahn-Teller coupling case A. Broken curves without, full curves with an additional vibrational broadening ($Z_0 = R_0$). Jahn-Teller energy $\varepsilon = 0, 16, 64\,\omega_0$; spin-orbit splitting $\lambda = 0, 10\,\omega_0$; natural line width $2\,\omega_0$. The dotted curves correspond to the two spin-components of the transition

5. An Experimental Example

The presented investigation has been induced by difficulties in the interpretation of the main absorption lines in the XUV-spectrum of XeF_4 in the 200 Å region [13], which correspond to excitations of a xenon $4\,d_{3/2}$ or $4\,d_{5/2}$ electron into the lowest empty molecular orbital. XeF_4 has D_{4h} symmetry (see Fig. 8) and its LEMO is of e_u type. It may be approximated by xenon $5\,p_{x,y}$ – AO's, which are occupied in xenon itself but are nearly empty in the molecule because of the strong electronegativity of the fluorine ligands [14].

The spin-orbit splitting of the $4d$ level has been estimated to be 1.95 ± 0.01 eV and that of the e_u level to be about $0.6 - 0.7$ eV [13]. The possible four one-electron transitions are shown in Fig. 9. They are split and shifted by a) the field of the $F^{\delta-}$ ligands and b) the $4d$ hole-e_u electron interaction. The corresponding parameters have been estimated from results of a molecular SCF calculation [14]. The main transition energies and intensities then calculated are given in Table 2.

From this Table we see two deviations of the calculated from the measured values: 1) the splittings between peaks 1 and 2 and between peaks 3 and 4 are about 0.15 eV larger than calculated on the basis of an e_u spin-orbit splitting of 0.7 eV; 2) peak 4 is calculated so weak that it would not at all be observable. Now the two xenon $5p$ – AO's correlate with the σ_u-LEMO's of the $F_1 - F_3$ and $F_2 - F_4$ entities (see Fig. 8) and, therefore, are strongly antibonding. From our

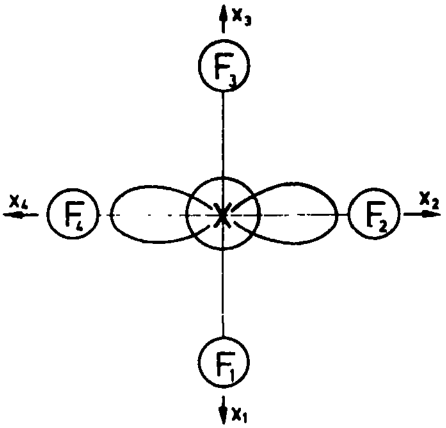

Fig. 8. Planar XF_4-molecule with D_{4h}-symmetry

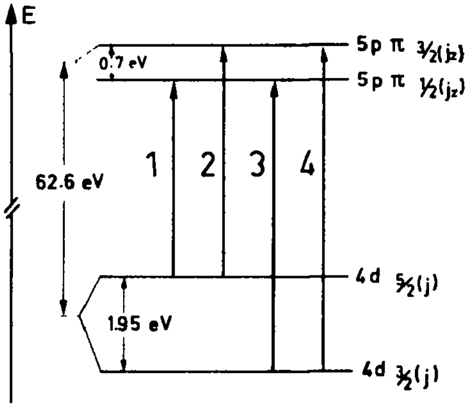

Fig. 9. One-electron levels engaged in the 60–65 eV excitations of XeF_4

Table 2. Xenon $4d \rightarrow$ "$5p$" transitions in XeF_4

Peak	Relative energy values in eV[a]			Relative intensities referring to a total of 2		
	Measured	Calculated		Measured	Calculated	
		With J. T. E.	Without J. T. E.		With J. T. E.	Without J. T. E
1	-1.5_0	-1.52	-1.45	0.3_5	0.3_8	0.3_3
2	-0.4_0	-0.36	-0.45	0.6_5	0.6_3	0.6_8
3	0.7_0	0.70	0.77	0.7	0.8_2	0.9_5
4	1.5_0	1.49	1.40	0.3	0.1_7	0.0_4

[a] The energy values refer to the center of gravity.

experience with XeF_2 [13] we expect an expansion of the corresponding Xe-F equilibrium distance of about $R_0 = 1/3$ Å leading to D_{2h} symmetry. This shoul give rise to a dynamical Jahn-Teller effect in the absorption spectrum.The A_1 ground state of XeF_4 shows 7 normal vibrations: three bond stretching one

(a_{1g}, b_{2g}, e_u), two in-plane bending ones (b_{1g}, e_u; the latter one is mixed to only a small degree with the e_u stretching mode [15]) and two out of plane bending ones (a_{2u}, b_{1u}). We expect that in the excited state only the bond lengths but not the equilibrium bond angles will be changed. Therefore the equilibrium values of the stretching symmetry coordinates only will change upon excitation. Furthermore, none of the bending modes will correlate with a_g under D_{2h} symmetry. Consequently there will occur no progressions of bending vibrations to any appreciable extent. This especially holds for the J. T. active b_{1g} mode and means that our problem is an example of J. T. case A. As the $4d-e_u$ hole-electron interaction is rather weak [13], we may treat the excitations within the one-electron picture, that is the transitions may be looked at as ${}^2A_{1g} \rightarrow {}^2E_u$ (and ${}^2E_g \rightarrow {}^2E_u$) transitions.

If we restrict ourselves to the internal stretching coordinates x_1, x_2, x_3, x_4 (see Fig. 8) and use the Modified Valence Force Field model, which is described in appendix C, the calculation leads to results which are also given in Table 2. We see that the theoretical energy splittings and the intensity values of peaks 3 and 4 are significantly improved, if the Jahn-Teller coupling is included. Furthermore the calculation with the parameters as chosen above reproduces the measured half width's of the absorption lines of about 0.7 eV [14].

The parameter values are near those of Fig. 7h: Each of the four one-electron transitions in XeF_4 roughly corresponds to one of the broken curves of Fig. 7h. They show the enhancement of the effective spin-orbit splitting by J. T. coupling and account for the energy difference of 0.15 – 0.2 eV mentioned at the beginning of this chapter. According to the mixing of pure spin-orbit states by the J. T. coupling, the broken curves exhibit a second shoulder which considerably contribute to the intensity of the two weak peaks 1 and 4.

6. Appendix

A. Calculational Details

All the quantum mechanical calculations have been performed numerically on an IBM 370 computer in a basis set of two- or three-dimensional harmonic oscillator functions. Most of the occuring integrals over generalized Laguerre polynomials $L_k^m(x)$ may be found in Refs. [5, 16]. Furthermore for the calculation of S_+-values (see chapter 3) one needs the integrals

$$S_{\mu\nu} = \int_0^\infty \frac{1}{\left(\frac{\mu-1}{2}\right)!} \cdot e^{-\frac{r^2}{2}} \cdot L^0_{\frac{\mu-1}{2}}(r^2) \times \frac{r}{\frac{\nu}{2}!\sqrt{\frac{\nu}{2}}} \cdot e^{-\frac{r^2}{2}} \cdot L^0_{\frac{\nu}{2}}(r^2) \times r\,dr$$

with μ odd and ν even. For these quantities, we obtained

$$S_{\mu\nu} = \sqrt{\frac{\pi}{2\nu}}\,(-1)^{\frac{\mu+\nu+1}{2}} \cdot \sum_{r=0}^{s} (-1)^r \cdot \prod_{t=0}^{\frac{\mu-1}{2}-r} \left(\frac{1.5}{t}-1\right) \cdot \prod_{t=1}^{\frac{\nu-2}{2}-r} \left(\frac{0.5}{t}-1\right) \cdot \prod_{t=1}^{r} \left(\frac{-0.5}{t}-1\right)$$

with s the smaller of the two integers $\frac{\mu-1}{2}$ and $\frac{\nu-2}{2}$. The products over t are to be set equal to unity, if their upper limit is zero.

For the calculation of the intensities we need the following integrals over the ususal harmonic oscillator functions $\varphi_n(z)$:

$$\int_{-\infty}^{+\infty} \varphi_0(z)\cdot\varphi_n(z+Z_0)\cdot dz = \sqrt{\frac{\eta^n}{n!}}\, e^{-\eta}$$

with $\eta = \frac{k_z}{2\omega_z} Z_0^2$. This result is obtained using the relation

$$\langle\varphi_0|Z^l|\varphi_n\rangle = \begin{cases} \dfrac{l!}{\sqrt{n!(2k_z/\omega_z)^l}\cdot 2^{\frac{l-n}{2}}\cdot\left(\frac{l-n}{2}\right)!} & \text{if } l-n \text{ even and non-negative} \\ \text{zero otherwise}. \end{cases}$$

B. Quasiclassical Energy Levels

Solving the integral of Eq. (2), one obtains after substitution by $\arcsin x = \frac{\pi}{2} - \arcsin\sqrt{1-x^2}$

$$\pi n\,\omega_0 = E_n\left(\arcsin\sqrt{1-\frac{\varepsilon}{E_n}} - \sqrt{\frac{\varepsilon}{E_n}\left(1-\frac{\varepsilon}{E_n}\right)}\right).$$

We are interested in the E_n-values for small n, for which $\delta = \sqrt{\frac{E_n}{\varepsilon}} - 1 \ll 1$. In terms of δ, the equation reads

$$\frac{\pi n\,\omega_0}{\varepsilon} = (1+\delta^2)\cdot\arcsin\sqrt{\frac{\delta^2}{1+\delta^2}} - \delta \approx \frac{2}{3}\delta^3 - \frac{2}{15}\delta^5 + O(\delta^7).$$

If we retain only the first term of the power series, which is justified in the case of small δ, that is small n and large ε, the equation can be solved approximately for the E_n:

$$E_n = \varepsilon\left[1+\left(\frac{3\pi n}{2}\,\frac{\omega_0}{\varepsilon}\right)^{2/3}\right].$$

C. Bond stretching MVFF *for* XeF_4

$x_i (i = 1, 2, 3, 4)$ are the internal stretching coordinates of XeF_4 as indicated in Fig. 8. The potential energy of the A_{1g} ground state of XeF_4 is then written as

$$V(A_{1g}) = \frac{k}{2}\sum_{i=1}^{4} x_i^2 + \frac{k'}{2}\sum_{i=1}^{4} x_i(x_{i+1}+x_{i+2}+x_{i+3}).$$

In terms of symmetry coordinates,

$$\alpha_{1g}=\tfrac{1}{2}(x_1+x_2+x_3+x_4)$$
$$\beta_{2g}=\tfrac{1}{2}(x_1-x_2+x_3-x_4) \qquad (3)$$
$$\varepsilon_{u1}=\tfrac{1}{2}(x_1-x_3) \quad \varepsilon_{u2}=\tfrac{1}{2}(x_2-x_4),$$

this reads as

$$V(A_{1g})=\frac{k+2k'}{2}\alpha_{1g}^2+\frac{k}{2}\beta_{2g}^2+\frac{k-k'}{2}(\varepsilon_{u1}^2+\varepsilon_{u2}^2)$$

leading to the following normal frequencies

$$\omega(a_{1g})=\sqrt{(k+2k')/M_F}$$
$$\omega(b_{2g})=\sqrt{k/M_F}$$
$$\omega(e_u)=\sqrt{(k-k')(1-2M_F/M_{Xe})/M_F}\,.$$

M_F and M_{Xe} are the masses of the atoms F and Xe, respectively. With the force constants $k=3.12\,\frac{\text{mdyn}}{\text{Å}}$ and $k'=\frac{k}{20}$ the measured values [15] can be reproduced nearly exactly. We now approximate the potentials of the excited E_u state by

$$V_1(E_u)=\frac{k}{2}[x_1^2+x_3^2]+\frac{\tilde{k}}{2}[(x_2-R_0)^2+(x_4-R_0)^2]+\frac{k'}{2}\sum_{i=1}^{4}x_i(x_{i+1}+x_{i+2}+x_{i+3})$$
$$V_2(E_u)=\frac{k}{2}[x_2^2+x_4^2]+\frac{\tilde{k}}{2}[(x_1-R_0)^2+(x_3-R_0)^2]+\frac{k'}{2}\sum_{i=1}^{4}x_i(x_{i+1}+x_{i+2}+x_{i+3})$$

where we have assumed, that the small coupling force constant k' as well as the force constant k of the Xe-F bonds, not directly engaged with the excited electron, have not changed. Transformation to the coordinates given by Eqs. (3) yields (despite a constant term)

$$V_{1,2}(E_u)=\frac{k_\alpha}{2}(\alpha_{1g}-\varrho_\alpha)+\frac{k_\beta}{2}(\beta_{2g}\mp\varrho_\beta)\pm\Delta\cdot\alpha_{1g}\cdot\beta_{2g}+\frac{k-k'}{2}\varepsilon_{u1,2}^2+\frac{\tilde{k}-k'}{2}\varepsilon_{u2,1}^2$$

with

$$k_\alpha=\frac{k+\tilde{k}}{2}+2k', \quad k_\beta=\frac{k+\tilde{k}}{2}$$

and

$$\varrho_\alpha=\frac{\tilde{k}}{k_\alpha}R_0, \quad \varrho_\beta=\frac{\tilde{k}}{k_\beta}R_0.$$

From our model, which will be correct to first order, we see, that only the a_{1g} and b_{2g} vibrational modes are strongly influenced by the electronic excitation, whereas the e_u mode is only slightly split (into b_{2u} and b_{3u} of D_{2h}) by different force constants but does not exhibit a change in the equilibrium value.

We have calculated the absorption line shape from $E_u\times a_{1g}\times b_{2g}$ vibronic states using the parameters as given above and $\tilde{k}=0.8\,k$. The final shape is not very sensitive to this latter choice.

Acknowledgement. We want to express our gratitude to Prof. Ballhausen, many comments of whom have greatly improved this manuscript.

The numerical calculations have been carried out on the IBM installation of the GMD at Bonn. We are grateful for computer time.

References

1. Jahn, H. A., Teller, E.: Proc. Royal Soc. (London) **A161**, 220 (1937).
2. Herzberg, G.: Molecular spectra and molecular structure, III. New York: Van Nostrand 1966; – Sturge, M. D.: Solid State Physics **20**, 91 (1967); – Ham, F. S.: In: Electron paramagnetic resonance, Ed. S. Geschwind. New York: Plenum Press 1971; Int. J. Quant. Chem. Symp. **5**, 191 (1971); – Englman, R.: The Jahn-Teller effect. London: Wiley 1972.
3. Ruch, E., Schönhöfer, A.: Theoret. chim. Acta (Berl.) **3**, 291 (1965).
4. Wagner, M.: Z. Physik **230**, 460 (1970).
5. Longuet-Higgins, H. C., Öpik, U., Pryce, M. H. L., Sack, H.: Proc. Royal Soc. (London) **A244**, 1 (1958); Ballhausen, C. J.: Theoret. chim. Acta (Berl.) **3**, 368 (1965).
6. Schenk, H. J., Schwarz, W. H. E.: Theoret. chim. Acta (Berl.) **24**, 225 (1972).
7. Öpik, U., Pryce, M. H. L.: Proc. Royal Soc. (London) **A238**, 425 (1957).
8. Ham, F. S.: Physic. Rev. **166**, 307 (1968).
9. O'Brien, M. C. M.: Proc. physic. Soc. (London) **86** 847 (1965).
10. Hartmann, H., Schläfer, H. L., Hansen, K. H.: Z. anorg. allg. Chem. **284**, 153 (1956); **289**, 40 (1957); – Pittel, B., Schwarz, W. H. E.: Ber. Bunsenges. **76**, 1025 (1972).
11. Cotton, F. A., Meyers, M. D.: J. Amer. chem. Soc **82**, 5023 (1960); Jones, G. D.: Physic. Rev. **155**, 259 (1967); Freeman, T. F., Jones, G. D.: Physic. Rev. **182**, 411 (1969).
12. Vekhter, B. G., Tsukerblat, B. S., Rosenfeld, Yu. B.: Theoret. chim. Acta (Berl.) **27**, 49 (1972).
13. Comes, F. J., Haensel, R., Nielsen, U., Schwarz, W. H. E.: J. chem. Physics **58** (1973).
14. Basch, H., Moskowitz, J. W., Hollister, C., Hankin, D.: J. chem. Physics **55**, 1922 (1971).
15. Tsao, P., Cobb, C. C., Claassen, H. H.: J. chem. Physics **54**, 5247 (1971).
16. Schrödinger, E.: Ann. Physik **80**, 483 (1926).

Dr. E. Schwarz
Lehrstuhl für Theoretische Chemie
der Universität Bonn
D-5300 Bonn
Wegelerstr. 12
Federal Republic of Germany

Theoret. chim. Acta (Berl.) 28, 283 -296 (1973)
© by Springer-Verlag 1973

On Radial Weighting Effects in Gaussian Expansions of Self-Consistent Field Atomic Orbitals*

S. Ehrenson and M. Wong**

Chemistry Department, Brockhaven National Laboratory, Upton, New York 11973

Received May 12, 1972

Gaussian expansions of the SCF functions for the first row atoms, boron through fluorine, in ground and low-lying electronic states have been generated under a wide range of radial weighting conditions by a full least-squares procedure. Typical results are presented and the quality of the wavefunctions obtained are analyzed in terms of regional electron densities and a variety of expectation values including energies. A novel method for recursive evaluation of repeated integrals of the error function, $F_l(\alpha, \zeta)$, is adopted and analyzed. These integrals are central quantities in the least-squares procedure employed.

Engendrement de représentations gaussiennes des fonctions SCF pour les atomes de la première ligne, du bore au fluor, dans les états électroniques fondamentaux et faiblement excités, avec un large éventail de conditions de pondération radiale obtenues par une procédure de moindres carrés. Des résultats typiques sont présentés et les qualités des fonctions d'onde obtenues sont analysées en fonction des densités électroniques par régions et de différentes valeurs moyennes dont les énergies. Adoption et analyse d'une nouvelle méthode pour l'évaluation récursive d'intégrales répétées de la fonction d'erreur $F_l(\alpha, \zeta)$. Ces intégrales sont des quantités centrales dans les procédures de moindres carrés utilisées.

Entwicklungen nach Gaußfunktionen für SCF-Funktionen von Elementen der ersten Reihe (Bor bis Fluor) wurden für den Grundzustand und niedrige angeregte Zustände einer Methode der kleinsten Quadrate berechnet, wobei eine Reihe von radialen Gewichtsfaktoren benutzt wurden. Einige typische Ergebnisse werden mitgeteilt und die Qualität der erhaltenen Wellenfunktion wird mit Hilfe von regionalen Elektronendichten und einer Reihe von Erwartungswerten sowie der Energie geprüft. Eine neue Methode für die rekursive Auswertung der mehrfachen Integrale der Fehlerfunktion $F_l(\alpha, \zeta)$ wird angewendet und analysiert. Diese Integrale sind von zentraler Bedeutung in der benutzten Methode der kleinsten Quadrate.

Introduction

Gaussian-type orbital (GTO) sets have recently supplanted minimal Slater-type atomic orbital (STO) sets as routine basis function choices in linear combination of atomic orbitals-molecular orbital (LCAO MO) calculations, principally because of differences in efficiency of calculation of two-electron integrals. Nevertheless, the extensive body of results obtained with the minimal STO bases have been, and continue to be of much use as benchmarks for calculations with GTO sets. Extrinsically, comparisons of goodness, usually in the sense of energy, are made of the LCAO MO SCF functions constructed from the alternative atomic functions [1]. More directly, considerable effort has been spent in obtaining accurate analytical GTO expansions of the STO's and optimized SCF STO atom ground state functions, with the purpose of simultaneously realizing the advantages of both types of functions in future calculations [2].

---

* Research performed under the auspices of the U.S. Atomic Energy Commission.

** Summer student program participant, 1971, from Swarthmore College, Swarthmore, Pa.

In a recent paper [3], the optimization method of least-squares fitting of GTO sums to 1*s*, 2*s* and 2*p* STO's was reexamined, and the conclusion was drawn that radial weighting in the fitting procedure was potentially useful, depending upon the intended application of the expansion function. In this paper further examination is made of the effects of weighting on AO representations. Specifically, modest size expansions of Clementi's SCF atomic functions [4] for first row atoms are generated under a wide range of radial weighting constraints, and various expectation values, regional electron densities and energies are computed. These are compared to those obtained from the SCF STO functions directly, and from GTO functions obtained by other expedients (i.e., direct energy minimization). Certain generalizations concerning these comparisons are discussed, as are their implications with regards to fitting of functions obtained from other sources, e.g., empirically, from experimental determination of electron densities by particle or photon scattering.

Expansion Methods

The least-squares error functions for the SCF STO AO expansions weighted by r^n and subject to explicit normalization are defined as,

$$\begin{aligned}\varepsilon_n &= \int(\psi-\psi'_n)^2\, r^n d\tau + \lambda_n\left(1-\int(\psi'_n)^2\, d\tau\right)\\ &= \iiint(\psi-\psi'_n)\, r^{n+2} dr \sin\theta\, d\theta\, d\phi + \lambda_n\left(1-\iiint(\psi'_n)^2\, r^2 dr \sin\theta\, d\theta\, d\phi\right),\end{aligned} \tag{1}$$

where,

$$\psi_k = \sum_j a_{jk}\, \phi_j\,, \tag{2}$$

and ϕ_k and a_{jk} are, here, respectively the STO's and combination coefficients for the ground state SCF AO's of the first row atoms [4]. The functions ψ'_n are,

$$\begin{aligned}\psi'_{ms,n} &= \sum_j d_{ms,n,k}\left(\frac{2\alpha_{ms,n,k}}{\pi}\right)^{3/4} \exp(-\alpha_{ms,n,k}\cdot r^2)\\ \psi'_{2p,n} &= \sum_j d_{2p,n,k}\left(\frac{128\alpha^5_{2p,n,k}}{\pi^3}\right)^{1/4} \cos\theta\, r \exp(-\alpha_{2p,nk}\cdot r^2)\,.\end{aligned} \tag{3}$$

Note, the 2*s* SCF AO's are expanded in terms of 1*s*-type GTO's and no interorbital constraints are placed on the exponents.

Eqs. (1–3) are identical in their origins and representation to those derived and used in Ref. [3], with the important exception that the functions to be expanded correspond closely to real atom states at or near the Hartree Fock level. Solution of these equations, i.e., minimization of ε_n at any expansion level as a function of the α and d parameters is accomplished in the same way as in Ref. [3] with the following noteworthy difference.

The STO- and GTO-containing integrals of the form,

$$\int_0^{\infty} r^l \exp(-\alpha r^2 - \zeta_{\text{STO}} r)\, dr\,, \tag{4}$$

lead in the course of evaluation to repeated integrals of the error function, $i^l \operatorname{erfc} Z$, where Z is $\zeta_{STO}/2\alpha^{1/2}$. Unlike the previous study, where unit exponent STO's limited the Z-range to less than 2.7, integrals with large Z are encountered here. Details of the novel method adopted for computation of these integrals, based on a recursive technique due to Gautschi [5], are presented in the Appendix. It is a matter of some interest that this technique, based on second-order difference equation solution methods, simultaneously generates all integrals (l, from zero to l_{max}) to controllable accuracy without recourse to Gauss-Laguerre quadrature procedures, an expedient followed by all other investigators of the least-squares GTO expansion problems cited.

Other procedural differences, as regards Ref. [3], of a more mechanical nature, include routine variation of initial choice of the Lagrangian multiplier, λ, to facilitate convergence of the least-squares method, and geometric mean extrapolation of parameters based on residuals of previous cycles when divergence in the iterative procedure is encountered. In many cases, especially for the 2*s* SCF expansions, initial guesses of λ (as well as of the α and d values) guided by converged results of neighboring weighted cases often speeded convergence. Where instability after several cycles led to divergence in the least-squares procedure, it was often found useful to adjust new initial guesses of the parameters by assuming proportionality of changes in these parameters with the changes in residuals, $\varepsilon'_{n,j}(P^0)$, see Ref. [3], Eq. (5), and then extrapolating by assuming a geometric mean relationship [6].

Expansion Results, Radial Densities and Simple Expectation Values

Tables 1–3 list the three-, four- and five-term GTO expansion coefficients and exponents for the 1*s*, 2*s* and 2*p* SCF functions for N(^{4}S), and, as well, various fitting measures, electron densities at arbitrarily chosen values of r and r-dependent expectation values. The results are typical for all the first row atoms in various electronic states examined; similar compilations for boron through fluorine and the unit-zeta STO functions are available from the author on request. The radial weighting factor range is from r^{-2}, stressing the region close to the nucleus, to r^3, stressing regions rather far away. The fitting measures EPSBAR ($\bar{\varepsilon}_n$) and $1 - S_n$ are defined in the footnotes, and are as in Ref. [3]. In all cases, for the square matrix of second derivatives over the coefficient and exponent parameters, the eigenvalues were positive, indicating a minimum in ε_n.

Most of the effects of weighting upon parameter sizes, measures of fitting, etc., noted for STO functions [3] are also observed for the SCF atomic functions. Important new details and differences, beyond the obvious scaling effects to be expected, are as follows.

In general, the $\bar{\varepsilon}_n$-values ($\varepsilon_n/\langle r^n \rangle$) at any level of expansion are larger for the SCF than the STO functions, being most noticeably so for the 2*s* functions and only somewhat less apparent for the 2*p* functions. The magnitude of the effect varies with the weighting constraint. It is also apparent when all the first row atomic state results are examined, that for the unweighted and positively weighted expansions, the fitting for all orbitals worsens proceeding from B to F. For the those obtained by direct energy optimization of GTO expansions of the same length [7].

The most immediate and striking observation, verified to be general for all the first row atoms in all states examined, is that *the r^{-1}-weighted expansions yield significantly better total energies than the unweighted expansions.* Functions generated under other weighting constraints are generally poorer. Of almost equal significance is the fact that the better 2s expansions (by ε_n criteria) are often poorer as regards total energy. In general, over all cases examined and independent of the level of expansion, around the coefficient crossover points, the better energy is associated with the expansion having the greater number of subtractive, highly contracted GTO terms.

Both of these observations, pertinent to the general issue of function expansion may be further examined and rationalized as follows. Of the components of total energy, the potential energy term is expected, and found to be most satisfactorily represented by r^{-1}-weighted expansion because its integrals have forms resembling $\langle r^{-1}\rangle$. The kinetic energy components are more complicated, the requisite Laplacians on GTO's leading to multiple-term, internally cancelling expectation values of powers of (αr). For the weighting variations considered, the potential energy dominates, and hence the best integral power for weighting is -1. That the 2s function with the maximum of subtractive, contracted GTO

TABLE [illegible]. COEFFICIENTS AND EXPONENTS FOR THE WEIGHTED GAUSSIAN EXPANSIONS OF THE 2S SCF FUNCTION OF NITROGEN (4S)

		3-TERM			4-TERM			5-TERM		
N	<R**N>	EXPONENT	COEFFICIENT	EPSHAR 1-S	EXPONENT	COEFFICIENT	EPSHAR 1-S	EXPONENT	COEFFICIENT	EPSHAR 1-S
-2	4.[illegible]5311([illegible])	[illegible]4(-1)	1.01347(0)	2.57(-3)	[illegible](-1)	1.02211(0)	5.69(-4)C	1.65258(-1)	3.60548(-1)	2.80(-4)
		[illegible](1)	-2.64741(-1)	5.78(-3)	1.0[illegible]69[illegible](1)	-2.50379(-1)	5.74(-3)	5.44351(-1)	7.24040(-1)	1.41(-4)
		[illegible]	-3.10943(-2)		6.51747(1)	-5.78860(-2)		9.21116(0)	-2.57515(-1)	
					[illegible](2)	-4.59717(-3)		5.72308(1)	-6.64981(-2)	
								6.95577(2)	-5.39844(-3)	
-1	1.[illegible]781[illegible]	[illegible](-1)	1.31859(0)	4.12(-3)A	1.79691(-1)	4.[illegible]7253(-1)	8.05(-4)D	1.96147(-1)	4.73270(-1)	9.57(-5)
		[illegible](1)	-2.55651(-1)	5.15(-3)	5.71513(-1)	6.78572(-1)	1.38(-4)	6.29242(-1)	6.26294(-1)	4.13(-5)
		[illegible](1)	-5.39714(-2)		9.29198(0)	-2.56240(-1)		7.34492(0)	-2.36895(-1)	
					[illegible](1)	-6.46615(-2)		3.33869(1)	-9.54704(-2)	
								2.47509(2)	-1.48764(-2)	
0	1.00000(0)	[illegible](-1)	[illegible]8854(-1)	[illegible](-3)B	1.90151(-1)	4.53826(-1)	1.81(-4)	1.92816(-1)	4.62512(-1)	9.60(-5)G
		[illegible](-1)	6.96[illegible]59(-1)	1.75(-3)	6.17295(-1)	6.45784(-1)	[illegible]92(-5)	6.22840(-1)	6.37994(-1)	3.69(-5)
		1.14[illegible](1)	-2.95026(-1)		[illegible]	-2.49889(-1)		7.03189(0)	-2.23924(-1)	
					4.5[illegible](1)	-8.85441(-2)		2.75775(1)	-1.00831(-1)	
								1.54073(2)	-2.20602(-2)	
1	1.33[illegible]	1.81[illegible](-1)	4.13[illegible](-1)	[illegible](-4)	1.84[illegible](-1)	4.[illegible]8253(-1)	7.39(-4)E	1.21878(-1)	1.42540(-1)	1.81(-5)H
		[illegible]2634[illegible](-1)	6.[illegible]61[illegible]5(-1)	1.35(-3)	5.92891(-1)	6.66147(-1)	9.49(-5)	2.91660(-1)	5.13280(-1)	8.51(-5)
		[illegible](1)	-2.305[illegible](-1)		[illegible]	-2.40369(-1)		7.51186(-1)	4.58358(-1)	
					[illegible]90451(1)	-9.24427(-2)		6.59701(0)	-2.32410(-1)	
								3.08203(1)	-1.15335(-1)	
2	[illegible]14890(0)	1.74[illegible](-1)	[illegible]887[illegible](-1)	5.41(-4)	1.15469(-1)	1.39247(-1)	8.39(-5)F	1.20256(-1)	1.37125(-1)	1.03(-5)
		[illegible](-1)	6.[illegible]7405(-1)	1.29(-3)	2.[illegible]235[illegible](-1)	4.92297(-1)	1.97(-3)	2.88565(-1)	5.14628(-1)	1.25(-4)
		1.2[illegible](1)	-2.89717(-1)		[illegible](-1)	4.98449(-1)		7.50395(-1)	4.63538(-1)	
					[illegible](0)	-2.91647(-1)		6.34569(0)	-2.21649(-1)	
								2.70469(1)	-1.25350(-1)	
3	4.[illegible]9116(0)	[illegible]4941(-1)	3.44442(-1)	[illegible](-4)	1.14477(-1)	1.16288(-1)	5.83(-5)	1.15684(-1)	1.20736(-1)	1.92(-5)
		[illegible](-1)	[illegible]1379(-1)	1.75(-3)	[illegible](-1)	4.44194(-1)	1.46(-3)	2.75324(-1)	5.01412(-1)	1.01(-4)
		1.15744(1)	-[illegible].2595[illegible](-1)		[illegible](-1)	4.97966(-1)		7.21287(-1)	4.88133(-1)	
					[illegible](1)	-2.96521(-1)		6.65583(0)	-2.25594(-1)	
								2.90716(1)	-1.21417(-1)	

SIX SIGNIFICANT FIGURES ARE TABULATED FOR EACH GAUSSIAN PARAMETER. THE APPROPRIATE POWER OF 10 IS ENCLOSED IN PARENTHESES TO THE RIGHT OF EACH ENTRY. THE RADIAL WEIGHTING FACTOR IS N, AND <R**(N)> IS THE EXPECTATION VALUE FOR THE OPERATOR (R**(N)) COMPUTED WITH THE SCF ORBITAL. EPSHAR IS EPS/<R**(N)> AND S IS THE OVERLAP BETWEEN THE SCF AND GAUSSIAN ORBITALS.

A) THE 2 POSITIVE, 1 NEGATIVE COEFFICIENT SET HAS EPSHAR(-1)= 1.21(-2) AND 1-S(-1)= 2.53(-3).
B) THE 1 POSITIVE, 2 NEGATIVE COEFFICIENT SET HAS EPSHAR(0)= 9.52(-3) AND 1-S(0)= 4.75(-3).
C) THE 2 POSITIVE, 2 NEGATIVE COEFFICIENT SET HAS EPSHAR(-2)= 2.23(-3) AND 1-S(-2)= 1.18(-3).
D) THE 1 POSITIVE, 3 NEGATIVE COEFFICIENT SET HAS EPSHAR(-1)= 3.73(-3) AND 1-S(-1)= 5.21(-3).
E) THE 3 POSITIVE, 1 NEGATIVE COEFFICIENT SET HAS EPSHAR(1)= 3.64(-4) AND 1-S(1)= 1.46(-3).
F) THE 2 POSITIVE, 2 NEGATIVE COEFFICIENT SET HAS EPSHAR(2)= 4.96(-4) AND 1-S(2)= 1.02(-4).
G) THE 3 POSITIVE, 2 NEGATIVE COEFFICIENT SET HAS EPSHAR(0)= 1.16(-4) AND 1-S(0)= 4.70(-5).
H) THE 2 POSITIVE, 3 NEGATIVE COEFFICIENT SET HAS EPSHAR(1)= 2.33(-4) AND 1-S(1)= 4.58(-5)

TABLE 2 (continued)

DENSITY ON A PER ELECTRON BASIS AT R (AU)

R	EXP FUNCT	GAUSS FUNCT (WTS) -2	-1	0	1	2	3
0.00000	59.92522	49.11954	39.94979	11.47949	7.43765	7.83172	17.31054
			19.89049	36.93854			
		54.90787	37.93398	29.44905	25.67388	5.12195	5.48563
		48.97632	50.28875		6.88615	37.19627	193.59472
		54.57808	47.51670	41.93715	22.13934	19.96362	22.04056
				28.76381	41.85230		
.05000	29.16707	31.84731	30.12376	10.56742	6.89578	7.25550	15.93565
			17.95266	28.54964			
		28.31609	29.49361	24.52540	21.83365	4.76813	5.10893
		31.92486	29.38485		6.39460	30.40052	113.83231
		28.32680	30.20836	29.72264	19.23003	17.55119	19.26003
				24.09070	29.74827		
.25000	.47997	.66340	.52578	.87776	.69742	.71997	1.45275
			.77184	.52130			
		.48397	.46556	.40751	.44242	.52680	.58205
		.67007	.47336		.67676	.44653	.53057
		.45955	.48065	.48780	.46927	.52524	.52677
				.40339	.47950		
.50000	.75919	.91870	.82408	.94910	.84573	.85081	.91568
			1.05982	.81377			
		.81154	.80567	.75044	.75507	.78839	.78545
		.92965	.79289		.83288	.78008	.82258
		.79994	.74755	.75190	.73735	.74835	.74750
				.74158	.75847		
1.00000	.79109	.72204	.73826	.74556	.76802	.76383	.77917
			.69933	.70358			
		.76062	.76258	.77713	.77518	.78666	.78677
		.71810	.74346		.77304	.75964	.72609
		.76113	.78105	.78222	.78816	.78896	.78480
				.78025	.77533		

EXPECTATION VALUES OF R**N

N	EXP FUNCT	GAUSS FUNCT (WTS) -2	-1	0	1	2	3
-2	4.75310	4.74692	4.48141	2.58304	2.02957	2.08231	3.42481
			3.53947	4.32459			
		4.75633	4.43046	3.99005	3.73260	1.69745	1.75805
		4.74359	4.68636		1.95725	4.64620	13.19169
		4.75190	4.65564	4.50141	3.47836	3.31360	3.51512
				3.95284	4.51187		
-1	1.07819	1.08166	1.07626	1.01436	.97117	.97442	1.07803
			1.06968	1.05996			
		1.08484	1.07762	1.06640	1.05692	.94559	.95088
		1.07682	1.07656		.96861	1 09859	1.37110
		1.07799	1.07811	1.07591	1.04782	1.04184	1.05293
				1.06568	1.07671		
0	1.00002	1.00000	1.00000	1.00000	1.00000	1.00000	1.00000
			1.00000	1.00000			
		1.00000	1.00000	1.00000	1.00000	1.00000	1.00000
		1.00000	1.00000		1.00000	1.00000	1.00000
		1.00000	1.00000	1.00000	1.00000	1.00000	1.00000
				1.00000	1.00000		
1	1.33225	1.30899	1.30597	1.33359	1.33951	1.33986	1.32748
			1.33852	1.33482			
		1.28999	1.33250	1.33231	1.33350	1.34175	1.34032
		1.34167	1.30506		1.33935	1.33135	1.31976
		1.33367	1.33192	1.33226	1.33125	1.33331	1.33235
				1.33229	1.33288		
2	2.14890	2.00525	1.98898	2.15217	2.15881	2.15985	2.14689
			2.17615	2.08412			
		1.93630	2.14974	2.14779	2.15060	2.16024	2.15729
		2.17785	1.98425		2.15861	2.14983	2.14043
		2.15381	2.14617	2.14746	2.15024	2.15011	2.14901
				2.14905	2.14976		
3	4.09116	3.45733	3.40386	4.09714	4.10313	4.10560	4.09454
			4.16855	3.66115			
		5.26248	4.08865	4.08013	4.08870	4.10639	4.10059
		4.18758	3.38829		4.10731	4.09218	4.08779
		4.10876	4.07166	4.07824	4.09327	4.09277	4.09146
				4.09167	4.08729		
4	9.06490	6.57107	6.41748	9.05694	9.05553	9.06942	9.06755
			9.32518	7.08892			
		6.05312	9.02674	8.98462	9.02207	9.08936	9.07750
		9.54070	6.37251		9.09662	9.04747	9.05862
		9.13814	8.94098	8.97434	9.06817	9.06702	9.06528
				9.06625	9.01904		

IN SUB-ROW ORDER, FOR THE 3-, 4- AND 5-TERM EXPANSIONS, OBTAINED WITH THE WEIGHTING SPECIFIED BY COLUMN HEADING. WHERE ENTRIES APPEAR IN THE EVEN NUMBERED SUB-ROWS, THEY ARE FOR THE ALTERNATIVE, POORER FITTING EXPANSIONS

terms is associated with the better energy, around the coefficient sign crossover point, is consistent with the observed energy advantage of the r^{-1}-weighted over the unweighted expansions. The greater the number of contracted GTO terms, the better fit are the functions in regions close to the nucleus, which are, of course, just the regions favored by r^{-1} weighting.

TABLE 1. COEFFICIENTS AND EXPONENTS FOR THE WEIGHTED GAUSSIAN EXPANSIONS OF THE 2P SCF FUNCTION OF NITROGEN (4S)

		3-TERM			4-TERM			5-TERM		
N	<R**(N)>	EXPONENT	COEFFICIENT	EPSBAR 1-S	EXPONENT	COEFFICIENT	EPSBAR 1-S	EXPONENT	COEFFICIENT	EPSBAR 1-S
-2	1.33630(0)	1.27889(-1)	4.97685(-1)	1.31(-3)	2.38190(-1)	5.24853(-1)	2.11(-4)	1.86634(-1)	3.86585(-1)	3.91(-5)
		1.66363(0)	4.38242(-1)	4.26(-3)	9.72339(-1)	5.14822(-1)	8.04(-4)	6.48961(-1)	5.19590(-1)	1.92(-4)
		1.09920(1)	6.89252(-2)		4.09944(0)	1.69143(-1)		2.23398(0)	2.65257(-1)	
					2.46140(1)	2.06549(-2)		8.07817(0)	6.20269(-2)	
								5.04176(1)	6.54723(-3)	
-1	9.57733(-1)	2.45467(-1)	5.50305(-1)	1.35(-3)	1.81998(-1)	3.77608(-1)	2.04(-4)	1.44820(-1)	2.55973(-1)	3.48(-5)
		1.05449(0)	5.31847(-1)	1.26(-3)	6.46487(-1)	5.38788(-1)	2.00(-4)	4.43955(-1)	4.92533(-1)	3.14(-5)
		5.45592(0)	1.42019(-1)		2.40114(0)	2.71245(-1)		1.39147(0)	3.55164(-1)	
					1.20705(1)	5.22089(-2)		4.81405(0)	1.21619(-1)	
								2.29914(1)	1.99759(-2)	
0	1.00001(0)	1.92197(-1)	4.15644(-1)	1.33(-3)	1.45557(-1)	2.61890(-1)	1.89(-4)	1.17733(-1)	1.65778(-1)	3.00(-5)
		7.45574(-1)	5.72017(-1)	6.60(-4)	4.61632(-1)	5.16008(-1)	8.95(-5)	3.28080(-1)	4.35619(-1)	9.70(-6)
		3.44669(0)	2.37401(-1)		1.56851(0)	3.60646(-1)		9.48360(-1)	4.05989(-1)	
					6.81282(0)	1.01930(-1)		2.95997(0)	1.93687(-1)	
								1.24142(1)	4.46204(-2)	
1	1.40925(0)	1.56651(-1)	3.05032(-1)	1.28(-3)	1.20700(-1)	1.78033(-1)	1.70(-4)	9.91595(-2)	1.06713(-1)	2.53(-5)
		5.45448(-1)	5.69184(-1)	1.17(-3)	3.50015(-1)	4.46984(-1)	1.92(-4)	2.56335(-1)	3.66731(-1)	3.03(-5)
		2.27451(0)	3.38579(-1)		1.10186(0)	4.21780(-1)		6.86158(-1)	4.22021(-1)	
					4.25268(0)	1.67483(-1)		1.99028(0)	2.65205(-1)	
								7.47105(0)	8.16175(-2)	
2	2.54464(0)	1.32859(-1)	2.74128(-1)	1.27(-3)	1.03460(-1)	1.21617(-1)	1.59(-4)	8.59592(-2)	6.92417(-2)	2.14(-5)
		4.26184(-1)	5.41770(-1)	2.68(-3)	2.79957(-1)	4.07957(-1)	5.79(-4)	2.08850(-1)	2.98341(-1)	1.27(-4)
		1.67092(0)	4.30157(-1)		8.23021(-1)	4.51898(-1)		5.72251(-1)	4.15897(-1)	
					2.93376(0)	2.41317(-1)		1.43495(0)	3.23413(-1)	
								4.92570(0)	1.29746(-1)	
3	5.66322(0)	1.16365(-1)	1.67658(-1)	1.34(-3)	9.12986(-2)	8.50560(-2)	1.49(-4)	7.64153(-2)	4.59839(-2)	1.89(-5)
		3.51553(-1)	5.04678(-1)	4.98(-3)	2.34047(-1)	3.50353(-1)	1.32(-3)	1.76304(-1)	2.39056(-1)	3.58(-4)
		1.33697(0)	5.07227(-1)		6.49666(-1)	4.61268(-1)		4.17533(-1)	3.95598(-1)	
					2.27002(0)	3.14111(-1)		1.09931(0)	3.62718(-1)	
								3.56154(0)	1.84504(-1)	

SIX SIGNIFICANT FIGURES ARE TABULATED FOR EACH GAUSSIAN PARAMETER. THE APPROPRIATE POWER OF 10 IS ENCLOSED IN PARENTHESES TO THE RIGHT OF EACH ENTRY. THE RADIAL WEIGHTING FACTOR IS N, AND <R**(N)> IS THE EXPECTATION VALUE FOR THE OPERATOR (R**(N)) COMPUTED WITH THE SCF ORBITAL. EPSBAR IS EPS/<R**(N)> AND S IS THE OVERLAP BETWEEN THE SCF AND GAUSSIAN ORBITALS.

DENSITY ON A PER ELECTRON BASIS AT R (AU)

		GAUSS FUNCT (WTS)					
R	EXP FUNCT	-2	-1	0	1	2	3
0.00000	0.00000	0.00000	0.00000	0.00000	0.00000	0.00000	0.00000
		0.00000	0.00000	0.00000	0.00000	0.00000	0.00000
		0.00000	0.00000	0.00000	0.00000	0.00000	0.00000
.05000	.17352	.11752	.08026	.05141	.03255	.02205	.01613
		.14654	.11278	.08117	.05615	.03955	.02944
		.16366	.13753	.10799	.08084	.05976	.04558
.25000	1.29528	1.39154	1.25071	.94087	.65307	.46564	.35090
		1.29551	1.35242	1.23045	.98906	.76155	.59734
		1.27952	1.30982	1.32606	1.21256	1.02377	.84711
.50000	1.43654	1.35751	1.49445	1.54009	1.35244	1.11292	.91582
		1.46070	1.39905	1.46454	1.50771	1.42285	1.27899
		1.43176	1.44585	1.41640	1.45674	1.49265	1.45978
1.00000	.64276	.67170	.65416	.60814	.65586	.72192	.75507
		.63514	.64137	.65415	.63144	.63926	.67668
		.64471	.64277	.63993	.64874	.64044	.63755

EXPECTATION VALUES OF R**N

		GAUSS FUNCT (WTS)					
N	EXP FUNCT	-2	-1	0	1	2	3
-2	1.33630	1.33816	1.31917	1.25592	1.16307	1.07277	.99516
		1.33673	1.33033	1.30781	1.26027	1.19807	1.13669
		1.33640	1.33449	1.32592	1.30334	1.26601	1.22278
-1	.95773	.96159	.95734	.94754	.92709	.90254	.87853
		.95854	.95767	.95514	.94730	.93467	.92001
		.95791	.95772	.95703	.95423	.94875	.94083
0	1.00001	1.00000	1.00000	1.00000	1.00000	1.00000	1.00000
		1.00000	1.00000	1.00000	1.00000	1.00000	1.00000
		1.00000	1.00000	1.00000	1.00000	1.00000	1.00000
1	1.40925	1.38091	1.40168	1.40938	1.41728	1.42793	1.44896
		1.40156	1.40774	1.40926	1.41108	1.41451	1.41937
		1.40714	1.40893	1.40724	1.40969	1.41078	1.41258
2	2.54464	2.36253	2.48720	2.53379	2.55562	2.57376	2.59508
		2.48629	2.53138	2.54264	2.54718	2.55204	2.55841
		2.52641	2.54150	2.54474	2.54524	2.54664	2.54865
3	5.66322	4.73654	5.31094	5.56611	5.66264	5.70282	5.73292
		5.31091	5.56056	5.64276	5.66441	5.67348	5.68059
		5.53677	5.63706	5.65078	5.66371	5.66602	5.66707
4	15.07293	10.67769	13.07417	14.37391	14.91318	15.09518	15.16469
		13.10147	14.41828	14.89897	15.04335	15.08333	15.09591
		14.25839	14.86811	15.02943	15.06675	15.07593	15.07865

IN SUB-ROW ORDER, FOR THE 3-, 4- AND 5-TERM EXPANSIONS, OBTAINED WITH THE WEIGHTING SPECIFIED BY COLUMN HEADING.

Table 4. Energies for N(^{4}S) from the Weighted Gaussian Expansions of the SCF Functions[a,b]

n	3-term	4-term	5-term
-2	-53.591496	-54.175475 (-54.114936)	-54.332092
	54.711468	54.261225 (54.360109)	54.261179
-1	-53.898145 (-53.621450)	-54.234054 (-54.244324)	-54.360021
	54.420081 (54.681354)	54.398677 (54.332928)	54.372410
0	-53.469122 (-53.688345)	-54.138958	-54.321897 (-54.260156)
	53.166807 (53.424447)	54.057232	54.295181 (54.224478)
1	-52.967555	-53.878588 (-53.662956)	-54.110339 (-54.199511)
	50.977425	53.129560 (52.538013)	53.673782 (53.910561)
2	-52.302572	-53.259828 (-53.470111)	-53.825663
	49.071870	51.206655 (52.258718)	52.825644
3	-51.525990	-52.685363	-53.426163
	47.645092	49.745718	51.807211

---

[a] In sub-row order, total energy and kinetic energy in hartrees. All AO (1s, 2s and 2p) expansions obtained with the same weighting, r^n. Parenthesized values are obtained using the alternative, poorer fitting (by $\bar{\varepsilon}_n$ criteria) 2s expansions.

[b] The Hartree-Fock energies are -54.400911 and 54.401562 [4]. The energy optimized 3-, 4- and 5-term expansions have total energies -54.062880, -54.319468 and -54.379474, respectively [7].

To pursue these matters further, r^{-1}-weighting improves the total energy (relative to the unweighted expansions) by from 56–66% of the improvement accomplished by freeing all the GTO parameters and energy optimizing them [7]. The larger the expansion, the greater the relative improvement. The absolute improvement (relative to the Hartree-Fock energy) accomplished by this weighting ranges from 30–48%, again being greater, the greater the expansion length. It is also of interest to note that regular, almost completely general progression trends exist for the GTO parameters themselves. The parameter values for the 1*s* and 2*p* orbital expansions obtained with r^{-1} weighting are fairly centrally

Table 5. Energies for C(^{3}P) from the Mixed Weighted Gaussian Expansions of the SCF Functions[a,b]

n_{2s} \ n_{1s}	0	-1	-2
	-37.19357,37.01441 -37.50473,37.44806 -37.63294,37.61454		
0	-37.20433,37.07250 -37.50919,37.46385 -37.63451,37.61891	-37.33789,37.60918 -37.56712,37.59288 -37.65857,37.64981	
	-37.19801,37.10101 *-37.50799,37.46940* *-37.63420,37.62009*	*-37.33148,37.63768* *-37.56592,37.59844* *-37.65832,37.65099*	
		-37.32873,37.64874 -37.57609,37.62783 -37.65822,37.66454	-37.15816,37.70946 -37.53259,37.52062 -37.64684,37.57091
-1	-37.20536,37.17651 -37.52239,37.51672 -37.63572,37.63817	-37.33945,37.70684 -37.58054,37.64362 -37.65978,37.66891	-37.16906,37.76756 -37.53701,37.53641 -37.64841,37.57527
	-37.19894,37.20501 *-37.52114,37.52227* *-37.63540,37.63935*	*-37.33293,37.73534* *-37.57929,37.64918* *-37.65953,37.67009*	
		-37.29478,37.75939 -37.57126,37.68285 -37.64985,37.67804	-37.11537,37.82779 -37.52766,37.57244 -37.63850,37.58606
-2		-37.30542,37.81748 -37.57571,37.69863 -37.65142,37.68241	-37.12621,37.88588 -37.53208,37.58823 -37.64008,37.59043

---

[a] The total energy, the kinetic energy, in hartrees. In sub-row order, the 3-, 4- and 5-term results. Variation in the 2p function weighting, r**n_{2p}, indicated by change in typeface; small typeface for the function determined without weighting, regular type for n_{2p} equal -1 and italics for -2.

[b] The Hartree-Fock energies are -37.68861 and 37.68854 [4]. The total energies are -37.45306, -37.63172, -37.67356 for the 3-, 4- and 5-term energy optimized GTO expansions [7].

located between those of the unweighted and energy optimized expansions. The 2s parameter comparisons are considerably more complicated because of the node production requirement, viz., the energy optimized 3- and 5-level sets have fewer subtractive contracted terms than those obtained by the space filling optimization methods. However, examination of the somewhat poorer (by ε_n standards) functions and their density contributions, combined with the above observation and the 4-term results reinforces the generalization that energy improvement accompanies contraction of the overlap optimized function.

Variations in the individual AO contributions to energy through use of GTO expressions obtained by variable weighting may be obtained by examination of Table 5. The results for C(^{3}P), which are typical, are shown; this is the ground state for the atom with equal numbers of 1*s*, 2*s* and 2*p* electrons which provides a useful normalization of the individual orbital effects[2]. It may be quickly ascertained that the greatest effects accompany changes in the 1*s* expansions. This is not a surprising result considering the relative AO contributions to total energy. The total energy increments are typically 0.01–0.1 hartrees (on the total energy), an order or more in magnitude greater than the effects noted upon variation in the 2*s* and 2*p* functions. The effects of variation in the latter are similar except as noted below.

The r^{-1}-weighted functions are most favorable as regards total energy for all AO's and for the 1*s* and 2*p* functions the effects of weighting are most profound for the 3-term and least important for the 5-term expansions. For the 2*s* AO, comparing the r^{-1}-weighted expansions, the greatest difference, by an order of magnitude, is noted for the 4-term expansion, an effect which may be a ramification of coefficient crossover. The r^{-1}-weighted 4-term expansion function has 3 negative coefficients, the unweighted has 2. In the 3-term expansions both have 2 negative coefficients and in the 5-term expansions both have 3. Comparison of the r^{-1}- and r^{-2}-weighted functions reveals for all AO's the effects of weighting decrease as the expansion length increases.

Discussion and Conclusions

The values of weighting, with relatively simple weighting functions, in the course of expansion of real molecule wavefunctions are apparent from the foregoing results. The weighting functions employed may be considered as useful first-order corrections in the process of orbital representation matching, the ultimate and usually completely impractical correction for optimization of a particular expectation value being in the use of the operator itself as weighting function (i.e., weighting with the Hamiltonian for energy matching). The previously recognized fact that least-squares fitting in an overlap maximization procedure tends to stress the more diffuse regions of space [2] is reiterated by the density and expectation value results as well as the energy comparisons presented. Weighting effects as exercised through parameter variation in the GTO's are smaller on the computed densities and $\langle r^n \rangle$, the larger are r and n, respectively. In fact, for the expectation values with large n, the unweighted or smaller n-weighted functions give as good and occasionally better results than those generated with matching n. Total energies are uniformly better from the r^{-1}-weighted functions; the expansions obtained under r^{-2}-weighting are uniformly as good or better for all the first row atoms at the 4-term or higher expansion levels than those obtained without weighting.

Limited tests of the effects on molecular properties of weighting of constituent AO's are in progress. In a most stringent test, one of the few completed so far, the variously weighted SCF atom expansions for $N(^4S)$ were used without scaling in the variational computation of geometry and energy optima for N_2. While the r^{-1}-weighted functions were found to be as good or better than the unweighted functions as far as binding energies go, they were as often as not poorer with respect to prediction of the equilibrium value of the internuclear distance, and both properties were never better than poorly represented at best. These results are not at all remarkable, considering the molecule chosen and that significant scaling is necessary to make the energy optimized GTO expansions for atoms acceptable for use in molecular calculations [8]. Weighting is clearly not a panacea for improvements of trial functions. Further tests are underway to better define the limits of what weighting of AO functions, both of SCF and STO type, can accomplish as regards molecular calculations.

---

[2] The best 2*s* expansion by total energy criteria is used at each weighting level. It should be noted that the 1*s* and 2*s* GTO expansions are not completely orthogonal because fit to the SCF AO's (which are of course orthogonal) is not perfect. The differences are however very small. In the course of the SCF procedure for energy calculation, orthogonality is assured by appropriate linear combination.

Another example worth mentioning of the potential utility of the radially-weighted expansions presented here, which does not explicitly involve their use in variational MO calculations, is to be found in the computation of X-ray scattering factors. Stewart [2] has found upon Fourier analysis that unweighted least-squares GTO expansions are satisfactory for low-angle scattering but poorer than those from variational fitting constraints at higher angles. It appears likely, since variation in the angle of scattering varies spatial regions stressed, that even better representations may be had employing the appropriately weighted functions. Direct expansion of empirical functions obtained from scattering, which represents a reverse situation, would also benefit from weighting, with regions of the highest and/or most reliable informational content stressed.

Apendix: Accurate Evaluation of the Error Function, $F_l(\alpha, \zeta)$

The integral of Eq. (4) may be cast in the error function form,

$$F_l(\alpha,\zeta) = \frac{\sqrt{\pi}}{2}\,\frac{e^{Z^2}}{\alpha^{(l+1)/2}}\, l!\, i^l \operatorname{erfc} Z \tag{A.1}$$

with,

$$Z = \zeta/2\alpha^{1/2}. \tag{A.2}$$

For small Z, the power series [9, Eq. (7.2.4)],

$$i^l \operatorname{erfc} Z = \sum_{k=0}^{l} \frac{(-1)^k Z^k}{2^{l-k} k!\, \Gamma\left(1 + \frac{l-k}{2}\right)} \tag{A.3}$$

may be used to accurately evaluate the error function for L and $L-1$, where L is the maximum value of l required, followed by downward recurrence employing the relationship [9, Eq. (7.2.5)],

$$i^{l-2} \operatorname{erfc} Z = 2l\, i^l \operatorname{erfc} Z + 2Z i^{l-1} \operatorname{erfc} Z\,, \tag{A.4}$$

which is unencumbered by serious differencing errors for small Z.

It is well known that for larger arguments, Z, power series representations for $i^l \operatorname{erfc} Z$ such as (A.3) cannot yield sufficiently accurate results [2, 10], especially if subsequent recursion is necessary. For very large Z (higher than 10 or 15, depending upon machine capacity, extent of recurrence necessary, accuracy desired, *etc.*), however, asymptotic series approximations are available [9, Eq. (7.1.23); 10].

Integral evaluation in the intermediate Z-range and definition of the range boundaries are therefore the central matters here. All previous investigators of the least-squares fitting problem cited have relied on Gauss-Laguerre quadrature in the intermediate range, with quadrature point choices ranging from 12 to 36, depending upon where the lower Z boundary was set, and upon similar criteria to those mentioned above for application of the asymptotic approximations.

We have employed the recursive non-quadrature technique of Gautschi [5] for intermediate and high Z-values.

Let the sequence $\omega_\mu^m(Z)$ ($\mu = m, m-1, \ldots, 1, 0, -1$) be generated by backward use of the recurrence relation,

$$\omega_{\mu-2}^m(Z) = 2m\omega_\mu^m(Z) + 2Z\omega_{\mu-1}^m(Z), \tag{A.5}$$

whose similarity to (A.4) is to be noted. Starting with $\omega_{m+2}^m = 0$ and $\omega_{m+1}^m = \gamma$, where $\gamma > 0$, then for any l, it may be shown,

$$\lim_{m \to \infty} \frac{\omega_l^m(Z)}{\omega_{-1}^m(Z)} = \frac{\sqrt{\pi}}{2} e^{Z^2} i^l \operatorname{erfc} Z \tag{A.6}$$

Since all $\omega_\mu^m(Z)$ values are generated in the course of obtaining $\omega_{-1}^m(Z)$, all $F_l(\alpha, \zeta)$ are obtained, and all exceed in accuracy the limit chosen for $F_L(\alpha, \zeta)$.

The number of terms in the sequence, m, required if $i^L \operatorname{erfc} Z$ is to have a fractional error less than 10^{-p} is known, [5, Eq. (5.3)],

$$m \approx \left(\frac{2\sqrt{2L}\, Z + p \ln 10 + \ln 2}{2\sqrt{2}\, Z} \right)^2 \tag{A.7}$$

or, for example, with $L = 12$ and a convergence limit of 3×10^{-11}, $m = 49$ with $Z = 2.5$, and $m = 37$ with $Z = 3.5$. Eq. (A.7) and these cited examples show how rapidly the sequence length decreases with increasing Z; the only practical limit for application in the high-Z range is machine overflow which can to a very great extent be extended by appropriate choice of γ.

At the lower end, Z-values much below 2 require extensive sequence generation. This introduces a time factor consideration, and the possibility of roundoff accumulation, both factors of course being machine dependent. (It should be recognized at the same time, however, that quadrature procedures suffer in a similar way.) A reasonable compromise for a machine having 14 significant figure carry would be a Z-boundary at 2.5. Here, 8 or more significant figures from (A.3) and (A.4), and 10 or more significant figures from (A.6) (with a 3×10^{-11} convergence criterion) are obtained for all l (zero to 12), as calibrated by a 24 point quadrature test.

Consequently, for the calculations described herein, only two Z-ranges are recognized and the boundary is set at Z equal 2.5.

It is a matter of some interest to note that the criterion used in Ref. [3] for judging accuracy of the error functions, i.e., comparison of $i^0 \operatorname{erfc} Z$ obtained from (A.3) and (A.4) with values for the same integral as obtained directly by power series representations, is deceptive. Even though agreement was found to 13 figures for Z up to 3.5 (using double precision arithmetic, or about 27 figure carry), the i^{12} erfc Z generated as the first step by (A.3) in this Z-region is seriously in error. Recurrence compensation, an effect of the type which enters favorably in the Gautschi method, is obviously responsible for this apparently enigmatic difference. Viz., ω_l^m/ω_{-1}^m can yield accurate estimations of $i^l \operatorname{erfc} Z$ for $m > l$, with the required difference $(m - l)$ dependent upon l and the goodness of choice of ω_{m+2}^m and ω_{m+1}^m [recall, the arbitrary choices of these sequence originators in (A.5) and (A.6)]. Similar recurrence compensation effects for simpler error functions have been pointed out by Shavitt [11].

Following this revelation, all error functions for all tabulated quantities in Ref. [3] were checked. They have been verified to be good to at least 8 significant figures: N.B., all correspond to $Z < 2.61$.

Acknowledgement. The authors wish to acknowledge the technical assistance of Mrs. Madeline Kinney.

References

1. See, for example, Hehre, W. J., Stewart, R. F., Pople, J. A.: J. chem. Physics **51**, 2657 (1969) and later members of the series
2. Stewart, R. F.: J. chem. Physics **50**, 2485 (1969); **52**, 431 (1970). Earlier work on analytical methods for expansion of STO functions are reviewed in these papers.
3. Ehrenson, S.: Chem. Physics Letters **9**, 521 (1971)
4. Clementi, E.: IBM J. Res. Develop. Suppl. **9**, 2 (1965).
5. Gautschi, W.: Math. Tables Aids Comp. **15**, 227 (1961).
6. Ehrenson, S.: Theoret. chim. Acta (Berl.) **14**, 136 (1969).
7. Ditchfield, R., Hehre, W. J., Pople, J. A.: J. chem. Physics **52**, 5001 (1970).
8. Hehre, W. J., Ditchfield, R., Pople, J. A.: J. chem. Physics **53**, 932 (1970). Hehre, W. J., Ditchfield, R., Radom, L., Pople, J. A.: J. Amer. chem. Soc. **92**, 4796 (1970).
9. Abramowitz, M., Stegun, I., (Eds.): Handbook of mathematical functions, Chap. 7. Washington: National Bureau of Standards 1964.
10. Cf., Silver, D. M.: Chem. Physics Letters **10**, 227 (1971).
11. Shavitt, I.: Methods in computational physics, Vol 2, p. 8. New York: Academic Press 1963.

Dr. S. Ehrenson
Chemistry Department
Brookhaven National Laboratory
Upton, New York 11973, USA

Theoret. chim. Acta (Berl.) 28, 297—305 (1973)
© by Springer-Verlag 1973

Statistische Modellrechnungen an den Molekülen CH_4, SiH_4, GeH_4, SnH_4 und PbH_4 nach der Einzentrenmethode

Karl Hensen, Manfred Achatz und Rolf Müller

Institut für physikalische Chemie der Universität Frankfurt am Main

Eingegangen am 4. August 1972

Statistical OCE-*Calculations on the Molecules* CH_4, SiH_4, GeH_4, SnH_4 *and* PbH_4

OCE-calculations are reported for ground state energies and bond distances of the hydrides CH_4, SiH_4, GeH_4, SnH_4 and PbH_4. The statistical atom model (Gombás and Ladányi [1]) is connected with the noble gas model (Hartmann and Gliemann [2]). The results are in good agreement with known experimental values. Bond distance and ground state energy of PbH_4 are presented for the first time.

Mit einem Einzentren-Ansatz werden Bindungsabstände und Gesamtenergien der Moleküle CH_4, SiH_4, GeH_4, SnH_4 und PbH_4 berechnet. Die statistische Betrachtungsweise der Elektronen nach Gombás und Ladányi [1] wird mit der Edelgas-Modellvorstellung nach Hartmann und Gliemann [2] verknüpft. Die Ergebnisse liegen in guter Übereinstimmung mit den vorliegenden experimentellen Daten. Bindungsabstand und Gesamtenergie des Moleküls PbH_4 werden erstmals berechnet.

Einleitung

Methan und die analogen Hydride der 4. Hauptgruppe sind der Gegenstand vieler experimenteller und theoretischer Untersuchungen.

Ziel der vorliegenden Arbeit ist, ein durchschaubares Modell zu entwickeln, das für *alle* oben angesprochenen Moleküle gute Aussagen über Bindungsabstand und Gesamtenergie liefert und dabei einen möglichst geringen Rechenaufwand erfordert.

Hartmann u. Gliemann [2] behandeln das CH_4-Molekül als Pseudo-Neon Atom unter der zusätzlichen Vereinfachung, daß die Rumpfelektronen des Zentralatoms in die Rechnung nur insofern eingehen, als sie die Kernladung des Zentralatoms abschirmen. Hartmann u. Gliemann rechnen mit der um die Anzahl der Rumpfelektronen verminderten Kernladung.

Das gute Ergebnis für den Bindungsabstand, das sie mit diesem stark vereinfachten Ansatz für CH_4 erhalten, wird schon bei SiH_4 – wie zu erwarten – nicht mehr erreicht. Überträgt man diese Modellvorstellung auf die Berechnung des Gleichgewichtsabstandes im SiH_4-Molekül, so ergibt sich für die Si—H-Bindung ein Wert von 5,113 at.E. [3] (exp. 2,787 at.E.); ein Zeichen dafür, daß die Verminderung der Kernladung um die Anzahl der Rumpfelektronen eine zu grobe Näherung darstellt.

Hartmann, Papula u. Strehl haben unter expliziter Berücksichtigung aller Rumpf- und Valenzelektronen das Edelgasmodell quantenmechanisch auf SiH_4 [4], GeH_4 [5] und später auch auf SnH_4 [6] ausgedehnt.

Selbst unter Verwendung einer minimalen Basis von Funktionen gelang e bisher nicht, das Molekül PbH_4 zu berechnen [7].

Die vorliegende Arbeit berichtet über Ergebnisse, die im Rahmen eine statistischen Behandlung von sowohl Rumpf- als auch Valenzelektronen erhalte werden. Dabei gelingt es u. a. erstmalig Aussagen über die Gesamtenergie de Moleküls PbH_4 im Grundzustand und die Länge der Pb—H-Bindung zu machen

Modellvorstellung und Rechenmethode

Die Moleküle CH_4, SiH_4, GeH_4, SnH_4 und PbH_4 besitzen im Rahmen de Modellvorstellung Pseudo-Edelgas-Konfiguration. Die Valenzschale des jeweiligen Zentralatoms wird durch die Elektronen der H-Atome zur Edelga konfiguration aufgefüllt, die vier Protonen sind tetraedrisch um den Kern de Zentralatoms angeordnet. Für die rechnerische Behandlung wird ein statistische Atommodell verwendet, in dem die Elektronen nach der Hauptquantenzah gruppiert sind.

Dabei werden die zu den einzelnen Hauptquantenzahlen gehörenden Elektronen gesondert behandelt und die Orthogonalitätsbedingungen für die Elektronen mit Hilfe eines von Gombás [8] hergeleiteten mittleren Zusatzpotential $G^{(n)}$ berücksichtigt.

$G^{(n)}$ ersetzt von statistischen Grundlagen ausgehend das Paulische Besetzungsverbot der vollbesetzten Elektronenzustände in der Form eines Abstoßungspotentials.

Die Energie der Elektronen der n-ten Schale setzt sich aus kinetischer un potentieller Energie zusammen. Austausch- und Korrelationswechselwirkung de Elektronen werden nicht berücksichtigt.

Die kinetische Energie zerfällt in 3 Teile:

$E_k^{(n)}$, den radialen Anteil, der mit der Weizsäcker-Korrektur identisch ist,

$E_\varphi^{(n)}$, den azimutalen Anteil,

$E_g^{(n)}$, die aus dem Zusatzpotential $G^{(n)}$ resultierende Energie, die den Elektrone der n-ten Schale die kinetische Mindestenergie zuführt, die benötigt wird um die Elektronen im Volumenelement $d\tau$ unterbringen zu können.

Die potentielle Energie zerfällt in 4 Teile:

$E_{pk}^{(n)}$, die coulombsche elektrostatische Wechselwirkungsenergie der Elektronen mit dem Zentralkern,

$E_{pe}^{(n)}$, die coulombsche elektrostatische Wechselwirkungsenergie der Elektronen mit den Elektronen der übrigen Schalen,

$E_{pw}^{(n)}$, die coulombsche elektrostatische Wechselwirkungsenergie der Elektronen mit den 4 Wasserstoffkernen,

$E_e^{(n)}$, die gegenseitige elektrostatische Wechselwirkungsenergie der Elektrone innerhalb der betrachteten Schale unter Ausschluß der elektrostatische Selbstwechselwirkung durch Benutzung der Korrektur von Fermi u. Amaldi [9].

Die einzelnen Energiebeiträge der Elektronen der n-ten Schale lauten damit (vgl. Gombás [1]):

$$E_k^{(n)} = \tfrac{1}{8} e^2 a_0 \cdot \int \frac{(\nabla \varrho_n)^2}{\varrho_n}\, d\tau\,,$$

$$E_\varphi^{(n)} = \sum_l \int n_l \cdot \tfrac{1}{2} \cdot e^2 a_0 \cdot \frac{l \cdot (l+1)}{r^2} \cdot \frac{\varrho_n}{N_n}\, d\tau\,,$$

$$E_g^{(n)} = -e \cdot \int G^{(n)} \varrho_n d\tau$$

$$G^{(n)} = \frac{1}{N_n} \cdot \sum_l n_l \cdot \left(-\frac{16\pi^4 r^4}{8(2l+1)^2} \cdot e a_0 \cdot \varrho_l^2 - \tfrac{1}{4} e a_0 \cdot \frac{1}{r^2} \right),$$

$$E_{pk}^{(n)} = -e^2 \cdot \int \frac{Z}{r} \cdot \varrho_n d\tau\,,$$

$$E_{pe}^{(n)} = e^2 \cdot \int \varrho_n \cdot \left(\sum_{n'=1}^{n-1} \int \frac{\varrho_{n'}(\boldsymbol{r}')}{|\boldsymbol{r} - \boldsymbol{r}'|}\, d\tau' \right) d\tau\,,$$

$$E_{pw}^{(n)} = -4e^2 \cdot \int \frac{\varrho_n(\boldsymbol{r})}{|\boldsymbol{r} - \boldsymbol{R}|}\, d\tau\,,$$

$$E_e^{(n)} = \tfrac{1}{2} \cdot \left(1 - \frac{1}{N_n} \right) \cdot e^2 \cdot \int \frac{\varrho_n(\boldsymbol{r}) \cdot \varrho_n(\boldsymbol{r}')}{|\boldsymbol{r} - \boldsymbol{r}'|}\, d\tau \cdot d\tau'\,.$$

Für die Dichteverteilungen der Elektronen in den einzelnen Schalen wird der kugelsymmetrische Ansatz

$$\varrho_n = A_n \cdot r^{2(n-1)} \cdot e^{-2\lambda_n r}$$

gewählt, mit A_n als Normierungskonstante, die sich aus der Bedingung

$$N_n = \int \varrho_n d\tau$$

zu

$$A_n = N_n \cdot \frac{(2\lambda_n)^{2n+1}}{4\pi \cdot (2n)!}$$

ergibt.

Mit diesem Ansatz ergeben sich zur n-ten Schale folgende Beiträge zur Gesamtenergie:

$$E_k^{(n)} = e^2 a_0 \cdot \frac{N_n}{2} \cdot \frac{1}{(2n-1)} \cdot \lambda_n^2\,;$$

$$E_\varphi^{(n)} = e^2 a_0 \cdot \left[\frac{1}{4n \cdot (2n-1)} \cdot \sum_l n_l \cdot l \cdot (l+1) \right] \cdot (2\lambda_n)^2\,;$$

$$E_g^{(n)} = e^2 a_0 \cdot \sum_{l=0}^{n-2} \sum_{n'=l+1}^{n-1} \sum_{n''=l+1}^{n-1} \tfrac{1}{2}\pi^2 n_l \cdot \frac{(2\lambda_{n'})^{2n'+1} \cdot (2\lambda_{n''})^{2n''+1} \cdot [2(\mathrm{n}' + \mathrm{n}'' + \mathrm{n})]!}{(2n')! \cdot (2n'')! \cdot (2n)!}$$
$$\cdot \frac{(2\lambda_n)^{2n+1}}{(2\lambda_{n'} + 2\lambda_{n''} + 2\lambda_n)^{2n'+2n''+2n+1}} + \tfrac{1}{4} e^2 a_0 \cdot \sum_{l=0}^{n-2} n_l \cdot \frac{(2\lambda_n)^2}{2n \cdot (2n-1)}\,;$$

$$E_{pk}^{(n)} = -e^2 \cdot \frac{N_n \cdot Z}{n} \cdot \lambda_n\,;$$

$$E_{pe}^{(n)} = e^2 \cdot \frac{N_n}{2n} \cdot \left(\sum_{n'=1}^{n-1} N_{n'} \cdot 2\lambda_n - \sum_{n'=1}^{n-1} N_{n'} \frac{(2\lambda_n)^{2n+1}}{(2\lambda_n + 2\lambda_{n'})^{2n}} \right.$$
$$- \sum_{n'=1}^{n-1} \sum_{\nu=1}^{2n'-1} N_{n'} \frac{(2n+2n'-\nu-1)! \cdot \nu}{(2n-1)! \cdot 2n' \cdot (2n'-\nu)!} \cdot (2\lambda_{n'})^{2n'-\nu}$$
$$\left. \cdot \frac{(2\lambda_n)^{2n+1}}{(2\lambda_n + 2\lambda_{n'})^{2n+2n'-\nu}} \right);$$

$$E_{pw}^{(n)} = -4e^2 \cdot \frac{N_n}{R} \cdot \left[1 - e^{-2\lambda_n R} \cdot \left(1 + \sum_{\nu=1}^{2n-1} \frac{2^{2n-\nu} \cdot \nu}{2n \cdot (2n-\nu) \cdot (2n-\nu-1)!} \cdot (\lambda_n R)^{2n-\nu} \right) \right]$$

$$E_e^{(n)} = \tfrac{1}{2} e^2 \cdot \frac{(N_n - 1) \cdot N_n}{2n} \cdot \left[\frac{2^{2n} - 1}{2^{2n}} - \sum_{\nu=1}^{2n-1} \frac{(4n-\nu-1)! \cdot \nu}{(2n)! \cdot (2n-\nu)! \cdot 2^{4n-\nu}} \right] \cdot 2\lambda_n .$$

Die Gesamtenergiefunktion des betrachteten Systems erhält man daraus in der Weise, daß man das Pseudo-Edelgasatom schalenweise aufbaut und dabei noch den aus der Coulombschen Wechselwirkung der 4 Protonen mit dem Kern des Zentralatoms sowie der Wechselwirkung der 4 Protonen untereinander resultierenden Energiebeitrag E_{pp} berücksichtigt.

Für diesen Beitrag ergibt sich bei tetraedrischer Anordnung der 4 Protonen um den Kern aus geometrischen Überlegungen der Wert:

$$E_{pp} = \frac{4}{R} \cdot \left(Z + \frac{3 \cdot \sqrt{6}}{8} \right).$$

Bezeichnet man mit n_μ die maximale in der angenommenen Edelgaskonfiguration auftretende Hauptquantenzahl, so enthält die Gesamtenergiefunktion als geometrischen Parameter den Gleichgewichtsbindungsabstand R und für jede besetzte Schale einen Variationsparameter λ_i.

$$E_{ges}(R, \lambda_1, \lambda_2, \ldots, \lambda_{n_\mu}) = E_{pp} + \sum_{i=1}^{n_\mu} E_k^{(i)} + E_\varphi^{(i)} + \cdots + E_e^{(i)}.$$

Die Gesamtenergiefunktion des Moleküls wird dann mit Hilfe der Prozedur Direct Search [10] bezüglich der Parameter (Bindungsabstand R und Funktionsexponenten λ_i) minimisiert.

Ergebnisse und Diskussion

Die Endwerte der Minimisierungen gehen aus Tab. 1 hervor.

Tabelle 1. Endwerte der Minimisierungen in atomaren Einheiten

Molekül	E	R_0	λ_1	λ_2	λ_3	λ_4	λ_5	λ_6
CH_4	− 38,426	2,123	5,719	1,255				
SiH_4	− 285,806	2,907	14,059	4,720	1,281			
GeH_4	− 2059,381	2,932	33,290	13,495	5,570	1,629		
SnH_4	− 6030,742	3,306	52,776	22,759	11,489	5,161	1,762	
PbH_4	− 19682,792	3,451	87,593	39,423	22,052	11,479	5,632	1,990

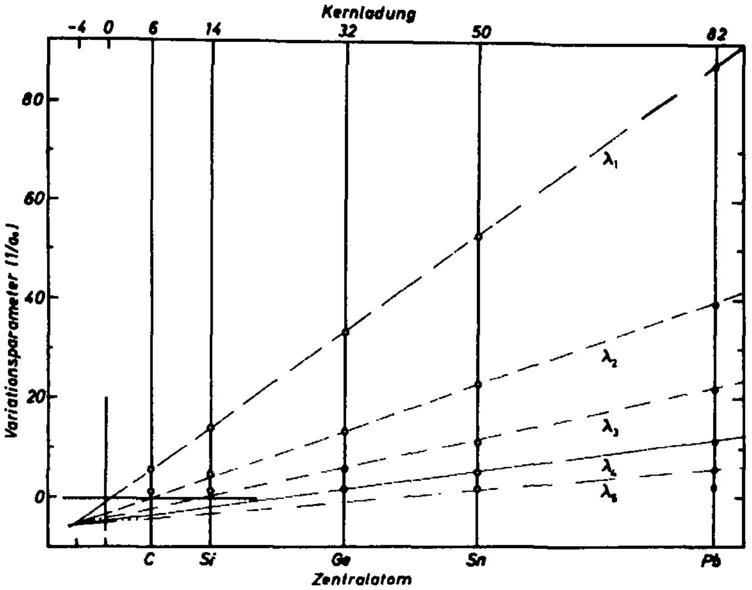

Fig. 1. Abhängigkeit der Variationsparameter λ_i von den Kernladungszahlen der Zentralatome

Es sei darauf hingewiesen, daß sowohl sämtliche Funktionsexponenten als auch der Bindungsabstand gleichzeitig minimisiert werden.

In Tab. 2 werden die Ergebnisse mit den bisher bekannten experimentellen und theoretischen Werten aus quantenmechanischen Rechnungen verglichen.

Den Rechnungen von Hartmann, Papula u. Strehl [2, 4–6] ist gemeinsam, daß sie alle nach der Pseudo-Edelgasnäherung durchgeführt werden und bisher die einzige in sich einheitliche Behandlung der Moleküle SiH_4, GeH_4 und SnH_4 darstellen.

Für SnH_4 liefern sie die einzigen theoretischen Vergleichsmöglichkeiten überhaupt und zum Molekül GeH_4 sind zusätzlich nur noch von Stevenson und Lipscomb LCAO-MO-SCF-Rechnungen mit einem minimalen STO-Basissatz

Tabelle 2. Vergleich der Ergebnisse mit den bisher bekannten experimentellen und theoretischen Daten

	experimentell		theoretisch			
	R (at.E.)	*E* (at.E.)	*R* (at.E.)	*E* (at.E.)	*R* (at.E.)	*E* (at.E.)
CH_4	2,067 [11]	− 40,51 [11]	2,187 [2]	− 6,642 [2][a]	2,123	− 38,426
SiH_4	2,787 [12]	−292,141 [12]	2,899 [4]	− 289,527 [4]	2,907	− 285,806
GeH_4	2,91 [13]		3,004 [5]	−2069,885 [5]	2,932	− 5059,381
SnH_4	3,215 [14]		3,385 [6]	−6012,924 [6]	3,306	− 6030,743
PbH_4					3,451	−19682,792

[a] Die Energie wird in diesem Fall nach dem 8-Elektronenmodell berechnet.

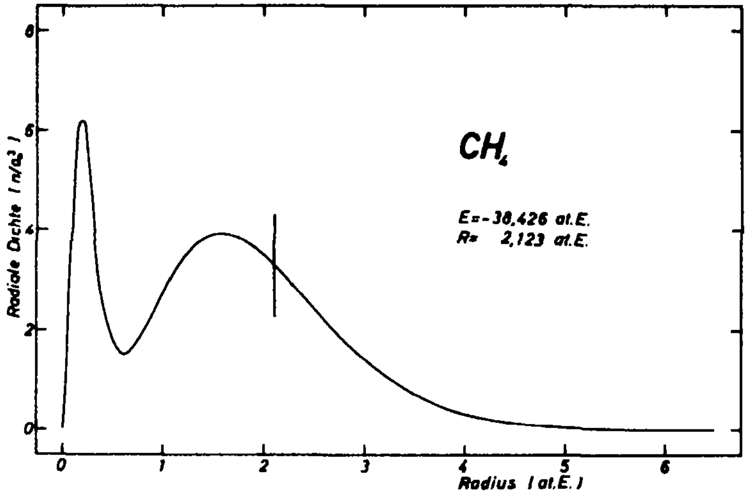

Fig. 2. Die gesamte radiale Elektronendichte des CH_4-Moleküls. Der senkrechte Strich markiert den Abstand *R* der vier H-Atome vom C-Atom

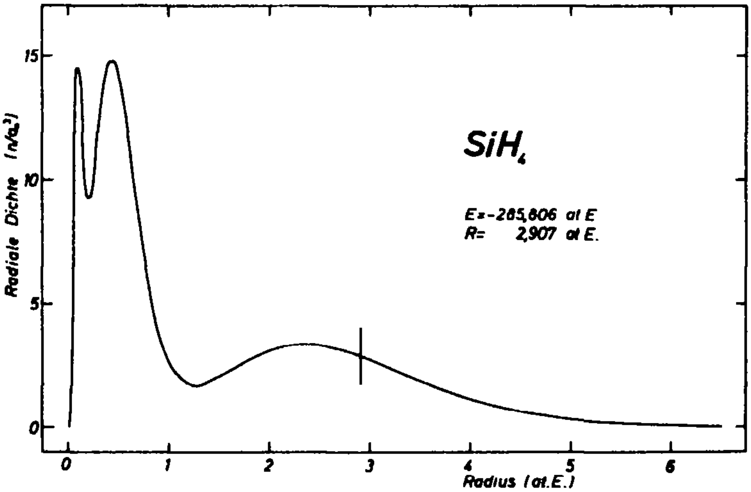

Fig. 3. Die gesamte radiale Elektronendichte des SiH_4-Moleküls. Der senkrechte Strich markiert den Abstand *R* der vier H-Atome vom Si-Atom

bekannt [15]. Zu den kleineren Molekülen SiH_4 und CH_4 finden sich ausführliche Literaturzitate bei Papula [4] und Grein [16].

Der Tab. 2 ist zu entnehmen, daß sich mit der einfachen statistischen Behandlungsweise der Moleküle bereits für CH_4 sehr brauchbare Werte für Bindungsabstand und Gesamtenergie ergeben.

Bei den Molekülen GeH_4 und SnH_4 werden die bisher bekannten Bindungsabstände besser approximiert als durch die quantenmechanischen Rechnungen von Hartmann, Papula und Strehl.

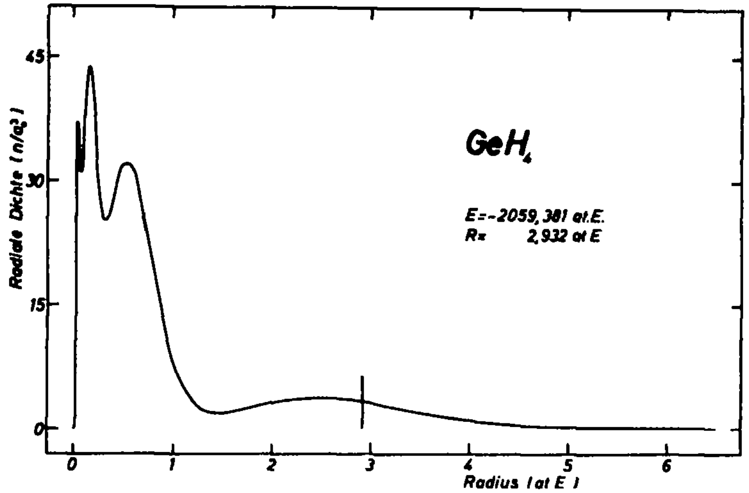

Fig. 4. Die gesamte radiale Elektronendichte des GeH_4-Moleküls. Der senkrechte Strich markiert den Abstand *R* der vier H-Atome vom Ge-Atom

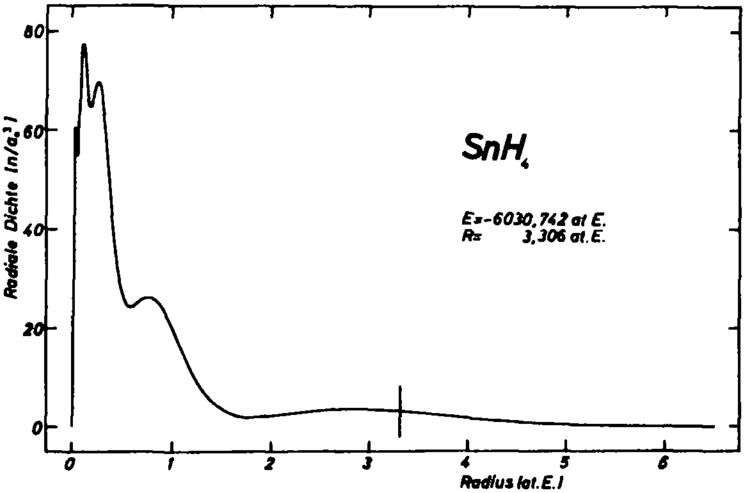

Fig. 5. Die gesamte radiale Elektronendichte des SnH_4-Moleküls. Der senkrechte Strich markiert den Abstand *R* der vier H-Atome vom Sn-Atom

In Fig. 1 sind die Endwerte der Parameter λ_i der Minimisierung als Funktion der Kernladung aufgetragen.

Nach erfolgter Minimisierung der Energie der Moleküle CH_4 und SiH_4 extrapolieren wir linear[1] aus einer ersten graphischen Darstellung die Startwerte für das Molekül GeH_4, und nach dessen Berechnung die Startwerte für SnH_4, danach für PbH_4. Die Rechnenzeit auf der Maschine TR 440 liegt bei gleich-

---

[1] Man vgl. hierzu die Abhängigkeit des Exponentialausdruckes von der Kernladungszahl bei den nach den Slaterschen Regeln zu erhaltenden Funktionen [17].

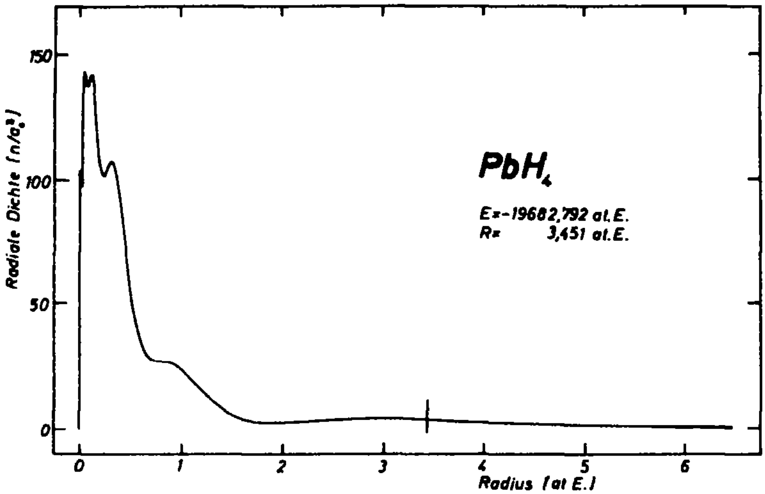

Fig. 6. Die gesamte radiale Elektronendichte des PbH_4-Moleküls. Der senkrechte Strich markiert den Abstand *R* der vier H-Atome vom Pb-Atom

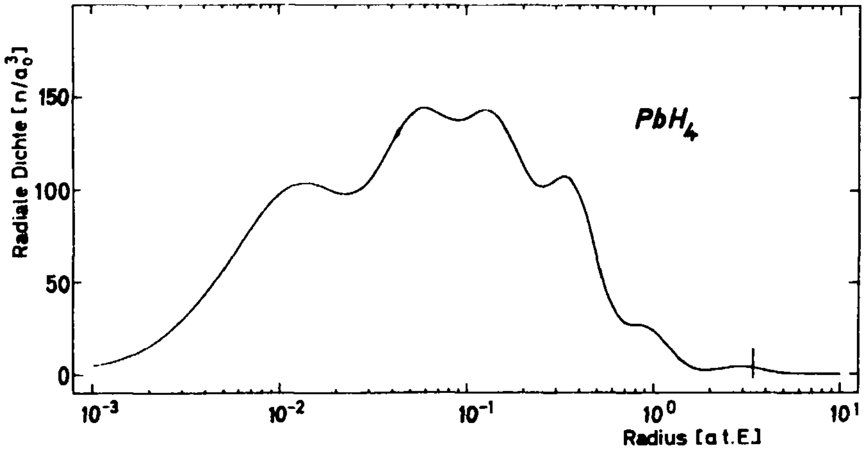

Fig. 7 Die gesamte radiale Elektronendichte des PbH_4-Moleküls in halblogarithmischer Darstellung. Der senkrechte Strich markiert den Abstand *R* der vier H-Atome vom Pb-Atom

zeitiger Minimisierung aller Parameter eines Moleküls, sogar bei PbH_4, noch unter einer Minute.

Es zeigt sich nach der Berechnung der Moleküle CH_4, SiH_4, GeH_4, SnH_4 und PbH_4, daß jeweils sich entsprechende Parameter λ_i nahezu auf einer Geraden liegen (Fig. 1).

Diese graphische Darstellung werten wir zusammen mit den erfolgreichen Rechnungen der Moleküle CH_4 bis SnH_4 als Indiz für die Richtigkeit von Bindungsabstand und Gesamtenergie bei PbH_4. Zusätzlich wird der Virialsatz für

Atome nachgeprüft; für das Verhältnis $-\frac{2E_{\text{kin}}}{E_{\text{pot}}}$ ergibt sich bei PbH_4 der Wert 1,0000.

Die radialen Dichteverläufe sind in Fig. 2–6 dargestellt. Für PbH_4 wird zur besseren Übersichtlichkeit der Radius in einer zusätzlichen Abbildung (Fig. 7) halblogarithmisch aufgetragen.

Wir danken der DFG für die finanzielle Unterstützung dieser Arbeit.

Literatur

1. Gombás, P, Ladányi, K.: Acta physica Acad. Sci. hung. **5**, 313 (1955).
2. Hartmann, H., Gliemann, G.: Z. physik. Chem. (N. F.) **15**, 108 (1958).
3. Eigene Rechnung.
4. Hartmann, H., Papula, L., Strehl, W.: Theoret. chim. Acta (Berl.) **17**, 131 (1970).
5. Hartmann, H., Papula, L., Strehl, W.: Theoret. chim. Acta (Berl.) **19**, 155 (1970).
6. Hartmann, H., Papula, L., Strehl, W.: Theoret. chim. Acta (Berl.) **21**, 69 (1971).
7. Papula, L.: Private Mitteilung.
8. Gombás, P.: Acta physica Acad. Sci. hung. **1**. 285 (1951).
9. Fermi, E., Amaldi, E.: Mem. Acc. Italia **6**, 117 (1934); man vergleiche weiter: Gombás, P.: Die statistische Theorie des Atoms und ihre Anwendung, S. 65. Wien: Springer 1949.
10. Kaupe, A. F., Jr.: Comm. ACM **6**, 313 (1963); as revised by: Bell, M., Pike, M. C.: Comm. ACM **9**, 684 (1966).
11. Bishop, D. M.: Mol. Physics **6**. 305 (1963).
12. Moccia, R.: J. chem. Physics **40**, 2175 (1964).
13. Tindal, Straley, Nielsen: Proc. nat. Acad. Sci. USA **27**, 208 (1941).
14. McKay, K. M.: Hydrogen compounds of metallic elements, p. 7. London: E. and F. N. Spon 1966.
15. Stevenson, P. E., Lipscomb, W. N.: J. chem. Physics **52**, 5343 (1970).
16. Grein, F.: Theoret. chim. Acta (Berl.) **1**, 52 (1962).
17. Eyring, Walter, Kimball: Quantum chemistry, p. 162. New York: Wiley 1965.

Prof. Dr. Karl Hensen
Institut für Physikalische Chemie
der Universität Frankfurt a. Main
D-6000 Frankfurt am Main
Robert-Mayer-Straße 11
Bundesrepublik Deutschland

Theoret. chim. Acta (Berl.) 28, 307—310 (1973)
© by Springer-Verlag 1973

Relatio

No N^4-Dependence in the Calculation of Large Molecules

Volker Dyczmons

Lehrstuhl für Theoretische Chemie der Universität Göttingen
Göttingen, Germany

Received September 18, 1972

It is shown that the time needed for computing large molecules is proportional to $N^2 \cdot (\ln N)^2$, when Gaussian functions are used and the molecule is larger than a well-definable limit. Some proposals to overcome this limit are made.

The time T needed for computing a molecule is proportional to the number of integrals one has to calculate. Now let us consider a four-center integral I_{abcd}:

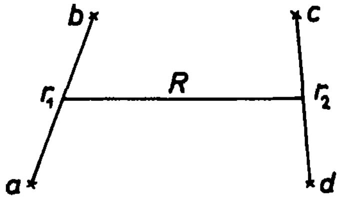

Fig. 1

Then, for large R (cf. Fig. 1)

$$I_{abcd} = \int \varphi_a(1)\,\varphi_b(1)\,\frac{1}{r_{12}}\,\varphi_c(2)\,\varphi_d(2)\,d\tau_1\,d\tau_2 \rightarrow S_{ab} S_{cd} \frac{1}{R} \,. \tag{1}$$

If we now use as basis-functions pure Gaussian functions (GF's):

$$\varphi_a(1) = \exp[-\eta_a(\boldsymbol{r} - \boldsymbol{r}_a)^2] \tag{2}$$

we get [1] (cf. Fig. (1)):

$$I_{abcd} \rightarrow \exp(-c_1 r_1^2) \cdot \exp(-c_2 r_2^2)\,\frac{1}{R} \tag{3}$$

with

$$c_1 = \frac{2\eta_a\eta_b}{\eta_a + \eta_b}, \quad c_2 = \frac{2\eta_c\eta_d}{\eta_c + \eta_d}. \tag{3a}$$

We now consider a linear molecule, which lies on the x-axis of a 3-dimensional coordinate system (Fig. 2).

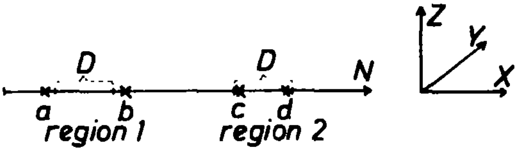

Fig. 2

Let N be the number of basis-functions which are used to describe this molecule. We choose the region 1 with length D in such a way that a and b lie both either within or outside the region. When a and b lie outside, the region should be between a and b. Let the same be true for region 2 with the same length D with regard to c and d.

Now one does not want to calculate all very small integrals. However, we require that the error due to neglect of these integrals ought to be smaller than ε.

Looking at Fig. 2 we note: If a, b lie both outside of region 1, then from (3) and with $R > 1$, one gets:

$$I_{abcd} < \exp(-c_1 D^2)\,. \tag{4}$$

We include in the calculation only such integrals where a, b, and c, d lie within their respective regions. The sum of all neglected integrals ΔI ought to be smaller than ε. This means:

$$\Sigma \Delta I < N^4 \cdot \exp(-c_M D^2) = \varepsilon \tag{5}$$

where c_M is the minimum of all c_1, c_2. It then follows:

$$D = \left[\frac{1}{c_M}\left(4 \ln N + \ln \frac{1}{\varepsilon}\right)\right]^{1/2} \propto \sqrt{\ln N} \tag{6}$$

summin over all positions of the regions 1 and 2 gives an additional factor N^2. The time T necessary for computing a linear molecule is then:

$$T \propto N^2 D^4 \propto N^2 \cdot (\ln N)^2\,. \tag{7}$$

For a nonlinear or nonplanar molecule we can repeat the same considerations for the y- and/or z-directions (see Fig. 2). Regions 1 and 2 then become spheres with the diameter D. With $N = N_x \cdot N_y \cdot N_z$ the total number of basisfunctions Eq. (5) is still valid. By summing over all positions one gets a factor $N_x^2 \cdot N_y^2 \cdot N_z^2 = N^2$ and the result is again Eq. (7).

Now what is the optimal way in calculating large molecules?:

a) First of all we note that GF's are of course better than Slater functions (for which $T \propto N^2 \cdot (\ln N)^4$).

b) There is a special kind of GF's which is optimal as basis-functions. They are grouped pure GF's with a *fixed* number of different η-values (the last point saves about 60% computing time).

c) One has to optimise molecular basis-sets for the different bonds (see e.g. [2]) and s-p-hybrids, as e.g. Huzinaga has done for atomic wave-functions [3].

d) One has to avoid small η-values as far as possible; cf. Eq. (6) and the definition of c_M in Eq. (3a).

After all this has been done one has to write computer programs in such a way that the estimate in Eq. (7) really holds. But this is easily done. One has only to test for which a, b (respectively c, d)

$$\int |\varphi_a(1)|\,|\varphi_b(1)|\,d\tau_1 > \frac{\varepsilon}{N^4} \tag{8}$$

holds. A better approximation than (5) shows that in (8) one gets $\text{const}\cdot\varepsilon/N$ instead of ε/N^4 [6].

In those cases where the correlation energy plays an important part, a SCF-calculation is not sufficient. For large molecules the following scheme is probably optimal as far as total computing time is concerned:

1) SCF-calculation.

2) *Complete* localization of the SCF-MO's; this is only possible by using non-orthogonal MO's.

3) Calculation of the pair-energies (see e.g. [4]). Interpair energies are calculated for neighbouring pairs only. The correlation energies of all these pairs are calculated only in the HF-field of neighbouring SCF-MO's. This is opposed to some methods which calculate the correlation energy for the molecule as a whole.

4) Calculation of the errors which arise by the additivity assumption for the pair-energies [5].

The great advantage of this scheme is that the time needed for the calculation of the correlation energy is *only* proportional to N, as compared to an N^2-dependence for the SCF-calculation.

This approach is probably good enough for most molecules. It may become possible to use tabulated values of intrapair and interpair energies and of pair additivity errors of small molecules for the computation of the correlation energy of larger systems.

Now we want to determine the molecular size for which Eq. (7) holds. For this purpose we consider a linear molecule: if it is larger than $2D$ (see Fig. 2), then Eq. (7) holds. For example, let us determine the critical size $2D$ for a chain of C-atoms with a C-C-distance of 2.5 a. u. With the choice of $\varepsilon = 10^{-6}$, 30 basis functions per C-atom and $c_M = 0.3$ we obtain with Eq. (6) a minimal number of 9 C-atoms. But Eq. (6) is not a very good approximation for this case since Eq. (6) was derived for the limit of molecule much larger than $2D$. 9 carbon atoms is a crude upper bound on the size of the molecule for which Eq. (7) applies. A better estimate of D in this case can be determined by the usual requirement that the smallest integral to be calculated should be equal to 10^{-8}. This means that $10^{-8} = S_{ab} = \exp(-c_M D^2)$. We also take $c_M = 0.3$ and get then $D = 7.8$ a. u. Therefore Eq. (7) holds if we have more than 6 C-atoms.

The essential point is this: Where is the limit from which the computing time increases quadratically? It is easily shown [6] that this limit is smaller than the one obtained above (i. e. about 5 C-atoms).

Another very important question is: How must the numerical accuracy of the individual integrals depend on N? In [6] it will be shown that this accuracy goes with $1/N$.

In conclusion, the techniques discussed in this paper should make *ab initio* calculations on larger molecules possible within a few years time.

I am grateful to Prof. Dr. W. A. Bingel for his encouragement of this work and to the „Deutsche Forschungsgemeinschaft" for its support.

References

1. Boys, S. F.: Proc. Roy. Soc. (London) A **200**, 542 (1950).
2. Dyczmons, V., Staemmler, V., Kutzelnigg, W.: Chem. Physics Letters **5**, No. 6, 361 (1970).
3. Huzinaga, S.: J. chem. Physics **42**, 1293 (1967).
4. Jungen, M., Ahlrichs, R.: Theoret. chim. Acta (Berl.) **17**, 339 (1970).
5. Dyczmons, V., Kebabcian, R.: to be published.
6. Dyczmons, V.: to be published.

V. Dyczmons
Lehrstuhl für Theoretische Chemie
der Universität Göttingen
D-3400 Göttingen, Bürgerstr. 50a
Federal Republic of Germany

Theoret. chim. Acta (Berl.) 28, 313–337 (1973)
© by Springer-Verlag 1973

Commentationes

A Semiempirical MO Study of the Electronic Structure and Excited States of the *Tris*(2,2′-Bipyridyl)Iron(II) and *Tris*(Glyoxal-*Bis*-N-Methylimine)Iron(II)Ions

Jan Blomquist
Institute of Physics, University of Stockholm, Vanadisvägen 9, 11346 Stockholm

Bengt Nordén
Dept. of Inorganic Chemistry, University of Lund, Box 740, 22007 Lund

Marianne Sundbom
Institute of Theoretical Physics, University of Stockholm, Vanadisvägen 9, 11346 Stockholm

Received May 23, 1972

A semi-empirical SCF–MO method, the PEEL method, has been applied in an investigation of the electronic structure and excited states of two iron compounds, $[Fe(II)-(GMI)_3]^{++}$ and $[Fe(II)-(bipy)_3]^{++}$. The electronic absorption spectra have been recorded. The calculations show that it is necessary to account for the trigonal distortion and the covalency in order to explain these spectra quantitatively. Mössbauer measurements have also been performed. The calculated electronic population of the iron is in accord with Mössbauer isomer shift data, indicating that a realistic electron distribution has been obtained by the PEEL method.

Eine semiempirische SCF–MO-Methode, die PEEL-Methode, wurde zur Untersuchung der Elektronenstruktur sowie von angeregten Zuständen der beiden Eisenverbindungen $[Fe(II)-(GMI)_3]^{++}$ und $[Fe(II)-(bipy)_3]^{++}$ angewendet.

Die elektronischen Absorptionsspektren wurden aufgenommen. Die Berechnungen zeigen, daß die trigonale Verzerrung und die Kovalenz berücksichtigt werden müssen, um die Spektren quantitativ zu erklären. Mössbauer-Messungen wurden ebenfalls durchgeführt. Die berechnete Elektronenverteilung am Eisenatom ist in Übereinstimmung mit den Daten der Isomerenverschiebung der Mössbauer-Messungen, wodurch gezeigt wird, daß mit der PEEL-Methode eine realistische Elektronen-Verteilung erhalten wurde.

Une méthode SCF–MO semi-empirique, la méthode PEEL, a été appliquée à une étude de la structure électronique et des états excités de deux composés ferreux: $[Fe(II)-(bipy)_3]^{++}$ et $[Fe(II)-(GMI)_3]^{++}$. Les spectres d'absorption électronique ont été enregistrés. Les calculs montrent qu'il est nécessaire de rendre compte de la distorsion trigonale et de la covalence pour expliquer ces spectres quantitativement.

Des mesures de l'effet Mössbauer ont aussi été effectuées. La population électronique calculée du fer est en bon accord avec les données sur le déplacement isomérique de Mössbauer, ce qui indique que la méthode PEEL fournit une distribution électronique réaliste.

1. Introduction

To obtain an understanding of the activity of organic molecules and organometallic complexes it is necessary to know more about their electronic structure. The present investigation is part of a project whose object is molecular orbital (MO)

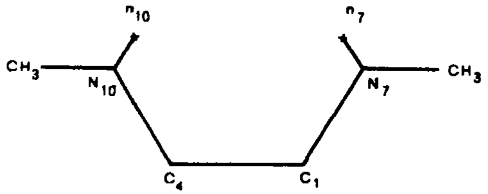

GMI
(ligand A)

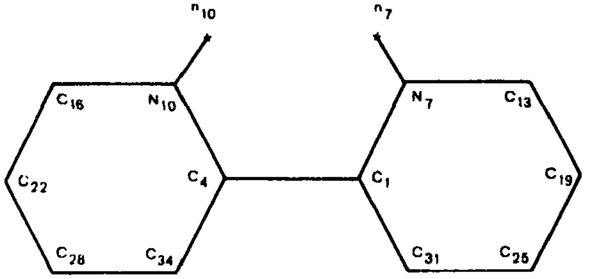

BIPYRIDYL
(ligand A)

Fig. 1. The numbering of the AO's of GMI and bipyridyl. Cf. Fig. 2 and text

studies of molecules of biological interest. This study uses the PEEL method, an extended Pariser-Parr-Pople (PPP) method, that has proved to be successful in accounting for many different properties of large organic molecules [1–3] and organic copper complexes [4 7]. It was found worthwhile to extend the method to complexes of other transition elements. In the present paper the semiempirical parameters for iron complexes are presented.

The two propellershaped ions[1] $[Fe(II)\text{–}(bipy)_3]^{++}$ and $[Fe(II)\text{–}(GMI)_3]^{++}$ (bipy = 2,2'-bipyridyl; GMI = glyoxal-*bis*-N-methylimine) have been used as model compounds for the determination of semiempirical parameters describing the amount of bonding between iron and the nitrogen ligands. These molecules were chosen because they have been extensively investigated by experimental methods. The calculations have been performed for the right-handed optical isomers (cf. Figs. 1 and 2). The present MO study gives information about the electronic distribution within the complexes, especially the effective electronic population on the iron ion, from which a value of the total electronic density at the iron nucleus can be deduced and compared with the experimental value obtained from Mössbauer isomer shift data. Further, the study permits a discussion of the different types of transitions in the electronic spectra.

Reviews of previous theoretical investigations and experimental findings for $[Fe(II)\text{–}(bipy)_3]^{++}$ and $[Fe(II)\text{–}(GMI)_3]^{++}$ can be found in some recent publications [8, 9]. In most discussions of the electronic spectra of these compounds, octahedral symmetry (O_h) and crystal field theory have been considered adequate for the assignments. The results of the present investigation, however, show that it is necessary to account for the trigonal distortion and the covalency in order to

---

[1] In this paper the convention has been used that Fe(II) stands for ferrous iron, Fe^{2+}.

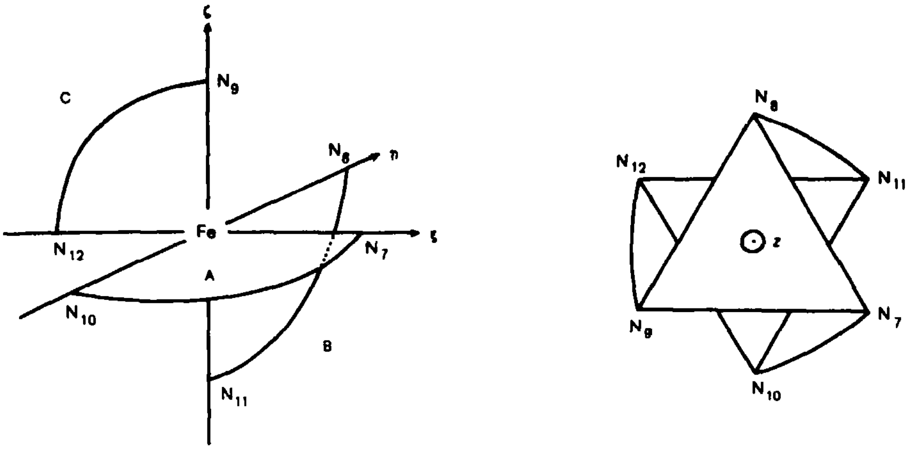

Fig. 2. The propellershaped structure of $[Fe(II)\ (GMI)_3]^{++}$ and $[Fe(II)\ (bipy)_3]^{++}$. *xyz* denotes the D_3 symmetry adapted right handed coordinate system with *z* as threefold axis and *x* through the twofold axis of ligand *A*. Cf. Fig. 1 and text

explain these spectra quantitatively. Day and Sanders [10, 11] discussed the CT band of the similar phenanthroline complex, using Hückel molecular orbitals and a simple treatment of CT states [12, 13]. In a more elaborate theoretical treatment of these molecules Ito, Tanaka, Hanazaki and Nagakura [14–16] were able to give a more quantitative discussion of the electronic transitions. They used an extension of the "molecules-in-molecule" method [13, 16] for their studies of metal complex ions, considered explicitly π orbitals of the ligands and *d* orbitals of the iron ion, and used locally excited ligand transitions together with electron transfer $(d \to \pi^*)$ transitions in their CI-treatment. Thus their methods did not allow for a discussion of transitions of $(d \to d)$ type.

In the present investigation 4*s* and 4*p* orbitals have been included, and the energy levels of excited states have been calculated by mixing all types of configurations obtained from single excitations. The theoretical model is discussed in Sections 3 and 4.

The electronic absorption spectra have been investigated experimentally and Mössbauer measurements have also been performed.

2. Experimental

Tris-(2,2'-bipyridyl) iron(II) sulphate was prepared according to a method of Jaeger and van Dijk [17]. The precipitate was washed with ether and dried over P_2O_5 for one week. It corresponded to a composition $Fe(bipy)_3 \cdot SO_4 \cdot 5H_2O$.

(*Analysis:* C 50.7, H 4.7, S 5, N 11.9; Calc. for $FeC_{30}N_6H_{24}SO_4 \cdot 5H_2$/: C 50.7, H 4.8, S 4.5, N 11.8.)

*Tris-(glyoxal-bis-*N*-methylimine) iron(II) iodide* was obtained in the way described by Krumholz [18] and dried over P_2O_5 for one week.

(*Analysis:* C 26.0, H 5.1, N 15.0; calculated for $FeC_{12}N_6H_{24}I_2$: C 25.6, H 4.3, N 14.9.)

The UV spectra in the range 15–54 kK were recorded on 10^{-4} M solutions (aqueous for the GMI complex, and methanolic for the bipyridyl complex) with a Cary 15 recording spectrophotometer. Spectrograde methanol was used without further purification. In the 10 kK range a Hitachi EPS-3T spectrophotometer was used on 0.3 M aqueous solutions. Concerning the iodide, it was carefully checked that no photolysis intervened. The UV spectrum could be exactly reproduced in several runs. The results are given in Tables 6, 7, 10 and 11 and Figs. 3 and 4.

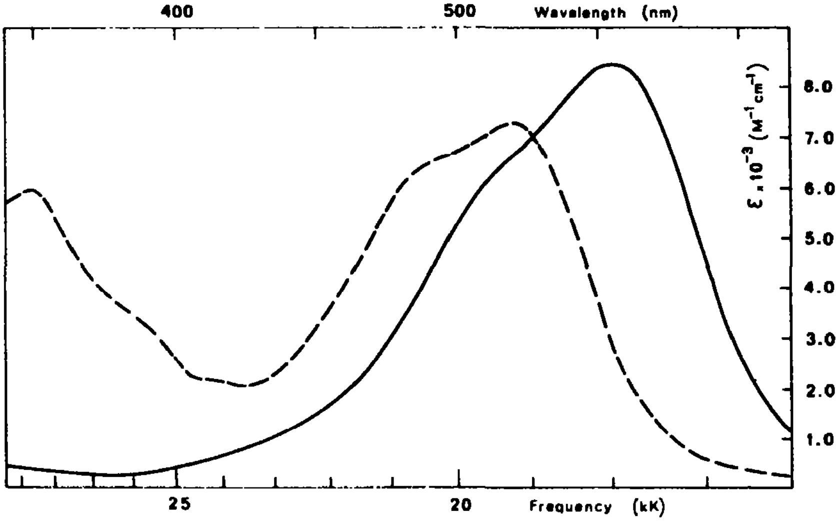

Fig. 3. The electronic absorption spectra of [Fe(II)-(GMI)$_3$]. I_2 in aqueous solution (———), and of [Fe(II)-(bipy)$_3$] · SO_4 · $5H_2O$ in methanol (- - ---). The visible region

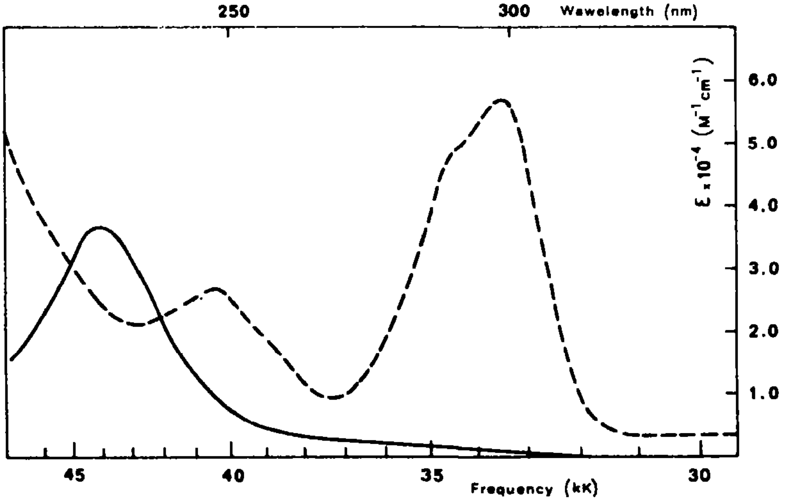

Fig. 4. The electronic absorption spectra of [Fe(II)-(GMI)$_3$]. I_2 in aqueous solution (---- ---), and of [Fe(II)-(bipy)$_3$] · SO_4 · $5H_2O$ in methanol (----). The UV region

Mössbauer spectra were measured at room temperature with an electromechanical transducer of Kankeleit type in combination with an Intertechnique 400-channel analyser and a Hilger and Watts P 1028 scintillation detector. The source was 5 mC ^{57}Co in Pd foil kept at the same temperature as the absorber. The velocity was calibrated using the magnetic splitting of natural iron. The Mössbauer lines were fitted to Lorentzians by means of a least squares method. Also in this case the spectra were satisfactorily reproduced in several runs with different samples. The results are given in Table 5.

More details about the Mössbauer study can be found in Ref. [47].

3. Theoretical Model

In applying the methods of quantum chemistry to large molecular systems, approximations must be made to simplify the work required and reduce the amount of computertime utilized drastically. Roos and Skancke [19] suggested a new scheme for the evaluation of semiempirical parameters in a modified PPP-method for π systems. In order to allow for a systematic study of large organic molecules, this scheme has been extended. The method is now applicable to the π-electron system of various heteroaromatic systems and to σ lone pair electrons (n) for nitrogen-containing molecules (see [3] for references). An extension of the PPP-method to organometallic molecules was suggested by Roos [4]. This method has been applied to Cu complexes [4–7] and has given very promising results. In the present work the scheme is extended to include iron complexes. The method has been thoroughly presented previously [4, 7] and will only be shortly outlined here:

1. The method is based on the Roothaan MO-SCF method for open shell systems [20].

2. The electrons have been divided into two groups, the core and the peel. The core group is not explicitly taken into account; it merely contributes a constant charge density, corresponding to a fixed electrostatic potential field. The Hamiltonian of the peel electrons can be written:

$$H = \sum_{i} H_{(i)}^{\text{core}} + \sum_{i<j} 1/r_{ij} \tag{1}$$

where $H_{(i)}^{\text{core}}$ is the sum of the kinetic and potential energy operator for electron i. The peel consists of the valence electrons of the metal atom, the ligand lone-pair electrons, and the π electrons of the ligands. The molecular orbitals are given as linear combinations of atomic orbitals, which are taken to be: $3d$, $4s$ and $4p$ orbitals on the metal atom, σ lone-pair orbitals for the ligand atoms, and one π orbital for each of the atoms contributing π-electrons to the system.

3. The zero differential overlap (ZDO) approximation is applied to all two-electron integrals except for the one-center exchange integrals.

4. Only resonance integrals between neighbouring atoms are retained, in correspondance with the nature of the ZDO approximation.

5. The method is semi-empirical. The following integrals are determined from atomic or molecular ionization potentials and spectral data:

Resonance integrals, $\beta_{\mu\nu} = H^{\text{core}}_{\mu\nu}$ (μ and ν neighbours),
two-center coulomb integrals, $\gamma_{\mu\nu}$ (μ and ν neighbours),
one-center coulomb integrals, $J_{\mu\nu}$,
one-center exchange integrals, $K_{\mu\nu}$,
parts of the one-center core integrals, $\alpha_\mu = H^{\text{core}}_{\mu\mu}$.

α_μ is decomposed according to a technique due to Goeppert-Mayer and Sklar [22], and described further in next section.

6. Excited states are calculated by means of the method of superposition of configurations. All types of singly excited configuration are included.

4. Semiempirical Iron Parameters

The extended PPP-method can be formulated in terms of two types of integrals: one-electron integrals occurring in the core matrix H^{core}, and two-electron integrals of coulomb and exchange type. In a semiempirical theory these integrals should be expressible in terms of a limited set of semiempirical parameters. The idea is to determine as many as possible of these parameters from experimental data. A general scheme using experimental data has been developed for the evaluation of semiempirical parameters of carbon and hetero atoms (see [3] for further references). In the present work previously determined carbon and nitrogen parameters [1, 3] have been used.

Semiempirical parameters for the iron atom and for the iron ligand bond have been derived in the present work and will be discussed in detail. It should be stressed that the procedure to obtain these parameters necessarily must be more uncertain depending on the greater complexity, e.g. the metal atom contributes nine AO's to the basis set, and the lack of sufficient experimental information.

Two-Electron Integrals

1. One-center coulomb, $J_{\mu\nu}$, and exchange, $K_{\mu\nu}$, integrals are considered and expressed in terms of Slater-Condon parameters F_k and G_k [40, 41]. These parameters were determined from iron atomic spectra and atomic Hartree-Fock calculations (see Appendix 1). They are considered dependent on charge, q, or number of d-electrons, n_d. Values obtained are given in Table 1.

2. Of the two-center two-electron integrals only the coulomb integrals, $\gamma_{\mu\nu}$, are retained. They were calculated by means of an interpolation formula suggested by Roos [4, 21]:

$$\gamma_{\mu\nu}(R) = \tfrac{1}{2}(\gamma_{\mu\mu} + \gamma_{\nu\nu}) \cdot f(z) \tag{2}$$

where R is the distance between the orbitals,

and

$$z = \tfrac{1}{2}(\gamma_{\mu\mu} + \gamma_{\nu\nu}) R \tag{3a}$$

$$f(z) = 1/(z + e^{-z}). \tag{3b}$$

Formula (2) is independent of the orientation of local coordinate axes.

Table 1. One-center semiempirical parameters (in kK) for Fe

SCP[a] \ q[b]	$q = 0$	$q = +1$	$q = +2$
ε_s	−490.37	−560.95	−612.78
$F_0(ss)$	49.70	58.29	—
$F_0(sd)$	62.17	73.12	84.06
$G_2(sd)$	1.290	1.560	1.830
ε_p	−356.83	−449.38	−481.79
$F_0(pp)$	43.74	55.24	—
$F_2(pp)$	0.919	1.160	
$F_0(sp)$	46.72	56.77	—
$G_1(sp)$	10.023	12.573	—
$G_1(pd)$	0.324	0.478	0.632
$G_3(pd)$	0.0162	0.0239	0.0316
$F_0(pd)$	46.66	61.42	68.47
$F_2(pd)$	0.275	0.351	0.411

SCP \ n_d[c]	$n_d = 8$	$n_d = 7$	$n_d = 6$	$n_d = 5$
ε_d	−734.40	−767.93	−793.83	−808.48
$F_0(dd)$	95.89	105.54	115.19	124.84
$F_2(dd)$	1.075	1.246	1.418	1.589
$F_4(dd)$	0.096	0.105	0.114	0.123

[a] SCP stands for Slater-Condon parameter.
[b] q is the charge of the iron ion.
[c] n_d is the number of 3d electrons of the iron ion.

One-Electron Integrals

The one-electron operator H^{core} has the following form:

$$H^{\text{core}} = T + U^{\text{core}}(\text{Me}) + \sum_i U^{\text{core}}(L_i) \tag{4}$$

where T denotes the kinetic energy operator, $U^{\text{core}}(\text{Me})$ the potential field from the metal core and $U^{\text{core}}(L_i)$ the corresponding field from the ligand atom i.

1. The core integral α_μ, where μ is a metal atomic orbital, can be decomposed in the following way:

$$\alpha_\mu = \varepsilon_\mu - \sum_i \sum_{v(i)} n_{v(i)} \gamma_{\mu v(i)} + \Delta\alpha_\mu \tag{5}$$

where

$$\varepsilon_\mu = \langle \mu | T + U^{\text{core}}(\text{Me}) | \mu \rangle \tag{6}$$

and

$$\Delta\alpha_\mu = \Sigma \langle \mu | U^0(L_i) | \mu \rangle \,. \tag{7}$$

This technique to rewrite α_μ is due to Goeppert-Mayer and Sklar [22]. ε_μ contains the interaction between a metal electron and the metal core. The matrix elements, ε_μ, were determined from atomic ionization potentials and atomic spectral data (see Appendix 1 and Table 1). In the second part of (5) $n_{v(i)}$ is the number of electrons associated with the atomic orbital $\nu(i)$ at the ligand atom i. $\Delta\alpha_\mu$ represents the penetration between a metal orbital and a neutral atom and was roughly estimated as follows: The nitrogen atoms were treated as point dipoles (in the center of the nitrogen atom) with a dipole moment of 2.25 D corresponding to the dipole moment of pyridine [23] and with a direction opposite to the vector connecting the center of the nitrogen atom to the center of charge of the sp^2-hybridized lone pair of nitrogen. $\Delta\alpha_\mu$ was estimated as the interaction between these dipoles and an electronic charge situated at the center of charge of the orbital μ. This method gave a value of 0.367 a.u. for the bipy complex and a value of 0.359 a.u. for the GMI complex. In this context it should be noted that it would be desirable to consider the sum of the first and third terms of (5) as one parameter to be determined from experimental data; e.g., ionization potentials of a series of similar iron complexes, thus applying a method similar to the one used for π systems. Unfortunately the lack of experimental data confines us to use the present much cruder method.

The core integrals $\alpha_{\nu_C(\pi)}$, $\alpha_{\nu_N(\pi)}$, and $\alpha_{\nu_N(n)}$, where $\nu_C(\pi)$, $\nu_N(\pi)$ and $\nu_N(n)$ are ligand atomic orbitals, are also decomposed according to the Goeppert-Mayer and Sklar method:

$$\alpha_{\nu_C(\pi)} = W_{\nu_C(\pi)} - \sum_{\nu' \neq \nu_C(\pi)} n_{\nu'} \gamma_{\nu' \nu_C(\pi)} - \sum_\mu n_\mu \gamma_{\mu \nu_C(\pi)} + \langle \nu_C(\pi) | U^0(\text{Me}) | \nu_C(\pi) \rangle ; \tag{8}$$

$$\begin{aligned} \alpha_{\nu_N(\pi)} = {} & W_{\nu_N(\pi)} - 2J_{\nu_N(\pi)\nu_N(n)} + K_{\nu_N(\pi)\nu_N(n)} - \sum_{\nu' \neq (\nu_N(\pi) \text{ and } \nu_N(n)} n_{\nu'} \gamma_{\nu' \nu_N(\pi)} \\ & - \sum_\mu n_\mu \gamma_{\mu \nu_N(\pi)} + \langle \nu_N(\pi) | U^0(\text{Me}) | \nu_N(\pi) \rangle ; \end{aligned} \tag{9}$$

$$\begin{aligned} \alpha_{\nu_N(n)} = {} & W_{\nu_N(n)} - J_{\nu_N(\pi)\nu_N(n)} + \tfrac{1}{2} K_{\nu_N(\pi)\nu_N(n)} \\ & - \sum_{\nu' \neq (\nu_N(\pi) \text{ and } \nu_N(n)} \quad - \sum_\mu n_\mu \gamma_{\mu \nu_N(n)} + \langle \nu_N(n) | U^0(\text{Me}) | \nu_N(n) \rangle ; \end{aligned} \tag{10}$$

ν' denotes a ligand atomic orbital and μ a metal atomic orbital. In the present work the terms expressing the ligand metal penetration, $\langle \nu | U^0(\text{Me}) | \nu \rangle$, have been neglected as was also done in previous calculations on copper complexes. The parameters W_ν are discussed in detail in previous papers [1, 3, 19].

2. The formula of Wolfsberg and Helmholtz [24] was used for the resonance integrals $\beta_{\mu\nu}$,

$$\beta_{\mu\nu} = -\frac{k_\mu}{2} \cdot S_{\mu\nu}(I_\mu + I_\nu) \tag{11}$$

where μ is a metal orbital ($3d$, $4s$, or $4p$) and ν an orbital of the nitrogen atoms.

Here I_μ and I_ν are valence state ionization potentials, $S_{\mu\nu}$ the overlap integral between μ and ν, and k_μ constants to be determined from molecular spectral data[2]. The overlap integrals were calculated theoretically from atomic Hartree-Fock orbitals for iron [25, 26] and nitrogen [26]. In line with previous studies on copper complexes, the preliminary intention was to investigate whether three different values, k_{3d}, k_{4s}, and k_{4p}, could be determined from the electronic spectral data of the bipyridyl and GMI complexes of iron(II). The initial values for these parameters were taken from previous studies of copper complexes [4, 5]. The calculated spectra were found to be predominantly determined by the value of k_{3d}. A satisfactory agreement between theory and experiment was obtaines for $k_{3d} = 3.26$ and $k_{4s} = k_{4p} = 1.0$. It should be noted, however, that the calculated spectra are insensitive to moderate changes in k_{4s} and k_{4p}.

---

[2] The assumed occupation numbers in determining the metal I_μ values are $3d^6 4s 4p$ for $4p$ and $3d^6 4s^2$ for $4s$ and $3d$.

5. Details of the Calculation

As far as we know there are no X-ray diffraction data for the iron(II) complexes with *tris*-(2,2′-bipy) and *tris*-(GMI). From an analysis of measured NMR spectra of [Fe(II)-(dipy)$_3$]Cl$_2$ Castellano, Günther and Ebersole [27] concluded that the *cis*-planar conformation of the bipyridyl groups was in line with the measured values of the chemical shifts. They also derived a metal-nitrogen distance of 2 Å. For a similar complex, *tris-o*-phenanthroline iron(II), Templeton, Zalkin and Ueki [28] obtained an average iron-nitrogen distance of 1.97 Å. In the present calculations of the two diamagnetic complexes [Fe(II)-(bipy)$_3$]$^{++}$ and [Fe(II)-(GMI)$_3$]$^{++}$ the Fe–N distance is assumed to be 2.0 Å. This is also in accord with recent X-ray data on a high-spin and a low-spin form of Fe(dipy)$_2$(NCS)$_2$ by König and Watson [29]. They obtained an average Fe–N distance of about 2.02 Å for the low spin (singlet) form. Both complexes are assumed to have D_3 symmetry. The dipyridyl ligands are assumed to have *cis*-planar structure with the same interatomic distances as found from electron diffraction measurements [30]. This structure was also used in a previous MO calculation [31] on the planar *cis*- and *trans*-forms of bipyridyl.

There are no experimental structural data of GMI. A first separate MO calculation was performed for GMI with the same reasonable assumption of geometry as was made by Ito *et al.* [14] in their theoretical investigation of GMI and the *tris*-(GMI) iron(II) complex. New bond distances were obtained from the calculated bond orders, $p_{\mu\nu}$, by means of the relations [1, 19]

$$R_{\mu\nu}(\mathrm{C,C}) = 1.517 - 0.18\,p_{\mu\nu}, \tag{12}$$

$$R_{\mu\nu}(\mathrm{C,N}) = 1.458 - 0.18\,p_{\mu\nu}. \tag{13}$$

The calculation on GMI was repeated with the obtained bond distances and with angles for GMI such that in the iron complex the N–Fe–N angle would be 90° for the Fe–N distance equal to 2.0 Å. The structures of GMI and dipy are shown in Fig. 1 and the interatomic distances used in the calculations are given in Table 2.

Table 2. Bond distances (*in* Å) for GMI and bipyridyl chosen for the calculations. The numbering of the atoms are given in Fig. 1 and in text (Section 5)

GMI		Bipyridyl	
Bond	Bond length	Bond	Bond length
4—1	1.4600	4- 1	1.4700
7—1	1.2878	7-- 1; 13— 7	1.3394
Fe-N	2.0000	19-–13; 31— 1	1.3958
		25—19; 31 –25	1.3936
		Fe-N	2.0000

Both in the calculation of GMI and $(Fe(II)-(GMI)_3]^{++}$ the influence of the CH_3 groups was neglected.

The propellershaped structure of the complexes is visualized in Fig. 2, where the three ligands are denoted A, B and C. The calculations were performed for the right-handed optical isomers [32].

In the following, x, y, z denotes the coordinate system adopted to D_3 symmetry. The z-axis is taken as the threefold symmetry axis, and the x- and y-axes are taken to form a right-handed system with the positive x-axis passing through the twofold axis of ligand A (cf. Fig. 2).

$$\begin{aligned}\hat{x} &= \frac{1}{\sqrt{2}}(\hat{\xi}-\hat{\eta})\\ \hat{y} &= \frac{1}{\sqrt{2}}(\hat{\xi}+\hat{\eta}-2\hat{\zeta})\\ \hat{z} &= \frac{1}{\sqrt{2}}(\hat{\xi}+\hat{\eta}+\hat{\zeta})\,.\end{aligned} \tag{14}$$

This same choice of axes was also made by Day and Sanders [11].

The numbering of the atomic orbitals in ligand A is given in Fig. 1. If i numbers an AO on ligand A, $(i+1)$ will number the corresponding AO on ligand B, and $(i+2)$ the corresponding AO on ligand C.

The atomic orbitals that constitute the basis for the calculations are 27 for the GMI complex and 51 for the dipy complex: the $3d$, $4s$ and $4p$ orbitals of the iron ion, one sp^2 hybridized lone pair orbital (n) from each nitrogen, and one π orbital from each of the carbon and nitrogen atoms of the ligands. For the GMI-complex the atomic orbitals with numbers from 1 12 refer to ligand π orbitals, while for the dipy complex, 1 36 refer to π orbitals. The number of electrons taken into account is 30 in the GMI complex and 54 in the dipy complex; in each complex, 6 electrons come from the iron ion and the rest from the ligands.

The self-consistent field molecular orbitals were evaluated by means of a computer program, SCF-OPSZDO, written by B. Roos and M. Sundbom. This program also calculates the energy levels of excited states by mixing configurations from single excitations. All computations were made on an IBM 360/75 computer. The program and the computer limit the number of configurations for each symmetry to 140. Thus for the bipy complex not all of the single excitations could be considered. The CI treatment was restricted for each symmetry to 140 configurations.

The values of the one-center semiempirical parameters of iron depend on the electronic population of the iron ion (see appendix). A reasonable guess of the electronic population was made from Mössbauer isomer shift data, according to a method presented in a previous publication [33]. The initial effective configuration of the iron ion was thus guessed to be $(3d)^{5.75}(4s)^{0.5}(4p)^{0.5}$. The values of the one-center parameters for this configuration were obtained by interpolation in Table 1 and were used in the preliminary calculations to obtain reasonable values of the parameters k_μ, which occur in the expressions for the resonance integrals (cf. Section 3). When reasonable values for k_μ had been obtained, new one-center iron parameters were determined from the calculated effective configuration. The whole calculation was repeated with these new parameters. This procedure was repeated until self-consistency was achieved. In view of the simplified electron configuration dependence of the one center iron parameters (see appendix) the calculation was repeated only if the calculated values of n_{3d} and q deviated from the input values by more than ±0.1. This selfconsistency in charge procedure was then repeated for each set of trial k_μ values.

6. Molecular Orbitals and Ground State Properties

The SCF molecular orbitals and eigenvalues of $[\mathrm{Fe(II)}\text{-}(\mathrm{GMI})_3]^{++}$ are presented in Tables 3 and 4. The orbital pattern is similar for both compounds.

$[\mathrm{Fe(II)}\text{-}(\mathrm{GMI})_3]^{++}$

From Table 4 where the total electron population of the atomic orbitals is given, the configuration of the Fe ion is found to be $(3d)^{5.46}$ $(4s)^{0.42}$ $(4p)^{0.42}$ with a net charge of + 1.70 on iron. The Table 4 contains a comparison with the elec-

Table 3. Molecular orbitals of $[\mathrm{Fe(II)}\ (\mathrm{GMI})_3]^{++}$. Orbital energies ε_i in a.u. The electronic population. The numbering system as in Fig. 1

MO[a]			The electron population[b,c]								
No.	Symmetry	ε_i	C_1	N_7	n_7	z^2	$xy+(x^2-y^2)$	$xz+yz$	s	$x+y$	z
1	$1a_1$	−1.0887	0.000	0.000	0.131	0.004	0	0	0.209	0	0
2;3	$1e$	−1.0706	0.000	0.000	0.260	0	0.147	0.292	0	0.001	0
4	$1a_2$	−0.9736	0.001	0.003	0.150	0	0	0	0	0	0.079
5;6	$2e$	−0.9642	0.004	0.013	0.290	0	0.019	0.013	0	0.126	0
7;8	$3e$	−0.8801	0.094	0.179	0.023	0	0.155	0.062	0	0.001	0
9	$2a_1$	−0.8597	0.014	0.090	0.000	0.372	0	0	0.002	0	0
10	$2a_2$	−0.8542	0.075	0.087	0.004	0	0	0	0	0	0.002
11;12	$4e$	−0.8027	0.072	0.249	0.000	0	0.050	0.019	0	0.001	0
13	$3a_1$	−0.6774	0.027	0.039	0.000	0.598	0	0	0.002	0	0
14;15	$5e$	−0.6567	0.141	0.024	0.001	0	0.754	0.245	0	0.000	0
16	$3a_2$	−0.4066	0.091	0.073	0.001	0	0	0	0	0	0.011
17;18	$6e$	−0.3407	0.100	0.121	0.001	0	0.507	0.120	0	0.038	0
19;20	$7e$	−0.2539	0.254	0.070	0.000	0	0.052	0.003	0	0.001	0
21	$4a_1$	−0.2490	0.126	0.037	0.000	0.025	0	0	0.000	0	0
22;23	$8e$	−0.1818	0.001	0.001	0.072	0	0.314	1.246	0	0.000	0
24	$5a_1$	−0.0964	0.000	0.000	0.035	0.001	0	0	0.788	0	0
25;26	$9e$	0.0107	0.001	0.008	0.018	0	0.002	0.000	0	1.831	0
27	$4a_2$	0.0252	0.000	0.003	0.012	0	0	0	0	0	0.908

[a] The 15 lowest orbitals are doubly occupied.

[b] Formal population of the virtual orbitals.

N_7 and C_1 denotes π orbitals on nitrogen and carbon. n_7 denotes a nitrogen σ lone pair orbital. z^2 stands for $3d_{z^2}$, s for $4s$ and x for $4p_x$ on iron.

[c] For orbitals of e symmetry the sum of population for e_x and e_y is given.

Table 4. The electronic population of the atomic orbitals in $[Fe(II)\text{-}(GMI)_3]^{++}$, GMI *(cis)* and GMI *(trans)*

AO	$[Fe(II)\text{-}(GMI)_3]^{++}$	GMI *(cis)*	GMI *(trans)*
GMI:			
C	0.856	0.981	0.979
N	1.372	1.019	1.021
n	1.721	2.000	2.000
Fe:			
z^2	1.947		
$x^2 - y^2$; xy	1.124	$n_{3d} = 5.457$	
yz; xz	0.631		
s	0.424	$n_{4s} = 0.424$	$q = 1.701$
x; y	0.128	$n_{4p} = 0.418$	
z	0.162		

tronic population in GMI. Further, this table shows that there is a synergic interaction between metal-ligand σ- and π-bonding, resulting in a net transfer of electrons from the ligand σ system to mainly the $4s$, $4p$ and $3d$ orbitals of Fe and in a backdonation from the $3d$ orbitals to the ligand π system.

The value of the electronic density at the iron nucleus, $|\psi(0)|^2$, deduced from the calculated effective configuration of valence electrons by a recently published method [33], is in good agreement with the value obtained from the measured Mössbauer isomer shift (Table 5).

As shown in Table 3 the molecular orbital $1a_1$ is mainly a ligand nitrogen lone pair orbital, stabilized by bonding to Fe $4s$ (21%). $2a_1$ is a bonding and $3a_1$ an antibonding metal-ligand (π) orbital with 37% and 60% d_{z^2}-character respectively. The orbital $1a_2$ is a ligand n orbital weakly stabilized by $4p_z$ (8%), while $2a_2$ can be considered as a pure ligand π orbital. As shown in Table 3 $1e$ is mainly a ligand n-orbital (22% d-character), $2e$ is a ligand n orbital, while $3e$ and $4e$ are ligand π orbitals. $5e$ has 50% metallic $3d$ and 50% ligand π character.

The results of the present MO study show that only one orbital ($3a_1$) is mainly (60%) metallic, indicating the difficulty in discussing this compound from the crystal field point of view. In many previous discussions the splitting of the octahedral levels have been considered small and generally neglected. This assumption is not justified by the present results.

$[Fe(II)\text{-}(bipy)_3]^{++}$

The orbital pattern resembles that of the GMI complex.

The configuration of the Fe ion is found to be $(3d)^{5.47}(4s)^{0.42}(4p)^{0.42}$ with a net charge of 1.69 on iron. As shown in Table 5, the calculated effective electronic configuration yields a value of the electronic density at the nucleus in accord with the value obtained from the observed Mössbauer isomer shift. The good agreement

Table 5. The electron density at the Fe nucleus, $|\psi(0)|^2$, for $[\mathrm{Fe(II)}\text{–}(\mathrm{GMI})_3]^{++}$ and $[\mathrm{Fe(II)}\text{–}(\mathrm{bipy})_3]^{++}$. *Calculated values compared with values derived from experimental Mössbauer isomer shifts, δ [33]*

	Calculation	Observations					
		Epstein [34]				Present work	
	$\lvert\psi(0)\rvert^2$	δ^a (mm/s) at 300° K	$\lvert\psi(0)\rvert^2$	δ^a (mm/s) at 80° K	$\lvert\psi(0)\rvert^2$	δ^a (mm/s) at 300° K	$\lvert\psi(0)\rvert^2$
$[\mathrm{Fe(II)}\text{–}(\mathrm{GMI})_3]^{++}$	11907.75	0.414 ±0.010[b]	11907.53 ±0.04	0.515 ±0.013[b]	11907.17 ±0.04	0.27 ±0.01[c]	11908.04 ±0.04
$[\mathrm{Fe(II)}\text{–}(\mathrm{bipy})_3]^{++}$	11907.66	0.367 ±0.008[b]	11907.70 ±0.03	0.403 ±0.005[b]	11907.57 ±0.02	0.41 ±0.01[d]	11907.55 ±0.04

[a] Relative stainless steel (SS). (Add 0.161 mm/s to convert to sodium nitroprusside as references substance.)

[b] The perchlorate salts.

[c] $\mathrm{Fe}\text{–}(\mathrm{GMI})_3\mathrm{I}_2$.

[d] $\mathrm{Fe}\text{–}(\mathrm{bipy})_3 \cdot \mathrm{SO}_4 \cdot 5\,\mathrm{H}_2\mathrm{O}$.

between theoretical and experimental values indicates that the present MO method can be used with some confidence for the determination of the electronic distribution in transition metal complexes.

The orbital pattern shows that O_h symmetry will not be adequate for the assignment of electronic transitions. Distortions due to the actual D_3 symmetry are considerable and cannot be neglected. Furthermore no orbital can be considered as purely metallic, thus indicating that crystal field theory cannot be used to give a realistic picture of the electronic energy levels.

7. Excited States

The present CI treatment allows a quantitative description of the excited electronic energy levels. The calculations show that it is possible to classify only a few of the excited states as pure $d-d$, $\pi-\pi^*(L)$, or CT transitions. This was also found in previous calculations on organic copper complexes [4–7]. The results are presented in Tables 6–12. For comparison the spectra of planar *cis*- and *trans*-forms of GMI and bipyridyl have also been calculated (for bipyridyl, see Ref. [31]). The values obtained are given together with experimental data in Table 12.

$[\mathrm{Fe(II)}\text{–}(\mathrm{GMI})_3]^{++}$

Most transitions can be classified as partly CT and partly *L*. The observed intense visible band at 18 kK is assigned to the $3\,{}^1E$ state (calc. 19.9 kK), which is mainly a combination of the configurations $(5e \rightarrow 6e)$ and $(5e \rightarrow 3a_2)$ (Table 8). They both have some $d \rightarrow \pi^*$ character. The amount of electron transfer is 0.25, as shown in Table 9, where the electronic populations for some of the excited states are given.

Table 6. Electronic singlet transitions in $[Fe(II)-(GMI)_3]^{++}$. Transition frequencies in kK

Type[a]	Symmetry	Calculated		Observed				
				Ito *et al.* [14][b]		Present investigation		
		ν	f	ν_{max}	$\log \varepsilon_{max}$	ν_{max}	Range	$\log \varepsilon_{max}$
CT + *L*	$1\,^1A_2$	14.1	0.0003					
CT + *d* – *d*	$1\,^1E$	14.3	0.00003					
CT	$2\,^1A_2$	15.2	0.004					
CT + *L*	$2\,^1E$	15.3	0.004					
CT + *L*	$3\,^1E$	19.9	0.38	18.5	3.9	18.0		3.94
d - *d*	$4\,^1E$	21.8	0.0008	19.4^{c}	3.8	19.8^{c}	17–22	3.79
CT + *d* – *d*	$5\,^1E$	30.9	0.03	29.1	2.3		28.5 29.4	very weak
CT + *d* - *d*	$3\,^1A_2$	31.0	0.0004					
CT + *d* - *d*	$1\,^1A_1$	32.3	0					
CT + *L*	$2\,^1A_1$	37.3	0					
CT + *L*	$4\,^1A_2$	48.4	0.17	45.0^{c}	4.0	44.3	42–47.5	4.55
CT + *L*	$6\,^1E$	48.5	0.01					
CT + *L*	$7\,^1E$	50.4	0.05					
CT + *L*	$8\,^1E$	50.6	0.21					
CT + *L*	$3\,^1A_1$	50.9	0					
CT + *L*	$9\,^1E$	51.5	0.16					
CT + *L*	$4\,^1A_1$	55.1	0					
L	$10\,^1E$	59.9	0.03					
CT + *L*	$5\,^1A_2$	60.2	0.40	54.7	4.6	54	47.5→54	4.8

[a] CT = charge transfer, *L* = intraligand $\pi - \pi^*$.

[b] *tris*(glyoxal-*bis*-N-methylimine) iron(II) tetrafluoroborate in an aqueous solution. The values are estimated from Fig. 1 in [14b]

Table 7. The lower electronic singlet and triplet transitions in $[Fe(II)\ (GMI)_3]^{++}$. Calculated values and the estimated range in which to search for the transition

Type	Symmetry	Calculated		Estimated range,
		ν (kK)	f	ν (kK) (cf. text)
CT + *L*	$1\,^3A_1$	4.6	0	3–10
CT + *L*	$1\,^3E$	5.7	0	4–11
CT + *d* – *d*	$2\,^3E$	7.9	0	6–13
CT + *L*	$1\,^3A_2$	8.6	0	7–12
CT + *L*	$3\,^3E$	12.7	0	17–18
d – *d*	$4\,^3E$	13.8	0	12—19
CT + *L*	$1\,^1A_2$	14.1	0.0003	10–12
CT + *L*	$2\,^3A_2$	14.1	0	12–13
CT + *d* – *d*	$1\,^1E$	14.3	0.00003	10–12
CT	$2\,^1A_2$	15.2	0.004	11–13
CT + *L*	$2\,^1E$	15.3	0.004	11–13
CT + *L*	$3\,^1E$	19.9	0.38	18.0[a]
d - *d*	$4\,^1E$	21.8	0.008	19.8[a]
CT + *d* – *d*	$3\,^3A_2$	24.4	0	22–29[b]
CT + *d* – *d*	$5\,^3E$	24.5	0	22—29[b]
CT + *d* – *d*	$2\,^3A_1$	24.7	0	22–29[b]
CT + *d* – *d*	$5\,^1E$	30.9	0.03	~29[a]

[a] Observed. See Table 6.

[b] Ito *et al.* [14] observed a shoulder band near 25 kK, that may be assigned to one or all of the three triplets: $3\,^3A_2$, $5\,^3E$ and $2\,^3A_1$.

Table 8. The lower excited states of $[Fe(II)\text{–}(GMI)_3]^{++}$. Configuration mixing[a]

Symmetry	Wave function
$1\,^3A_1$	$0.96\,(5e\rightarrow 6e)^T$
$1\,^3E$	$-0.62\,(5e\rightarrow 6e)^T+0.25\,(3a_1\rightarrow 6e)^T+0.72\,(5e\rightarrow 3a_2)^T$
$2\,^3E$	$0.45\,(5e\rightarrow 6e)^T+0.83\,(3a_1\rightarrow 6e)^T$
$1\,^3A_2$	$0.52\,(5e\rightarrow 6e)^T+0.81\,(3a_1\rightarrow 3a_2)^T$
$3\,^3E$	$0.59\,(5e\rightarrow 6e)^T-0.38\,(3a_1\rightarrow 6e)^T+0.66\,(5e\rightarrow 3a_2)^T$
$4\,^3E$	$0.92\,(3a_1\rightarrow 8e)^T+0.39\,(2a_1\rightarrow 8e)^T$
$1\,^1A_2$	$0.98\,(5e\rightarrow 6e)^S$
$2\,^3A_2$	$0.82\,(5e\rightarrow 6e)^T-0.51\,(3a_1\rightarrow 3a_2)^T$
$1\,^1E$	$0.28\,(5e\rightarrow 6e)^S+0.91\,(3a_1\rightarrow 6e)^S-0.23\,(2a_1\rightarrow 6e)^S$
$2\,^1A_2$	$0.99\,(3a_1\rightarrow 3a_2)^S$
$2\,^1E$	$0.66\,(5e\rightarrow 6e)^S-0.25\,(3a_1\rightarrow 6e)^S+0.66\,(5e\rightarrow 3a_2)^S$
$3\,^1E$	$-0.61\,(5e\rightarrow 6e)^S+0.72\,(5e\rightarrow 3a_2)^S$
$4\,^1E$	$0.92\,(3a_1\rightarrow 8e)^S-0.36\,(2a_1\rightarrow 8e)^S$
$3\,^3A_2$	$0.95\,(5e\rightarrow 8e)^T$
$5\,^3E$	$0.96\,(5e\rightarrow 8e)^T$
$2\,^3A_1$	$0.96\,(5e\rightarrow 8e)^T$
$5\,^1E$	$0.95\,(5e\rightarrow 8e)^S$
$3\,^1A_2$	$0.96\,(5e\rightarrow 8e)^S$
$1\,^1A_1$	$0.96\,(5e\rightarrow 8e)^S$
$2\,^1A_1$	$0.83\,(5e\rightarrow 6e)^S-0.42\,(3a_1\rightarrow 4a_1)$
$4\,^1A_2$	$0.96\,(5e\rightarrow 7e)^S$
$6\,^1E$	$0.79\,(5e\rightarrow 7e)^S+0.56\,(5e\rightarrow 4a_1)$
$7\,^1E$	$0.85\,(4e\rightarrow 3a_2)^S+0.39\,(3a_1\rightarrow 7e)$
$8\,^1E$	$-0.50\,(5e\rightarrow 7e)^S+0.80\,(5e\rightarrow 4a_1)+0.20\,(4e\rightarrow 3a_2)$
$3\,^1A_1$	$0.85\,(5e\rightarrow 7e)^S-0.52\,(3a_1\rightarrow 4a_1)$
$9\,^1E$	$0.95\,(3a_1\rightarrow 7e)^S-0.43\,(4e\rightarrow 3a_2)$
$4\,^1A_1$	$0.52\,(4e\rightarrow 6e)^S+0.34\,(5e\rightarrow 7e)+0.28\,(5e\rightarrow 6e)$
$10\,^1E$	$0.96\,(4e\rightarrow 6e)^S$

[a] T stands for triplet, and S for singlet.

Table 9. Populations for some excited states in $[Fe(II)\text{–}(GMI)_3]^{++}$

State	$3d_{z^2}$	$3d_{x^2-y^2}+3d_{xy}$	$3d_{xz}+3d_{yz}$	$4s$	$4p_x+4p_y$	$4p_z$	C(π)	N(π)	N(n)
Ground[a]	1.947	2.248	1.262	0.424	0.256	0.162	5.139	8.229	10.328
$1\,^3A_1$[b]	0.000	−0.172	−0.081	0.000	0.018	0.000	−0.064	0.302	−0.002
$2\,^1E$[b]	−0.057	−0.232	−0.108	0.000	0.012	0.006	0.074	0.301	0.004
$3\,^1E$[b]	−0.043	−0.242	−0.024	0.000	0.010	0.006	0.036	0.330	0.000
$4\,^1E$[b]	−0.881	0.222	0.553	−0.002	0.001	0.000	−0.074	−0.035	0.217
$5\,^1E$[b]	−0.001	−0.368	0.518	0.000	0.000	0.000	−0.270	−0.075	0.196
$4\,^1A_2$[b]	−0.003	−0.379	−0.123	0.000	0.000	0.000	0.389	0.122	−0.007
$7\,^1E$[b]	−0.107	−0.042	−0.011	0.001	0.000	0.012	0.380	−0.231	−0.003
$8\,^1E$[b]	−0.004	−0.363	−0.117	0.000	0.000	0.001	0.410	0.079	−0.006
$9\,^1E$[b]	−0.526	−0.017	−0.006	−0.001	0.001	0.003	0.581	−0.035	−0.001
$5\,^1A_2$[b]	−0.207	0.039	0.015	0.005	0.004	0.014	0.362	−0.205	−0.026

[a] Populations.

[b] Change from the ground state population.

Table 10. Electronic singlet transitions in $[Fe(II)\text{-}(bipy)_3]^{++}$. *Transition frequencies in kK*

Type	Symmetry	Calculated		Observed				
				Present investigation[a]			Hanazaki and Nagakura[b] [15]	
		ν	f	ν_{max}	range	$\log\varepsilon_{max}$	ν	$\log\varepsilon$
CT + *L*	$1\,^1A_2$	11.2	0.004					
CT + *L*	$1\,^1E$	13.1	0.03					
CT	$2\,^1E$	15.9	0.35	19.2	18—23	3.86	19.5	3.93
CT + *d* − *d*	$3\,^1E$	17.3	0.003	20.5^{c}		3.80	20.4^{c}	3.87
CT	$2\,^1A_2$	22.4	0.003	24.1	23—24.5	3.18	24.2^{c}	3.38
CT + *L*	$1\,^1A_1$	25.6	*F*	25.5^{c}	24.5—31	3.45	25.6^{c}	3.54
CT + *L*	$4\,^1E$	27.7	0.04					
CT + *L*	$3\,^1A_2$	28.1	0.29	28.6		3.75	28.74	3.81
CT + *L*	$5\,^1E$	29.0	0.20	29.8^{c}		3.67		
CT + *L*	$2\,^1A_1$	31.5	*F*					
CT + *L*	$6\,^1E$	31.8	0.00004					
d - *d*	$7\,^1E$	32.8	0.0005					
CT + *L* + *d* − *d*	$8\,^1E$	33.6	0.004					
CT + *L* + *d* − *d*	$4\,^1A_2$	33.8	0.02					
CT + *L*	$9\,^1E$	33.9	0.10					
CT + *L*	$5\,^1A_2$	34.6	0.18					
CT + *L*	$10\,^1E$	36.7	0.15					
CT	$11\,^1E$	37.5	0.39	33.4	32—36	4.77	33.56	4.81
CT + *L*	$6\,^1A_2$	37.9	0.91	34.5^{c}		4.72	34.5^{c}	4.74
CT + *L*	$12\,^1E$	40.4	0.02					
CT + *L*	$7\,^1A_2$	40.7	0.31	38.6^{c}	36 43	4.22	38.8^{c}	4.26
CT + *L*	$13\,^1E$	42.2	0.13					
CT + *L*	$14\,^1E$	44.4	0.07					
CT + *L*	$8\,^1A_2$	44.7	0.95	40.5		4.41	40.49	4.44
CT + *L*	$15\,^1E$	44.9	0.29	42.0^{c}		4.36	41.5^{c}	4.38

The calculations give four singlets with energies lower than $3\,^1E$ and with low intensities.

A shoulder (19.8 kK) is observed on the high energy side of the 18 kK band and is probably due to the vibrational structure. A weak electronic transition, $4\,^1E$, is predicted to be found in that region. According to the form of the orbitals and the population analysis, the transition to $4\,^1E$ is a $d-d$ transition.

The three singlets $5\,^1E$ (30.9 kK), $3\,^1A_2$ (31.0 kK) and $1\,^1A_1$ (32.3 kK) all have ($5e \rightarrow 8e$) as the main configuration, indicating that each of them can be classified as partly $d \rightarrow d$ and partly CT ($\pi \rightarrow d + d \rightarrow \pi$) in character, as also shown in Table 9. The calculated weak transitions to $5\,^1E$ and $3\,^1A_2$ probably correspond to the observed weak band at 29 kK. Transitions to $^1A_1$ states are symmetry forbidden. Ito *et al.* [14] did not obtain any transition in this region, probably because ($d-d$) transitions were not considered in their method.

Table 10 (continued)

Type	Symmetry	Calculated		Observed				
				Present investigation[a]			Hanazaki and Nagakura[b] [15]	
		ν	f	ν_{max}	range	$\log \varepsilon_{max}$	ν	$\log \varepsilon$
L	$16\,^1E$	47.6	0.07					
L	$17\,^1E$	47.7	0.01					
L	$9\,^1A_2$	47.7	0.10					
CT + L	$18\,^1E$	48.1	0.05					
CT + L	$10\,^1A_2$	48.8	0.11					
L	$19\,^1E$	50.1	0.009					
L	$20\,^1E$	50.7	0.03					
L	$11\,^1A_2$	52.1	0.005					
L	$21\,^1E$	52.7	0.31	48.3[d]	43.5→	4.84	48[d]	4.70
CT + L	$22\,^1E$	53.9	0.07					
L	$23\,^1E$	54.1	0.21					
L	$12\,^1A_2$	54.3	1.43					
L	$24\,^1E$	55.8	0.83					
L	$25\,^1E$	56.5	0.34					
L	$13\,^1A_2$	56.8	0.38					
L	$26\,^1E$	57.1	0.12					
L	$27\,^1E$	58.0	0.08					

[a] $[\mathrm{Fe(bipy)_3}]\cdot \mathrm{SO_4}\cdot 5\mathrm{H_2O}$ in methanol.

[b] $[\mathrm{Fe(bipy)_3}]\cdot \mathrm{Cl_2}\cdot 7\mathrm{H_2O}$ in aqueous solution.

[c] ^1E transitions are polarized perpendicular ($\perp$) to the C_3 axis.
$^1A_2$ transitions are polarized parallel ($\parallel$) with the C_3 axis.
$^1A_1$ transitions are symmetry forbidden.

[d] shoulder.

The 4 $^1A_2$ (48.4 kK) state is a combined CT ($d \rightarrow \pi^*$) and $L(\pi \rightarrow \pi^*)$ state (Table 9) and may be referred to the observed strong band at 44.3 kK.

Observations indicate a strong UV band at around 54 kK, also observed by Ito *et al.* [14]. It may be assigned to the 5 $^1A_2$ state that, according to the population analysis, can be classified as partly CT ($d \rightarrow \pi^*$) and partly $L(\pi \rightarrow \pi^*)$.

In Table 7 the lower calculated triplet and singlet transitions are given together with an estimated range in which to search for the transition. Calculated singlets with fairly safe assignments to observed transitions have been found to be around 2–4 kK too high in energy. The singlet-triplet gap will come out too large from the calculations, by 2–7 kK in the present method [3]. In the region 10–13 kK we predict two singlet transitions polarized parallel to the threefold z-axis, 1 $^1A_2$ and 2 $^1A_2$, and two singlets polarized perpendicular to the threefold z-axis, 1 ^1E and 2 ^1E. The calculations further predict four low-lying triplets with some CT character, 1 $^3A_1$, 1 ^3E, 2 ^3E and 1 $^3A_2$.

Table 11. The lower electronic singlet and triplet transitions in $[Fe(II)-(bipy)_3]^{++}$. Calculated values and the estimated range in which to search for the transition. Transition frequencies in kK

Type	Symmetry	Calculated		Estimated range, ν (cf. text)	Observed Present investigation[c]	
		ν	$\bar{f}$		ν_{max}	$\log\varepsilon_{max}$
CT + *L*	$1\,^3A_1$	3.3		5—13[a]		
CT + *L*	$1\,^3E$	6.0		8—16[a]	8.85[d]	0.7
CT + *L*	$1\,^3A_2$	10.4		10—14[b]		
CT + *L*	$1\,^1A_2$	11.2	0.004	11—14[b]		
CT	$2\,^3E$	11.3		16—19[b]	11.8[d]	0.9
CT + *L*	$1\,^1E$	13.1	0.03	13—16[b]		
CT	$3\,^3E$	13.5		15—20[b]		
CT	$2\,^1E$	15.9	0.35	→	19.2	3.86
CT + *d* – *d*	$3\,^1E$	17.3	0.003	→	20.5[c]	3.80
CT + *L*	$2\,^3A_2$	18.7		22—24		
CT + *L*	$4\,^3E$	20.5		22—28		
CT + *L*	$3\,^3A_2$	21.8		23—28		
CT	$2\,^1A_2$	22.4	0.003	→	24.1[c]	3.18

[a] König and Schläfer [39] assigned a sharp peak at 8.98 kK to a triplet. This peak was later considered by Palmer and Piper [38] as the second overtone of the C–H stretching vibration.

[b] Palmer and Piper [38] observed a weak band located at 11.5 kK and assigned it as a spinforbidden transition ($^3T_1 \leftarrow {}^1A_1$)

[c] $[Fe(bipy)_3]SO_4 \cdot 5H_2O$ in methanol (10^{-4} M).

[d] $[Fe(bipy)_3]SO_4 \cdot 5H_2O$ in aquaeus solution (0.3 M).

Table 12. Electronic singlet transition in *cis*- and *trans*-forms of bipyridyl. Transition frequencies in kK

Calculated						Observed [31] (cyclohexane)	
cis-			*trans*-				
Symmetry[a]	ν	f	Symmetry[a]	ν	f	ν_{max}	$\varepsilon_{max}\cdot 10^{-4}$
$^1B_1(n-\pi^*)$	36.0		$^1A_u(n-\pi^*)$	36.5			
$^1A_1$	39.0	0.02	^1B_u	38.8	0.08	35.5	1.50
$^1B_2$	39.3	0.05	^1A_g	39.4	0		
$^1B_2$	43.5	0.92	^1B_u	43.7	0.99	42.2	1.20
$^1B_1(n-\pi^*)$	47.5		$^1A_u(n-\pi^*)$	48.1			
$^1A_1$	51.8	0.17	^1A_g	50.4	0		
$^1B_2$	51.9	0.57	^1B_u	54.1	1.27	52.4	4.0
$^1B_2$	55.8	0.56	^1A_g	54.5	0		
$^1A_1$	57.3	0.42	^1A_g	57.4	0		
$^1A_1$	57.5	0.79	^1B_u	57.8	1.18		

[a] All transitions are $\pi-\pi^*$ unless otherwise indicated.

$[Fe(II)-(bipy)_3]^{++}$

The electronic spectra of this complex have been thoroughly investigated experimentally. A review of observed data can be found in three recent articles by König [35], Krumholz [36] and by Bryant, Fergusson and Powell [37]. Characteristic for the observed spectra are two intense bands in the visible at about 19 and 28 kK, and two strong bands in the ultraviolet at about 33 and

40 kK. In the following, these four bands and the region above 40 kK and below 20 kK will be discussed in more detail.

The Region Around 19 kK. The intense visible band at around 19 kK has been characterized as a CT band. Its intensity and its structure in crystal spectra [38] excludes a transition of $d-d$ type. It cannot be a perturbed ligand transition as no band is found for the ligand bipyridyl in that region (cf. Table 12).

The present calculations give only one strong band in this region, $2\,{}^1E$ (15.9 kK, Table 10), which is a CT ($d \rightarrow \pi^*$) transition, in accord with previous assignments.

The observed shoulder towards higher energy (20.4 kK) has been ascribed to a vibrational structure of the 19 kK band [32, 38]. The calculated $3\,{}^1E - 2\,{}^1E$ separation (1.4 kK) indicates that the $d-\pi^*$ transition to $3\,{}^1E$ is to be found in that region. But as $3\,{}^1E$ is predicted to be much weaker than $2\,{}^1E$ (the calculated oscillator strength of $2\,{}^1E$ is 0.35 while it is only 0.003 for $3\,{}^1E$) it is probably hidden in the absorption spectra.

In between the two strong visible bands we have observed a weak band at 24.1 kK for $[\mathrm{Fe(bipy)_3}] \cdot \mathrm{SO_4} \cdot 5\,\mathrm{H_2O}$ in methanol. Hanazaki and Nagakura [15] report a shoulder at 24.2 kK for $[\mathrm{Fe(bipy)_3}] \cdot \mathrm{Cl_2} \cdot 7\,\mathrm{H_2O}$ in aqueous solution. This band may be assigned to the calculated weak $2\,{}^1A_2$ transition (22.4 kK, $f = 0.003$) of $d \rightarrow \pi^*$ type. For a definite assignment to be made, a more careful analysis of polarization data in the narrow region (23–24.5 kK) remains to be done.

The Region Around 28 kK. Like Hanazaki and Nagakura [15] we assign the observed 28.6 kK band to three probably operlapping transitions, $4\,{}^1E$ (27.7 kK), $3\,{}^1A_2$ (28.1 kK) and $5\,{}^1E$ (29.0 kK) with f-values: 0.04, 0.29 and 0.20 respectively. They can all be classified as partly CT ($d \rightarrow \pi^*$) and partly $L(\pi \rightarrow \pi^*)$. As mentioned previously, in the GMI complex the transitions in this region have very low calculated f-values (0.03 and 0.0004) in accord with experimental findings. The difference of intensity for this band in the GMI and the bipyridyl complexes mirrors the fact that the bands are of different character in the two compounds.

The observed shoulder at 25.5 kK is most probably attributed to one of these three transitions, but it is interesting to note that the calculations also give an electronically forbidden transition in that region, to $1\,{}^1A_1$ (25.6 kK) characterized as CT $(d \rightarrow \pi^*) + L(\pi \rightarrow \pi^*)$.

The Region Around 33 kK. The observed strong band at 33.4 kK with a shoulder at 34.5 kK has been assigned to an internal ligand transition [37, 15] shifted to lower energy in comparison with the free ligand. According to the present calculation these bands are clearly due to $11\,{}^1E$ (37.5 kK) and $6\,{}^1A_2$ (37.9 kK). Calculations for planar bipyridyl *(trans)*, with the same carbon and nitrogen parameters as used in the present study, give the lowest $\pi-\pi^*$ transition at 38.8 kK (Table 12). The MO calculation of the iron complex thus gives two transitions "shifted" to lower energy compared with the lowest $\pi-\pi^*$ transition of bipyridyl. But $11\,{}^1E$ and $6\,{}^1A_2$ cannot be classified as internal ligand transitions. They both have some $d-\pi^*$ character, transferring 0.70 resp. 0.36 electrons from iron d orbitals to the ligand π system.

The Region Around 40 kK. The observed band at 40.5 kK, with a shoulder on the low energy side at 38.6 kK and a shoulder on the high energy side at 42.0 kK has previously been considered as due to the second $\pi-\pi^*$ transition in bipyridyl

[37]. In this region the present calculation gives one strong transition, $8\,^1A_2$, surrounded by two weaker transitions, $14\,^1E$ and $15\,^1E$. The low energy shoulder may be assigned to $7\,^1A_2$ and $13\,^1E$. All of these five states can be classified as CT $(d \rightarrow \pi^*) + L(\pi \rightarrow \pi^*)$ states with an electron transfer of about 0.3–0.4.

The Region in Far UV. Observations have not been extended further than 48 kK. They show a region with increasing intensity from 43.5 kK (Table 10). The calculations give two strong transitions, $12\,^1A_2$ (54.3 kK) and $24\,^1E$ (55.8 kK), classified as transitions within the π-system of the bipyridyl molecules. The calculated spectral pattern for $[\mathrm{Fe(II)\text{-}(bipy)_3}]^{++}$ in this region resembles the one for *cis*-bipyridyl, as can be seen from Tables 10 and 12. For bipyridyl in cyclohexane solution there is an observed strong band at 52.4 kK (Table 12).

The Region Below 20 kK. The lower singlet and triplet transitions are given in Table 11. Palmer and Piper [38] observed in crystal spectra a weak band at 11.5 kK polarized perpendicular to the threefold z-axis. They assigned it as a spinforbidden $d-d$ transition ($^1A_1 - {}^3T_1$ in O_h) gaining intensity through spin-orbit coupling with the visible CT band around 19 kK. They further attributed a weak sharp peak at 8.89 kK to the second overtone of the C–H stretching vibration. König and Schläfer [39] made a different assignment of the corresponding peak at 8.98 kK in solution spectra. They considered it to be a $^1A_1 - {}^3T_1(O_h)\,d\text{–}d$ transition. According to the present calculation there are no d–d singlets or triplets in this low energy region. The observed band at 11.5 kK in crystal spectra [38] and 11.8 kK in solution spectra (Table 11) can most probably be assigned to the weak perpendicularly polarized $1\,^1E$ transition. According to the present calculations the tail of the observed strong band at 19.2 kK may be constituted of two weak singlets, $1\,^1E$ and $1\,^1A_2$, and three triplets, $1\,^3A_2$, $2\,^3E$ and $3\,^3E$.

Two low-lying triplets, $1\,^3A_1$ and $1\,^3E$, are predicted. Both or one of them may be attributed to the 8.85 kK peak, but it should be stressed that as yet there exist no clear experimental evidence for them. They might be revealed in luminescence spectra or by the aid of ESR measurements.

8. Conclusions

The method used in the present calculations had previously been applied in studies of organic copper complexes [4–7] and proven to be capable of giving a quantitative account for many different properties depending on the electronic structure. The present investigation shows that the method is also well suited for studies of iron organic compounds. The scheme for evaluation of one-center iron parameters and parameters describing the iron-ligand bond can of course be extended to other transition elements.

The results can be summarized as follows: For both $[\mathrm{Fe(II)\text{-}(GMI)_3}]^{++}$ and $[\mathrm{Fe(II)\text{-}(bipy)_3}]^{++}$ the calculated electronic population of the iron is in accord with Mössbauer isomer shift data, indicating that a realistic electron distribution has been obtained for the normal state. The electronic spectra of both compounds are quantitatively analyzed. Ligand field, charge transfer, and intraligand transitions are treated simultaneously and the interaction between them is properly taken into account. The method makes it possible to explain detailed properties of the electronic spectra, e.g. the difference in intensity for the visible band in the neighbourhood of 29 kK in the two similar compounds.

Previous assignments based on O_h symmetry and crystal field theory can only be expected to give a rough qualitative picture of the spectral pattern, as trigonal distortion and covalency have been neglected. It is thus not astonishing that the present assignments for some bands differ considerably from previous conventional assignments.

For both compounds triplet $[\mathrm{CT}(d \to \pi^*) + L(\pi - \pi^*)]$ states are predicted to be found in the near IR. The experimental verification of these bands remains to be done.

Appendix

One-Center Parameters for Iron from Observed Atomic Spectra and Atomic Analytical Hartree-Fock Wave Functions

In a semiempirical method considering the valence electrons (3*d*, 4*s* and 4*p*) of the transition metal ion, it would be desirable to obtain from experimental data the numerical values of the metal one-center parameters for different electronic populations and charges of the ion. Atomic spectral data can be used for the determination of the two-electron Slater-Condon parameters, $F_k(\mu, \nu)$, $G_k(\mu, \nu)$, and the one-electron parameters ε_μ (Eq. 6, Section 4). This is so because the energy of a spectroscopic term of an atom can be expressed in terms of these parameters [40–42]. With the assumption of a "frozen core" the energy is given by the expression:

$$E^{i,g} = C + \sum_{\mu} a^g(\mu)\varepsilon_\mu + \sum_{\mu > \nu}\sum \Big\{ b^g(\mu,\nu) F_0(\mu,\nu) + \sum_{k \neq 0} [c_k^{i,g}(\mu,\nu) F_k(\mu,\nu) - d_k^{i,g}(\mu,\nu) G_k(\mu,\nu)] \Big\} \tag{15}$$

where C is a constant particular to the element, μ and ν denote atomic valence orbitals, and i detones the i^{th} term of the configuration g.

Hinze and Jaffé [42] in an extensive study of the first transition elements using atomic term energies determined the Slater-Condon parameters with $k \neq 0$ for the neutral atom and the monopositive ion. Later Tondello *et al.* [43] using certain theoretical conditions together with spectral data made a new determination of the Slater-Condon parameters ($k \neq 0$) assuming the parameters to be charge dependent. Because of the lack of enough experimental information, it will not be possible to deduce from observed data only, the charge and configuration dependence of all one-center parameters needed in semiempirical calculations. Some extra assumptions have to be made.

In the present work a procedure for obtaining $F_k(\mu, \nu)$, $G_k(\mu, \nu)$ (including $k = 0$) and ε_μ for iron is presented. Atomic spectral data [44] are used in combination with some relations between theoretical Slater-Condon parameters, obtained from atomic analytical Hartree-Fock wave functions [25, 26, 45]. Recently a different approach was given by Anno and Teruya [46] in an elaborate study of the Slater-Condon parameters of all first transition elements.

The experimental spectroscopic energy of a multiplet was determined from Moore's tables [44] as a weighted mean of the J states. The following configurations and multiplets were considered.

d^8 : ^3F
d^7s : $^5F, ^5P, ^3H, ^1H, ^3G, ^1G$
d^6s^2: $^5D, ^3H, ^3G, ^3D, ^1I$
d^7p : $^5F, ^5G, ^5S, ^5P, ^3I, ^1I$
d^6sp: $^7D, ^7F, ^7P$

d^7 : $^4F, ^4P, ^2G, ^2H, ^2F$
d^6s : $^6D, ^4H, ^4G, ^2H, ^2I$
d^5s^2: $^6S, ^4D$
d^6p : $^6D, ^6F, ^6P, ^4I, ^2K$
d^5sp: ^8P

d^6 : $^5D, ^3H, ^3G, ^3D, ^1I, ^3\overline{F}, ^1F, ^1\overline{G}$
d^5s : $^7S, ^5S, ^5G, ^5D, ^5F, ^3H, ^1H$
d^5p : $^7P, ^5H, ^3K, ^1K$.

For $^3\overline{F}$ and $^1\overline{G}$ in the configuration d^6, an average over two multiplets was used.

$F_k(\mu, \nu)$ *and* $G_k(\mu, \nu)$ *for* $k \neq 0$

The parameters $F_2(d, d)$, $F_4(d, d)$ and $G_2(s, d)$ were determined in the classical manner by a least-squares procedure from term energies for each considered configuration not containing $4p$. Different values for different configurations were obtained. An analysis of these values shows that $F_2(d, d)$ and $F_4(d, d)$ depend strongly and almost linearly on the number of $3d$-electrons (n_{3d}) and weakly on n_{4s}. Thus $F_2(d, d)$ and $F_4(d, d)$ are assumed to be linear functions of n_{3d} and a least-squares procedure gives:

$$F_2(d, d) = 1.418 - 0.171\,(n_{3d} - 6) \text{ in kK}, \tag{16}$$

$$F_4(d, d) = 0.114 - 0.009\,(n_{3d} - 6) \text{ in kK}. \tag{17}$$

It is also reasonable to describe $G_2(s, d)$ as a linear function of the charge, q.

$$G_2(s, d) = 1.290 + 0.269\,q \text{ in kK}. \tag{18}$$

The values of $F_2(d, d)$, $F_4(d, d)$ and $G_2(s, d)$ determined from Eqs. (16), (17) and (18) were then used in the expressions for the term energies in configurations with $4p$. Different values of $F_2(p, d)$ and $G_3(p, d)$ for different configurations were obtained. (No value of $F_2(p, d)$ could be determined for d^5p.)

$G_3(p, d)$ can be described as a linear function of q:

$$G_3(p, d) = 0.0162 + 0.0077\,q \text{ in kK}. \tag{19}$$

As there are not enough experimental spectroscopic data to allow for an analysis of the configuration dependence of $F_2(p, d)$, a comparison was made with theoretical values of this parameter. The theoretical data indicates that $F_2(p, d)$ is nonlinearly q-dependent. In Table 1 the values of $F_2(p, d)$ for $q = 0$ and $q = 1$ are the experimentally derived values; the value for $q = 2$ is a "scaled" theoretical value, where the scaling factor is the average quotient between experimental and theoretical values for $q = 0$ and 1.

As $G_1(p, d)$ could not be determined from the observed term energies, used in the present investigation, the values of this parameter are determined as:

$$G_1^e(p, d) = \left[\frac{G_1^t(p, d)}{G_3^t(p, d)}\right]_{\text{average value}} \cdot G_3^e(p, d) \tag{20}$$

where the index e stands for experimental and t for theoretical. As the quotient between $G_1^t(p, d)$ and $G_3^t(p, d)$ is found to be almost constant for different configurations, an average value of the quotient is used. It was not possible to determine $G_1(s, p)$ from the term energies considered, as it always occurs in the combination:

$$F_0'(s, p) = [F_0(s, p) - G_1(s, p)] \,. \tag{21}$$

ε_μ and $F_0(\mu, \nu)$

The parameters ε_μ and $F_0(\mu, \nu)$ ($F_0'(s, p)$ replacing $F_0(s, p)$) cannot be determined from term energies of just one configuration. "Average" values, over different ionic states and configurations, for these parameters, were derived from expressions of the barycenter energies of each configuration considered.

The values of $F_k(\mu, \nu)$ and $G_k(\mu, \nu)$ for $k \neq 0$, derived in the manner described above, were inserted in the expressions for the barycenter energies, giving linear equations for ε_μ and $F_0(\mu, \nu)$. The "average" values, $\bar{\varepsilon}_\mu$ and $\bar{F}_0(\mu, \nu)$ were determined from a least-squares fit to the equations thus obtained.

Theoretical values of $F_0^t(\mu, \nu)$ were calculated and corresponding average values, $\bar{F}_0^t(\mu, \nu)$ derived. An analysis of theoretical $F_0^t(\mu, \nu)$ values was made. It turned out that $F_0^t(d, d)$ with rather good accuracy can be described as a linear function of n_{3d}, while $F_0^t(s, s)$, $F_0^{\prime t}(s, p)$, $F_0^t(s, d)$ and $F_0^t(p, d)$ can be considered as non-linear functions of q. This simplified population dependence of the theoretical F_0^t values is transformed to the semiempirical parameters by the formula:

$$F_0^e(\mu, \nu) = \left[\frac{\bar{F}_0^e(\mu, \nu)}{\bar{F}_0^t(\mu, \nu)}\right] \cdot F_0^t(\mu, \nu) \,. \tag{22}$$

The obtained values of $F_0^e(\mu, \nu)$ (see Table 1) were then inserted in the expressions for the barycenter energies of each configuration, giving linear equations for ε_μ. These equations can be solved assuming ε_{3d} to be a function of n_{3d}, and ε_{4s} and ε_{4p} to be functions of q. These assumptions are in line with the results for $F_k(\mu, \nu)$. The obtained semiempirical values of the one-center parameters are presented in Table 1. The values of $G_1^e(s, p)$ and $F_0^e(s, p)$, given in Table 1, are obtained from the values of $F_0^{\prime e}(s, p)$ assuming $[G_1^e(s, p)/F_0^e(s, p)]$ equal to the average theoretical value of $[G_1^t(s, p)/F_0^t(s, p)]$. $F_0(p, p)$ and $F_2(p, p)$ cannot be derived from experimental data. The values given in Table 1 have been roughly estimated as:

$$F_0^e(p, p) = 2F_0^e(s, p) - F_0^e(s, s) \,, \tag{23}$$

$$F_2^e(p, p) = \left[\frac{F_2^t(p, p)}{F_0^t(p, p)}\right]_{\text{average value}} \cdot F_0^e(p, p) \,. \tag{24}$$

The semiempirical parameters obtained are found to reproduce the spectroscopic energy terms of Fe in different ionic states with a standard deviation of 1.63 kK.

The present procedure can be considered as a method to "scale" theoretical parameter values in those cases where a direct determination from experimental data is not possible. The values in Table 1 must be looked upon as "a first trial" to these important parameters. New experimental data in combination with wave functions accounting for correlation (and eventually relativistic effects) will probably allow for a more detailed description of the configuration dependence of the parameters. A similar procedure can of course be used in a systematic study of all transition elements.

Acknowledgement. This investigation has been supported by grants from the Swedish Natural Science Research Council. The authors wish to express gratitude to Prof. Inga Fischer-Hjalmars for her encouraging interest throughout the work and also to Dr. Björn Roos for valuable discussions. Thanks are also due to Mr. Lars Norén for assistance in numerical computations.

References

1. Fischer-Hjalmars, I., Sundbom, M.: Acta chem. scand. **22**, 607 (1968).
2. Sundbom, M.: Acta chem. scand. **22**, 1317 (1968).
3. Sundbom, M.: Acta chem. scand. **25**, 487 (1971).
4. Roos, B.: Acta chem. scand. **20**, 1673 (1966).
5. Roos, B.: Acta chem. scand. **21**, 1855 (1967).
6. Roos, B.: Svensk kem. Tidskr. **80**, 204 (1968).
7. Roos, B., Sundbom, M.: J. molecular Spectroscopy **36**, 8 (1970).
8. McWhinnie, W. R., Miller, J. D.: Advances inorg. Chem. Radiochem. **12**, 135 (1969).
9. Krumholz, P.: Structure and Bonding **9**, 139 (1971).
10. Day, P., Sanders, N.: J. chem. Soc. (A), 1530 (1967).
11. Day, P., Sanders, N.: J. chem. Soc. (A), 1536 (1967).
12. Mulliken, R. S.: J. Amer. chem. Soc. **72**, 600 (1950); **74**, 811 (1952).
13. Murrell, J. N.: Quart. Rev. **15**, 191 (1961).
14. Ito, T., Tanaka, N., Hanazaki, I., Nagakura, S.: a) Bull. chem. Soc. Japan **41**, 365 (1968). b) Sci. Rep. Tohoku Univ., Ser. I, **50**, 168 (1967).
15. Hanazaki, I., Nagakura, S.: Inorg. Chemistry **8**, 648 (1969).
16. Hanazaki, I., Hanazaki, F., Nagakura, S.: J. chem. Physics **50**, 265 (1969).
17. Jaeger, F. M., van Dijk, J. A.: Z. anorg. allg. Chem. **227**, 273 (1936).
18. Krumholz, P.: J. Amer. chem. Soc. **75**, 2163 (1953).
19. Roos, B., Skancke, P. N.: Acta chem. scand. **21**, 233 (1967).
20. Roothaan, C. C. J.: Rev. mod. Physics **32**, 179 (1960).
21. Roos, B.: Acta chem. scand. **19**, 1715 (1965).
22. Goeppert-Mayer, M., Sklar, A. L.: J. chem. Physics **6**, 645 (1938).
23. McClellan, A. L.: Tables of experimental dipole moments. San Fransisco: Freeman 1963.
24. Wolfsberg, M., Helmholtz, L.: J. chem. Physics **20**, 837 (1952).
25. Blomquist, J., Roos, B., Sundbom, M.: USIP Report 71-07. This report is available upon request from Dr. Jan Blomquist, Inst. of Physics, University of Stockholm, Vanadisvägen 9, 11346 Stockholm.
26. Clementi, E.: IBM J. Res. Develop., Suppl. 9, 2 (1965).
27. Castellano, S., Günther, H., Ebersole, S.: J. physic. Chem. **69**, 4166 (1965).
28. Templeton, D. H., Zalkin, A., Ueki, T.: Acta crystallogr. **21**, A 154 (1966).
29. König, E., Watson, K. J.: Chem. Physics Letters **6**, 457 (1970).
30. Almenningen, A., Bastiansen, O.: Det Kgl. Nordiske Videnskabers Selskabs Skrifter 1958, Nr. 4.
31. Nordén, B., Håkansson, R., Sundbom, M.: Acta chem. scand. **26**, 429 (1972).
32. Hanazaki, I., Nagakura, S.: Inorg. Chemistry **8**, 654 (1969).
33. Blomquist, J., Roos, B., Sundbom, M.: J. chem. Physics **55**, 141 (1971).

34. Epstein, L. M.: J. chem. Physics **40**, 435 (1964).
35. König, E.: Coordin. Chem. Reviews **3**, 471 (1968).
36. Krumholz, P.: Structure and Bonding **9**, 139 (1971).
37. Bryant, G. M., Fergusson, J. E., Powell, H. K. J.: Austral. J. Chem. **24**, 257 (1971).
38. Palmer, R. A., Piper, T. S.: Inorg. Chemistry **5**, 864 (1966).
39. König, E., Schläfer, H. L.: Z. Physik. Chem. Neue Folge **34**, 355 (1962).
40. Slater, J. C.: Quantum theory of atomic structure, Vol. 1, Chapter 13. New York: McGraw-Hill Book Co. 1960.
41. Condon, E. U., Shortley, G. H.: The Theory of Atomic Structure, p. 174 183. New York: Cambridge University Press 1935.
42. Hinze, J., Jaffé, H. H.: J chem. Physics **38**, 1834 (1963).
43. Tondello, E., de Michelis, G., Oleari, L., di Sipio, L.: Coord. Chem. Rev. **2**, 65 (1967).
44. Moore, C. E.: Circular of the National Bureau of Standards 467, Washington 1952.
45. Roos, B., Salez, C., Veillard, A., Clementi, E.: A General Program for Calculation of Atomic SCF Orbitals by the Expansion Method. Special IBM Technical Report, San José, California. IBM Research Laboratory 1968.
46. Anno, T., Teruya, H.: J. chem. Physics **52**, 2840 (1970).
47. Blomquist, J., Moberg, L.: USIP-Report 72-03, Jan. 1972.

Dr. M. Sundbom
Institute of Theoretical Physics
University of Stockholm
Vanadisvägen 9
11346, Stockholm, Sweden

Theoret. chim. Acta (Berl.) 28, 339–353 (1973)
© by Springer-Verlag 1973

The Electronic Structure of the NF_2 Radical

R. D. Brown, F. R. Burden, B. T. Hart, and G. R. Williams

Department of Chemistry, Monash University, Clayton, Victoria, Australia 3168

Received May 25, 1972

Ab initio unrestricted Hartree-Fock (UHF) calculations (with and without single annihilation) have been performed on the radical NF_2 using four different basis sets; namely, a minimal basis Slater set, two minimal basis Gaussian sets and a Gaussian set of approximately double zeta accuracy.

Several one-electron charge dependent properties have been calculated with each basis set and it is most apparent that near double zeta accuracy $2p$ functions are necessary to produce reliable values.

Single annihilation of the UHF wavefunctions calculated with the two basis sets containing near double zeta $2p$ functions, was found to give an accurate representation of the anisotropic coupling constants at both the nitrogen and fluorine atoms. Less satisfactory agreement with the experimental isotropic coupling constants was found with all calculations.

This investigation of the NF_2 radical indicates that, providing a good quality basis set is used, the single annihilated UHF method can provide accurate values for most charge and spin dependent observable properties of open shell molecules.

Ab initio-Rechnungen nach der uneingeschränkten Hartree-Fock-Methode (UHF-Methode) (mit und ohne einfache Auslöschung) wurden für das Radikal NF_2 mit verschiedenen Basissätzen durchgeführt. Die vier Basissätze sind: ein minimaler Basissatz von Slaterfunktionen, zwei minimale Basissätze von Gaußfunktionen und ein größerer Satz von Gaußfunktionen von angenäherter Genauigkeit einer Doppelzeta-Basis. Der Vergleich der Basissätze bei der Berechnung von ladungsabhängigen Einelektron-Eigenschaften zeigt, daß der angenäherte Doppelzeta-Basissatz zur Berechnung geeigneter Werte notwendig ist. Eine einfache Auslöschung in den UHF-Wellenfunktionen, die mit den beiden Basissätzen mit genäherten Doppelzeta-$2p$-Funktionen berechnet wurden, führte auf eine genaue Darstellung der anisotropen Kopplungskonstanten am Stickstoff und an Fluor. Die Übereinstimmung der berechneten isotropen Kopplungskonstanten war bei allen Rechnungen weniger gut. Diese Ergebnisse für das NF_2-Radikal zeigen, daß bei Verwendung einer geeigneten Basis mit Hilfe der UHF-Methode mit einfacher Auslöschung genaue Werte für die meisten von der Ladung oder vom Spin abhängigen Eigenschaften von Molekülen mit offenen Schalen gewonnen werden können.

Introduction

Only a very small number of molecules which contain an odd number of electrons are sufficiently unreactive under normal conditions of temperature and pressure to permit investigations by physical methods. Two members of this select group which have been extensively studied, both experimentally and theoretically, are NO and NO_2 [1]. Another member of the group which has been given some experimental, but little theoretical [2], attention is the molecule NF_2. An electron diffraction study of its geometry [3] and some infra-red [4], ultraviolet [5], e.s.r. [6] and photoelectron [7] studies have been made. However, no definitive study of the microwave spectrum has been reported [8].

In collaboration with our microwave group, who are currently engaged in the analysis of a complex spectrum which has been observed in *K*-, *R*- and *F*-bands [8], we have investigated the electronic structure of NF_2 using *ab initio* SCF procedures based on both Slater-type orbitals (STO's) and Gaussian functions. A particular aim of the work has been to compute the various spin-coupling parameters involved in the Hamiltonian of the freely rotating molecule in order to aid the spectral analysis. We report here the results of this study.

Method

We have investigated the charge and spin properties of NF_2 using the unrestricted Hartree-Fock method (UHF) [9]. The spin-dependent properties were all calculated from the modified UHFAA (unrestricted Hartree-Fock after single annihilation) wavefunction in which the contaminating quartet spin state of the UHF wavefunction had been annihilated [10]. It is reassuring to note that recent work by Claxton and Weiner [11] on hydrocarbon radicals has shown that spin densities calculated using the UHFAA method are of comparable accuracy to those obtained using the much more time consuming SCF configuration interaction (SCFCI) and multi-configuration SCF (MSCF) methods.

The calculations reported here have employed both STO's and Gaussian functions. For the calculations based on STO's the Multicentre Gaussian Expansion (MGE) method [12, 28] has been employed. In this method, all one-electron integrals are computed exactly (in the Slater basis) by the use of analytical or C-function techniques. Two electron integrals involving the overlaps of two monocentric charge distributions are also calculated by the use of analytical of C-function techniques. The remaining repulsion integrals are computed via the Gaussian expansion method [15] employing an expansion of 3 GTO/STO. Trial calculations on a number of small molecules have shown that the use of this expansion technique to evaluate repulsion integrals leads to the following levels of error in the resultant mean values of one electrons operators: r^2 : $<0.1\%$; r : 0.2%; r^{-1} : 0.1%; r^{-3} : 1%. The level of error in the calculated total energy is even lower – about 1 in 5000. These errors are significantly lower than those resulting from the limited size of the basis (and of course lower than those arising from the inadequate treatment of correlation in the Hartree Fock formulation).

The exponents [29] used for the STO's were:

$$\text{Nitrogen:}\quad \zeta_{1s} = 6.6652,\quad \zeta_{2s} = 1.9236,\quad \zeta_{2p} = 1.9170\,.$$

$$\text{Fluorine:}\quad \zeta_{1s} = 8.6501,\quad \zeta_{2s} = 2.5639,\quad \zeta_{2p} = 2.5485\,.$$

Hereafter, this STO set is referred to as the S basis set.

Three Gaussian lobe basis sets were used, two which have been shown [13] to be of minimal basis Slater accuracy and one of double zeta accuracy. A summary of these basis sets is as follows:

(a) The LG basis set consists of a five component 1*s* function, a three component 2*s* function and a three component 2*p* function. The exponents and coefficients were obtained from Stewart's work [14], the final exponents being obtained after the usual scaling procedure [15] (multiply Stewart's exponent

Table 1. LW basis set 2*p* functions

Nitrogen			Fluorine		
Coefficients	Exponents	Distances[a]	Coefficients	Exponents	Distances[a]
11.4992	0.3271	0.0525	11.1035	0.5174	0.0417
7.3312	1.6332	0.0235	7.8209	2 7128	0.0182
1.2518	9.9557	0.0095	1.4534	16.5056	0.0074

[a] All distances in atomic units.

by ζ^2 where ζ is the relevant STO exponent). The distances of the lobe centres from the orbital centre were obtained using the relation $R = 0.03\,\alpha^{-\frac{1}{2}}$ [16] where R is the required distance and α is the Gaussian exponent. We have shown that this basis set may be regarded as identical to the corresponding cartesian Gaussian set for molecular calculations [17].

(b) The LW basis set employs the same *s* functions as the LG set but the three component 2*p* function was obtained by a least squares fit to a five component lobe function of double zeta accuracy [18]. The values of the exponents, coefficients and lobe distances for the *p* functions are given in Table 1. This basis set has been shown in calculations on small polyatomic molecules [13] to produce one-electron expectation values which are generally closer to the experimental values than those produced by the LG set.

(c) The W basis set consists of the large Gaussian lobe basis set produced by Whitten [18] and is of double zeta STO accuracy [19].

For the geometrical model of NF_2 we have chosen, from the small amount of experimental work available [3], an NF bond length of 1.37 Å (137 pm) and an angle of 103°.

Results and Discussion

The ground state of NF_2 is $^2B_1$ [20]. If electrons of opposite spin are paired in spatial orbitals of the same symmetry we obtain, for all calculations, the following ground state configuration:

$$(1a_1)^2(1b_2)^2(2a_1)^2(3a_1)^2(2b_2)^2(4a_1)^2(1b)_1)^2(5a_1)^2(3b_2)^2(1a_2)^2(4b_2)^2(6a_1)^2(2b_1)^1 .$$

This pairing of electrons has merit in providing a conceptually simple picture, however, it negates the major advantage of the UHF method in allowing the use of different orbitals for different spins.

Fig. 1 is a diagram of the spatial orbital energies for the two spin sets, calculated with the W basis set. It is significant that molecular orbitals (MO) of the same symmetry often have quite different energies and may be concentrated in different regions of space. This is best shown by the π-type $1b_1$ MO, which is noticeably more stable (by 0.0994 a.u.) for the α-electron spin set than for the β-electron spin set. The $1b_1$ MO coefficients for each spin set are recorded in Table 2 and show that the α-electron distribution is very different to the β-electron distribution with the latter closer to the fluorine nucleus. Thus although the overall charge

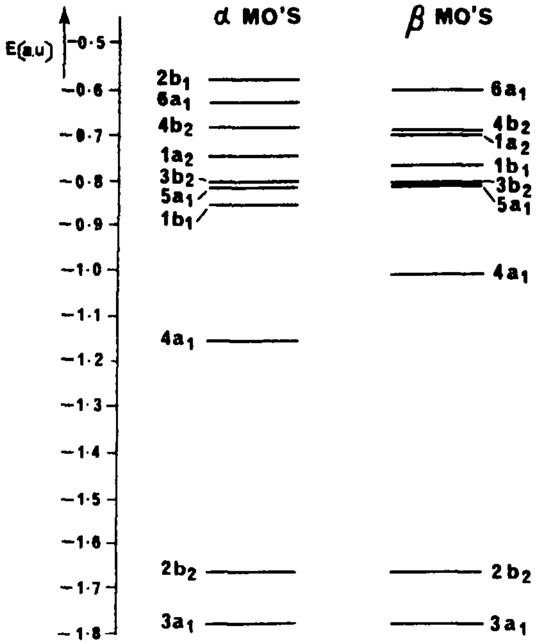

Fig. 1. UHF energy levels of NF_2 calculated with the W basis set

Table 2. The $1b_1$ MO coefficients in NF_2 with the W basis set

Spin set	Coefficients	
	$C_1{}^a$	C_2^a
α set	0.5637	0.4937
β set	0.2338	0.6435

[a] $\chi(1b_1) = C_1 p_x(N) + C_2(p_x(F_1) + p_x(F_2))$.

Table 3. Total energy of the NF_2 molecule (in a.u.)

Energy	Basis set			
	S	LG	LW	W
E	−252.1476	−251.7269	−252.4081	−253.0485
ΔE^a	−0.4207	-	−0.6812	−1.3216

[a] ΔE is the amount by which the energy from each set is lower than that from the LG set.

distribution may not be significantly altered by allowing extra MO freedom (as in the UHF method), the spin distribution may be quite radically changed.

Total energies are reported in Table 3 for each basis set and, as expected, the large double zeta W basis set gives the lowest energy. However, care must be exercised in using the total energy to judge the accuracy of a wavefunction; we prefer to use the calculated one-electron properties as the criteria.

Table 4. One-electron charge properties for NF_2

Property[a]	Basis set S	LG	LW	W
$\langle z_N \rangle^e$ [a.u.]	28.7505	28.8092	29.0646	29.0627
$\langle z_N \rangle^n$	29.0084	29.0084	29.0084	29.0084
$\langle z_N \rangle^t$	0.2579	0.1992	− 0.0562	− 0.0543
μ [Debye]	0.656	0.506	− 0.143	− 0.138
$\langle x^2 \rangle^b$ [a.u.]	9.2655	9.2878	10.4691	11.0562
$\langle y^2 \rangle$	83.7116	83.7732	85.6371	86.3073
$\langle z^2 \rangle$	23.6076	23.4904	24.5267	25.1170
$\langle r^2 \rangle$	116.5847	116.5514	120.6329	122.4806
χ^d_{av} [10^{-6} emu mole^{-1}]	−92.3337	−92.3073	−95.5398	−97.0032
$\theta_{xx}e$[a] [$10\ ^{26}$ esu cm^2]	59.7064	59.6391	60.8471	60.0586
$\theta_{xx}n$	−58.5006	−58.5006	−58.5006	−58.5006
$\theta_{xx}t$	1.2058	1.1385	2.3465	1.5580
$\theta_{yy}e$	−90.4796	−90.6264	−92.6916	−91.7514
$\theta_{yy}n$	90.5795	90.5795	90.5795	90.5795
$\theta_{yy}t$	0.0999	− 0.0469	− 2.1122	− 1.1720
$\theta_{zz}e$	30.7730	30.9872	31.8443	31.6927
$\theta_{zz}n$	−32.0787	−32.0787	−32.0787	−32.0787
$\theta_{zz}t$	− 1.3057	− 1.0915	− 0.2346	− 0.3860
$\langle r_N{}^1 \rangle$ [a.u.]	25.0876	25.0460	24.9339	24.9342
$\sigma^d_{av}(N)$ [ppm]	445.3	444.6	442.6	442.6
$\langle r_F{}^1 \rangle$	31.3524	31.2767	31.3884	31.4379
$\sigma^d_{av}(F)$	556.5	555.2	557.1	558.6
Q_N[c]	0.08	0.08	0.32	0.36
Q_F	− 0.04	− 0.04	− 0.16	− 0.18

[a] e = electronic contribution, n = nuclear contribution, t = total contribution.

[b] Refered to the centre of mass.

[c] Mulliken net charges.

Table 5. Molecular quadrupole moments for molecules related to NF_2[a]

	θ_{xx}[b]	θ_{yy}	θ_{zz}
OF_2[c]	−(0.5 ± 1.9)	−(1.6 ± 1.4)	(2.1 ± 1.0)
O_3[c]	(7.9 ± 7.9)	−(17.1 ± 5.2)	(9.2 ± 4.7)
NO_2[d]	2.17	− 3.65	1.48

[a] In units of 10^{-26} esu · cm^2.

[b] Axis system is same as for NF_2 (see Fig. 6).

[c] Experimental values.

[d] Ref. [1a].

To simplify the discussion of the electronic structure of NF_2, the calculated one-electron properties have been divided into two sections, namely, those dependent on the total charge density matrix and those dependent on the spin density matrix. The former properties are recorded in Tables 4–6 and the latter properties in Tables 7–9. All charge properties have been calculated using both

Table 6. Field gradients and quadrupole coupling constants for NF_2

Property	Basis set			
	S	LG	LW	W
$q_{xx}(N)$[a]	−0.3905	−0.4257	−0.8633	−0.8554
$q_{yy}(N)$	0.8228	0.7729	1.2809	1.3067
$q_{zz}(N)$	−0.4323	−0.3472	−0.4176	−0.4514
$\chi^{Q}_{xx}(N)$[b]	−1.3488	−1.4703	−2.9819	−2.9545
$\chi^{Q}_{yy}(N)$	2.8420	2.6696	4.4242	4.5136
$\chi^{Q}_{zz}(N)$	−1.4932	−1.1993	−1.4424	−1.5591
$q_{xx}(F)$[a]	−1.9944	−1.7672	−2.2118	−2.2458
$q_{yy}(F)$	1.7424	1.6200	2.0558	2.0405
$q_{zz}(F)$	0.2518	0.1472	0.1560	0.2053
$q_{yz}(F)$	3.2104	2.8099	3.5209	3.6132

[a] Total field gradient in a.u.

[b] In MHz with nuclear quadrupole moment
$Q(N) = 1.47 \times 10^{-26}$ esu · cm^2.

Table 7. Isotropic spin properties for NF_2

Property	Basis set								Expt.
	S		LG		LW		W		
	UHF	UHFAA	UHF	UHFAA	UHF	UHFAA	UHF	UHFAA	
$\langle S^2 \rangle$	0.7690	0.7502	0.7631	0.7501	0.7596	0.7501	0.7613	0.7501	0.7500
$\varrho(O)$ N [a.u.$^{-3}$]	0.2362	0.0816	0.1432	0.0492	0.1555	0.0532	0.1366	0.0472	
$\varrho(O)$ F [a.u.$^{-3}$]	0.0926	0.0321	0.0683	0.0235	0.0627	0.0215	0.0903	0.0311	
A_N [MHz]	76.2889	26.3616	46.2624	15.8924	50.2110	17.1890	44.1212	15.2382	45.1[a]
A_F [MHz]	389.4319	135.1151	287.2509	99.0039	263.8497	90.4839	379.6799	130.6276	168.8

[a] Ref. [6].

Table 8. Spin polarization and spin delocalization contributions to the total spin density in NF$_2$ for the W basis set calculations

	ϱ_{Total}	ϱ_{SP}	ϱ_{SD}
$\varrho^{\mathrm{N}}_{\mathrm{UHF}}$	0.1366	0.1341 (98%)[a]	0.0025 (2%)
$\varrho^{\mathrm{N}}_{aa}$[b]	0.0472	0.0447 (95%)	0.0025 (5%)
$\varrho^{\mathrm{F}}_{\mathrm{UHF}}$	0.0903	0.0888 (98%)	0.0015 (2%)
$\varrho^{\mathrm{F}}_{aa}$	0.0311	0.0296 (95%)	0.0015 (5%)

[a] % contribution to total spin density i.e. $\frac{\varrho_{\mathrm{SP}}}{\varrho_{\mathrm{Total}}} \times 100$.

[b] aa = after annihilation; Ref. [10].

Table 9. Anisotropic spin properties for NF$_2$

Component	Basic set								Expt.[b]
	S		LG		LW		W		
	UHF	UHFAA	UHF	UHFAA	UHF	UHFAA	UHF	UHFAA	
T_{xx}(N)[a]	62.0502	65.2756	56.7861	59.1935	84.1903	86.8772	86.3527	89.4633	90.3
T_{yy}(N)	− 29.5530	− 32.1280	− 27.4107	− 29.2580	− 40.5467	− 42.9304	− 41.7926	− 44.2667	− 45.1
T_{zz}(N)	− 32.4972	− 33.1476	− 29.3754	− 29.9355	− 43.6436	− 43.9467	− 44.5600	− 45.1966	− 45.1
T_{xx}(F)	274.1254	200.1356	241.1852	186.1943	353.8130	299.3238	389.1121	310.6073	425.6
T_{yy}(F)	−162.8328	−104.3112	−139.9636	− 95.3584	−206.4200	−155.5809	−224.2910	−161.1502	−212.8
T_{zz}(F)	−111.2927	− 95.8244	−101.2216	− 90.8359	−147.3939	−143.7429	−164.8211	−149.4571	−212.8
T_{yz}(F)	−141.8653	− 29.1633	− 98.3980	− 15.4896	−131.2122	− 27.6945	−152.0354	− 33.4644	

[a] Units MHz.

[b] Experimental values, from Ref. [6], are within ±0.5%.

the UHF and UHFAA wavefunctions but only the UHF results are tabulated since annihilation is found to cause insignificant changes. The properties were calculated using computer programs which were written by us and thoroughly tested [28, 31, 32].

Simple Picture of the Electronic Distribution of NF_2

In an attempt to obtain a simple orbital picture of NF_2 we have localized the α- and β-electron sets of MO's obtained from the UHF calculation. The localization method used was that proposed by Foster and Boys [21] and involves maximizing the squares of the distances of the orbital centroids from each other.

The most interesting result obtained by using the local orbitals is the arrangement of the electrons around the nitrogen atom. In terms of simple valence theory the structure would be written as depicted in Fig. 2, were only the valence electrons are considered. The localized orbital picture gives a very similar structure and shows the arrangement of the three non-bonding electrons around nitrogen very clearly. The electrons are arranged as shown in Fig. 3. The two electrons with α spin occupy orbitals that are directed out of the molecular plane while the electron with β spin is in an orbital lying between those of the two α-electrons and concentrated in the molecular plane. This simple picture is appealing in that it allows for spin polarization in spreading the two α-electrons further apart than suggested by the simple valence structure.

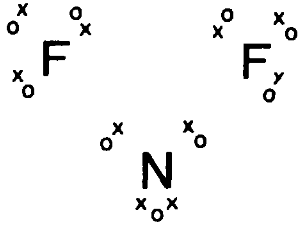

Fig. 2. Simple valence bond electron distribution for NF_2

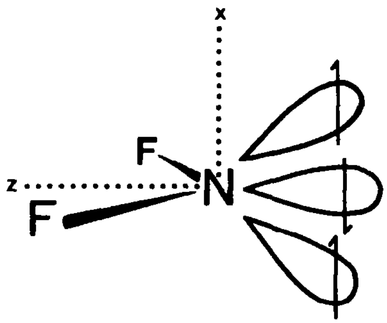

Fig. 3. Schematic diagram of the localized orbitals in NF_2 showing the three non-bonding electrons on nitrogen

Dipole Moment

Table 4 records the electronic contribution to mean z at nitrogen ($\langle z_N \rangle$) and the dipole moment (μ) for each basis set; note that the dipole moment is very sensitive to changes in basis set. Values calculated with the S and LG basis sets are in close agreement with one another, which might have been expected from our previous work [17] where we demonstrated that results obtained with LG basis sets are of comparable accuracy to calculations with equivalent cartesian Gaussian basis sets known to be of minimal basis Slater accuracy.

Note also that the S and LG basis set calculations give the dipole moment with the positive end towards the fluorine as in Fig. 4 (a), while the LW and W basis sets predict a small dipole in the opposite direction as in Fig. 4 (b).

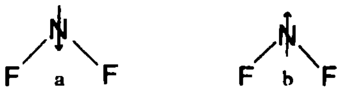

Fig. 4 a and b. Dipole moment directions for NF_2 (arrow points towards the positive end of the dipole). a Direction calculated with the S and LG basis sets. b Direction calculated with the LW and W basis sets

Pople has performed both CNDO/2 and INDO calculations on NF_2 [2b] and obtains dipole moments of magnitude 0.12 D and 0.38 D respectively, both in the same direction as the LW and W predictions, while Del Bene [2a], using an expansion set of three Gaussian functions per STO, calculates a dipole moment of 0.49 D in the opposite direction.

From these calculations we see that the overall value of the electronic contribution $\langle r \rangle^e$ (which in turn decides the magnitude and direction of μ after combination with the nuclear contribution $\langle r \rangle^n$) is dependent on quite small and subtle changes in the electron distribution due to the bonding between the atoms.

$\langle r^2 \rangle$, *average diamagnetic susceptibility, molecular quadrupole moment*

The second moments of the electronic charge distribution $\langle x^2 \rangle$, $\langle y^2 \rangle$, $\langle z^2 \rangle$ and $\langle r^2 \rangle$, referred to the centre of mass, give a measure of how diffuse or compact the charge distribution is in each direction. From the results in Table 4 the W basis set gives a charge distribution which is more diffuse than that given by the smaller basis sets. The S and LG basis sets again give quite comparable results while the LW basis set predicts values which are between those given by W and S basis sets.

On the basis of previous work in which the LW basis set has been shown to give quite accurate values for the average diamagnetic susceptibility, χ^d_{av} [13], we predict the value of -95.5×10^{-6} emu mole^{-1} as the most probable experimental result.

Molecular quadrupole moments, denoted θ_{xx}, θ_{yy}, θ_{zz}, measure the deviation of the change distribution from spherical symmetry by calculating the difference between an electronic and a nuclear contribution. They have been shown to be extremely sensitive to the accuracy of the wavefunction and hence the choice of basis set [19, 22]. This sensitivity to the basis set is noted in the results for θ_{xx}, θ_{yy} and θ_{zz} recorded in Table 4. Thus, while all basis sets give an approximately prolate spheroidal shape (elongated in the y direction) for the electronic distribution of NF_2, the more contracted electronic charge given by the S and LG basis sets when combined with the nuclear contribution gives a quite different result for the molecular quadrupole moments than is given by the LW and W basis sets.

To assist in determining the most likely experimental values of θ_{xx}, θ_{yy} and θ_{zz} we have recorded in Table 5 the relevant experimental values for OF_2 and O_3 together with the results from a near Hartree-Fock calculation on NO_2 [1a]. In each of these related molecules θ_{yy} is negative, indicating an excess of negative charge in the y direction. If this trend is maintained in NF_2 we expect the LW and W basis set values to be the best predictions of the experimental results.

$\langle r^{-1} \rangle$, *Diamagnetic Nuclear Shielding*

The potential at the nuclei are given in Table 4, together with the corresponding values of the average diamagnetic shielding constant ($\sigma^{\mathrm{d}}_{\mathrm{av}}$).

Since this property is closely coupled to the energy one would expect the larger basis calculation, which gives the lowest energy 1.3216 a.u. or 0.5%, to produce the most reliable values of $\langle r^{-1} \rangle$ and $\sigma^{\mathrm{d}}_{\mathrm{av}}$ at each nucleus.

$\langle r^{-1} \rangle$ may be interpreted as the electronic contribution to the potential at a particular nucleus. The total potential $\Phi(n)$ at nucleus n is given by:

$$\Phi(n) = -\langle r_n^{-1} \rangle + \sum_{k \neq n} \frac{Z_k}{R_{kn}}$$

where

Z_k = charge of nucleus k,

R_{kn} = distance of nucleus k from n

and may be used as a measure of the atomic environment of atom n [23]. For example, the less negative the potential, the more positive the average atomic environment. In using the calculated $\langle r^{-1} \rangle$ data note that the nuclear contribution will be the *same* for each calculation and thus the *larger* the magnitude of $\langle r^{-1} \rangle$ the more *negative* is the atomic environment.

The $\langle r^{-1} \rangle$ values at the nitrogen nucleus indicate that the environment is calculated most negative by the S basis set and more positive by the LW and W basis sets. This trend is also given by the net charge on nitrogen (Q_{N}) calculated from the Mulliken population analysis (see Table 4).

At the fluorine atoms the average atomic environment predicted by each basis set is in qualitative agreement with that given by the net changes (Q_{F}). Thus fluorine is predicted to be most negative by the W basis set.

$\langle r^{-3} \rangle$, *the Electric Field Gradient and Quadrupole Coupling Constant*

The components of the field gradient tensor ($q_{\alpha\beta}$) at both nitrogen and fluorine are reported in Table 6 together with the quadrupole coupling constants at nitrogen ($\chi^Q_{\alpha\beta}$). For nitrogen all basis sets predict the same trends for q(N) and χ^Q(N). These quantities are negative in the out-of-plane x direction and in the z direction, and positive in the y direction.

The magnitude of χ^Q_{xx}(N) and χ^Q_{yy}(N), calculated using the LW and W basis sets, are approximately twice those obtained with the S basis set, while the value of χ^Q_{zz}(N) is almost the same for all three basis sets. The difference between the S basis set and the LW and W basis sets is probably in the description of the α-electron distribution around the nitrogen atom.

From Table 6 the agreement between the calculated field gradient tensor elements at fluorine is closer than is the case at nitrogen. This presumably indicates that the charge asymmetry around the fluorine atoms is less influenced by the basis set.

Importance of the Representation of the 2p Function

A wide variation in the calculated one-electron properties is noted for the LG and LW basis sets. Since these two basis sets only differ in their representation of the 2*p* function, we see the importance of this function in accounting for the asymmetry of the charge distribution. Fig. 5 is a plot of the nitrogen 2*p* functions from each basis set. A Hartree-Fock (HF) 2*p* function [24] is also plotted for comparison. The curves for fluorine produced the same trends. Similar curves are noted for the LW and W basis set 2*p* functions but the curves differ from those representing the S and LG 2*p* functions both close to the nucleus and at distances far from it.

The greater reliability of the one-electron property values calculated with the double zeta accuracy W basis set, coupled with the very close resemblance between the 2*p* function from this basis set and the HF 2*p* function, suggests the desirability of using double zeta accuracy 2*p* functions for molecular calculations.

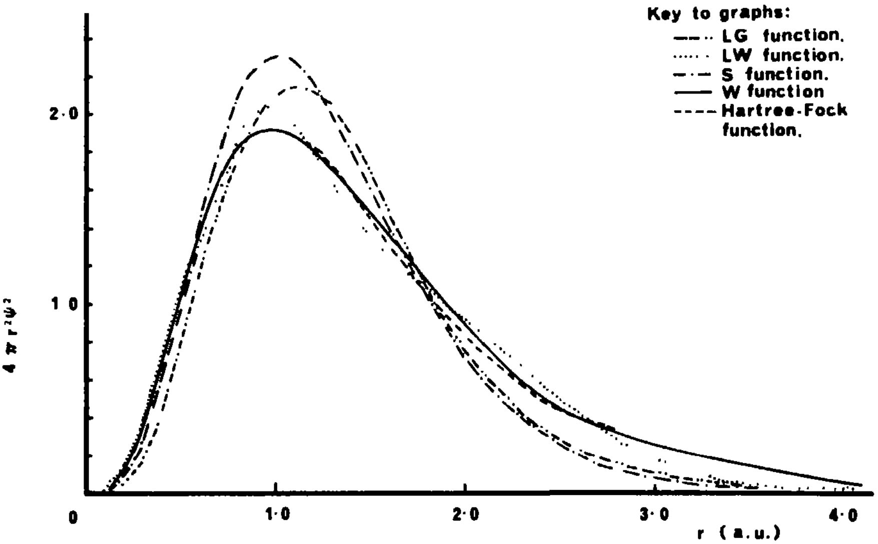

Fig. 5. Graphical comparison of the 2*p*-functions from the different basis sets used in calculations on NF_2

Spin Dependent Properties

The microwave spectrum of NF_2 shows hyperfine structure from the interaction of the electron spin with both the nitrogen and the fluorine nuclear spins.

To assist in the interpretation of the hyperfine structure we have calculated the isotropic coupling constants at each nucleus, (A_N, A_F, or Fermi contact term) and the anisotropic coupling constant tensor (T_{xx}, T_{yy}, T_{zz}, etc. or dipole-dipole term). The coupling constants derived from both the UHF and UHFAA wavefunctions are reported for each basis set to indicate the sensitivity of these terms to spin contamination in the wavefunction.

The results reported in Table 7 show that annihilation of the contaminating quartet spin state reduces the spin density $\varrho(O)$, and hence the isotropic coupling constant at each nucleus, by around one third. This change occurs with all four basis sets.

To explain this observation we make use of a recent analysis of the UHF wavefunction [25-27] which allows the computed spin density to be separated into components arising from the spin polarization and spin delocalization mechanisms. Spin polarization is the production of spin density due to correlation between electrons while spin delocalization is the spin density which would be due to the singly occupied orbital in a restricted HF wavefunction.

The spin polarization (SP) contributions to the spin density for the UHF and UHFAA (denoted here *aa*) wavefunctions, are given by:

$$(\varrho^{A}_{\mathrm{UHF}})_{\mathrm{SP}} = \tfrac{3}{2}(\varrho^{A}_{\mathrm{UHF}} - \varrho^{A}_{aa}),$$

$$(\varrho^{A}_{aa})_{\mathrm{SP}} = \tfrac{1}{2}(\varrho^{A}_{\mathrm{UHF}} - \varrho^{A}_{aa}).$$

The corresponding spin delocalization (SD) contributions are obtained from the general expression:

$$(\varrho^{A})_{\mathrm{SD}} = \varrho^{A} - (\varrho^{A})_{\mathrm{SP}}.$$

Note that when only the SP mechanism is important we have

$$\varrho^{A}_{\mathrm{UHF}} = 3\varrho^{A}_{aa}.$$

The W basis set UHF and UHFAA wavefunctions have been analysed for the SP and SD contributions to the spin density and the results are given in Table 8. It is evident that the majority of the spin density at both the nitrogen and fluorine atoms arises from the SP mechanism giving the expected reduction of spin density on single annihilation of the UHF wavefunction. The dominance of the SP mechanism in π-radicals has been shown previously [28].

Note also from Table 7 that the isotropic coupling constants calculated with the S basis set (UHFAA results) are in closest agreement with the experimental values. This result is not unexpected since the isotropic constants are dependent upon the square of the wavefunction at the nucleus (predominantly the 1*s* functions) and it is well known that Gaussian functions give a less accurate representation in this region.

The higher spin density on the nitrogen atom is consistent with the simple pictures of the unpaired electron being essentially centred on this atom.

The anisotropic coupling constants, recorded in Table 9, are not as significantly affected by the application of a single annihilator to the UHF wavefunction as are the isotropic coupling constants; however the absolute magnitudes of the anisotropic coupling constants at nitrogen are increased slightly while at fluorine they are decreased substantially after annihilation of the UHF wavefunction.

As the T values are dependent on the asymmetry of the spin density around the nucleus and therefore most influenced by the $2p$ orbital populations, these results are possibly due to annihilation of the quartet spin state allowing spin density to be transferred from the fluorine $2p$ orbitals to the nitrogen $2p$ orbitals.

The theoretical values obtained for the anisotropic tensor at nitrogen, with all four basis sets, correctly predict the relative signs and magnitudes of the diagonal elements. The double zeta accuracy W basis set gives excellent agreement with the experimental values while the values from the S basis set are in error by about 30%. Note that the largest anisotropic coupling constant in NF_2 is the out-of-plane T_{xx} element and that the tensor is almost axially symmetric (i.e. $|T_{yy}| \simeq T_{zz}| \simeq \frac{1}{2} T_{xx}$). These results are due to the unpaired electron mainly residing in the $2p_x$ orbital on nitrogen.

e.s.r. data are available for the anisotropic coupling at the fluorine atom in NF_2 and are tabulated, together with the theoretically calculated values, in Table 9. Note that the tensor elements are quoted in terms of the molecular axis system and not the principal axis system of the tensor. The "experimental" values for T_{yy} and T_{zz} are quoted as being equal because there is insufficient information available from the e.s.r. experiment (the magnitude of the T_{yz} component is needed) to enable explicit values to be assigned to these elements.

It is evident that the anisotropic coupling constants calculated with the LW and W basis sets are in much better agreement with experiment than those values calculated with the S and LG basis sets. This indicates the sensitivity of the anisotropic coupling tensor to the $2p$ function chosen in the basis; for fluorine it appears that single exponent STO's are inadequate and one needs to use at least double zeta accuracy $2p$ functions to correctly describe the anisotropy of the charge distribution around the fluorine atom.

An interesting aspect of single annihilation on UHF wave-functions is the effect on the principal axis directions for the anisotropic coupling constant tensor at fluorine. From Fig. 6 we see that one principal axis is almost along the N–F bond and that this axis is rotated by around 3.5° (for the W basis set results) after annihilation. Thus we have another indication of the sensitivity of the electron spin distribution to single annihilation.

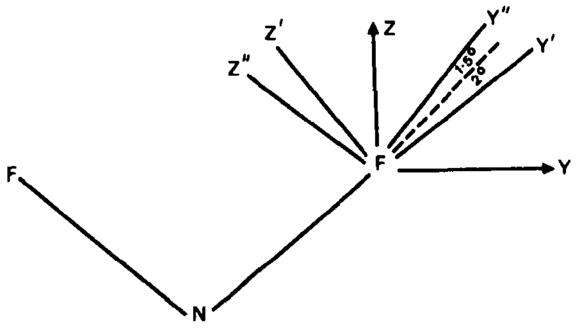

Fig. 6. Axis systems for NF_2. (X, Y, Z) coordinate axis system. (X', Y', Z') principal axis system for UHF calculated anisotropic coupling tensor. (X'', Y'', Z'') principal axis system for UHFAA calculated anisotropic coupling tensor. $X = X' = X''$ out of plane axis

Conclusion

The calculations we have performed on the NF_2 radical, using four different basis sets, underline the importance of a flexible $2p$ function for describing the asymmetry of the electronic distribution. The LW and W Gaussian function basis sets, which have near double zeta accuracy $2p$ functions, are found to give more reliable values for most one-electron properties than does a single STO basis set.

The accuracy of the predicted properties derived from any gaussian basis set depends upon the reliability of that basis set in the appropriate region of space. For instance, predictions of the isotropic spin parameters, A, are less reliable since they depend on the value of the wavefunction at the various nuclei and only large, carefully chosen representations of the $1s$ functions will achieve consistent accuracy. Presumably this inaccuracy in the representation of the $1s$ functions near the nuclei is also the cause of the large variation in the A values upon annihilation.

Thus we recommend the following one-electron properties as being the best theoretical predictions to date:

$$\chi^{d}_{av} = -95.5 \times 10^{-6}\ \text{emu mole}^{-1}; \quad \theta_{xx} = 1.6,\ \theta_{yy} = -1.2,$$
$$\theta_{zz} = -0.4 \text{ in units of } 10^{-26}\ \text{esu cm}^{-2}; \quad \sigma^{d}_{av}(\mathrm{N}) = 442.6\ \text{ppm},$$
$$\sigma^{d}_{av}(\mathrm{F}) = 558.6\ \text{ppm}; \quad \chi^{Q}_{xx}(\mathrm{N}) = -2.95\ \text{MHz},\ \chi^{Q}_{yy} = 4.51\ \text{MHz},$$
$$\chi^{Q}_{zz} = -1.56\ \text{MHz}.$$

The dipole moment is uncertain since it is predicted to be $-0.14D$ by the LW and W Gaussian basis sets and $+0.66D$ by the STO basis set (see Fig. 2). In view of the generally poor representation of the fluorine atom by STO's, the value given by the Gaussian basis sets is possibly more reliable. It seems there may be a near cancellation of oppositely directed lone "pair" and bond moments.

Single annihilated UHF wavefunctions, from the LW or W basis sets, give an accurate representation of the anisotropic coupling constants at both the nitrogen and fluorine atoms. However, rather poor agreement with the experimental isotropic coupling constants was found with all basis sets.

Thus this investigation of the NF_2 radical indicates that, providing a good quality basis set is used, the single annihilated UHF method can provide values for most charge and spin dependent observable properties of open shell molecules.

References

1a. Rothenberg, S., Schaefer, H. F.: Molecular Physics **21**, 317 (1971).
1b. Fink, W. H.: J. chem. Physics **54**, 2911 (1971).
1c. Schaefer, H. F., Rothenberg, S: J. chem. Physics **54**, 1423 (1971).
1d. Lefebvre-Brion, H., Moser, C. M.: J. molecular Spectroscopy **15**, 211 (1965).
2a. Del Bene, J.: J. chem. Physics **54**, 3487 (1971).
2b. Pople, J. A., Beveridge, D. L.: Approximate molecular orbital theory. New York: McGraw-Hill 1970.
2c. Kaufman, J. J.: J. chem. Physics **37**, 759 (1962).
3. Bohn, R. K., Bauer, S. H.: Inorg. Chemistry **6**, 304 (1967).
4. Hormony, M. D., Myers, R. J.: J. chem. Physics **37**, 636 (1962).
5. Goodfriend, P. L., Woods, H. P.: J. molecular Spectroscopy **13**, 63 (1964).

6. McDowell, C. A., Nakajima, H., Raghunathan, P.: Canad. J. Chem. **48**, 805 (1970).
7. Cornford, A. B., Frost, D. C., Henning, F. G., McDowell, C. A.: J. chem. Physics **54**, 1872 (1971).
8. Hrubesh, L. W., Rinehart, E. A., Anderson, R. E.: J. molecular Spectroscopy **36**, 354 (1970).
9. Pople, J. A., Nesbet, R. K.: J. chem. Physics **22**, 571 (1954).
10. Amos, A. T., Snyder, L. C.: J. chem. Physics **41**, 1773 (1964).
11. Claxton, T. A., Weiner, B.: Trans. Faraday Soc. **66**, 2213 (1970).
12. Brown, R. D., Burden, F. R., Williams, G. R.: Theoret. chim. Acta (Berl.) **18**, 98 (1970).
13. Brown, R. D., Burden, F. R., Hart, B. T.: To be published.
14. Stewart, R. F.: J. chem. Physics **52**, 431 (1970).
15. Taketa, H., Huzinaga, S., O-ohata, K.: J. physic. Soc. Japan **21**, 2313 (1966).
16. Shih, S., Buenker, R. J., Peyerimhoff, S. D., Wirsam, B.: Theoret. chim. Acta (Berl.) **18**, 277 (1970).
17. Brown, R. D., Burden, F. R., Hart, B. T.: Theoret. chim. Acta (Berl.) **25**, 49 (1972).
18. Whitten, J. L.: J. chem. Physics **44**, 359 (1966).
19. Harrison, J. F.: J. chem. Physics **47**, 2990 (1967).
20. Herzberg, G.: Electronic spectra of polyatomic molecules, p. 606. New York: Van Nostrand Reinhold Co. 1966.
21. Boys, S. F., Foster, J. M.: Rev. mod. Physics **32**, 300 (1960).
22. Neumann, D. B., Moskowitz, J. W.: J. chem. Physics **50**, 2216 (1969).
23. Schwartz, M. E.: Chem. Physics Letters **6**, 631 (1970).
24. Clementi, E.: IBM, J. Res. Develop. Suppl. **9**, 2 (1965).
25. Yonezawa, T., Nakatsuji, H., Kawamura, T., Kato, H.: Chem. Physics Letters **2**, 454 (1968).
26. Yonezawa, T., Nakatsuji, H., Kawamura, T., Kato, H.: J. chem. Physics **51**, 669 (1969).
27. Nakatsuji, H., Kato, H., Yonezawa, T.: J. chem. Physics **51**, 3175 (1969).
28. Williams, G. R.: Ph. D. Thesis, Monash University (1971).
29. Ransil, B. J.: Rev. mod. Physics **32**, 239 (1960).

Prof. Dr. R. D. Brown
Department of Chemistry
Monash University
Wellington Road
Clayton, Victoria, Australia 3168

Theoret. chim. Acta (Berl.) 28, 355-361 (1973)
© by Springer-Verlag 1973

Spectres et étude conformationnelle des dérivés méthyles de l'acide benzoïque

Yves G. Smeyers et Carlos Sieiro

Laboratorio de Química Cuántica. Instituto de Química Física «Rocasolano», et Departamento de Química, Nueva Universidad Autónoma de Madrid

Reçu le 16 fevrier 1972

Spectra and Conformational Analysis of Methyl Derivatives of Benzoic Acids

Using the well known Pariser-Parr-Pople procedure, with Configuration Interaction, the absorption maxima, oscillator strengths, and effective torsion angles of the methyl benzoic acids are determined. The results agree sufficiently well with the experimental data.

A l'aide de la méthode bien connue de Pariser-Parr et Pople, avec Interaction de Configurations, on détermine les maxima d'absorption, forces de l'oscillateur, et angles effectifs de torsion des dérivés méthylés de l'acide benzoïque. Les résultats obtenus sont en bon accord avec les données expérimentales.

Mit Hilfe der Pariser-Parr-Pople-Methode mit Konfigurationswechselwirkung werden die Absorptionsmaxima, die Oszillatorenstärken und die effektiven Torsionswinkel der Methylderivate der Benzoesäure bestimmt. Die Resultate stimmen gut mit experimentellen Ergebnissen überein.

Introduction

Il y a quelques années déjà que Wepster [1] et Ossorio [2] étudièrent expérimentalement les spectres Ultraviolets, en solution, des dérivés méthylés du nitrobenzène et de l'acide benzoique respectivement. Ces deux auteurs ont observé les caractéristiques suivantes:

1) Les dérivés méthylés en position ortho présentaient toujours une franche diminution de l'intensité de la Bande Principale, B_{1u}, par rapport à l'intensité de la même bande du dérivé non-méthylé correspondant.

2) Les dérivés méthylés deux fois en position ortho présentaient une diminution beaucoup plus marquée.

3) Les dérivés méthylés en position para présentaient par contre un accroissement de cette intensité.

4) Tandis que les dérivés en position méta ne présentaient pas de variation importante.

Wepster et Ossorio attribuèrent cette diminution d'intensité, chez les dérivés ortho, à une diminution de la conjugaison entre les électrons pi de l'anneau benzénique et du substituant X, due à une torsion de la liaison C–X. La torsion serait provoquée par la présence d'un ou deux groupes méthyles en position ortho, pour des raisons stériques. Ces auteurs ont même essayé de déterminer cet angle de torsion, en utilisant une relation linéaire entre la force de l'oscillateur et le carré du cosinus de l'angle:

$$f = k\cos^2\varphi \tag{1}$$

qui avait été antérieurement établie empiriquement par le propre Wepster [1, 3], ainsi que d'autres chercheurs [4].

L'existence d'une torsion, chez les dérivés ortho, fut confirmée plus tard. Certaines valeurs de l'angle de torsion, calculées par Ossorio [2], furent même retrouvées approximativement par diffraction de Rayons X, à l'état cristallin [5, 6 et 7]. Il n'y a pas de raison pour que cette torsion ne se maintienne pas en solution.

Dans ce travail, nous allons déterminer théoriquement les énergies de transition, les forces de l'oscillateur des dérivés méthylés de l'acide benzoïque, ainsi que l'angle de torsion effectif, défini par l'expression (1). D'un autre côté, nous allons essayer d'évaluer directement la valeur de l'angle de torsion, en sélectionnant la configuration angulaire qui reproduit le mieux les spectres, c'est à dire, la situation et l'intensité des bandes.

La méthode de calcul

Pour déterminer les spectres électroniques, on a utilisé la méthode bien conue de Pariser-Parr et Pople [8], avec Interaction de Configurations sur toutes les mono-excitations.

On pourrait croire qu'un procédé qui tiendrait compte de tous les électrons de valence serait plus indiqué pour l'étude de molécules non-planes. Toutefois nous avons vérifié que les méthodes accessibles habituelles, comme le CNDO et l'INDO, ne conduisent pas à des résultats raisonables pour les barrières de rotation. Concrètement, nous avons trouvé, dans le cas de l'acide benzoïque, comme configuration angulaire la plus basse, une structure non-plane, où le groupe carboxyle serait tordu à 90°. Des résultats négatifs analogues ont été aussi signalés ailleurs [9]. Par contre, il existe dans la littérature scientifique, de nombreux exemples de calculs conformationnels satisfaisants de molécules non-planes, réalisés dans le cadre de l'approximation électronique pi, [10, 11 et 12]. Finalement, certains auteurs affirment même que la séparation sigma-pi est sauvegardée dans les molécules non-planes à condition de paramétriser convenablement les intégrales [13].

Pour tenir compte du défaut de coplanarité des dérivés méthylés en position ortho, on a multiplié l'intégrale d'échange, béta, correspondante à la liaison affectée, par le cosinus de l'angle de torsion:

$$\beta^{\theta}_{pq} = \cos\theta\,\beta_{pq}\,.$$

Quant aux intégrales de répulsion bicentriques $\langle pp|qq\rangle$, on a préféré ne pas les affecter directement par l'angle de torsion, vu qu'il agissait d'intégrales de Coulomb, qui allaient d'ailleurs être évaluées par une approximations de charges sphériques. En fait, la torsion affecte généralement ces intégrales indirectement aux travers des distances interatomiques qui changent avec l'angle de torsion. Il semble d'ailleurs que l'inclusion de termes, qui tiendraient compte explicitement de l'angle, n'apporterait pas d'améliorations importantes [11].

Pour calculer l'angle de torsion effectif, on a employé l'expression (1), en posant $k=f_0$, où f_0 est la force de l'oscillateur de l'acide benzoïque supposé plan. Pour calculer les forces de l'oscillateur on a eu recours à la méthode habituelle [14].

Pour introduire les groupements méthyles dans le formalisme pi, on a adopté le modèle hyperconjugatif, qui centre un pseudo-atome sur le prolongement de la liaison C–CH$_3$. Simultanément, on a introduit un effet inductif sur l'atome de carbone substitué. Les avantages de ce modèle mixte ont été discutés dans un travail antérieur [15].

La paramétrisation

Pour estimer les intégrales monocentriques, on a utilisé les approximations habituelles suivantes:

$$\alpha_p = W_p - (N_p - 1)\langle pp|pp\rangle$$
$$\langle pp|pp\rangle = -W_p + I_p .$$

Les valeurs du potentiel d'ionisation, W_p, et de l'électroaffinité, I_p, correspondantes au groupement méthyle et à l'atome de carbone substitué, ont été empruntées au travail cité ci-dessus [15]. Dans les autres cas, elles ont été tirées des tables de Hinze et Jaffé [16].

Les intégrales de répulsion bicentriques ont été évaluées, dans tous les cas, au moyen de l'approximation de Mataga [17]:

$$\langle pp|qq\rangle = e^2\left[R_{pq} + \frac{2e^2}{\langle pp|pp\rangle + \langle qq|qq\rangle}\right]^{-1}.$$

Quant aux intégrales d'échange, béta, elles ont été estimees de la façon suivante:

1) Les intégrales correspondantes à l'anneau ont été paramétrisées à nouveau de façon à reproduire la première transition du benzène, dans les conditions actuelles du calcul, c'est à dire, en employant les intégrales de Mataga avec $R_{pq} = 1{,}39$ Å, etc. ...

2) Les intégrales correspondantes aux liaisons C=O et C–OH ont été paramétrisées de façon à reproduire les deux premières bandes de l'acide benzoïque, B_{2u} et B_{1u}.

3) Les intégrales correspondantes aux liaisons C–CH$_3$ et C≡H$_3$ ont été empruntées au travail cité ci-dessus [15].

Dans le calcul des intégrales de répulsion, on a employé les valeurs de R_{pq} déduites à partir des distances standard de liaison, signalées dans le Tableau 1, en considérant des angles de valence de 120°. Dans ce même tableau, on a résumé les paramètres employés dans ce travail.

Tableau 1. Valeurs des potentiels d'ionisation, intégrales de répulsion et d'échange, en eV, ainsi que longueurs de liaison, en Å, employées dans ce travail

Centre	W_p	$\langle pp\|pp\rangle$	Liaison	R_{pq}	β_{pq}
$-CH-$	−11,16	11,13	$CH-CH$	1,39	−2,386
$-C(CH_3)-$	−10,66	11,13	—	—	—
$-C(OOH)$	−11,16	11,13	$C-COOH$	1,48	−1,70
$=O$	−17,70	15,30	$C=O$	1,23	−2,70
$-OH$	−30,46	15,30	$C-OH$	1,30	−1,80
$-C(H_3)$	−11,16	11,13	$C-CH_3$	1,52	−1,22
$\equiv H_3$	−8,5	8,5	$C\equiv H_3$	0,45	−3,00

Réalisation des calculs et résultats

A. Les spectres électroniques

Avec ces paramètres, on a étudié la série entière des dérivés méthylés de l'acide benzoïque. Notamment, on a calculé les énergies de transition correspondantes aux bandes benzenoïdes B_{2u}, B_{1u}, mesurées par Ossorio [2], et E_{1u}.

Quand la molécule ne possédait aucun groupement méthyle en position ortho, on l'a considérée comme étant plane.

Quand la molécule ne possédait qu'un groupe méthyle en position ortho, on a introduit dans les calculs une torsion de la liaison C–COOH, comme on l'a décrit ci-dessus, en envisageant des torsions de 30°, 35°, 40° et 45°. On s'est limité à ces valeurs, étant donné qu'Ossorio avait trouvé des chiffres de cet ordre de grandeur (36°) pour l'angle de torsion effectif.

Finalement, quand il existait deux groupements méthyles en position ortho, on a realisé les calculs à un angle de torsion de 60°. On s'est limité à cette valeur, vu qu'elle était en assez bon accord avec les données expérimentales connues alors, par diffraction de Rayons X, [5] et [6], ainsi qu'avec l'angle de torsion effectif calculé par Ossorio. Les spectres des dérivés di-méthylés en ortho ne présentaient pas d'ailleurs non plus de bande B_{1u} bien définie qui permettrait établir approximativement l'angle de torsion, comme dans le cas des dérivés mono-méthylés.

Comme on pouvait s'y attendre, on a vérifié alors que la torsion exerce un effet hypsochrome sur les transitions électroniques. Si l'angle de torsion est le même pour tous les dérivés mono-méthylés en ortho, on a trouvé que l'angle qui permet le mieux de reproduire la situation des bandes (B_{1u}), vaut approximativement 40°. L'effet de la torsion est toutefois relativement faible.

De même, on a trouvé que la torsion provoque une diminution de l'intensité. Dans le cas des dérivés monométhylés en ortho, l'angle qui permet le mieux de reproduire les intensités (c'est à dire l'angle de torsion effectif) vaut approximativement 35°.

Dans le Tableau 2, on donne les énergies de transition et forces de l'oscillateur de la série entière des dérivés méthylés de l'acide benzoïque, obtenues dans ces conditions. Dans le cas des dérivés mono-méthylés en ortho, ce sont les résultats calculés à 35°, que l'on a préféré donner, vu que les

Tableau 2. Energies de transition en mμ, forces de l'oscillateur, intensités, angles de torsion effectifs obtenus, dans ce travail (a) et par Ossorio (b), des différents dérives méthylés de l'acide benzoïque. Les valeurs entre parenthèses sont des *inflexions*

Acide	Transition B_{2u}				Transition B_{1u}						E_{1u}	
	calc.^{a}		exp.^{b}		calc.^{a}			exp.^{b}			calc.^{a}	
	mμ	f	mμ	log$E$	mμ	f	φ	mμ	log$E$	φ	mμ	f
Benzoïque	265	0,011	279	2,84	230	0,353		226	3,99		197	0,280
ortho-m-	266	0,028	278	3,07	233	0,221	37°	228	3,81	36°	206	0,403
méta-m-	270	0,032	279	3,07	232	0,289		230	3,95		204	0,645
para-m-	266	0,004	(280)	2,72	240	0,442		234	4,14		188	0,501
2-3-m-	271	0,037	281	3,04	232	0,198	42°	(229)	3,73	42°	204	0,504
2-4-m-	266	0,015	278	3,04	238	0,305	21°	236	3,98	9°	207	0,377
2-5-m-	271	0,056	286	3,18	232	0,181	44°	(230)	3,80	37°	210	0,470
2-6-m-	263	0,021	273	2,72	232	0,091	60°	(229)	3,33	62°	206	0,218
3-4-m-	270	0,029	(284)	2,96	240	0,349		236	4,10		205	0,485
3-5-m	274	0,034	285	3,13	233	0,285		234	3,92		202	0,604
2-3-4-m-	270	0,017	282	2,98	241	0,278	28°	237	3,82	35°	205	0,362
2-3-5-m-	275	0,061	288	3,13	234	0,171	46°	(234)	3,68	46°	208	0,482
2-3-6-m-	268	0,045	276	2,88	235	0,059	66°			(67°)	211	0,314
2-4-6-m-	263	0,007	272	2,63	240	0,130	53°			(58°)	216	0,106
3-4-5-m-	273	0,015	281	3,07	243	0,362		240	4,01		203	0,461
2-4-5-m-	271	0,053	285	3,17	240	0,241	34°	239	3,95	18°	212	0,453
2-3-4-5-m-	273	0,035	288	3,07	243	0,252	33°	241	3,81	36°	208	0,352
2-3-4-6-m-	267	0,030	276	2,70	243	0,051	68°			(67°)	212	0,179
2-3-5-6-m-	271	0,062	278	2,96	236	0,064	65°			(70°)	214	0,305
2-3-4-5-6-m-	270	0,027	277	2,68	229	0,030	73°			(69°)	216	0,171

intensitées sont beaucoup plus sensibles que les énergies à un changement de conformation angulaire.

Dans même tableau, on donne aussi les angles de torsion effectifs théoriques. De même, on y a inclus les résultats expérimentaux mesurés par Ossorio [2].

B. *Les stabilités relatives*

Comme on sait, l'énergie électronique pi (à l'intérieure d'un même groupe d'isomères) est une mesure de l'énergie de résonance, c'est à dire, de la stabilité relative de ces isomères. C'est la raison pour laquelle, on donne, en Tableau 3, les différences d'énergies électroniques pi, en kcal/mol, pour un même groupes d'isomères dans leur état fondamental. Les énergies correspondantes aux dérivés méthylés une fois et deux fois en position ortho ont été déduites à un angle de torsion de 35° et 60° respectivement.

Dans même tableau, on donne aussi les différences correspondantes des enthalpies de formation, à l'état gazeux et à 25°C, mesurées experimentalement [18]. On constate alors qu'il existe une corrélation évidente entre les résultats théoriques et expérimentaux. L'accord est respectivement très satisfaisant, bon et moins bon, dans le cas des dérivés mono-, di- et tri-méthylés. Dans le cas des dérivés tetra-méthylés, on n'observe aucune corrélation. C'est pourquoi,

Tableau 3. Différences d'énergies électroniques pi théoriques, et d'enthalpies de formation expérimentales (gaz et à 25° C), en kcal/mol, à l'intérieur d'un même groupe d'isomères correspondants aux dérivés méthylés de l'acide benzoïque

Dérivés	$-\Delta E$ calc.	$-\Delta H$ exp.
Ortho-m-	0	0
Méta-m-	3,8	2,6
Para-m-	4,1	3,3
2-6-m-	0	0
2-3-m-	2,7	2,0
2-5-m-	2,9	3,1
2-4-m-	3,3	4,3
3-4-m-	6,8	5,0
3-5-m-	6,9	5,4
2-3-6-m-	0	0
2-4-6-m-	0,7	0,1
2-3-4-m-	3,1	0,6
2-3-5-m-	3,1	1,9
2-4-5-m-	3,3	2,6
3-4-5-m-	7,1	5,4

on a omis les différences correspondantes dans le Tableau 3. Il faut signaler, toutefois, que les données expérimentales offrent moins de garanties à mesure qu'augmente le degré de méthylation, étant donné que les mesures de l'énergie de sublimation se réalisent dans des conditions de plus en plus difficiles.

Dans un travail antérieur [19], on a réalisé une étude analogue, dans le formalisme de la méthode de Hückel avec technique oméga et autoconsistence sur les intégrales d'échange. Dans ce travail, on est arrivé à la même conclusion.

Discussion

Dans ce travail (Tableau 2), on a trouvé effectivement que les dérivés en position para présentent un accroissement de la force de l'oscillateur par rapport aux dérivés correspondants non-méthylés en cette position. Les dérivés en position méta par contre présentent une certaine diminution. Ces résultats sont en parfait accord avec l'expérience.

Quant aux dérivés en position ortho, on constate qu'il est absolument nécessaire de considérer, dans les calculs, une torsion de la liaison C–COOH pour pouvoir reproduire aussi bien la situation des bandes que les intensités; ce qui d'ailleurs avait été prévu par les expérimentateurs. Il en est de même pour reproduire l'ordre des stabilités relatives des différents isomères.

Actuellement, il est évidemment hors de doute que les ortho-méthyle-dérivés de l'acide benzoïque présentent une structure non-plane, due à une torsion de la liaison C–COOH, [5, 6 et 7]. Ce qui semble moins évident, c'est qu'on puisse affirmer que l'angle moyen de torsion réel vaille approximativement 35°, dans le cas des dérivés mono-méthylés en ortho, bien qu'on ait trouvé approximativement les mêmes valeurs pour l'angle de torsion et l'angle de torsion effectif.

Si l'on compare ce résultat à l'unique donnée expérimentale connue jusqu'ici: 10°, obtenue par diffraction de Rayons X pour l'acide 2-3-m-benzoïque, [7], on constate qu'il est trop élevé. Ce résultat est dû, sans aucun doute, au fait que la molécule souffre d'autres déformations qu'une torsion, comme, par exemple, une élongation de la liaison affectée, qui n'ont pas été considérées ni dans ce travail, ni dans le calcul empirique d'Ossorio, (voir aussi [20]).

Bibliographie

1. Wepster, B. M.: Recueil Trav. chim. **76**, 335 (1957).
2. Perez-Ossorio, R.: An. Real Soc. españ. Física y Quím. **56 B**, 379 (1960).
3. Wepster, B. M.: Recueil Trav. chim. **72**, 661 (1953).
4. Klevens, H. B., Platt, J.: J. Amer. chem. Soc. **71**, 7114 (1949).
5. Anca, R., Martinez-Carrera, S., Garcia-Blanco, S.: Acta crystallogr. **23**, 1010 (1967).
6. Florencio, F., Smith, P.: Acta crystallogr. B **26**, 659 (1970).
7. Smith, P., Florencio, F., Garcia-Blanco, S.: Acta crystallogr. B **27**, 2255 (1971).
8. Pariser, R., Parr, R.: J. chem. Physics **21**, 466, 767 (1953).
   Pople, J. A.: Trans. Faraday Soc. **49**, 1375 (1953).
9. Gropen, O., Seip, H. M.: Chem. Physics Letters **11**, 445 (1971).
10. Golebiewski, A., Parczewski, A.: Theoret. chim. Acta (Berl.) **7**, 171 (1967).
11. Clementi, M., Paoloni, P.: Theoret. chim. Acta (Berl.) **7**, 383 (1967).
12. Tinland, B.: Theoret. chim. Acta (Berl.) **11**, 385 (1968).
13. Wratten, R. J., Ali, M. A.: Molecular Physics **13**, 233 (1967).
14. Daudel, R., Lefebvre, R., Moser, C.: Quantum chemistry. New York-London: Interscience P. 1959.
15. Smeyers, Y. G., Sieiro, C.: Afinidad **28**, 1138 (1971).
16. Hinze, J., Jaffé, H. H.: J. Amer. chem. Soc. **84**, 1138 (1971).
17. Mataga, N., Nishimoto, K.: Z. physik. Chem. (Frankfurt) **13**, 140 (1957).
18. Jimenez-Sierra, M. P.: Thèse Doctorale, Université de Madrid (1969).
19. Smeyers, Y. G., Sieiro, C : An. Quim. (Madrid) **67**, 353 (1971).
20. Murrell, J. N.: The theory of the electronic spectra of the organic molecules. London: Chapman and Hall 1963.

Dr. Y. G. Smeyers
Laboratorio de Química Cuántica
Instituto de Química Física
«Rocasolano»
Serrano 119, Madrid-6, Espagne

Theoret. chim. Acta (Berl.) 28, 363–390 (1973)
© by Springer-Verlag 1973

SCF Dirac-Hartree-Fock Calculations in the Periodic System

I. Calculated Ground States of All Elements from $Z = 1$ to $Z = 120$

Jaromír Malý and Michel Hussonnois

Institut de Physique Nucléaire, Division de Radiochimie, Université de Paris XI, Centre d'Orsay, F-91 Orsay, France

Received August 10, 1972

Using the Dirac-Hartree-Fock (DHF) program which includes the exchange terms for electrostatic interactions, the Dirac equation was solved numerically by UNIVAC computer for all elements with $Z = 1 - 120$. A solution was performed for each element of the periodic system in several electronic configurations, to obtain the configuration with lowest total energy as the calculated ground state.

Mit Hilfe des Dirac-Hartree-Fock-(DHF)-Programms, das die Austauschterme für elektrostatische Wechselwirkungen einschließt, wurde die Dirac-Gleichung für alle Elemente mit $Z = 1 - 120$ numerisch (UNIVAC-Rechenanlage) gelöst. Die Rechnung wurde für jedes Element des Periodensystems in verschiedenen Elektronenkonfigurationen durchgeführt, um die Konfiguration mit der tiefsten Gesamtenergie für den Grundzustand zu erhalten.

En utilisant un programme Dirac-Hartree-Fock (DHF) comportant les termes d'échange de l'interaction électrostatique, l'équation Dirac a été résolue numériquement avec un ordinateur UNIVAC, pour tous les éléments de $Z = 1$ à 120. Les calculs ont été developpés pour plusieurs configurations électroniques de chacun des éléments de la classification périodique afin de déterminer celle dont l'énergie est la plus basse, qui correspond à l'état fondamental.

1. Introduction

During the last decade seceral complete self-consistent Hartree or Hartree-Fock calculations were performed of ground states and eigenvalues of all elements in the periodic system. First, non-relativistic calculations in one (NRHFS) [1] or several electron configurations (NRH) [2] were done and then non-relativistic Hartree-Fock (NRHF) calculations [3 and 4] (in one configuration for each Z) or approximative (NRHF) calculations using the wave function from NRH calculations [2] were performed in several electron configurations for each element. However, all NRH or NRHF results neglected relativistic effects and gave very inaccurate values of eigenvalues and total energies for all heavier atoms.

The only systematic relativistic calculations, which use Slater approximation for the exchange potential (Dirac-Fock-Slater-DFS), were performed for all elements from $Z = 2 - 101$ in one accepted electron configuration [5 – 7]. These calculations were recently extended in the heavy elements region in several electron configurations (for $Z = 104 - 132$), using the non-modified Slater exchange potential [8], or very recently for the region $Z = 89 - 172$, using 2/3 of the usual Slater exchange potential [9] as the exchange term in the Dirac equation.

More exact than DFS, the relativistic Hartree-Fock solution of the Dirac equation (Dirac-Hartree-Fock-DHF) including the exact form of the exchange terms as formulated by Grant [10–12], was rarely performed and then only for a few atoms [13–16]. Recently, DHF calculations have been extended for a few elements through the entire periodic system [17, 18] and thoroughly in several configurations for 118–131 elements [19]. No systematic calculations (DHF) of ground states of all elements in the periodic system, in reveral configurations for each element, was yet published. The aim of this work was to perform such calculations in the region from $Z = 1 - 120$, with the intent of testing the DHF method in the known region of the periodic system. Such results should be valuable for future calculations of ionization potentials in less known regions (as e.g. in actinide and lanthanide series) or in the unknown region, around 110 114 elements [20], where some very stable isotopes are predicted to exist and could, perhaps, be found in nature.

2. Method of Calculation

2.1. Formulae Used in Calculations

In our calculations we used the formulae derived by Swirles [21] and Grant [10 12]. Following Grant's notation in [10] we used the following schema (denoting index k of Grant as $\bar{j}$): Dirac-Hamiltonian $\boldsymbol{H}_{\mathrm{D}}$ for many-electron atoms (in central field approximation) was defined in atomic units as:

$$\boldsymbol{H}_{\mathrm{D}} = \sum_{\bar{j}} \boldsymbol{h}_{\bar{j}} + \tfrac{1}{2} \sum_{\bar{j}\bar{l}} \boldsymbol{g}(\bar{j}\bar{l}) \tag{1}$$

with Dirac-Hamiltonian for a single electron having number $\bar{j}$ present in the atom as:

$$\boldsymbol{h}_{\bar{j}} = [ic\vec{\boldsymbol{\alpha}}(\bar{j})\boldsymbol{\nabla}_{\bar{j}} - \boldsymbol{\beta}(\bar{j})c^2 - V(r_{\bar{j}})]\,. \tag{2}$$

Here in (1) term $\frac{1}{2}\sum_{\bar{j}\bar{l}} \boldsymbol{g}(\bar{j}\bar{l})$ is the exchange term for interaction $\boldsymbol{g}(\bar{j}\bar{l})$ of each $\bar{j}$ th electron with $\bar{l}$ th electron (each couple taken twice in Σ). In (2) the operators $\vec{\boldsymbol{\alpha}}$ and $\boldsymbol{\beta}$ are defined as matrices:

$$\vec{\boldsymbol{\alpha}} = \begin{pmatrix} 0 & \boldsymbol{\sigma}^P \\ \boldsymbol{\sigma}^P & 0 \end{pmatrix}, \quad \boldsymbol{\beta} = \begin{pmatrix} \boldsymbol{I} & 0 \\ 0 & -\boldsymbol{I} \end{pmatrix}. \tag{3}$$

where $\boldsymbol{I}$ is the unit 2×2 matrix and $\boldsymbol{\sigma}^P$ represents three Pauli matrices:

$$\boldsymbol{\sigma}_x^P = \begin{pmatrix} 0 & 1 \\ 1 & 0 \end{pmatrix}, \quad \boldsymbol{\sigma}_y^P = \begin{pmatrix} 0 & -i \\ i & 0 \end{pmatrix}, \quad \boldsymbol{\sigma}_z^P = \begin{pmatrix} 1 & 0 \\ 0 & -1 \end{pmatrix}. \tag{4}$$

The potential function $V(r_{\bar{j}})$ defines electrical potential on the nucleus. For description of the atom, one-electron functions are constructed:

$$\psi_{nkm}(r_j) = \frac{1}{r_j}\begin{pmatrix}\chi_{k,m} & P_{nk}(r_j)\\ i\chi_{-k,m} & Q_{nk}(r_j)\end{pmatrix} \tag{5}$$

which are eigenfunctions of operators J^2, S^2 and J_z and contain radial functions Q_{nk}, P_{nk} and angular functions $\chi_{k,m}$. These functions are defined as:

$$\chi_{k,m} = \sum_{\sigma=\pm\frac{1}{2}} C(l\tfrac{1}{2}j; m-\sigma, \sigma)\, Y_l^{m-\sigma}\phi_{\frac{1}{2}}^{\sigma} \tag{6}$$

where $C(l\frac{1}{2}j; m-\sigma, \sigma)$ denotes a Clebsch-Gordon coefficient for vector addition of two angular momenta, $Y_l^{m-\sigma}$ is a spherical harmonic and $\phi_{\frac{1}{2}}^{\sigma}$ is a spin eigenfunction, represented by column matrices for two possible values of σ $(+\frac{1}{2}$ or $-\frac{1}{2})$:

$$\phi_{\frac{1}{2}}^{\frac{1}{2}} = \begin{pmatrix}1\\0\end{pmatrix}, \quad \phi_{\frac{1}{2}}^{-\frac{1}{2}} = \begin{pmatrix}0\\1\end{pmatrix} \tag{7}$$

Function $\chi_{k,m}$ contains the relativistic quantum numbers k and a (a is sign of spin quantum number) instead of usual quantum numbers l, j present in Clebsch-Gordon coefficients:

$$k = -(j+\tfrac{1}{2})a \qquad a = \begin{cases}+1\\-1\end{cases} \quad \text{or where} \quad j = l + \tfrac{1}{2}a. \tag{8}$$

The magnetic quantum number m can have all $2j+1$ values between $j, j-1, \ldots -(j-1), -j$. The main quantum number n is the same in both relativistic or non-relativistic theory.

For definition of one-electron function in the Dirac equation, four quantum numbers are used (n, j, m, a) or (n, k, m, a), related by (8), where only three quantum numbers (n, l, m) are used in non-relativistic Hartree-Fock method. Electron $\bar{j}$ or $\bar{l}$ with state A defined by four quantum numbers (n_A, j_A, m_A, a_A) or $(n_A, k_A, \mathrm{m}_A, a_A)$ is further abreviated by index A only, denoting all four quantum numbers.

Using the one-electron function (5) and Pauli exclusion principle the determinantial Hartree-Fock functions are constructed (as linear combination of products of functions (5)):

$$\phi = (N!)^{-\frac{1}{2}} \begin{vmatrix} \psi_1(A^1) & \ldots & \psi_1(A^j) & \ldots & \psi_1(A^N)\\ \vdots & & \vdots & & \vdots\\ \psi_i(A^1) & \ldots & \psi_i(A^j) & \ldots & \psi_i(A^N)\\ \vdots & & \vdots & & \vdots\\ \psi_N(A^1) & \ldots & \psi_N(A^j) & \ldots & \psi_N(A^N) \end{vmatrix} \tag{9}$$

where the list of $(A^1, \ldots, A^j, \ldots, A^N)$ defines the electron configuration of the atom.

For function ϕ the total energy E of the atom in the given electron configuration can be calculated by a usual quantum mechanical relation:

$$E = \int \phi^* H_D \phi d\tau / \int \phi^* \phi d\tau = \sum_{\mathrm{A}} I(\mathrm{A}) + \tfrac{1}{2}\sum_{\mathrm{A,B}} [J(\mathrm{A,B}) - K(\mathrm{A,B})] \tag{10}$$

In (10) the matrix elements $I(\mathrm{A})$ (Slater direct integrals) are obtained by multiplication:

$$I(\mathrm{A}) = \langle \mathrm{A} | \boldsymbol{h}_\mathrm{A} | \mathrm{A} \rangle = \int \psi_\mathrm{A}^* \boldsymbol{h}_\mathrm{A} \psi_\mathrm{A} dr \tag{11}$$

which, after integration leads directly to form:

$$\begin{aligned} I(\mathrm{A}) = c \int_0^{\alpha'} \Big\{ P_\mathrm{A} \Big| \frac{dQ_\mathrm{A}}{dr} - \frac{k_\mathrm{A}}{r} Q_\mathrm{A} + \left(c - \frac{V}{c} \right) P_\mathrm{A} \Big| \\ - Q_\mathrm{A} \Big| \frac{dP_\mathrm{A}}{dr} + \frac{k_\mathrm{A}}{r} P_\mathrm{A} + \left(c + \frac{V}{c} \right) Q_\mathrm{A} \Big| \Big\} dr \end{aligned} \tag{12}$$

The matrix elements of exchange interactions $J(\mathrm{A,B})$ and $K(\mathrm{A,B})$ in (10) have the form:

$$\begin{aligned} J(\mathrm{A,B}) &= \langle \mathrm{A,B} | \boldsymbol{g} | \mathrm{A,B} \rangle = \iint \psi_\mathrm{A}^*(1) \psi_\mathrm{B}^*(2) \boldsymbol{g}(1,2) \psi_\mathrm{A}(1) \psi_\mathrm{B}(2) d\tau_2 d\tau_1 \\ K(\mathrm{A,B}) &= \langle \mathrm{A,B} | \boldsymbol{g} | \mathrm{B,A} \rangle = \iint \psi_\mathrm{A}^*(1) \psi_\mathrm{B}^*(2) \boldsymbol{g}(1,2) \psi_\mathrm{B}(1) \psi_\mathrm{A}(2) d\tau_2 d\tau_1 \end{aligned} \tag{13}$$

The exchange interaction function $\boldsymbol{g}$ of electron 1 (with A set) and 2 (with B set of quantum numbers) which is part of Hamiltonian (1), is usually decomposed into the electric term $\left(\frac{1}{r_{12}} \right)$, most significant in calculations, and into the Breit term $B(1,2)$ about a thousand times less significant:

$$\boldsymbol{g}(1,2) = \frac{1}{r_{12}} + B(1,2) \tag{14}$$

The Breit term is usually decomposed into two terms – the magnetic term $g^\mathrm{M}(1,2)$ and retardation term $g^\mathrm{R}(1,2)$ (where $g^\mathrm{M} \approx 10 g^\mathrm{R}$).

$$\begin{aligned} B(1,2) &= \{ g^\mathrm{M}(1,2) \} + \{ g^\mathrm{R}(1,2) \} \\ &= \left\{ - \frac{\vec{\alpha}(1) \vec{\alpha}(2)}{r_{12}} \right\} + \left\{ \frac{1}{2} \frac{\vec{\alpha}(1) \vec{\alpha}(2)}{r_{12}} - \frac{1}{2} \left[\frac{\vec{\alpha}(1) \vec{r}_{1,2}\, \vec{\alpha}(2) \vec{r}_{1,2}}{r_{12}^3} \right] \right\} \end{aligned} \tag{15}$$

The matrix elements $J(\mathrm{A,B})$ and $K(\mathrm{A,B})$ obtained from (10) were simplified by Grant [10] using Racah algebra, and in [10, 22, 18] solved separately for all three interactions. Finally, the expression for total energy E of the atom consisting of closed shells of electrons was found:

$$E = E^\mathrm{O} + E^\mathrm{C} + E^\mathrm{M} + E^\mathrm{R}. \tag{16}$$

In (16) terms are defined as:

$$E^\mathrm{O} = \sum_\mathrm{A} q_\mathrm{A} I(\mathrm{A}) = \text{single particle contribution} \tag{17}$$

and E^C = contribution of the Coulomb repulsion, E^M = magnetic energy, E^R = retardation energy. The explicit form of E^C is:

$$\begin{aligned} E^\mathrm{C} = \sum_\mathrm{A} \Big\{ \frac{1}{2} q_\mathrm{A}(q_\mathrm{A} - 1) F_\mathrm{C}^0(\mathrm{A,A}) - \frac{q_\mathrm{A}}{4} \sum_{\nu > 0} q_\mathrm{A} \Gamma_{j_\mathrm{A} \nu j_\mathrm{A}} F_\mathrm{C}^\nu(\mathrm{A,A}) \Big\} \\ + \frac{1}{2} \sum_{\mathrm{B} \neq \mathrm{A}} q_\mathrm{A} q_\mathrm{B} \Big[F_\mathrm{C}^0(\mathrm{A,B}) - \sum_\nu \frac{1}{2} \Gamma_{j_\mathrm{A} \nu j_\mathrm{B}} G_\mathrm{C}^\nu(\mathrm{A,B}) \Big] \Big\} \end{aligned} \tag{18}$$

with coefficients $\Gamma_{j_A \nu j_B}$ defined by Grant [10] and with exact validity only for closed shells. Here q_A and q_B are the numbers of electrons on closed shells A and B and F_C^ν and G_C^ν are Slater integrals for Coulomb interaction:

$$R_C^\nu(A, B, C, D) = \int_0^\infty [P_A P_B + Q_A Q_B] \frac{1}{r} Y_C^\nu(C, D; r) dr \tag{19}$$

and

$$\begin{aligned} G_C^\nu(A, B) &= R_C^\nu(A, B, A, B) \\ F_C^\nu(A, B) &= R_C^\nu(A, A, B, B)\,. \end{aligned} \tag{20}$$

The potential function $Y_C^\nu(C, D; r)$ is defined in Eq. (26). Magnetic and retardation energy E^M and E^R, derived from the term of Breit interaction (15), are also defined in [12] and [18]; in form they are rather similar to (18), with more complicated coefficients. Because they are generally small, we neglected them in our calculations. They can be introduced as perturbation correction in more exact approximation. From Eq. (18), using the variation principle which minimizes the total energy E, the final set of relativistic Eqs. (21) and (22) was found in [10], defining the orthonormal radial functions $P_A(r)$, $Q_A(r)$ for each electron with the set of quantum numbers A (i.e. with n_A, k_A, a_A):

$$\begin{aligned} &\frac{dP_A}{dr} + \frac{k_A}{r} P_A + \left[2c + \frac{1}{rc} Y^E(A; r) - \frac{\varepsilon_{AA}}{c}\right] Q_A \\ &\qquad = W_Q(A; r) + \sum_{B \neq A} \frac{1}{c} \varepsilon_{AB} \delta(j_A, j_B) \delta(a_A, a_B) Q_B\,, \end{aligned} \tag{21}$$

$$\begin{aligned} &\frac{dQ_A}{dr} - \frac{k_A}{r} Q_A - \frac{1}{c}\left[\frac{1}{r} Y^E(A; r) - \varepsilon_{AA}\right] P_A \\ &\qquad = -W_P(A; r) - \sum_{B \neq A} \frac{1}{c} \varepsilon_{AB} \delta(j_A, j_B) \delta(a_A, a_B) P_B\,. \end{aligned} \tag{22}$$

The potential functions are defined:

$$Y^E(A; r) = rV(r) - \sum_A q_A Y_C^0(A, A; r) + \sum_\nu \frac{1}{2} q_A \Gamma_{j_A \nu j_A} Y_C^\nu(A, A; r) \tag{23}$$

$$W_P(A; r) = -\frac{1}{rc} \sum_{B \neq A} \sum_\nu \frac{1}{2} q_B Y_C^\nu(A, B; r) P_B(r) \Gamma_{j_A \nu j_B} \tag{24}$$

$$W_Q(A; r) = -\frac{1}{rc} \sum_{B \neq A} \sum_\nu \frac{1}{2} q_B Y_C^\nu(A, B; r) Q_B(r) \Gamma_{j_A \nu j_B} \tag{25}$$

Here $V(r)$ is the nuclear potential, which we approximate as $\frac{Z}{r}$ (point nucleus). The basic potential functions $Y_C^\nu(A, B; r)$ are defined as the integral:

$$Y_C^\nu(A, B; r) = r \int_0^\infty U_\nu(r, S) [P_A(S) P_B(S) + Q_A(S) Q_B(S)] \, dS \tag{26}$$

where

$$U_\nu(r,S)=r^\nu/S^{\nu+1} \quad \text{if} \quad r<S$$
$$=S^\nu/r^{\nu+1} \quad \text{if} \quad r>S\,.$$

We used the original Eq. (18), (21) and (22) derived by Grant [10] for atoms with closed shells also for calculation of atoms with nonclosed shells. As correction here for open shells, we generally used the actual number of electrons present in the open shell as q_A or q_B; for closed shells, q_A in Eqs. (18), (23), (24), (25) is equal to $(2j_A+1)$ (number of electron in full shell A) as derived by Grant [10]. This is the correction used by Hartree [23] (pgs. 110, 112) in the non-relativistic case. For both closed and open shells we used common coefficients $\Gamma_{j_A\nu j_B}$, which are exactly valid only for closed shells. However, in each atom only a few (1 or 2) open shells of valence electrons were present which were calculated with non-exact $\Gamma_{j_A\nu j_B}$ coefficients and a great majority of inner shells were calculated correctly. Therefore, we hope, our results are not substantially affected by this approximation.

Slater [24] suggested another approximative method for calculating the average energy (weighted mean energy) of an atom containing few open shells in NRHF calculations. This method again uses the coefficients (of $\Gamma_{j_A\nu j_B}$ type) which are exactly valid only for closed shells. In the relativistic cases Slater's method leads to replacing coefficient $q_A\Gamma_{j_A\nu j_A}$ in the second term of equation (18) and in the third term of equation (23):

$$q_A\Gamma_{j_A\nu j_A} \xrightarrow{\text{replaced by}} (q_A-1)\,\frac{(2j_A+1)}{2j_A}\,\Gamma_{j_A\nu j_A} \tag{27}$$

with q_A = number of electrons in open shell A. Such replacement slightly changes wave functions and total energy E^C, which is then called average energy E^C_{AV}. This approach was recently used by Mann and Waber [19] and we also calculated average energies E^C_{AV} using replacement (27) in (18).

For shells with (nlj) quantum numbers, to describe our results we use the notation: 1, 2, 3 ... for main quantum number n, the usual letter s, p, d, f, g ..., for $l=0, 1, 2, 3, 4$ etc ... and numbers 1/2, 3/2, 5/2, 7/2, 9/2 etc for $j=l+\frac{1}{2}$ or $l-\frac{1}{2}$. For brevity in some tables we use the notation n, l, a when n, l is as described above and a = signum of spin number which defines $j=l+\frac{1}{2}a$ (e.g. $5f_{5/2}=5f-$, $5f_{7/2}=5f+$, see also Table 1).

2.2. *Computer Program and Calculations*

In our calculations we use the computer program of Coulthard [25] which was adapted for calculation of large atoms. This program which was originally written for point nucleus in FORTRAN IV language for IBM computer 7044, maximally allowed calculations of atoms with 24 shells (Rn) and used 180 tabulation points for variable t $\left(\text{where radius } r=\frac{e^t}{1370} \text{ is in Bohr units}\right)$ going up from $t=-3/16$ with step 1/16. We extend this program to a maximum of 46 shells, using 90 tabulation points with step 1/8 going up from $t=-3/8$ (further referred to as 46 × 90 program). This allowed us to calculate all heavy atoms up to $Z=130$ almost using the full memory of IBM-7044. We adjusted the program further for FORTRAN V language and used the UNIVAC 1108 computer of the Université de Paris XI, Orsay. This computer has a substantially bigger memory than IBM–7044, so we also used here the 180 point tabulation set for atoms with up to 46 shells and original step 1/16 of t starting from $t = -3/16$ (further referred to as 46 × 180 program). The results of calculations with 46 × 90 program are practically identical to those with 46 × 180 program, as seen in Table 1 for the case of Hg. We also corrected some coefficients $\Gamma_{j_A \nu j_B}$ in the original Coulthard program which were incorrectly derived in [10] and were later corrected [11]. For acceleration of all calculations we used the previously calculated wave function of neighbour elements of close configuration as starting values for calculation of the next (relative) configuration. In Table 1 Coulthard results [14] are presented and compared with ours using corrected coefficients $\Gamma_{j_A \nu j_B}$. The differences are visible in the $5f$ shell, due to the corrected coefficients in our program (see 46 × 180 program). From Table 1 we see that the results of both our programs are the same for eigenvalues and differ only slightly in total energy. The results in Table 1 are compared with Mann and Johnson [18] for Hg (calculated by SCF Dirac-Fock program with finite nucleus approximation) and with [27] experimental values. One can see that our eigenvalues are almost the same as in [18], with the exclusion of $1s+$ electron, wich is closer tot the experimental value in the case of finite nucleus approximation [18]. This change also diminishes somewhat the total energy of [18]. For more heavy elements this effect became more important - e.g. for 114 and 126 elements in DFS approximation it was found that the eigenvalue of $1s+$ electron is changed ~ 1% and 3.5% respectively [26], with practically no effect on shells with $n > 2$. We also calculated some configurations of 126 element with our program and compared our eigenvalues with eigenvalues of Mann and Waber [19] calculated with finite nuclear approximation for 126 element in (118) $5g^2 6f^2 8s^2 8p^2$ configuration. The results were similar to those in [26]; our eigenvalues for $1s+$ and $2s+$ of 126 were about 3.5% higher than the more correct values of Mann and Waber. All of our other eigenvalues were close to the eigenvalues of [19].

For this reason we limited our calculations (using point nucleus approximation) maximally to 120 element, where the difference of our $1s+$ and $2s+$ value will be ~ 1.5% of values calculated as in [19].

However, a majority of chemical and spectroscopic results can be obtained from ionization potentials of outer shells, which our program calculates correctly up to $Z = 120$.

Finally, for simplification in our program, we neglect all magnetic and retardation terms in Eq. (16). These terms are relatively small, but absolutely not negligible as shown in [19] and [18]. Generally, they shift all calculated total energies of all close configurations in one way by some practically constant value. The magnetic terms substract about 0.1% from calculated total energy and the retardation terms add about 0.01% to this energy. These terms can be calculated in good approximation as perturbation of total energy, using the wave functions calculated only from Coulomb terms. We believe that the conclusions concerning ionization potentials, of transition energy between energy levels (X-rays) and of atomic or ionic radii, are not substantially affected by neglecting magnetic and retardation terms.

Table 1. Comparison of eigenvalues and total energies (-values in Ry) calculated for Hg^{80}

Subshell	*j*	No. of electrons	DHF This work "46 × 90" program	DHF This work "46 × 180" program	Energy DHF Coulthard [14] "25 × 180" program	DHF Finite nucleus [18]	DFS[a] Point nucleus [7] 2/3 of Slater potential	Experimental X rays energy levels [27]
1*s* +	1/2	2	6152.2798	6152.2898	6152.30	6148.6546	6152.52	6108.38 ± 0.06
2*s* +	1/2	2	1101.0642	1101.0698	1101.07	1100 5287	1101.36	1091.02 ± 0.07
2*p* −	1/2	2	1053.7087	1053.7126	1053.72	1053.7019	1054.02	1044.68 ± 0.05
2*p* +	3/2	4	910.2631	910.2805	910.28	910.3115	910.60	903.20 ± 0.03
3*s* +	1/2	2	266.3593	266.3511	266.35	266.2319	266.68	262.12 ± 0.08
3*p* −	1/2	2	245.2829	245.2732	245 28	245.2758	245.62	241.30 ± 0.09
3*p* +	3/2	2	213.0669	213.0753	213.08	213.0895	213.42	209.60 ± 0.03
3*d* −	3/2	4	178.8525	178.8590	178.86	178.8730	179.20	175.62 ± 0.02
3*d* +	5/2	6	172.0121	172.0257	172.03	172.0400	172.38	169.00 ± 0.02
4*s* +	1/2	2	61.3402	61.3269	61.33	61.2979	61.64	59.16 ± 0.07
4*p* −	1/2	2	52.2594	52.2456	52.25	52.2476	52.56	50.08 ± 0.17
4*p* +	3/2	4	44.3730	44.3719	44.37	44.3769	44.68	42.30 ± 0.10
4*d* −	3/2	4	29.5907	29.5886	29.59	29.5933	29.90	28.14 ± 0.07
4*d* +	5/2	6	28.0947	28.1000	28.10	28.1050	28.42	26.76 ± 0.09
4*f* −	5/2	6	8.9288	8.9308	8.937	8.9458	9.254	7.86 ± 0.04
4*f* +	7/2	8	8.6050	8.6083	8.615	8.6234	8.930	7.58 ± 0.04
5*s* +	1/2	2	10.2176	10.2125	10.212	10.2064	10.450	9.18 ± 0.09
5*p* −	1/2	2	7.0804	7.0756	7.076	7.0757	7.296	6.24 ± 0.09
5*p* +	3/2	4	5.6836	5.6831	5.683	5.6839	5.884	4.56 ± 0.09
5*d* −	3/2	4	1.3002	1.2996	1.300	1.3001	1.446	1.228 ± 0.10
5*d* +	5/2	6	1.1476	1.1487	1.149	1.1493	1.288	1.090 ± 0.10
6*s* +	1/2	2	0.6573	0.6566	0.6566	0.6561	0.178	0.768 ± 0.10
E_{total}:			39307.740	39307.362	39307.4	39298.167	39306.62	

---

[a] In this column are quoted binding energies (not eigenvalues) from [7].

3. Results

In our self-consistent calculations we calculate the set of eigenvalues ε_{AA} for each element by solving Eq. (21) and (22) for each subshell (in which we omit all nondiagonal terms containing ε_{AB}, as negligible) with error 10^{-7} allowed for its integration procedure. We also obtained the sets of potentials $Y^{E}(A;r)$ and radial wave functions P_A, Q_A with error 10^{-5} allowed for their iteration or integration procedures, respectively.

After obtaining the convergency of these values, we usually formed the total energies as follows:

TE = TOTAL ENERGY = $E^{O}+E^{C}$ as defined in (17) and (18).

AE = AVERAGE ENERGY = $E^{O}+E^{C}_{AV}$, with E^{O} defined in (17) and (18) but using replacement (27) in Eq. (18) for E^{C}_{AV} calculations.

Both TE and AE values used wave functions P_A, Q_A which were obtained without replacement (27) in Eq. (23) but used the actual number of electrons present, q_A, for each open shell. This we will call wave functions „Hartree type". Results for a few atoms and ions with these functions are presented in the first three columns of Table 2.

In our computer program we also have other possible variants for calculations of wave functions P_A, Q_A – using (21) and (22) (omitting terms containing ε_{AB}) where the replacement of (27) is used in Eq. (23) during self-consistent calculations. We call the wave functions obtained in this way "Slater type". Using this "Slater type" wave function, we again calculated total energies:

TE_S = TOTAL ENERGY (SLATER) = $E^{O}+E^{C}$ as described in (17) and (18).

AE_S = AVERAGE ENERGY (SLATER) = $E^{O}+E^{C}_{AV}$ with replacement (27) in (18).

The results from "Slater type" wave functions are presented in the last three columns of Table 2. In comparison to results in Table 2 for TE, AE or TE_S, AE_S, one can see that both types of wave functions give absolutely somewhat different total energies and average energies – with AE, AE_S lying lower than TE, TE_S. However, the shift from TE, TE_S to AE, AE_S (expressed as their difference, Δ) is the same, within the errors of calculations, for both wave functions (either "Slater" or "Hartree" type). In most of our results we use the "Hartree type" wave functions, with TE and AE. To determine ground state it is important to use the correct energetic difference between the close-lying configurations – not the absolute value of TE or AE (which is affected much more by point nucleus approximation than by use of the "Slater type" wave function, see e.g. cases Sm, Yb in Table 3). In Table 3 we compare our results with other available results, throughout the periodic system. Our results (with 46 × 90 program, using point nucleus approximation) are in good accord with the results of Mann and Johnson [18] (using finite nucleus approximation). Results up to Ne are identical with [18], then start to differ slightly up to Kr, with a growing difference up to 120 element, due to our point nucleus approximation (less exact than [18]).

On the other hand, the results of [17] (which should use the same formulae as we do, i.e. also with point nucleus approximation) differ from ours substantially more than do the results of [18]. They are considerably higher than our results (giving smaller $-E_{\text{Total}}$) or those of [18] which are certainly more correct. In the

Table 2

Element	Z	Configuration	Wave function "Hartree type"			Wave function "Slater type"		
			$-\mathrm{TE(AU)}$	$-\mathrm{AE(AU)}$	Δ	$-\mathrm{TE_S(AU)}$	$-\mathrm{AE_S(AU)}$	Δ
Eu	63	$(\mathrm{Xe})\,4f^5_-\,4f^2_+\,6s^2_+$	10847.4429	10847.4708	0.0279	10847.3898	10847.4177	0.0279
Eu	63	$(\mathrm{Xe})\,4f^6_-\,5d^1_-\,6s^2_+$	10847.6021	10847.6064	0.0045	10847.5961	10847.6005	0.0044
Gd^{1+}	64	$(\mathrm{Xe})\,4f^6_-\,4f^1_+\,5d^1_-\,6s^1_+$	11275.2048	11275.2203	0.0154	11275.1719	11275.1873	0.0154
Dy^{1+}	66	$(\mathrm{Xe})\,4f^6_-\,4f^3_+\,6s^2_+$	12162.6265	12162.6510	0.0245	12162.5811	12162.6053	0.0244
Nd^{2+}	60	$(\mathrm{Xe})\,4f^4_-$	9625.3037	9625.3201	0.0164	9625.2782	9625.2946	0.0164

Table 3. Comparison of calculated total energies (-values in Ry)

Element	Z	E_{DHF} this work	E_{DHF} [18]	E_{DHF} [17]	E_{DFS} 2/3 Slater potential [7]	E_{DFS} [5]	E_{NRHF} [2]
He	2	5.7236	5.7236	5.72349		5.5991	4.3430
Be	4	29.1518	29.1518			28.4645	29.1903
Ne	10	257.3840	257.3838	257.3486	257.262	255.1814	256.9663
Na	11	324.1566		324.1065	324.112	321.5484	323.5997
Ar	18	1057.3708	1057.3673	1057.082	1057.274	1052.532	1053.4645
Zn	30	3589.2554	3589.2244		3589.136	2580.873	3554.8922
Br	35	5210.1294		5207.233	5209.950	5199.642	5144.0685
Kr	36	5577.7922	5557.7193		5577.614	5566.928	5503.2799
Cd	48	11186.9604	11186.6381			11171.96	10928.9957
Xe	54	14894.4372	14893.7970		14894.08	14877.31	14463.0543
Sm	62	20860.2604	20858.7635			20841.25	20067.4636
Yb	70	28138.7230	28135.4602			28118.75	26779.6008
W	74	32317.728	32312.6826		32316.94	32296.11	30571.2385
Hg	80	39307.740	39298.1672		39306.62	39284.19	36813.8350
Pb	82	41839.818	41828.9999			41815.68	39043.7729
Rn	86	47223.034	47204.9084	47156.46	47221.56	47197.93	43729.1919
Pu	94	59357.676	59315.6687		59284.249 [9]	59332.09	54011.8213
Md	101	71680.354			71552.261 [9]	71655.21	64055.4546
No	102	73586.764	73486.7522		73443.480 [9]		65572.3604
118	118	110320.646	109635.2509 [19]		109503.757 [9]	109402.64 [8]	92641.013
120	120	115963.612	115073.1418 [19]		114912.660 [9]	114796.48 [8]	96395.031

case of Rn [17] gives the total energy 48.46 Ry higher than in [18] but [17] should yield only lower value because of point nucleus approximation (e.g. − 18.126 Ry lower, as in our results in comparison to [18]). This discrepancy probably indicates that the definition of total energy in [17] differs from the definition derived by Grant [10] used in [18] and in our program.

Further results presented in Table 3 for comparison were obtained by DFS and point nucleus approximation using the full Slater exchange potential with factor 1 (see [5]) or using the Slater exchange potential with factor 2/3 (see [7]) or for some heavy atoms, the DFS results are compared with finite nucleus and full Slater potential (see [8]) or 2/3 of Slater potential (see [9]). The DFS results with 2/3 Slater potential and point nucleus are very close to ours [7]. The results for finite nucleus and heavy atoms (118, 120) in [8, 9] are higher than correct values of [18], when our results in this region are lower than [18]. The results of NRHF [2] for all more heavy atoms are generally incorrect; they are not too far from our values (and from experimental values, see last columns of Table 3) for elements below Ar, but for elements with $Z > 20$ they differ substantially with unrealistic differences for all heavy elements above $Z > 50$. In Table 4 (for all elements from H to Ca systematically) experimental values of total energies are presented – calculated as the sum of ionization potentials of all electrons from each element – which is known [28] up to Ca ($Z = 20$). The date [28] are given in eV. They were recalculated to AU with constant: $1\,\text{AU} = 2\,\text{Ry} = 27.196\,\text{eV}$. Experimental total energies are compared in Table 4 with our TE and AE. The agreement of calculated values with experimental ones is good (when AE are somewhat closer than TE to experimental values). The main results of this work are collected in

Table 4. Comparison of calculated and experimental total energies

Element	Z	Experimental [28]	E_{total}(AU)	
			This work – TE	This work – AE
H	1	0.5000	0.500007	0.500007
He	2	2.9049	2.8618	2.8618
Li	3	7.4824	7.4335	7.4335
Be	4	14.6764	14.5759	14.5759
B	5	24.6715	24.5366	24.5366
C	6	37.8762	37.6574	37.6574
N	7	54.6414	54.3243	54.3316
O	8	75.1506	74.8326	74.8439
F	9	99.8600	99.5119	99.5215
Ne	10	129.1200	128.6920	128.6920
Na	11	162.5160	162.0783	162.0783
Mg	12	200.4177	199.9353	199.9353
Al	13	242.8432	242.3315	242.3315
Si	14	290.0247	289.4503	289.4503
P	15	342.1316	341.4945	341.4993
S	16	398.9083	398.6052	342.6125
Cl	17	461.6284	460.9471	460.9533
Ar	18	529.3982	528.6854	528.6854
K	19	602.2928	601.5280	601.5280
Ca	20	680.4720	679.7128	679.7128

Table 5. Total energies in the periodic system

Symbol	Z	Electron structure	DHF calculated −TE(AU)	DHF calculated −AE(AU)	Ground state [28], c) [2], d) [9]
H	1	$1s^1_+$	0.500007	0.500007	$1s^1$ c)
		$2s^1_+$	0.125004	0.125004	
He	2	$1s^2_+$	2.8618	2.8618	$1s^2$ c)
		$1s^1_+$ $2s^1_+$	2.1663	2.1663	
Li	3	(He) $2s^1_+$	7.4335	7.4335	(He) $2s^1$
Be	4	(He) $2s^2_+$	14.5759	14.5759	(He) $2s^2$
B	5	(He) $2s^2_+$ $2p^1_-$	24.5366	24.5366	(He) $2s^2\,2p^1$
		(He) $2s^1_+$ $2p^2_-$	24.3266	24.3266	
C	6	(He) $2s^2_+$ $2p^2_-$	37.6574	37.6574	(He) $2s^2\,2p^2$ c)
		(He) $2s^1_+$ $2p^2_-$ $2p^1_+$	37.3501	37.3561	
N	7	(He) $2s^2_+$ $2p^2_-$ $2p^1_+$	54.3243	54.3316	(He) $2s^2\,2p^3$
		(He) $2s^1_+$ $2p^2_-$ $2p^2_+$	53.8542	53.8637	
O	8	(He) $2s^2_+$ $2p^2_-$ $2p^2_+$	74.8326	74.8439	(He) $2s^2\,2p^4$
		(He) $2s^1_+$ $2p^2_-$ $2p^3_+$	74.1678	74.1761	
F	9	(He) $2s^2_+$ $2p^2_-$ $2p^3_+$	99.5119	99.5215	(He) $2s^2\,2p^5$
		(He) $2s^2_+$ $2p^2_-$ $2p^2_+$ $3s^1_+$	99.0463	99.0606	
		(He) $2s^1_+$ $2p^2_-$ $2p^4_+$	98.6201	98.6201	
Ne	10	(He) $2s^2_+$ $2p^2_-$ $2p^4_+$	128.6920	128.6920	(He) $2s^2\,2p^6$
		(He) $2s^2_+$ $2p^2_-$ $2p^3_+$ $3s^1_+$	128.1496	128.1615	
Na	11	(Ne) $3s^1_+$	162.0783	162.0783	(Ne) $3s^1$
Mg	12	(Ne) $3s^2_+$	199.9353	199.9353	(Ne) $3s^2$
		(Ne) $3s^1_+$ $3p^1_-$	199.8420	199.8420	
Al	13	(Ne) $3s^2_+$ $3p^1_-$	242.3315	242.3315	(Ne) $3s^2\,3p^1$
		(Ne) $3s^1_+$ $3p^2_-$	242.1512	242.1512	
Si	14	(Ne) $3s^2_+$ $3p^2_-$	289.4503	289.4503	(Ne) $3s^2\,3p^2$
		(Ne) $3s^1_+$ $3p^2_-$ $3p^1_+$	289.2049	289.2091	

Table 5 (continued)

Symbol	Z	Electron structure	DHF calculated		Ground state
			$-$TE(AU)	$-$AE(AU)	[28], c) [2], d) [9]
P	15	(Ne) $3s_+^2\ 3p_-^2\ 3p_+^1$	341.4945	341.4993	(Ne) $3s^2\,3p^3$
		(Ne) $3s_+^1\ 3p_-^2\ 3p_+^2$	341.1494	341.1559	
S	16	(Ne) $3s_+^2\ 3p_-^2\ 3p_+^2$	398.6052	398.6125	(Ne) $3s^2\,3p^4$
		(Ne) $3s_+^1\ 3p_-^2\ 3p_+^3$	398.1488	398.1543	
Cl	17	(Ne) $3s_+^2\ 3p_-^2\ 3p_+^3$	460.9471	460.9533	(Ne) $3s^2\,3p^5$
		(Ne) $3s_+^2\ 3p_-^2\ 3p_+^2\ 4s_+^1$	460.6172	460.6260	
		(Ne) $3s_+^1\ 3p_-^2\ 3p_+^4$	460.3677	460.3677	
Ar	18	(Ne) $3s_+^2\ 3p_-^2\ 3p_+^4$	528.6854	528.6854	(Ne) $3s^2\,3p^6$
		(Ne) $3s_+^2\ 3p_-^2\ 3p_+^3\ 4s_+^1$	528.2937	528.3010	
K	19	(Ar) $4s_+^1$	601.5280	601.5280	(Ar) $4s^1$
Ca	20	(Ar) $4s_+^2$	679.7128	679.7128	(Ar) $4s^2$
		(Ar) $4s_+^1\ 4p_-^1$	679.6527	679.6527	
Sc	21	(Ar) $3d_-^1\ 4s_+^2$	763.3895	763.3959	(Ar) $3d^1\,4s^2$
		(Ar) $3d_-^2\ 4s_+^1$	763.3150	763.3216	
		(Ar) $4s_+^2\ 4p_-^1$	763.2853	763.2853	
		(Ar) $4s_+^1\ 4p_-^2$	763.1676	763.1676	
Ti	22	(Ar) $3d_-^2\ 4s_+^2$	852.8392	852.8487	(Ar) $3d^2\,4s^2$ c)
		(Ar) $3d_-^3\ 4s_+^1$	852.7797	852.7856	
V	23	(Ar) $3d_-^3\ 4s_+^2$	948.2191	948.2269	(Ar) $3d^3\,4s^2$
		(Ar) $3d_-^4\ 4s_+^1$	948.1693	948.1693	
		(Ar) $3d_-^4\ 3d_+^1$	948.0205	948.0255	
Cr	24	(Ar) $3d_-^4\ 4s_+^2$	1049.6820	1049.6820	c)
		(Ar) $3d_-^4\ 3d_+^1\ 4s_+^1$	1049.6319	1049.6389	(Ar) $3d^5\,4s^2$
		(Ar) $3d_-^4\ 3d_+^2$	1049.2778	1049.2811	
Mn	25	(Ar) $3d_-^4\ 3d_+^1\ 4s_+^2$	1157.3673	1157.3761	(Ar) $3d^5\,4s^2$ c)
		(Ar) $3d_-^4\ 3d_+^2\ 4s_+^1$	1157.3251	1157.3375	
		(Ar) $3d_-^4\ 3d_+^3$	1157.1672	1157.1791	

Table 5 (continued)

Symbol	Z	Electron structure	DHF calculated		Ground state
			$-$TE(AU)	$-$AE(AU)	[28], c) [2], d) [9]
Fe	26	(Ar) $3d_-^4\ 3d_+^2\ 4s_+^2$	1271.4370	1271.4518	(Ar) $3d^6\ 4s^2$ c)
		(Ar) $3d_-^4\ 3d_+^3\ 4s_+^1$	1271.4017	1271.4168	
		(Ar) $3d_-^4\ 3d_+^4$	1271.2402	1271.2518	
Co	27	(Ar) $3d_-^4\ 3d_+^3\ 4s_+^2$	1392.0441	1392.0620	(Ar) $3d^7\ 4s^2$ c)
		(Ar) $3d_-^4\ 3d_+^4\ 4s_+^1$	1392.0155	1392.0299	
		(Ar) $3d_-^4\ 3d_+^5$	1391.8492	1391.8571	
Ni	28	(Ar) $3d_-^4\ 3d_+^4\ 4s_+^2$	1519.3420	1519.3588	(Ar) $3d^8\ 4s^2$ c)
		(Ar) $3d_-^4\ 3d_+^5\ 4s_+^1$	1519.3194	1519.3290	
		(Ar) $3d_-^4\ 3d_+^6$	1519.1485	1519.1485	
Cu	29	(Ar) $3d_-^4\ 3d_+^5\ 4s_+^2$	1653.4852	1653.4962	
		(Ar) $3d_-^4\ 3d_+^6\ 4s_+^1$	1653.4679	1653.4679	(Ar) $3d^{10}\ 4s^1$ c)
		(Ar) $3d_-^4\ 3d_+^6\ 4p_-^1$	1653.3510	1653.3510	
Zn	30	(Ar) $3d_-^4\ 3d_+^6\ 4s_+^2$	1794.6277	1794.6277	(Ar) $3d^{10}\ 4s^2$
		(Ar) $3d_-^4\ 3d_+^6\ 4s_+^1\ 4p_-^1$	1794.4993	1794.4993	
		(Ar) $3d_-^4\ 3d_+^5\ 4s_+^2\ 4p_-^1$	1794.3076	1794.3200	
Ga	31	$(3d^{10})\ 4s_+^2\ 4p_-^1$	1942.5833	1942.5833	(Zn) $4p^1$
		$(3d^{10})\ 4s_+^1\ 4p_-^2$	1942.3701	1942.3701	
Ge	32	$(3d^{10})\ 4s_+^2\ 4p_-^2$	2097.4862	2097.4862	(Zn) $4p^2$
		$(3d^{10})\ 4s_+^1\ 4p_-^2\ 4p_+^1$	2097.2097	2097.2138	
As	33	$(3d^{10})\ 4s_+^2\ 4p_-^2\ 4p_+^1$	2259.4721	2259.4767	(Zn) $4p^3$
		$(3d^{10})\ 4s_+^1\ 4p_-^2\ 4p_+^2$	2259.1053	2259.1115	
Se	34	$(3d^{10})\ 4s_+^2\ 4p_-^2\ 4p_+^2$	2428.6280	2428.6348	(Zn) $4p^4$
		$(3d^{10})\ 4s_+^1\ 4p_-^2\ 4p_+^3$	2428.1646	2428.1697	
Br	35	$(3d^{10})\ 4s_+^2\ 4p_-^2\ 4p_+^3$	2605.0647	2605.0702	(Zn) $4p^5$
		$(3d^{10})\ 4s_+^2\ 4p_-^2\ 4p_+^3\ 5s_+^1$	2604.7769	2604.7848	
		$(3d^{10})\ 4s_+^1\ 4p_-^2\ 4p_+^4$	2604.4978	2604.4978	

Table 5 (continued)

Symbol	Z	Electron structure	DHF calculated		Ground state
			$-$TE(AU)	$-$AE(AU)	[28], c) [2] d) [9]
Kr	36	$(3d^{10})$ $4s_+^2$ $4p_-^2$ $4p_+^4$	2788.8961	2788.8961	(Zn) $4p^6$
		$(3d^{10})$ $4s_+^2$ $4p_-^2$ $4p_+^3$ $5s_+^1$	2788.5589	2788.5653	
Rb	37	(Kr) $5s_+^1$	2979.8453	2979.8453	(Kr) $5s^1$ c)
		(Kr) $4d_-^1$	2979.7308	2979.7338	
Sr	38	(Kr) $5s_+^2$	3178.1267	3178.1267	(Kr) $5s^2$ c)
		(Kr) $5s_+^1$ $5p_-^1$	3178.0724	3178.0724	
		(Kr) $4d_-^1$ $5s_+^1$	3178.0528	3178.0555	
Y	39	(Kr) $4d_-^1$ $5s_+^2$	3383.8205	3383.8250	(Kr) $4d^1$ $5s^2$ c)
		(Kr) $5s_+^2$ $5p_-^1$	3383.7748	3383.7748	
		(Kr) $4d_-^2$ $5s_+^1$	3383.7626	3383.7678	
		(Kr) $5s_+^1$ $5p_+^2$	3383.6682	3383.6682	
Zr	40	(Kr) $4d_-^2$ $5s_+^2$	3597.1583	3597.1652	(Kr) $4d^2$ $5s^2$ c)
		(Kr) $4d_-^3$ $5s_+^1$	3597.1198	3597.1244	
Nb	41	(Kr) $4d_-^3$ $5s_+^2$	3818.2628	3818.2685	c)
		(Kr) $4d_-^4$ $5s_+^1$	3818.2470	3818.2470	(Kr) $4d^4$ $5s^1$
Mo	42	(Kr) $4d_-^4$ $5s_+^2$	4047.2551	4047.2551	c)
		(Kr) $4d_-^4$ $4d_+^1$ $5s_+^1$	4047.2517	4047.2572	(Kr) $4d^5$ $5s^1$
		(Kr) $4d_-^4$ $4d_+^2$	4047.1823	4047.1903	
Tc	43	(Kr) $4d_-^4$ $4d_+^2$ $5s_+^1$	4284.2622	4284.2718	c)
		(Kr) $4d_-^4$ $4d_+^1$ $5s_+^2$	4284.2423	4284.2488	(Kr) $4d^5$ $5s^2$
		(Kr) $4d_-^4$ $4d_+^3$	4284.2075	4284.2174	
Ru	44	(Kr) $4d_-^4$ $4d_+^3$ $5s_+^1$	4529.3901	4529.4017	(Kr) $4d^7$ $5s^1$ c)
		(Kr) $4d_-^4$ $4d_+^4$	4529.3587	4529.3683	
		(Kr) $4d_-^4$ $4d_+^2$ $5s_+^2$	4529.3535	4529.3646	
Rh	45	(Kr) $4d_-^4$ $4d_+^4$ $5s_+^1$	4782.7806	4782.7917	(Kr) $4d^8$ $5s^1$ c)
		(Kr) $4d_-^4$ $4d_+^5$	4782.7568	4782.7632	
		(Kr) $4d_-^4$ $4d_+^3$ $5s_+^2$	4782.7094	4782.7226	

Table 5 (continued)

Symbol	Z	Electron structure	DHF calculated −TE(AU)	DHF calculated −AE(AU)	Ground state [28]. c) [2] d) [9]
Pd	46	(Kr) $4d^4$ $4d^5_+$ $5s^1_+$	5044.5316	5044.5390	c)
		(Kr) $4d^4_-$ $4d^6_+$	5044.5269	5044.5269	(Kr) $4d^{10}$
		(Kr) $4d^4_-$ $4d^4_+$ $5s^2_+$	5044.4352	5044.4477	
Ag	47	(Kr) $4d^4_-$ $4d^6_+$ $5s^1_+$	5314.7757	5314.7757	(Kr) $4d^{10}$ $5s^1$ c)
		(Kr) $4d^4_-$ $4d^6_+$ $5p^1$	5314.6644	5314.6644	
		(Kr) $4d^4_-$ $4d^5_+$ $5s^2_+$	5314.6508	5314.6590	
Cd	48	(Kr) $4d^4_-$ $4d^6_+$ $5s^2_+$	5593.4802	5593.4802	(Kr) $4d^{10}$ $5s^2$ c)
		(Kr) $4d^4_-$ $4d^6_+$ $5s^1_+$ $5p^1$	5593.3640	5593.3640	
		(Kr) $4d^4_-$ $4d^5_+$ $5s^2_+$ $5p^1_-$	5593.0917	5593.1007	
In	49	$(4d^{10})$ $5s^2_+$ $5p^1_-$	5880.6194	5880.6194	(Cd) $5p^1$
		$(4d^{10})$ $5s^1_+$ $5p^2_-$	5880.4324	5880.4324	
Sn	50	$(4d^{10})$ $5s^2_+$ $5p^2_-$	6176.3416	6176.3416	(Cd) $5p^2$
		$(4d^{10})$ $5s^1_+$ $5p^2_-$ $5p^1_+$	6176.0967	6176.1004	
Sb	51	$(4d^{10})$ $5s^2_+$ $5p^2_-$ $5p^1_+$	6480.7646	6480.7686	(Cd) $5p^3$
		$(4d^{10})$ $5s^1_+$ $5p^2_-$ $5p^2_+$	6480.4471	6480.4525	
Te	52	$(4d^{10})$ $5s^2_+$ $5p^2$ $5p^2_+$	6793.9838	6793.9897	(Cd) $5p^4$
		$(4d^{10})$ $5s^1_+$ $5p^2_-$ $5p^3_+$	6793.5842	6793.5887	
I	53	$(4d^{10})$ $5s^2_+$ $5p^2_-$ $5p^3_+$	7116.0977	7116.1025	(Cd) $5p^5$
		$(4d^{10})$ $5s^2_+$ $5p^2_-$ $5p^2_+$ $6s^1_+$	7115.8535	7115.8603	
		$(4d^{10})$ $5s^1_+$ $5p^2_-$ $5p^4_+$	7115.6124	7115.6124	
Xe	54	$(4d^{10})$ $5s^2_+$ $5p^2_-$ $5p^4_+$	7447.2186	7447.2186	(Cd) $5p^6$
		$(4d^{10})$ $5s^2_+$ $5p^2_-$ $5p^3_+$ $6s^1_+$	7446.9369	7446.9424	
		$(4d^{10})$ $5s^2_+$ $5p^2_-$ $5p^3_+$ $5d^1_-$	7446.8801	7446.8869	
Cs	55	(Xe) $6s^1_+$	7787.1333	7787.1333	(Xe) $6s^1$ c)
		(Xe) $5d^1_-$	7787.0727	7787.0763	
Ba	56	(Xe) $6s^2_+$	8136.0530	8136.0530	(Xe) $6s^2$ c)
		(Xe) $5d^1$ $6s^1_+$	8136.0154	8136.0185	

Table 5 (continued)

Symbol	Z	Electron structure	DHF calculated		Ground state
			$-$TE(AU)	$-$AE(AU)	[28], c) [2], d) [9]
La	57	(Xe) $5d_-^1$ $6s_+^2$	8494.1045	8494.1086	(Xe) $5d^1$ $6s^2$ c)
		(Xe) $5d_-^2$ $6s_+^1$	8494.0874	8494.0923	
		(Xe) $4f_-^1$ $6s_+^2$	8494.0054	8494.0136	
Hf	72	(Xe) $4f_-^6$ $4f_+^8$ $5d_-^2$ $6s_+^2$	15090.919	15090.926	(Xe) $4f^{14}$ $5d^2$ $6s^2$ c)
		(Xe) $4f_-^6$ $4f_+^8$ $5d_-^3$ $6s_+^1$	15090.837	15090.841	
		(Xe) $4f_-^6$ $4f_+^7$ $5d_-^3$ $6s_+^2$	15090.463	15090.483	
Ta	73	$(4f^{14})$ $5d_-^3$ $6s_+^2$	15619.018	15619.024	(Xe) $4f^{14}$ $5d^3$ $6s^2$ c)
		$(4f^{14})$ $5d_-^4$ $6s_+^1$	15618.957	15618.957	
		$(4f^{14})$ $5d_-^4$ $5d_+^1$	15618.950	15618.952	
W	74	$(4f^{14})$ $5d_-^4$ $6s_+^2$	16158.864	16158.864	(Xe) $4f^{14}$ $5d^4$ $6s^2$
		$(4f^{14})$ $5d_-^4$ $5d_+^1$ $6s_+^1$	16158.809	16158.814	
		(Xe) $4f_-^6$ $4f_+^7$ $5d_-^4$ $5d_+^1$ $6s_+^2$	16157.811	16157.833	
Re	75	$(4f^{14})$ $5d_-^4$ $5d_+^1$ $6s_+^2$	16710.606	16710.612	(Xe) $4f^{14}$ $5d^5$ $6s^2$
		$(4f^{14})$ $5d_-^4$ $5d_+^2$ $6s_+^1$	16710.562	16710.571	c)
		$(4f^{14})$ $5d_-^4$ $5d_+^3$	16710.465	16710.474	
Os	76	$(4f^{14})$ $5d_-^4$ $5d_+^2$ $6s_+^2$	17274.417	17274.427	(Xe) $4f^{14}$ $5d^6$ $6s^2$
		$(4f^{14})$ $5d_-^4$ $5d_+^3$ $6s_+^1$	17274.390	17274.402	c)
		$(4f^{14})$ $5d_-^4$ $5d_+^4$	17274.305	17274.314	
Ir	77	$(4f^{14})$ $5d_-^4$ $5d_+^3$ $6s_+^2$	17850.468	17850.480	(Xe) $4f^{14}$ $5d^7$ $6s^2$ d)
		$(4f^{14})$ $5d_-^4$ $5d_+^4$ $6s_+^1$	17850.459	17850.469	c)
		$(4f^{14})$ $5d_-^4$ $5d_+^5$	17850.393	17850.399	
Pt	78	$(4f^{14})$ $5d_-^4$ $5d_+^5$ $6s_+^1$	18438.953	18438.960	(Xe) $4f^{14}$ $5d^9$ $6s^1$ c) d)
		$(4f^{14})$ $5d_-^4$ $5d_+^4$ $6s_+^2$	18438.937	18438.948	
		$(4f^{14})$ $5d_-^4$ $5d_+^6$	18438.902	18438.902	
Au	79	$(4f^{14})$ $5d_-^4$ $5d_+^6$ $6s_+^1$	19040.044	19040.044	(Xe) $4f^{14}$ $5d^{10}$ $6s^1$ c) d)
		$(4f^{14})$ $5d_-^4$ $5d_+^5$ $6s_+^2$	19040.005	19040.012	
		$(4f^{14})$ $5d_-^4$ $5d_+^6$ $6p_-^1$	19039.895	19039.895	

Table 5 (continued)

Symbol	Z	Electron structure		DHF calculated		Ground state
				−TE(AU)	−AE(AU)	[28], c) [2], d) [9]
Hg	80	$(4f^{14})$	$5d^4\ 5d^6_+\ 6s^2_+$	19653.870	19653.870	(Xe) $4f^{14}\ 5d^{10}\ 6s^2$
		$(4f^{14})$	$5d^4_-\ 5d^6_+\ 6s^1_+\ 6p^1_-$	19653.713	19653.713	
		$(4f^{14})$	$5d^4_-\ 5d^5_+\ 6s^2_+\ 6p^1_-$	19653.594	19653.602	
Tl	81	$(5d^{10})$	$6s^2_+\ 6p^1_-$	20280.397	20280.397	(Hg) $6p^1$
		$(5d^{10})$	$6s^1_+\ 6p^2_-$	20280.183	20280.183	
Pb	82	$(5d^{10})$	$6s^2_+\ 6p^2_-$	20919.909	20919.909	(Hg) $6p^2$
		$(5d^{10})$	$6s^1_+\ 6p^2_-\ 6p^1_+$	20919.599	20919.602	
		$(5d^{10})\ 5f^2_-$	$6s^2_+$	20919.311	20919.313	
		$(4f^{14})$	$5d^4_-\ 5d^5_+\ 6s^2_+\ 6p^2_-\ 6p^2_+$	20919.276	20919.289	
Bi	83	$(5d^{10})$	$6s^2_+\ 6p^2_-\ 6p^1_+$	21572.572	21572.576	(Hg) $6p^3$
		$(5d^{10})$	$6s^1_+\ 6p^2_-\ 6p^2_+$	21572.177	21572.182	
Po	84	$(5d^{10})$	$6s^2_+\ 6p^2_-\ 6p^2_+$	22238.584	22238.589	(Hg) $6p^4$
		$(5d^{10})$	$6s^1_+\ 6p^2_-\ 6p^3_+$	22238.101	22238.105	
At	85	$(5d^{10})$	$6s^2_+\ 6p^2_-\ 6p^3_+$	22918.167	22918.171	
		$(5d^{10})$	$6s^2_+\ 6p^2_-\ 6p^2_+\ 7s^1_+$	22917.961	22917.967	
		$(5d^{10})$	$6s^1_+\ 6p^2_-\ 6p^4_+$	22917.583	22917.583	
Rn	86	$(5d^{10})$	$6s^2_+\ 6p^2_-\ 6p^4_+$	23611.517	23611.517	(Hg) $6p^6$
		$(5d^{10})$	$6s^2_+\ 6p^2_-\ 6p^3_+\ 7s^1_+$	23611.289	23611.294	
		$(5d^{10})$	$6s^2_+\ 6p^2_-\ 6p^3_+\ 6d^1_-$	23611.225	23611.231	
Fr	87	(Rn)	$7s^1_+$	24318.616	24318.616	c)
		(Rn)	$6d^1_-$	24318.557	24318.558	
Ra	88	(Rn)	$7s^2_+$	25039.773	25039.773	(Rn) $7s^2$
		(Rn)	$6d^1_-\ 7s^1_+$	25039.719	25039.722	
		(Rn)	$7s^1_+\ 7p^1_-$	25039.719	25039.719	
Ac	89	(Rn)	$6d^1_-\ 7s^2_+$	25775.221	25775.224	(Rn) $6d^1\ 7s^2$
		(Rn)	$6d^2_-\ 7s^1_+$	25775.165	25775.169	

Table 5 (continued)

Symbol	Z	Electron structure	DHF calculated		Ground state
			$-$TE(AU)	$-$AE(AU)	[28], c) [2] d) [9]
	104	$(5f^{14})\ 6d_-^1\ 7s_+^2\ 7p_-^1$	38758.899	38758.903	
		$(5f^{14})\ 6d_-^2\ 7s_+^2$	38758.894	38758.899	d)
		$(5f^{14})\ 7s_+^2\ 7p_-^2$	38758.831	38758.831	
		$(5f^{14})\ 6d_-^3\ 7s_+^1$	38758.776	38758.780	
		$(5f^{14})\ 6d_-^1\ 7s_+^1\ 7p_-^2$	38758.758	38758.763	
		$(\mathrm{Rn})\ 5f_-^6\ 5f_+^7\ 6d_-^3\ 7s_+^2$	38758.436	38758.451	
	105	$(5f^{14})\ 6d_-^3\ 7s_+^2$	39772.180	39772.185	d)
		$(5f^{14})\ 6d_-^2\ 7s_+^2\ 7p_-^1$	39772.163	39772.169	
		$(5f^{14})\ 6d_-^1\ 7s_+^2\ 7p_-^2$	39772.076	39772.081	
		$(5f^{14})\ 6d_-^4\ 7s_+^1$	39772.070	39772.070	
	106	$(5f^{14})\ 6d_-^4\ 7s_+^2$	40806.599	40806.599	d)
		$(5f^{14})\ 6d_-^4\ 6d_+^1\ 7s_+^1$	40806.473	40806.477	
		$(\mathrm{Rn})\ 5f_-^6\ 5f_+^7\ 6d_-^4\ 6d_+^1\ 7s_+^2$	40805.719	40805.735	
	107	$(5f^{14})\ 6d_-^4\ 6d_+^1\ 7s_+^2$	41862.784	41862.789	d)
		$(5f^{14})\ 6d_-^4\ 6d_+^2\ 7s_+^1$	41862.646	41862.654	
		$(5f^{14})\ 6d_-^4\ 6d_+^3$	41862.484	41862.492	
	108	$(5f^{14})\ 6d_-^4\ 6d_+^2\ 7s_+^2$	42941.395	42941.403	d)
		$(5f^{14})\ 6d_-^4\ 6d_+^3\ 7s_+^1$	42941.260	42941.269	
		$(5f^{14})\ 6d_-^4\ 6d_+^4$	42941.100	42941.108	
	109	$(5f^{14})\ 6d_-^4\ 6d_+^3\ 7s_+^2$	44043.206	44043.216	d)
		$(5f^{14})\ 6d_-^4\ 6d_+^4\ 7s_+^1$	44043.088	44043.097	
		$(5f^{14})\ 6d_-^4\ 6d_+^5$	44042.923	44042.928	
	110	$(5f^{14})\ 6d_-^4\ 6d_+^4\ 7s_+^2$	45169.029	45169.038	d)
		$(5f^{14})\ 6d_-^4\ 6d_+^5\ 7s_+^1$	45168.909	45168.915	
		$(5f^{14})\ 6d_-^4\ 6d_+^6$	45168.749	45168.749	c)
	111	$(5f^{14})\ 6d_-^4\ 6d_+^5\ 7s_+^2$	46319.724	46319.730	d)
		$(5f^{14})\ 6d_-^4\ 6d_+^6\ 7s_+^1$	46319.621	46319.621	c)
		$(5f^{14})\ 6d_-^4\ 6d_+^6\ 7p_-^1$	46319.385	46319.385	

Table 5 (continued)

Symbol	Z	Electron structure		DHF calculated		Ground state
				$-$TE(AU)	$-$AE(AU)	[28], c) [2] d) [9]
	112	$(5f^{14})$	$6d_-^4\ 6d_+^6\ 7s_+^2$	47496.244	47496.244	d)
		$(5f^{14})$	$6d_-^4\ 6d_+^5\ 7s_+^2\ 7p_-^1$	47496.125	47496.132	
		$(5f^{14})$	$6d_-^4\ 6d_+^6\ 7s_+^1\ 7p_-^1$	47496.026	47496.026	
	113	$(6d^{10})$	$7s_+^2\ 7p_-^1$	48699.491	48699.491	d)
		$(6d^{10})$	$7s_+^1\ 7p_-^2$	48699.198	48699.198	
		$(6d^{10})$	$7s_+^1\ 7p_-^1\ 7p_+^1$	48699.101	48699.104	
	114	$(6d^{10})$	$7s_+^2\ 7p_-^2$	49930.620	49930.620	d)
		$(5f^{14})$	$6d_-^4\ 6d_+^5\ 7s_+^2\ 7p_-^2\ 7p_+^1$	49930.202	49930.213	
		$(6d^{10})$	$7s_+^1\ 7p_-^2\ 7p_+^1$	49930.160	49930.163	
		$(6d^{10})$	$7s_+^2\quad 6f_-^2$	49929.888	49929.890	
	115	$(6d^{10})$	$7s_+^2\ 7p_-^2\ 7p_+^1$	51190.773	51190.776	d)
		$(6d^{10})$	$7s_+^1\ 7p_-^2\ 7p_+^2$	51190.165	51190.169	
	116	$(6d^{10})$	$7s_+^2\ 7p_-^2\ 7p_+^2$	52481.367	52481.372	d)
		$(6d^{10})$	$7s_+^1\ 7p_-^2\ 7p_+^3$	52480.659	52480.663	
	117	$(6d^{10})$	$7s_+^2\ 7p_-^2\ 7p_+^3$	53803.978	53803.982	d)
		$(6d^{10})$	$7s_+^2\ 7p_-^2\ 7p_+^2\quad 8s_+^1$	53803.873	53803.878	
		$(6d^{10})$	$7s_+^1\ 7p_-^2\ 7p_+^4$	53803.123	53803.123	
	118	$(6d^{10})$	$7s_+^2\ 7p_-^2\ 7p_+^4$	55160.323	55160.323	d)
		$(6d^{10})$	$7s_+^2\ 7p_-^2\ 7p_+^3\ 8s_+^1$	55160.206	55160.210	
		$(6d^{10})$	$7s_+^2\ 7p_-^2\ 7p_+^3\ 7d_-^1$	55160.108	55160.114	
	119	(118)	$8s_+^1$	56552.178	56552.178	d)
		(118)	$7d_-^1$	56552.081	56552.083	
		(118)	$8p_-^1$	56551.774	56551.774	
	120	(118)	$8s_+^2$	57981.806	57981.806	
		(118)	$8s_+^1\ 8p_-^1$	57981.738	57981.738	
		(118)	$8s_+^1\quad 7d_-^1$	57981.707	57981.709	

When only one accepted electron structure for an atomic number Z was calculated [2], entries c) in Table 5 were omitted

Table 5: the calculated TE and AE for all elements up to $Z = 120$. Each element was calculated in two or more electron configurations. In Table 5 when only one configuration is presented (case Li, Be, Na, K), the second calculated configuration was not converging.

Table 5 contains all chemical periods from H up to $Z = 120$: lanthanides and actinides are separated from other elements in Tables 6, 7. Symbol and Z in the first two columns are self-explanatory. Electron structure in the third column of Table 5 is denoted by n, l, a symbols for the last electrons which follow the electron configuration of a core with all closed shells. As cores the symbols (Ne), (Ar), (Kr), (Xe), (Rn), (118) are used for the configuration of ground states of elements Ne, Ar, Kr, Xe, Rn and 118. When symbols ($3d^{10}$), ($4d^{10}$), ($4f^{14}$), ($5d^{10}$), ($5f^{14}$) and ($6d^{10}$) are used, they correspond to closed shell configurations of (Ar) $3d^4_- 3d^6_+$, (Kr) $4d^4_- 4d^6_+$, (Xe) $4f^6_- 4f^8_+$, (Xe) $4f^6_- 4f^8_+ 5d^4_- 5d^6_+$, (Rn) $5f^6 5f^8_+$ and (Rn) $5f^6_- 5f^8_+ 6d^4_- 6d^6_+$, respectively.

In columns 4 and 5 our calculated values in atomic units taken with - sign are presented. The value with the lowest energy among them is underlined, corresponding to our calculated ground states. In the last column experimentally known ground states spectroscopically determined up to $Z = 96$ are presented – according to [28], by non-relativistic symbols similar to relativistic ones in column 3. Besides the cores of noble gases, here we use (Zn), (Ce) and (Hg), each corresponding to the electron ground states of Zn, Cd or Hg respectively for cores.

In the last column, when available, the ground state determined by NRHF calculations according to [2] is marked by the symbol *c*). Also, when available, the gound state determined by DFS according to [9] is marked by the symbol *d*). In the case of lanthanides (Table 6) full TE values calculated in [2] are presented. In the case of actinides (Table 7) our results are compared with full NRHF data from [2] and DFS data from [9] and are discussed in the following section.

4. Discussion

Table 5 presents our results for total energies (– TE or – AU) of all elements in the periodic system up to $Z = 120$ (exclusive of $4f$ and $5f$ elements) in comparison with spectroscopically determined ground states of [28]. It is visible that our calculated ground states as TE or AE (under-lined in Table 5) show the same electron structure. One exclusion is the case of Mo, where TE shows (Kr) $4d^4_- 5s^2_+$ structure and AE (Kr) $4d^4_- 4d^1_+ 5s^1_+$ structure. However, energetically, they are within the limits of calculating errors and are, therefore, equally possible. The errors of calculation, taken as the difference between two calculations repeated in sequence (using the first results as the starting point for the second calculation) is usually ± 0.001 – 0.002 AU. In comparison with experimentally determined ground states, our results in Table 5 reproduce them completely, with the following few exclusions: Cr, Cu, Nb, Tc, Pd. It is necessary to bear in mind that experimentally the ground state is determined as the electron structure giving the lowest lying multiplet. Our program is able to calculate only a mean energetic level of each configuration (AE), i.e., the barycentrum of all multiplets of the determined ground state configuration. If two configurations exist with a

Table 6. Total energies of lanthanides in AU ($-E_T$ values)

Symbol	Z	Electron structure	This work (−TE)	DHF (−AE)	NR − HF [2]	NR − H [2]	Experimental [28] ground state
La	57	(Xe) $5d^1_- 6s^2_+$	8494.1045*	8494.1086*	8220.473*	8141.964*	(Xe) $5d^1 6s^2$
		(Xe) $5d^2_- 6s^1_+$	8494.0874	8494.0923			
		(Xe) $4f^1_-$ $6s^2_+$	8494.0054	8494.0137	8220.291	8141.887	
Ce	58	(Xe) $4f^1_-$ $5d^1_- 6s^2_+$	8861.5974*	8861.6117*	8566.201*	8484.990*	(Xe) $4f^1$ $5d^1 6s^2$
		(Xe) $4f^2_-$ $6s^2_+$	8861.5277	8861.5422	8566.109	8484.834	
		(Xe) $5d^2_- 6s^2_+$	8861.4690	8861.4751	8565.985	8484.976	
Pr	59	(Xe) $4f^2_-$ $5d^1_- 6s^2_+$	9238.8064*	9238.8278*	8920.320	8836.331*	
		(Xe) $4f^3_-$ $6s^2_+$	9238.7565	9238.7738	8920.324*	8836.200	(Xe) $4f^3$ $6s^2$
		(Xe) $4f^1_-$ $5d^2_- 6s^2_+$	9238.6512	9238.6689	8920.076	8836.275	
		(Xe) $5d^3_- 6s^2_+$			8919.610	8836.031	
Nd	60	(Xe) $4f^3_-$ $5d^1_- 6s^2_+$	9625.8666*	9625.8910*	9282.884	9196.042*	
		(Xe) $4f^4_-$ $6s^2_+$	9625.8381	9625.8544	9282.909*	9195.923	(Xe) $4f^4$ $6s^2$
		(Xe) $4f^2_-$ $5d^2_- 6s^2_+$	9625.6908	9625.7163			
Pm	61	(Xe) $4f^4_-$ $5d^1_- 6s^2_+$	10022.9266*	10022.9495*	9653.980	9564.213*	
		(Xe) $4f^5_-$ $6s^2_+$	10022.9133	10022.9240	9654.023*	9564.103	(Xe) $4f^5$ $6s^2$
		(Xe) $4f^3_-$ $5d^2_- 6s^2_+$	10022.7258	10022.7544			
Sm	62	(Xe) $4f^6_-$ $6s^2_+$	10430.1302*	10430.1302	10033.732*	9940.806	(Xe) $4f^6$ $6s^2$
		(Xe) $4f^5_-$ $5d^1_- 6s^2_+$	10430.1179	10430.1343*	10033.674	9940.910*	
		(Xe) $4f^4_-$ $5d^2_- 6s^2_+$	10429.9022	10429.9291			
Eu	63	(Xe) $4f^6_-$ $5d^1_- 6s^2_+$	10847.6027*	10847.6072*	10422.037	10326.204*	
		(Xe) $4f^6_- 4f^1_+$ $6s^2_+$	10847.5153	10847.5247	10422.108*	10326.107	(Xe) $4f^7$ $6s^2$
		(Xe) $4f^5_- 4f^2_+$ $6s^2_+$	10847.4429	10847.4709			
		(Xe) $4f^5_-$ $5d^2_- 6s^2_+$	10847.3660	10847.3856			
Gd	64	(Xe) $4f^6_- 4f^1_+$ $5d^1_- 6s^2_+$	11275.3958*	11275.4109*	10819.139	10720.165*	(Xe) $4f^7$ $5d^1 6s^2$
		(Xe) $4f^6_- 4f^2_+$ $6s^2_+$	11275.3201	11275.3370	10819.225*	10720.075	
		(Xe) $4f^6_-$ $5d^2_- 6s^2_+$	11275.2588	11275.2654			

Table 6 (continued)

Symbol	Z	Electron structure	This work (−TE)	DHF (−AE)	NR − HF [2]	NR − H [2]	Experimental [28] ground state
Tb	65	(Xe) $4f^6_- \, 4f^2_+ \, 5d^1_- \, 6s^2_+$	11713.7535*	11713.7769*	11225.080	11122.892*	
		(Xe) $4f^6_- \, 4f^3_+ \, 6s^2_+$	11713.6898	11713.7118	11225.175*	11122.803	(Xe) $4f^9 \; 6s^2$
		(Xe) $4f^6_- \, 4f^1_+ \, 5d^2_- \, 6s^2_+$	11713.6038	11713.6221	11224.741	11122.765	
Dy	66	(Xe) $4f^6_- \, 4f^3_+ \, 5d^1_- \, 6s^2_+$	12162.8253*	12162.8542*	11639.912	11534.437*	
		(Xe) $4f^6_- \, 4f^4_+ \, 6s^2_+$	12162.7717	12162.7960	11640.014*	11534.349	(Xe) $4f^{10} \; 6s^2$
		(Xe) $4f^6_- \, 4f^2_+ \, 5d^2_- \, 6s^2_+$	12162.6650	12162.6924			
Ho	67	(Xe) $4f^6_- \, 4f^4_+ \, 5d^1_- \, 6s^2_+$	12622.7719*	12622.8030*	12063.708	11954.872*	
		(Xe) $4f^6_- \, 4f^5_+ \, 6s^2_+$	12622.7266	12622.7500	12063.818*	11954.784	(Xe) $4f^{11} \; 6s^2$
		(Xe) $4f^6_- \, 4f^3_+ \, 5d^2_- \, 6s^2_+$	12622.5966	12622.6298			
Er	68	(Xe) $4f^6_- \, 4f^5_+ \, 5d^1_- \, 6s^2_+$	13093.7330*	13093.7632*	12496.560	12384.288*	
		(Xe) $4f^6_- \, 4f^6_+ \, 6s^2_+$	13093.7018	13093.7211	12496.673*	12384.196	(Xe) $4f^{12} \; 6s^2$
		(Xe) $4f^6_- \, 4f^4_+ \, 5d^2_- \, 6s^2_+$	13093.5581	13093.5581			
Tm	69	(Xe) $4f^6_- \, 4f^6_+ \, 5d^1 \, 6s^2_+$	13575.8969*	13575.9224*	12938.520	12822.738*	
		(Xe) $4f^6_- \, 4f^7_+ \, 6s^2_+$	13575.8540	13575.8656	12938.633*	12822.647	(Xe) $4f^{13} \; 6s^2$
		(Xe) $4f^6_- \, 4f^5_+ \, 5d^5_- \, 6s^2_+$	13575.7059	13575.7404			
Yb	70	(Xe) $4f^6_- \, 4f^7_+ \, 5d^1_- \, 6s^2_+$	14069.4034*	14069.4203*	13389.685	13270.315*	
		(Xe) $4f^6_- \, 4f^8_+ \, 6s^2_+$	14069.3615	14069.3615	13389.800*	13270.209	(Xe) $4f^{14} \; 6s^2$
		(Xe) $4f^6_- \, 4f^6_+ \, 5d^2_- \, 6s^2_+$	14069.2041	14069.2335			
Lu	71	(Xe) $4f^6_- \, 4f^8_+ \, 5d^1_- \, 6s^2_+$	14574.4121*	14574.4164*	13850.105*	13727.072*	(Xe) $4f^{14} \, 5d^1 \, 6s^2$
		(Xe) $4f^6_- \, 4f^8_+ \, 5d^2_- \, 6s^1_+$	14574.3276	14574.3324	13850.022	13736.962	
		(Xe) $4f^6_- \, 4f^7_+ \, 5d^2_- \, 6s^2_+$	14574.2155	14574.2356			

Table 7. Total energies of actinides in AU (− E values)

Symbol	Z	Electron structure		This work (− TE)	DHF (− AE)	DFS Finite nucleus [9]	NR - HF [2]	NR - H [2]	Experimental [28, 30] ground state
Ac	89	(Rn)	$6d^1_- \ 7s^2_+$	25775.221*	25775.224*	25748.8215*	23719.989	23529.981	(Rn) $6d^1 \ 7s^2$
		(Rn)	$6d^2_- \ 7s^1_+$	25775.165	25775.169				
		(Rn)	$5f^1_- \ 7s^2_+$	not converging		25748.7235			
Th	90	(Rn)	$6d^2_- \ 7s^2_+$	26525.270*	26525.275*	26497.1235*	24357.353	24163.507*	(Rn) $6d^2 \ 7s^2$
		(Rn) $5f^1_-$	$6d^1_- \ 7s^2_+$	26525.195	26525.205	26497.102	24357.453*	24163.481	
		(Rn) $5f^2_-$	$7s^2_+$	26525.088	26525.097	26497.036	24357.425	24163.377	
Pa	91	(Rn) $5f^1_-$	$6d^2_- \ 7s^2_+$	27290.293*	27290.306*	27260.451	25004.576	24806.696	
		(Rn) $5f^2_-$	$6d^1_- \ 7s^2_+$	27290.261	27290.276	27260.473*	25004.724	24806.714*	(Rn) $5f^2 \ 6d^1 \ 7s^2$
		(Rn) $5f^2_-$	$6d^2_- \ 7s^1_+$	27290.221	27290.237				
		(Rn)	$6d^3_- \ 7s^2_+$	27290.212	27290.216				
		(Rn) $5f^3_-$	$7s^2_+$	27290.148	27290.160	27290.237	25004.746*	24806.641	
U	92	(Rn) $5f^3_-$	$6d^1_- \ 7s^2_+$	28070.689*	28070.707*	28038.6875*	25661.828	25459.711*	(Rn) $5f^3 \ 6d^1 \ 7s^2$
		(Rn) $5f^2_-$	$6d^2_- \ 7s^2_+$	28070.672	28070.690	28038.6235	25661.628	25459.651	
		(Rn) $5f^4_-$	$7s^2_+$	28070.613	28070.624	28038.680	25661.887*	25459.660	
		(Rn) $5f^1_-$	$6d^3_- \ 7s^2_+$	28070.547	28070.560				
Np	93	(Rn) $5f^4_-$	$6d^1_- \ 7s^2_+$	28866.774*	28866.791*	28832.6635	26328.820	26122.532*	(Rn) $5f^4 \ 6d^1 \ 7s^2$
		(Rn) $5f^5_-$	$7s^2_+$	28866.722	28866.730	28832.6845*	26328.930*	26122.519	
		(Rn) $5f^3_-$	$6d^2_- \ 7s^2_+$	28866.711	28866.732	28832.563	26328.590	26122.458	
Pu	94	(Rn) $5f^5_-$	$6d^1_- \ 7s^2_+$	29678.838*	29678.850*	29642.1245	27005.753	26795.231	
		(Rn) $5f^6_-$	$7s^2_+$	29678.812	29678.812	29642.176*	27005.911*	26795.252*	(Rn) $5f^6 \ 7s^2$
		(Rn) $5f^4_-$	$6d^2_- \ 7s^2_+$	29678.747	29678.767	29641.987	27005.481	26795.114	
Am	95	(Rn) $5f^6_-$	$6d^1_- \ 7s^2_+$	30507.231*	30507.235*	30467.781	27692.695	27477.876	
		(Rn) $5f^6_- \ 5f^1_+$	$7s^2_+$	30507.135	30507.142	30467.8205*	27692.884*	27477.916*	(Rn) $5f^7 \ 7s^2$
		(Rn) $5f^5_-$	$6d^2_- \ 7s^2_+$	30507.109	30507.124	30467.608	27692.366	27477.713	

Table 7 (continued)

Symbol	Z	Electron structure	This work (−TE)	DHF (−AE)	DFS Finite nucleus [9]	NR−HF [2]	NR−H [2]	Experimental [28, 30] ground state
Cm	96	(Rn) $5f^6_- \; 5f^1_+ \; 6d^1_- \; 7s^2_+$	31352.179*	31352.191*	31309.039	28389.681	28170.503	(Rn) $5f^7 \; 6d^1 \; 7s^2$
		(Rn) $5f^6_- \; 6d^2_- \; 7s^2_+$	31352.133	31352.139	31308.881	28389.304	28170.301	
		(Rn) $5f^6_- \; 5f^2_+ \; 7s^2_+$	31352.116	31352.128	31309.1055*	28389.907*	28170.569*	
Bk	97	(Rn) $5f^6_- \; 5f^2_+ \; 6d^1_- \; 7s^2_+$	32215.135*	32214.152*	32167.4905	29096.792	28872.193	
		(Rn) $5f^6_- \; 5f^3_+ \; 7s^2_+$	32214.106	32214.122	32167.5805*	29097.055*	28873.282*	
		(Rn) $5f^6_- \; 5f^1_+ \; 6d^2_- \; 7s^2_+$	32214.053	32214.067	32167.301	29096.376	28872.962	
		(Rn) $5f^6_- \; 5f^4_+ \; 7s^1_+$	32213.894	32213.909				
Cf	98	(Rn) $5f^6_- \; 5f^4_+ \; 7s^2_+$	33093.492*	33093.510*	33043.7585*	29814.350*	29586.081*	
		(Rn) $5f^6_- \; 5f^3_+ \; 6d^1_- \; 7s^2_+$	33093.475	33093.496	33043.642	29814.037	29585.955	
		(Rn) $5f^6_- \; 5f^2_+ \; 6d^2_- \; 7s^2_+$	33093.377	33093.397	33043.423			
Es	99	(Rn) $5f^6_- \; 5f^5_+ \; 7s^2_+$	33990.664*	33990.681*	33936.8105*	30541.883*	30309.055*	
		(Rn) $5f^6_- \; 5f^4_+ \; 6d^1_- \; 7s^2_+$	33990.643	33990.666	33936.6725	30541.541	30308.912	
		(Rn) $5f^6_- \; 5f^3_+ \; 6d^2_- \; 7s^2_+$	33990.497	33990.522	33936.4235			
Fm	100	(Rn) $5f^6_- \; 5f^6_+ \; 7s^2_+$	34906.063*	34906.077*	34847.5135*	31279.643*	31042.192*	
		(Rn) $5f^6_- \; 5f^5_+ \; 6d^1_- \; 7s^2_+$	34906.019	34906.041	34847.352	31279.253	31042.014	
		(Rn) $5f^6_- \; 5f^7_+ \; 7s^1_+$	34905.868	34905.876				
		(Rn) $5f^6_- \; 5f^4_+ \; 6d^2_- \; 7s^2_+$	34905.851	34905.878	34847.0745			
Md	101	(Rn) $5f^6_- \; 5f^7_+ \; 7s^2_+$	35840.177*	35840.186*	35776.1305*	32027.727*	31785.589*	
		(Rn) $5f^6_- \; 5f^6_+ \; 6d^1_- \; 7s^2_+$	35840.094	35840.113	35775.948	32027.327	31785.414	
		(Rn) $5f^6_- \; 5f^8_+ \; 7s^1_+$	35839.979	35839.979				
		(Rn) $5f^6_- \; 5f^5_+ \; 6d^2_- \; 7s^2_+$	35839.869	35839.895	35775.6415			
No	102	(Rn) $5f^6_- \; 5f^8_+ \; 7s^2_+$	36793.382*	36793.382*	36721.740*	32786.180*	32539.291*	
		(Rn) $5f^6_- \; 5f^7_+ \; 6d^1_- \; 7s^2_+$	36793.300	36793.313	36721.533	32785.739	32539.087	
		(Rn) $5f^6_- \; 5f^6_+ \; 6d^2_- \; 7s^2_+$	36793.048	36793.060	36721.1985			
Lr	103	(Rn) $5f^6_- \; 5f^8_+ \; 6d^1_- \; 7s^2_+$	37766.134*	37766.138*	37682.363	33554.555	33303.099	
		(Rn) $5f^6_- \; 5f^8_+ \; 6d^2_- \; 7s^1_+$	37766.025	37766.030				
		(Rn) $5f^6_- \; 5f^7_+ \; 6d^2_- \; 7s^2_+$	37765.893	37765.909				

close barycentrum of their multiplets (e.g. a difference of only 0.01 AU = 0.27 eV) it is possible that the lowest lying multiplet is in the configuration with the higher lying barycentrum. Furthermore, our calculations for open shells are in error, using coefficients $\Gamma_{j_A v j_B}$ (valid exactly only for closed shells). The magnitude of error introduced by such approximation is visible if we compare our TE with AE, both of which are calculated with different coefficients in the terms containing $\Gamma_{j_A v j_A}$. In the case of Cr, Cu, Nb, Tc and Pd, the maximal difference between TE and AE is 0.011 AU – so here we could accept ±0.013 AU as a reasonably estimated error in total energy (covering incorrect $\Gamma_{j_A v j_B}$ coefficients and including calculation errors). From this point of view the experimental and theoretical ground states of Cu, Nb, Tc and Pd which differ less than 0.026 AU are still within the ±0.013 AU error limits. Only the case of Cr clearly indicates some discrepancy between experiment and theory. On the other hand, in almost all cases in Table 5 it is visible that the use of incorrect $\Gamma_{j_A v j_B}$ coefficients in the last few open shells is not very critical because ground states here were correctly calculated. The ground state position found by NRH in [2], available for most of the periodic system (denoted by *c*)) in Table 5, are in accord with our DHF values, including the cases of Cr, Cu, Nb, Tc, Pd – however, they differ in the cases of Re, Os, Ir, 110 and 111 element. The positions of ground states found by DFS calculations [9] (using finite nucleus approximation denoted by *d*)) in Table 5 for Ir, Pt, Au and 105-120 element agree exactly with ours. For 104 element DFS values [9] present $(5f^{14})\,6d_-^2\,7s_+^2$, as the ground state configuration. However, in [9] $(5f^{14})\,6d_-^1\,7s_+^2\,7p_-^1$ state was not calculated by the DFS method which we found to be the ground state. The same ground state as ours was reported by Mann [29].

In contrast to the good accord of calculated ground state with experimental ones in Table 5, the case of lanthanides and actinides in Tables 6 and 7 presents systematical discrepancies. The lowest lying states calculated as DHF (this work), DFS (9), NRH (2) and NRHF (2) in Tables 6 and 7 are denoted by *. From the comparison of our −TE and −AU values in the lanthanides series with spectroscopic data [28, 30], our results of −AE show one $5d_-^1$ electron present in all lanthanides. Our results of −TE indicate the same, with the exclusion of Sm^{62}, where no $5d_-^1$ is present in the ground state. If we accept the value ±0.02 AU (i.e., maximal allowed difference between two states 0.04 AU) as a reasonably estimated error of −AE or −TE – due to computing errors and incorrect use of $\Gamma_{j_A v j_B}$ also for open shells – we could explain the discrepancy between theory and experiment in the case of Pm and Sm and, perhaps, for Nd and Er. The discrepancies are to great in the cases of Tb, Dy, Ho and especially, of Eu. It is very difficult to explain them in the same way; their calculated ground states, each containing one $5d_-^1$ electron are 0.05 to 0.085 AU lower than states without $5d$ electrons.

In the lanthanide series the positions of ground states from NRH calculations [2] are in exact accord with ours. On the other hand the NRHF calculations [2] are apparently giving wrong results (see Table 6 and Table 7) they are systematically indicating the same structure in both lanthanides and actinides: no $5d_-^1$ electrons in any lanthanide below Ce and no $6d_-^1$ electrons below Th, with similar structure of Ce and Th, each containing one $5d_-^1$ or $6d_-^1$ electron respectively. Systematic DFS results for lanthanides are not available. Our results in the actinide series for both $-$TE or $-$AE values are in accord with experimentaly determined ground state positions for Ac, Th, U, Np and Cm. For Pa and Pu our calculated ground states are 0.03 AU or 0.038 AU lower than those experimentally determined (i.e. still within the estimated 0.04 AU difference, as mentioned in the lanthanide case). In the case of Am (also of Eu) we have a strong discrepancy with experimental results (we found $5d^1_-$ present in the ground state). In the region from Cf to No our results indicate the absence of $6d$ electrons and again the presence of one $6d^1_-$ electron in Lr. DFS results, calculated for actinides in [9], agree with experimental results in the case of Ac, Th, Pa, U, Pu, Am and disagree for Np and Cm. DFS calculations indicate the absence of $6d$ electrons in all actinides, starting from Np. NRH calculations are in the best accord with experiments agreeing in the cases of Ac, Th, Pa, U, Np, Pu and Am and disagreeing for Cm. They indicate the absence of $6d$ electrons in the actinide series starting from Pu.

Generally, the disagreement in the lanthanides and some actinides between calculated and spectroscopically determined ground states known to us from 1969 [16] is disturbing. We realize that it is very important to remove these discrepancies. The most simple way to do it is to find the exact position of both barycentrums in the two neighbor configurations (of experimental ground state and DHF ground state). This can be done by finding its experimental average energies – as the weighted average energetic position of all their multiplets (using the present assignment of spectral lines). This could lead to a natural explanation of discrepancies – without necessitating the reclassification of spectral lines. Another way is to calculate exactly the ground state configuration terms, using the exact complicated coefficients for open shells, in place of $\Gamma_{j_A v j_B}$. This method should give final results, and could, eventually, suggest some need for the change in the ground state assignment of some lanthanides and actinides. However, it needs substantial change in our program and extensive computer time. From this point of view, the present predictions of chemistry of superheavy elements [9, 29], based on DFS [9] and DHF [19] calculations (using calculations of barycentrum of ground state only) are only preliminary – as is natural for the first step in the unknown region. We believe that a thorough investigation of atoms and ions in the known region of the periodic system is crucial in order to predict the chemistry of some superheavy elements by the DHF or DFS methods.

Acknowledgement. The authors are indebted to Professor G. Bouissières for discussions and continuous support of this work.

References

1. Hermann, F., Skillman, S.: Atomic structure calculations. Englewood Cliffs, New Jersey: Prentice Hall, Inc. 1963.
2. Larson, A. C., Waber, J. T.: Self-consistent field hartree calculations for atoms and ions. Los Alamos: Los Alamos Scientific Laboratory, preprint LA-DC-8508, 1967.
3. Froese, Ch.: J. chem. Physics 45, 1417 (1966); Froese, Ch.: Hartree-Fock parameters for the atoms helium to radon. Vancouver: Department of Mathematics, University of Columbia 1966.
4. Mann, J. B.: Atomic structure calculations. 1. Hartree-Fock energy results for the elements hydrogen to lawrencium. Los Alamos: Los Alamos Scientific Laboratory preprint LA-3690, 1967.

5. Snow, E.C., Canfield, J.M., Waber, J.T.: Physic. Rev. **135** A, 969 (1964).
6. Liberman, D., Waber, J.T., Cromer, D.T.: Physic. Rev. **137** A, 27 (1965).
7. Rosen, A., Lindgren, I.: Physic. Rev. **176**, 114 (1968).
8. Waber, J.T., Cromer, D.T., Liberman, D.: J. chem. Physics **51**, 664 (1969).
9. Fricke, B., Greiner, W., Waber, J.T.: Theoret. chim. Acta (Berl.) **21**, 235 (1971).
10. Grant, I.P.: Proc. Royal Soc. (London) A **262**, 555 (1961).
11. Grant, I.P.: Proc. physic. Soc. **86**, 523 (1965).
12. Grant, I.P.: Advances in Physics **19**, 747 (1970).
13. Mayers, D.F.: (results for Hg) quoted by Liberman, D. *et al.*: Physic. Rev. **137** A, 27 (1965).
14. Coulthard, M.A.: Proc. physic. Soc. **91**, 44 (1967).
15. Mann, J.B., Waber, J.T.: (results for Md and No) quoted as Ref. 181 by Seaborg, G.T.: Annu. Rev. nuclear Sci. **18**, 53 (1958).
16. Malý, J.: (results for ground states of actinides and ions of Pa) quoted by Chauchois, Y.: Tagungsbericht der 3. Internationalen Protaktiniumkonferenz, Schloss Elmau bei Mittenwald, 15 april 1969, Preprint BMBW-FBK 71-17, München (1971).
17. Desclaux, J.P., Mayers, D.F., Brien, F.O.: J. Physics B. Atom Molec. Physics **4**, 631 (1971).
18. Mann, J.B., Johnson, W.R.: Physic. Rev. A **4**, 41 (1971).
19. Mann, J.B., Waber, J.T.: J. chem. Physics **53**, 2397 (1970).
20. Nilsson, S.G., Nix, J.R., Sobciewski, A., Szymanski, Z., Wyczech, S., Gustafson, C., Möller, P.: Nuclear Physics A **115**, 545 (1968).
21. Swirles, B.: Proc. Royal Soc. A, **152**, 625 (1935).
22. Kim, Y.K.: Physic. Rev. **154**, 17 (1967).
23. Hartree, D.R.: The calculation of atomic structure. New York, John Wiley; London, Chapman & Hall, 1957.
24. Slater, J.C.: Quantum theory of atomic structure, Vol. 1. New York Toronto - London: Mac Graw Hill 1960.
25. Coulthard, M.A.: University of Melbourne, Internal Report UM-P-66/4 (1966).
26. Tucker, T.C., Roberts, L.D., Nestor, C.W., Carlson, T.A., Malik, F.B.: Physic. Rev. **174**, 118 (1968).
27. Bearden, J.A., Burr, A.F.: Rev. mod. Physics **39**, 125 (1967).
28. Moore, Ch. E.: NSRDS-NBS 34, Nat. Stand. Ref. Data, National Bureau of Standards, Washington 1970.
29. Fricke, B., Waber, J.T.: Actinide Rev. **1**, 433 (1971), Ref. 46
30. Moore, Ch. E.: Appl. Optics **2**, 665 (1963)

Dr. J. Malý
Institut de Physique Nucléaire,
Division de Radiochimie
Université de Paris XI
Centre d'Orsay, B.P. 1
F-91 Orsay, France

[illegible] numbers
38966
24.4.82